The University of Nottingham
Faculty of Engineering
Department of Civil Engineering
Institute of Engineering Surveying and Space Geodesy

Estimation of Arabian rigid plate motion and strain rate accumulation within the Arabian plate using GPS measurements

By
Bandar Saleh Almuslmani
BSc, MSc

Thesis submitted to the University of Nottingham
for the degree of Doctor of Philosophy
July 2009

BRITISH LIBRARY

IMAGING SERVICES NORTH

Boston Spa, Wetherby
West Yorkshire, LS23 7BQ
www.bl.uk

NO CD/DVD ATTACHED

PLEASE APPLY TO THE UNIVERSITY

Abstract

The Arabian plate is classified as medium sized. It is surrounded by the Nubian, Somalian, Eurasian and Indian plates. Previous investigations of present-day kinematics of the Arabian plate using GPS measurements were primarily obtained from stations located on surrounding plates, with few stations actually located on the Arabian plate itself. Due to the inhomogeneous distribution of these GPS stations and the fact that some of these were actually located in the plate boundary zone, the motion of Arabia was only sensed in a few locations of the rigid plate interior.

Through the establishment of GPS networks in Saudi Arabia, the aim of this study was to compute an updated estimate for the absolute and relative motion of the Arabian plate Euler pole and rotation rate. Then to investigate, at the regional scale, the strain rate accumulation within the Arabian plate. Then, to investigate, at a local scale, the strain rate accumulation in the tectonically active south-western part of Saudi Arabia.

The results of this study are on absolute motion model for the Arabian plate which is significantly different from those obtained in previous studies, as a result of the number of stations used and their distribution. This does not mean that the previous studies were in error, but that they suffered from a lack of evenly distributed geodetic data for Arabia. Hence, this study result is a new contribution to the knowledge of Arabian plate motion. The results of this study for the relative motion model of the Arabian plate with respect to the Eurasian, Nubian and Somalian plates confirms the results from previous studies, and confirms that the Arabian plate motion is slowing down.

This study has also shown that, in general, the strain values are low in most of the Arabian plate, where there is a compression in the north-east to south-west directions and an extension in the north-west to south-east direction, except in two areas, the north-west, close to the Aqaba Gulf and the Dead Sea fault, and the south-west where there are high strain values and variable directions for the principle strain. Furthermore, this study agrees with geologic studies in that there is a compression north-east to south-west and extension north-west to south-east between Farasan Island and the coast of the Red Sea.

Acknowledgments

I would be grateful to my parents who encourage and support me all the time. My grateful goes to the Lieutenant General Morraye Al-shahrani for giving me this opportunity to do this research and for his encourage and support during all the stage of this research as well as providing the research data.

Likewise, I am very grateful to my supervisors Professor Terry Moore, Dr. Richard Bingley and Dr. Norman Teferle for their continuous advice, support, help and guidance during my study, without them this piece of work could not have been possible. A very special thank you to Dr. Norman Teferle for his patient on the lengthy discussions during this research. Also, I thank Dr. Richard Bingley for the proof reading of this thesis. As well, my gratitude goes to all IESSG staff.

The author is thankful to David Lavallée for the provision of the TANYA software used for the plate motion model computations. Also I like to acknowledge the IGS community for the use of IGS data and products [*Beutler et al.,* 1999] and GFZ re-processed orbits and ERPS product [Steigenberger et al., 2006].

I owe many special thanks to Brigadier Saeed Alzahrani for his support and encouragement during this research. My thanks must goes to Brigadier Abdullah Aloraini for his support for this research and during the field campaigns. Furthermore, thanks should also go to my colleagues in GCS Col. Turkey Alotaibi, Lt.Col. DR. Eid Almoitari and Mr. Mubarak Aldosari for their continuous encouragement, advice and help on the field campaigns arrangements. Also my thanks to Professor Sadiq Oqleuo the consultant of GCS for his advice.

Also, I would like to thank my colleagues in GCS who participate in the field campaigns Brigadier Ali Alzahrani, Col. Saeed Alamri, Lt.Col.Dr. Abdilaziz Alothman, Lt.Col.Eng. Abdulmohsan Althydi, Maj.Eng. Talaq Alotaibi and all other participate in the field campaign because without them this work has not been achieved.

Contents

List of Figures

List of Tables

Acronyms and abbreviations

BIH	Bureau International de l'Heure
BPE	Bernese Processing Engine
BSW	Bernese software
CATS	Coordinate time series analysis
CM	Centre of Mass of the earth
CTSAna	Coordinate Time Series Analysis
DCB	differential code bias
DORIS	Doppler Orbit determination and Radio-positioning Integrated by Satellite
EOF	Empirical Orthogonal Filter
EOP	Earth Orientation Parameters
GCS	GCS General Commission for Survey
GMF	Global Mapping Function
GMT	Generic Mapping Tools
GNSS	The International Global Navigation Satellite System
GPS	Global Positioning System
IMF	isobaric mapping function
IERS	International Earth Rotation Service
IESSG	Institute of Engineering Surveying and Space Geodesy
IGS	International GNSS Service
ITRS	International Terrestrial Reference System
ITRSF	International Terrestrial Reference Frame
LLR	Lunar Laser Ranging
LOD	Length of Day
MLE	maximum likelihood estimation
NNR	No-Net-Rotation
OTL	Ocean tide loading
PCV	phase centre variation

QIF	Quasi Ionosphere-Free
SLR	Satellite Laser Ranging
UT	Universal Time
VMF	Vienna mapping function
ZHD	Zenith Hydrostatic Delay
ZTD	Zenith Total Delay

1. Introduction

The earth surface is subject to external forces, such as the gravitational attraction of the moon and the sun and of other planets, and interior forces, such as mantle convection or surface boundary and plate forces, as slabs pull and ridges push. In 1912, Alfred Wegener revealed his continental drift theory, stating that some 200 million years ago the super continent Pangaea started to split apart. Shortly afterwards, this theory was supported by a number of scientists. Hence, the continental drift theory led to the new scientific concept of plate tectonics, a model in which the outer shell of the earth is divided into a number of thin, rigid plates that are in relative motion with each other [Turcotte and Schubert, 2002]. The rigid plates are massive, irregularly shaped slabs of solid rock, with a size varying between hundreds to thousands of square kilometres. The continuous splitting and moving of the lithosphere (super continent) of 200 million years ago has resulted in seven major plates and numerous small plates at the present time [Martha, 1996].

A plate's motion can be in the form of a rotation, a translation or a deformation. Moreover, the magnitudes of velocities for these plates are of the order of a few tens of millimetres per year. Furthermore, earthquakes, volcanic eruptions and mountains occur at the plate boundaries. Therefore, the estimation of the motion of tectonic plates and their deformations is quite important, since these motions and deformations play a key role in seismic hazard mapping as well as other applications. Therefore, scientists and researchers have carried out more and more investigations to estimate these plate motions and deformations using different techniques and methods, the main three being geologic techniques, geophysics techniques and geodetic techniques.

Space geodetic techniques, such as Satellite Laser Ranging (SLR), Very Long Baseline Interferometry (VLBI) and Global Positioning System (GPS) are used to investigate plate motion and their deformation. However, in recent years, GPS has been most widely used for a variety of reasons, mainly because it is capable of estimating plate motions when sufficient observations are available over a fairly lengthy time period and secondly because of the low cost of GPS equipment and processing compared to other techniques. GPS techniques have developed dramatically in recent years, with millimetre level accuracy now being achievable. These developments have been in all aspects of GPS, starting with the constellation, receivers, antenna and station monument specification, but also considering GPS bias and error mitigation and reference frame.

The Arabian plate is classified as medium sized compared to others such as the Eurasian plate. It is surrounded by Nubia and Somalia on the west and south-west, Eurasia on the north and east, and India on the south-east. Arabia divides into two main geological parts, namely the Arabian shield, which covers one third of the plate on the west along the Red Sea and the Arabian platform, which covers two thirds of the plate on the east. Most seismicity associated with the plate occurs along the plate boundary zone, for example, along the Zagros Belt [e.g. Reilinger *et al.*, 2006] and the Dead Sea Fault [e.g. Wdowinski *et al.*, 2004]. Clusters of seismic events exist along the continuation of the Dead Sea Fault through the Gulf of Aqaba and along the Red Sea spreading axis [e.g. McClusky *et al.*, 2003], which continues into the East African Rift [e.g. Fernandes *et al.*, 2004; Stamps *et al.*, 2008], and along the Gulf of Aden.

Previous investigations of the present-day kinematics of the Arabian plate using GPS measurements were primarily obtained from stations located on surrounding plates, often with few stations actually located on the Arabian plate itself. Due to the inhomogeneous distribution of these GPS stations and the fact that some of these were actually located in the plate boundary zone, the

motion of the Arabia plate was only sensed in a few locations on the rigid plate interior [Sella *et al.*, 2002], [Kreemer *et al.*, 2003], [McClusky *et al.*, 2003], [Prawirodirdjo and Bock, 2004], [Vernant *et al.*, 2004], [Drewes and Angermann, 2001], [Drewes, 2006], [Vigny *et al.*, 2006], [Reilinger *et al.*, 2006], [Kreemer *et al.*, 2006], [Altamimi *et al.*, 2007].

In order to advance the knowledge of the dynamics of the Arabian plate and its intra-plate deformations, the General Commission for Survey (GCS), through collaboration with the Institute of Engineering Surveying and Space Geodesy (IESSG), densified the GPS network in Saudi Arabia, to cover nearly two thirds of the tectonic plate. Much of the early work for this was detailed in Almotairi [2006], who used the early data from the GCS network to investigate Arabian plate motion and large scale deformations. For this continuing study there were three aims. The first aim was the computation of an updated estimate for the absolute and relative motion of the Arabian plate Euler pole and rotation rate, now in ITRF2005, using a near global reference frame and a new processing strategy. In contrast to Almotairi [2006], this study also uses the recent absolute phase centre models for satellite and receiver antennas' as well as the new GPS products, introduced by the IGS in November 2006, and the first reprocessing products [Steigenberger *et al.*, 2006]. The second aim was to investigate, at the regional scale, the strain rate accumulation within the Arabia plate using the GPS network. The third aim was to investigate, at a local scale, the strain rate accumulation in the tectonically active south-western part of Saudi Arabia using a densified GPS network of 27 stations.

The following items summarize the objectives of this study.

- To establish a dense GPS network for Arabian plate geodynamic studies.
- To develop a processing strategy.
- To compute the daily coordinates for GPS network stations.
- To estimate the velocity field for the GPS network stations.

- To estimate the velocity uncertainties for the GPS network stations.
- To estimate the absolute Arabian plate motion.
- To estimate the relative Arabian plate motion with respect to the surrounding plates (Eurasian, Nubian and Somalian).
- To investigate, at the regional scale, the strain rate accumulation within the Arabia plate using the GPS network.
- To investigate, at a local scale, the strain rate accumulation in the tectonically active south-western part of Saudi Arabia.

The novelty of this study is expected to be the first reliable result concerning the Arabian plate Euler pole and rotation rate estimation in ITRF2005, since it was densified with a well distributed station network (minimum time span for most stations being four years). Furthermore, this study is the first of its kind, at the regional scale and local scale, for strain rate accumulation within the Arabia plate.

This thesis is structured into eight chapters and the overviews of these chapters are summarized as follows. In Chapter Two, (**Earth's interior and Arabian plate structure**) the earth interior (crust, mantle and core) and the Arabian plate structures are briefly described with the present shape of the tectonic plates. Also, the drivers of plate tectonics are discussed, and the main types of plate movement are explained. A detailed introduction to the Arabian plate structure, including the Arabian shield, Arabian platform and Red Sea, are then given. Finally, the Arabian plate seismicity is described.

Chapter Three, **(GPS for geodynamic investigations)** start by briefly describing the developments of reference frames and their importance in geodetic work, with a short explanation of the latest ITRF2005 realization. Then the IGS products and community are outlined, followed by the criteria for station positions for regional networks and how they are optimally expressed in an ITRF. Then, the GPS constellation is discussed with its recent developments, followed by a short explanation of the GPS observables with

their linear combinations, ambiguity resolution and differencing techniques. Finally, GPS bias and error mitigation is outlined.

Chapter Four, **(The GPS data set and processing strategy)** describes the GPS networks and their station specifications, the campaigns carried out and the data quality checking considered. Details are then given of the reference frame implementation applied and the processing strategy used in this study. Finally, the stages of GPS data processing when using the Bernese processing software version 5.0 are outlined.

Chapter Five, **(Velocity and uncertainty estimation using time series Analysis)** briefly revisits the theory of geodetic time series analysis, including the modelling of periodic signals, coordinate offsets, and stochastic noise. Regional filtering is introduced as a means of improving the signal-to-noise ratio in the coordinate time series and is then applied to both continuous and episodic data. The Coordinate Time Series Analysis (CTSAna) tools used in the analysis are also briefly described, and the velocities and uncertainties estimated for the continuous and episodic GPS stations in this study are presented.

Chapter Six, **(Estimation of the Arabian rigid plate motion)**, presents the previous studies on Arabian plate motion and the background theory for plate motion estimation. Results for the estimated absolute motion for the rigid Arabian plate are presented. Also, the impact of the number of stations and their distribution on the Arabian plate are tested and the influence of stations in active areas, or near the plate boundary, are evaluated. Following that, the results for the preferred estimation of Arabian plate motion from this study are compared to the estimations of previous studies. Furthermore, the relative motion of the Arabian plate with respect to the surrounding plates (Eurasian, Nubian and Somalian) is estimated and compared to other studies.

Chapter Seven, (**Strain rate accumulation within the Arabian plate**), discusses the background theory of strain and its estimations. Strain rate accumulations within the Arabia plate at a regional scale and at a local scale in the south-west part are then estimated and analysed.

Chapter Eight, (**Conclusions and recommendations for further work**) presents the conclusions of this study.

Chapter 2: Earth interior and Arabian plate structure

2.1 Introduction

The theory of plate tectonics has been a unifying concept that has revolutionized earth science over the last century. In order to understand tectonic plate motion, the interior structure of the earth should be studied and understood, since the activities happening in the earth's interior produce the forces that act on the plates and cause them to move.

In this chapter, the earth's interior structure will be outlined briefly, followed by a review of the type of forces causing different plate movement types. Elements of the Arabian plate structure will then be discussed, such as the tectonic setting of the Arabian shield, Arabian platform and the Red Sea, and seismicity.

2.2 Earth's interior structure and tectonics

The radius of the Earth is approximately 6,300 km and there are three main layers in the interior structure of the Earth (crust, mantle and core). In a simple description, these layers are similar to a boiled egg, where the crust is the outside rigid and thin shell, the mantle is the white and the core is the yolk. The thickness of the crust varies between 0–100 km, with an average value beneath the continents of 38 km and beneath the oceans of 5–8 km [Donald and Schubert, 2002; Fowler, 2005]. The second layer, the mantle is below the crust and is approximately 2,900 km thick, extending down towards the Earth's central core. The mantle consists of iron, magnesium and silicates. It is denser than the crust, because the temperature and pressure increase with depth. The mantle is divided into two main parts: the upper part and the lower part. The third layer is the core, which is below the mantle and surrounds the centre of the Earth, with a radius of approximately 3,400 km. The core consists of iron and nickel. It is divided into two parts: the liquid outer core (2,200 km) and the inner solid core (1,200 km) [Fowler, 2005]. For an illustration, see Figure 2.1.

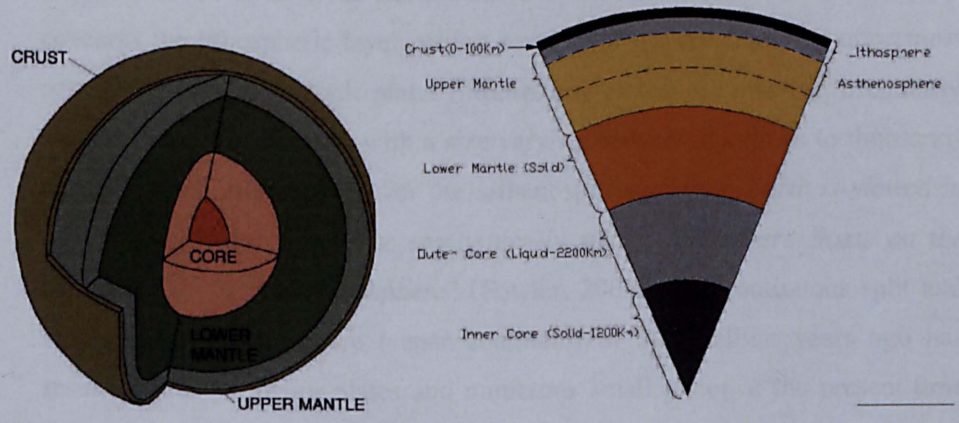

Figure 2.1. Interior structure of the Earth (http://pubs.usgs.gov/gip/interior/).

The upper part of the mantle is cooler and rigid. Therefore, the layer comprising the crust and the uppermost part of the mantle is called the lithosphere (from the Greek word lithos, meaning ROCK or STONE). The average thickness of the lithosphere is approximately 100 km, but it is thinner under the oceans (less than 15 km) and thicker in continental areas (up to or more than 200 km). The layer directly beneath the lithosphere in the upper mantle layer is called the asthenosphere (from the Greek word asthenia, meaning WEAK or SICK). This is hot and a semi-solid (heavy liquid) material [Martha, 1996].

In 1912, the German meteorologist Alfred Wegener published a scientific theory called continental drift, stating that some 200 million years ago the super continent Pangaea started to split apart. His theory was supported a short time later by a number of scientists. The continental drift theory led to the new scientific concept of plate tectonics.

In geological terms, a plate is a large rigid slab of solid rock and the word tectonics comes from the Greek for "to build". Therefore, the term plate tectonics refers to how the Earth's surface is built of plates. Plate tectonics concerns the lithospheric layer, which consists of the crust and the uppermost part of the mantle. Tectonic plates (lithospheric plates) are massive, irregularly shaped slabs of solid rock, with a size varying between hundreds to thousands of km^2, which are moving over the asthenosphere. "*If the Earth is viewed in purely mechanical terms, the mechanically strong lithosphere floats on the mechanically weak asthenosphere*" [Fowler, 2005]. The continuous split and moving of the lithosphere (super continent) of 200 million years ago has resulted in seven major plates and numerous small plates at the present time [Martha, 1996]. Figure 2.2 illustrates their general shape at present.

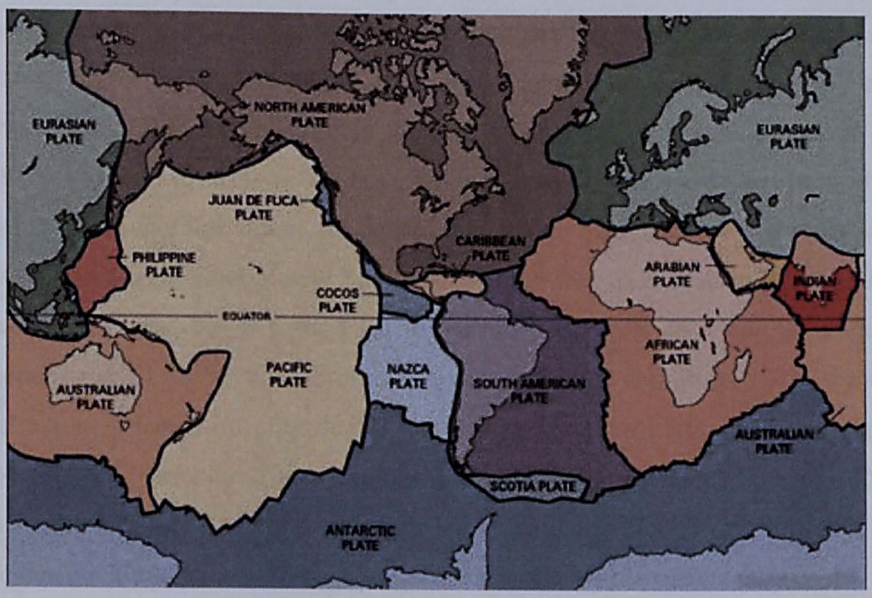

Figure 2.2. Present shapes of Earth plates [Martha, 1996].

The continuous movements of plates relative to each other in different directions and at different rates do not affect the size of the Earth, because any movement on one side of a plate has an effect on its other side.

Moreover, the geological and geophysics communities argue about what drives plate tectonics. There are two major concerns: whether mantle convection dominates or whether surface boundary and plate forces, as slabs pull and ridges push, are the most important. These are illustrated in Figure 2.3.

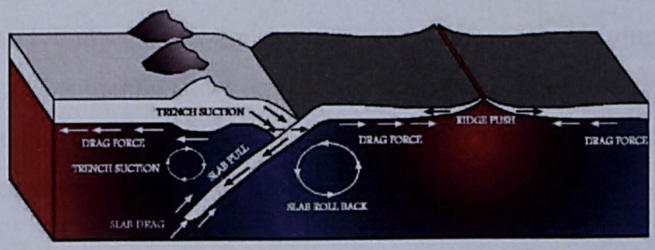

Figure 2.3. Different plate driving forces. (www.umich.edu/~gs265/tecpaper.htm#Discussion)

Geophysicists and geologists use three techniques to quantify the plate driving forces. First is the deformational modelling technique, which uses intra-plate stress fields. This was popular in the late 1970s and used by Soloman *et al.* [1975] and Bott [1991]. In this case, finite element models are used to predict both global and individual plate motions based on the forces driving and resisting the individual plates. The results found this technique to be good for individual plates, but not good for the earth, because it does not adequately account for all of the appropriate complex boundary conditions. The second technique is based on empirical relationships between plate size, age, type, geometry and velocity. This technique was used by Forsyth and Uyeda [1975], and is based on the strong correlation between plate velocities and the age of the oceanic lithosphere, but does not allow for other types of forces.

The third technique is the Net Torque Method, which studies the driving mechanism of plate motion by balancing the net torque acting on each plate. The advantage of this method is in accounting for all plate forces in the equation, both driving and resistive. The rigid rotation law is defined as if there is no acceleration and/or inertia acting on that body; then all applied forces or torques should sum to zero, so the net torque acting on that body must be zero. This follows Newton's second law of motion: the acceleration of any object is directly proportional to the net forces acting on it and inversely proportional to its mass. Moreover, in order for the Net Torque Method to work, a number of assumptions are made: firstly, the acceleration and inertia of each plate are negligible so the plates are in dynamic equilibrium; secondly, the surface boundary and body forces are considered as the main driving forces, as opposed to active mantle flow; thirdly, since the plates move on the surface of the Earth, their respective motions are described as a rotation about an axis passing through the centre of the Earth.

As stated previously, surface boundary and body forces occur as slabs pull and ridges push. Ridge push can be considered as both a body force and a surface

boundary force. As a body force, ridge push has been attributed to the cooling and thickening of the oceanic lithosphere with age [McKenzie, 1970],. As a surface boundary force, ridge push is caused by the gravity effect, which results from warm buoyant mantle up-welling beneath the ridge crest, causing a topography-induced horizontal pressure gradient. Slab pull derives from the negative buoyancy of the cold subducting lithosphere and is dependent on the temperature, age, angle and volume of the subducting slab, as well as the length of the respective trench.

Studies have classified plate movement into three main types: divergent, convergent and transform. Divergent movement (accreting or constructive) is a linear movement between two plates where these plates are moving away from each other and new crust is created by magma pushing up from the mantle, such as the opening ridge of the Red Sea. Convergent (consuming or destructive) movement is where two plates slide into each other and usually collide forming either a subduction zone or an orogenic belt. Transform movement (lithosphere is neither created nor destroyed) is where the plates move laterally relative to each other.

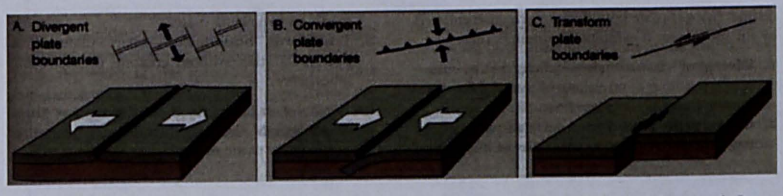

Figure 2.4. Types of plate movement [http://pubs.usgs.gov/gip/dynamic].

2.3 Arabian plate structure

The Arabian plate is 25–30 million years old, and consists of crystalline Precambrian (545–4550 Ma), phanerozoic sedimentary (545–0 Ma) and volcanic rocks [Al-Amri, 1998; Rodgers *et al.*, 1999]. The Arabian plate is classified as medium sized compared to others plates such as the Eurasian one. It is surrounded by the African (Nubian, Somalian) plate to the west and south-west, the Eurasian plate to the north and east and the Indian plate to the south-east (see Fig. 2.5).

The geological history of the Arabian plate (Arabian lithosphere) has not been investigated widely, especially the uppermost part of the mantle, but a number of research projects have been carried out on selected areas of the Arabian plate to study and investigate the geology of the Arabian crust (top layer of the Arabian lithosphere). These studies show that the Arabian plate divides into two main parts, namely: the Arabian shield, which covers one third of the plate and is in the west, along the Red Sea; and the Arabian platform, which covers the other two thirds of the plate [Sanvol *et al.*, 1998; Al-Amri, 1999a], as shown in Figure 2.5.

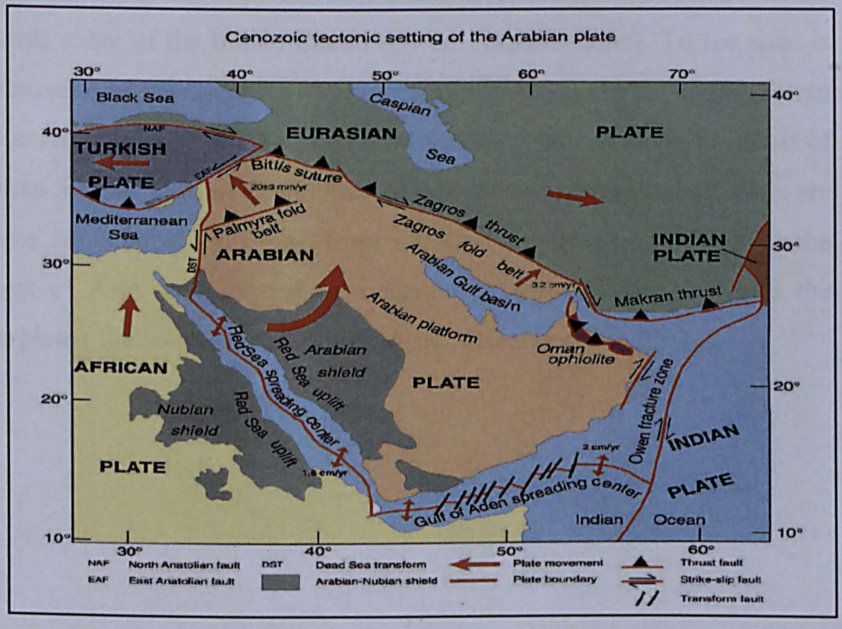

Figure 2.5. The geological map of the Arabian plate [Saudi Geological Survey, 2006].

Seismological studies show that the Arabian shield thickness averages 40 km [Badri, 1991], 51 km [Al-Amri, 1999a] and 39 km [Al-Damegh *et al.*, 2005]. The shield is gradually thinning towards the Red Sea where new oceanic crust is forming and it consists of different layers. The Arabian platform is covered by phonerozoic sediments and the thickness averages 45 km, gradually thickening towards the Zagros Mountains, where continental collision is taking place. Here, the uppermost mantle thickness averages 51 km [Al-Amri, 1999a]. The total displacement of Arabian plate is estimated at about 107 km since Oligocene times (30 Ma), with an annual rate of about 0.5 cm over the last 7 to 10 million years [Grünthal *et al.*, 2006].

The separation between the Arabian plate and the African plate 30 million years ago created the Great Rift Valley, which starts in northern Syria (south-west of Asia) and runs to central Mozambique (in East Africa), a distance of about 5,000 km, with the valley being 30–100 km in width. It starts with the Jordan River running in the northern part down to the Dead Sea; then continues with the Wadi Arabah running from the Dead Sea in a southern direction; then the rift continues through the Gulf of Aqaba and the Red Sea. The southern end of the Red Sea marks a fork in the rift. To the east is the Gulf of Aden, then the mid-oceanic ridge of the Indian Ocean (Owen Fracture Zone). To the west is the continuation of the Great Rift Valley into East Africa. In the south-eastern part of the Arabian plate are the Makran Mountains that run along the coast of the Arabian Sea and Gulf of Oman. East and north-east of the Arabian plate are the Zagros Mountains, extending from the Gulf of Oman 1,500 km to the south-west of Asia, and formed by collision of the Arabian plate and the Eurasian plate (the so-called the Zagros thrust) [Nehlig *et al.*, 2002].

2.3.1 Arabian Shield

The Arabian shield and Nubian shield were attached to each other and then separated by the Red Sea in the Oligocene age (30 Ma). The Arabian shield was formed by Precambrian terranes. These terranes are Midyan, Hijaz, Jeddah, Asir, Afif, Hail, Ad Dawadimi and Ar Rayn, as shown in Figure 2.6. Moreover, these terranes are separated from each other by suture zones.

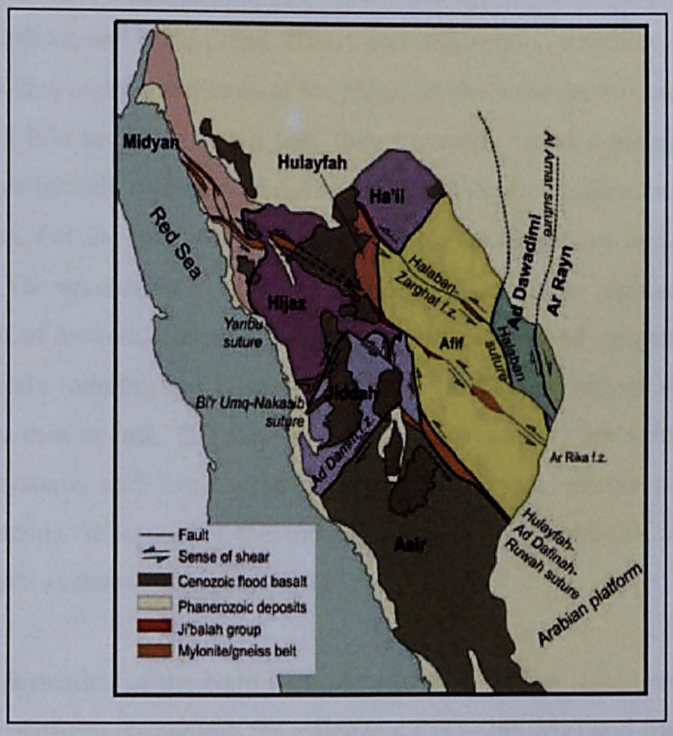

Figure 2.6. The Arabian shield tectonic structure from the Precambrian age, [compiled by Peter R. Johnson in 1998].

The Midyan, Hijaz, Jeddah and Asir terranes form the western part of the Arabian shield and Afif, Hail, Ad Dawadimi and Ar Aayn terranes form the eastern side of the shield. The eastern build-up may have started by about 680–640 Ma when the Afif terrane collided with the western shield along the Nabitah suture. At about 670 Ma, a subduction complex formed west of the

Amar arc. Along this subduction zone, the Afif terrane and Ar Rayn terrane collided from about 640–620 Ma [Al-Husseini, 2000].

The Arabian shield is a very old area of about 770,000 km^2. Its slightly arched surface sloping very gently toward the north, north-east and east. The Arabian shield is composed of sedimentary Precambrian rocks. The fold fault pattern of the shield, together with some layer relationships, suggests that the shield has undergone two orogenic cycles. The first cycle was the Hijaz orogeny, which was the more intense and widespread. East-west compression was dominant so that strongly folded and faulted beds of the shield in the west-central part trend north-easterly while in the southern part they generally trend northerly. The tectonic features include transcurrent normal and high angle reverse faults and major fold axes. For the orogeny, folding and intrusion may have occurred at greater depth. The second cycle was the Najd orogeny, and this represents the younger period of mountain building. The effects of the second orogeny were the north-westerly trending left lateral faults. The faults may reflect shearing from shallower movements. The fault systems in this orogeny are subsequent to the other systems and have offset and truncated many of the previous tectonic lineaments. It is one of the most prominent Precambrian/Cambrian hard wrench fault systems [Chapman, 1978].

Following the formation of the Najd fault system, the Arabian shield remained a rather stable platform throughout the Paleozoic (545–248 Ma) and Mesozoic (248–65 Ma) except for several episodes of movement along older faults. The only major event that affected the region since early Cambrian was the deformation and magmatism associated with the Red Sea rifting. Recently, various speculations have indicated that the Arabian-Nubian shield was formed through a process of arc and terranes accretion. On the basis of this interpretation, the evolution of the Arabian shield is in terms of three stages: magmatic arc, continental collision and intra-cratonic.

Two distinct phases of continental magmatism are evident in western Saudi Arabia. The first phase produced tholeiitic-to-transitional lavas emplaced along north-west trends from about 30 to 20 Ma. The second phase produced transitional-to-strongly alkalic lavas emplaced along north–south trends about 12 Ma to recent. The first phase is attributed to passive mantle up-welling during an extension of the Red Sea basin, whereas the second phase is attributed to active mantle up-welling but was facilitated by a minor continental extension perpendicular to the plate collision [Camp and Roobol, 1992]. The second phase is largely contemporaneous with a major period of crustal uplift to produce the west Arabian swell. The central axis of the uplift and magmatism of the Arabian swell is symmetric and coincides with two fundamental features, which are the Hail-Ruthbah arch in the north and the Makkah-Madinah-Nafud volcanic line in the south [Camp and Roobol, 1992]. Volcanism was widespread in western Saudi Arabia during the Tertiary period (65–2 Ma). The oldest lavas are called the Trap series on Cretaceous clastics in Yemen; these are associated closely with the rifting of the Red Sea. Northwards thick effusions of basalt and andesite cover vast areas. The effusions have been subdivided on the basis of radioactive dating and these range from the Oligocene to Holocene (33–0 Ma). The Oligocene and Holocene flows were like those of the Trap series. Thus, volcanism has continued up to the present time [Chapman, 1978].

2.3.2 Arabian Platform

The Arabian platform consists of the Paleozoic and Mesozoic sedimentary rocks that uncomfortably overlay the shield and dip very gently and uniformly to the east and north-east towards the Arabian Gulf [Powers *et al.*, 1966]. The accumulated sediments in the Arabian platform represent the south-eastern part of the vast Middle East basin that extends eastward into Iran, westward into the eastern Mediterranean, and northward into Jordan and Syria.

The Arabian shield isolated the Arabian platform from the North African Tethys and played an active paleogrographic role through gentle subsidence of its northern and eastern sectors during the phanerozoic, allowing almost 5,000 metres of continental and marine sediments to be deposited over the platform. This accumulation of sediments represents several cycles from the Cambrian onward and now forms a homocline dipping very gently away from the Arabian shield [Al-Amiri and Alkhalifah, 2004].

The Amar collision occurred along the north-trending Amar suture, that bisects the Arabian peninsula at about 45° E, when the Rayn terrane in the east was fused to the western part of the Arabian craton [Looseveld *et al.*, 1996; Al-Husseini, 2000]. The Amar collision was followed by a widespread extensional collapse of the Arabian-Nubian shield between about 620–530 Ma. The extensional collapse culminated in the regional development of the extensive Najd fault and its complimentary rift basins, Zagros suture, the north-east trending Oman salt basins, and the Sinai triple junction.

The Sinai triple junction is composed of the Najd fault system, the Egypt rift, the Jordan valley and Derik rift. During the final extensional stage about 570–530 Ma, the north-west trending Najd fault system dislocated the Arabian shield left-laterally by about 250–300 km. This dislocation appears to compliment the north-east oriented intra-continental rifts in Oman, the Zagros mountains and the Arabian Gulf. These rift basins accumulated thick sequences of clastic and carbonate rocks and salt such as the Ara group in Oman, and the Hormuz series in the Arabian Gulf and the Zagros Mountains [Ziegler, 2001]. During the extensional collapse, the north-trending anticlines probably remained elevated as elongated horst bounded by normal faults.

The striking geometric pattern appears to have formed in two tectonic stages, namely, the Precambrian Amar collision between about 640–620 Ma followed by the development of the Najd rift system between about 570–530 Ma.

2.3.3 The Red Sea and Gulf of Aqaba

The Red Sea is a 1,800 km extended channel trending north-west to south-east from the Sinai Peninsula in the north down to the strait of the Gulf of Aden in the south. The Red Sea can be divided into two main units. These are firstly the shelf area, which is composed of the coastal area and the marginal shelves, and secondly the main and axial trough. The shelf is narrow in the north and wide in the south, whereas the trough is wide in the north and narrow in the south. The Red Sea structure is a graben along the crest of an anticline that formed in the Arabian-Nubian shield. The inner margins of the shield were apparently subjected to considerable uplift that formed prominent scarps at the edge of the Red Sea rift. A zone 1–2 km wide, composed of high and tensional faults concealed by coastal sediments, lies at the foot of the escarpments. On the seaward side of this zone, the basement has been step faulted downward in blocks and lies beneath the shelf area at depths of 2–3 km below sea level [Chapman, 1978].

Three sets of faults seem to have controlled the development of the Red Sea. These were the north-west to south-east trending main line of faults, which are associated with step faulting and the west-north-west to east-south-east major fault trend in the Precambrian basement, which caused many irregularities in the coastline [Chapman, 1978]. The regional distribution of seismicity in the Red Sea indicates a concentrated distribution of events proximal to the main and axial trough in the southern portion. However, the concentration is not uniformly distributed but occurs in clusters on the ridge crests or near transform faults of the rift axis. Other significant activities appear to occur along other portions of the central rift not having transform faults. The activities may be related to intrusive mechanisms of normal fault movements associated with the down-dropping of blocks or movements along undetected transform faults. Focal mechanisms for two earthquakes located near the southern Red Sea rift axis indicate a nearly pure strike-slip mechanism on north-east trending planes that suggest seismic activity on rift transform faults.

The Gulf of Aqaba forms the southern part of the Levantine transform fault. This forms the boundary between the Arabian and Nubian plates. The fault is composed of four straight segments. The first is along the Gulf of Aqaba, the second runs along the Dead Sea, Jordan and Hula valley, the third passes through the Beka'a and Orontes valley, and from Orontes the transform extends up to the Taurus-Zagros thrust. With a total of 105–110 km dominant left lateral shear, minor components of extension compression and up-warping occur in many places. Normal faults were generated along the margins of the transform due to these systems, with variable displacements in the localities of these faults. Changes in the trend of the transform resulted in the formation of rhomb-shaped basins such as the four deeps in the gulf and the Dead Sea. On either side of the gulf, long early Neogene dykes trending north-west parallel to each other were believed to have accompanied the initial rifting of the Red Sea. This volcanism was followed by the shear along the Gulf of Aqaba. A system of faults sub-parallel to the gulf exists within a zone tens of kilometres wide on either side. A study of active faulting in the Dead Sea rift [Al-Amri *et al.*, 1991] indicated that there were two types of fault activities: strike-slip and normal faults, the former being the more prominent in activity.

2.3.4 Arabian plate seismicity

The Arabian plate is surrounded by active plate boundaries as evidenced by earthquake locations. Figure 2.6 shows these locations and densities. Active tectonics of the region is dominated by the collision of the Arabian plate with the Eurasian plate along the Zagros and Bitlis thrust systems, and rifting and seafloor spreading in the Red Sea and Gulf of Aden. Strike-slip faulting occurs along the Gulf of Aqabah and the Dead Sea transform fault systems [Al-Amri and Alkhalifah, 2004; Al-Damegh *et al.*, 2004].

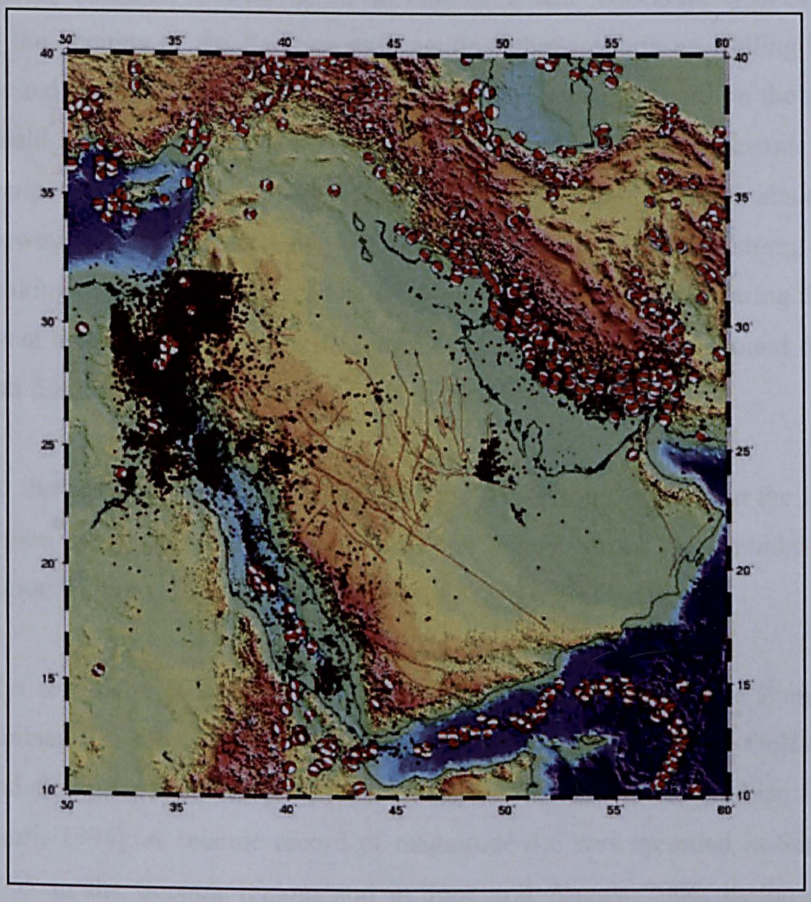

Figure 2.7. Arabian plate seismicity plot. The circles show all the seismic events from 1960 up to July 2008 from the Saudi Geological Survey (SGS) up to latitude 32° N. The peach ball show the seismic events from 1976 up to July 2008 from (http://www.globalcmt.org/CMTsearch.html) of magnitude > 4. The red lines show the faults from the Precambrian age, digitized from the tectonic map of Saudi Arabia and adjacent areas, compiled by Peter R. Johnson in 1998.

The Arabian shield consists of Precambrian terranes separated by suture zones [Schmidt *et al.*, 1979]. During the late Oligocene (30 Ma) and early Miocene (24 Ma) the Arabian shield was disrupted by the development of the Red Sea and Gulf of Aden rifts, and from the mid-Miocene (14 Ma) to the present the region has experienced volcanism and uplift [Bohannon *et al.*, 1989]. The uplift and volcanism are generally assumed to be the result of hot, buoyant material in the upper mantle that may have eroded the base of the lithosphere [Camp and Roobol, 1992]. However, details about the nature of the upper mantle such as its thermal and compositional state are not known. Volcanic

activity (Harrats) is observed on the Arabian shield. This is likely to be related to the opening of the Red Sea and mantle asthenospheric up-welling beneath western Arabia [Camp and Roobol, 1992]. The seismic record on the Arabian shield is low compared to other regions. Only a few moderate seismic events, composed of 25 (4.0<M>5.9) and 1 (M>6.0), have occurred since 1900. However, historical accounts [Ambraseys, 1988] indicate that strong ground shaking has been felt in the north-western portion of the shield during the 1068 event and 1588 event. The 1068 event was accompanied by ground cracking and fissuring that caused widespread destruction.

To the south, the majority of earthquakes and tectonic activity in the Red Sea region are concentrated along a belt that extends from the central Red Sea region south to Afar and then east through the Gulf of Aden.

The seismicity record of the Gulf of Aden and Owen Fracture Zone in the Arabian Sea shows seismic activity along the Sheba Ridge, in the Gulf of Aden and along the lateral fault of the Owen Fracture Zone in the Arabian Sea [Al-Amri, 1994]. A seismic record of magnitude 4.6 was recorded in September 2005 in the Socotra region, and in June and August 2006, earthquakes of magnitudes 4.6 and 5.0, respectively, were recorded in the Owen Fracture Zone. In December 1982, 4,000 people were killed in a destructive earthquake of magnitude 6.0 in Daamar (central Yemen). This followed the January 1941 earthquake in the north-west of Yemen (M=5.9) with an aftershock on February 1941 (M=5.2), and an earthquake in October 1955, highlighted the hazards that may result from nearby seismic sources and demonstrated the vulnerability of northern Yemen to moderate magnitude and larger earthquakes. The historical and instrumental records of strong shaking in the southern Arabian shield and Yemen (1845,1932, 1941,1982 and 1991) indicate that the return period of severe earthquakes affecting the area is about 60 years [Al-Amri, 1994, 1995].

The Arabian plate boundary extends north-east from the Afar region through the Gulf of Aden and into the Arabian Sea and Zagros fold belt. The boundary is clearly delineated by teleseismic epicentres, although there are fewer epicentres bounding the eastern third of the Arabian plate south of Oman. Most seismicity occurs in the crustal part of the Arabian plate beneath the Zagros folded belt [Jackson and Fitch, 1981]. The Zagros is a prolific source of large magnitude earthquakes with numerous magnitude 7+ events occurring in the last few decades. The seismicity record of recent years for and around the Zagros Mountains shows that the area is very active, where almost every day there is a seismic record, with most being less than 6.0 in magnitude. However, on average one major earthquake (above 6.0) has occurred every year for the last 10 years. In May 1997, an earthquake of magnitude 7.3 occurred north of Zagros, where 1,567 people were killed, 2,300 injured, 50,000 made homeless, 10,533 houses destroyed and 5,474 houses damaged. In March 1998, an earthquake of magnitude 6.6 occurred in northern Iran, in which five people were killed, 50 injured, 10,000 made homeless, 2,000 houses destroyed and major damage was done to service utilities. In June 2002, a magnitude 6.5 earthquake occurred in the middle of the Zagros Mountains (western part of Iran) and in August 2003 one of magnitude 5.9 occurred in the south-east of Iran but caused no reported damage. However in December 2003, a quake of magnitude 6.6 occurred in Bam (southeast part of Iran), where 30,000 were killed, 30,000 injured, 85 per cent of buildings were damaged or destroyed, and the infrastructure seriously damaged. Following this, in May 2004, an earthquake of magnitude 6.3 occurred in Mazandaran (northern Iran) killing 35, injuring 400 and damaging many buildings. There is February 2005, there was a magnitude 6.4 earthquake in Kerman (Central Iran) which killed 602 and injured 991 and in November 2005, a 6.0 earthquake occurred in Usfyog (southern Iran) which killed 13, injured 100 and damaged or destroyed 80 per cent of buildings. The last major earthquake occurring was in March 2006 in Loresten (western Iran), and had a magnitude of 6.1, killing 70 people, injuring 1,300 and leaving 40 villages completely destroyed.

The Gulf of Aqaba and Dead Sea region is distinct from the Arabian shield as this region is characterized by a high seismicity record. Active tectonics in this region is associated with the opening of the northern Red Sea and Gulf of Aqaba as well as a major continental strike-slip plate boundary. The Dead Sea transform system connects the active spreading centres of the Red Sea to the area where the Arabian plate is converging with Eurasia in southern Turkey. The Gulf of Aqaba in the southern portion of the rift system has experienced left-lateral strike-slip faulting with a 110 km offset since the early Tertiary to the present, with major historical earthquakes recorded in the years 1068, 1072, 1212, 1293 and 1588 [Garfunkel and Ben-Avraham, 1996]. Ben Menahem [1979] indicated that about 26 major earthquakes between 6.1 and 7.3 occurred in the southern Dead Sea region between 2100 B.C. and 1900 A.D. In the last century, the seismic records of the Gulf of Aqaba show activity in September 1927 of magnitude 4.9, May 1934 of magnitude 4.2, April 1983 of magnitude 5.1, September 1989 of magnitude 4.1, April 1990 of magnitude 4.2, July 1993 of magnitude 5.9. The last major event of the last century was in November 1995 and was of magnitude 6.2 in the Gulf of Aqaba, when 6 people were killed, 40 injured and many buildings damaged. On February 2004, an earthquake of magnitude 5.3 in the Dead Sea also injured 4 people, damaged a number of buildings and a landslide occurred at Ma`in [Wdowinski *et al.*, 2004]. Therefore, these indicate that the Gulf of Aqaba is one of the most seismically active zones in the Dead Sea transform system (see Table 2.1). Earthquake locations provide evidence for continuation of the faulting regime from the Gulf north-eastwards inland beneath thick sediments, suggesting that the northern portion of the Gulf is subjected to more severe seismic hazards than the southern portion [Thenhaus *et al.*, 1986; Al-Amri *et al.*, 1991].

Table 2.1. Historical seismicity record on the Arabian Plate.

Zone	Mag. 2.0–2.99	Mag. 3.0–3.99	Mag. 4.0–4.99	Mag. 5.0–5.99	Mag. >6
Gulf of Aqaba	2694	2413	557	41	5
North Red Sea	191	216	52	10	2
Central Red Sea	86	79	67	26	6
South Red Sea	182	201	110	101	15
interior of Arabian plate	9	19	2	2	0
South Arabian Gulf	12	60	736	243	14

The overall seismicity in the interior of the Arabian plate suggests that little internal deformation is presently occurring. There is widespread quaternary volcanism along the Red Sea coast with at least one documented historical eruption in 1256 A.D and some seismicity was associated with that eruption. Seismicity may also be related to transform faults in the Red Sea continuing onto land, as well as other causes. But, to date, few on-land epicentres have been accurately located and there are few focal mechanisms available.

Moreover, a volcanic eruption occurred on 1 October 2007 at the island of Jazirt Atta-Ir, located about 85 miles (140 km) from Yemen in the Red Sea south of our GPS network. Furthermore, a volcanic activity has been occurring since last May 2009 up to the time of writing this thesis in Harrah Al-shaqah, located on north-west Arabian shield about 240 km north of Almadineenaa city. This volcanic activity have made a series of earthquakes on a daily basis, on some occasions greater than four in magnitude and the strongest reaching 5.7 according the to Saudi Geological Surveys (SGS). Therefore, from these evidences a number of agencies in that area expect that a new cycle of volcanic activities has started in the Red Sea and on the Arabian shield.

2.4 Kinematic and dynamic modelling for tectonic plate motion study

The Earth's interior structure (crust, mantle and core) and the drivers of plate tectonics briefly described here can help to develop an advanced dynamic model for plate tectonics over the region under the assumption that additional quantitative information and data are available. But, the fact that this study's intention is to apply the GPS technique to describe the tectonic motions (which is a purely geometric approach) supports only the application of kinematic modelling. The difference between kinematic and dynamic approaches will be briefly discussed and their link will be explained in order to justify the application of the kinematic approach for describing a dynamic system like tectonic plate motions.

Furthermore, motion studies are divided into two categories kinematics and dynamics: where the kinematics is the motion study without regard to forces that cause it; while the dynamics is the motion study that result from forces. Moreover, kinematics analysis is simpler than dynamic analysis and is adequate for many applications involving moving parts. Also, all the physical positions parts in an assembly are shown in kinematic simulations with respect to the time as it goes through a cycle. Therefore, simulating steady state motion (no acceleration) is useful to use this technology as well as for evaluating motion for interference purposes, such as assembly sequences of complex mechanical system. However, dynamic simulation is more complex since the problem needs to be defined more and more data is needed to account for the forces. In addition to that dynamics are required to accurately simulate the actual motion of a mechanical system. In general, kinematic simulation helps to evaluate form, while dynamic simulation assists in analyzing function.

Following this study's goal to use a pure geometric technique (without additional information about driving forces) to only describe the plate tectonic motions in a steady-state manner the most suitable approach is the kinematic one, estimating only displacements and velocities. Also, the task of this study

is to investigate the type and the form of tectonic motions on the earth surface, without going into an explanation about the driving forces. In order to find the link with the dynamics of the system it is possible to estimate the acceleration of reaction forces but for this purpose more than one observation epochs (covering a huge territory with a high density of observation points) and very long time span (period) are necessary for the description of very slow tectonic movements. The same model can be used for GPS time series analysis in order to evaluate very fast displacements (for very short time span) during seismic events. Both cases can be considered in a future continuation of the plate tectonic study over the Arabian plate structure when other sources of data and information will be available. Furthermore, most of the previous studies on Arabian plate use a pure geometric technique (see 6.2), where geological plate motion models determined from seafloor spreading rates, transform fault azimuths and earthquake slip vectors describe relative motion between plates [DeMets *et al.*, 1990], geological study by NNR-NUVEL-1A [DeMets *et al.*, 1994] and the geological and geophysical study by the PB2002 model [Bird, 2003]. A comparison of this study and these studies results are discussed on sections (6.5 and 6.6).

2.5 Summary

This chapter has briefly described the Earth's interior structure (crust, mantle and core) and the present shape of the tectonic plates. After discussing the drivers of plate tectonics, the main types of plate movement were explained as well.

A detailed introduction to the Arabian plate structure, including the Arabian shield, Arabian platform and Red Sea was then given. It was explained that: the Arabian shield was formed by Precambrian terranes; the Arabian platform consists of Palaeozoic and Mesozoic sedimentary rocks; and the Red Sea can be divided into the shelf area and the marginal shelves , and the main and axial trough.

Arabian plate seismicity was then described, with details of earthquakes that have occurred. It was shown that there have been ver few earthqukes in the interior of the Arabian plate but many of magnitude >5 in the Gulf of Aqaba, Red Sea and Southern Arabian Gulf. The driving motivation for using Kinematic approach for description of the plate tectonics dynamic system has been discussed as well.

Chapter 3: GPS for geodynamic investigations

3.1 Introduction

Space geodesy is used to investigate a wide range of scientific questions and applications, particularly those related to plate motions and the rotational dynamics of the earth, where the surface expression of these processes can be at the millimetre level or less per year. Current space geodetic techniques are capable of measuring to such precisions when sufficient observations are available for fairly lengthy periods of time and the reference frame is consistently defined throughout the observation period, so that the rate of station motion can be derived from the time series of coordinates. Furthermore, the GPS bias and errors should be mitigated, either by direct computation or using models to estimate them, as part of the processing techniques.

In this chapter, the development of the terrestrial reference frame will be outlined briefly, followed by details of IGS product development. After that, the GPS constellation, GPS observables and linear combinations of observables will be briefly explained. Then, the GPS bias and error mitigation is outlined in terms of the atmosphere delay, earth tide and loading, and antenna issues.

3.2 Terrestrial reference frame

A Terrestrial Reference System (TRS) is a mathematical model, with no physical existence, used to describe the deformable earth. It is an affine Euclidian frame with an origin, a scale and orientation [Altamimi *et al.*, 2002]. The International Terrestrial Reference System (ITRS) is an accurate geodetic reference system, comprising a set of right-handed orthogonal axes, where the origin is defined at the Centre of Mass of the earth (CM), including oceans and atmosphere, and the axes oriented to the corresponding axes of the International Earth Rotation Service (IERS) system, i.e. consistent with BIH (Bureau International de l'Heure) orientation at 1984.0. The orientation time evolution is ensured by using a No-Net-Rotation (NNR) condition with respect to horizontal tectonic motions over the whole earth. The IERS maintain a precise global frame known originally as the IERS Terrestrial Reference Frame (ITRF), but now more commonly known as the International Terrestrial Reference Frame. This is a realization of ITRS and is updated periodically. This realization consists of estimating station positions at a given epoch and their linear velocities using five space geodetic techniques: Very Long Baseline Interferometry (VLBI), Lunar and Satellite Laser Ranging (LLR and SLR), GPS, and Doppler Orbit determination and Radio-positioning Integrated by Satellite (DORIS). Each of the space geodetic techniques has strengths and weaknesses for the determination of the reference frame parameters. VLBI is used for defining accurate earth orientation in an inertial frame; SLR is used in the determination of the centre and accurate scale for the earth. Although GPS was not used in defining the origin or scale, it makes a large contribution in terms of the velocity field. DORIS, with its homogeneous network coverage, provides an excellent tracking system for low earth orbiting satellites.

The first realization of ITRS was the ITRF88, and 10 others ITRF versions (ITRF89, ITRF90, ITRF91, ITRF92, ITRF93, ITRF94, ITRF96, ITRF97, ITRF2000 and ITRF2005) have been established and published since, where each version superseded and replaced its predecessor [http://itrf.ensg.ign.fr].

The most recent realization of the ITRS is ITRF2005, where the input data are the time series for station position in each technique (weekly in GPS and SLR, and daily in VLBI) and Earth Orientation Parameters (EOP), i.e. Polar Motion (x_p, y_p), Universal Time (UT1) and Length of Day (LOD), which was the first time this had been used in the realization. There are a number of advantages when using the time series of station positions; it allows the monitoring of station non-linear motion and station discontinuities and also the examination of the temporal behaviour of the physical parameters (origin and scale) of the frame [Altamimi *et al.*, 2007]. The ITRF2005 origin is defined as zero translations and translation rates with respect to CM, averaged by the SLR time series spanning 13 years of observations. The ITRF2005 scale and its rate are defined using VLBI time series spanning 26 years of observations. A series of weekly station coordinates and daily pole coordinates has been computed using 13 years (January 1993 to December 2005) of DORIS measurements collected by the instruments onboard SPOT2, SPOT3, SPOT4, SPOT5, TOPEX/Poseidon and ENVISAT [http://itrf.ensg.ign.fr]. The ITRF2005 orientation (at epoch 2000.0) and its rate are aligned to ITRF2000 using 70 stations of high geodetic quality [Altamimi *et al.*, 2007]. The No-Net-Rotation condition is ensured for ITRF2000 by minimizing the three rotation rate parameters between ITRF2000 and NNR-NUVEL-1A using a core set of 50 stations [Altamimi *et al.*, 2002]. Since ITRF2005 is aligned to ITRF2000 over the same three rotation rate parameters using a set of 70 stations, the same condition is then applied to ITRF2005.

Furthermore, a new ITRF2008 will be realized in the near future; with three more years of data available, new stations included and improved processing strategies for each technique [IGSMAIL-5855 on 11 Nov 2008].

3.3 IGS

The International Global Navigation Satellite System (GNSS) Service (IGS) is a voluntary federation of more than 200 agencies from all over the world. IGS gather the GPS and GLONASS station data and produce the highest quality GPS and GLONASS products in support of earth science research, multidisciplinary applications and education. The IGS formally began on 1 January 1994 under the name of the International GPS Service for Geodynamics and, due to an expansion of IGS objectives, the name changed to the International GPS Service on 1 January 1999. Moreover, the IGS continues its expansion, integrating data from the Russian GLONASS system and the coming European Galileo system; the name has therefore changed again to the current title of the International GNSS Service on 14 March 2005, but the acronym "IGS" has been retained in all the names.

IGS products include high accuracy satellite ephemeris, earth rotation parameters, coordinates and velocities of the IGS tracking stations, satellite clock information, timescale products, ionosphere information and troposphere information. The accuracies of these products are sufficient to support scientific objectives such as the realization of the ITRF and monitoring the deformation of the solid earth. Moreover, the IGS has produced its own realization of the ITRF, of which the latest realization is IGS05, using 132 IGS stations, where the IGS05 and ITRF2005 velocity vectors are identical [Ferland in IGSMAIL-5447 on 19 Oct 2006].

Regional GNSS networks are used for plate motion investigation as well as for reference frame densifications. Moreover, since the computing facilities and the GNSS data analysis software have improved dramatically in recent years, more people now have the possibility to process regional GNSS networks. A regional GNSS network solution of station positions is derived using the IGS products. The expression of the IGS product in ITRF is ensured by aligning the global IGS combined solution of station positions and velocities to ITRF. This alignment is performed using 14 transformation parameters between the IGS

TRF and ITRF, in the case of IGS05 and ITRF2005 estimated over 132 stations distributed globally [Ferland, 2006]. The estimated station coordinates for a regional GNSS network solution using IGS products are theoretically expressed in ITRF. When a regional GNSS network is integrated into the ITRF, some technical issues need to be considered to achieve the optimal integration. Firstly, there must be a link between the ITRF and the regional GNSS network by selecting high quality ITRF stations with the selection criteria to include IGS stations:

- Among the regional network.
- Surrounding the regional network.
- With at least of 3 years of continuous data.
- With a station velocity residual less than 3 mm/yr.

Also, the expression of the regional GNSS network solution in the ITRF can be achieved by two methods. Firstly, the coordinates of the selected IGS stations can be constrained to their ITRF values; this method is used by EUREF for their weekly solution with 12 IGS stations being constrained to their ITRF2000 values. Secondly, by aligning the regional GNSS network solution to the ITRF using transformation parameters, which should be estimated using the selected IGS stations.

3.4 GPS constellation

The GPS constellation consists of 24 plus satellites distributed in six orbital planes, where each plane contains at least four satellites and these planes are equally spaced 60° apart about the equator. The orbital radius is approximately 26,600 km with respect to CM and the inclination of the orbital planes is 55° with respect to the equatorial plane. The nominal orbital period of a GPS satellite is one-half of a sidereal day (11 hours 58 minutes) [Kaplan, 1996]. The orbital altitude is such that the satellite repeats the same track and configuration over any point approximately every 24 hours (4 minutes earlier each day) [Dana, 2000]. The GPS constellation provides between 5 and 12 satellites visible at any point on the earth surface.

There are three different notations that can give each satellite its orbital position. The first one is to assign a letter to each orbital plane (A, B, C, D, E, and F) and a number from 1 to 4 to each satellite within a plane; for example D4 refers to satellite number 4 in orbital plane D. The second notation, assigned by the U.S. Air Force, is in the form of a space vehicle number (SVN); 13 refers to satellite number 13. The third notation is the configuration of the pseudorandom (PRN) code generators on the satellite. The PRN code generators are configured uniquely on each satellite. Hence, a satellite can be identified by the PRN code that it generates.

The GPS satellite consists of a radio transmitter, an atomic clock, computers and other auxiliary equipment such as solar panels and a propulsion system. There are seven generations of GPS satellite, called block I, block II, block IIA, block IIR, block IIR-M, block IIF and block III. Block I satellites were first launched in 1978 and are no longer operational, but some of them were operational for more than 10 years, whereas their design life was only 4.5 years. Block II is slightly different from block I; the orbital inclination is 55° in block II, but was 63° in block I. Also, block II differs in aspects of security access and design life (7.5 years). Block IIA ("A" denotes advanced) was first launched at the end of 1990 and equipped with a mutual communication capability [Hofmann-wellenhof, 2001]. Block IIR ("R" denotes replacement) was first launched in July 1997 and there were 12 satellites of this type, equipped with advanced communications and tracking between satellites. Block IIR-M ("M" denotes modernized) was first launched in September 2005 and seven satellites of this type have been launched so far, with the last satellite launched in March 2009 and one more to be launched later on. This block IIR-M satellites transmit a second civil signal (L2C) on the L2 frequency and a new military code "M" on both frequencies L1 and L2. Moreover, 12 satellites of block IIF ("F" denotes follow on) will be launched in the future with an intended design life of 15 years and equipped with improved on-board systems such as inertial navigation. Finally, 30 satellites of block III will be launched

and this generation is expected to carry GPS up to 2030 and beyond [Hofmann-wellenhof, 2001].

The GPS constellation is maintained by a number of control stations, at which data are continuously collected from all satellites with the view of monitoring the satellites operational status, its solar arrays and battery levels, to resolve satellite anomalies, control selective availability (before it was switched off), anti-spoofing and updates for each satellite clock, ephemeris and almanac. The master control station is located at Falcon Air Force Base, Colorado Springs, USA.

The L-band radio frequency was chosen for GPS satellite transmissions, since it is good for long distance communication, operates under all weather conditions and the hardware that receives the L-band is inexpensive. The fundamental satellite signal frequency is 10.23 MHz. The satellite transmits two microwave L-band carrier frequencies. The primary carrier is L1 and the secondary is L2. The L1 frequency of 1575.42 MHz results from multiplying the fundamental 10.23 MHz by 154. The L2 frequency of 1227.60 MHz results from multiplying the fundamental 10.23 MHz by 120. The chipping rate of the P(Y)-code is 10.23 MHz and that of the C/A-code is 1.023 MHz. The C/A code is a member of a gold codes group that has a weak cross-correlation between all members of the group. This advantage makes it easy to quickly distinguish between different satellite signals that are received simultaneously. The C/A code repeats every 1023 bits (one millisecond). Moreover, there is a different C/A code PRN for each satellite gold code. The P (Y) code modulates both L1 and L2 and it is 38 weeks long, one week per satellite. The P-code is encrypted into the Y-code when anti-spoofing is in operation.

3.5 The GPS observables

3.5.1 The pseudo-range observable

The time it takes a signal to travel a given distance is the basis of the pseudo-range observable. GPS receivers compare the received satellite code and a replica code generated in the receiver. There is a difference between the two codes in time. This time is the elapsed time for the signal to travel from satellite to receiver. This time is not free of errors because there are some factors that have effects on the signal path such as the ionosphere, troposphere delay and clock offsets. Hence it is known as the pseudo-range. The algorithms that are used to compute the pseudo-range are as follows:

Distance = speed of light in vacuum × time

$$D = C \times T \tag{3.1}$$

Therefore, the distance between the GPS satellite and the receiver antenna is equal to the product of the speed of light and the elapsed time for the signal to travel from the satellite to the receiver antenna.

$$PR = C \times \Delta T \tag{3.2}$$

where PR is the pseudo-range between the satellite and the antenna of the GPS receiver.

$$PR_r^s(\tau_r) = \rho_r^s(T^s, T_r) - c[\delta\tau_r(\tau_r) - \delta t^s(t^s)] + d_{atm} \tag{3.3}$$

where PR_r^s is the pseudo-range between the satellite (s) and the antenna of the GPS receiver (r) and time (τ_r)

T_r: the receiver clock time after correction.

T^s: the satellite clock time after correction (the true GPS time).

$\rho_r^s(T^s, T_r)$: the geometric range obtained from signal transmitted at the satellite (s) and the signal received at receiver (r) with regard to the true GPS time.

$\delta\tau_r(\tau_r)$: the receiver (r) clock offset at the receiver time.

$\delta t^s(t^s)$: the satellite (s) clock offset at the satellite time.

d_{atm}: the ionosphere and troposphere delay.

3.5.2 The carrier phase observable

The carrier is radio energy created from an oscillator and fed to a power amplifier in a transmitter whose amplitude, frequency, or phase may be modulated to convey several types of information [Dye and baylin, 1997]. The carrier phase means the number of complete cycles and the fractional cycle between satellite and receiver antenna. There are two phases, L1 and L2, where L1 is at 1575.42 MHz with a wavelength of approximately 19 cm and L2 is at 1227.60 MHz with a wavelength of 24 cm. The carrier phase observable can be very precise if simultaneous carrier phase measurements are taken at more than one point. Then, these measurements are post-processed using the carrier phase algorithms that are summarized below.

$$\Phi_r^s(\tau_r) = (\frac{f}{c}).\rho_r^s(T^s, T_r) - f[\delta\tau_r(\tau_r) - \delta t^s(t^s)] + N_r^s + d_{atm} \qquad (3.4)$$

where:

$\Phi_r^s(\tau_r)$: the observed carrier phase between the satellite (s) and the antenna of the GPS receiver (r) and time (τ_r).

T_r :the receiver clock time after correction.

T^s: the satellite clock time after correction (the true GPS time).

$\rho_r^s(T^s, T_r)$: the geometric range obtained between satellite (s) and receiver (r) related to the true GPS time.

$\delta\tau_r(\tau_r)$: the receiver (r) clock offset in the receiver time.

$\delta t^s(t^s)$: the satellite (s) clock offset in the satellite time.

N_r^s: the integer ambiguity between the satellite (s) and the antenna of the GPS receiver (r).

d_{atm}: the ionosphere and troposphere delay.

However, the carrier phase observations are ambiguous since only the fractional part of the wavelength and the change in the integer number of wavelengths since lock-on can be measured. The integer number of wavelengths (integer ambiguity) between satellite and receiver antenna when the receiver first locks on is unknown. It is necessary to solve this ambiguity and various GPS techniques can be applied to do this.

3.6 Linear combinations of observable

The linear combinations of observables is a technique to minimize the effect of bias delay or to improve the integer ambiguity estimation. The drawbacks of linear combinations are the noise level and the possibility of losing the integer nature of the ambiguities. In fact, the L1 and L2 carrier phase can be combined to form a number of observables; however the widely known and used combinations are summarised as follows.

3.6.1 Ionosphere-free linear combination (L_3)

The ionosphere-free combination (L_3) is used to eliminate ionosphere delay from the observables. The drawback of the L3 observable is that the integer nature of the ambiguities is lost.

$$L_3 = \frac{f_1^2}{f_1^2 - f_2^2} L_1 - \frac{f_2^2}{f_1^2 - f_2^2} L_2 \tag{3.5}$$

3.6.2 Geometry-free linear combination (L4)

The geometry-free linear combination (L4) is independent of receiver clocks, satellite clocks and geometry (orbits, station coordinates). However, it contains the ionosphere delay and the initial phase ambiguities. Therefore, it is used for ionosphere model estimation. It is formed as follows:

$$L_4 = L_1 - L_2 \tag{3.6}$$

3.6.3 Wide lane combination (L_5)

The wide lane combination (L_5) is used for fixing the cycle slips and to resolve ambiguities to their integer values. The L_5 wavelength is about 86 cm and is approximately four times larger than L_1 and L_2: therefore, this linear combination is called wide lane. It is formed as follows:

$$L_5 = \frac{f_1 L_1}{f_1 - f_2} - \frac{f_2 L_2}{f_1 - f_2} \tag{3.7}$$

3.6.4 Melbourne-Wubbena linear combination (L_6)

The Melbourne-Wubbena linear combination (L_6) is a linear combination that uses both the carrier phase (L_1 and L_2) and the code (P_1 and P_2). The L_6 eliminates the effect of the ionosphere, the geometry, the clocks and the troposphere. It is formed as follows:

$$L_6 = \frac{f_1 L_1}{f_1 - f_2} - \frac{f_2 L_2}{f_1 - f_2} - \frac{f_1 P_1}{f_1 + f_2} - \frac{f_2 P_2}{f_1 + f_2} \tag{3.8}$$

3.6.5 Initial phase ambiguities and ambiguity resolution

The initial ambiguity parameters in the original observation equations are integer numbers of cycles, but they contain a number of other linear terms such as receiver clock corrections, satellite clock corrections, hardware effects and the initial phase shift between satellite and receiver. So these linear terms prevent access to the integer character of the carrier phase ambiguities. The double differencing cancels out or can allow these receiver clock corrections, satellite clock corrections, hardware effects and initial phase shifts to be neglected. Hence, the integer nature of the initial phase ambiguities becomes accessible. There are many techniques available to resolve the ambiguities. Most of these techniques are carried out in two steps: the first step estimates the ambiguities as a real number; in the second step, the integer value of the ambiguities are resolved using the real number of the ambiguities and the variance-covariance from step one, as well as statistical testing, to have a reliable way of resolving the ambiguities.

The four most popular techniques used in static positioning are round, search, sigma and QIF. The round algorithm is a simple strategy that only rounds the real value estimated in step one to the nearest integer. This round algorithm is simple, but is not safe, especially on long baselines. The search algorithm is also called the fast ambiguity resolution approach, where all real numbers of ambiguities in the solution vector and variance-covariance are found, then the *a posteriori* variance factor is computed. Then all possible combinations of integer values are estimated. After that, a statistical test is used where the lowest standard deviation is selected to indicate the best solution. The drawback of this search algorithm is that either all the ambiguities or none are resolved. The sigma algorithm is an iteration using the least squares adjustment technique, since in the first iteration the *a posteriori* RMS error for each ambiguity parameter is computed in the initial least squares adjustment. Then the RMS errors are sorted in ascending order; after that the maximal number of ambiguities fixed within one iteration step is assumed to be the best determined ambiguity or the differences between ambiguities are then resolved by

rounding to the nearest integers. However, the iteration process is terminated if all ambiguities have been resolved or if in the last step no ambiguity could be resolved based on the above criteria. The sigma algorithm can be applied to almost every linear combination. Hence, it can be used in baseline mode and session mode. Moreover, this algorithm is suitable when high quality code data are available on both frequencies, so the Melbourne-Wubbena linear combination can be used when the baselines are very long. The QIF (Quasi Ionosphere Free) algorithm is also an iteration algorithm using the least squares adjustment technique, where the RMS error is computed for each L_3 ambiguity bias associated with a pair L_1 and L_2. Then the ambiguity pairs are sorted in ascending order using their RMS error. After that, the search range is defined for the pair of L1 and L2 ambiguities and the number of integers for pair L1 and L2 are tested with the smallest value being accepted. If no ambiguity pair passes the test, then the next pair of ambiguities associated with the second smallest RMS error is used. Once a pair is accepted, then the whole process is repeated; hence the ambiguities are resolved iteratively.

3.6.6 Differencing

Differencing is a method of removing or reducing some of the GPS biased and errors, such as satellite clock offsets, orbital errors, atmospheric errors and receiver clock offsets. Differencing is defined as simultaneously observing at two or more receivers, two or more satellites and combining their resulting phase observables. There are three types of differencing: single, double and triple, where each eliminates or reduces one more GPS bias or error. Now, assume there are two receivers (a,b) and four satellites (i,j,k,l). The phase observation equations would be:

$$\Phi_a^i(\tau_a) = (\frac{f}{c}).\rho_a^i(T^i,T_a) - f[\delta\tau_a(\tau_a) - \delta t^i(t^i)] + N_a^i + d_{atm} \qquad (3.9)$$

$$\Phi_a^j(\tau_a) = (\frac{f}{c}).\rho_a^j(T^j,T_a) - f[\delta\tau_a(\tau_a) - \delta t^j(t^j)] + N_a^j + d_{atm} \qquad (3.10)$$

$$\Phi_a^k(\tau_a) = (\frac{f}{c}).\rho_a^k(T^k,T_a) - f[\delta\tau_a(\tau_a) - \delta t^k(t^k)] + N_a^k + d_{atm} \qquad (3.11)$$

$$\Phi_a^l(\tau_a) = (\frac{f}{c}).\rho_a^l(T^l, T_a) - f[\delta\tau_a(\tau_a) - \delta t^l(t^l)] + N_a^l + d_{atm} \quad (3.12)$$

$$\Phi_b^i(\tau_b) = (\frac{f}{c}).\rho_b^i(T^i, T_b) - f[\delta\tau_b(\tau_b) - \delta t^i(t^i)] + N_b^i + d_{atm} \quad (3.13)$$

$$\Phi_b^j(\tau_b) = (\frac{f}{c}).\rho_b^j(T^j, T_b) - f[\delta\tau_b(\tau_b) - \delta t^j(t^j)] + N_b^j + d_{atm} \quad (3.14)$$

$$\Phi_b^k(\tau_b) = (\frac{f}{c}).\rho_b^k(T^k, T_b) - f[\delta\tau_b(\tau_b) - \delta t^k(t^k)] + N_b^k + d_{atm} \quad (3.15)$$

$$\Phi_b^l(\tau_b) = (\frac{f}{c}).\rho_b^l(T^l, T_b) - f[\delta\tau_b(\tau_b) - \delta t^l(t^l)] + N_b^l + d_{atm} \quad (3.16)$$

where the single difference can be formed by simultaneous observations at two receivers of one satellite. The observation equations can be expressed as:

$$\Phi_{ab}^l(\tau_a, \tau_b) = \Phi_b^i(\tau_b) - \Phi_a^i(\tau_a) \quad (3.17)$$

$$\Phi_{ab}^j(\tau_a, \tau_b) = \Phi_b^j(\tau_b) - \Phi_a^j(\tau_a) \quad (3.18)$$

$$\Phi_{ab}^k(\tau_a, \tau_b) = \Phi_b^k(\tau_b) - \Phi_a^k(\tau_a) \quad (3.19)$$

$$\Phi_{ab}^l(\tau_a, \tau_b) = \Phi_b^l(\tau_b) - \Phi_a^l(\tau_a) \quad (3.20)$$

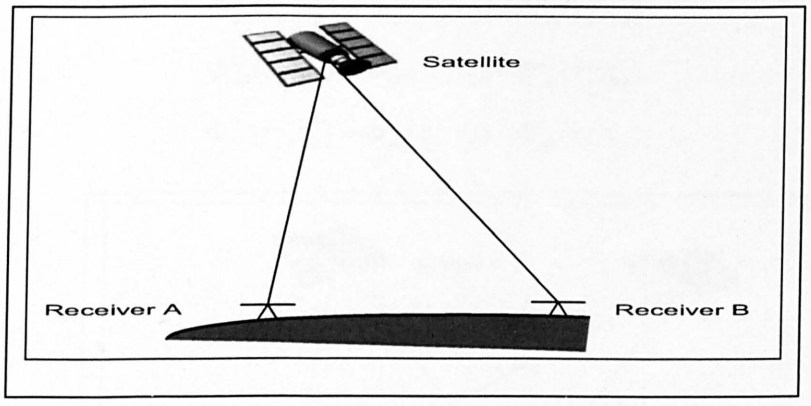

Figure 3.1. The single difference.

Substituting equations 3.9 and 3.13 into 3.17, 3.10 and 3.14 into 3.18, 3.11 and 3.15 into 3.19 and 3.12 and 3.16 into 3.20 gives:

$$\Phi_{ab}^{i}(\tau_a,\tau_b)=(\frac{f}{c}).\rho_{ab}^{i}(T^i,T_a,T_b)-f[\delta\tau_{ab}(\tau_a,\tau_b)]+N_{ab}^{i}+d_{atm} \quad (3.21)$$

$$\Phi_{ab}^{j}(\tau_a,\tau_b)=(\frac{f}{c}).\rho_{ab}^{j}(T^j,T_a,T_b)-f[\delta\tau_{ab}(\tau_a,\tau_b)]+N_{ab}^{j}+d_{atm} \quad (3.22)$$

$$\Phi_{ab}^{k}(\tau_a,\tau_b)=(\frac{f}{c}).\rho_{ab}^{k}(T^k,T_a,T_b)-f[\delta\tau_{ab}(\tau_a,\tau_b)]+N_{ab}^{k}+d_{atm} \quad (3.23)$$

$$\Phi_{ab}^{l}(\tau_a,\tau_b)=(\frac{f}{c}).\rho_{ab}^{l}(T^l,T_a,T_b)-f[\delta\tau_{ab}(\tau_a,\tau_b)]+N_{ab}^{l}+d_{atm} \quad (3.24)$$

As can be seen from the equations above, the single difference eliminates satellite clock offset and reduces orbital atmospheric errors. Also, the atmospheric effects will be cancelled out if the observation area is small and stations are at the same altitude since the atmosphere can be assumed to be identical at all receivers.

Moreover, the double difference can be formed by simultaneous observations by two receivers of two satellites. The observation equations can be expressed as:

$$\Phi_{ab}^{ij}(\tau_a,\tau_b)=\Phi_{ab}^{j}(\tau_a,\tau_b)-\Phi_{ab}^{i}(\tau_a,\tau_b) \quad (3.25)$$

$$\Phi_{ab}^{ik}(\tau_a,\tau_b)=\Phi_{ab}^{k}(\tau_a,\tau_b)-\Phi_{ab}^{i}(\tau_a,\tau_b) \quad (3.26)$$

$$\Phi_{ab}^{il}(\tau_a,\tau_b)=\Phi_{ab}^{l}(\tau_a,\tau_b)-\Phi_{ab}^{i}(\tau_a,\tau_b) \quad (3.27)$$

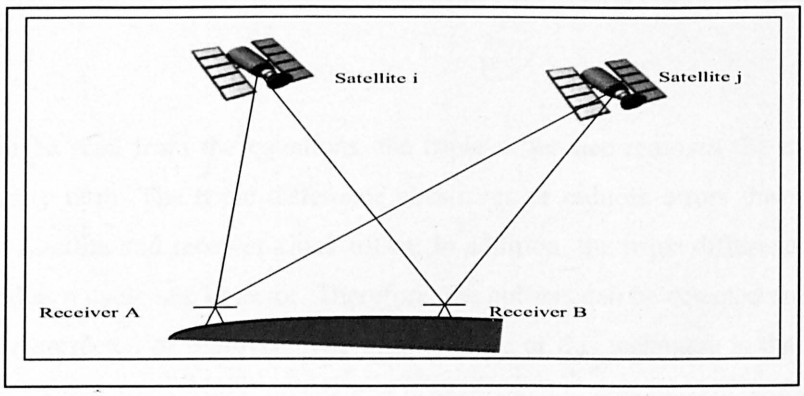

Figure 3.2. The double difference.

Substituting equations 3.21 and 3.22 into 3.25, 3.21 and 3.23 into 3.26 and 3.21 and 3.24 into 3.27 gives:

$$\Phi_{ab}^{ij}(\tau_a,\tau_b) = (\frac{f}{c}).\rho_{ab}^{ij}(T^i,T^j,T_a,T_b) + N_{ab}^{ij} + d_{atm} \quad (3.28)$$

$$\Phi_{ab}^{ik}(\tau_a,\tau_b) = (\frac{f}{c}).\rho_{ab}^{ik}(T^i,T^k,T_a,T_b) + N_{ab}^{ik} + d_{atm} \quad (3.29)$$

$$\Phi_{ab}^{il}(\tau_a,\tau_b) = (\frac{f}{c}).\rho_{ab}^{il}(T^i,T^l,T_a,T_b) + N_{ab}^{il} + d_{atm} \quad (3.30)$$

It can be seen from these equations that the double difference eliminates or reduces errors that occur at the satellite. Also, the double difference eliminates the receiver clock offsets.

Finally, the triple difference can be formed by differencing the double difference observation equation at two epochs (m, n).

$$\Phi_{ab}^{ij}(\tau_a,\tau_b)_{mn} = \Phi_{ab}^{ij}(\tau_a,\tau_b)_n - \Phi_{ab}^{ij}(\tau_a,\tau_b)_m = (\frac{f}{c}).\rho_{ab}^{ij}(T^i,T^j,T_a,T_b)_{nm} + d_{atm} \quad (3.31)$$

$$\Phi_{ab}^{ik}(\tau_a,\tau_b)_{mn} = \Phi_{ab}^{ik}(\tau_a,\tau_b)_n - \Phi_{ab}^{ik}(\tau_a,\tau_b)_m = (\frac{f}{c}).\rho_{ab}^{ik}(T^i,T^k,T_a,T_b)_{nm} + d_{atm} \quad (3.32)$$

$$\Phi_{ab}^{il}(\tau_a,\tau_b)_{mn} = \Phi_{ab}^{il}(\tau_a,\tau_b)_n - \Phi_{ab}^{il}(\tau_a,\tau_b)_m = (\frac{f}{c}).\rho_{ab}^{il}(T^i,T^l,T_a,T_b)_{nm} + d_{atm} \quad (3.33)$$

As can be seen from the equations, the triple difference removes the integer ambiguity term. The triple difference eliminates or reduces errors that occur due to satellite and receiver clock offset. In addition, the triple difference can be used as a cycle slip detector. Therefore, the outliers can be detected and can then be corrected or removed. The disadvantage of this technique is that it is noisy.

3.7 Receiver and satellite antenna

The observed range between a receiver antenna and a satellite antenna is the distance between the electrical phase centres of the two antennas. However, the physical phase centres (geometric antenna centre) and electrical phase centres for receiver antenna and satellite antenna do not coincide, since the electrical phase centres are theoretical points in space, and the difference in a receiver antenna can be centimetres and in a satellite antenna can be up to one metre [Mader and Czopek, 2001]. In terms of antenna height, neither the electrical phase centre nor the physical phase centre are points that can be measured to; hence the offset of the physical phase centre from an external point on the antenna must be known and is commonly referenced to an antenna reference point (ARP) at the base (bottom) of the antenna pre-amplifer.

Using the correct phase centre offsets becomes very important when different antenna types are used. The antenna heights at GPS stations are measured vertically from the survey marker to the ARP. The offset from the ARP to the physical phase centre is then added to give the height of the physical phase centre above the survey marker. The receiver antenna has two phase centres: one for the L1 frequency and the other for L2. Moreover, the electrical phase centre will change with the changing direction of the signal from a satellite; this phase centre variation (PCV) mainly depends on the satellite elevation.

For GPS satellites the physical phase centre (geometric antenna centre) is the satellite centre of mass, since the equations of motion governing the satellite orbit refer to the centre of mass, whereas the electrical phase centre for the satellite is along the transmitting antenna. Therefore, the vector offset between the physical phase centre (satellite centre of mass) and the electrical phase centre must be determined accurately. This vector offset has been assumed to be constant for a specific satellite block type. The IGS uses offsets for block I, II, IIA, IIR-A, IIR-B and IIR-M.

In order to get high precision, the exact position of the phase centre for both the satellite transmitting antenna and the receiver antenna should be known. Originally, the relative phase centres were used in the GPS community, where the relative phase centre offsets and variations were obtained by estimation from GPS data collected on a short, well known baseline and based on the assumption that the PCV for the AOAD/M_T reference antenna were zero. More recently, the GPS community has agreed to move from relative to absolute antenna phase centre offsets and variations, starting from the GPS week 1400 (4 Nov 2006) for both satellite and receiver. For this case, the absolute phase centre offsets and variations for the receiver antenna are estimated by two methods. Firstly, the method reported by Schupler and Clark [1991], which involves measurements in an anechoic chamber. In this method, the antenna is mounted in a position that enables rotations around two independent axes and shifts in three directions. While the transmitting antenna is kept fixed, the receiving antenna is rotated through zenith angles from -90° to +90° in different azimuths. Secondly, in the method developed by Wubbena *et al.* [1998], the antenna is mounted onto a precise robot, which rotates the antenna around a fixed point. For the GPS satellite antenna, offsets and absolute antenna phase centre variations are determined by absolute tracking antenna [Schmid and Rothacher, 2003].

Moreover, the GPS receiver antenna is covered by radar domes to protect the antenna from environmental effects such as snow, sand and weather. These radar domes are supposed to be transparent to GPS frequencies, however, they have been shown to have an affect on the GPS signals, causing a bias on station coordinate estimates, especially on the height component. Therefore, the geodetic community uses a list of corrections for different antenna and radar dome combinations to be applied in the processing stage to minimize these bias effects.

3.8 Earth tides and loading effects

The earth surface is perpetually deformed due to a variety of internal and external forces acting on time scales from seconds to millions of years. These effects require careful attention and good model estimation using the IERS standards, because any errors remaining in periodic models are likely to propagate into other frequencies; therefore, care must be taken when making geophysical interpretations from geodetic time series. A brief description of solid earth tides, ocean tide loading, atmospheric pressure loading and hydrological loading will be given.

3.8.1 Solid earth tides

The earth surface undergoes periodic deformations under the gravitational forces of the moon, and sun and other planets. The solid Earth is deformed at tidal periods and its response is usually determined by the Earth's elasticity. Besides the direct effect of the gravitational attraction of the Moon and Sun, solid earth tides are dependent on the latitude and local factors such as geology and elasticity. It is believed that "*the Earth has physical properties that obey very complex, and as yet little known, laws whose study is the subject of rheology and which combine parameters of elasticity, viscosity and plasticity*" [Melchior, 1983]. Where, Earth tides can lead to surface motions of up to 40 cm in semi-diurnal and diurnal time scales.

Unmodelled sub-daily periodic signals can propagate into time series of daily geodetic coordinates. Therefore, poorly modeled periodic signals in the geodetic analysis may lead to misinterpreting geodetic analysis bias as geophysical signal. Watson *et al.*, [2006] carry out a comparison study between two solid Earth tide models IERS2003 and IERS1992 using analyses of global GPS data. Where, this study shows that aliased annual and semi-annual signals are evident in the vertical component of the GPS time series, with the amplitudes increasing as a function of latitude up to approximately 2 and 0.4 mm, respectively.

Therefore, corrections for the earth tide should be applied to ensure that highly precise station coordinates are estimated, especially for long baselines, since the earth tide will not difference away as in the case of the shorter baselines. Models for the solid earth tides have been estimated and are updated from time to time. The latest model is that used in IERS conventions 2003 [McCarthy and Petit, 2004].

3.8.2 Ocean tide loading

Ocean tide loading (OTL) is defined as the deformation of the earth surface as a result of the ocean tides. OTL is produced mainly by the gravitational forces of the moon and sun. The moon effects are twice larger than the sun effects. This is due to the fact that the Sun is at a greater distance which is more important than mass of the Sun. The tidal frequencies are generally expressed in terms of fundamental frequencies namely that result in classification of tides as semi-diurnal, diurnal and long period. Since the water moves back and forth so the mass is redistributed causing the periodic loading of the ocean bottom. Also, the surface of the earth is viscous elastic, so it deforms under this load which in some low latitude regions deforms the Earth's surface about 10 cm [Baker, 1984].

The ocean tide loading can affect horizontal and vertical components; so in precise geodetic work the OTL effect should be removed. Where, Penna *et al.*, [2008] reported that the surface of South-West of England moves through a (predominantly) vertical range of over 10cm in around 6 hours.

There are a number of OTL models, the latest being GOT00.2 and FES2004. The corrections for these models are available from the provider at the Onsala space observatory (www.oso.chalmers.se/~loading). GOT00.2 is a long wavelength adjustment of the previous model FES94.1 using TOPEX/Poseidon data and is given on a 0.5 × 0.5 degree grid. FES2004 is a further development

of the FES series using TOPEX/Poseidon data and is given on a 0.125 degree resolution.

3.8.3 Atmospheric pressure loading

The movement of air particles due to the density variations accompanied by changes in temperature is called atmospheric dynamics. Where the atmospheric mass and its periodic movements affect the earth; since the mass of the atmosphere induces some gravitational attraction as it is composed of gases and other particles. Therefore, the changes of the weight of the column of atmosphere due to variations of pressure result in the earth crust and sea surface deforming, called atmospheric pressure loading.

The effect of the atmospheric pressure loading is of long wavelengths from 1000 to 2000 km, where the largest effect is at high latitudes. Where this loading signals effects the horizontal one third the amplitude of the vertical [van Dam *et al,*. 2002]. Where the atmospheric pressure variations are causing surface displacements up to 3 cm for the vertical component at high latitudes [van Dam *et al.,* 1994]. Petrov and Boy [2004] reported that the atmospheric pressure loading can cause deformation of the Earth's crust up to 20 mm for the vertical component and 3 mm for horizontal components. Petrov and Boy [2004] have detected the atmospheric pressure loading signal for the first time at the horizontal component, where this signal has never been before taken into account in routine reduction of geodetic observations, since it adds noise to the horizontal site position with an rms of 0.6mm If it is not modeled. Also, the effect on the annual component has amplitudes between 0.5 and 3 mm [van Dam *et al.,* 2002]. Atmospheric pressure loading is evident in GPS measurements and can causes vertical surface displacement of about 24% of the total variance in the GPS vertical estimates [Van Dam *et al.,* 1994].

Moreover, one of the problems with atmospheric pressure loading is the ocean response. The relationship between the atmosphere and the oceans is

represented by a common factor, called the Inverted Barometer (IB). Where the IB is equivalent to an increase in atmospheric pressure of 1 mbar causing the underlying ocean surface to depress by 1 cm [Ponte *et al.*, 1991]. Furthermore, the oceanic response to the atmospheric pressure is approximately close to the inverse barometer [Ponte *et al.*, 1991] and hence the oceans are considered separately from land. Therefore, precise estimation of the deformations and gravity field variations of the Earth, require correction to atmosphere pressure for seasonal variations. If the atmospheric pressure loading correction is not applied, GPS orbits may introduce regional perturbations at the stage of orbit computations [Johansson *et al.*, 2002]. Furthermore, Petrov and Boy [2004] reported that when applying atmospheric pressure loading corrections this causes a small change in the resulting terrestrial reference frame; where the maximum station position change which observed one year or more is 2 mm, the velocity change is typically below 0.1 mm/yr with the maximum change of 0.4 mm/yr, and the scale factor is increased by 0.05 ± 0.02 ppb.

3.8.4 Hydrological loading

The changes of the water mass stored in continents results in the Earth's crust being deformed, called hydrological loading. This deformation is subject to seasonal and long term variability in the hydrological cycle, where the main contributors are changes in groundwater storage, soil moisture, snow coverage, lake water, river water and vegetation water. However, only soil moisture variations are considered to be significant. Furthermore, little is known about the spatial and temporal variability of water storage on a global scale [Rodell and Famiglietti, 2002]. Where, the continental water mass is an important variable in the earth time varying gravity field, but it is the least known of the mass redistribution variables [Minster, 1999]. Moreover, surface groundwater is the dominant contributor to the variations in the Earth's gravitational field at the annual frequency [Dong *et al.*, 1996]. Due to its contribution to time dependent gravity field, monthly, seasonal and annual changes in continental water were predicted to be detectable by GRACE satellite mission [Rodell and Famiglietti, 1999].

The contribution of the hydrological cycle to loading deformation is of increasing interest to many researchers [Mangiarotti *et al.*, 2001]. Where the earth system is affected by mass redistribution as result of changing in continental water storage. For example, at seasonal time scale, it contributes to the time varying gravity field [Wahr and Bryan, 1998], loads and deforms the Earth's surface, causes Earth rotation variations, causes the position of the centre of mass to vary [Bouille *et al.*, 2000], and is regarded as a primary cause of sea level variations when transferred from the continents to the oceans [Chen *et al.*, 1998].

Snow and rain are visible variables in the hydrological cycle over the continents. Over a global scale, these two represent the water mass balance between the oceans and land. Where, soil moisture is a measure of the water content in the upper earth's surface. The time dependent variability in soil moisture depends upon soil type, plant cover and precipitation. This variable of the global hydrological cycle is the most difficult to estimate and, subsequently not many models are available. Remote sensing satellite missions can provide information about surface water but can not estimate the deeper soil moisture. The GRACE mission is intended to help in resolving estimating the problem of continental water.

3.9 Atmospheric delay

When the GPS signals propagate through the atmosphere, they are affected by refraction; hence this should be mitigated in the processing stage, otherwise it will affect the station coordinate estimates. The earth atmosphere is divided into two main layers, the troposphere layer and the ionosphere layer and the signal propagation conditions are quite different in these two parts.

3.9.1 Tropospheric delay

The troposphere (neutral atmosphere) is the lower layer of the atmosphere; it extends approximately 50 kilometres up from the earth surface. Here, the signal propagation is mainly affected by pressure, temperature and water vapour content of the troposphere. This layer is considered to be the ultimate accuracy-limiting factor for geodetic applications [Dach *et al.*, 2007]. The bias caused by the troposphere can be divided into two types: relative and absolute troposphere bias. The relative troposphere bias is due to an error of (mis-modelled) tropospheric refraction at one endpoint of a baseline relative to the other endpoint. The absolute tropospheric bias is due to an error of (mis-modelled) tropospheric refraction at both endpoints of a baseline [Dach *et al.*, 2007]. The relative tropospheric bias affects the height component and the absolute bias makes a scale bias for the baseline between the two stations [Beutler *et al.*, 1999]. Also, the troposphere is a non-dispersive layer and since the GPS signal is of the microwave type, the refractive index of the signal is independent of the signal frequency. Moreover, the troposphere bias is of a magnitude above the noise level of the phase observable, hence the effect of this bias should be minimized. There are two methods: firstly by modelling the troposphere refraction using ground meteorological measurements or water vapour radiometers (in this method, there is no use of GPS observables); secondly, tropospheric parameters can be estimated using GPS observables.

In high precision geodetic work the signal delay due to the troposphere layer using GPS observables can be estimated along with the geodetic parameters as the Zenith Total Delay (ZTD), i.e. the delay at 90° from the horizon (at the zenith). The ZTD estimates are highly correlated with other biases e.g. ocean tide loading [Baker, 1998; Dragert *et al.*, 2000] or antenna phase centre variations [Rothacher, 2002]. The ZTD are separated into a hydrostatic delay and a wet delay. The Zenith Hydrostatic Delay (ZHD) is due to the dry components of the atmosphere, while the Zenith Wet Delay (ZWD) is due to the dipole moment of the water vapour in the atmosphere. The hydrostatic contribution accounts for 90% of the delay and can be modelled by assuming

that the atmosphere is in a state of hydrostatic equilibrium [Langley, 1996]. The wet delay is correlated with water vapour content along the path of the signal; it is highly variable so it is difficult to estimate. Flouzat *et al,*. [2009] show that there is strong seasonal fluctuation of zenithal delays consistent with meteorological data and strong horizontal tropospheric gradients.

Moreover, at the GPS station the satellites appear at different elevation angles from 0° to 90°; hence the signals at a low elevation may travel longer [Dodson *et al.*, 1996]. Therefore, mapping functions for the troposphere delay are required to take into account the satellite elevation. The most popular mapping function for both the hydrostatic and wet mapping functions is the mapping function developed by Niell (NMF) [Niell, 1996]. However, more mapping functions have been developed recently, for example, the Isobaric mapping function (IMF) [Niell, 2001] and the Vienna mapping function (VMF) [Boehm *et al.* 2006], where both mapping functions are derived using numerical weather models. Furthermore, Boehm *et al.* [2006] also developed a Global Mapping Function (GMF). Vey *et al,*. [2006] carry out a comparison between Niell hydrostatic mapping function (NMF) and the isobaric hydrostatic mapping function (IMF) based on numerical weather fields; the result shows that the most pronounced differences is in the height component.

3.9.2 Ionospheric delay

The ionosphere is the upper layer of the atmosphere; it is approximately 70 to 1000 kilometres or more above the earth surface. The ionosphere is a layer of electrons and electrically charged atoms and molecules [Langley, 1996]. Here, the signal propagation is mainly affected by free charged particles [Jakowski, *et. al.*, 2008]. The ionization of ionosphere depends on the Sun's radiation activity which mainly includes X-rays, extreme ultraviolet radiation and corpuscular radiation from the Sun. The structures and peak electron densities of ionosphere vary with time such as sunspot cycle and season, geographical location (polar and equatorial regions). The ionosphere layer is divided into

four major regions called D, E, F and topside. Where these major regions are sub-divided into several regularly occurring layers, for example, F1 and F2 [Bassiri and Hajj, 1993]. The D region is the innermost between 70-90 Km above the surface of the earth. The ionization in D region is extremely low at night, but during the day becomes more heavily ionized. The E region is the middle region between 90-150 km above the earth surface. The E region is sub-divided into different layers which isolate separate layers of irregular occurrence within this region. These sub-divided layers are named with an E prefix such as the thick layer, E2, and a highly variable thick layer, Sporadic E. The F region is the upper region 150-500 km above earth surface. Where, the ionization in F region is mostly based on extreme ultraviolet radiation so that the electron density is controlled by the zenith angle of the sun. The ionospheric effect on GPS signal will be greater in summer because the daytime period which means high solar activity is longer than those in winter for every day. The most important reflecting layer F2 is found in this region. The other sub-divided layers in this region are also labeled with an F prefix, such as temperate-latitude stratification, F1. The topside region starts at the height of the maximum density of the F2 ionosphere layer and extends upward with decreasing density to a transition height. Where, the transition height is not regular and often vary, sometimes, it may lie as high as 1100 km. Generally, it rarely drops below 500 km at night or 800 km in daylight. Furthermore, the ionization above the transition height is weak, thus it has little effect on GPS signal propagation.

The state of the ionosphere can be described by the electron density in units of electrons per cubic metre. This density can vary rapidly where the number of electrons along the path of the signals varies. Hence, the GPS receiver cannot keep track of the signal due to these variations in density of the ionosphere. When the GPS receiver loses lock for a short period of time on a satellite signal, this is called a cycle slip [Langley, 1996]. The density variations are correlated with solar activity, where these solar activities are characterized by the sunspot numbers, which follow an 11-year cycle. Figure 3.3 shows solar

cycle sunspot numbers observed from 1 January 2000 to 30 June 2008 and predicted from 1 July 2008 to 1 Jan 2016.

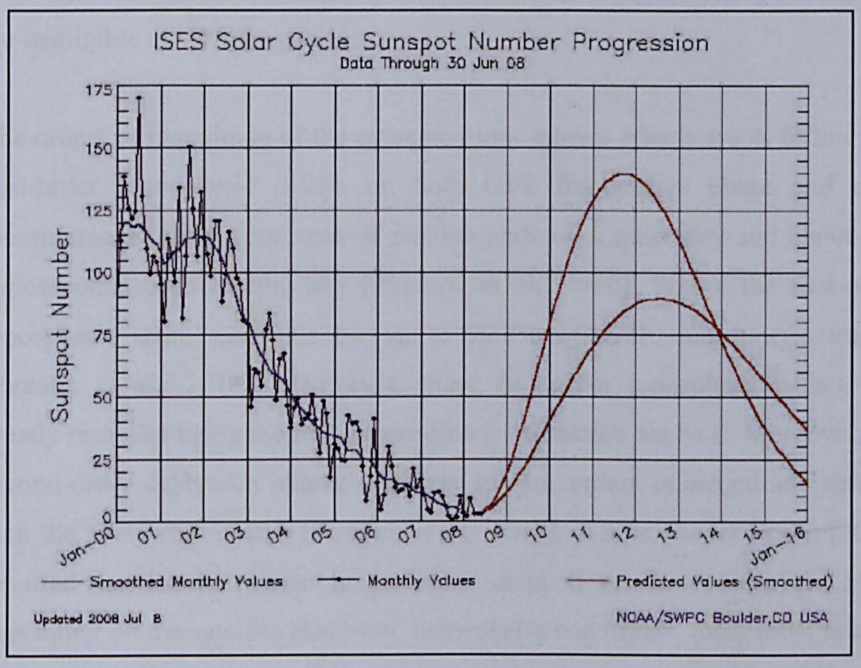

Figure 3.3. ISES sunspot numbers [http://www.smeter.net/ propagation/sunspots/current-sunspot-cycle.php].

When the GPS signals pass through the ionosphere, the variation of the electron density will cause error to the signals and it is reflected by the refractive index. The ionospheric impact on GPS signal means a signal delay, where this delay may reach up to several tens of nanoseconds [Pireaux *et al,*. 2010] and it is increase dramatically on ionosphere storm. The ionosphere is dispersive for microwave signals so the refractive index of a signal is dependent on the signal frequency. Therefore, this characteristic has been used widely in the analysis of dual frequency GPS observations to greatly reduce the effect of the ionospheric delay on GPS signals by creating the ionosphere free (L_3) linear combinations of the two carrier signals L_1 and L_2. Furthermore, the geomagnetic field is another essential component for estimating the second-order ionoshperic error. Similar to ionosphere, it is needed to model the geomagnetic field in order to determine the magnetic field along the signal

propagation path. Petrie *et al,*. [2010] reported that the ionospheric electron content and the geomagnetic field affect the second order term, while the geomagnetic field does not affect the third order term; also subsequent terms are negligible at GPS frequencies.

The orders of magnitude of the estimated ionospheric effects are as follow: the first-order ionospheric delays on both GPS frequencies phase and code measurements are several tens of nanoseconds on a quiet day and about 100 nanoseconds on a stormy day [Pireaux, et al,. 2010]. Where the first-order ionospheric term accounts for up to 99.9% of total ionospheric impact [Pireaux *et al,*. 2010]. However, these first-order ionospheric effects are greatly removed using the ionosphere-free combination analysis. Moreover, the second-order delays on phases are three to four orders of magnitude smaller than the first order delays [Pireaux *et al,*. 2010]. Where, Kedar *et al,*. [2003] reported that the first order ionospheric delay is on the order of 1– 50 m depending on the satellite elevation, ionospheric conditions, local time, season, and solar cycle. The remaining effect due to higher-order terms is estimated to be on the order of sub-millimeter to several centimeters. Also, Lutz *et al.*, [2010] reported that the second order correction term of one observation can reach 1cm in position depending on station latitude, elevation angel and time of the day. Herna´ndez-Pajares *et al.,* [2007] show that the Second order ionospheric term effects is in general the position shifts at sub millimeter level and are directed southward for low latitude stations and northward for high latitude stations. Furthermore, Petrie *et al,*. [2010] reported that the bias in the estimated vertical velocity caused by higher order ionospheric effects on the range 0.0 to 0.29 mm/yr over the period 1996-2000 and -0.34 to 0.0 mm/yr over the period 2001-2005. Therefore, Petrie *et al,*. [2010] suggest that when millimeter level coordinate precision is required, the higher order ionospheric effects should be considered, particularly over the maximum ionospheric periods and in equatorial regions. Also, Kedar *et al,*. [2003] recommend that higher order ionospheric terms correction should be applied when proper interpretation of station motions is required; otherwise uncorrected higherorder

ionospheric terms can alias into artificial diurnal, seasonal and inter-annual station motions, which may be misinterpreted as tidal effects and crustal deformation.

3.10 Summary

This chapter has briefly described the developments of reference frames and their importance in geodetic work, with a brief explanation of the latest ITRF2005 realization. Then the IGS products and community were outlined, followed by the criteria for regional GNSS networks and how they are optimally expressed in the ITRF.

The GPS constellation was briefly outlined with its recent developments; then a short explanation of the GPS observables with their linear combinations was presented. The initial phase ambiguity and ambiguity resolution were outlined, followed by quick explanations of the differencing techniques.

Finally, GPS biases and errors, and their mitigation were discussed. The antenna bias from both the receiver antenna and satellite antenna was briefly explained and then an outline was given as to how to reduce this bias, which was in the past by applying relative phase centre models and is now by using the absolute phase centre models. Also, the earth tide and ocean tide loading effects were outlined briefly and the latest models used to reduce these biases were introduced. Lastly, the atmospheric delay was described in terms of the troposphere and ionosphere.

Chapter 4: The GPS data set and processing strategy

4.1 Introduction

In order to design a GPS network for plate motion investigation, two main criteria should be taken into account when a station location is chosen, one concerning geological factors, the other geodetic factors. The first geological criterion concerns the choice of a suitable location from a geological point of view in or near the area of interest. Secondly, the stability of the ground at the local site should be considered. The main geodetic criteria are its suitability for GPS observations, i.e. clear sky to avoid possible satellite signal block or multipath, no nearby electrical power lines, power stations or radio communication stations to avoid signal disturbances and the station should be as far as possible from future civil engineering developments, so that the station can be used for long-term geodetic monitoring. Additionally, the available budget is another major factor to be considered when designing a GPS network. Other essential factors to be carefully considered when studying plate motion are the reference frame implementation and the processing strategy to be used.

In this chapter, the GPS networks and their station specifications, and the campaigns carried out are discussed. Then the data quality checking is considered. Finally, details are given of the reference frame implementation applied and processing strategy used in this study.

4.2 The GPS data set

The General Commission for Survey (GCS) in Saudi Arabia in collaboration with the Institute of Engineering Surveying and Space Geodesy (IESSG) designed a densified GPS network in Saudi Arabia taking into account the criteria given in §4.1 above. The decision was made not to establish new station monuments, as the existing stations that are part of Saudi Arabia's geodetic network satisfy the geological and geodetic criteria, and their use minimizes the research cost. Hence, 31 geodetic stations from the Saudi Arabia geodetic network were selected. The selection criteria for these stations were for them to be: evenly distributed within Saudi Arabia and their monuments thought to be stable and in a suitable geophysical setting (Fig. 4.1). Moreover, the distribution of these stations also takes account of the geological structure of the Arabian plate as explained in Chapter 2. Fifteen stations are located in the Arabian shield, distributed as follows:

- Along the Red Sea coast: seven stations (F001, F002, F005, F006, F007, F008 and F009)
- Farasan island: one station (F074)
- Asir terrane: two stations (F016 and F031)
- Afif terrane: three stations (F033, F013 and F041)
- Hail terrane: one station (F024)
- Jiddah terrane: one station (F012)

The other 16 stations were distributed on the Arabian platform as follow:

- Wajid basin in the south of Saudi Arabia: two stations (F078 and DATM)
- Central Arabian arch and graben: ten stations (F077, F019, F035, F036, F020, F037, F030, F039, F029 and F040)
- Widyan basin on the north of Saudi Arabia: two stations (F026 and F027)
- Sirhan-turayf basin in the north of Saudi Arabia: one station (F045)

- Tabuk basin in the north-west of Saudi Arabia: one station (F010)

Figure 4.1 below illustrates these distributions.

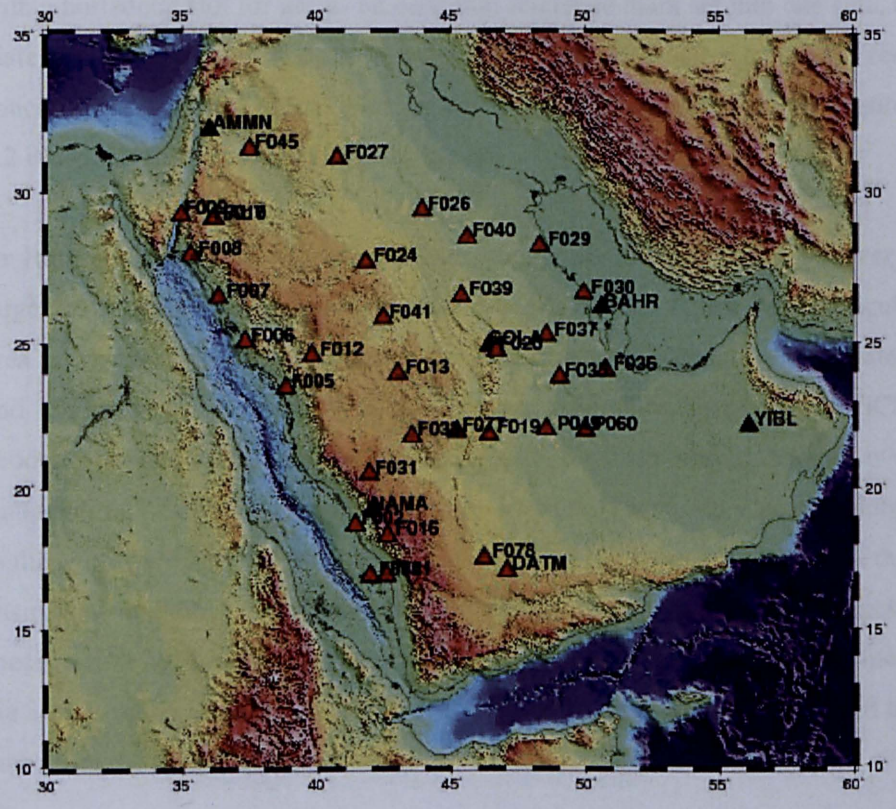

Figure 4.1. The regional GPS network.

The monument specification is another crucial factor to be considered when designing a GPS network for plate motion investigation. This specification is addressed by the IGS community, where very high standards are listed to minimize errors due to local monument deformation. All the 31 stations selected from the Saudi Arabia geodetic network have the same monument specification, even the DATM station that was initially established as a datum station in Saudi Arabian territory for the Saudi/Yemeni border in the south in early 2000. These monument pillars were constructed of concrete fitted with a brass forced centring device on the top surface, with a domed bronze tablet with a horizontal slot for use as an elevation reference mark set into one side, a plate set into one side and an underground mark. High strength reinforced concrete was specified to make the pillars very strong and long lasting. Figure 4.2 illustrates these monument specifications.

Ar Rub al Khali basin (the name means the Empty Quarter basin) is a very large basin in the south and south-east of Saudi Arabia. It is a very difficult area in which to live since there are high and long sand dunes, a lack of water and it is very hot, especially in the summer. Therefore, there are no GCS geodetic stations in this area up to now. Hence, for this research, another two stations (P049 and P060) were added to the network. These two stations belong to the Ministry of Petroleum and Mineral Resources and are to the north of the basin, their addition giving a more even network distribution. The monument specification for these two stations is different from the previous stations since the area is sandy. Here, a 30 metre pipe, installed with drills, was employed to make sure the monument was stable.

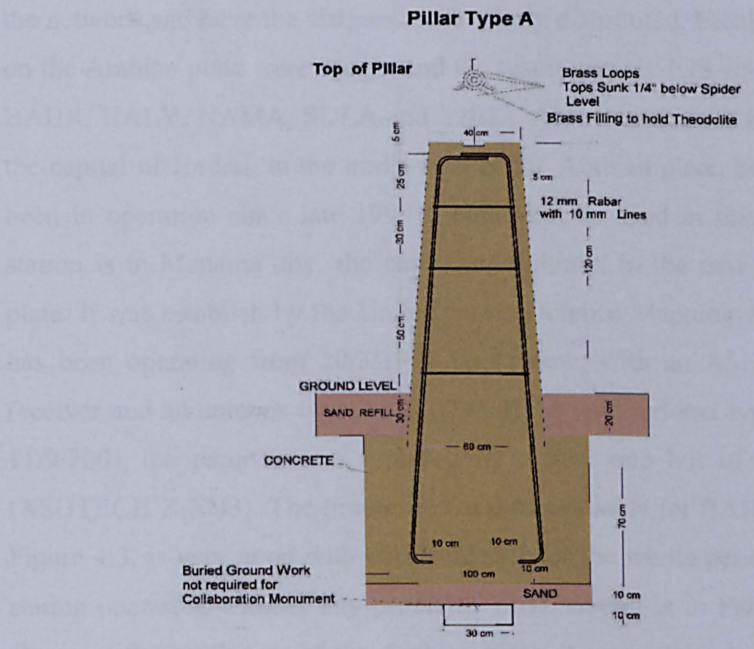

Figure 4.2. The Saudi Arabia geodetic station monument.

Furthermore, the author searched for more suitable GPS stations on the Arabian plate, to add to the stations available from the GCS in order to densify the network and have the stations more evenly distributed. Firstly, IGS stations on the Arabian plate were sought and the result was six IGS stations (AMMN, BAHR, HALY, NAMA, SOLA and YIBL). AMMN station is in Amman city, the capital of Jordan, in the north-west of the Arabian plate, but as it had not been in operation since late 1999 it could not be used in this study. BAHR station is in Manama city, the capital of Bahrain, in the east of the Arabian plate. It was establish by the United States Defence Mapping Agency. BAHR has been operating from 20/3/1995 up to now, with an ASHTECH Z-XII3 receiver and an antenna type ASH700936B_M with radome type SNOW . On 11/9/2001 the receiver was replaced by a new one but of the same type (ASHTECH Z-XII3). The time series of data available for BAHR, as shown in Figure 4.3, is very good with data available for the whole period and with the station operating without any problem. YIBL station is in Fahud province in Oman in the south-east of the Arabian plate. It was established by petroleum development Oman. YIBL operated from 13/7/2003 up to now and at first used an ASHTECH UZ-12 receiver type and antenna type ASH701945C_M with an undefined radome type but on 12/11/2006 the receiver was replaced by a TRIMBLE NETRS receiver. The monument at YIBL is a short drilled braced monument and the time series of data availability for YIBL, as shown in Figure 4.3, is mostly complete, except for a number of short gaps in mid-2004 and early 2005 and discrete data periods in 2005, 2006 and 2007.

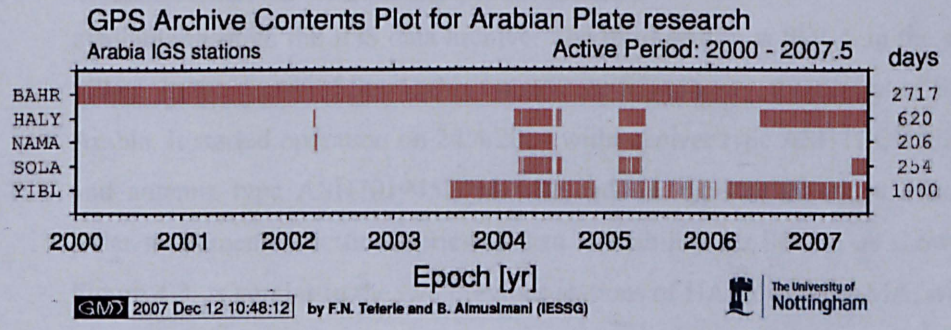

Figure 4.3. Time series of data available for IGS stations on the Arabian plate.

The other three IGS stations (HALY, NAMA and SOLA) are in Saudi Arabia and were established by King Abdulaziz City for Science and Technology (KACST) and the Massachusetts Institute of Technology (MIT). HALY is near Halat Ammar town in the north-west of Saudi Arabia and has been operating since 26/3/2002 with receiver type ASHTECH Z-XII3 and antenna type ASH701945C_M with radome type SCIT. Its monument type is short drilled braced stainless steel. The time series of data availability for HALY, as shown in Figure 4.3, was not continuous as expected as a result of data transmission technical problems occurring from time to time. There are three gaps where data have been lost. The first gap occurred after 15 days of operation in March 2002 and lasted about two years to early 2004. The second gap was from the middle of 2004 up to early 2005 (seven months) and the third gap was from the middle of 2005 up to the middle of 2006 (about one year). NAMA station is near Namas city on the top of Asir terrene with an elevation of 2,700 m in the south-west of Saudi Arabia. It started operation on 31/3/2002 with receiver type ASHTECH Z-XII3 and antenna type ASH701945C_M with radome type SCIT. Its monument type is short drill braced stainless steel. The time series of data availability for NAMA, as shown in Figure 4.3, is similar to the previous station HALY as a result of the same data transmission problems with a gap of data directly after it started operation in March 2002 up to early 2004. The second gap of data is from the middle of 2004 up to early 2005. Unfortunately, the data from mid-2005 up to the time of writing this thesis are not available. The early data in March 2002 for both HALY and NAMA stations were downloaded from the UNAVCO archive through the following web link: http://facility.unavco.org/data/gnss/perm_sta.php because the data are not available through the IGS data archive. The third station is SOLA in the solar village in the centre of the Arabian plate near Riyadh city, the capital of Saudi Arabia. It started operation on 24/4/2004 with receiver type ASHTECH UZ-12 and antenna type ASH701945E_M with radome type SCIS and a concrete pillar monument. The time series of data availability for SOLA, as shown in Figure 4.3, is similar to the two previous stations of HALY and NAMA, with a

gap of data after mid-2004 up to early 2005 and from mid-2005 up to mid-2007.

The author tried to add the stations used in previous studies on the Arabian plate, so the authors of these studies were contacted; for example, Vernant *et al.* [2004] for stations in Iran, Reilinger *et al.* [2006] and Vigny *et al.* [2006] but these authors did not make their stations' GPS data available.

Therefore, the network consists of 38 stations on the Arabian plate, 31 stations from the geodetic network of the GCS, two stations from the Ministry of Petroleum and Mineral Resources network and five IGS stations.

Furthermore, since this study also aims to investigate the strain rate accumulation within the Arabian plate, a local network was designed and added in the active south-western part of Saudi Arabia. These local network stations are part of the Saudi geodetic network and the distances between them vary between tens to two hundred kilometres as illustrated in Figure 4.4. The selection of these stations was as follows:

- Farasan island: three stations (F074, O643 and O644).
- Along the Red Sea coast: six stations (F001, M589, M591, O229, O231 and O632).
- Along the Asir terrane gradients: eight stations (M586, M587, M588, O629, O630, O634, O639 and O641).
- On top of the Asir terrane: eight stations (F016, O235, O258, O260, O627, O628, O633 and O635).

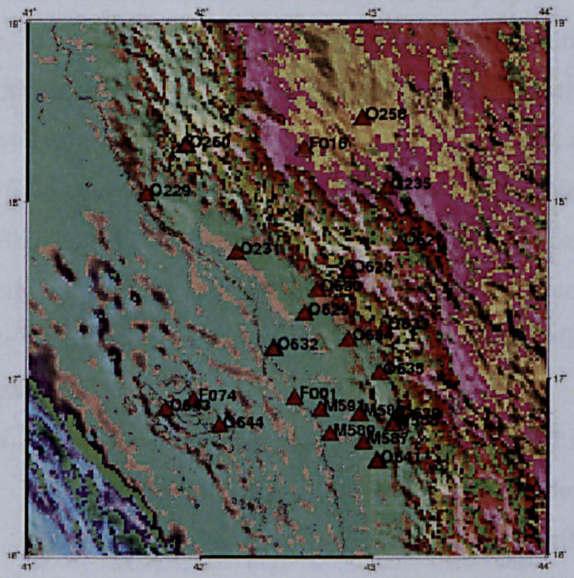

Figure 4.4. The local GPS network on the south-west of the Arabian plate.

4.2.1 Field campaigns

GCS decided to buy 11 Trimble GPS receivers model 5700 dual frequency and 11 Zephyr geodetic antennas, mainly for the purpose of this research. Also, GCS bought 13 4x4 vehicles, suitable for the hard topography of the area. In accord with the number of receivers available, it was arranged to have 11 field crews, each crew consisting of three people, two surveyors and one driver. Moreover, it was decided to carry out these campaigns in the winter season when the weather is much better for field work. Therefore, the initial plan was to carry out the first field campaign in early winter (January), but because of the late delivery of the receivers from the United States to Saudi Arabia the field campaign was shifted to the late winter and early spring seasons (March). GCS funded the field operation costs, which included the crews' field allowances and field logistical support (petrol, accommodation, food, etc.).

The design of the observation plan was mainly for the purpose of this research and, if possible, to ensure maximum benefit of this data for other projects for the GCS but without effecting the requirements of this research. For example, the epoch interval was set to 15 seconds instead of 30 seconds at IGS stations, since the GCS field operation standard is 15 seconds. Moreover, four stations (F001, F009, F020 and F035) were used as references stations for the GCS geodetic network adjustment in 1991. Therefore, it was recommended that these stations be observed continuously in each campaign of this research for the following reasons:

- their locations are distributed evenly within the Arabian plate, with F009 up in the north-west of the Arabian plate near Aqabha Gulf, F001 is down to the south-west in Jazan city, F020 is in the centre in Riyadh (GCS compound) and F035 is in the centre of the Arabian platform near Harat;
- it is good to have a number of network stations with the maximum period of observation;
- they give more chances to process the network data in more than one stage, if required; and
- they can be used for reprocessing and adjustment of the GCS geodetic network.

The time span of the observations is a major factor in this type of research. Therefore, the time span was arranged to be four years with three campaigns, giving two two-year spans between consecutive campaigns. Also, the field campaigns were arranged to be carried out almost at the same time of the year to minimize the systematic bias that may occur in the annual signal. The observation session was set to be 24 hours starting at 00:00 GMT time (+3 hours in local time of Saudi Arabia) to be consistent with IGS station specifications. The elevation cut-off angle was set at 10°.

The first campaign was carried out in March 2003 for 22 days, when the four Saudi fiducial stations (F001, F009, F020 and F035) were observed

continuously except for two days (66 and 77) used for logistic support. The other stations were observed between one to four days (for more details, see Table 4.1 below). The second campaign was carried out in March 2005 for 18 days, when the four Saudi fiducial stations were observed continuously and the other stations were observed between one and eight days (for more details, see Table 4.2 below). The third campaign was carried out in March 2007 for 18 days, when the four Saudi fiducial stations were observed continuously, but two days (81 and 82) of data for station F020 were not available because of a battery problem. The other stations were observed between two and seven days (for more details, see Table 4.3 below). The initial plan of the GCS and the IESSG was to use the 1988–1991 GPS data available at GCS that was collected when establishing the GCS geodetic network in 1991 for estimating the Arabian plate model in Phase One of this research. Unfortunately, this data was not good enough for the purpose of this research. Therefore, another campaign between the 2003 and 2005 campaigns was added and this campaign was carried out in April 2004 for eight stations only for 16 days, with the four Saudi fiducial stations again being observed continuously, but one day (125) of data for station F001 was not available because of a battery problem. The other four stations were observed between seven and nine days (for more details, see Table 4.4 below). The purpose of this campaign was to give more reliability on the estimation of the Arabian plate model from the first two epochs (2003 and 2005) carried out in phase one.

Table 4.1. Data available for the regional network campaign 2003.

	Julian day of the year 2003																			
Stations	62	63	64	65	66	67	68	69	70	71	72	73	74	75	76	77	78	79	80	81	82	83
F001	X	X	X	X		X	X	X	X	X	X	X	X	X	X		X	X	X	X	X	X
F009	X	X	X	X		X	X	X	X	X	X	X	X	X	X		X	X	X	X	X	X
F020	X	X	X	X		X	X	X	X	X	X	X	X	X	X		X	X	X	X	X	X
F035	X	X	X	X		X	X	X	X	X	X	X	X	X	X		X	X	X	X	X	X
F002									X													
F005									X			X										
F006												X		X								
F007														X			X					
F008																	X					
F010																	X					
F012												X		X								
F013									X			X										
F016							X		X													
F019	X																					
F024														X			X			X		
F026																				X		X
F027																	X			X		
F029	X																			X		X
F030	X																					X
F031				X			X															
F033				X			X															
F036	X			X																		
F037	X																					X
F039												X		X						X		X
F040																				X		X
F041												X		X								
F045																	X					
P049	X			X																		
P060	X																					
F074							X		X													
F077				X			X															
F078							X		X													
DATM				X																		

Table 4.2. Data available for the regional network campaign 2005.

	Julian day of year 2005																	
Stations	65	66	67	68	69	70	71	72	73	74	75	76	77	78	79	80	81	82
F001	X	X	X	X	X	X	X	X	X	X	X	X	X	X	X	X	X	X
F009	X	X	X	X	X		X	X	X	X	X	X	X	X	X	X	X	X
F020	X	X	X	X	X	X	X	X	X	X	X	X	X	X	X	X	X	X
F035	X	X	X	X	X	X	X	X	X	X	X	X	X	X	X	X	X	X
F002						X	X											
F005										X								
F006										X	X	X	X					
F007													X					
F008													X					
F010													X					
F012										X								
F013			X							X								
F016						X	X											
F019	X	X	X															
F024													X	X	X	X	X	X
F026																X		
F027																X		
F029	X															X	X	X
F030	X																	X
F031						X	X	X	X	X								
F033			X	X	X	X	X	X	X	X								
F036	X																	
F037	X																	
F039	X															X	X	X
F040																X	X	X
F041										X	X	X	X					
F045													X	X	X	X		
P049	X																	
P060																		
F074						X	X											
F077			X															
F078			X	X	X	X	X											
DATM			X	X	X	X	X											

Table 4.3. Data available for the regional network campaign 2007.

	Julian day of year 2007																	
Stations	73	74	75	76	77	78	79	80	81	82	83	84	85	86	87	88	89	90
F001	X	X	X	X	X	X	X	X	X	X	X	X	X	X	X	X	X	X
F009	X	X	X	X	X	X	X	X	X	X	X	X	X	X	X	X	X	X
F020	X	X	X	X	X	X	X	X			X	X	X	X	X	X	X	X
F035	X	X	X	X	X	X	X	X	X	X	X	X	X	X	X	X	X	X
F002							X	X	X									
F005	X	X																
F006															X	X	X	X
F007											X	X	X					
F008						X	X	X	X									
F010	X	X	X	X														
F012				X	X	X												
F013																X	X	X
F016															X	X	X	X
F019	X	X	X															
F024													X	X	X	X	X	X
F026										X	X							
F027						X	X	X										
F029				X	X	X	X											
F030									X	X								
F031	X	X	X	X	X													
F033								X	X	X	X	X	X	X				
F036												X	X	X				
F037																X	X	X
F039	X	X															X	X
F040													X	X	X			
F041								X	X	X	X							
F045	X	X	X	X														
P049																	X	X
P060																		
F074											X	X	X					
F077					X	X												
F078									X	X		X	X	X				
DATM	X	X	X	X	X	X	X											

Table 4.4. Data available for the regional network campaign 2004.

	Julian day of year 2004															
Stations	117	118	119	120	121	122	123	124	125	126	127	128	129	130	131	132
F001	X	X	X	X	X	X	X	X		X	X	X	X	X	X	X
F009	X	X	X	X	X	X	X	X	X	X	X	X	X	X	X	X
F020	X	X	X	X	X	X	X	X	X	X	X	X	X	X	X	X
F035	X	X	X	X	X	X	X	X	X	X	X	X	X	X	X	X
F002																
F005																
F006																
F007																
F008																
F010																
F012																
F013			X	X	X	X	X	X	X							
F016																
F019																
F024																
F026																
F027	X	X	X	X	X	X	X	X	X							
F029	X	X	X	X	X	X	X	X	X							
F030																
F031																
F033																
F036																
F037																
F039																
F040																
F041																
F045																
P049																
P060																
F074																
F077																
F078																
DATM	X	X	X	X	X	X	X	X	X							

In this study, the time span of the observations for the local network was two years with one campaign in the middle, giving a one year gap between consecutive campaigns. Also, the field campaigns were arranged to be similar to the regional network campaigns with the local network campaigns' observations being carried out almost at the same time of the year in January to minimize the systematic bias that may occur in the annual signal. Moreover, the observation sessions were set to be 24 hours starting at 00:00 GMT time (+3 hours in local time of Saudi Arabia) to be consistent with IGS station specifications. The elevation cut-off angle was set as 10° and the epoch interval was 15 seconds. The first campaign was carried out in January 2006 for five days, with the three Saudi fiducial stations (F001, F016 and F074) observed on each day of this campaign, except for station F074 that could not be observed for one day (21) due to logistic support problems. The other stations were observed between one and three days (for more details, see Table 4.5 below). The second campaign was carried out in January 2007 for 5 days, with the three Saudi fiducial stations observed on each day of this campaign, except for station F001 that could not be observed for one day (26) due to logistic support problems. The other stations were observed between one and three days (for more details, see Table 4.5 below). In this campaign, station O642 was destroyed and station M588 was its replacement. The third campaign was carried out in January 2008 for 9 days, with the three Saudi fiducial stations observed on each day of this campaign. The other stations were observed between one and five days (for more details, see Table 4.5 below). In this campaign, station O260 was destroyed and more observations were taken at station O632 since there was one redundant crew and there was no replacement station available as this campaign was the last campaign for this study.

Table 4.5. Data available for the local network campaigns 2006, 2007 and 2008.

	Julian day of 2006					Julian day of 2007					Julian day of 2008								
Stations	21	23	25	27	29	26	29	31	33	35	20	21	22	23	24	25	26	27	28
F001	X	X	X	X	X		X	X	X	X	X	X	X	X	X	X	X	X	X
F016	X	X	X	X	X	X	X	X	X	X	X	X	X	X	X	X	X	X	X
F074		X	X	X	X	X	X	X	X	X	X	X	X	X	X	X	X	X	X
O229	X									X							X	X	X
O231	X	X							X	X							X		X
O235	X									X									X
O258	X									X									X
O260	X									X									
O627	X	X							X	X									X
O628	X	X							X	X							X		X
O629		X	X					X	X										
O630		X	X					X	X						X		X		
O632		X	X	X			X	X	X				X		X		X	X	X
O633			X					X									X		
O634			X					X							X				
O635			X	X			X	X					X		X				
O639				X	X	X	X				X								
O641					X	X					X								
O642					X														
O643				X			X						X						
O644					X	X					X								
M586				X			X	X					X		X				
M587				X	X	X	X				X		X						
M588						X					X								
M589					X	X					X								
M591				X	X	X	X				X		X						

The author actively participated in field crews in Saudi Arabia during 2003, 2004 and 2005 campaigns, while in the 2006, January 2007, March 2007 and 2008 campaigns, he designed the field observation plans as well as being the technical supervisor for all crews in the field.

4.2.2 Checking data quality

When the raw GPS data of the campaigns were received, two essential and important steps were carried out. The first step was to archive the data in a secure and safe storage and the second was to check the quality of the raw data. Therefore, storage was arranged and the data archived in one of the IESSG servers where the data were accessible only by the author. For data quality checking, a tool called TEQC was used. This tool is widely employed in the GNSS community. TEQC is a toolkit developed at the University Navstar Consortium (UNAVCO) and is used in the pre-processing stage of GNSS data. TEQC is capable of translating the binary data of most popular receivers to RINEX format, of editing and cutting/splicing RINEX files, and of quality checking of GNSS data. TEQC gets its name from Translation, Editing and Quality Check and it is pronounced "tek". TEQC can be executed on Unix/Linux and Windows platforms, with all the information it uses to run being supplied on the command line.

In this research, the TEQC quality check mode was used for all data of the IGS stations and the regional GPS network. Scripts by Dr. F. N. Teferle were used and the summary files (S-files) were then stored. The summary files (S-files) contain important statistical analysis information, which can clearly present the quality of the data. The summary files (S-files) may show satellite windows and observation status, station information, session length, sample rate, expected observations, actual observations, percentage rate, RMS MP1, RMS MP2 and the number of cycle slips. Where Figures 4.5 and 4.6 are two examples plots for the station data quality check.

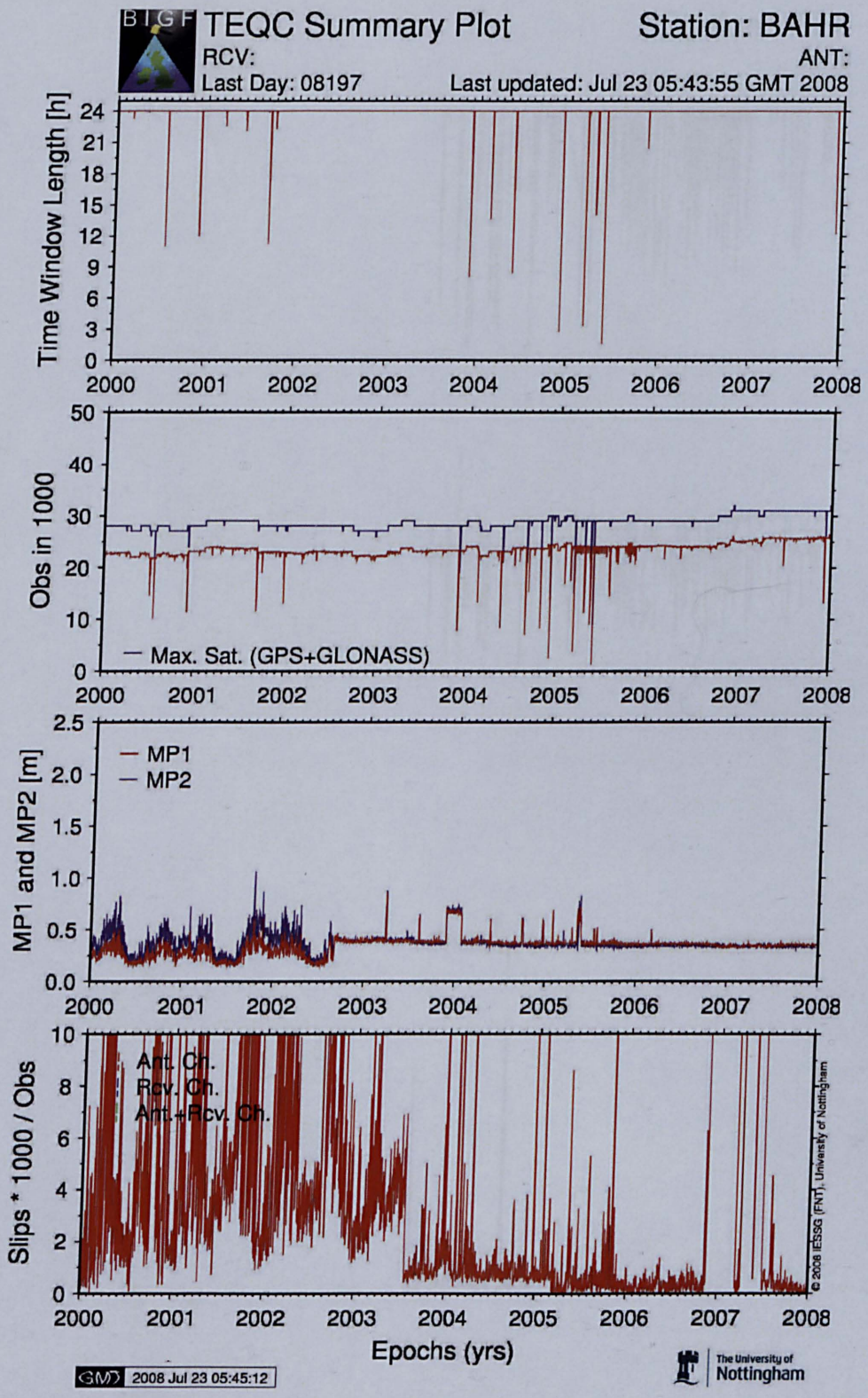

Figure 4.5. Daily TEQC summary plot for BAHR (from S-file).

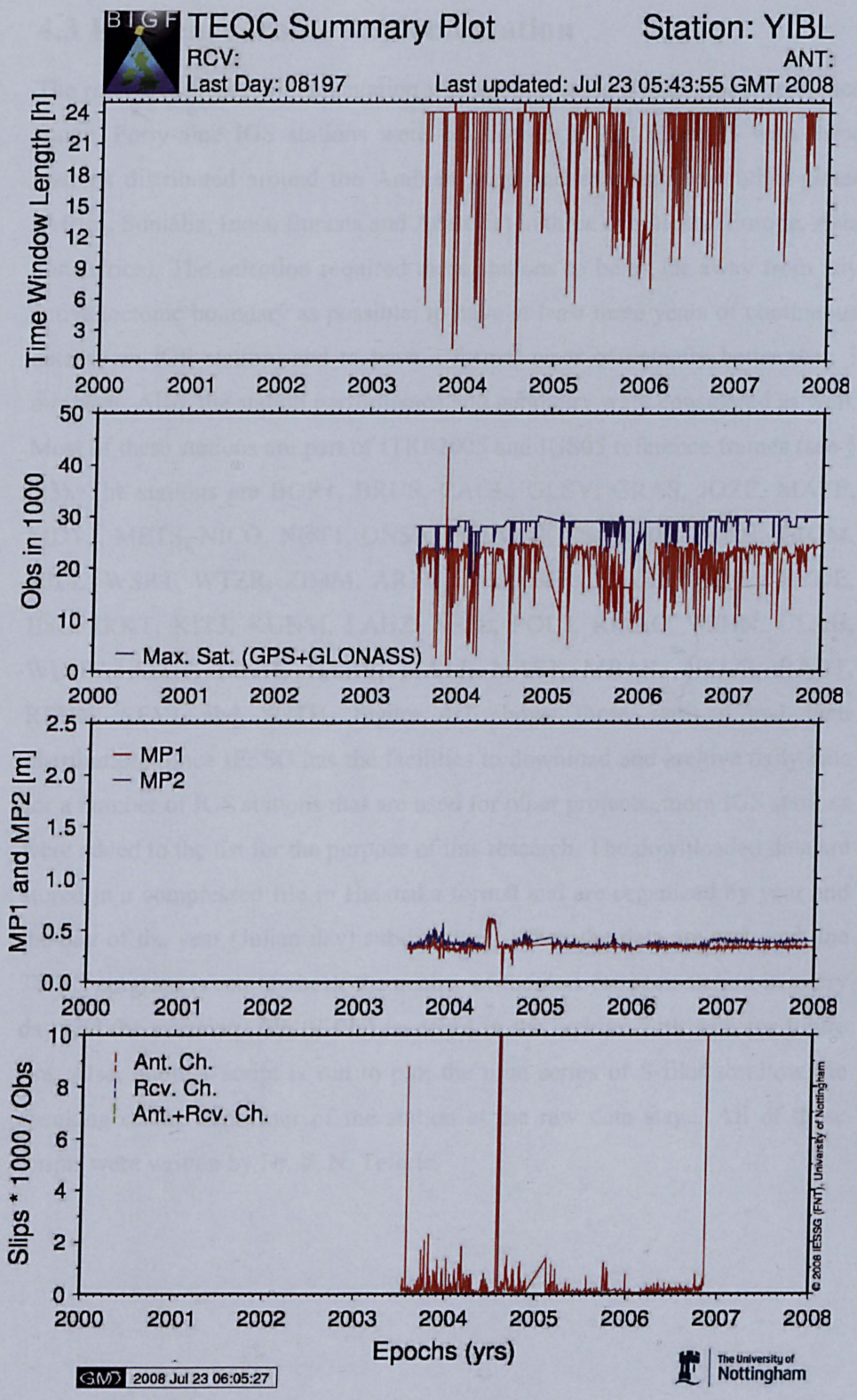

Figure 4.6. Daily TEQC summary plot for YIBL (from S-file).

4.3 Reference frame implementation

The reference frame implementation was applied using a near global reference frame. Forty-nine IGS stations were considered in this research, with these stations distributed around the Arabian plate and spanning five other plates (Africa, Somalia, India, Eurasia and Anatolia) in three continents (Europe, Asia and Africa). The selection required these stations to be as far away from any active tectonic boundary as possible; to have at least three years of continuous data as an IGS station; and to have a formal error of velocity better than 3 mm/year. Also, the station performance and geometry were considered as well. Most of these stations are part of ITRF2005 and IGS05 reference frames (see § 3.3). The stations are BOR1, BRUS, CAGL, GLSV, GRAS, JOZE, MATE, MDVJ, METS, NICO, NOT1, ONSA, POLV, POTS, SFER, TRAB, TROM, VILL, WSRT, WTZR, ZIMM, ARTU, BILI, BJFS, DAEJ, GUAO, HYDE, IISC, IRKT, KIT3, KUNM, LAHZ, NRIL, POL2, RMAO, TEHN, ULAB, WUHN, ASC1, DGR1, HARB, MALI, MAS1, MBAR, NKLG, RABT, REUN, SEY1 and SUTH. Figure 4.7 shows these stations and their distribution. Since IESSG has the facilities to download and archive daily data for a number of IGS stations that are used for other projects, more IGS stations were added to the list for the purpose of this research. The downloaded data are stored in a compressed file in Hatanaka format and are organized by year and the day of the year (Julian day) subdirectory. When the data are archived, the TEQC program is run to check the quality of the data for each station in every day and the summary file (S-file) is stored in the archive with data for future use. Also, another script is run to plot the time series of S-files to allow the checking of the behaviour of the station at the raw data stage. All of these scripts were written by Dr. F. N. Teferle.

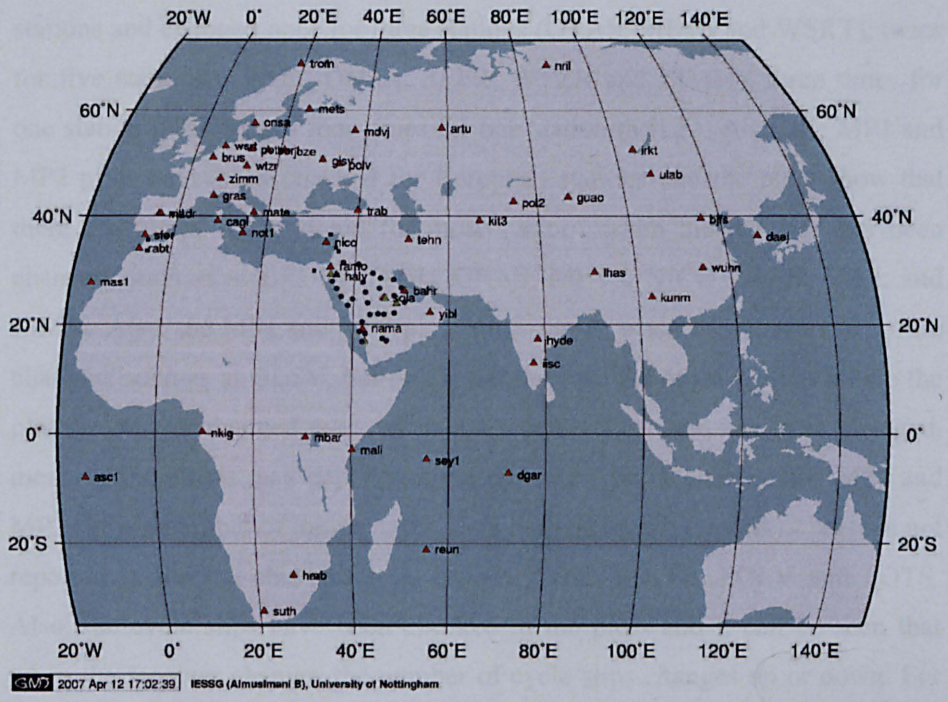

Figure 4.7. The IGS stations used in the reference frame implementation, (where the red triangles are the IGS stations outside the Arabian plate, the green triangles are the IGS stations on the Arabian plate and the blue circles are the stations of the regional network).

From the IGS stations in the European region, it was rather easy to find enough high quality stations to provide good coverage. In other areas, the choice was much more limited. Therefore, 21 IGS stations in Europe were selected (BOR1, BRUS, CAGL, GLSV, GRAS, JOZE, MATE, MDVJ, METS, NICO, NOT1, ONSA, POLV, POTS, SFER, TRAB, TROM, VILL, WSRT, WTZR and ZIMM), all in the Eurasian plate except for TRAB and NICO that are in the Anatolian plate. Moreover, the data of these stations were available for the full time period 1 January 2000 to 30 June 2007, except for short gaps for some stations such as CAGL, GRAS, ONSA, TRAB, TROM and VILL. There are other stations, such as MDVJ, NOT1 and POLV, which commenced operation after the starting date (for more details, see Figure 4.8 below). Also, the quality of data for these stations was assessed using the TEQC tool. The antennas were not changed at most of them during the period 1 January 2000 to 30 June 2007, the exceptions being the following three stations: BRUS and CAGL changed once, and GRAS was changed twice. The receivers were not changed for 11

stations and changed once for three stations (GRAS, METS and WSRT), twice for five stations (CAGL, ONSA, SEFR, WTZR and ZIMM), three times for one station (BRUS) and four times for one station (VILL). Also, the MP1 and MP2 plots have been checked for European stations and the plots show that there are jumps up or down for most stations when the receiver has been changed, such as at BRUS, CAGL, GRAS, METS, NICO, SEFR, VILL and ZIMM. Also, the MP1 and MP2 plots show jumps when the receiver firmware changed, such as at GLSV, but this is not the case for other stations where the plot remains unchanged even when the receiver firmware has been changed, meaning the jumps may depend on the receiver type. Moreover, the MP1 and MP2 show a number of jumps in the plots with unknown reasons or reasons not reported in the log sheet such as BOR1, JOZE, MATE, POLV and POTS. Also, the cycle slips have been checked in the plots and it can be seen that when the receiver changes the number of cycle slips changes up or down. For example, the number of cycle slips when the receiver changed at CAGL in March 2004 decreased to less than 0.2 per 1000 observations, except on a number of days with jumps to 8 per 1000 observations, whereas it was 1.5 per 1000 observations except for a number of days with jumps to 8 per 1000 observations as a result of changing the receiver in March 2004. After July 2006, most days reached 8 per 1000 observations. The number of cycle slips in GLSV was less than 1 per 1000 observations until mid-2005 when it jumped to 9 per 1000 observations. In GRAS station, there was a decrease from 2 per 1000 observations to less than 1 per 1000 observations in October 2004 when the receiver and antenna changed. For station JOZE, the number of cycle slips was about 2 per 1000 observations but sometimes jumped to 9 per 1000 observations. For station MATE, it was less than 10 per 1000 observations between mid-2001 and late 2004 and mid-2005 to 2006. MESTS had a very low value, less than 0.5 per 1000 observations except for a few days when it increased to 10 per 1000 observations. At ONSA the number of cycle slips decreased dramatically after a change of receiver on August 2003 (from 6 to 2 per 1000 observations). For station POLV, there were almost no cycle slips from mid-2006 to mid-2007, when it jumped to 8 per 1000 observations.

TORM had a few cycle slip with a number of days that jumped to 6–8 per 1000 observations. For VILL, the number of cycle slip on average was 2 per 1000 observations with a number of days jumping to 10 per 1000 observations but when the receiver changed in early 2005 the number of cycle slips decreased dramatically to zero. At WSRT station, there were less than 1 per 1000 observations but in early 2005 they went up and down (1 to 10 per 1000 observations). WTZR station had less than 1 per 1000 observations. ZIMM station had an average number of cycle slips but when the receiver changed on August 2003 they jumped to between 8 per 1000 observations and more than 10 per 1000 observations, then in early 2006 down to less than 2 per 1000 observations.

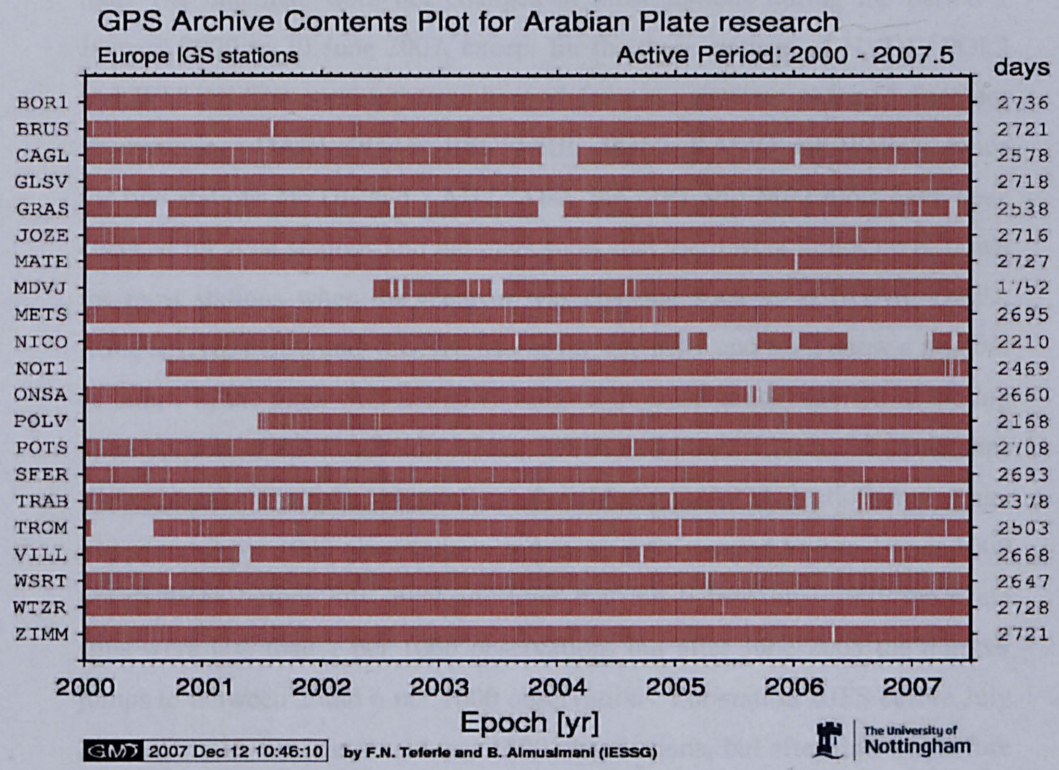

Figure 4.8. Time series of data available for IGS stations in Europe.

Eighteen IGS stations were selected in Asia (ARTU, BILI, BJFS, DAEJ, DGAR, GUAO, HYDE, IISC, IRKT, KIT3, KUNM, LHAZ, NRIL, POL2, RAMO, TEHN, ULAB and WUHN), most in the Eurasian plate except for

DGAR, HYDE and ISSC in the Indian plate and RAMO in the Sinai microplate. Moreover, the data from these stations were available most of the time for the period 1 January 2000 to 30 June 2007, except for short gaps from time to time. Also, a number of stations started operation during the chosen period, such as GUAO that commenced operation in mid-2002, HYDE started in late 2002, NRIL started in mid-2000, TEHN started operation in late 2004 and finally ULAB started operation in late 2000. Also, TEHN station is the only station that is not part of ITRF2005 or IGS05 reference stations out of the Arabian plate, but it has been chosen because there is no IGS station close to the east of the Arabian plate. Therefore, it has been chosen to strengthen the network geometry. For more details of data time series availability, see Figure 4.9 below. The quality of data for these stations was assessed using the TEQC tool. The antennae were not changed at most stations during the period 1 January 2000 to 30 June 2007, except for the three stations of HYDE, POL2 and WUHN. The receiver was changed for nine stations: changed once for seven stations DAEJ, DGAR, IISC, NRIL, POL2, RAMO and WUHN, twice for two stations HYDE and LAHZ. Also, the MP1 and MP2 plots have been checked for Asia stations and the plots show that there were jumps up or down for most stations when the receiver was changed such as at DGAR, DAEJ, IISC, LAHZ, POL2 and WUHN. Moreover, the MP1 and MP2 show a number of jumps in the plots with unknown reasons or reasons not reported in the log sheet such as at ARTU, BJFS, NRIL, TEHN and ULAB. Also, the cycle slips show that, for example, the number of cycle slip at ARTU station on average was about 2 per 1000 observations and many days jumped to 6 to 10 per 1000 observations before July 2002 and after that but before June 2005 the cycle slips were less than 1 per 1000 observations but after June 2005 the number jumps to between 2 and 6 per 1000 observations. For station BJFS before July 2001, the rate was less than 1 per 1000 observations, but after that and before October 2003 it was less than 2 per 1000 observations but afterwards it varied between 1 and 2 with 10 per 1000 observations on some days. For station DAEJ, the number of cycle slips before May 2005 on average was less than 2 per 1000 observations with some days between 4 and 8 per 1000 observations,

but after that the number was less than 200. For stations GUAO and HYDE, the number of cycle slips was less than 1 per 1000 observations, but for stations IISC and RAMO there were almost no cycle slips. For station IRKT, the number of cycle slips on average was 2 per 1000 observations, but with a number of days at more than 10 per 1000 observations. At station KIT3 the number on average was 8 per 1000 observations and for station KUNM it was 4 per 1000 observations. For LAHZ station as a result of changing the receiver, the number of cycle slips changed before October 2003 with many days having more than 10 per 1000 observations; after that and before May 2006 there were less than 2 per 1000 observations and after that date less than 0.5 per 1000 observations. Also at station NRIL, when the receiver was changed, the number changed as well; before November 2005 there were on average 4,000 and a number of days at 6 to 10 per 1000 observations but after that on average less than 2 per 1000 observations with some days less than 4 per 1000 observations. For station TEHN there were not many cycle slips. For station ULAB before 2005, cycle slips varied between 1 and 10 per 1000 observations and after that less than 2 per 1000 observations. At WUHN station the number before June 2000 was less than 2 per 1000 observations, but after that the number varied between 2 to more than 10 per 1000 observations.

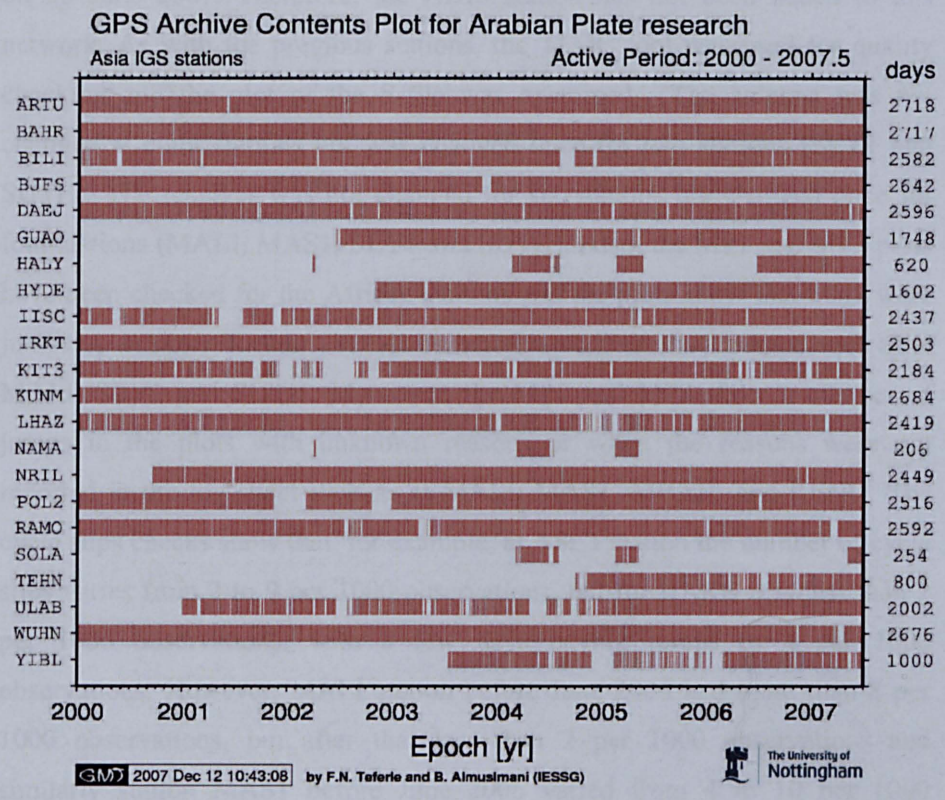

Figure 4.9. Time series of data available for IGS stations in Asia.

Unfortunately, the selection of IGS stations on the African continent is very limited since there are not many IGS stations, especially across the Red Sea in Egypt, Sudan, Ethiopia and Somalia. There are no IGS stations in north or central Africa. Therefore, ten IGS stations in Africa have been selected where seven of them (ASC1, HARB, MAS1, MBAR, NKLG, RABT and SUTH) are on the Nubian plate and the other three (MALI, REUN and SEY1) are on the Somalia plate. For more details of data time series availability, see Figure 4.10 below. Also, the quality of data for these stations was assessed using the TEQC tool. For information, a new IGS station has just been installed called ADIS in Addis Ababa, the capital of Ethiopia, in the Nubian plate, which started operation on 29 June 2007 at the end of data processing for this research

on 30 June 2007. Therefore, the ADIS station has not been added to this network. As with the previous stations, the TEQC tool was used for quality checking and the plot of the S-file was examined. The antenna was not changed at eight stations but was changed once for two stations (SEY1 and SUTH). The receiver was not changed for six stations but changed once for four stations (MALI, MAS1, SEY1 and SUTH). Also, the MP1 and MP2 plots have been checked for the African stations and the plots show that there were jumps up or down for most stations when the receiver was changed such as at MALI, SEY1 and SUTH. Moreover, the MP1 and MP2 show a number of jumps in the plots with unknown reasons or when the reasons were not reported in the log sheet such as at MALI, MAS1, MBAR, and RENU. The cycle slips checks show that, for example, at ASC1 station the number of cycle slips varies from 2 to 9 per 1000 observations, but for HARB it is less than 2 per 1000 observations, with a few days having jumps to 4 per 1000 observations. However, MALI station before June 2006 had more than 8 per 1000 observations, but after that less than 2 per 1000 observations and similarly station MAS1 before June 2006 varied from 4 to 10 per 1000 observations but after that was less than 0.5 per 1000 observations. For MBAR station, the number of cycle slips before 2004 varied from 0.5 to 10 per 1000 observations and after that on average was 1 per 1000 observations. For station NKLG, the number of cycle slips ranged from 4 to 10 per 1000 observations, RABT station had on average 4 per 1000 observations. For station RENU before May 2003 there were not too many, but afterwards between 2 per 1000 observations and 10 per 1000 observations. For SEY1 station before March 2005, there were less than 4 per 1000 observations and afterwards more than 6 per 1000 observations. Finally, the number of cycle slips at SUTH station before February 2002 was on average 2 per 1000 observations and after that less than 0.5 per 1000 observations.

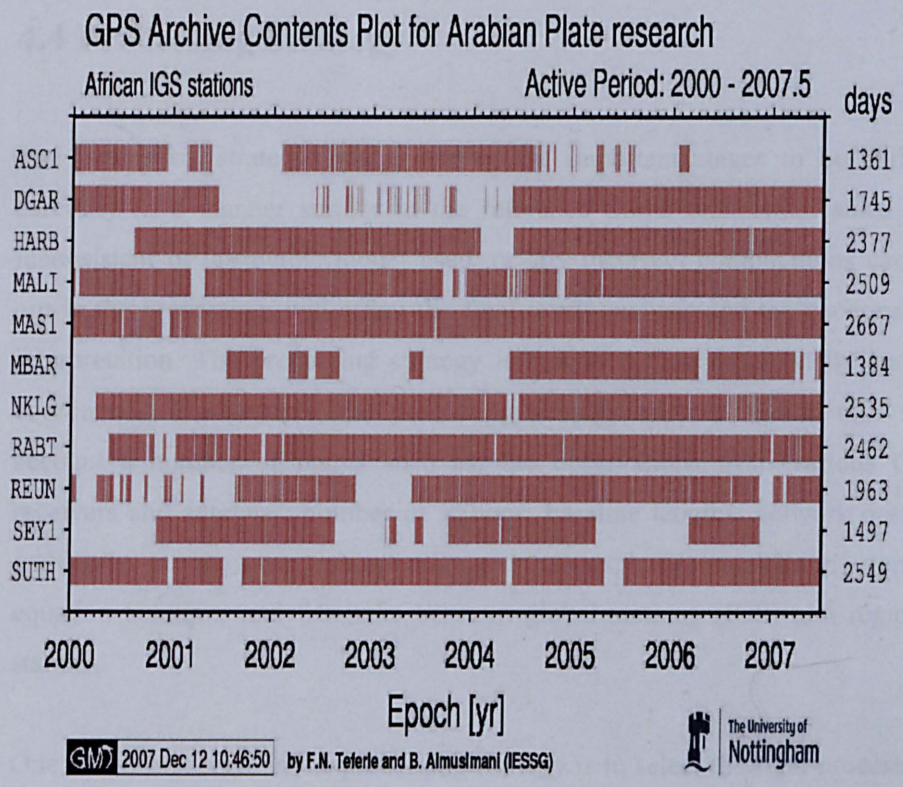

Figure 4.10. Time series of data available for IGS stations on African plate.

4.4 Processing Strategy

The processing strategy is also one of the important stages to be defined carefully in a manner similar to the reference frame realization, since any inconsistent or unsuitable model used, or any incorrect computations carried out in the processing, will affect the final result analysis and the geodynamic interpretation. The processing strategy is designed to compute daily station coordinates. Furthermore, the processing strategy adopted should take into account a number of points such as: the observations from various GPS receivers and antennas; number of stations; baseline lengths; network design; ambiguity resolutions; ionospheric and tropospheric modelling; normal equation solution; and the links between global stations (IGS) and regional stations.

One of the first steps in the processing strategy is to select the right processing and adjustment software for the study of GPS data. There are many GPS data processing and adjustment packages available and most of them are commercial software. However, there are other software packages designed for high geodetic accuracy requirements where the typical users are research scientists or agencies responsible for first order networks. The three most popular of these software are also employed at IGS analysis centers. These are first the GAMIT and GLOBK processing software, which was developed and is maintained in the Department of Earth, Atmospheric and Planetary Sciences at the Massachusetts Institute of Technology (MIT) in the USA. The second software is the GIPSY-OASIS (GOA II) processing software, developed and maintained by the National Aeronautics and Space Administration (NASA) and Jet Propulsion Laboratory (JPL) at Pasadena, California in the USA. The third software is Bernese GPS software, developed and maintained by the Astronomical Institute at the University of Bern in Switzerland. The Bernese GPS software (BSW) version 5.0 was used in this study and for this the author attended a training course for five days in Bern in September 2006. BSW 5.0 will be outlined briefly in Section 4.5.

The models used for the elimination or reduction of the GPS biases and errors are other crucial and important issues in the processing and analysis. In this study, the solid earth tides and ocean tide loading effects were modelled using the best model available at the time. For instance, the solid earth tides model follows the IERS conventions 2003 [McCarthy and Petit, 2004], while the ocean tide loading model used was GOT00.2, since the study network is almost global and GOT00.2 is a long wavelength adjustment of the previous model FES94.1. Figure 4.11 shows the global ocean tide amplitude, and the model parameters for all network stations were obtained from the ocean tide loading provider on [www.oso.chalmers.se/-/loading].

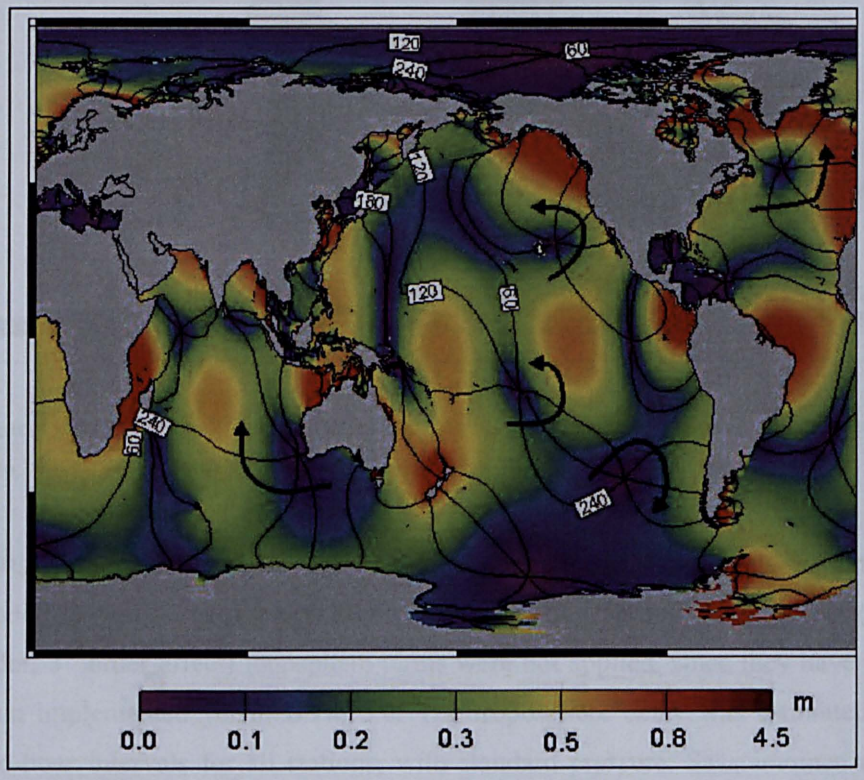

Figure 4.11. The ocean tides for harmonic M2
[http://www.oso.chalmers.se/~loading/loadingprimer.html].

The other widely used model is FES2004. However, Figure 4.12 show the missing data in this model and it can be seen that there are no data available for the Red Sea and the Arabian Gulf.

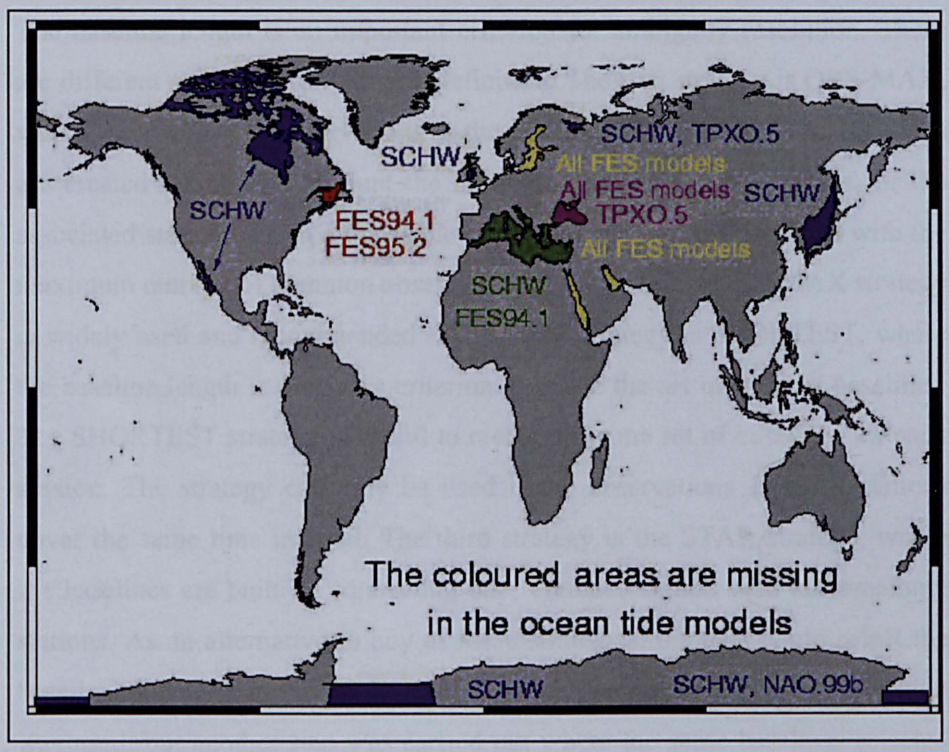

Figure 4.12. Water areas that are missing in the ocean tide models [http://www.oso.chalmers.se/~loading/tidemodels.html].

Furthermore, the ionosphere delay model used is the CODE global ionosphere model, as well as the iospherically free observable, where the higher-order (2^{nd} order, 3^{rd} order effect) ionosphere terms were not applied, since they have not been implemented yet in BSW 5.0. The troposphere delay was estimated at two-hour intervals for all stations, with standard pressure, Saastamoinen and the dry and wet-Neill mapping functions. Again, the latest isobaric mapping function (IMF), Vienna Mapping Functions (VMF) and Global Mapping Function (GMF), were not used since they are not implemented in BSW 5.0. The atmospheric pressure loading and hydrological loading effects were also

not modelled, since there is no conventional model and they also have not been implemented in BSW 5.0.

The baseline length is an important criterion for ambiguity resolution. There are different strategies for baseline definition. The first strategy is OBS-MAX, where the number of observations is the optimization criterion. The baselines are created taking into account the number of common observations for the associated stations. From all possible combinations, a set of baselines with the maximum number of common observations is chosen. The OBS-MAX strategy is widely used and recommended. The second strategy is SHORTEST, where the baseline length is used as a criterion to create the set of shortest baselines. The SHORTEST strategy is useful to create the same set of baselines for each session. The strategy can only be used if the observations from all stations cover the same time interval. The third strategy is the STAR strategy, where the baselines are built by connecting one reference station with all remaining stations. As an alternative to any of these strategies, the user could select the baseline manually. In this study, the OBS-MAX strategy for phase observation was used, but another step was carried out where the same baselines selected on phase observation were formed again using CODE single differences.

The ambiguity resolution strategy used in this study when the baseline was less than 2000 km was the QIF (Quasi Ionosphere-Free), since all receivers in this study are dual frequencies, so the L1 and L2 observations were available and the L1 and L2 ambiguities could be resolved using QIF. When the baseline length was longer than 2000 km but less than 4000 km, it was solved in two stages. The first stage used wide-lane ambiguity resolution using sigma ambiguity resolution, the Melbourne-Wubbena linear combination (L_6) observable and by introducing the P1-C1 differential code bias (DCB). The second stage was solved using narrow-lane ambiguity resolution using sigma ambiguity resolution, the ionosphere-free linear combination (L_3) observable and by introducing the wide-lane ambiguities solved in stage one.

The data sampling rate used in the processing was 30 seconds, even though the regional GCS stations used 15 seconds, to be consistent with the data sampling rate of 30 seconds at IGS stations. Furthermore, the elevation cut-off angle was 10°. The CODE distributed files (PHAS COD.I05 and satellite.I05) were used for the absolute satellite and receiver antenna phase centre models, with the appropriate receiver antenna and radome combinations assigned. The IGS switched to using absolute phase centre models starting from week 1400 (5 Nov 2006), i.e. in the middle of this research, therefore it was decided to use the new products (IGS final precise orbits and earth rotation parameters (ERP)) starting from week 1400 and for the period before that to use the first GFZ re-processed products' [Steigenberger *et al.*, 2006]; the only ones available at the time.

Datum definition used the constraining technique to constrain the coordinates of reference stations to their *a priori* values. The tight constraint is similar to fixing reference coordinates and the loose constraint is similar to a free network solution. Therefore, by varying the constraints, it is possible to move smoothly between the above two cases (tight and loose constraining), with each case having advantages and disadvantages. Since it estimates the position of all stations, it needs at least one station to be fixed to its *a priori* position. Therefore, the minimum constraint condition is optimal to define the geodetic datum with the minimum number of constraints without fixing or constraining particular station coordinates.

The free network conditions are based on the assumption that there are two reference frames, where the first is an a priori reference frame e.g. ITRF(X_L) and the second is the reference frame of the resulting coordinates e.g. regional (X_R).The relation between a regional solution (X_R) and ITRF (X_L) over selected stations could be written as in vector form [Dach *et al.*, 2007; Altamimi *et al.*, 2002]

$$X_L = X_R + A\varepsilon \tag{4.1}$$

in matrix form

$$\begin{bmatrix} X_L^i \\ Y_L^i \\ Z_L^i \end{bmatrix} = \begin{bmatrix} X_R^i \\ X_R^i \\ X_R^i \end{bmatrix} + \begin{bmatrix} 1 & 0 & 0 & 0 & -Z^i & Y^i & X^i \\ 0 & 1 & 0 & Z^i & 0 & -X^i & Y^i \\ 0 & 0 & 1 & -Y^i & X^i & 0 & Z^i \end{bmatrix} \begin{bmatrix} \Delta X \\ \Delta Y \\ \Delta Z \\ \alpha \\ \beta \\ \gamma \\ \mu \end{bmatrix} \tag{4.2}$$

where A is the design matrix of partial derivatives and ε is the vector of seven transformation parameters. The idea of minimum constraint conditions is based on the requirement that some of these seven parameters are set equal to zero. Using the observation equation to compute the parameters

$$\theta = A\varepsilon - (X_L - X_R) \tag{4.3}$$

this result in the following system of normal equations

$$A^T A\varepsilon = A^T (X_L - X_R) \tag{4.4}$$

where $X_L - X_R$ is the difference between the estimated and the a priori value

$$X_L - X_R = \rho \tag{4.5}$$

and the parameters of the seven parameter transformation are given by

$$\varepsilon = (A^T A)^{-1} A^T \rho \tag{4.6}$$

The free network condition thus may be imposed by adding the following fictitious observation

$$B\rho = 0 \tag{4.7}$$

Where $B = (A^T A)^{-1} A^T$

The advantage of a minimum constraint technique is that small errors in the coordinates of a reference station do not distort the network geometry and do not degrade the datum definition significantly [Dach *et al.*, 2007]. Altamimi *et al.* [2002] demonstrated that the minimum constraint is an efficient method to optimally express a regional solution in a global frame such as ITRF; hence they suggested this method instead of the classical constraints. Moreover, the minimum constraints condition is used in a number of IGS analysis centres as well. Table 4.6 shows a summary of the processing strategy used in this study.

Table 4.6. Summary of processing strategy used in this study.

Software	Bernese GPS Software (BSW) V5.0
Elevation cut-off	10 degrees
Sampling rate	30 seconds
Tropospheric delay modelling	The tropospheric delay was estimated at 2-hour intervals for all stations using : 1. Dry-Neill as *a priori* model 2. Dry and Wet-Neill Mapping functions
Ionospheric delay modelling	CODE global ionosphere model is used as well as the ionspherically free observable
Ocean Tide Loading	GOT00.2 model as obtained from the ocean tide loading provider on (www.oso.chalmers.se/~/loading)
Processing criteria	1. Automatic selection of baselines to form phase single difference using OBS-MAX strategy. 2. The same baselines selected in step (1) to form CODE single difference.
Observables	L3 (Ionspherically free)
Ambiguity resolution	< 2000 km QIF (Quasi-ionosphere-free) < 4000 km Wide lane techniques 1. Wide-lane ambiguity resolution (SIGMA, MELWUEBB, introduce P1-C1 DCB) 2. Narrow-lane ambiguity resolution (SIGMA, L3, Introduce wide-lane ambiguities)
Antenna phase centre modelling	Absolute satellite and receiver antenna phase centre model by application of the CODE distributed file (PHAS COD.I05)
Orbits and ERP products	< 1400 week (5 Nov 2006) using GFZ re-processed orbits and ERPS [Steigenberger *et al.*, 2006] > 1400 week (5 Nov 2006) using IGS final precise orbits and ERPS products
Reference frame	ITRF2005 using minimum constrained on IGS stations (except for IGS stations on Arabia plate and TEHN)
Post-processing	CTSAna tools with CATS (Williams, 2003) and ADDNEQ2

A comparison of the data sets between this study and Almotairi [2006] shows that in this study the time span of observations was arranged to be four years with three campaigns giving two-year span between consecutive campaigns. Whereas in Almotairi [2006] the time span of observations was only two years. Furthermore, the data available for each station of GCS are three sets for this study, whereas in Almotairi [2006] only two sets for each station were available. Therefore care should be taken when considering the results of Almotairi [2006] since any bad data for one set will affect the result. Also, this study has four years time span, which gives the plate a longer time of movement and more reliable results when compared to Almotairi [2006] who used two years only. Moreover, in this study more IGS stations on the Arabian plate were included (BAHR, HALY, NIMA, SOLA, YIBL), whereas in Almotairi [2006] only BAHR station was included. Furthermore, the full data of seven and half years (1 Jan 2000 to 30 Jun 2007) available for these stations were used in this study, whereas in Almotairi [2006] only data during the campaigns was used for BAHR station.

In terms of, the reference frame implementation, in this study this was applied using a near global reference frame; forty-nine IGS stations were considered, with these stations distributed around the Arabian plate and spanning five other plates (Africa, Somalia, India, Eurasia and Anatolia) in three continents (Europe, Asia and Africa). In contrast, Almotairi [2006] only used fourteen IGS stations, all of them on the Eurasia plate, and only constrained six of them. Therefore, care should again be taken when considering the results of Almotairi [2006] since the regional network was tied to the reference frame by only one baseline.

In addition to all of the above, this study also used a significantly processing strategy to Almotairi [2006]. A comparison between the two is illustrated in table 4.7

Table 4.7 the processing strategy comparison between this study and Almotairi [2006]

	This study	Almotairi [2006]
Software	Bernese GPS Software V5.0	Bernese GPS Software V4.2
Elevation cut-off	10 degrees	15 degrees
Sampling rate	30 seconds	30 seconds
Tropospheric delay modelling	The tropospheric delay was estimated at 2-hour intervals for all stations using : 1. Dry-Neill as *a priori* model 2. Dry and Wet-Neill Mapping functions	At the IGS stations the tropospheric delay is introduced using the global solutions and estimated only for the other stations using: 1. No *a priori* model. 2. Dry Neill Mapping function.
Ionospheric delay modelling	CODE global ionosphere model is used as well as the ionspherically free observable	The global ionosphere model is used as well as the ionospherically free observable.
Solid Earth Tide Model	IERS conventions 2003	Applied according to IERS standards (1996)
Ocean Tide Loading	GOT00.2 model as obtained from the ocean tide loading provider on (www.oso.chalmers.se/~/loading)	FES99 model at www.oso.chalmers.se/~loading for each station.
Processing criteria	1. Automatic selection of baselines to form phase single difference using OBS-MAX strategy. 2. The same baselines selected in step (1) to form CODE single difference.	Shortest Baseline strategy is used in the single difference observable at the pre-processing stage. In the network stage the double difference observable is used.
Observables	L3 (Ionspherically free)	L3 (Ionspherically free)
Ambiguity resolution	< 2000 km QIF (Quasi-ionosphere-free)	QIF strategy is used to resolve the ambiguities.
	< 4000 km Wide lane techniques 1. Wide-lane ambiguity resolution (SIGMA, MELWUEBB, introduce P1-C1 DCB) 2. Narrow-lane ambiguity resolution (SIGMA, L3, Introduce wide-lane ambiguities)	
Antenna phase centre modelling	Absolute satellite and receiver antenna phase centre model by application of the CODE distributed file (PHAS COD.I05)	The IGS file is used to account for variations for different combinations of receivers and antennas.
Orbits and ERP products	< 1400 week (5 Nov 2006) using GFZ re-processed orbits and ERPs [Steigenberger *et al.*, 2006]	The IGS (final) Precise ephemeris
	> 1400 week (5 Nov 2006) using IGS final precise orbits and ERPs products	
Reference frame	ITRF2005 using minimum constrained on IGS stations (except for IGS stations on Arabia plate and TEHN)	ITRF2000 using constrained on six IGS station on Europe on first stage to estimate the coordinate for stations (F001, F009, F020, F035), then the second stage constrained these four GCS stations to estimate the other GCS stations.
Post-processing	CTSAna tools with CATS (Williams, 2003) and ADDNEQ2	Using ADDNEQ and FORTRAN program

From table 4.7, it can be seen that in all cases, except for sampling rate and observables, this study used a much more up-to-date processing strategy, notably including the use of BSW 5.0, IERs conventions 2003,, absolute satellite and receiver antenna phase centre models, re-processed satellite orbits and ERPs and ITRF2005.

4.5 Bernese processing software (V5.0)

The Bernese software (BSW) is a scientific GPS/GLONASS processing software, developed at the University of Bern in Switzerland. Typical users are research scientists and surveyors looking for high accuracy, or using permanently operating GPS receivers. The latest version is 5.0, released on 27 June 2006. BSW 5.0 can be operated in either a Unix/Linux or Windows environment and accepts data in RINEX format. It has a new powerful Bernese Processing Engine (BPE), which can be run using the Perl scripting language, and multi-session processing and jumps within the process control file (PCF) are supported.

The input and output data in BSW 5.0 are organized to allowed easy management by the user. The term campaign (project) is used for a set of data that should be processed together. Each campaign consists of a directory and subdirectories, where all input and output data are stored. There are nine main directories in each campaign, as illustrated in Table 4.2.

Table 4.8. Main directories for each campaign.

Directory	Description
ATM	Atmosphere files (e.g. ION and TRP)
BPE	Output of BPE runs
OBS	Bernese observation files
ORB	Orbit related files (orbit files, ERP files, satellite clock files, DCB files ....)
ORX	Original Rinex files
OUT	Output files
RAW	Rinex files ready to import into the processing
SOL	Solution files (normal equations, Sinex)
STA	Campaign specific station files (STA, FIX, CRD, ...)

The processing of data in BSW 5.0 passes through four main stages (for more details, it is recommend that the reader consults the Bernese Manual [Dach *et al.*, 2007]).

4.5.1 Preparation stage

The preparation stage is where all the input files are checked and made ready for the pre-processing stage. The first input data are the RINEX (observation) data, which need to be copied to the ORX directory for all stations to be processed. Secondly, the final precise orbits in SP3 format with extension *.PRE, earth orientation parameters in weekly files with extension *.IEP, and monthly means for the differential Code Biases (DCB) are input. Thirdly, the global ionosphere model files in the Bernese format, obtained from the IGS processing at CODE, are copied to the atmosphere directory (ATM).

The station related files are in the directory (STA) as summarised below:

- Session table file (*.SES) contains the time interval covering all observations that should be processed together.
- Station abbreviations table file (*.ABB) contains 4- and 2-character station abbreviations. They are used for automatic generation of filenames by other programs. Abbreviations should be unique; otherwise, files may be overwritten by other files.
- Station information file (*.STA) contains station name, receiver, antenna and antenna height and is divided into the following types:

  Type 001: Renaming of stations.
  Type 002: Station information
  Type 003: Handling of station problems
  Type 004: Station coordinates and velocities
  Type 005: Handling station types

- Station coordinates file (*.CRD) contains the geocentric station coordinates that are used in the processing programs as *a priori* coordinates. If these coordinates are not in the required epoch, then COOVEL or HELMR1 programs and velocity files are used to propagate the coordinates to the required epoch.
- Station velocities file (*.VEL) contains station velocity information. They are used as *a priori* velocity information in ADDNEQ2 or as the output file for the velocity estimate in COOVEL and HELMR1 programs.

- Tectonic plate assignment file (*.PLD) contains tectonic plate assignment of stations.
- Ocean Tidal Loading Table file (*.BLQ) contains ocean tidal loading amplitudes and phases and is used to take into account the effects on site coordinates of ocean tide loading. It contains station specific amplitudes and phase of the elevation largest tidal constituents for the vertical as well as for the horizontal.
- Station selection file (*.FIX) contains the selection list for coordinate fixing and definition of no-translation conditions.

Also, in the preparation stage, all the general files should be checked and brought up-to-date, such as:

CONST: All constants used in the Bernese GPS software

DATUM: Definition of geodetic datum

RECEIVER: Receiver information

PHAS_IGS.I05: Phase centre eccentricities and variations

SATELLIT.I05: Satellite information file

GPSUTC: Leap seconds

IAU2000.NUT: Nutation model coefficients

IERS2000.SUB: Sub-daily pole model coefficients

JGM3: Earth potential coefficients

OT_CSRC.TID: Ocean tides coefficients

4.5.2 Pre-processing stage

In this stage, the RINEX observation files are imported into the Bernese software using the program RXOBV3. This program makes a number of checks on the RINEX header information. Also, the POLUPD program converts the earth orientation information from IERS standard format (with extension *.IEP) provided by IGS into the internal Bernese EOP format (with extension *.ERP). After that, the orbit files are generated in two programs. The first program is PRETAB, where the main task is to create tabular files, which means transforming the precise orbits from the terrestrial into the celestial reference frame. The second program is ORBGEN, which prepares the standard orbits using the satellite positions in the tabular orbit files. The most important information in the output of the statistical analysis for each satellite is the RMS errors, which should not be larger than 2 cm. Then, the CODSPP program is used to compute the receiver clock corrections. The *a posteriori* RMS error for each zero difference should be checked in the output, where a value of 3 m is expected if the P-code is available and without selective availability (SA).

4.5.3 Processing stage

The single differences are created by the SNGDIF program. This program creates single differences for phase and code, which are usually required for further computations. The baseline length is formed using the strategy OBS-MAX.

The cycle slips are detected and repaired using the MAUPRP program. The task of this program is to:

- Mark observations to be excluded from processing when observations were at low satellite elevations, epochs with unpaired observations (L1 without L2 or vice versa) and small pieces of observations.
- Identify large outliers.
- If possible, repair the cycle slips; otherwise, a new ambiguity must be introduced when the cycle slip is large.

The epoch difference solution is used as the reference for the data screening. For a successful phase processing, the RMS of the epoch difference solution has to be below 2 cm. The estimates for the coordinates in the epoch difference solution are expected to be smaller than about 0.5 m.

The GPSEST program could be run initially to produce an ambiguity free L_3 solution. The aim of this run is not to compute the final solution, but to check the quality of data and to save the residuals after the least squares adjustment. The important information in the output file is the *a posteriori* RMS error. An *a posteriori* RMS error of about 1.0 to 1.5 mm is expected if elevation dependant weighting is used. A significantly higher RMS error indicates that the data stems from low quality receivers, the data was collected under extremely bad conditions, or that the pre-processing step in the MAUPRP program or CODSPP program was not successfully performed.

The RESRMS program analyses a set of selected residual files. It provides statistical information for the residuals of the stations or baselines. The main purpose of RESRMS is the screening of post-fit residuals. The residual file from a GPSEST solution is analysed for outliers and an edit information file is written. For each station or baseline, an output is provided by the RESRMS containing the total RMS for all satellites (Total RMS), the median of all residuals (med.Resi), the width of the histogram (Sigma), the number of observations (num Obs), the number of satellites (nSat) and the number of observation pieces rejected (nDel).

Marking of observations means that individual observations may be flagged with a so-called marking flag. The marking flags are used to mark outliers, observations at low elevation and small pieces of observations. The SATMRK program is used in BSW 5.0 to set and reset marking flags or to remove observations. Then, the GPSEST program is re-run to create the final (clean) residual files and store the normal equation files.

The next step is to check the screening results from the previous step and reject data of any misbehaving station. Two programs are used to carry out this step. The first program is RESRMS, which creates summaries from the first (unscreened) and final residual files. The second program is RESCHK, which creates residual screening statistics and deletes bad stations based on their overall performance. Stations or satellites having problems are indicated by large residuals or by a very high percentage of deleted data. The RESCHK program is allowed to delete one (the worst) station per iteration step, because the misbehaving station may affect other stations.

4.5.4 Post-processing stage

Parameter estimation in BSW 5.0 is based on Least Squares Estimation. There are two main programs, GPSEST and ADDNEQ2, which can carry out the parameter estimation by least squares. The GPSEST program processes the observations and sets up the observation equations and solves the normal equation. The ADDNEQ2 program manipulates and combines solutions on the normal equation level. The ADDNEQ2 program in BSW 5.0 is a replacement for the ADDNEQ program in BSW 4.2. ADDNEQ2 was developed to compute multi-session solutions from the combination of a set of single-session solutions. The sequential adjustment technique is used in ADDNEQ2, where in general it is independent of the observation types of the individual solutions. Moreover, the definition of the geodetic datum and estimation of station velocities are available in ADDNEQ2.

The first run for ADDNEQ2 is to compute an ambiguity-float network solution, where a network solution with real value ambiguities is computed based on NEQ files stored in the GPSEST after the residual screening. Also, in this run, the coordinate and troposphere estimates are saved for further use in the ambiguity resolution. The *a posteriori* RMS should be not higher than 1.4 mm.

The ambiguity resolution strategies used in program GPSEST are SIGMA and QIF (Quasi Ionosphere-Free). The BASLST program is then used to select baselines. If the baseline length is less than 2000 km, the GPSEST runs for each baseline to be processed and L1 and L2 ambiguities are resolved using QIF. However, if the baseline length is longer than 2000 km and less than 4000 km, then the GPSEST runs for each baseline to be processed for wide-lane and narrow lane ambiguities are resolved using sigma. Also, a summary file is created for the previous steps showing percentages of successfully resolved ambiguities (on average, about 70% of ambiguities are resolved).

The final step of the daily solution is to compute the ambiguity-fixed network solution. The GPSEST program is used and an ambiguity fixed solution is computed and NEQ information is stored. Also, in this GPSEST run, estimated parameters include coordinates, zenith path delays and horizontal tropospheric gradients. After that, the ADDNEQ2 program is used to compute the final daily solution using NEQ from the previous GPSEST. Also, in this ADDNEQ2 run, the datum definition is realized by three no-net translation conditions imposed on a set of fiducial stations. A summary file of the ambiguity fixed network solution from ADDNEQ2 is produced. The *a posteriori* RMS should not exceed about 1.5 mm.

After the final daily solution has been computed, usually the campaign or multi-session solution is computed by combining the NEQs from each session in the ADDNEQ2 program. All coordinate parameters belonging to the same station are combined to one single set of coordinates referred to an epoch.

When combining several NEQs, consistency is very important. For example, combining station coordinates before and after a reported event, such as a receiver change, may cause a jump in the coordinates. The coordinate repeat abilities should be carefully monitored; jumps or outliers will degrade the quality of the results. Moreover, the coordinate residuals solutions with respect to the combined solution are computed. The residuals allow the identification of problems for each station. In addition, the velocity field could be estimated using ADDNEQ2 if the multi-solution covers a long time, such as one year or more.

4.5.5 Bernese Processing Engine (BPE)

The Bernese Processing Engine (BPE) has been developed to allow for a much-automated GPS data processing. The BPE is very important as it allows large campaigns and permanent GPS networks to be processed automatically. The first version of BPE was in BSW 4.0. The latest version of BSW 5.0 has a new powerful BPE, which can be run using the Perl scripting language, and multi-session processing and jumps within the process control file (PCF) are supported

The PCF contains a list of scripts that help the user for specific needs, such as the script COOVEL that runs the BSW COOVEL program. There are PCF examples providing an overview and description of the scripts in logically connected blocks. For more details of script sequences or a description and flow chart used in this study, see Appendix K. For further details, the author recommends reading the Bernese manual [Dach *et al.*, 2007].

4.6 Summary

In this chapter, the GPS networks were detailed, both regional and local, including the IGS stations on Arabian plate. Then the campaigns carried out were outlined, along with the data quality checks carried out.

This chapter than, detailed the reference frame implemented in this study, i.e. a near global reference frame, where forty nine IGS stations were considered. Then the processing strategy adopted in this study was discussed and BSW 5.0 was briefly outlined, showing the stages of the data processing carried out.

Chapter 5: Velocity and uncertainty estimation using time series analysis

5.1 Introduction

Station velocities, i.e. the rate of change in a station's position, and their uncertainties can be estimated from time series of daily coordinate estimates by fitting of an appropriate model, in a least square sense, to these time series. This model will often include, depending on the characteristics of the time series, additional parameters, e.g. for periodic variations, besides the velocity parameter. Furthermore, it is important that this model and the estimation process are capable of producing realistic error bounds for the estimated parameter.

Sophisticated mathematical and statistical methods, such as spectral analysis and maximum likelihood estimation (MLE), have been applied to the analysis of time series of GPS coordinate estimates since the late 1990s. By exporting the time series in their north, east and up components and by assuming that the time series contain a combination of random and time-correlated noise, the aim of estimating velocities together with realistic uncertainties can be achieved.

In this chapter, the theory of geodetic time series analysis is briefly revisited, including the modelling of periodic signals, coordinate offsets, and stochastic noise. Regional filtering is introduced as a means of improving the signal-to-noise ratio in the coordinate time series and is applied to both the continuous and episodic data used in this study. The application of regional filtering to episodic data to the knowledge of the author has not then attempted by other scientists. The Coordinate Time Series Analysis (CTSAna) tools used in the analysis are also briefly described. Finally, the velocities and uncertainties for all continuous and episodic GPS stations used in this study are estimated.

5.2 Background theory

GPS coordinate time series are known to experience a range of deformation signals with permanent and/or seasonal character. Therefore, the accurate estimation of station velocities and their associated uncertainties requires the modelling of offsets, periodic signals and noise. Regional filtering can also be considered in the time series analysis.

Station velocities can be estimated using the basic form of the linear regression problem as illustrated in equation (5.1)

$$y_i = x_0 + rt_i + \varepsilon_x(t_i) \tag{5.1}$$

where y_i is the points at time t_i $(i = 1,.....,N)$, x_0 is the initial position, r is the rate of station velocity and $\varepsilon_x(t_i)$ is the error term.

5.2.1 Periodic signals

Periodic signals are caused by various processes with dominant seasonal character such as un-mitigated atmospheric pressure and hydrological loading, non-tidal ocean loading, and the thermal expansion of monuments and bedrock. Furthermore, inadequately modelled systematic biases, e.g. multipath, can also introduce periodic variations at a number of frequencies which can alias into annual periods. All of these signals have been identified and reported in a large number of studies of continuous GPS time series [Heki, 2001; Dong *et al.*, 2002; Prawirodirdjo, 2006; Dixon and Mao, 1997; Scherneck *et al.*, 1998; Calais, 1999; Mao *et al.*, 1999; Braitenberg *et al.*, 2001; Kenyeres *et al.*, 2001; Poutanen *et al.*, 2001; Zerbini *et al.*, 2001; Johansson *et al.*, 2002; Kleijer, 2002; Mazzotti *et al.*, 2003; Penna and Stewart, 2003; Williams *et al.*, 2004; Stewart *et al.*, 2005; Bos *et al.*, 2008; Penna *et al.*, 2007; Wöppelmann *et al.*, 2009; Yan *et al.*, 2009].

Lavallée [2000] and Blewitt and Lavallée [2002] showed that station velocities are affected by the periodic signals in coordinate time series. The effects of periodic signals can be mitigated by different approaches. One of these can removes periodic signals from all coordinate time series indirectly by removing a common mode bias from these [Wdowinski *et al.*, 1997; Nikolaidis, 2002; Wdowinski, *et al.*, 2004; Teferle, 2003; Teferle et al., 2009]. Moreover, Dixon and Mao [1997] reported that the errors in station velocities as a result of annual periodic signals are at their minimum at integer years, but Blewitt and Lavallée [2002] showed this to be false and suggested that the effect in station velocities is a minimum at integer-plus-half years.

Here, a periodic signal in the coordinate time series is represented by a sine or and cosine curve and can be estimated using a least squares fit using Equation (5.1) with the inclusion of any periodic terms.

A periodic signal y_i at time t_i (where $i = 1,.....,N$) can be described by [e.g. Teferle, 2003]

$$y_i = a\cos(2\pi f t_i - \phi) + \varepsilon_x(t_i) \tag{5.2}$$

where a is the amplitude at the fundamental frequency f with a phase shift ϕ and $\varepsilon_x(t_i)$ is an arbitrary term accounting for noise. Equation (5.2) can be expanded into form [e.g. Teferle, 2003]

$$y_i = p\sin(2\pi f t_i) + q\cos(2\pi f t_i) + \varepsilon_x(t_i) \tag{5.3}$$

where the parameters p and q are related to the amplitude a and phase shift ϕ as

$$a = \sqrt{p^2 + q^2} \qquad \phi = \operatorname{atan}(\frac{p}{q}) \tag{5.4}$$

A simple model consisting of a linear trend with an additional periodic signal, can be derived by combination of Equations 5.1 and 5.3 giving [e.g. Teferle, 2003]

$$y_i = x_0 + rt_i + p\sin(2\pi ft_i) + q\cos(2\pi ft_i) + \varepsilon_x(t_i) \tag{5.5}$$

Any additional periodic variations (e.g. the semi-annual signal) can be modeled in a similar manner as in equation (5.5).

5.2.2 Offsets

Coordinate offsets are defined as discontinuities or jumps in coordinate time series, where the causes of these discontinuities might be known or unknown [Williams, 2003]. Known offsets can be a result of a real physical displacement, e.g. an earthquake, or related to changes in the station equipment (receiver, antenna and/or radome) and reference frame, e.g. ITRF2000 to ITRF2005 [Scherneck *et al.*, 1998; Bruyninx *et al.*, 2002; Johansson *et al.*, 2002; Kaniuth and Stuber, 2002; Vespe *et al.*, 2002; Williams, 2003; Teferle, 2003]. Moreover, any change in the environment of an antenna can cause an offset; e.g. Dong *et al.* [2002] illustrated that the trimming of a tree to less than half its height near a GPS antenna resulted in an offset of 1 cm in the horizontal and 4 cm in the vertical directions. Also, snow on an antenna may cause an offset in the height time series at the centimetre level [Jaldehag *et al.*, 1996; Scherneck *et al.*, 1998; Johansson *et al.*, 2002].

Since the change of receiver, antenna and/or radome can cause an offset to the coordinate time series, the IGS community has agreed that each station should have a history file (IGS station information log) [http://igscb.jpl.nasa.gov/network/list.html], which details equipments changes for a particular station. The IGS community makes these files available for all IGS stations.

When the offset x_{off} is known to occur at time t_{off} where $t_1 < t_{off} < t_N$ in coordinate time series, then equation (5.1) becomes [e.g. Teferle, 2003]

$$y_i = x_0 + rt_i + o_i x_{off} + \varepsilon_x(t_i) \tag{5.6}$$

where

$$o_i = \begin{cases} 1 & t_i \geq t_{off} \\ 0 & t_i < t_{off} \end{cases} \tag{5.7}$$

in the case of more offsets, then an additional term is required for each additional offset in equation (5.6). Therefore, it is possible to build a parameter model for the coordinate time series estimating a linear plus annual term and and offset magnitude at a given epoch as follows [e.g. Teferle, 2003] :

$$y_i = x_0 + rt_i + p\sin(2\pi ft_i) + q\cos(2\pi ft_i) + o_i x_{off} + \varepsilon_x(t_i) \tag{5.8}$$

5.2.3 Stochastic noise

Traditionally, geodetic coordinate time series were assumed to contain only random (white noise) errors, but over the last decade a number of authors showed that coordinate time series follow more a combination of white and coloured (time-correlated) noise that can be modelled as a power-law process [Agnew, 1992; Zhang *et al.*, 1997; Mao *et al.*, 1999; Johnson and Agnew, 2000; Williams, 2003; Williams *et al.*, 2004; Le Bail, 2006; Amiri-Simkooei, 2009]. It is now well established that this time-correlated noise in the coordinate time series needs to be taken into account in order to obtain realistic estimates for the uncertainties associated with the coordinate component velocities. While white noise has equal power at all frequencies, coloured noise

as modelled by a power-law process is defined by its power spectrum [Agnew, 1992; Kasdin, 1995]. Furthermore, white noise can be reduced greatly by frequent measurements and averaging but this is not the case for coloured noise.

Two special cases of coloured noise have been discussed widely in the published literature, namely, flicker and random walk noise [Zhang et al., 1997; Mao et al., 1999; Williams *et al.*, 2004; Langbein, 2008]. Flicker noise was observed as fluctuations (average seasonal temperature, annual amount of rainfall or the rate of traffic flow) and is the main noise contribution to the common mode (see Section 5.2.4) [Williams *et al.* 2004]. Therefore, it is suggested that flicker noise depends on the GPS system, e.g. the modelling of orbits, etc. In contrast to flicker noise random walk noise has been attributed to station-specific sources, such as monument motions [Wyatt, 1982, 1989; Langbein et al., 1995; Johnson and Agnew, 2000; Langbein, 2008]. Johnson and Agnew [2000] reported that well-monumented stations show a random walk process at low frequencies.

Meaningful interpretation of GPS stations velocities, especially for strain analyses, requires realistic uncertainties [Leonard *et al.*, 2007]. Also, Williams *et al.* [2004] reported that it is important to understand the noise content of GPS position data so that realistic uncertainties can be assigned to parameters estimated from them. Williams *et al.* [2004] carried out a comprehensive noise analysis using 11 years of data for 877 global and regional continuous GPS stations. Their result shows that for global GPS solutions the combination of white plus flicker noise is the most suitable stochastic model and for regional GPS solutions, when spatial correlations were reduced by regional filtering, different stations and networks had different noise sources dominating, including residual common mode noise (white plus flicker noise), monument instabilities (random walk noise) and localized deformation due to changes in the groundwater table (unknown power-law noise plus annually repeating

signals) [Williams *et al.*, 2003]. Zhang *et al.* [1997] reported that the noise in the data was best described as a combination of white noise and flicker noise.

Mao *et al.* [1999] concluded that white noise plus flicker noise best described the noise content of the time series. Calais [1999] reported that a combination of white noise and flicker noise was the preferred model. Teferle [2003] and Teferle *et al.* [2006] reported that white noise and flicker noise best described the noise content of the time series in the British Isles. However, the importance of random walk was reported in other studies such as Johnson and Agneew [1995] and Langbein and Johnson [1997].

There are several methods for investigating the noise characteristics of the coordinate time series, but the most widely used method, and also believed to be the most accurate is Maximum Likelihood Estimation (MLE) [e.g. Zhang *et al.*, 1997; Langbein and Johnson, 1997, Mao *et al.*, 1999; Williams, 2003; Williams *et al.*, 2004]. Using MLE it is possible to estimate the noise amplitudes for several stochastic models together with parameters for a linear trend, periodic signals and coordinate offsets. The methodology of MLE is explained in more detail in Zhang *et al.* [1997] and Williams [2003] and has been implemented in the coordinate time series software CATS [Williams, 2008]. Empirical methods to estimate the noise amplitudes such as these reported by Williams [2003]; Le Bail, [2006] and Amiri-Simkooei, [2009] are less accurate than MLE, however, they have been shown to be more time-efficient. The empirical method by Williams [2003] does not estimate the noise amplitudes simultaneously with the other parameters. After these have been determined from least squares, the noise amplitudes are derived from the residual time series in a second step. This method is also implemented in CATS. For more details on the equations used by the author to compute the noise amplitudes, the reader is referred to Appendix A.

5.2.4 Regional filtering

Time series of daily coordinate solutions in a region contain spatial correlations. Wdowinski *et al.* [1997] reported that this common mode signature can be seen in all station time series are the result of errors that affect each station within a region in a similar manner. The characteristic of these correlations suggests a common source for this effect, in particular satellite orbits and clock products and the reference frame. Other sources may include modelling of systematic biases and errors such as satellite antenna phase centres, the neglecting of high-order ionosphere terms, and un-mitigated tropospheric delay. These biases and errors cause an increase in the day-to-day scatter in the coordinate time series, which will affect the accuracy of the estimated parameters. Therefore, by applying spatial filtering, the common mode can be removed and the day-to-day scatter minimized, improveing the signal-to-noise ratio [Wdowinski *et al.*, 1997, 2004; Nikolaidis, 2002].

As outlined in Teferle *et al.* [2009] care must be taken in order to avoid a departure from a given reference frame of the filtered coordinate time series. There are two different methods for the spatial filtering: unweighted or weighted staching of daily residuals [Wdowinski *et al.*, 1997; Nikolaidis, 2002; Wdowinski, *et al.*, 2004; Teferle *et al.* 2006, 2009] and Empirical Orthogonal Filter (EOF) [Johansson *et al.*, 2002; Dong *et al.*, 2006; Teferle *et al.* 2008]. Following Teferle *et al.* [2006], the author applied weighted stacking to compute the daily common mode bias as the weighted mean coordinate residual from a selection of stations on a particular day. Then this bias was subtracted from all unfiltered coordinate time series forming the filtered coordinate time series.

It is recommended by different authors (Wdowinski *et al.* [1997]; Nikolaidis [2002]) that the stations used for the computation of the common mode bias should be of high quality to answer that the computed bias contains only the common systematic variations of the coordinate time series and not station-specific noise. Also, it was recommend [Wdowinski *et al.* 1997; Nidolaidis,

2002; Teferle *et al.* 2006] that if more stations are included in the stacking process, then the estimation of the common mode bias would be better since the averaged daily residual is improved by having more stations.

When carrying out spatial filtering using the stacking method, the annual and semi-annual signals in the coordinate time series can be regarded as part of the spatially correlated noise [Wdowinski *et al.*, 1997; Wdowinski *et al.*, 2004; Nikolaidis 2002]. However, Prawirodirdjo *et al.* [2006] removed the annual and semi-annual signals during the stacking process as these were considered to be due to thermoelastic expansion of the monument. On the other hand, Teferle *et al.* [2009] argued that not including annual and semi-annual signals during common mode bias computation may lead to a non-zero, artificial linear trend in the daily common mode bias time-series itself, which in turn will affect the trend of the filtered coordinate time-series, thus biasing station velocity estimates.

In this study the common mode bias ε_i is estimated for each day based on the coordinate residuals $v_{i,s}$ of each station s for each day $i = 1,.....,N$ and the standard errors $\sigma_{i,s}$ of the coordinates. The following equation is applied [Nikolaidis, 2002]:

$$\varepsilon_i = \begin{cases} 0 & S_i(t_i) < 3 \\ \dfrac{\sum_{s=1}^{S_i} \dfrac{v_{i,s}}{\sigma_{i,s}^2}}{\sum_{s=1}^{S_i} \dfrac{1}{\sigma_{i,s}^2}} & S_i(t_i) \geq 3 \end{cases} \tag{5.9}$$

Where S_i is the number of available continuous GPS stations in the network per day. If $S_i < 3$,then no common mode bias was computed for the day i. After that, the daily coordinate common mode biases are subtracted from the raw coordinate time series y_i of all stations. Hence the spatially filtered coordinate time series

$\tilde{y}_i$ is derived as follow:

$$\tilde{y}_i = y_i - \varepsilon_i \tag{5.10}$$

Can be formed for these filtered coordinate time series. Using least squares the best fitting model parameters. Further more, a new RMS statistic of the residual coordinate time series obtained at this stage can be computed and compared to the RMS statistic of the residual coordinate time series based on the unfiltered data. The amount of change in the RMS scatter can then be expressed as improvement [in %]using the following ratio [e.g. Teferle, 2003]

$$\%\text{Improvement} = \frac{RMS_{unfilter} - RMS_{filter}}{RMS_{unfilter}} \tag{5.11}$$

5.2.5 CTSAna Tools

The Coordinate Time Series Analysis (CTSAna) tools are a set of scripts developed mostly by Dr. F. N. Teferle to carry out time series analysis for velocity and velocity uncertainty. For more details of this tool, the reader is advised to consult Teferle [2003]. These scripts are written in Korn and C shell, the Perl scripting language, forming a wrapper around the CATS program for time series analysis [Williams, 2003, 2008] and use the Generic Mapping Tools (GMT) [Wessel and Smith, 1998] to produce graphs and maps.

The CTSAna tools are organized to be in a consistent order, with the whole coordinate time series analysis being under one project name. Each project has a number of subdirectories (`cmb`, `emp`, `eof`, `inf`, `mle`, `raw`, `psd`, `sta`, and `tqc`) for common mode bias estimation, empirical coordinate time series analysis, EOF analysis, general information, MLE, the raw coordinate time series, power spectral analysis, station information and time series of teqc quality parameters [Estey and Meertens, 1999]. The main analysis sub directories (`cmb`, `emp`,...) are further subdivided into subdirectories (`figures`, `gmt`, `inputs`, `results` and `tables`).

This organization allows easy execution of the scripts and the results are presented in a common structure. Once a project has been created, the daily coordinates with their associated uncertainties are extracted from a series ADDNEQ2 output or SINEX files provided by the Bernese software and placed into a coordinate time series file with extension (`*.cts`) in the `raw` subdirectory. Also, at this stage it is essential to prepare/update a number of files (`stationlist_file`, `coordinates_file`, `offsets_file`, `modelfits_file` and `exclusions_file`) in the `sta` subdirectory. Naturally the station-list file contains the names of all stations to be analyzed, the coordinates file the *a priori* station coordinates, the offsets file the epochs of known discontinuities for each station, the model-fits file the definition of the parameters of any periodic terms to be included in the model fit, and the exclusions file the station-specific periods to be excluded from the analysis. The following step converts coordinate time series in the `raw` subdirectory into the CATS-formatted coordinate time series file for both Cartesian (xyz) and topocenteric (neu) coordinates with respect to a reference cooridinate, either computed as the weightd mean coordinate or from the coordinates file. Also, in this step the offset epochs specific to a particular station in the offsets file will be entered into the header of the new CATS-formatted coordinate time series file. After this, outliers are detected and removed by fitting a model comprising offsets and periodic terms as stipulated in the offsets and model-fits files to the coordinate time series based on weighted least squares.

Residual coordinate time series are then computed as the difference between the daily coordinates and model values. The weighted root mean square (WRMS) is then computed for these residuals.

Finally, an outlier is defined when the residual is greater than three times the WRMS. Hence, these daily coordinates have outliers removed from the coordinate time series.

Once the cleaned coordinate time series have been obtained a number of scripts can then perform either an empirical or an MLE time series analysis using the CATS program. As mentioned above, the computation of the common mode bias can also be carried out for filtering of the coordinate time series. These are the placed into a subdirectory `flt` which is futher subdivided (`figures`, `gmt`,...). If futher analysis of the filtered coordinate time series is required, both empirical and MLE time series analysis can now be applied to the filtered coordinate time series. It should be mentioned here that Teferle *et al.* [2009] recommend to be consistent in the analysis (empirical or MLE) prior to the common mode bias computation and afterwards during the analysis of the filtered coordinate time series.

5.3 Continuous GPS stations

As outlined in §5.2.5, time series of the daily coordinates computed using BSW5.0 were used as input to CATS [Williams, 2008] by the CTSAna tools in order to estimate station velocities and their associated uncertainties. CATS takes account of the linear velocity offsets and periodic signals and their uncertainties are estimated with full white plus flicker noise covariance based on a maximum likelihood estimation (MLE) [Williams, 2003; Williams *et al.*, 2004] as explained in §5.2.

In this study periodic signals (annual and semi-annual) were taken into account in all stages for all CGPS stations. However, the final list of offset epochs to be included for CGPS station term srem from an iterative process. In the first run of CTSAna all reported changes from the IGS station information log and the ITRF2005 discontinuity file were applied to all IGS stations. Table B.1 in Appendix B shows all changes applied in the first step. Then a visual inspection of all coordinate (north, east, up) time series was carried out to see if there were any further offsets in the time series and these were added to the list in Table B.1 of Appendix B. Moreover, since a large number of potentially unnecessary offsets in the coordinate time series can make the estimation of the station velocities unstable, the number of offsets applied was kept as low as possible.

From these checks it was found that BILI had two offsets in the up components on 15 January 2002 and 3 March 2002, and BRUS had an offset in the up component as a result of a receiver change on 21 March 2001. In addition, it was suggested that the data from 1 January 2000 to 28 April 2000 of BRUS station be excluded from time series analysis since the time series plot showed large scatter and inconsistency as a result of changing the receiver twice and the antenna once during this short period of time (IGS mail: 2682, 2691, 2765, 2807 and 2814). CAGL had offsets in all three components on 11 July 2001 as a result of a receiver and antenna change. The Sumatra earthquake on 26

December 2004 caused noticeable offsets in all three components of DGAR and in two components (northing and easting) at HYDE, IISC and KUNM. RAMO, located on the Sinai micro plate close to the Dead Sea fault, showed large differences, especially in the east component, between the computed and known coordinate values from ITRF2005; hence it was suggested that the data obtained before the monument was repaired on 17 March 2004 be excluded to see the effect of this exclusion on the result. There were offsets for SEY1 on 21 June 2004 in all three components. SFER station shows an offset on 4 March 2002 in the north component as a result of receiver and antenna change and another offset on 8 June 2003 in the north and east components (see Figure 5.1). Finally, WUHN has an offset in the up component on 23 January 2002 as a result of an antenna change.

Therefore, CTSAna was run for a second time applying all the noticeable offsets and exclusions suggested after the first run described above and the results showed that more offsets and exclusions needed to be applied for a number of stations. There is an offset in the north component on 18 May 2004 at DGAR station, as receiver and antenna were changed. Two offsets in all components at GRAS station on 22 April 2003 and 20 October 2004 occurred as a result of the receiver and antenna both being changed. Also, HARB station had an offset in all components as the receiver was changed. There was an offset in the north and east components on 6 December 2004 at JOZE station. More offsets were found due to antenna change at LAHZ, MATE and REUN on 28 Feb 2007, 10 Feb 2004 and 4 April 2003, respectively. The difference was still large at RAMO station, so it was suggested that no data be excluded, but two offsets be applied in all components for 17 July 2000 as the antenna was changed, and at 15 March 2004 as monument repair was carried out. Also, another offset was added in all components for SEY1 station as the receiver and antenna were changed on 6 Feb 2003. SUTH station has two offsets in the north and up components as receiver and antenna were both changed on 27 Feb 2002 and 1 June 2004. Also, VILL station has four offsets in all components: one because the receiver was changed on 23 April 2001 and the other three as

the antenna was changed on 28 September 2004, 29 November 2006 and 18 April 2007. Moreover, WTZR station had an offset in all components on 2 July 2002 due to an antenna change. WUHN station had two offsets in the up component on 7 June 2000 as receiver and antenna were changed and on 31 October 2002 as a ITRF2005 offset. In addition to the above offsets, it was suggested that the result in all components for BILI and IRKT stations from 15 January 2002 to 3 March 2002 and from 1 January 2000 to 31 March 2000, respectively, be excluded. All the offset plots for these stations can be seen in Appendix B.

With both offset lists and exclusions lists in place, the final coordinate time series were prepared for all CGPS stations. Figure 5.1 shows an example coordinate time series for SFER. The figure includes the WRMS statistic and the station velocities with their associated uncertainties and for others stations can be seen in Appendix C. Table 5.1 summarises the station velocities and their associated uncertainties for all CGPS stations.

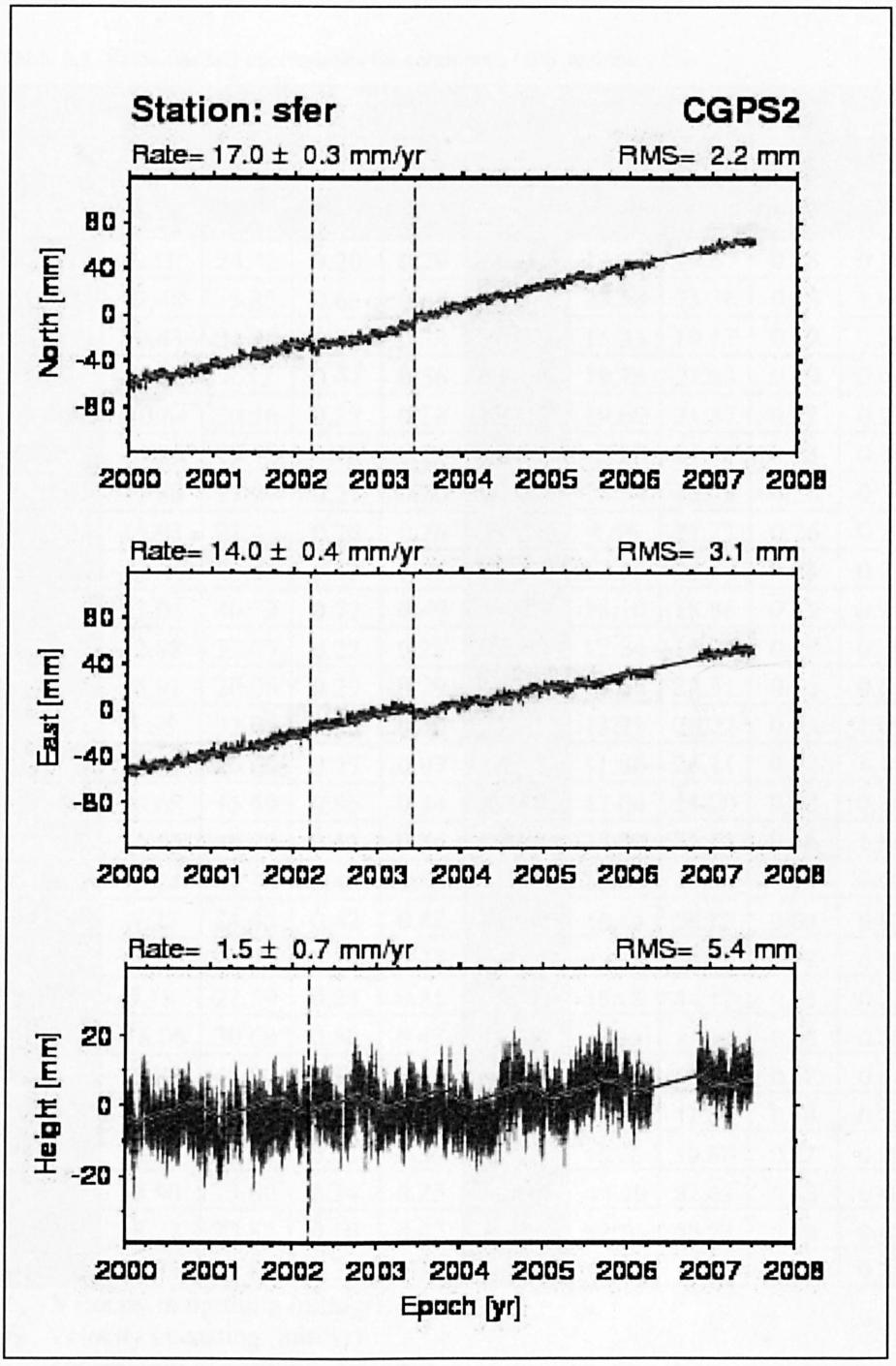

Figure 5.1. SFER station coordinate time series plot and the error bars were three sigmas

Table 5.1. Velocities and uncertainties for continuous GPS stations.

	Velocity		Uncertainty			Velocity		Uncertainty	
Stations	V_N	V_E	U_N	U_E	Stations	V_N	V_E	U_N	U_E
	mm/yr	mm/yr	mm/yr	mm/yr		mm/yr	mm/yr	mm/yr	mm/yr
ARTU	6.31	24.42	0.20	0.29	METS	12.78	19.67	0.23	0.20
ASC1	12.48	-5.85	0.65	0.68	NAMA	28.58	33.36	0.45	1.60
BAHR	30.43	31.20	0.26	0.28	NICO	15.33	19.17	0.20	0.20
BILI	-20.43	8.52	0.44	0.36	NKLG	19.76	21.63	0.40	0.44
BJFS	-10.64	30.16	0.37	0.38	NOT1	19.69	21.37	0.22	0.23
BOR1	14.85	19.72	0.18	0.21	NRIL	-2.22	21.71	0.28	0.36
BRUS	15.88	17.07	0.21	0.26	ONSA	14.54	16.73	0.20	0.24
CAGL	15.93	21.41	0.26	0.26	POL2	5.56	27.27	0.26	0.31
DAEJ	-12.49	26.45	0.42	0.40	POLV	12.85	22.58	0.24	0.23
DGAR	33.04	46.72	0.72	0.49	POTS	15.10	18.86	0.19	0.20
GLSV	12.98	22.05	0.22	0.23	RABT	17.84	15.96	0.27	0.29
GRAS	15.91	20.06	0.29	0.29	RAMO	19.66	22.52	0.35	0.51
GUAO	5.65	32.02	0.38	0.40	REUN	13.23	20.22	0.93	1.09
HALY	23.39	26.60	0.27	0.97	SEY1	11.86	26.11	0.98	1.11
HARB	18.68	16.69	0.85	0.74	SFER	17.04	14.00	0.32	0.36
HYDE	34.66	40.80	0.61	0.54	SOLA	28.00	31.53	0.46	1.66
IISC	35.24	42.34	0.40	0.45	SUTH	21.02	16.64	0.93	0.60
IRKT	-7.22	24.45	0.42	0.42	TEHN	18.49	26.72	0.60	0.83
JOZE	14.19	20.73	0.24	0.24	TRAB	13.55	25.01	0.17	0.19
KIT3	5.78	27.59	0.24	0.31	TROM	15.23	14.17	0.33	0.27
KUNM	-18.06	30.69	0.50	0.49	ULAB	-8.30	27.60	0.36	0.39
LHAZ	15.89	45.97	0.34	0.33	VILL	16.56	18.69	0.37	0.41
MALI	16.72	26.21	0.42	0.55	WSRT	16.36	17.30	0.18	0.23
MAS1	17.25	16.30	0.31	0.34	WTZR	15.56	19.67	0.27	0.26
MATE	18.90	23.00	0.24	0.23	WUHN	-11.29	32.43	0.45	0.40
MBAR	18.22	23.82	0.50	0.42	YIBL	32.70	36.23	0.49	0.43
MDVJ	11.95	22.65	0.31	0.34	ZIMM	16.18	19.44	0.18	0.22

V_N : Velocity in northing (mm/yr)
V_E : Velocity in easting (mm/yr)
U_N : Uncertainty in northing (mm/yr)
U_E : Uncertainty in easting (mm/yr)

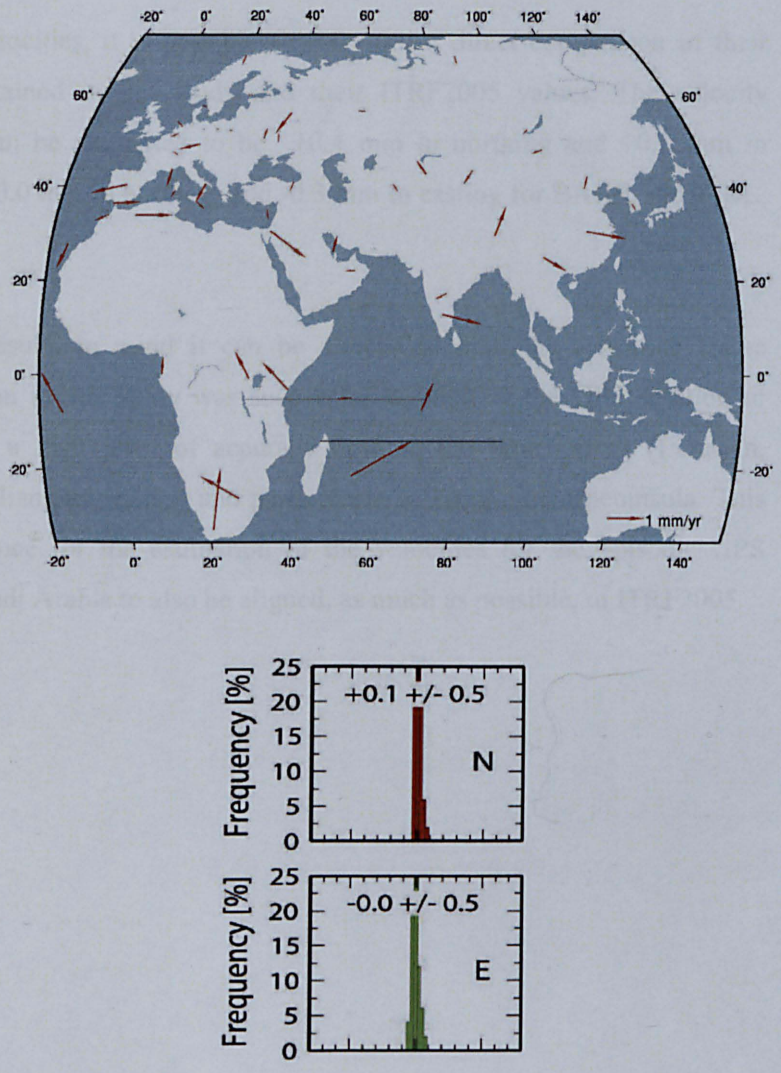

Figure 5.2. a) Velocity differences (this study minus ITRF2005). b) Distribution of velocity differences (this study minus ITRF2005).

In order to investigate the reference frame implementation, the distribution of the residual station velocities for reference frame stations, computed from their station velocity estimates obtained in this study minus their official ITRF2005 velocities was investigated. As can be seen, in Figure 5.2 in general there is a good station velocity recovery of less than 1 mm/year for both horizontal components. Although no significant bias can be found, a few stations show larger residual velocities in their east component. Furthermore, Since BAHR and YIBL are IGS stations on the Arabian plate and they have official

ITRF2005 velocities, it is possible to carry out a direct comparison of their velocities obtained in this study and their ITRF2005 values. The velocity differences can be computed to be +0.4 mm in northing and +0.1 mm in easting and +0.0 mm in northing and -0.3 mm in easting for BAHR and YIBL, respectively.

With these results in mind it can be concluded that, the reference frame implementation in this study was successful in aligning the GPS solution to ITRF2005 at a high level of accuracy both in the larger areas (Eurasian, Nubian, somalian and Indian) and particularly on the Arabian peninsula. This gives confidence for the estimation of the velocities for the episodic GPS stations in Saudi Arabia to also be aligned, as much as possible, to ITRF2005.

5.4 Episodic GPS stations

As the campaign network relies on two or more surveys with a few days of data, periodic signals and offsets can generally not be estimated. However, these limitations must be considered in the uncertainty budget of the campaign data. The GCS stations were observed during episodic campaigns; hence the periodic signals propagation biases explained in §5.2.1 and coordinates offsets explained in §5.2.2 could not be applied. However, all campaigns for the regional network were conducted between March and April of the year and for the local network in January of the year, respectively, in order to minimize biases from annual and semi-annual signals [e. g. Mazzotti *et al.*, 2003]. Furthermore, all GCS stations were observed by one type of receiver (Trimble 5700) and geodetic antenna (Trimble Zephyr:TRM41249.00).

5.4.1 Velocity estimation

The station velocity estimation for episodic GPS stations assumes a constant rate between all episodic campaigns. Hence, the station velocities were obtained by a weighted least-squares fit to all daily positions of the two or more campaign occupations.

A regional filter (explained in §5.2.4) was computed using six CGPS stations in the region (BAHR, NICO, RAMO, TEHN, TRAB and YIBL) and applied to the episodic GPS coordinate time series. Wdowinski *et al.* [2004] used ten stations and Nikolaidis [2002] eight stations after careful selection of these. The number of CGPS stations in and around the Arabic peninsula is very limited, therefore the author was not able to carry out a specific selection process [e.g. Teferle, 2003; Teferle *et al.*, 2009] for finding an optimal set of CGPS stations for the computation of the daily common mode.

Figure 5.3 shows the common mode bias in each component (north, east and up). Also, this figure shows the number of stations used on each day for the computation of the common mode bias, which is between four and six stations,

as no common mode bias was computed when there were fewer than three stations on a day.

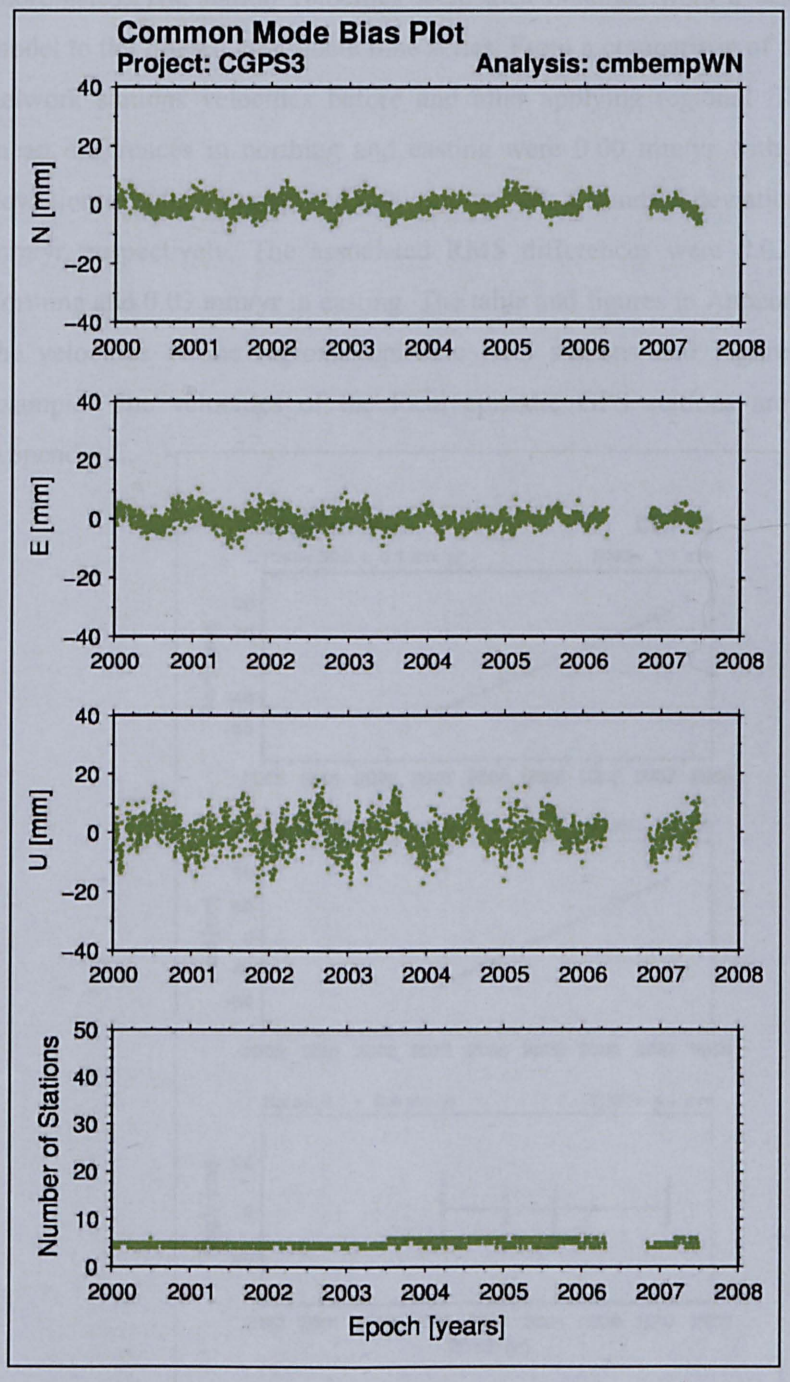

Figure 5.3. The common mode bias in each component (north, east and up) computed from six stations and the number of stations used on each day for the computation.

Then the filtered coordinate time series of the episodic GPS stations were computed by subtracting the daily common mode bias values from the raw coordinates. The station velocities were then obtained from a best fit linear model to the filtered coordinate time series. From a comparison of the regional network stations velocities before and after applying regional filtering, the mean differences in northing and easting were 0.00 mm/yr with a standard deviation of ± 0.03 mm/yr and 0.00 mm/yr with a standard deviation of ± 0.03 mm/yr, respectively. The associated RMS differences were 0.03 mm/yr in northing and 0.03 mm/yr in easting. The table and figures in Appendix D show the velocities of the regional episodic GPS stations and Figure 5.4 is an example. The velocities of the local episodic GPS stations are shown in Appendix E.

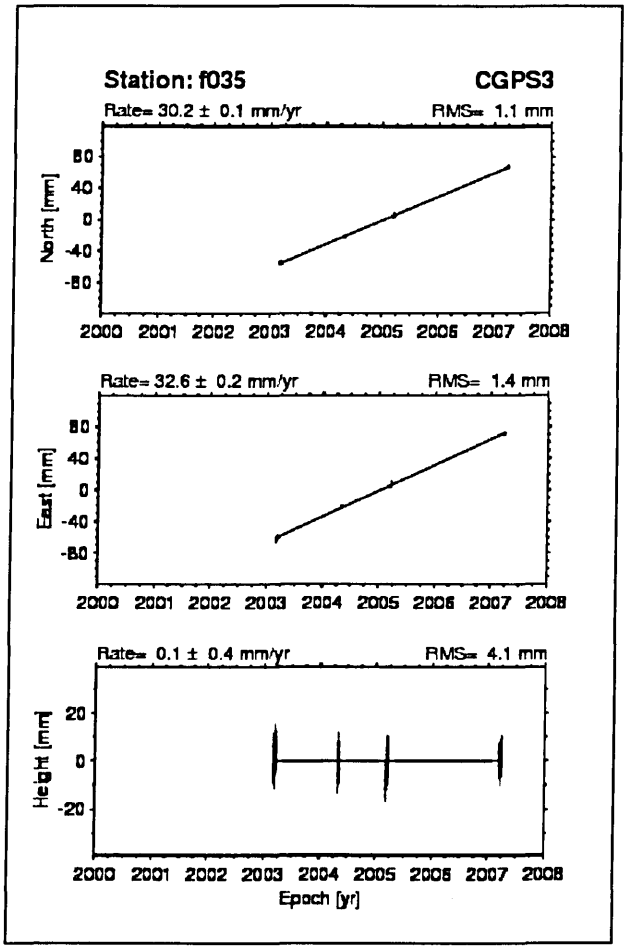

Figure 5.4. The coordinate time series for an episodic GPS station (station F035).The error bars are 3-sigmas .

5.4.2 Uncertainty Estimation

As neither the MLE nor the empirical methods can be reliably applied to episodic GPS station data an alternative method had to be derived. The uncertainties of episodic GPS stations are expected to be greater than those for CGPS stations mostly due to the limited amount of data and the greater possibility of outliers affecting the estimated velocity [e.g. Leonard *et al.*, 2007; Geirsson *et al.*, 2006; Williams *et al.*, 2004]. To obtain more realistic uncertainties for the velocities of episodic GPS stations the author carried out a comparison between three different methods:

- Method 1

  Geirsson *et al.* [2006] computed the velocity uncertainty σ_{vel} from the standard deviation of the residual σ_v and the length of the time series T in years in the form of

$$\sigma_{vel} = \frac{\sigma_v}{T} \tag{5.12}$$

- Method 2

  This method based on noise amplitude using formulaes by Zhang *et al.* [1997] or Mao *et al.* [1999] where for the white noise $(k = 0)$ it can be shown for n equally spaced data such that $t_i = (i-1)\Delta T$ and $T = (n-1)\Delta T$ with T is the total observation time span in years and ΔT the interval, that the velocity uncertainty σ_j^2 can be computed from

$$\sigma_j^2 = \frac{a^2}{\Delta T^2} \times \frac{12}{n^3 - n} = \frac{a^2}{T^2} \times \frac{12(n-1)}{n(n+1)} \quad ; \; n \geq 2 \tag{5.13}$$

  For the flicker noise $(k = -1)$, following Zhang *et al.* [1997] or Mao *et al.* [1999] the velocity uncertainty σ_j^2 can be computed from

$$\sigma_j^2 = \frac{9b^2}{16\Delta T^2(n^2-1)} \tag{5.14}$$

If it assumes that noise at EGPS stations is equivalent to close by CGPS stations then there have several option to obtain these. the Zhang *et al.* [1997] or Mao *et al.* [1999] method use the average amplitudes of the white and flicker noise for the regional network taken from the CATS output from this study. Also, Williams *et al.* [2004] produced the white noise and flicker noise amplitudes as functions of latitude on a global scale.Table 5.4 shows the average white and flicker noise amplitudes for the latitude from this study and Williams *et al.* [2004]. In this study, the author carried out two tests using the average of noise amplitudes from this study (method 2a) and the extract noise amplitudes from [Williams *et al.*, 2004] for latitude 25° N (method 2b).

- Method 2a

  In this method the average of noise amplitudes were computed from this study using three stations (method 2a3) and six stations (method 2a6). As the white and flicker noise depends on the latitude [Williams *et al.*, 2004], the author selected three stations (BAHR, YIBL and RAMO) which are the available continuous stations that almost cover the area (method 2a3), then added three more stations bringing the total to six (BAHR, YIBL, RAMO, NICO, TRAB and TEHN) (method 2a6), even although NICO and TRAB are quite far north in the network area but these are the nearest stations that can be added. CTSAna was run to estimate the average white noise and flicker noise for the three components (north, east and up) using three and six stations, and the values are given in Table 5.2

- Method 2b

  The global result of Williams *et al.* [2004] were used for estimating the average for the white noise and flicker noise in the network area assuming Latitude 25° N to be the middle of this network.

Table 5.2. The average white and flicker noise for the network area from this study and Williams *et al.* [2004].

		White noise (mm)			Flicker noise (mm)			
	Stns	north	east	up	north	east	up	stations
This study	3	1.2±0.4	4.1±0.2	6.5±2.1	1.7±0.4	6.1±0.2	16.8±4.5	BAHR, RAMO, YIBL
This study	6	1.2±0.2	3.8±0.9	5.4±1.8	1.5±0.5	5.2±1.1	15.9±3.0	BAHR, NICO, RAMO, TEHN, TRAB, YIBL
Williams *et al.* [2004]	Global	1.6	3.5	4.8	2.3	8.5	22	Lat 25°

Remark: For the white and flicker noise amplitudes for Williams *et al.*, [2004] the uncertainties are available. At uncertainties one 1-σ .

As can be seen from Table 5.2, when using six stations the average white and flicker noise amplitudes are smaller than or equal to when using three stations for all components.. In general, the avarege white and flicker noise amplitudes agree well with those at 25° N from Williams *et al* [2004] even though the amplitudes for flicker noise are slightly smaller when based on the coordinate time series analysis from this study. There are several reasons that explain this:

- Williams *et al* [2004] showed that the noise content in global GPS coordinate times series analysis was higher than in those for regional ones. This is particularly true for the flicker noise component with the implementation of the common mode, i.e. largely flicker noise are removed.
- The use of the re-processed GPS products [Steinberger et al., 2006] in this study has less day-to-day scatter in the coordinate time series analysis bringing about reduced noise amplitudes.

The velocity uncertainty for each station of the regional episodic GPS network was then computed using equations (5.13 and 5.14) with the three sets of average white and flicker noise amplitudes from Table 5.2, the number of observation days per year and the data time span associated with each station. Therefore, the horizontal station velocity uncertainties were estimated four times in total, i.e. when also considering method 1 [Geirsson *et al.* 2006]. The results are shown in Tables 5.3 and 5.4, and compared in Table 5.5.

Table 5.3. Velocity uncertainties for episodic campaign stations when using *Zhang et al.* [1997] or *Mao et al.* [1999] equations with the average amplitudes of the white and flicker noise for the regional network taken from this study when applying three and six stations.

	Method 2a3		Method 2a6			Method 2a3		Method 2a6	
Stations	U_N	U_E	U_N	U_E	Stations	U_N	U_E	U_N	U_E
	mm/yr	mm/yr	mm/yr	mm/yr		mm/yr	mm/yr	mm/yr	mm/yr
DATM	0.53	1.88	0.48	1.63	F033	0.54	1.91	0.49	1.66
F001	0.44	1.56	0.39	1.34	F035	0.42	1.51	0.38	1.30
F002	0.68	2.41	0.63	2.12	F036	0.68	2.39	0.63	2.10
F005	0.72	2.53	0.67	2.24	F037	0.68	2.38	0.63	2.10
F006	0.60	2.13	0.55	1.86	F039	0.58	2.06	0.53	1.80
F007	0.68	2.41	0.64	2.12	F040	0.64	2.26	0.59	1.98
F008	0.69	2.42	0.64	2.13	F074	0.66	2.31	0.61	2.03
F009	0.43	1.53	0.38	1.31	F077	0.72	2.52	0.67	2.22
F010	0.69	2.43	0.64	2.14	F078	0.58	2.05	0.53	1.79
F012	0.69	2.42	0.64	2.13	HALY	0.27	0.97	0.24	0.82
F013	0.58	2.05	0.53	1.78	NAMA	0.45	1.60	0.40	1.37
F016	0.63	2.23	0.58	1.96	SOLA	0.46	1.66	0.41	1.42
F019	0.66	2.32	0.61	2.04					
F020	0.43	1.55	0.39	1.33					
F024	0.55	1.97	0.50	1.71					
F026	0.72	2.54	0.67	2.24					
F027	0.57	2.04	0.52	1.77					
F029	0.53	1.90	0.48	1.64					
F030	0.68	2.40	0.63	2.11					

U_N : Uncertainty in northing (mm/yr)
U_E : Uncertainty in easting (mm/yr)
Method 2 & 3: *Zhang et al.* [1997] or *Mao et al.* [1999] equations were used with the average amplitudes of the white and flicker noise for the regional network taken from the CATS output for three station (BAHR, YIBL and RAMO) from this study.
Method 2 & 6: *Zhang et al.* [1997] or *Mao et al.* [1999] equations were used with the average amplitudes of the white and flicker noise for the regional network taken from the CATS output for six stations (BAHR, YIBL, RAMO, NICO, TEHN and TRAB) from this study.

Table 5.4. Velocity uncertainties for episodic campaign stations when using Geirsson *et al.* [2006] equations and *Zhang et al.* [1997] or *Mao et al.* [1999] equations with the average amplitudes of the white and flicker noise for the global model taken from Williams *et al.*, [2004].

	Method 2b		Method 1			Method 2b		Method 1	
Stations	U_N	U_E	U_N	U_E	Stations	U_N	U_E	U_N	U_E
	mm/yr	mm/yr	mm/yr	mm/yr		mm/yr	mm/yr	mm/yr	mm/yr
DATM	0.71	2.47	0.59	0.59	F033	0.73	2.49	0.52	0.84
F001	0.59	2.11	0.62	0.69	F035	0.57	2.06	0.44	0.60
F002	0.92	2.96	0.88	0.36	F036	0.91	2.93	0.46	0.74
F005	0.97	3.07	0.46	0.98	F037	0.91	2.93	0.38	0.73
F006	0.81	2.71	0.29	0.62	F039	0.78	2.65	0.34	0.76
F007	0.92	2.96	0.41	0.63	F040	0.86	2.83	0.37	0.44
F008	0.92	2.97	0.18	0.57	F074	0.88	2.87	1.08	0.87
F009	0.58	2.08	0.48	0.61	F077	0.96	3.06	0.58	0.71
F010	0.93	2.98	0.19	0.41	F078	0.78	2.63	0.60	0.59
F012	0.92	2.97	0.37	1.10	HALY	0.36	1.34	0.44	0.34
F013	0.78	2.63	0.56	0.56	NAMA	0.61	2.21	0.77	0.59
F016	0.85	2.80	0.71	0.57	SOLA	0.63	2.29	0.69	0.61
F019	0.88	2.88	0.42	0.48					
F020	0.59	2.10	0.55	0.68					
F024	0.75	2.55	0.45	0.74					
F026	0.97	3.08	0.37	0.44					
F027	0.77	2.63	0.23	0.50					
F029	0.72	2.48	0.47	0.62					
F030	0.91	2.94	0.51	0.95					

U_N : Uncertainty in northing (mm/yr)
U_E : Uncertainty in easting (mm/yr)
Method 2b: Zhang *et al.* [1997] or Mao *et al.* [1999] equations were used with the average amplitudes of the white and flicker noise for the global network taken from Williams *et al.* [2004].
Method 1: Geirsson *et al.* [2006] equations were used.

Table 5.5. Statistical analysis of the differences between the different methods of estimating velocity uncertainty for episodic campaign stations

Diff. of		RMS	Mean	S.dev	min	max
Method 1	N	0.25	0.09	0.24	-0.42	0.50
Method 2a3	E	1.48	1.43	0.39	0.63	2.10
Method 1	N	0.24	0.04	0.24	-0.47	0.45
Method 2a6	E	1.22	1.17	0.36	0.48	1.80
Method 1	N	0.39	0.29	0.26	-0.20	0.74
Method 2b	E	2.03	1.99	0.39	1.00	2.63
Method 2a3	N	0.05	0.05	0.00	0.03	0.05
Method 2a6	E	0.27	0.26	0.03	0.14	0.30
Method 2a3	N	0.21	-0.20	0.04	-0.25	-0.10
Method 2b	E	0.56	-0.56	0.04	-0.63	-0.37
Method 2a6	N	0.25	-0.25	0.04	-0.30	-0.13
Method 2b	E	0.82	-0.82	0.06	-0.87	-0.51

Method 1: when using Geirsson *et al.* [2006] equation.
Method 2a3 when using *Zhang et al.* [1997] or *Mao et al.* [1999] equations with the average amplitudes of the white and flicker noise for three stations
Method 2a6: when using *Zhang et al.* [1997] or *Mao et al.* [1999] equations with the average amplitudes of the white and flicker noise for six stations.
Method 2b is when using the global model taken from Williams *et al.*, [2004].

As can be seen from Table 5.5, the difference between the station velocity uncertainties (method 2a3 and method 2a6) using three or six stations to obtain the average noise amplitude is very small, especially in the north component. Furthermore, the difference in the velocity uncertainties between using method 2a and method 2b is very similar. It can also be seen also that the difference between method 2 and method 1 is almost the same for the north component but differs for the east component, with differences up to 2 mm. For more information about the value of uncertainty of each station for all methods, as well as their differences, please consult Appendix F.

A further test of the four sets of velocity uncertainties can be obtained from a plate motion model estimation for each set and through comparison of the reduced chi squared (χ^2) value. The results show that using method 2a6 [Williams *et al.* 2004] the velocity uncertainties seem over-estimated as indicated by ($\chi^2 = 0.635$). For method 1 [Geirsson *et al.* 2006] the velocity

uncertainties seem under-estimated($\chi^2 = 1.42$). However, when using method 2a3 (this study with averged white and flicker noise amplitude from 3 stations and equation (5.13 and 5.14)) the χ^2 is almost equal to unity ($\chi^2 = 1.05$). Therefore, the best velocities uncertainty estimation for the episodic GPS stations in this study seems to be method 2a3. For more details, please consult Appendix D and E.

5.5 Summary

In this chapter the background theory of GPS coordinate time series analysis was briefly outlined, including the modelling of periodic signals, coordinate offsets and stochastic noise. Furthermore, the regional filtering was also briefly outlined. Also, previous studies carried out in the field of coordinate time series analysis were mentioned and referenced. Then the CTSAna tool used in the analysis was briefly described.

The Continuous GPS station (CGPS) and the Episodic GPS station (EGPS) velocities and their associated uncertainties were estimated using the time series of the daily coordinates computed using BSW5.0 as input to CATS by CTSAna tools. For CGPS stations the linear velocity offsets and periodic signals and their uncertainties were estimated with full white plus flicker noise covariance based on maximum likelihood estimation (MLE). Whereas, for the EGPS stations a regional common mode bias was estimated using six CGPS stations in the region and applied to the episodic GPS coordinate time series. After that, the filtered coordinate time series of the episodic GPS stations were obtained, then the station velocities were computed from a best fit linear model to the filtered coordinate time series. For EGPS stations velocity uncertainties, two methods were then tested to estimate realistic velocity uncertainties

Chapter 6: **Estimation of the Arabian rigid plate motion**

6.1 **Introduction**

Previous investigations of present-day Arabian plate motion using GPS measurements were primarily carried out from stations located on surrounding plates, with few stations actually located on the Arabian plate itself. Due to the inhomogeneous distribution of these GPS stations and the fact that some of these were actually located in the plate boundary zone, Arabian plate motion was only sensed in a few locations on the stable plate interior. In order to advance the knowledge of the dynamics of the Arabian plate, the General Commission for Survey (GCS) in Saudi Arabia, in collaboration with the Institute of Engineering Surveying and Space Geodesy (IESSG), has created a dense GPS network of 32 stations in Saudi Arabia, covering nearly two thirds of the Arabian plate. In addition to the 32 network stations, IGS stations located on the Arabia plate, such as BAHR, YIBL, HALY, SOLA and NAMA, were also considered in the analysis.

In this chapter, details of the previous studies on Arabian plate motion and the background theory for plate motion estimation will be presented. Results for, the absolute motion for the rigid Arabian plate estimated using the 37 GPS stations will be presented. Also, the impact of the number of stations and their distribution on the Arabian plate will be tested and the influence of stations in active areas, or near the plate boundary, will be evaluated. Following that, the results for the preferred estimation of Arabian plate motion from this study will be compared to the estimations of previous studies. Furthermore, the relative motion of the Arabian plate with respect to the surrounding plates (Eurasian, Nubian and Somalian) will be estimated and compared to other studies as well.

Within this chapter, there arises the question of whether the Arabian plate is rigid. This question is addressed through the tests carried out, in an attempt to show that any apparent instability of Arabian plate is a very interesting scientific result from this study, and not just simply due to systematic errors at the same sites or underestimation of formal errors.

6.2 Previous studies of Arabian plate motion

An overview of the previous studies and the GPS stations used in them is given in Figure 6.1 and a summary, in chronological order of publication; is given below:

Drewes and Angermann [2001] presented a global model (APKIM2000) for absolute motion, but for the Arabian plate they used only SOLA (SLR station) in Riyadh plus two GPS stations: BAHR IGS station and DYR2 to the north of the Arabian plate, near the Bitlis suture.

Sella *et al.* [2002] presented a global model (REVEL2000) for absolute and relative motion, but for the Arabian plate they used only two GPS stations: BAHR IGS station and KATZ, which is very close to the Dead Sea fault.

Kreemer *et al.* [2003] presented a global model (GSRM v1.2) for absolute and relative motion, but for the Arabian plate they also only used two GPS stations: BAHR IGS station and SANA, which had a time span of 5 years but is in the tectonically active south-west area (in Yemen).

McClusky *et al.* [2003] focused on the relative motion between the Nubian, Arabian, Anatolian and Eurasian plates using four GPS stations on the Arabian plate: BAHR IGS station and three others (KIZ2, KRCD, GAZI) located to the north of the Arabian plate in south-east Turkey, near the East Anatolian Fault, with time spans varying from four to ten years (MCCL 2003).

Prawirodirdjo and Bock [2004] estimated a global plate motion model (CGPS2004) for absolute and relative motion using 12 years of continuous GPS observations; for the Arabian plate they used seven GPS stations: BAHR IGS station on the Arabian plate, three others (DRAG, ELAT, GILB) that are

not on the Arabian plate but on the Sinai micro plate [Wdowinski *et al.*, 2004], two (ELRO, KATZ) that are very close to the deformation boundary of the Dead Sea fault and UDMC in Syria, which had a short time span (1.2 years).

Vernant *et al.* [2004] focused on Iran, where a collision between the Arabian and Eurasian plates occurs, and studied relative motion only (VERN 2004). They used seven GPS stations on the Arabian plate: BAHR IGS station, three others (KHAS, KHOS, MUSC) along the east of the Arabian plate, but with a short time span of only 2 years, and the three (KIZ2, KRCD, GAZI) previously used by McClusky *et al.* [2003].

Drewes [2006] re-estimated his previous global model [Drewes and Angermann, 2001] as APKIM2005. This time, for the Arabian plate motion estimation, he used eight stations: SOLA (SLR station) plus seven GPS stations: BAHR and YIBL IGS stations, two others (ELAT, DRAG) that are not on the Arabian plate but on the Sinai micro plate, two others (KATZ, ELRO) that are very close to the deformation boundary of the Dead Sea fault, and AMMN in Jordan.

Vigny *et al.* [2006] used ten GPS stations from (VIGN 2006) the south-western and eastern Arabian plate (Djibouti, Yemen, Oman, Bahrain and Iran). However, three (RSB0, KHAS, REIH) of the ten stations are very close to the plate boundary and, moreover, the data available from six of the ten stations were only for two epochs and the time span between these two epochs varied from between two years for three stations (MUSC, KHAS, KHOS) and ten years for three stations (DHAM, HODD, JNAR), which are all in the tectonically active south-west area, where it is dangerous to assume that no local deformation occurred between the two epochs.

Reilinger *et al.* [2006] considered the whole middle East area (REIL 2006) and the complex tectonic plate zone (Arabian, Nubian, Somalian, Indian and Eurasian), but they studied relative motion only and although they used 33 GPS stations on the Arabian plate, including BAHR IGS station, most of them were distributed along the deforming boundary (Yemen, Oman, Saudi Arabia, Iran, Bahrain, Jordan, Lebanon, Syria and Turkey) with few stations actually

located on the stable plate interior. Moreover, these stations had different time spans and most of them had less than four years of data.

Almotairi [2006] estimated Arabian plate motion model for absolute and relative to Eurasian plate using 27 stations of the GCS as illustrated on chapter 4 figure 4.1. Where the time span is two years and only two sets for each station were available.

Kreemer *et al.* [2006] re-estimated their previous global model [Kreemer *et al.*, 2003] as GSRM-NNR-2. For the Arabian plate motion estimation, they used nine stations: the two stations used in their previous model complemented with stations from other studies, for example Vigny *et al.* [2006].

For absolute Euler pole and rotation rate estimation in ITRF2005, Altamimi *et al.* [2007] used SOLA SLR station plus four GPS stations: BAHR, DRAG, ELAT and RAMO IGS stations. However, these are not well distributed on the Arabian plate, DRAG, ELAT and RAMO are on the Sinai micro plate, according to their IGS station information log files and several published papers, and SOLA is an SLR station with a residual velocity of more than 2 mm/yr.

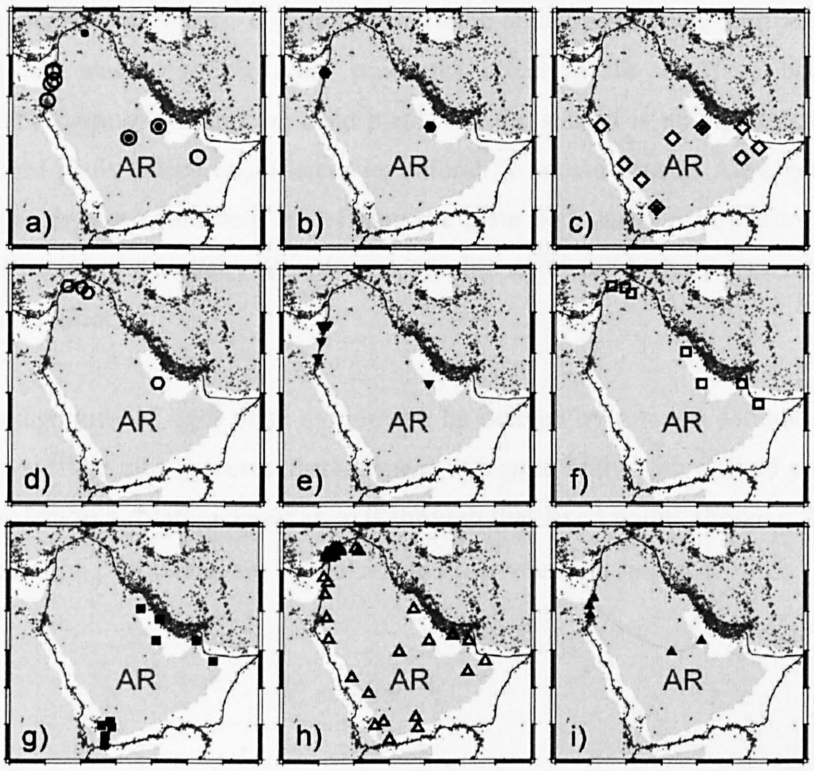

Figure 6.1. GPS stations used in previous studies: (a) solid circle is APKIM2000 [Drewes and Angermann, 2001] and open circle is APKIM2005 [Drewes, 2008]; (b) solid pentagon is REVEL-2000 [Sella *et al.*, 2002]; (c) solid diamond is GSRM v1.2 [Kreemer *et al.*, 2003] and open diamond is GSRM-NNR-2 [Kreemer *et al.*, 2006]; (d) open pentagon is MCCL2003 [McClusky *et al.*, 2003]; (e) solid inverted triangle is CGPS2004 [Prawirodirdjo and Bock, 2004]; (f) open square is VERN2004 [Vernant *et al.*, 2004]; (g) solid square is VIGN2006 [Vigny *et al.*, 2006]; (h) open triangle is REIL2006 [Reilinger *et al.*, 2006]; (i) solid triangle is ITRF2005 [Altamimi *et al.*, 2007].

6.3 Background theory for plate motion estimation

When using geodetic data, the number and distribution of the stations are the most important factors for modelling rigid plate motions, as stations near to the plate boundary cannot move with the rigid plate due to elastic deformation. Moreover, plates could be subject to deformation as well within their interiors, which is known as intra-plate deformation. In addition, station velocities have errors; the previous chapters explained how these could be minimized. For example, errors could occur by using a short data span, there could be

equipment set-up errors, or errors in periodic signal estimation. Furthermore, there are many possible local processes affecting the interface between geodetic monuments and the rigid plate, e.g. the station is poorly attached to the rigid plate, which could occur by natural or human causes. Also, geology and geophysics could help in defining the plate boundary or the deformation zones by using seismicity records, topographic relief and bathometric mapping of the seafloor.

The magnitude of rigid plate motion can be defined by rotation parameters as follows: "The most general displacement of a rigid body with a fixed point is equivalent to a rotation about an axis through that fixed point" [Fowler, 2005]. The rotation parameters are known as the Euler vector $[\omega_i, \omega_j, \omega_k]$.

$$X = \omega \times X \tag{6.1}$$

X : is the velocity vector of the stations
X : is the position vector of the stations
ω : is the rotation parameters of the plate (Euler vector)
$\times$: is the cross product
m : is the number of unknowns
n : is the number of observations
r : is the number of equations

$$\begin{bmatrix} X_i \\ X_j \\ X_k \end{bmatrix}_n = \begin{bmatrix} \omega_i & \omega_j & \omega_k \end{bmatrix} \times \begin{bmatrix} X_i \\ X_j \\ X_k \end{bmatrix}_n \tag{6.2}$$

$$\begin{bmatrix} X_i \\ X_j \\ X_k \end{bmatrix}_n = [\omega_j X_k - \omega_k X_j]_{in} + [\omega_k X_i - \omega_i X_k]_{jn} + [\omega_i X_j - \omega_j X_i]_{kn} \tag{6.3}$$

$$\begin{aligned} x_{in} &= \omega_j x_{kn} - \omega_k x_{jn} \\ x_{jn} &= \omega_k x_{in} - \omega_i x_{kn} \\ x_{kn} &= \omega_i x_{jn} - \omega_j x_{in} \end{aligned} \tag{6.4}$$

$$\begin{aligned} \omega_j x_{kn} - \omega_k x_{jn} - x_{in} &= 0 \\ \omega_k x_{in} - \omega_i x_{kn} - x_{jn} &= 0 \\ \omega_i x_{jn} - \omega_j x_{in} - x_{kn} &= 0 \end{aligned} \tag{6.5}$$

In matrix form

$$A^n = \begin{bmatrix} 0 & x_{kn} & -x_{jn} \\ -x_{kn} & 0 & x_{in} \\ x_{jn} & -x_{in} & 0 \end{bmatrix} \quad v^n = \begin{bmatrix} v_{in} \\ v_{jn} \\ v_{kn} \end{bmatrix} \quad \hat{\omega} = \begin{bmatrix} \hat{\omega}_i \\ \hat{\omega}_j \\ \hat{\omega}_k \end{bmatrix} \quad l^n = \begin{bmatrix} x_{in} \\ x_{jn} \\ x_{kn} \end{bmatrix}$$

$$W_l^n = \begin{bmatrix} \sigma^2_{x_{in}} & \sigma_{ijn} & \sigma_{ikn} \\ \sigma_{ijn} & \sigma^2_{x_{jn}} & \sigma_{jkn} \\ \sigma_{ikn} & \sigma_{jkn} & \sigma^2_{x_{kn}} \end{bmatrix} \quad v = \begin{bmatrix} v^1 \\ v^2 \\ \\ v^n \end{bmatrix} \quad l = \begin{bmatrix} l^1 \\ l^2 \\ \\ l^n \end{bmatrix} \quad A = \begin{bmatrix} A^1 \\ A^2 \\ \\ A^n \end{bmatrix}$$

$$W = \begin{bmatrix} W_l^1 & 0 & 0 \\ 0 & W_l^2 & 0 \\ & & \\ 0 & 0 & W_l^n \end{bmatrix}$$

The least squares can be used to determine the estimates of ω and v, which will be donated by $\hat{\omega}$ and $\hat{v}$. The definition of least squares is "the least

squares estimates are defined as those which minimize a specified quadratic form of the residuals" [Cross, 1994].

$$V^T W_l V = \text{minmum} \tag{6.6}$$

Then the least squares solution is:

$$\hat{\omega} = (A^T W_l A)^{-1} A^T W_l l \tag{6.7}$$

$$\hat{v} = A\hat{\omega} - b \tag{6.8}$$

Moreover, the rotation rate Ω in both absolute and relative motion is equal to the magnitude of the Euler vector:

$$\Omega = \sqrt{\hat{\omega}_i^2 + \hat{\omega}_j^2 + \hat{\omega}_k^2} \tag{6.9}$$

and the pole coordinates can be computed as:

$$\hat{\phi} = \tan^{-1} \frac{\hat{\omega}_k}{\sqrt{\hat{\omega}_i^2 + \hat{\omega}_j^2}} \tag{6.10}$$

$$\hat{\lambda} = \tan^{-1} \frac{\hat{\omega}_j}{\hat{\omega}_i} \tag{6.11}$$

It is important to assess the quality of the result, and using least squares the residuals can be employed for this. Also, the unit variance or the chi square value can be used to assess the model's fit to the data. This is used in most rigid plate motion estimations using geodetic techniques. The disadvantages of the least squares method is that when there is an error in one observation it may

propagate into other residuals and this could be absorbed into the estimated parameters.

The reduced χ^2 is used to measure the correctness of the formal errors, where it is defined as follows:

$$\chi^2 = \frac{1}{n-\mu}\sum_{i=1}^{n}\frac{v_i^2}{\sigma_i^2} \tag{6.12}$$

where n is the number of observations, μ the number of unknowns, v_i the residuals and σ_i the standard errors.

When the reduced χ^2 equals one, it means that a good fit of data to the model has been achieved and that the formal error estimates are reasonable. However, when the reduced χ^2 is less than one, it may be that the formal errors are overestimated; and when the reduced χ^2 is greater than one, the formal errors may be underestimated or the model poorly fits the data [Dixon *et al.*, 2000].

Moreover, the *F*-test allows the comparison of variances of two normal distributions. Therefore, the *F*-test can be used to compare two models; the two estimated variances σ_1 and σ_2 for the two models are indicators of the model fit, since if both models fit the data then the ratio σ_1/σ_2 is nearly equal to one. In this study, the *F*-test is employed using the reduced χ^2 quantity, which relates to the variance and has a χ^2 distribution with number of degrees of freedom *v*. Therefore, the ratio of the χ_1^2 and χ_2^2 for model one and model two, respectively, is:

$$F = \chi_1^2/\chi_2^2 \tag{6.13}$$

where this follows the F distribution with v_1 and v_2 degrees of freedom. So the null hypothesis $H_o : \sigma_2^2 = \sigma_1^2$ is that both models fit the data at approximately the same level, against the alternate hypothesis $H_A : \sigma_2^2 > \sigma_1^2$ that the variance estimated from model 2 is larger than the variance estimated from model 1. The probability $P(F \leq c) = 1 - \alpha$, $\alpha = 5\%$ is assumed and c is obtained from the tabulated values of the F-test. If the F-test for the two models is less than this value, then the null hypothesis holds, namely that the two variances are equal with a 95% confidence, and any difference is due to random error. A 1-tailed test was used in this case because the only information of interest is whether model 1 is more precise than model 2.

6.4 The Tanya software for plate motion estimation

The Tanya software is processing and analysis software, developed at the Newcastle University. It was originally written by Phil Davies in 1997 on a UNIX platform. The Tanya software is a complete package of software used for processing, velocity estimation, time series tools, Euler pole estimation and loading/ geocenter motion estimation (Reference of some of David's papers). Major modifications were made to the Tanya software by David Lavallée in 2000. After that, a new two version of Tanya software existed. Where one version (Newcastle version) was modified by Konstantin Nurutditinov from 1999 to 2004. This version maintains to implementations ERP and ILRS. The second version (Reno version) was modified by David Lavallée e from 2001 to 2005. The Reno version was given a nickname TANYAK (K for Kinematics) and was first implemented on a Linux platform in 2003. After that, in 2005 Lavallée took Nuruditinov's modifications necessary for ERP estimation and applied them to the original TANYA models under the umbrella of the Linux-based TANYAK software. This version is called Tanyak version 1.6 on September 2006.

The author used the TANYAK software in this study for Euler pole estimation for describing the absolute and relative Arabian rigid plate motion. Where the

input file used contains the velocities of stations with their associated uncertainties estimated on chapter 5. Furthermore, the weight matrix is a diagonal matrix with the diagonal elements formed using the station velocity variances.

The formulation used in the TANYA software is explained in the previous section 6.3, where the two equations 6.14 and 6.15 form the basis of all plate tectonic models.

The velocity vector of the stations X at a position X on plate A with rotation described by the absolute Euler vector ω_A is given by the vector cross product $\times$:

$$X = \omega_A \times X \tag{6.14}$$

The relative 3x1 Euler vector describing the rotation of plate A to plate B is:

$$_A\omega_B = \omega_B - \omega_A \tag{6.15}$$

For further details on TANYAK software, the author recommends reading Lavallée [2000 and 2006].

6.5 Absolute Arabian rigid plate motion

This section discusses the estimation of an absolute rigid plate motion model for the Arabian plate and presents a comparison between the estimation of this study and the estimations of previous studies.

6.5.1 Estimation of the absolute Arabian rigid plate motion

Station velocity estimates from 37 GPS stations were considered for the computation as illustrated in Figure 6.2 Four episodic GPS stations (F031, F041, F045 and P049) were excluded from the estimation for the following reasons: damaged monuments at F031 and F041; different monument specifications and antenna location issues at P049; motorway construction at F045. Hence, the velocity estimates from 33 GPS stations were taken forward and used in the model inversion: 28 network stations in Saudi Arabia, three IGS stations (HALY, SOLA and NAMA) in Saudi Arabia, one IGS station (YIBL) in Oman and one IGS station (BAHR) in Bahrain as illustrated in Figure 6.3.

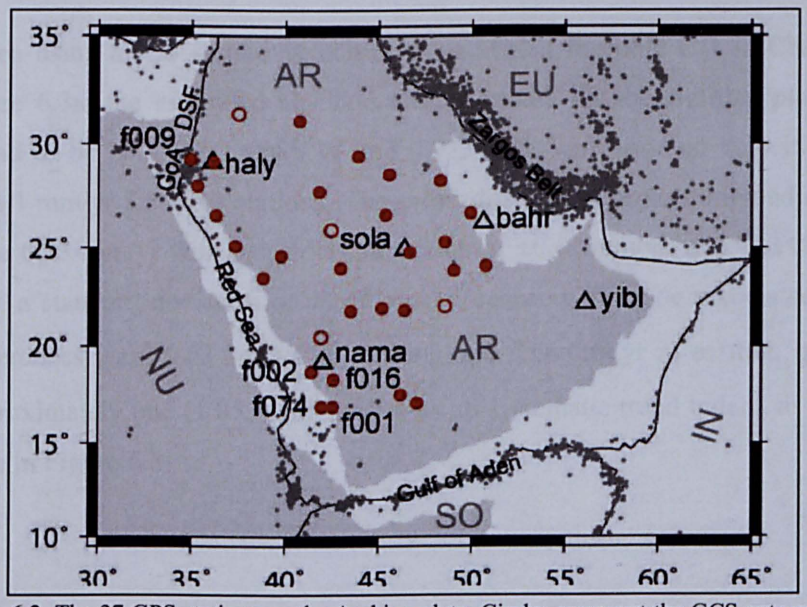

Figure 6.2. The 37 GPS stations on the Arabian plate. Circles represent the GCS network and open triangles are the IGS stations. Also, the solid circles and the open triangles were used in the estimation of the Arabian plate motion parameters and the open circles were excluded from the Arabian plate motion parameter estimations. Where, AR: Arabian plate, EU: Eurasian plate, IN: Indian plate, NU: Nubian plate, SO: Somalian plate, DSF: Dead sea fault, GoA: Gulf of Agaba.

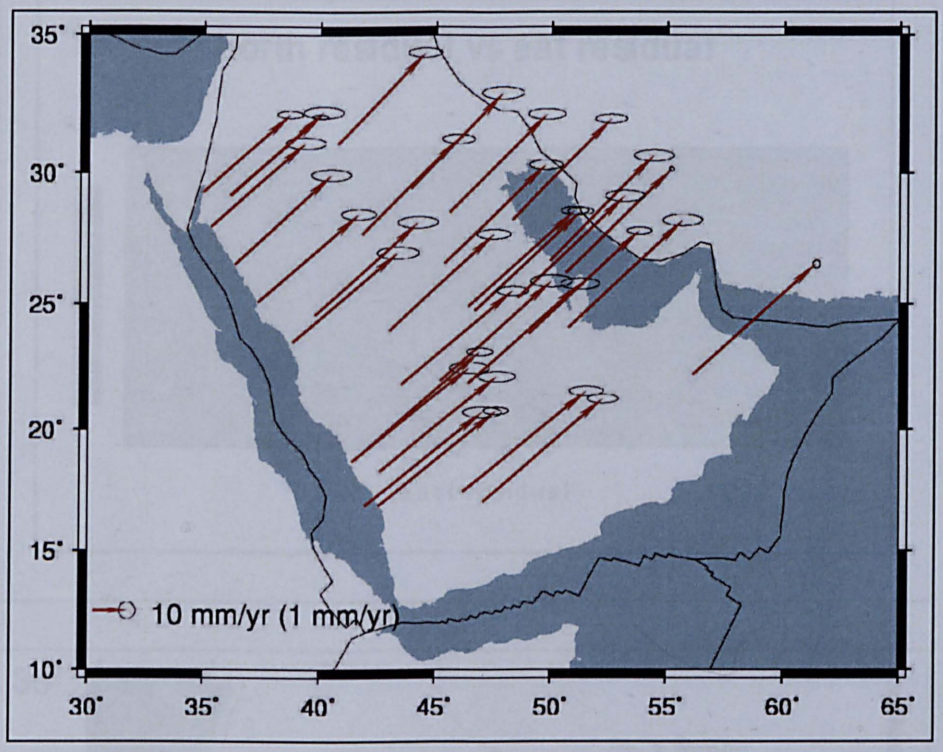

Figure 6.3. Absolute GPS station velocity estimates for stations in this study at 95% confidence level.

When using all 33 station velocities as estimated in Table C.1 in Chapter 5 figure 6.3a, the estimated absolute motion model for the Arabian plate was found to be 50.420°N, 4.089°W and 0.533°/Ma, with residual velocities less than 1 mm/yr for most stations. The mean differences in northing and easting were 0.23 mm/yr with a standard deviation of ±0.62 mm/yr, and -0.11 mm/yr with a standard deviation of ±0.66 mm/yr, respectively. The associated RMS differences were 0.65 mm/yr in northing and 0.66 mm/yr in easting, χ^2 was approximately one (1.053) and there was no systematic trend indent, as can be seen in Figure 6.3.

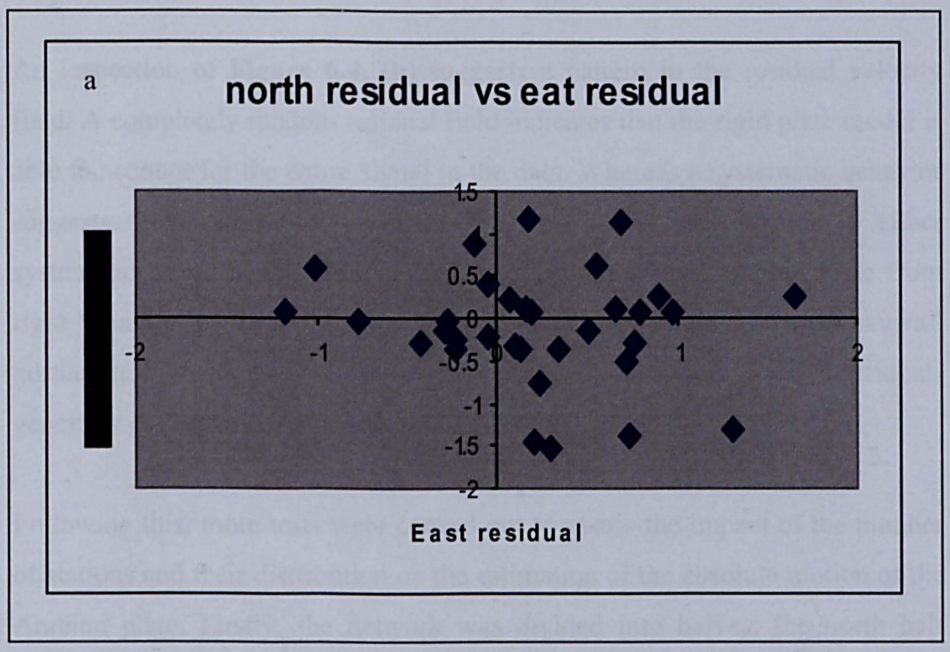

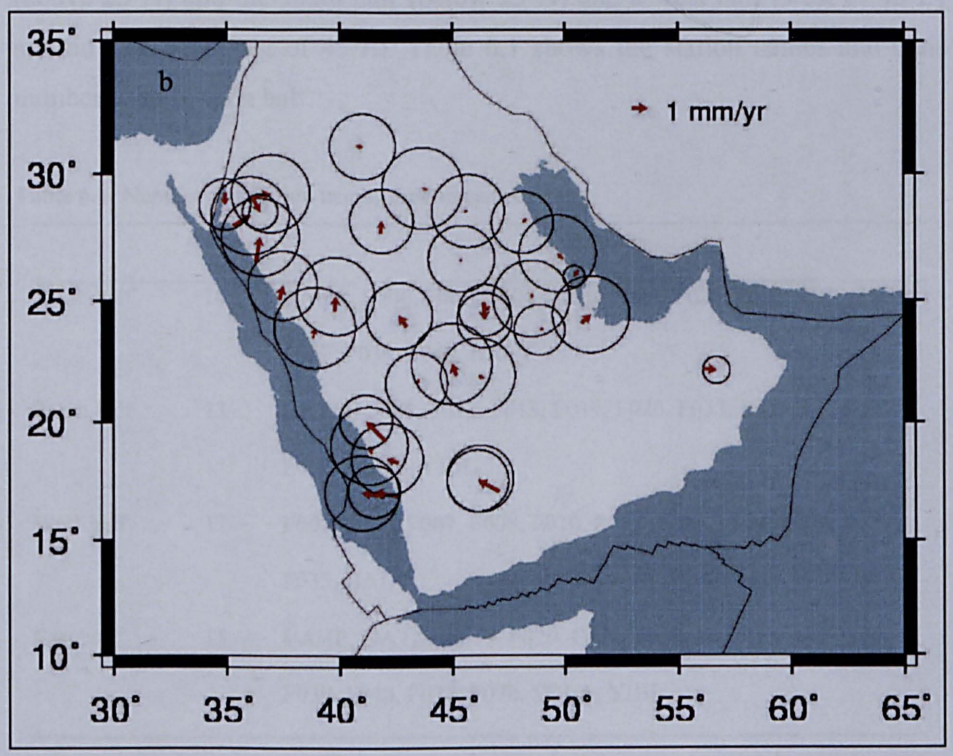

Figure 6.4. (a) The residual velocities for north residual versus east residual with respect to a plate motion model estimated in this study. (b) The residual velocities with respect to a plate motion model estimated in this study.

An inspection of **Figure 6.4. (b)** suggests a pattern in the residual velocity field. A completely random residual field indicates that the rigid plate model is able to account for the entire signal in the data. Whereas a systematic behavior suggests the existence of un-modeled signal which may be due to either systematic errors in the observations or deviation of the Arabian Plate from rigid behavior, i.e. deformation. A group of stations in the northwest have all northeasterly residuals whereas several stations in the southwest have residuals generally in northwesterly direction.

Following this, more tests were carried out to assess the impact of the number of stations and their distribution on the estimation of the absolute motion of the Arabian plate. Firstly, the network was divided into halves: the north half (above 25°N) and the south half (below 25°N) and a west half (west of 45°E) and an east half (east of 45°E). Table 6.1 shows the station names and their number used in each half.

Table 6.1. Number and station names used in each half test.

	# stns	Stations
North half	14	BAHR, F006, F007, F008, F010, F024, F026, F027, F029, F030, F037, F039, F040, HALY
South half	13	DATM, F005, F012, F013, F019, F020, F033, F035, F036, F077, F078, SOLA, YIBL
West half	12	F005, F006, F007, F008, F010, F012, F013, F024, F026, F027, F033, HALY
East half	15	BAHR, DATM, F019, F020, F029, F030, F035, F036, F037, F039, F040, F077, F078, SOLA, YIBL

Table 6.2 and Figure 6.5 demonstrate the effect on pole location and rate when choosing a set of stations on one part of the Arabian plate. This shows that when using south stations only, the pole is pushed further west and up to the north. On other hand, when using stations on the west only, the pole location

moved further to the east and down to the south, and this is what happened in a number of previous studies, when they had fewer stations on one part of the Arabian plate, which will be discussed later in Section 6.5.2.

Table 6.2. Different absolute Arabian plate motion parameters when applying half tests. Uncertainty in the pole location is given by semi major (σ_{maj}) and semi minor (σ_{min}) axes of the 1σ error ellipse (AZ is the azimuth of the major axis), and # stns is the number of stations used in plate motion parameters estimation.

	# stns	Lat [°]	Lon [°]	Rate [°/Ma]	σ_{maj} [°]	σ_{min} [°]	AZ [°]	σ_{rate} [°/Ma]	χ^2
North half	14	50.462	-4.237	0.530	1.39	0.20	-10.0	0.009	1.149
South half	13	51.179	-6.949	0.523	2.68	0.25	-9.10	0.013	0.742
West half	12	49.598	-0.037	0.570	2.56	0.37	-15.4	0.023	1.353
East half	15	50.403	-3.207	0.537	2.83	0.17	-8.40	0.016	0.711

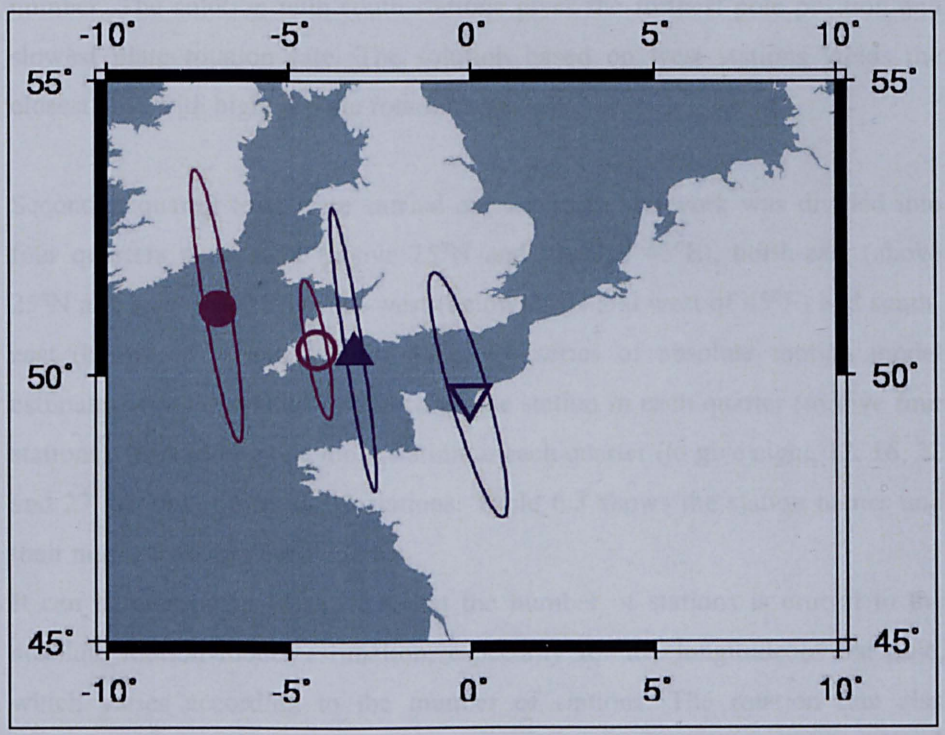

Figure 6.5. Pole location plots for absolute motion from different half tests. Open circles are when using north half stations; solid circles are for south half stations; open inverted triangles are for west half stations; and solid triangles are for east half stations.

The four regional solutions given in **Figure 6.5** yield solutions which are significantly different. All four confidence ellipses are distinct, and they do not contain the remaining pole positions. This suggests that either the a posteriori variances are too optimistic or a part of the observed velocity field is due to ongoing crustal motion which is not accounted for in the rigid plate model. Another likely reason is that the least squares solution depends on the distribution of the GPS stations, and that there is a trade off between the estimates of the unknowns. The velocity vector at a GPS point may be explained equally well by several combinations. That is, a slow plate rotation rate together with rotation pole located further away from the plate is able to yield similar station velocity based on a closer pole with higher rotation rate. In fact an inspection of pole positions together with rotation rate estimates in Table 6.2 confirms the sensitivity of the solution to the station positions and number. The solution with south stations gives the furthest pole position and slowest plate rotation rate. The solution based on west stations yields the closest pole with highest plate rotation rate.

Secondly, quarter tests were carried out where the network was divided into four quarters north-west (above 25°N and west of 45°E), north-east (above 25°N and east of 45°E), south-west (below 25°N and west of 45°E) and south-east (below 25°N and east of 45°E). A series of absolute motion model estimates were computed by selecting one station in each quarter (to give four stations), then adding one more station to each quarter (to give eight, 12, 16, 22 and 27 stations) up to all 33 stations. Table 6.3 shows the station names and their number used in each quarter.

It can be seen from Figure 6.6 that the number of stations is crucial to the absolute motion model estimation, especially for the longitude of the pole, which varies according to the number of stations. The rotation rate also changes, i.e. as the pole moves to the west, the rotation rate decreases.

Table 6.3. Number and station names used in each quarter test.

	# stns	Stations
Test 1	4	HALY, BAHR, YIBL, F033
Test 2	8	Test 1 stations plus F006, F029, F078, F012
Test 3	12	Test 2 stations plus F027, F030, SOLA, F013
Test 4	16	Test 3 stations plus F024, F037, F036, F005
Test 5	22	Test 4 stations plus F008, F026, F039, F040, F019, DATM
Test 6	27	Test 5 stations plus F007, F010, F020, F035, F077
Test 7	33	All stations included

Table 6.4. Different absolute Arabian plate motion parameters when applying quarter tests. Uncertainty in the pole location is given by semi-major (σ_{maj}) and semi-minor (σ_{min}) axes of the 1σ error ellipse (AZ is the azimuth of the major axis) and # stns is the number of stations used in plate motion parameters estimation.

	# stns	Lat [°]	Lon [°]	Rate [°/Ma]	σ_{maj} [°]	σ_{min} [°]	AZ [°]	σ_{rate} [°/Ma]	χ^2
Test 1	4	50.234	-0.469	0.551	1.33	0.19	-11.8	0.009	0.938
Test 2	8	50.363	-2.013	0.544	1.29	0.18	-11.3	0.009	1.478
Test 3	12	50.401	-2.343	0.542	1.26	0.17	-11.1	0.008	1.321
Test 4	16	50.405	-2.782	0.540	1.23	0.17	-10.8	0.008	1.215
Test 5	22	50.399	-3.221	0.538	1.18	0.16	-10.6	0.008	1.020
Test 6	27	50.507	-4.064	0.533	1.13	0.15	-10.2	0.007	0.999
Test 7	33	50.420	-4.089	0.533	1.03	0.15	-10.9	0.006	1.053

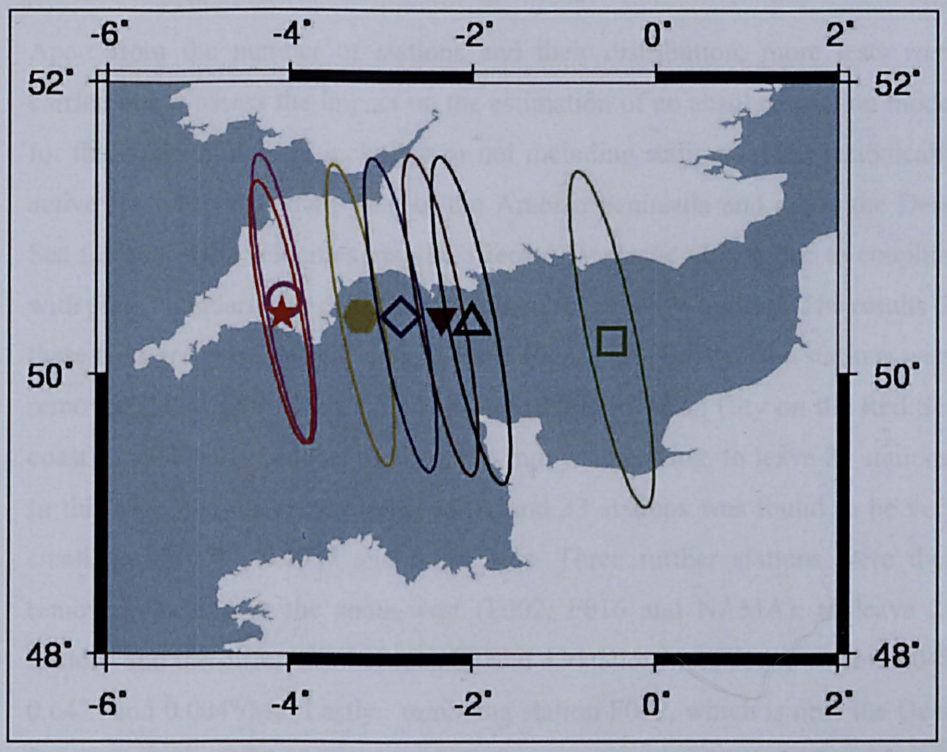

Figure 6.6. Pole location plots for absolute motion from different quarter tests. Open square is test 1 when using 4 stations; open triangle is test 2 when using 8 stations; solid inverted triangle is test 3 when using 12 stations; open diamond is test 4 when using 16 stations; solid pentagon is test 5 when using 22 stations; open circle is test 6 when using 27 stations; and solid star is test 7 when using all 33 stations.

The same trade off between the distance of the rotation pole to the GPS stations and the plate rotation rate is also apparent in the present test solutions. The Test 1 with only 4 GPS points results in the closest pole with the fastest rotation rate. The rotation pole is pushed further away from the Arabian plate with the accompanying decrease in the rotation rate as the number of stations included in the model increases. The solution becomes stable after 27 stations. This clearly demonstrates that absolute plate motion estimates based on a few stations may not be reliable at all. There should be sufficient number of GPS stations to form a robust configuration to be able to resolve the trade off problem.

Apart from the number of stations and their distribution, more tests were carried out to assess the impact on the estimation of an absolute motion model for the Arabian plate of including or not including stations in the tectonically active region to the south-west of the Arabian peninsula and along the Dead Sea fault, as their velocities may be affected by elastic effects due to coupling with plate boundaries or distributed strain in these active regions. The results of these tests are presented in Table 6.5 and Figure 6.7. Firstly, two stations were removed (F074 in the Farasan Islands and F001 in Jazan City on the Red Sea coast), which had residuals of about 1.4 mm/yr in easting, to leave 31 stations. In this case, the difference between 31 and 33 stations was found to be very small, i.e. 0.001°, 0.193° and 0.002°/Ma. Three further stations were then removed, located in the south-west (F002, F016 and NAMA), to leave 28 stations and the difference between 28 and 33 stations was found to be 0.004°, 0.647° and 0.004°/Ma. Lastly, removing station F009, which is near the Dead Sea fault to leave 27 stations, gave differences between 27 and 33 stations of 0.087°, 0.025° and 0.000°/Ma. However, all four estimates are almost the same size with similar error ellipses and the reduced χ^2 is close to one for all four estimations.

Table 6.5. Different absolute Arabian plate motion parameters when excluding a number of stations in the deforming regions. Uncertainty in the pole location is given by semi-major (σ_{maj}) and semi-minor (σ_{min}) axes of the 1σ error ellipse (AZ is the azimuth of the major axis), and # stns is the number of stations used in plate motion parameters estimation.

		Lat	Lon	Rate	σ_{maj}	σ_{min}	AZ	σ_{rate}	χ^2
Excluded stns	# stns	[°]	[°]	[°/Ma]	[°]	[°]	[°]	[°/Ma]	
	33	50.420	-4.089	0.533	1.03	0.15	-10.9	0.006	1.053
F001 & F074	31	50.421	-3.896	0.535	1.03	0.15	-10.8	0.007	1.091
F001, F074, F002, F016 & NAMA	28	50.416	-3.442	0.537	1.04	0.15	-10.8	0.007	1.002
F001, F074, F002, F016, NAMA & F009	27	50.507	-4.064	0.533	1.13	0.15	-10.2	0.007	0.996

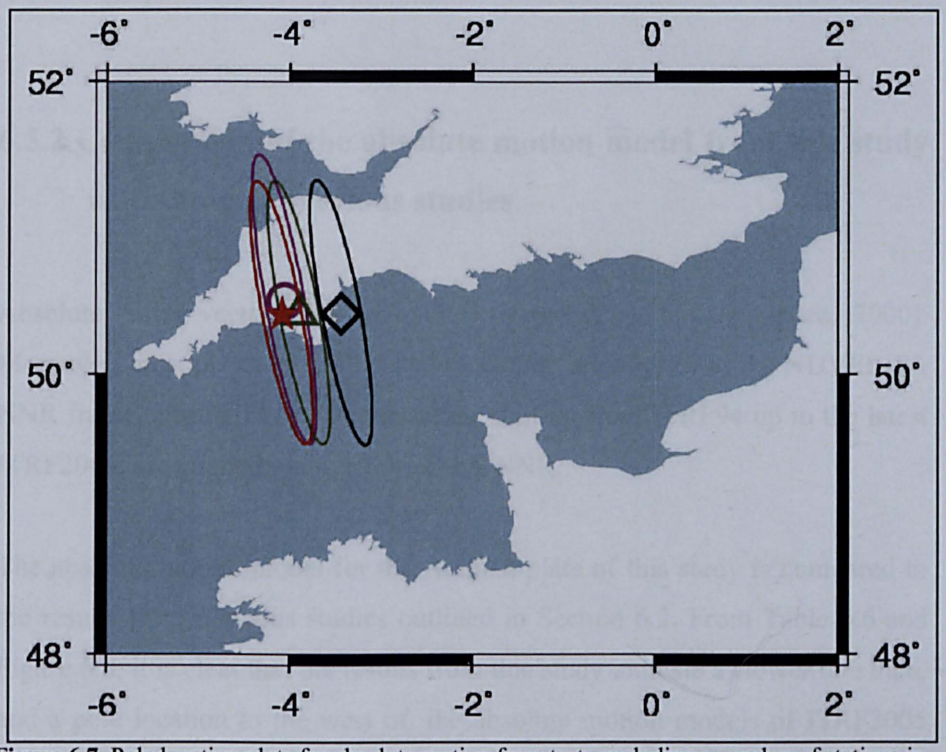

Figure 6.7. Pole location plots for absolute motion from tests excluding a number of stations in the deforming regions. Solid star is this study when using 33 stations; open circle is when using 27 stations; open triangle is when using 31 stations; open diamond is when using 28 stations.

Further statistical analysis showed that the reduced χ^2 was very close to one for all four estimations and the Fisher test showed that all four estimations were effectively of equal quality. Overall, therefore, it can be concluded that excluding these stations had a small effect on the absolute plate motion estimation, which may be because the velocities of these stations are not affected by local deformation or that their small number out of a total of 33 stations has little effect on absolute plate motion estimation. Therefore, for this study, we consider the use of 33 stations to provide the preferred absolute plate motion estimates for the Arabian plate.

6.5.2 Comparison of the absolute motion model from this study with those of previous studies

Absolute Euler vectors are completely frame dependent [Lavallee, 2000]. Moreover, most previous studies and this study are aligned to the NUVEL-1A NNR frame, since all ITRF frame series, starting from ITRF94 up to the latest ITRF2005, are aligned to the NUVEL-1A NNR.

The absolute motion model for the Arabian plate of this study is compared to the results from previous studies outlined in Section 6.2. From Table 6.6 and Figure 6.8, it is clear that the results from this study indicate a slower rate than, and a pole location to the west of, the absolute motion models of ITRF2005 [Altamimi *et al.*, 2007], APKIM2005 [Drewes, 2006], CGPS2004 [Prawirodirdjo and Bock, 2004] and REVEL-2000 [Sella *et al.*, 2002], which only used five, eight, seven and two stations, respectively, all on the northern half of the Arabian plate. It is clear that the results from this study indicate a faster rate than, and a pole location to the east of, the absolute motion model of VIGN2006 [Vigny *et al.*, 2006], who used ten stations but with most of them on the southern half of the Arabian plate. Also, the results from this study indicate a slower rate than, and a pole location to the east of APKIM2000 [Drewes and Angermann, 2001], who used two stations on the northern half of the Arabian plate and a third station to the north, near the Bitlis suture.

Considering again Table 6.6 and Figure 6.8, it is clear that the results from this study agree most closely with the absolute motion model GSRM v1.2 of Kreemer *et al.* [2003]. However, it should be noted that our uncertainties are three to four times better for the pole location. Kreemer *et al.* [2003] only used two stations with BAHR on the north-east and SANA on the south-west of the Arabian plate. The absolute motion model GSRM-NNR-2 [Kreemer *et al.*, 2006] is not as close as the previous model. There are two possible reasons for

this: firstly, the no-net-rotation condition is ensured for ITRF2000 by minimizing the three rotation rate parameters between ITRF2000 and NNR-NUVEL-1A and the ITRF2005 is aligned to ITRF2000 [Altamimi *et al.*, 2007]. The no-net-rotation condition of GSRM-NNR-2 is significantly different from that of ITRF2005 [Kreemer *et al.*, 2006]. However, Altamimi *et al.* [2007] argue that the accuracy level of the no-net-rotation condition implementation is still about 2 mm/yr. Secondly, the updated model included additional data. However, our best estimate still agrees to within 1σ with GSRM-NNR-2.

Comparisons with NNR-NUVEL-1A [DeMets *et al.*, 1994] show that this is close in rate and longitude to the results from this study, but significantly different in latitude (by 5.22°). Furthermore, the difference between the results from this study and the geological and geophysical study carried out by Bird [2003] were found to be 3.750°, 2.111° and -0.060°/Ma.

The absolute motion model for the Arabian plate of this study is compared to the results from Almotairi [2006] and Table 6.6 and Figure 6.8 show that the results from this study indicate a faster rate, and a pole location that is higher in latitude; the difference between the results from this study and Almotairi [2006] were found to be 0.85°, 0.31° and 0.025°/Ma. From a comparison of the station velocities based on the absolute motion models, the mean differences in the northing and easting components from Almotairi [2006] were 0.99 mm/yr with a standard deviation of ±0.06 mm/yr, and 2.22 mm/yr with a standard deviation of ±0.14 mm/yr, respectively. The associated RMS differences were 0.99 mm/yr in northing and 2.22 mm/yr in easting. Furthermore, the significant and new contribution of this study over Almotairi [2006] is the reliability of this study, since it involved the computation of an updated estimate for the absolute and relative motion of the Arabian plate Euler pole and rotation rate, now in ITRF2005, using a near global reference frame and a new processing strategy, as outlined in section 4.4.

Table 6.6. Absolute Arabian plate motion parameters from this study and previous studies. Uncertainty in the pole location is given by semi-major (σ_{maj}) and semi-minor (σ_{min}) axes of the 1σ error ellipse (AZ is the azimuth of the major axis) and # stns is the number of stations used in plate motion parameter estimations.

Reference	Model	# stns	Lat [°]	Lon [°]	Rate [°/Ma]	σ_{maj} [°]	σ_{min} [°]	AZ [°]	σ_{rate} [°/Ma]
This study		33	50.420	-4.089	0.533	1.03	0.15	-10.9	0.006
Altamimi *et al.* [2007]	ITRF2005	5	49.642	5.061	0.579	2.28	0.58		0.019
Almotairi [2006]		27	49.57	-3.77	0.508	0.68	0.14		0.009
Kreemer *et al.* [2006]	GSRM-NNR-2	9	52.525	-2.229	0.549				
Vigny *et al.* [2006]	VIGN2006	10	52.59	-15.74	0.461	2.98	0.42	81	0.011
Drewes *et al.* [2006]	APKIM2005	8	49.48	4.83	0.596	3.27	0.83		0.029
Prawirodirdjo & Bock [2004]	CGPS2004	7	51.341	3.576	0.546	1.49	0.28	157	0.014
Bird et al [2003]	PB2002		46.67	-6.20	0.593				
Kreemer *et al.* [2003]	GSRM v1.2	2	50.6	-2.7	0.550	3.4	0.6	35	0.007
Sella *et al.* [2002]	REVEL-2000	2	51.47	2.89	0.521	3.1	0.7	-70	0.024
Drewes & Angermann [2001]	APKIM2000	3	51.8	-9.3	0.467	38.7	2.8		0.155
DeMets *et al.* [1994]	NNR-NUVEL-1A		45.2	-4.5	0.546				

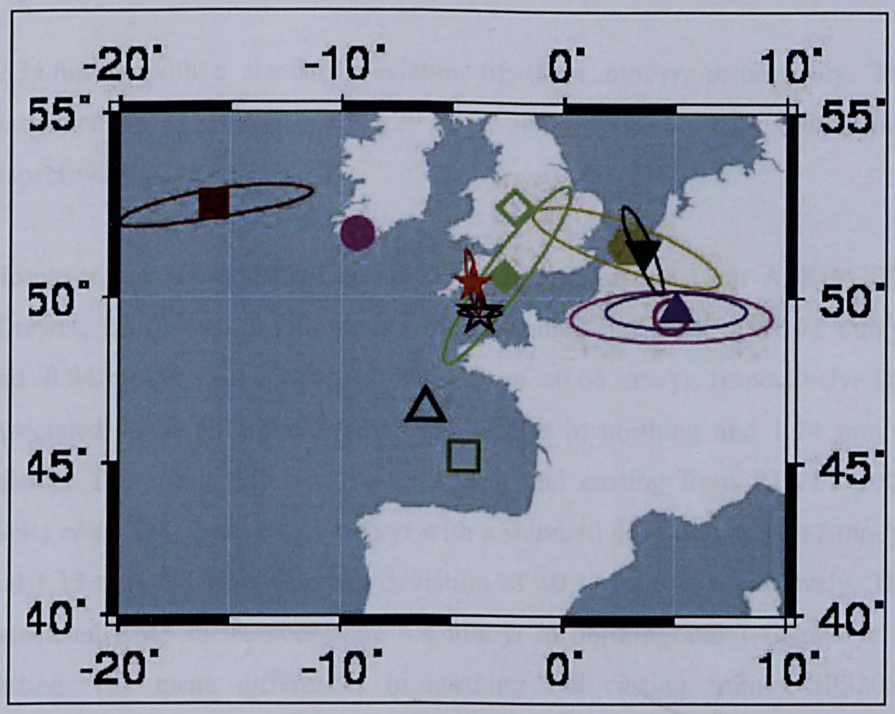

Figure 6.8. Pole location plots for absolute motion from this study and other studies. Solid star is this study; open star is Almotairi [2006]; solid triangle is ITRF2005 [Altamimi *et al.*, 2007]; solid square is VIGN2006 [Vigny *et al.*, 2006]; open circle is APKIM2005 [Drewes, 2006]; solid inverted triangle is CGPS2004 [Prawirodirdjo and Bock, 2004];open triangle is PB2002 [Bird *et al.*, 2003]; solid diamond is GSRM v1.2 [Kreemer *et al.*, 2003]; open diamond is GSRM-NNR-2 [Kreemer *et al.*, 2006]; solid pentagon is REVEL-2000 [Sella *et al.*, 2002]; solid circle is APKIM2000 [Drewes and Angermann, 2001]; and open square is NNR-NUVEL-1A [DeMets *et al.*, 1994].

From a comparison of the station velocities based on the absolute motion models, the mean differences in northing and easting from ITRF2005 [Altamimi *et al.*, 2007] were 1.98 mm/yr with a standard deviation of ±0.63 mm/yr, and -0.14 mm/yr with a standard deviation of ±0.55 mm/yr, respectively. The associated RMS differences were 2.07 mm/yr in northing and 0.56mm/yr in easting, whereas the mean difference in northing and easting from GSRM v1.2 [Kreemer *et al.*, 2003] were only -0.11 mm/yr with a standard deviation of ±0.12 mm/yr and -0.84 mm/yr with a standard deviation of ±0.14 mm/yr, respectively, and associated RMS differences of only 0.17 mm/yr in northing and 0.85 mm/yr easting. These small differences in station velocities confirm the good agreement between this study and GSRM v1.2 in both the pole location and the rotation rate. However, the mean difference in northing and easting from GSRM-NNR-2 [Kreemer *et al.*, 2006] is higher at 1.29 mm/yr with a standard deviation of ±0.04 mm/yr and

-2.34 mm/yr with a standard deviation of ±0.11 mm/yr, respectively. The associated RMS differences are 1.29 and 2.34 mm/yr in northing and easting, respectively.

Moreover, the mean differences in northing and easting from APKIM2005 [Drewes, 2006] were 0.99 mm/yr with a standard deviation of ±0.71 mm/yr and -0.94 mm/yr with a standard deviation of ±0.66 mm/yr, respectively. The associated RMS differences were 1.21 mm/yr in northing and 1.14 mm/yr easting. The mean differences in northing and easting from REVEL-2000 [Sella *et al.*, 2002] were 4.40 mm/yr with a standard deviation of ±0.17 mm/yr and 1.13 mm/yr with a standard deviation of ±0.17 mm/yr, respectively. The associated RMS differences were 4.4 mm/yr in northing and 1.14 mm/yr in easting. The mean differences in northing and easting from CGPS2004 [Prawirodirdjo and Bock, 2004] were 3.55 mm/yr with a standard deviation of ±0.32 mm/yr and -0.09 mm/yr with a standard deviation of ±0.28 mm/yr, respectively. The associated RMS differences were 3.57 mm/yr in northing and 0.28 mm/yr in easting. The mean differences in northing and easting from VIGN2006 [Vigny *et al.*, 2006] were 1.15 mm/yr with a standard deviation of ±0.83 mm/yr and 0.66 mm/yr with a standard deviation of ±0.78 mm/yr, respectively. The associated RMS differences were 1.41 mm/yr in northing and 1.02 mm/yr in easting. The mean differences in northing and easting from APKIM2000 [Drewes and Angermann, 2001] were 4.40 mm/yr with a standard deviation of ±0.17 mm/yr and 1.13 mm/yr with a standard deviation of ±0.17 mm/yr, respectively. The associated RMS differences were 4.40 mm/yr in northing and 1.14 mm/yr in easting. The mean differences in northing and easting from NNR-NUVEL-1A [DeMets *et al.*, 1994] were -3.88 mm/yr with a standard deviation of ±0.27 mm/yr and 3.68 mm/yr with a standard deviation of ±0.22 mm/yr, respectively. The associated RMS differences were 3.89 mm/yr in northing and 3.69 mm/yr in easting. The north absolute velocity of this study shows slowing of the Arabian plate by 12% compared to the geological study by NNR-NUVEL-1A [DeMets *et al.*, 1994]. For example, at the longitude of HALY (36°) in the north-west, BAHR (50°) in the east and

F001 (42°) in the south-west, the velocities in the north direction are 24.40 mm/yr, 30.86 mm/yr and 27.5 mm/yr, respectively, less than those predicted by DeMets *et al.*, [1994], namely, 27.85 mm/yr, 35.12 mm/yr and 31.34 mm/yr, respectively. The mean differences in northing and easting from PB2002 [Bird, 2003] were -6.59 mm/yr with a standard deviation of ±0.33 mm/yr and -0.50 mm/yr with a standard deviation of ±0.46 mm/yr, respectively. The associated RMS differences were 6.59 mm/yr in northing and 0.68 mm/yr in easting. Also, the north absolute velocity of this study shows a slowing of the Arabian plate by 19% compared to the geological and geophysical study by the PB2002 model [Bird, 2003], where for the same stations HALY, BAHR and F001, the velocities in the north direction are 24.40 mm/yr, 30.86 mm/yr and 27.5 mm/yr, respectively, less than those predicted by *Bird* [2003], namely, 30.38 mm/yr, 37.88 mm/yr and 34.05 mm/yr, respectively. It can be concluded that the result of this study is significantly different from recent geodetic published studies such as Altamimi *et al.* [2007], Drewes [2006] and Vigny *et al.* [2006], but this does not mean that the previous studies are in error just that they lacked evenly distributed geodetic data on the Arabian plate. This was confirmed by the subset result in this study agreeing with the pole of Altamimi *et al.* [2007] if similar stations in terms of geometry and distribution are used.

The trade off between the estimates of plate rotation pole and rotation rate also becomes evident in a comparison of these various studies. The solution of Vigny et al. [2006] yields the smallest rotation rate with rotation pole furthest away from the Arabian plate. This is followed by APKIM2000 [Drewes and Angermann, 2001]. The solutions with the largest rate and smallest pole distance are ITRF2005 [Altamimi et al. 2007] and APKIM2005 [Drewes at al. 2006]. Our tests using varying number of stations reveal that the least squares solution becomes stable with 27 or more stations in the model._It is clear, therefore, that this study is a new contribution to the knowledge of Arabian plate motion, since this study is more reliable as it is the first study using evenly distributed stations and these stations have a minimum of four years of time span, these two factors being crucial for plate motion estimation.

According to the estimations of residual velocities and their uncertainties (see figure 6.4) Arabian plate is rigid, because they can be considered as non-significant. However, residual velocities have different orientation for different parts of Arabian plate and the estimates of the pole location for different studies are different. This can be explained by either systemic errors or different partial movements of parts of Arabian plate. The fact that the configuration of GPS networks in different studies is different – using different stations from different parts of the Arabian plate (including even stations from neighbouring plate (e.g. Altamimi *et. al.*, [2007]) can explain the differences in the pole location estimation. The author assumes that this fact indicates that the differences in residual velocities in different parts of the Arabian plate are mostly due to existing partial movements inside the main plate. In other words, Arabian plate can be considered as non-rigid.

This study uses maximum possible stations and best possible station distribution and the conclusions can be considered as most representative. According to that it is expected that Arabian plate has parts with different movements, but additional research need to be conducted in order to confirm this conclusion. Other type of earth observations like InSAR data can be used in order to compliment the recent study and to provide independent proof of the major findings in this study.

Figure 6.9 shows the absolute velocities estimates for the GPS stations in this study based on the model of this study and the models from previous studies. For more details on the station velocity estimates from the model of this study and the differences between these and previous studies, see Appendix F.

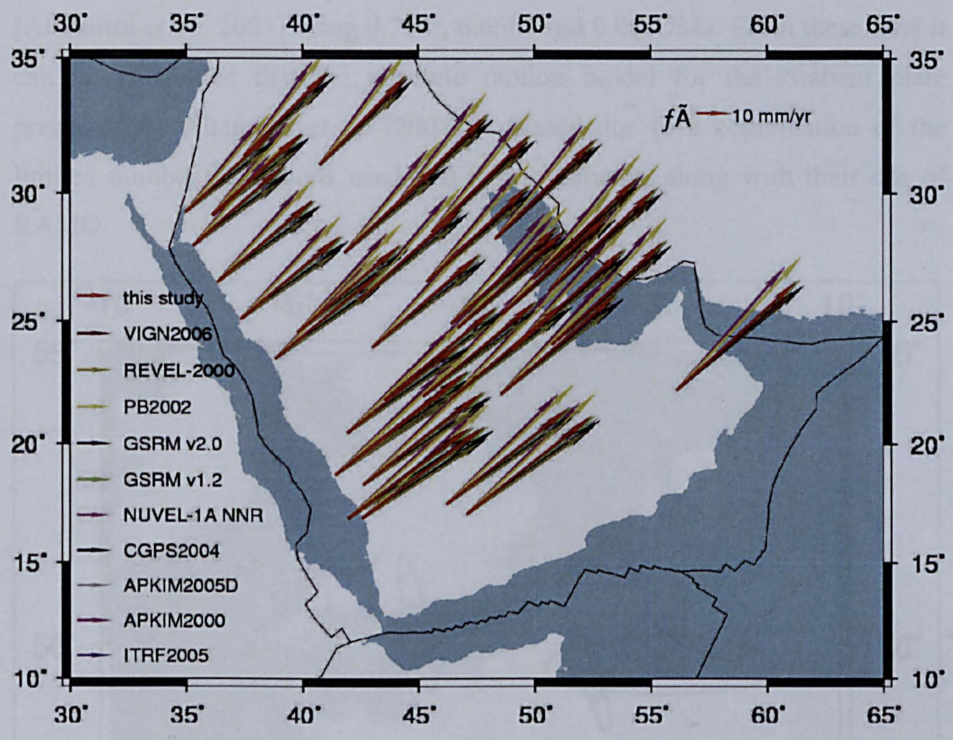

Figure 6.9. Absolute velocity estimates for the GPS stations in this study based on the model of this study and the models from previous studies. VIGN2006 [Vigny *et al.*, 2006]; REVEL-2000 [Sella *et al.*, 2002]; PB2002 [Bird *et al.*, 2003]; GSRM-NNR-2 [Kreemer *et al.*, 2006]; GSRM v1.2 [Kreemer *et al.*, 2003]; NUVEL-1A NNR [DeMets *et al.*, 1994]; CGPS2004 [Prawirodirdjo and Bock, 2004]; APKIM2005 [Drewes, 2006]; APKIM2000 [Drewes and Angermann, 2001]; ITRF2005 [Altamimi *et al.*, 2007].

Figure 6.10 shows the pole location from ITRF2005 [Altamimi *et al.*, 2007], which is clearly significantly different to the preferred estimate of this study. For a fairer comparison with ITRF2005 [Altamimi *et al.*, 2007], the author re-estimated the absolute plate motion model using a similar number of stations and similar geometry (BAHR, SOLA (GPS station), HALY, F009 and RAMO) to ITRF2005 [Altamimi *et al.*, 2007]. The re-estimated absolute motion model with five stations was found to be 49.317°N, 3.233°E and 0.572°/Ma; the difference from ITRF2005 [Altamimi *et al.*, 2007] being 0.325°, 1.828° and 0.007°/Ma. The author then re-estimated the absolute motion model using only four GPS stations (BAHR, SOLA, HALY and F009), i.e. without RAMO as it has been reported that this station is on the Sinai micro-plate [Wdowinski *et al.*, 2004]. The re-estimated absolute motion model with four stations was found to be 50.379°N, 1.605°W and 0.54°/Ma; the difference from ITRF2005

[Altamimi *et al.*, 2007] being 0.737°, 6.666° and 0.039°/Ma. From these tests it can be concluded that the absolute motion model for the Arabian plate presented by Altamimi *et al.* [2007] is biased due to a combination of the limited number of stations used and their geometry, along with their use of RAMO.

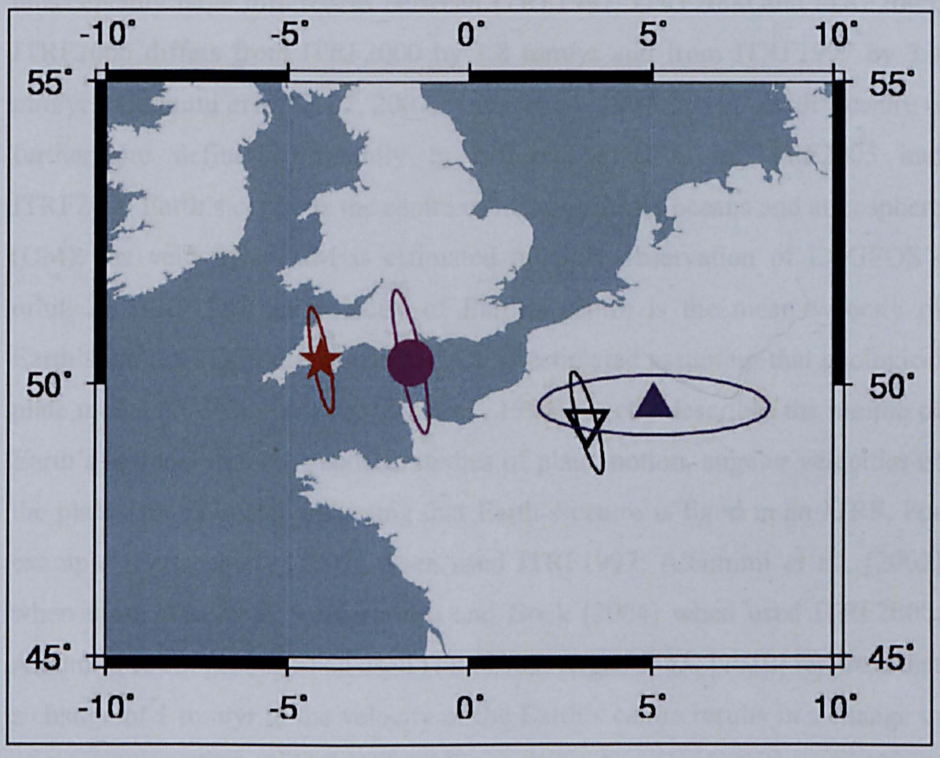

Figure 6.10. Pole location plots for absolute motion from different tests in this study and previous studies. Solid star is this study using 33 stations; solid triangle is ITRF2005 [Altamimi *et al.*, 2007]; open inverted triangle is this study when using five stations with similar geometry to ITRF2005 [Altamimi *et al.*, 2007]; and solid circle is this study when using four stations with similar geometry to ITRF2005 [Altamimi *et al.*, 2007].

6.6 **Relative Arabian rigid plate motion**

One of the main aims of satellite geodesy is positioning of points on the Earth's surface by determining the point coordinates and their velocities (evaluation in time) in a reference frame. In order to realize a reference frame, its origin and orientation of the reference frame and their translation rates must be defined precisely. In space geodesy Earth Centred Earth Fixed (ECEF) International Terrestrial Reference Frames (ITRF) have been developed and improved by

IERS having the orientation consistent with the International Celestial Reference Frame (ICRF) and Earth Orientation Parameter (EOP) series and the origin at the Earth's centre at a selected time epoch.

The translation rate (velocity) of Earth's centre is uncertain, as is evident in the unacceptably large differences between ITRF1997, ITRF2000 and ITRF2005. ITRF2005 differs from ITRF2000 by 1.8 mm/yr and from ITRF1997 by 3.4 mm/yr [Altamimi *et al.*, 2002, 2007; Argus *et al.*, 2007, 2010]. Earth's centre is furthermore defined differently in different ITRF's. In ITRF2005 and ITRF2000 Earth's centre is the centre of mass of Earth, oceans and atmosphere (CM); the velocity of CM is estimated by SLR observation of LAGEOS's orbit. In ITRF1997 the velocity of Earth's centre is the mean velocity of Earth's surface (CF); the velocity of CF is estimated assuming that geological plate model NUVEL-1A [DeMets *et al.*, 1994] exactly describes the motion of Earth's surface. In most geodetic studies of plate motion, angular velocities of the plates are estimated assuming that Earth's centre is fixed in an ITRF. For example Sella *et al.*, [2002] when used ITRF1997; Altamimi *et al.*, [2002] when used ITRF2000; Prawirodirjo and Bock [2004] when used ITRF2000; Altamimi *et al.*, [2007] when used ITRF2005. Argus *et al.*, [2010] reported that a change of 1 mm/yr in the velocity of the Earth's centre results in a change in plate angular velocity of 0.012 deg/Myr, and angular velocity estimates depend on the estimate of the velocity of the Earth's centre. Argus *et al.*, [2010] developed a space geodesy plate motion model, GEODVEL which refers to the centre of mass of the solid Earth (CE) and estimates of the velocity of CE. The GEODVEL estimates differ from other geodetic angular velocity estimates partly due to different velocity of the Earth's centre, for instance, 0.028 deg/Myr from REVEL [Sella *et al.*, 2002], 0.015 deg/Myr from ITRF2005 [Altamimi *et al.*, 2007] and 0.068 deg/Myr from NUVEL-1A [Demets *et al.*, 1994] which indicates a slowing down of relative plate motion [Argus *et al.*, 2010]. Demets *et al.*, [2010] reported also that convergence between the Nazca and South America plates across the Peru–Chile trench has also slowed rapidly since 3.16 Ma; the 3.16-Myr-average NUVEL-1A convergence rate is 14 ± 2

mm/yr higher than the GPS estimate for this plate pair, respectively. Lavallee [2000] reported that the relative Euler vectors are frame dependent the effect of an error in defining the velocity origin on relative Euler vectors and model predictions is dependent on the size and direction of the error and the plate/tracking network geometry.

The orientation rate of ITRF should have a geophysical meaning due to plate motions. Therefore the orientation rates are usually aligned to a no net rotation (NNR) frame, such as NNR-NUVEL-1A [Altamimi *et al.*, 2003]. However realization of the NNR constraint may cause biases since it is sensitive to adopted plate geometries and plate motion estimates. Kreemer *et al.*, [2006] reported a few millimetre level differences between various NNR models. Therefore, Geodesists usually look at relative Euler poles because relative Euler poles are independent of the rotational frame used for the GPS, thus one should avoid errors in aligning different solutions to an external frame. The concept of plate tectonics is based on the approximate assumptions that the plates are rigid, plate boundaries are narrow and plate motions are steady during at least last 3 my. Ggeological plate motion models determined from seafloor spreading rates, transform fault azimuths and earthquake slip vectors describe relative motion between plates [DeMets *et al.*, 1990]. Then absolute plate motions can be obtained by using the NNR constraint. The geological plate motion models have some weaknesses: (1) earthquake slip vectors along subduction zones give biased estimates of the direction of relative plate, (2) some plates have few or no spreading rates or transform azimuths along their boundaries, (3) the relative motion between adjacent plates estimated indirectly using a circuit through several plates may be biased if one of the plates in the circuit contains a deforming zone and two or more plates, for instance, in NUVEL-1A Nubia and Somalia are assumed to be part of a single Africa Plate [Argus *et al.*, 2010]. Plate tectonic assumptions and geologic plate motion models can be evaluated by space geodesy based angular velocity vectors which describe present-day motions of the major tectonic plates. Space geodesy based angular velocities and linear velocities referring to the ITRF/the

ECEF-NNR global frame correspond to absolute plate motions, whereas relative angular/linear velocity, referring to a frame fixed to plate, providing relative plate motions is of most interest to geologist and geophysicists. Immediate applications of such relative angular/linear velocities include; (1) identification of stable plate interiors and assessment of intra-plate deformation, (2) assessment of where the plate boundary deformation zone begins, (3) rigorous accounting for precisely where the full relative plate motion is accommodated between the stable plate interiors, (4) unambiguous determination of block rotations in the plate boundary zone relative to the far field (stable part of a plate), and (5) testing whether the geologic plate motion is steady through time or not [Beavan *et al.*, 2002].

6.6.1 The motion of the Arabian plate relative to the Eurasian plate

The author computed a series of relative motion model estimates between the Arabian plate and the Eurasian plate, where the 33 stations used in the absolute Arabian plate estimations were used all the time, while the stations in the Eurasian plate were selected in each test (see table 6.7). Furthermore, the southern margin of the Eurasian plate is subject to deformation as a result of its collision with the Nubian plate, the Arabian plate, the Anatolian plate and the Indian plate. The first test started with 29 stations (excluding LAHZ, MATE, NOT1 and TRAB) on the southern margin of the Eurasian plate. The 29 stations were ARTU, BJFS, BOR1, BRUS, CAGL, DAEJ, GLSV, GRAS, GUAO, IRKT, JOZE, KIT3, KUNM, MDVJ, METS, NRIL, ONSA, POL2, POLV, POTS, SFER, TEHN, TROM, ULAB, VILL, WSRT, WTZR, WUHN and ZIMM. In test 2, 19 stations were used with another 10 stations excluded, namely CAGL, SFER and TEHN in the southern margin of the Eurasia plate, BIFS, DAEJ, IRKT, KUNM, ULAB and WUHN near the margin on the east and south east, and TROM in the north of the Eurasian plate because of possible horizontal motions as a result of postglacial rebound. It can be seen in

Table 6.8 that the results of the two tests are close to each other, with the differences in latitude, longitude and rate being 0.56°, 0.36° and 0.012 °/Ma, respectively, but χ^2 is very large for both of tests at 19.56 and 7.24. Therefore, the relative parameters were estimated by selecting stations from these 19 stations in test 2 with χ^2 closest to one. The result was test 3, where seven stations were used (see Table 6.7 for stations used in each test, where all of them in Europe had χ^2 = 1.21). Then more tests were carried out by adding more stations to test 3. In test 4, five stations in Asia (KIT3, POL2, GUAO, NRIL, and ARTU) were added to the test 3 stations, but the result again shows a large value for χ^2 (7.23). In test 5, KIT3 and POL2 were excluded since these are located on the northern margin of the deformation in the Tien Shan range, POL2 being in the east and KIRT on the west [Shen et al., 2000] [Larson et al., 1999]. The result of this test showed again a large χ^2 (6.34). Hence, in test 6 two more stations were excluded (GUAO and NRIL) and this test was carried out using eight stations, the seven stations used in test 3 and the ARTU station in Asia. The result showed a low χ^2 (1.32). More tests were carried out to include more stations in Europe, so the stations in test 3 and seven more stations (BOR1, GRAS, JOZE, METS, MDVJ, ONSA, POLV) were used in test 7, but the result showed χ^2 (1.98) to be larger than test 3 (1.21). Therefore, test 8 was carried out where METS and ONSA in Scandinavia were excluded and the result showed χ^2 (1.38) to be larger than in test 3 (1.21).

Table 6.7. Number and station names used in each Arabian and Eurasian relative motion test in this study

	# stns	Stations
Test 1	29	Excludes LAHZ, MATE, NOT1, TRAB
Test 2	19	Test 1 stations excluding BIFS, CAGL, DAEJ, IRKT, KUNM SFER, , TEHN, TROM , ULAB, WUHN
Test 3	7	BRUS, GLSV, POTS, VILL, WSRT,WTZR, ZIMM
Test 4	12	Test 3 stations plus ARTU, GUNO, KIT3, NRIL, POL2
Test 5	10	Test 3 stations plus ARTU, GUAO, NRIL
Test 6	8	Test 3 stations plus ARTU
Test 7	14	Test 3 stations plus BOR1, GRAS, JOZE, METS, MDVJ, ONSA, POLV
Test 8	12	Test 3 stations plus BOR1, GRAS, JOZE, MDVJ, POLV

Table 6.8. Relative Arabian and Eurasian motion parameters from different tests in this study. Uncertainty in the pole location is given by semi-major (σ_{maj}) and semi-minor (σ_{min}) axes of the 1σ error ellipse (AZ is the azimuth of the major axis) and # stns is the number of stations used in each parameters estimation.

		Lat	Lon	Rate	σ_{maj}	σ_{min}	AZ	σ_{rate}	χ^2
	# stns	[°]	[°]	[°/Ma]	[°]	[°]	[°]	[°/Ma]	
Test 1	29	27.73	19.12	0.423	0.53	0.25	-1.9	0.0083	19.56
Test 2	19	27.17	18.76	0.411	0.55	0.28	-0.2	0.0084	7.24
Test 3	7	28.17	18.93	0.431	0.56	0.40	-17.8	0.010	1.21
Test 4	12e	27.34	19.02	0.410	0.55	0.29	-0.6	0.0084	7.23
Test 5	10	27.21	18.98	0.414	0.55	0.30	-0.8	0.0085	6.34
Test 6	8	28.50	18.81	0.435	0.53	0.31	-5.4	0.0088	1.32
Test 7	14	28.21	18.69	0.431	0.54	0.32	-5.4	0.009	1.98
Test 8	12w	27.94	18.96	0.426	0.54	0.34	-5.7	0.0092	1.38

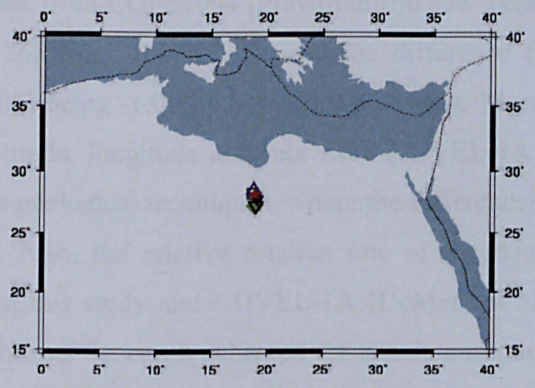

Figure 6.11. Pole location plots for relative motion between the Arabian and Eurasian plate from different tests in this study. Solid inverted triangle is test 1 when using 29 stations; solid diamond is test 2 when using 19 stations; solid star is test 3 when using 7 stations; solid pentagon is test 4 when using 12 stations (test 3 stations and 5 stations in Asia); open square is test 5 when using 14 stations; open diamond is test 6 when using 12 stations (all of them in Europe); open triangle is test 7 when using 8 stations; and open inverted triangle is test 8 when using 10 stations (test 3 stations and 3 stations in Asia).

It can be seen from Table 6.8 and Figure 6.11 that the differences between the tests are small in pole location and rate, but they vary in χ^2. Therefore, the author's preferred estimation for this study is the result of test 3, as χ^2 is the smallest.

The estimated relative motions of the Arabian plate with respect to the Eurasian plate from this study were 28.17° N, 18.93° E and 0.431 °/M (Table 6.9 and Figure 6.12) and this confirms the results from a number of previous studies, where the pole is close (within 1σ) in location and rate to those of previous studies using geodetic techniques, since the difference from REIL2006 [Reilinger *et al.*, 2006] is -0.23°, 0.53° and 0.003 °/Ma, the difference from MCCL2003 [McClusky *et al.*, 2003] being 0.77°, 0.53° and 0.031 °/Ma, the difference from VERN2004 [Vernant *et al.*, 2004] being 0.270°, -0.57° and 0.021 °/Ma and the difference from GSRM v1.2 [Kreemer *et al.*, 2003] being 1.97°, -1.47° and -0.006 °/Ma, this difference being higher than the previous ones, but still within (1σ). However, this study differs, especially in longitude with other studies using geodetic techniques. For example, the difference from REVEL-2000 [Sella *et al.*, 2002] being 1.95°, -3.94° and 0.004

°/Ma, the difference from CGPS2004 [Prawirodirdjo and Yehuda Bock, 2004] being 0.663°, -4.268° and -0.008 °/Ma and the difference from VIGN2006 [Vigny *et al.*, 2006] being -1.00°, 6.81° and 0.067 °/Ma. Moreover, this study differs in both latitude, longitude and rate from NUVEL-1A [DeMets *et al.*, 1994], which uses geological techniques, where the differences are 3.57°, 5.23° and -0.069 °/Ma. Also, the relative rotation rate of the Arabia plate to the Eurasia plate from this study and NUVEL-1A [DeMets *et al.*, 1994] is 12% slower, which confirms the result achieved for absolute rotation. Furthermore, in the European Geosciences Union, General Assembly 2009 (EGU 2009) McClusky *et al.*, [2009] presented a poster showing new relative motion parameters estimated between the Arabian plate and the Eurasian plate as 27.5° ± 0.5°, 17.6° ± 0.3° and 0.404 ± 0.004 Ma. These values are written from the poster by Dr. R. M. Bingley who attended the conference. The author tried to contact the authors of this poster to get confirmation of these values but the author received no reply. However, in this new study the pole is close (within 1σ) in location and rate to McClusky *et al.*, [2009], since the difference is only 0.67°, 1.33° and 0.027 °/Ma.

The difference of the estimated relative motions of the Arabian plate with respect to the Eurasian plate from this study and those from Almotairi [2006] is quite small in rate and latitude, but it is quite large in longitude, since the differences are -0.03°, 3.79° and -0.012 °/Ma. Moreover, a comparison of the station velocities based on the relative motion model between the Arabian and Eurasian plates from this study and Almotairi [2006] was also carried out here it was found that the mean differences in northing and easting between this study and Almotairi [2006] at the 37 common stations were -3.05 mm/yr with a standard deviation of ± 0.02 mm/yr in northing and -0.69 mm/yr with a standard deviation of ± 0.12 mm/yr in easting. The associated RMS differences were 3.05 mm/yr in northing and 0.70 mm/yr in easting. In addition to these differences it should also be noted this study was also able to estimate the relative motions of the Arabian plate with respect to the Nubian and Somalian

plates, whereas Almotairi [2006] could only estimate the relative motion to Eurasian plate only.

Table 6.9. Relative motion models for Arabia-Eurasia from this and previous studies. Uncertainty in the pole location is given by semi-major (σ_{maj}) and semi-minor (σ_{min}) axes of the 1-σ error ellipse (AZ is the azimuth of the major axis).

Reference	Model	Lat [°]	Lon [°]	Rate [°/Ma]	σ_{maj} [°]	σ_{min} [°]	AZ [°]	σ_{rate} [°/Ma]
This study		28.17	18.93	0.431	0.56	0.40	-17.8	0.0103
Almotairi [2006]		28.20	15.14	0.443	0.90	0.15		0.026
Reilinger *et al.* [2006]	REIL2006	28.4	18.4	0.428	1.0	0.9		0.009
Vigny *et al.* [2006]	VIGN2006	28.27	12.12	0.364	2.5	0.66	276	0.017
Vernant *et al.* [2004]	VERN2004	27.9	19.5	0.41	1.4	0.5		0.1
Prawirodirdjo & Bock [2004]	CGPS2004	27.507	23.198	0.439	0.96	0.35	13	0.019
McClusky *et al.* [2003]	MCCL2003	27.4	18.4	0.40	2.5	1.0		0.04
Kreemer *et al.* [2003]	GSRM v1.2	26.2	20.4	0.437	3.7	0.9	77	0.023
Sella *et al.* [2002]	REVEL-2000	26.22	22.87	0.427	2.1	1.1	76	0.029
DeMets *et al.* [1994]	NUVEL-1A	24.6	13.7	0.50	5.2	1.7	-72	0.05

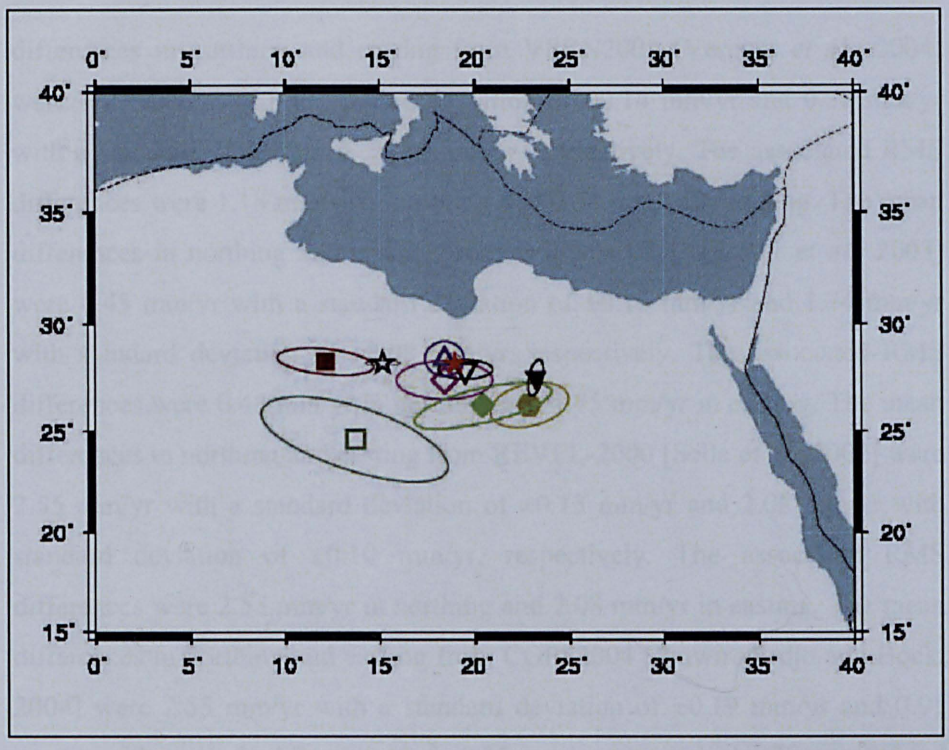

Figure 6.12. Pole location plots for relative motion between the Arabian and Eurasian plates from this and previous studies. Solid star is this study; open star Almotairi [2006]; open triangle is REIL2006 [Reilinger *et al.*, 2006]; solid square is VIGN2006 [Vigny *et al.*, 2006]; open diamond is MCCL2003 [McClusky *et al.*, 2003]; solid inverted triangle is CGPS2004 [Prawirodirdjo and Bock, 2004]; open inverted triangle is VERN2004 [Vernant *et al.*, 2004]; solid diamond is GSRM v1.2 [Kreemer *et al.*, 2003]; solid pentagon is REVEL-2000 [Sella *et al.*, 2002]; and open square is NUVEL-1A [DeMets *et al.*, 1994].

Moreover, for a comparison of the station velocities based on the relative motion model between the Arabian and Eurasian plates, 37 GPS stations relative velocities were estimated using the model computed in this study and the model parameters of other studies, to see the impact of these differences on pole location and rate. It was found that the mean differences in northing and easting from REIL2006 [Reilinger *et al.*, 2006] at the 37 stations were -0.20 mm/yr with a standard deviation of ±0.04 mm/yr and -0.22 mm/yr with a standard deviation of ±0.03 mm/yr, respectively. The associated RMS differences were 0.20 mm/yr in northing and 0.22 mm/yr in easting. The mean differences in northing and easting from MCCL2003 [McClusky *et al.*, 2003] were 0.81 mm/yr with a standard deviation of ±0.23 mm/yr and 0.88 mm/yr with a standard deviation of ±0.25 mm/yr, respectively. The associated RMS differences were 0.84 mm/yr in northing and 0.91 mm/yr in easting. The mean

differences in northing and easting from VERN2004 [Vernant *et al.*, 2004] were 1.17 mm/yr with a standard deviation of ±0.14 mm/yr and 0.51 mm/yr with a standard deviation of ±0.16 mm/yr, respectively. The associated RMS differences were 1.18 mm/yr in northing and 0.54 mm/yr in easting. The mean differences in northing and easting from GSRM v1.2 [Kreemer *et al.*, 2003] were 0.45 mm/yr with a standard deviation of ±0.15 mm/yr and 1.74 mm/yr with standard deviation of ±0.08 mm/yr, respectively. The associated RMS differences were 0.48 mm/yr in northing and 1.75 mm/yr in easting. The mean differences in northing and easting from REVEL-2000 [Sella *et al.*, 2002] were 2.55 mm/yr with a standard deviation of ±0.13 mm/yr and 2.08 mm/yr with standard deviation of ±0.10 mm/yr, respectively. The associated RMS differences were 2.55 mm/yr in northing and 2.08 mm/yr in easting. The mean differences in northing and easting from CGPS2004 [Prawirodirdjo and Bock, 2004] were 2.53 mm/yr with a standard deviation of ±0.19 mm/yr and 0.95 mm/yr with a standard deviation of ±0.15 mm/yr, respectively. The associated RMS differences were 2.54 mm/yr in northing and 0.96 mm/yr in easting. The mean differences in northing and easting from VIGN2006 [Vigny *et al.*, 2006] were -0.99 mm/yr with a standard deviation of ±0.70 mm/yr and -0.11 mm/yr with a standard deviation of ±0.61 mm/yr, respectively. The associated RMS differences were 1.21 mm/yr in northing and 0.61 mm/yr in easting. The mean differences in northing and easting from NUVEL-1A [DeMets *et al.*, 1994] were -7.54 mm/yr with a standard deviation of ±0.47 mm/yr and 1.75 mm/yr with a standard deviation of ±0.53 mm/yr, respectively. The associated RMS differences were 7.56 mm/yr in northing 1.82 mm/yr in easting. It could be concluded from the above and the Figure 6.12 below that the significant difference in the north direction between this study and the geological model NUVEL-1A [DeMets *et al.*, 1994]. Moreover, this study agrees with other studies such as REIL2006 [Reilinger *et al.*, 2006], MCCL2003 [McClusky *et al.*, 2003], VERN2004 [Vernant *et al.*, 2004], REVEL-2000 [Sella *et al.*, 2002] and VIGN2006 [Vigny *et al.*, 2006] in that the Arabian plate slows down in the north direction as it moves to the north and collides with Eurasia. The crustal thickening forms the Zagros and Caucaus mountains, increasing the

gravitational body force that opposes Arabia northward, hence causing the gradual slowing of the Arabia – Eurasia convergence and Red Sea divergence (spreading) [Sella *et al.*, 2002].

Figure 6.13 shows the relative velocity estimates for the GPS for stations in this study based on the model of this study and the models from previous studies between the Arabian and Eurasian plates. See Appendix G for more details on stations velocity estimates from the model of this study and the differences between these and pervious studies.

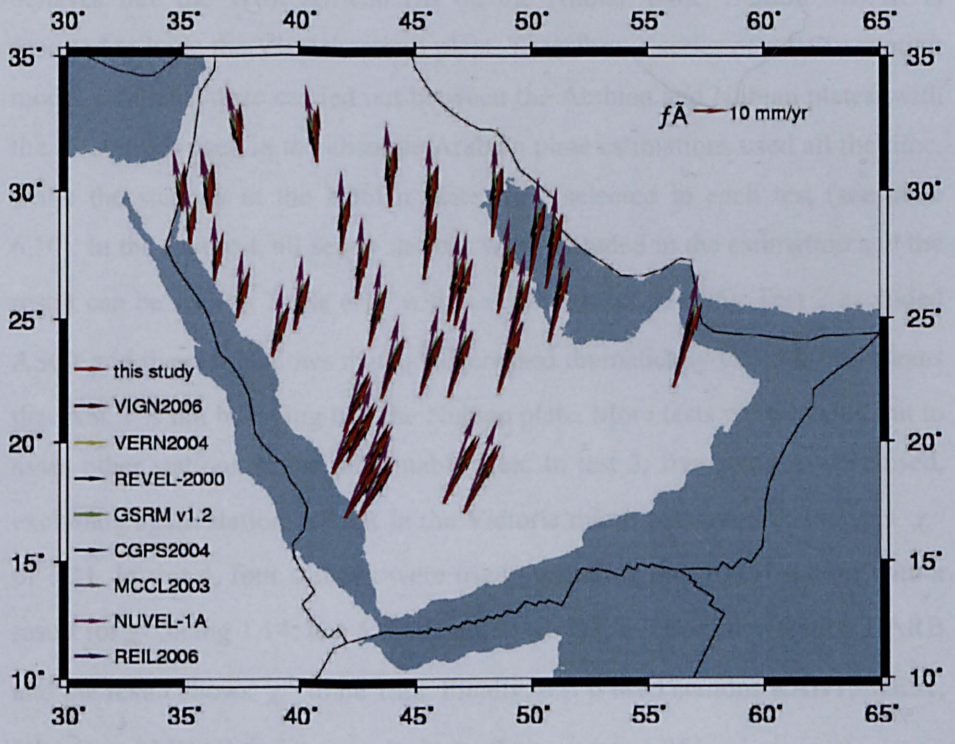

Figure 6.13. Relative velocity estimates for the GPS stations in this study based on the model of this study and the models from previous studies between the Arabian and Eurasian plates. VIGN2006 [Vigny *et al.*, 2006]; VERN2004 [Vernant *et al.*, 2004]; REVEL-2000 [Sella *et al.*, 2002]; GSRM v1.2 [Kreemer *et al.*, 2003]; CGPS2004 [Prawirodirdjo and Bock, 2004]; MCCL2003 [McClusky *et al.*, 2003]; NUVEL-1A [DeMets *et al.*, 1994]; REIL2006 [Reilinger *et al.*, 2006].

6.6.2 The motion of the Arabian plate relative to the Nubian plate

There are no stations on the stable part of the Nubian plate; the only stations available are near the boundary of the plate or in a deformable area. These stations are ASC1, HARB, MAS1, MBAR, NKLG, RABT and SUTH, where ASC1 is in the boundary between the Nubian plate and the South America plate (it has been reported as in the Nubian plate, but in other reports in the South America plate). Stations SUTH and HARB are in a deformable area between the Nubian plate and Somalia. Some have SUTH behaving as the East African rift on the Somalian plate but according to the most recent reports it behaves like the West African rift on the Nubian plate. Station MBAR is reported to be in the Victoria micro plate. Therefore, a series of relative motion model estimates were carried out between the Arabian and Nubian plates, with the 33 stations used in the absolute Arabian plate estimations used all the time, while the stations in the Nubian plate were selected in each test (see table 6.10). In the first test, all seven stations were included in the estimation and the result can be seen in Table 6.11 with a very high χ^2 (24.95). Test 2 excluded ASC1 and the result shows that χ^2 decreased dramatically to 1.34; this means that ASC1 is not behaving like the Nubian plate. More tests were carried out to asses other stations in the deformable area. In test 3, five stations were used, excluding again station MBAR in the Victoria micro plate, and this gave a χ^2 of 1.21. In test 4, four stations were used, excluding the SUTH station with a result for χ^2 being 1.14; test 5 used station SUTH, but excluded station HARB and the result shows χ^2 to be 1.22. Finally, test 6 used stations RABT, MES1, NKLG and MBAR and the result shows that χ^2 was 1.25.

Table 6.10. Number and station names used in each Arabian and Nubian relative motion test in this study.

	# stns	Stations
Test 1	7	ASC1, HARB, MAS1, MBAR, NKLG, RABT and SUTH,
Test 2	6	Test 1 stations excluding ASC1
Test 3	5	Test 2 stations excluding MBAR
Test 4	4	Test 3 stations excluding SUTH
Test 5	4	Test 3 stations excluding HARB
Test 6	4	Test 2 stations excluding HARB and SUTH

Table 6.11. Relative Arabian and Nubian motion parameters from different tests in this study. Uncertainty in the pole location is given by semi-major (σ_{maj}) and semi-minor (σ_{min}) axes of the 1σ error ellipse (AZ is the azimuth of the major axis) and # stns is the number of stations used in each parameters estimation.

		Lat	Lon	Rate	σ_{maj}	σ_{min}	AZ	σ_{rate}	χ^2
	# stns	[°]	[°]	[°/Ma]	[°]	[°]	[°]	[°/Ma]	
Test 1	7	32.59	22.93	0.428	0.57	0.33	-10.7	0.0089	24.95
Test 2	6	31.23	25.25	0.399	0.57	0.35	-9.4	0.009	1.34
Test 3	5	31.44	24.82	0.405	0.61	0.36	-8.2	0.0092	1.21
Test 4	4	31.42	24.47	0.407	0.65	0.36	-6.7	0.0096	1.14
Test 5	4	31.41	24.82	0.404	0.64	0.36	-7.0	0.0094	1.22
Test 6	4	31.19	25.37	0.395	0.61	0.36	-7.0	0.0094	1.25

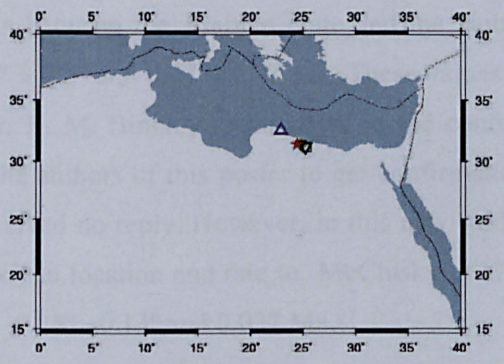

Figure 6.14. Pole location plots for relative motion between the Arabian and Nubian plates from different tests in this study. Open triangle is test 1 when using 7 stations; open inverted triangle is test 2 when excluding ASC1 station; solid inverted triangle is test 3 when using 5 stations; solid star is test 4 when excluding stations ASC1, MBAR, and SUTH; solid diamond is test 5 when excluding stations ASC1, MBAR, HARB; open square is test 6 when excluding stations ASC1, HARB, SUTH.

It can be seen from Table 6.11 and Figure 6.14 that the differences between the tests (2 to 6) are small in pole location and rate, but they vary slightly in χ^2. Therefore, the preferred estimation for this study is the result of test 4, as χ^2 is the smallest.

The estimated relative motion model of the Arabian plate to the Nubian plate from this study was 31.42° N, 24.47° E and 0.407 °/M (Figure 6.15 and Table 6.12) and this confirms the results from most previous studies. The pole is close (within 1σ) in location and rate to those of previous studies using geodetic or geological techniques, since the difference from REIL2006 [Reilinger *et al.*, 2006] is -0.08°, -0.73° and 0.014 °/Ma, the difference from MCCL2003 [McClusky *et al.*, 2003] being 0.92° , -1.23° and 0.037 °/Ma, the difference from CHU1998 [Chu and Gordon, 1998] being -0.08°, 1.47° and 0.004 °/Ma and the difference from JESTIN1994 [Jestin *et al.*, 1994] being 1.17°, 0.77° and -0.011 °/Ma. However, this study differs in longitude and rate from VIGN2006 [Vigny *et al.*, 2006], since the differences were -0.22°, 4.18° and 0.099 °/Ma. Also, this study differs in longitude from REVEL-2000 [Sella *et al.*, 2002], since the differences were 0.16°, -5.08° and 0.007 °/Ma. Furthermore, in the European Geosciences Union, General Assembly 2009 (EGU 2009) McClusky *et al.*, [2009] presented a poster showing new relative

motion parameters between the Arabian plate and the Nubian plate being as 31.7° ± 0.2°, 24.6° ± 0.3° and 0.37 ± 0.01 Ma. These values were written from the poster by Dr. R. M. Bingley who attended the conference. The author tried to contact the authors of this poster to get confirmation of these values, but the author received no reply. However, in this new study the pole is close (within 1σ) as well in location and rate to McClusky *et al.*, [2009], since the difference is only -0.28°, -0.13° and 0.037 Ma.

Table 6.12. Relative motion models for Arabia-Nubia from this study and previous studies. Uncertainty in the pole location is given by semi-major (σ_{maj}) and semi-minor (σ_{min}) axes of the 1-σ error ellipse (AZ is the azimuth of the major axis).

Reference	Model	Lat [°]	Lon [°]	Rate [°/Ma]	σ_{maj} [°]	σ_{min} [°]	AZ [°]	σ_{rate} [°/Ma]
This study		31.42	24.47	0.407	0.65	0.36	-6.7	0.0096
Reilinger *et al.* [2006]	REIL2006	31.5	25.2	0.393	0.7	0.6		0.005
Vigny *et al.* [2006]	VIGN2006	31.64	20.29	0.308	2.5	1.1	290	0.018
McClusky *et al.* [2003]	MCCLU2003	30.5	25.7	0.37	2.3	1.0		0.04
Sella *et al.* [2002]	REVEL-2000	31.26	29.55	0.400	1.8	1.3	-85	0.030
Chu and Gordon (1998)	CHU1998	31.5	23.0	0.403	2.7	1.2		0.050
Jestin *et al.* (1994)	JESTIN1994	32.59	23.70	0.418				

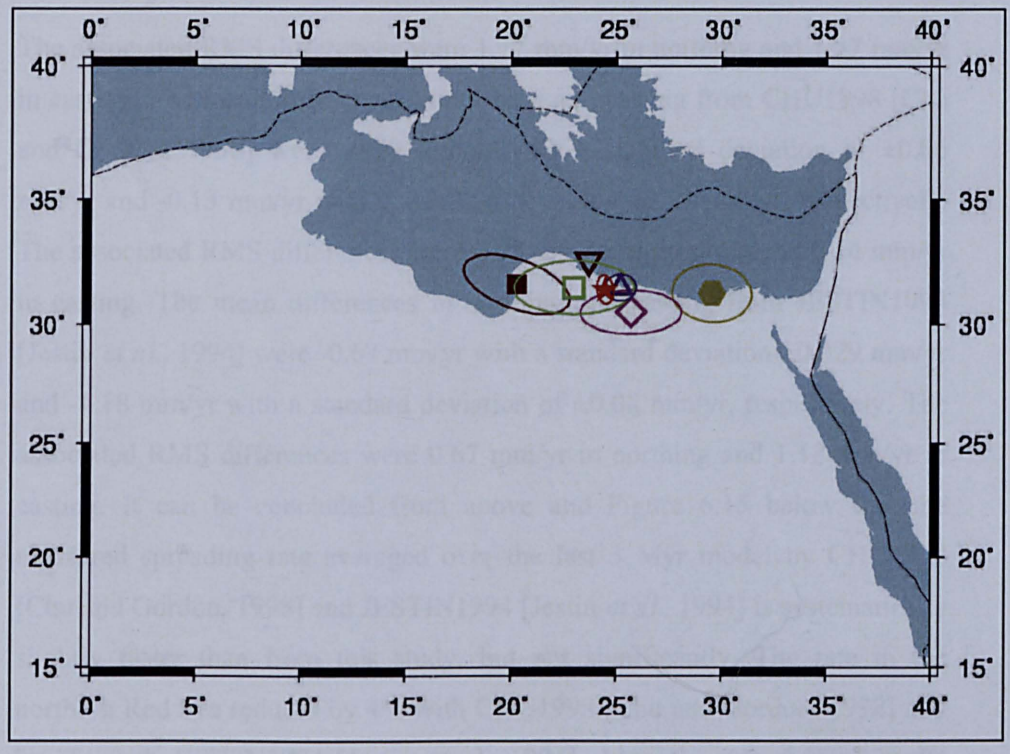

Figure 6.15. Pole location plots for relative motion between the Arabian and Nubian plates from this study and other studies. Solid star is this study; open triangle is REIL2006 [Reilinger *et al.*, 2006]; solid square is VIGN2006 [Vigny *et al.*, 2006]; open diamond is MCCL2003 [McClusky *et al.*, 2003]; open inverted triangle is JESTING1994 [Jestin *et al.*, 1994]; solid pentagon is REVEL-2000 [Sella *et al.*, 2002]; and open square is CHU1998 [Chu and Gordon, 1998].

From a comparison of the station velocities based on the relative motion model between the Arabian and Nubian plates, the 37 stations velocities were computed using this study's model and other studies' model parameters to see the impact of these differences in pole location and rate. It was found that the mean differences in northing and easting from REIL2006 [Reilinger *et al.*, 2006] at the 37 stations were 0.89 mm/yr with a standard deviation of ±0.10 mm/yr and 0.23 mm/yr with a standard deviation of ±0.11 mm/yr, respectively. The associated RMS differences were 0.90 mm/yr in northing and 0.25 mm/yr in easting. The mean differences in northing and easting from MCLL2003 [McClusky *et al.*, 2003] were 1.75 mm/yr with a standard deviation of ±0.24 mm/yr and 1.35 mm/yr with a standard deviation of ±0.29 mm/yr, respectively.

The associated RMS differences were 1.77 mm/yr in northing and 1.37 mm/yr in easting. The mean differences in northing and easting from CHU1998 [Chu and Gordon, 1998] were -0.79 mm/yr with a standard deviation of ±0.06 mm/yr and -0.13 mm/yr with a standard deviation ±0.05 mm/yr, respectively. The associated RMS differences were 0.79 mm/yr in northing and 0.14 mm/yr in easting. The mean differences in northing and easting from JESTIN1994 [Jestin *et al.*, 1994] were -0.67 mm/yr with a standard deviation ±0.029 mm/yr and -1.18 mm/yr with a standard deviation of ±0.08 mm/yr, respectively. The associated RMS differences were 0.67 mm/yr in northing and 1.18 mm/yr in easting. It can be concluded from above and Figure 6.15 below that the measured spreading rate averaged over the last 3 Myr model by CHU1998 [Chu and Gordon, 1998] and JESTIN1994 [Jestin *et al.*, 1994] is systematically slightly faster than from this study, but not significantly. The rate in the northern Red Sea reduces by 4% with CHU1998 [Chu and Gordon, 1998] and by 7% with JESTIN1994 [Jestin *et al.*, 1994]. Also, the rate reduces in the southern Red Sea by 9% with CHU1998 [Chu and Gordon, 1998] and by 11% with JESTIN1994 [Jestin *et al.*, 1994]. The mean differences in northing and easting from VIGN2006 [Vigny *et al.*, 2006] were 1.1 mm/yr with a standard deviation of ±0.85 mm/yr and 1.17 mm/yr with a standard deviation of ±0.81 mm/yr, respectively. The associated RMS differences were 1.38 mm/yr in northing and 1.42 mm/yr in easting. The mean differences in northing and easting from REVEL-2000 [Sella *et al.*, 2002] were 3.42 mm/yr with a standard deviation of ±0.04 mm/yr and 0.62 mm/yr with a standard deviation of ±0.13 mm/yr, respectively. The associated RMS differences were 3.42 mm/yr in northing and 0.63 mm/yr in easting.

Figure 6.16 shows the relative velocity estimates for the GPS stations in this study based on the model of this study and the models from previous studies between the Arabian and Nubian plates. For more details on the stations velocity estimates from the model of this study and the differences between these and previous studies, please refer to Appendix H.

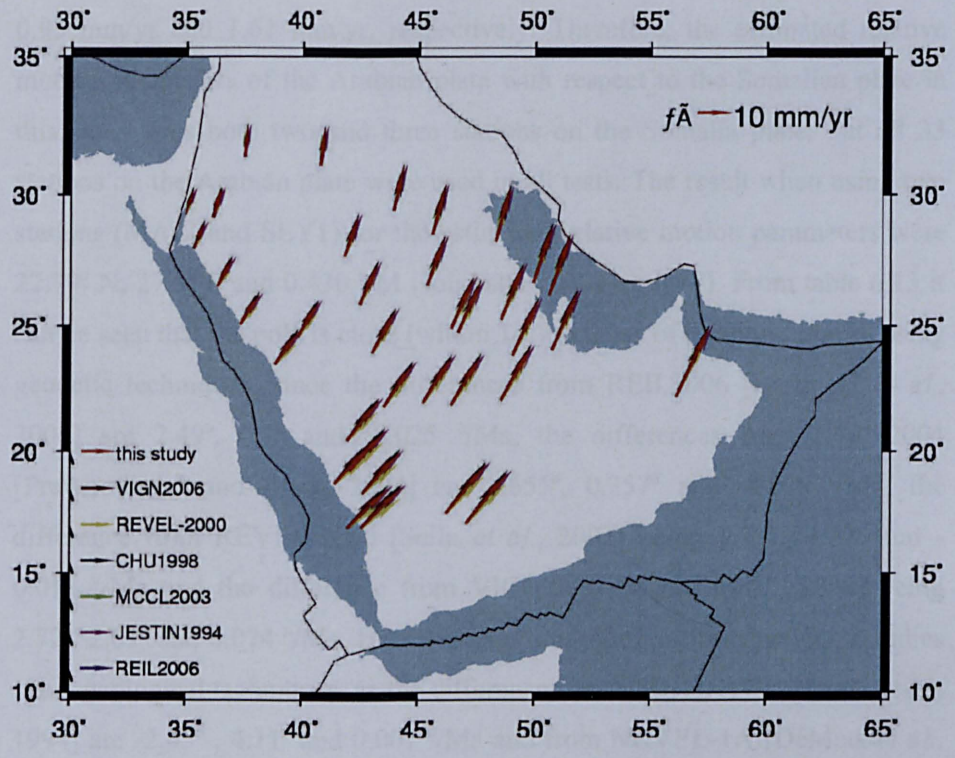

Figure 6.16. Relative velocity estimates for the GPS stations in this study based on the model of this study and the models from previous studies between the Arabian and Nubian plates. VIGN2006 [Vigny *et al.*, 2006]; REVEL-2000 [Sella *et al.*, 2002]; CHU1998 [Chu and Gordon, 1998]; MCCL is MCCL2003 [McClusky *et al.*, 2003]; JESTIN1994 [Jestin *et al.*, 1994]; REIL2006 [Reilinger *et al.*, 2006].

6.6.3 The motion of the Arabian plate relative to the Somalian plate

The estimation of the relative motion of the Arabian plate to the Somalian plate was not well constrained, because only three stations (MALI, REUN and SEY1) were available on the Somalian plate and they are very close to the equator. Moreover, these stations are not very stable; two stations (REUN and SEY1) are on a small island in the middle of the Indian Ocean. The station velocities computed for the three stations in this study show that the difference from the ITRF2005 values are less than 1 mm/yr for MALI and SEY1 in both

components, whereas the differences for REUN in northing and easting were 0.93 mm/yr and 1.61 mm/yr, respectively. Therefore, the estimated relative motion parameters of the Arabian plate with respect to the Somalian plate in this study uses both two and three stations on the Somalia plate, but all 33 stations on the Arabian plate were used in all tests. The result when using two stations (MALI and SEY1) for the estimated relative motion parameters were 22.79° N, 27.5° E and 0.430 °/M (solid star in Figure 6.17). From table 6.13 it can be seen that the pole is close (within 1σ) to those of previous studies using geodetic techniques, since the differences from REIL2006 [Reilinger *et al.*, 2006] are 2.49°, 0.1° and -0.025 °/Ma, the differences from CGPS2004 [Prawirodirdjo and Bock, 2004] are 2.655°, 0.257° and -0.029 °/Ma, the difference from REVEL-2000 [Sella *et al.*, 2002] being 1.73°, -1.12° and -0.011 °/Ma and the difference from VIGN2006 [Vigny *et al.*, 2006] being 2.72°, 2.01° and 0.074 °/Ma. However, this study differs from previous studies using geological techniques, as the differences from JESTIN1994 [Jestin *et al.*, 1994] are -2.45° , 4.11° and 0.007 °/Ma and from NUVEL-1A [DeMets *et al.*, 1994] -1.31°, 3.5° and 0.03 °/Ma. Moreover, the rate determined by this study when using two stations on the Somalian plate compromising all others studies using geodesy and geological techniques, with the maximum difference being 0.074 °/Ma from VIGN2006 [Vigny *et al.*, 2006].

The estimated relative motion parameters between the Arabian and Somalian plates when using three stations (MALI, SEY1 and REUN) were 24.92° N, 26.05° E and 0.398 °/M (open star in Figure 6.17). The pole is close (within 1σ) in latitude and longitude to those of previous studies using geological techniques, since the differences from JESTIN1994 [Jestin *et al.*, 1994] are -0.32°, 2.66° and -0.025 °/Ma and from NUVEL-1A [DeMets *et al.*, 1994] 0.82°, 2.05° and -0.002 °/Ma. However, this study's estimation when using three stations were significantly different from previous studies using geodesy techniques, since the difference from REIL2006 [Reilinger *et al.*, 2006] were

4.62° , -1.35° and -0.057 °/Ma, the difference from CGPS2004 [Prawirodirdjo and Bock, 2004] were 4.785°, -1.193° and -0.061 °/Ma, the difference from REVEL-2000 [Sella *et al.*, 2002] being 3.86°, -2.57° and -0.043 °/Ma and the difference from VIGN2006 [Vigny *et al.*, 2006] being 4.85° , 0.56° and 0.042 °/Ma. Moreover, the rate determined by this study when using three stations on the Somalian plate was slower than all other studies using geodesy and geological techniques, except VIGN2006 [Vigny *et al.*, 2006], where the maximum difference was -0.061 °/Ma from CGPS2004 [Prawirodirdjo and Bock, 2004].

Moreover, it can be seen from Table 6.13 and Figure 6.17 that the locations of the pole for each technique (geodetic and geological) are close to each other in the other studies, and so we have two separated sets of pole locations. The first set is for the geological techniques by NUVEL-1A [DeMets *et al.*, 1994] and JESTIN1994 [Jestin *et al.*, 1994], where the differences are -1.14° and 0.61°. The second set is for the geodetic techniques of REIL2006 [Reilinger *et al.*, 2006], CGPS2004 [Prawirodirdjo and Bock, 2004], REVEL-2000 [Sella *et al.*, 2002] and VIGN2006 [Vigny *et al.*, 2006], where the maximum differences between REVEL-2000 [Sella *et al.*, 2002] and VIGN2006 [Vigny *et al.*, 2006] were -0.99° and 3.13°. The location of the pole in the two sets was significantly different, as the differences of the mean between the two sets were 4.28° and -3.49°. However, the rotation rate of the geological techniques compromising the rotation rate of the geodetic techniques. Moreover, it can be seen that this study, which used geodetic techniques, is closer in pole location to others studies using the same geodetic techniques when using two stations in the Somalian plate, but it differs from other studies using geological techniques. However, it is the other way round when using three stations in the Somalia plate, since the pole location from this study is closer to the pole location from other studies using geological techniques and it differs from other studies using geodetic techniques.

Table 6.13. Relative motion models for Arabia-Somalia from this study and previous studies. Uncertainty in the pole location is given by semi-major (σ_{maj}) and semi-minor (σ_{min}) axes of the 1-σ error ellipse (AZ is the azimuth of the major axis).

Reference	Model	Lat [°]	Lon [°]	Rate [°/Ma]	σ_{maj} [°]	σ_{min} [°]	AZ [°]	σ_{rate} [°/Ma]
This study	2 stns on SO	22.786	27.497	0.430	2.53	0.63	-56.8	0.0326
This study	3 stns on SO	24.925	26.052	0.398	1.95	0.65	-54.90	0.0196
Reilinger *et al.* [2006]	REIL2006	20.300	27.400	0.455	1.00	0.60		0.0080
Vigny *et al.* [2006]	VIGN2006	20.070	25.490	0.356	2.30	1.20	286.00	0.0260
[Prawirodirdjo and Bock, 2004]	CGPS2004	20.135	27.243	0.459	0.78	0.33	42.00	0.0340
[Sella *et al.*, 2002]	REVEL-2000	21.060	28.620	0.441	1.80	1.00	55.00	0.0290
[DeMets *et al.*, 1994]	NUVEL-1A	24.100	24.000	0.400	4.90	1.30	-65.00	0.0500
Jestin *et al.* [1994]	JESTIN1994	25.240	23.390	0.423	4.50	2.40		0.0500

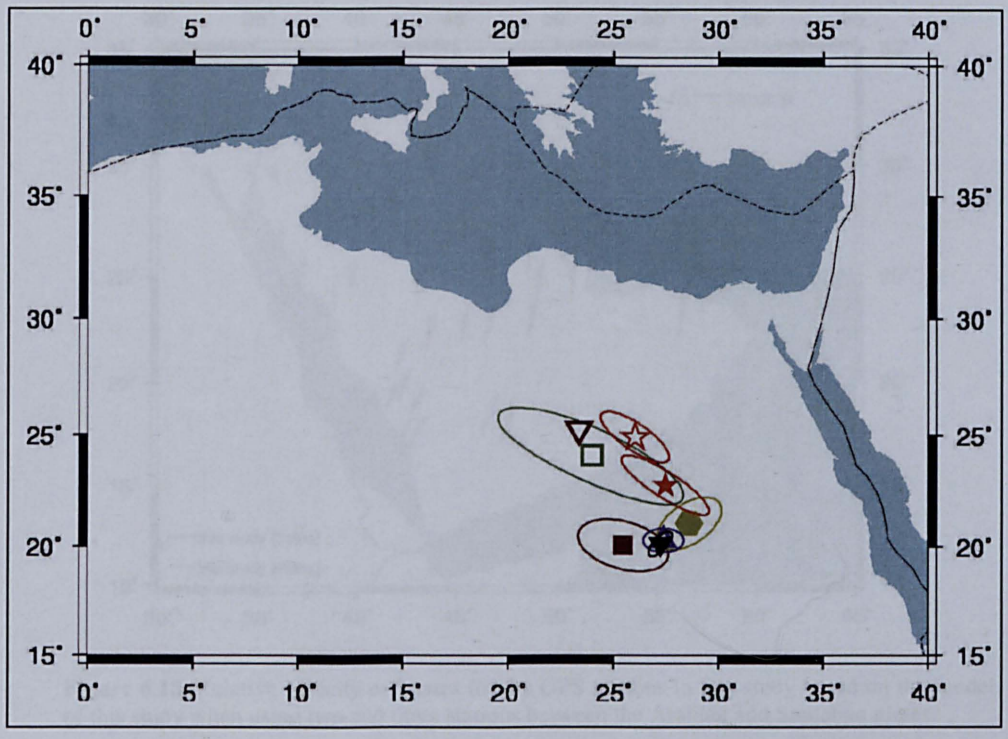

Figure 6.17. Pole location plots for relative motion between the Arabian and Somalian plates from this study and other studies. Solid star is this study when using two stations on the Somalian plate; open star is this study when using three stations on the Somalian plate; open triangle is REIL2006 [Reilinger *et al.*, 2006]; solid square is VIGN [Vigny *et al.*, 2006]; solid inverted triangle is CGPS2004 [Prawirodirdjo and Bock, 2004]; open inverted triangle is JESTIN1994 [Jestin *et al.*, 1994]; solid pentagon is REVEL-2000 [Sella *et al.*, 2002]; and open square is NUVEL-1A [DeMets *et al.*, 1994].

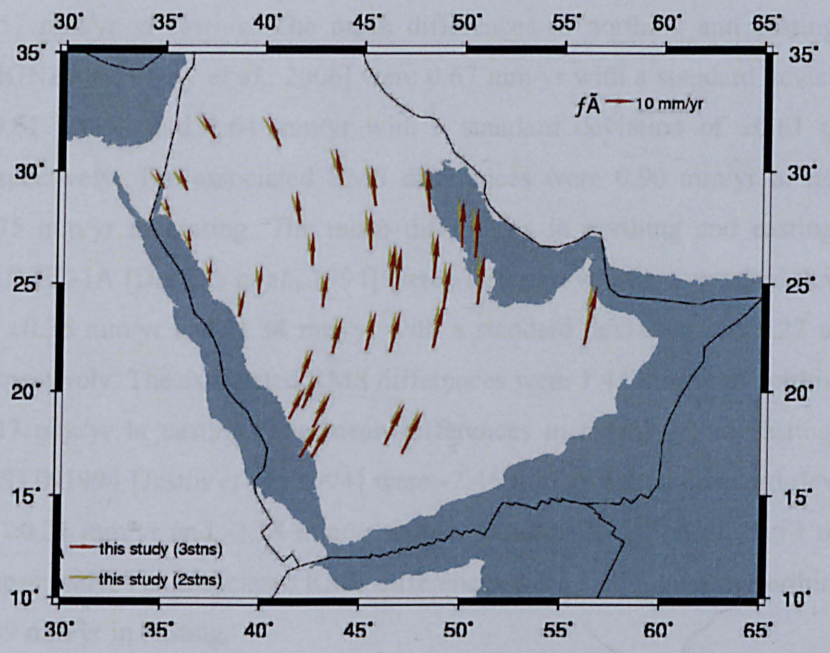

Figure 6.18. Relative velocity estimates for the GPS stations in this study based on the model of this study when using two and three stations between the Arabian and Somalian plates.

From a comparison of the station velocities based on the relative motion model between the Arabian and Somalian plates, the 37 stations relative velocities were computed using this study's computed model and other studies' model parameters to see the impact of these differences in pole location and rate. It was found that the mean differences in northing and easting of this study when using two stations in the Somalian plate and from CGPS2004 [Prawirodirdjo and Bock, 2004] at the 37 stations were -1.26 mm/yr with a standard deviation of ±0.31 mm/yr and 2.34 mm/yr with a standard deviation of ±0.23 mm/yr, respectively. The associated RMS differences were 1.29 mm/yr in northing and 2.35 mm/yr in easting. The mean differences in northing and easting from REIL2006 [Reilinger *et al.* 2006] were -1.0 mm/yr with a standard deviation of ±0.28 mm/yr and 2.19 mm/yr with a standard deviation of ±0.20 mm/yr, respectively. The associated RMS differences were 1.04 mm/yr in northing and 2.20 mm/yr in easting. The mean differences in northing and easting from REVEL-2000 [Sella *et al.*, 2002] were 0.41 mm/yr with a standard deviation of ±0.16 mm/yr and 1.57 mm/yr with a standard deviation of ±0.09 mm/yr, respectively. The associated RMS differences were 0.43 mm/yr in northing and

1.57 mm/yr in easting. The mean differences in northing and easting from VIGN2006 [Vigny *et al.*, 2006] were 0.67 mm/yr with a standard deviation of ±0.61 mm/yr and 1.64 mm/yr with a standard deviation of ±0.61 mm/yr, respectively. The associated RMS differences were 0.90 mm/yr in northing 1.75 mm/yr in easting. The mean differences in northing and easting from NUVEL-1A [DeMets *et al.*, 1994] were -1.39 mm/yr with a standard deviation of ±0.36 mm/yr and -1.34 mm/yr with a standard deviation of ±0.27 mm/yr, respectively. The associated RMS differences were 1.43 mm/yr in northing and 1.37 mm/yr in easting. The mean differences in northing and easting from JESTIN1994 [Jestin *et al.*, 1994] were -2.46 mm/yr with a standard deviation of ±0.21 mm/yr and -2.38 mm/yr with a standard deviation of ±0.13 mm/yr, respectively. The associated RMS differences were 2.47 mm/yr in northing and 2.39 mm/yr in easting.

Figure 6.19 shows the relative velocities for the GPS stations in this study based on the model of this study estimation and the model from previous studies between the Arabian and Somalian plates. For more details on the station velocity estimates from the model of this study and the differences between these and previous studies, please refer to Appendix I.

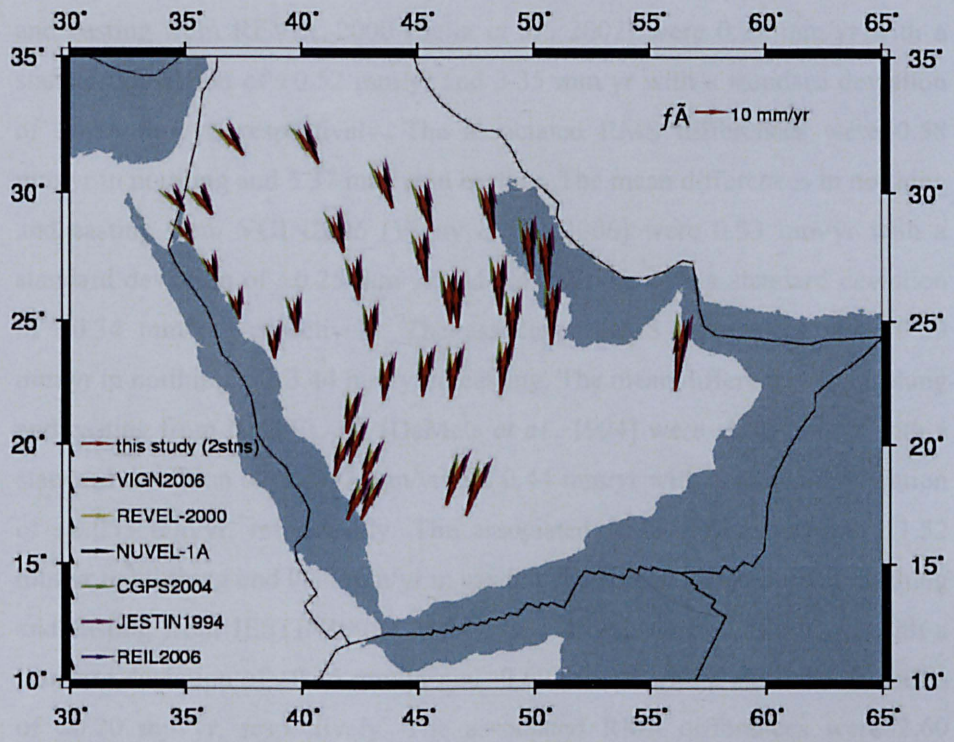

Figure 6.19. Relative velocity estimates for the GPS stations in this study based on the model of this study (2 stations) and the models from previous studies between the Arabian and Somalian plates. VIGN2006 [Vigny *et al.*, 2006]; REVEL-2000 [Sella *et al.*, 2002]; NUVEL-1A [DeMets *et al.*, 1994]; CGPS2004 [Prawirodirdjo and Bock, 2004]; JESTIN1994 [Jestin *et al.*, 1994]; REIL2006 [Reilinger *et al.*, 2006].

On the other hand, it was found that the mean differences in northing and easting when using three stations in the Somalian plate and from CGPS2004 [Prawirodirdjo and Bock, 2004] at the 37 stations were -1.39 mm/yr with a standard deviation of ±0.67 mm/yr and 4.12 mm/yr with a standard deviation of ±0.49 mm/yr, respectively. The associated RMS differences were 1.54 mm/yr in northing and 4.15 mm/yr in easting. The mean differences in northing and easting from REIL2006 [Reilinger *et al.*, 2006] were -1.13 mm/yr with a standard deviation of ±0.64 mm/yr and 3.97 mm/yr with a standard deviation of ±0.46 mm/yr, respectively. The associated RMS differences were 1.29

mm/yr in northing and 4.0 mm/yr in easting. The mean differences in northing and easting from REVEL-2000 [Sella *et al.*, 2002] were 0.27 mm/yr with a standard deviation of ±0.52 mm/yr and 3.35 mm/yr with a standard deviation of ±0.36 mm/yr, respectively. The associated RMS differences were 0.58 mm/yr in northing and 3.37 mm/yr in easting. The mean differences in northing and easting from VGIN2006 [Vigny *et al.*, 2006] were 0.53 mm/yr with a standard deviation of ±0.25 mm/yr and 3.42 mm/yr with a standard deviation of ±0.34 mm/yr, respectively. The associated RMS differences were 0.59 mm/yr in northing and 3.44 mm/yr in easting. The mean differences in northing and easting from NUVEL-1A [DeMets *et al.*, 1994] were -1.52 mm/yr with a standard deviation of ±0.007 mm/yr and 0.44 mm/yr with a standard deviation of ±0.055 mm/yr, respectively. The associated RMS differences were 1.52 mm/yr in northing and 0.44 mm/yr in easting. The mean differences in northing and easting from JESTIN1994 [Jestin *et al.*, 1994] were -2.59 mm/yr with a standard deviation of ±0.15 mm/yr and -0.60 mm/yr with a standard deviation of ±0.20 mm/yr, respectively. The associated RMS differences were 2.60 mm/yr in northing and 0.63 mm/yr in easting.

Figure 6.20 shows the relative velocities estimates for the GPS stations in this study based on the model of this study (3 station) and the models from previous studies between the Arabian and Somalian plates. For more details on the station velocity estimates for the model of this study and differences between these and previous studies, please refer to appendix I.

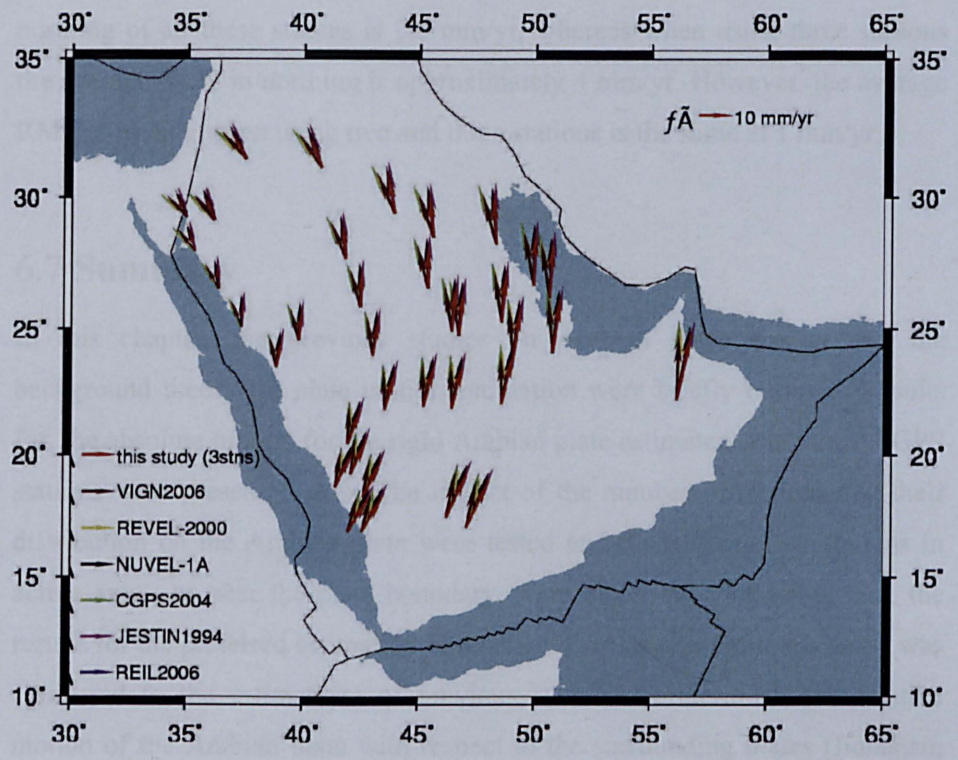

Figure 6.20. Relative velocity estimates for the GPS stations in this study based on the model (3 stations) and the model from previous studies between the Arabian and Somalian plates. VIGN2006 [Vigny *et al.*, 2006]; REVEL-2000 [Sella *et al.*, 2002]; NUVEL-1A [DeMets *et al.*, 1994]; CGPS2004 [Prawirodirdjo and Bock, 2004]; JESTIN1994 [Jestin *et al.*, 1994]; REIL [Reilinger *et al.*, 2006].

This statistical analysis above shows that the measured spreading rate averaged over the last 3 Myr model by NUVEL-1A [DeMets *et al.*, 1994] and JESTIN1994 [Jestin *et al.*, 1994] is systematically faster than determined in this study, when using both two and three stations in the Somalian plate, being slightly faster in the case of two stations than with three stations. The rate in the southern Red Sea (Gulf of Aden) from this study using two stations reduces by 8~12% compared to NUVEL-1A [DeMets *et al.*, 1994] and by 16~20% compared to JESTING1994 [Jestin *et al.*, 1994]. Also, the rate reduces in the southern Red Sea (Gulf of Aden) by 7~8% with NUVEL-1A [DeMets *et al.*, 1994] and by 15~17% with JESTIN1994 [Jestin *et al.*, 1994] when compare to this study using three stations. Also, the statistical analysis above shows that the 37 station velocities of this study using two stations in Somalia are closer in northing to other studies using geodetic techniques, since the average RMS in

northing of all these studies is 2.0 mm/yr, whereas when using three stations the average RMS in northing is approximately 4 mm/yr. However, the average RMS in easting when using two and three stations is the same at 1 mm/yr.

6.7 Summary

In this chapter, the previous studies on Arabian plate motion and the background theory for plate motion estimation were briefly outlined. Results for, the absolute motion for the rigid Arabian plate estimated using the 37 GPS stations were presented. Also, the impact of the number of stations and their distribution on the Arabian plate were tested and the influence of stations in active areas, or near the plate boundary, were evaluated. Following that, the results for the preferred estimation of Arabian plate motion from this study was compared to the estimations of previous studies. Furthermore, the relative motion of the Arabian plate with respect to the surrounding plates (Eurasian, Nubian and Somalian) were estimated and compared to previous studies.

Chapter 7: Strain rate accumulation within the Arabian plate

7.1 Introduction

Investigations of strain rate accumulation on the Arabian plate using GPS measurements had not been carried out previously because of a lack of a homogeneous distribution of GPS stations. Therefore, the General Commission for Survey (GNS) in Saudi Arabia, in collaboration with the Institute of Engineering Surveying and Space Geodesy (IESSG), created a regional GPS network in Saudi Arabia, covering nearly two-thirds of the Arabian plate, and a local network covering the south-western part of Saudi Arabia, in order to advance the knowledge of the strain rate accumulation within the Arabian plate.

This chapter, details the theory of strain and its estimation, presents estimates of strain rates within the Arabian plate (regional network) and the south-west part of Saudi Arabia (local network), and provides an interpretation based on the available seismic record and faults map.

7.2 Strain

Stresses are defined as the forces per unit area that are transmitted through a material by inter atomic force fields [Turcotte and Schubert, 2002]. When forces are applied to an object, it can change its size and shape; this is called deformation. Furthermore, the forces per unit area in an elastic solid, called stress, result in strain or deformation of the solid. The response of a body to forces may have many forms, where the body is displaced, or rotated, or distorted. Deformation describes the collective displacements of points in a body. In other words, it describes the complete transformation from the initial to the final geometry of a body, and this change may include a translation (i.e. movement from one place another), a rotation (spin around an axis) and a distortion (change in shape). Strain describes the changes of points in a body relative to each other; hence strain describes the distortion of a body. When the distortion and rotation components are zero, there is only translation, which is formally called rigid-body-translation since the body undergoes no shape change as it moves. Moreover, when the distortion and translation are both zero, there is only rotation. This rotation is called rigid-body-rotation. When the translation and rotation components are both zero, there is only distortion. This distortion is described by strain. Therefore, it can be seen from the above explanations that strain is a component of deformation; hence care should be taken when talking about deformation and strain (i.e. deformation and strain are not synonymous). Furthermore, deformation describes the complete displacement of points in a body relative to an external reference frame. However, strain describes the displacement field of points relative to each other or, in other words, it requires an internal reference frame within the body. This is why strain is independent of an external reference frame [Ayhan *et al.*, 2002].

The basics of the theory of elasticity were formulated by Helmholtz in the fundamental theorem of kinematics in 1858: "the change of position in an infinitesimal region around a point of a deformable body corresponds in a first approximation to the sum of a translation, a rotation and a dilatation". The

stresses cause solids to deform, so the stresses make changes in the distances separating adjacent small elements of the solid. Figure 7.1 shows a small element of the solid in the shape of a rectangular parallelepiped. Before deformation, it has sides $\delta x, \delta y$ and δz, where the element may be deformed by changing the dimensions of its sides while maintaining its shape in the form of a rectangular parallelepiped. Then after the deformation the sides of the element are $\delta x - \varepsilon_{xx}\delta x$, $\delta y - \varepsilon_{yy}\delta y$ and $\delta z - \varepsilon_{zz}\delta z$. The quantities $\varepsilon_{xx}, \varepsilon_{yy}$ and ε_{zz} are normal components of strain where ε_{xx} is the change in length of the side parallel to the x axis divided by the original length of the side and ε_{yy} and ε_{zz} are similar in the y and z axes.

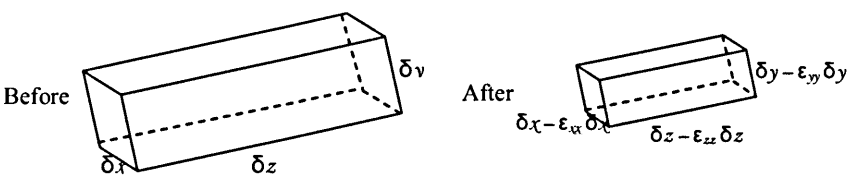

Figure 7.1. Change of dimensions of rectangular parallelepiped. .

Moreover, the deformation of the element is considered to be so small that squares and higher order products of the strain components can be neglected in computing the change in volume of the element and the fractional change in volume (i.e. volume change divided by original volume) is $\varepsilon_{xx} + \varepsilon_{yy} + \varepsilon_{zz}$. This quantity of the element is known as the dilatation Θ.

Furthermore, the strain components of a small element of a solid can be related to the displacement of the element. For simplicity, the two-dimensional case will be explained. Figure 7.2 shows the corners of a rectangle before deformation a, b, c, d and after deformation a', b', c', d' with the assumption that the rectangular shape is maintained.

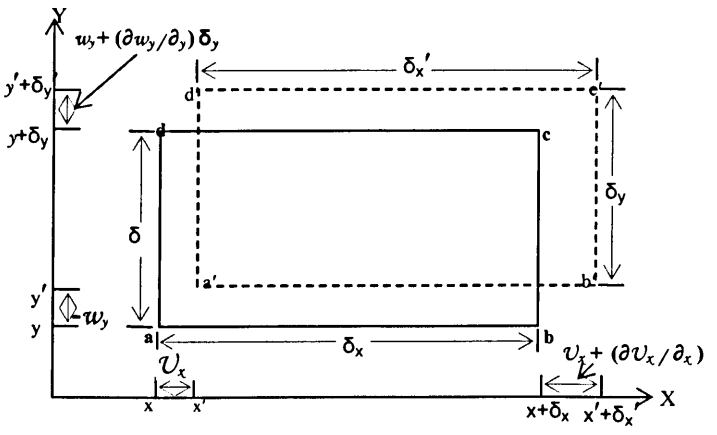

Figure 7.2. Distortion in two-dimensions for a rectangle. δ_x and δ_y are the length of the rectangular before deformation while δ_x' and δ_y' are after deformation

The coordinates of corner a before the strain are (x, y) and the coordinates of corner a' after the strain are (x', y'). Therefore, the displacement of the corner a as a result of the strain is

$$U_x(x, y) = x - x' \tag{7.1}$$

in the $x$direction and

$$U_y(x, y) = y - y' \tag{7.2}$$

in the y direction. Also, corner b with coordinates before strain of $(x+\delta x, y)$ is displaced to position b' with coordinates $(x'+\delta x', y')$ after the strain. Therefore, the displacement of b in the $x$direction is

$$U_x(x+\delta x, y) = x+\delta x-(x'+\delta x') \tag{7.3}$$

Similarly, the displacement of corner d in the y direction $U_y(x, y+\delta y)$ is given by the difference in the $y$coordinates of d and d'

$$U_y(x, y+\delta y) = y+\delta y-(y'+\delta y') \tag{7.4}$$

since the strain $(\delta x-\delta x')/\delta x$ and $(\delta y-\delta y')/\delta y$ is assumed to be small. Also since δx and δy are infinitesimal, $U_x(x+\delta x, y)$ and $U_y(x, y+\delta y)$ can be expanded as follows:

$$U_x(x+\delta x, y) = U_x(x, y)+\frac{\partial U_x}{\partial x}\delta x \tag{7.5}$$

$$U_y(x, y+\delta y) = U_y(x, y)+\frac{\partial U_y}{\partial y}\delta y \tag{7.6}$$

Substitution of (7.5) into (7.3) gives:

$$U_x(x, y)+\frac{\partial U_x}{\partial x}\delta x = x+\delta x-(x'+\delta x') \tag{7.7}$$

Then considering (7.1) and re-arranging gives:

$$\delta x = \delta x'+\frac{\partial U_x}{\partial x}\delta x \tag{7.8}$$

Similarly, in the y direction:

$$\delta y = \delta y'+\frac{\partial U_y}{\partial y}\delta y \tag{7.9}$$

According to the strain component definitions and (7.8) and (7.9),

$$\varepsilon_{xx} = \frac{\delta x-\delta x'}{\delta x} = \frac{\partial U_x}{\partial x} = \frac{l_x-l_x}{l_x} \tag{7.10}$$

$$\varepsilon_{yy} = \frac{\delta y - \delta y'}{\delta y} = \frac{\partial U_y}{\partial y} = \frac{l_y - l_y}{l_y} \tag{7.11}$$

where l_x^o is the original distance in the X direction, l_y^o is the original distance in the Y direction, l_x is the deformed distance in the X direction and l_y is the deformed distance in the Y direction. When e_{xx} and e_{yy} are positive, there is an extension, but when e_{xx} and e_{yy} are negative there is a compression.

In three-dimensional strain, the ε_{zz} is

$$\varepsilon_{zz} = \frac{\delta z - \delta z'}{\delta z} = \frac{\partial U_z}{\partial z} \tag{7.12}$$

Therefore, the components of strain in the x, y and z directions are proportional to the derivatives of the associated displacements in the respective directions. Moreover, the dilatation Θ, i.e. the volumetric deformation, can be computed by:

$$\Theta = \frac{\partial U_x}{\partial x} + \frac{\partial U_y}{\partial y} + \frac{\partial U_z}{\partial z} = \frac{V - V}{V} \tag{7.13}$$

where V^o is the original volume and V is the deformed volume. When Θ is positive, there is an extension, but when Θ is negative there is a compression.

So far, shape was assumed to be maintained, but this is not necessarily the case, because shear strains can distort the shape of the small elements. Figure 7.3 shows a rectangular element in two dimensions that has been distorted into a parallelogram.

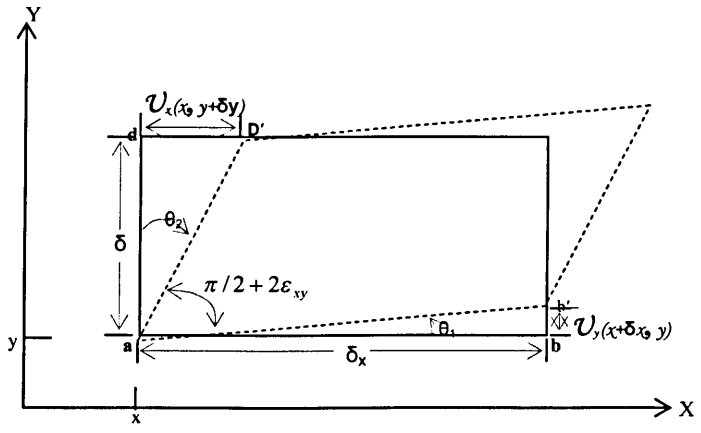

Figure 7.3. Distortion of a rectangle by a strain including shear.

Figure 7.3 illustrates that the shear strain ε_{xy} is defined to be one half of the decrease in the angle *bad* .

$$\varepsilon_{xy} = -\frac{1}{2}(\theta_1 + \theta_2) \tag{7.14}$$

where θ_1 and θ_2 are the angles through which the sides of the original rectangular element are rotated. As in the case of stress, the shear strain is symmetric so $\varepsilon_{xy} = \varepsilon_{yx}$. Also, θ_1 and θ_2 are related to the displacements.

$$\tan\theta_1 = \frac{U_y(x+\delta x, y)}{\delta x} = \theta_1 \tag{7.15}$$

$$\tan\theta_2 = \frac{U_x(x, y+\delta y)}{\delta y} = \theta_2 \tag{7.16}$$

Since the rotations are assumed to be infinitesimal, hence the tangents of the angles are almost equal to the angle values. Therefore, $U_y(x+\delta x, y)$ and $U_x(x, y+\delta y)$ can be expressed in terms of the spatial derivatives of the displacements.

$$U_y(x+\delta x, y) = \frac{\partial U_y}{\partial x}\delta x \tag{7.17}$$

$$U_x(x, y+\delta y) = \frac{\partial U_x}{\partial y}\delta y \tag{7.18}$$

For simplicity, we can assume $U_x(x, y) = 0$ and $U_y(x, y) = 0$; then substitution of (7.17) and (7.18) into (7.15) and (7.16) leads to the result in (7.14) giving the following equation:

$$\varepsilon_{xy} = \frac{\partial U_y}{\partial x} + \frac{\partial U_x}{\partial y} \tag{7.19}$$

Moreover, the shear strain could be used to compute the solid-body rotation of the element if $\theta_1 \neq \theta_2$. Where the solid body rotation $U_z = \omega$,

$$\omega = U_z = -\frac{1}{2}(\theta_1 - \theta_2) \tag{7.20}$$

Considering (7.15), (7.16), (7.17) and (7.18) with (7.20) gives:

$$\omega = U_z = \frac{1}{2}\left(\frac{\partial U_y}{\partial x} - \frac{\partial U_x}{\partial y}\right) \tag{7.21}$$

From the above, the other commonly used strain terms can be computed, i.e. the principal strain rate components ($\varepsilon_1, \varepsilon_2$). Also, the maximum and minimum strains, called the principal strains, can be computed, where the maximum and minimum normal strains are perpendicular to each other and oriented in directions for which the shear strains are zero. Therefore, a transformation is required to determine the principal axes of strains, where the shear strain is equal to zero.

$$\varepsilon_1 = \frac{1}{2}\left(e_{xx} + e_{yy}\right) + \sqrt{\left(\frac{e_{xx} + e_{yy}}{2}\right)^2 + e_{xy}^2} \tag{7.22}$$

$$\varepsilon_2 = \frac{1}{2}\left(e_{xx} + e_{yy}\right) - \sqrt{\left(\frac{e_{xx} + e_{yy}}{2}\right)^2 + e_{xy}^2} \tag{7.23}$$

The principal strain angle (i.e. direction of ε_1) is then

$$\tan(2\beta) = \frac{2e_{xy}}{e_{xx} + e_{yy}} \tag{7.24}$$

7.3 Strain rate estimation

The author decided to use the method of deriving horizontal geodetic strain rates because it is independent of geological preferences, and as there is no up-to-date geological information that could help with the strain analysis. Hence the method of applying interpolation between points was used to calculate the strain. Moreover, Shen *et al.* [1996] developed a strain rate modelling method, which like most other methods, e.g. Frank [1966] and Prescott [1976], interpolates the strain rates using the discretized geodetic measurements (Fig. 7.4). However, Shen *et al.* [1996] method differs from the others, as it models strain rates as continuous functions within the whole network. For this, a uniform strain rate field is assumed at each location. Then a least squares inversion is performed over the station velocities and their covariances to solve for the unknown parameters. There being six unknown parameters: two velocity components V_x and V_y; three strain rate components e_{xx}, e_{yy} and e_{xy}; and lastly the rotation rate ω. The modelling algorithm can be written in the following form:

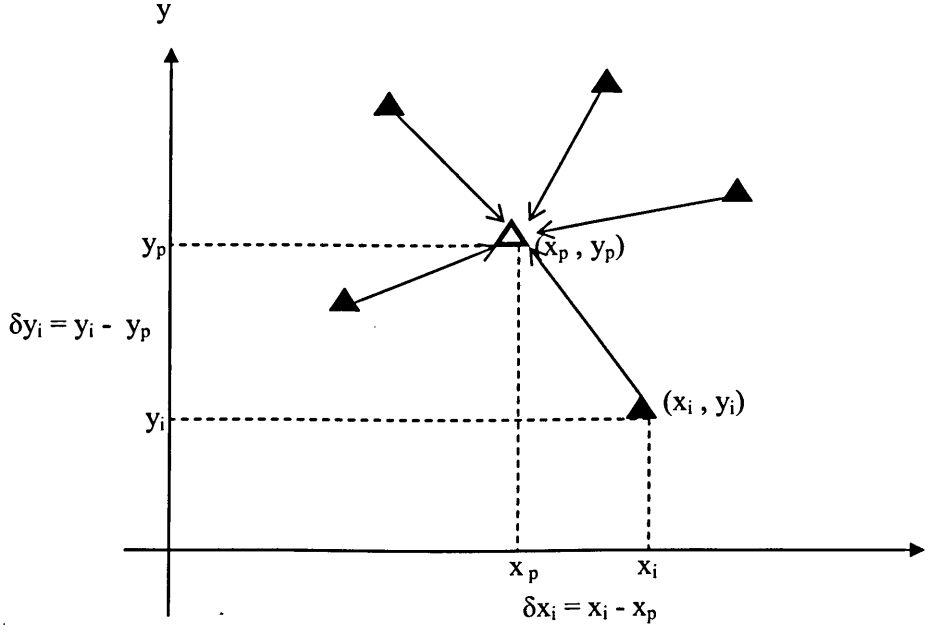

Figure 7.4. Predicting the grid node velocity. The solid triangle is the known station velocity and the open triangle is the predicted station velocity.

$$\begin{bmatrix} V_x^i \\ V_y^i \end{bmatrix} = \begin{bmatrix} 1 & 0 & \delta x^i & \delta y^i & 0 & \delta y^i \\ 0 & 1 & 0 & \delta x^i & \delta y^i & -\delta x^i \end{bmatrix} \begin{bmatrix} V_x \\ V_y \\ e_{xx} \\ e_{xy} \\ e_{yy} \\ \omega \end{bmatrix} + \begin{bmatrix} \sigma_x^i \\ \sigma_y^i \end{bmatrix} \qquad (7.9)$$

V_x^i and V_y^i are the observed ith station velocity components at location R^i

V_x and V_y are the unknown station velocity components at location R

e_{xx}, e_{yy} and e_{xy} are the unknown strain rate components at location R

ω is the unknown rotation rate at location R

σ_x^i and σ_y^i are the errors of the corresponding velocity components

$R^i = \begin{bmatrix} R_x^i & R_y^i \end{bmatrix}^T$ is the vector location components at the ith observed station

$R = \begin{bmatrix} R_x & R_y \end{bmatrix}^T$ is the vector location components of the unknown station

$\delta R^i = \begin{bmatrix} \delta R_x^i & \delta R_y^i \end{bmatrix}^T = \begin{bmatrix} R_x^i - R_x & R_y^i - R_y \end{bmatrix}^T = \begin{bmatrix} \delta x^i & \delta y^i \end{bmatrix}^T$

so $\delta x^i = R_x^i - R_x$ and $\delta y^i = R_y^i - R_y$

When there are n station velocity estimations, the observation equations in matrix form are as follows:

$$L = AX + V \qquad (7.18)$$

L : The observation matrix of dimension 2n x 1

A : The design matrix of dimension 2n x 6

X : The parameters matrix of dimension 6 x 1

V : The residual matrix of dimension 2n x 1

Since the infinitesimal strain calculates the predicted station velocity from the surrounding (neighbouring) stations, care should be taken because the surrounding stations sometimes are not at the same distance from the predicted stations, so their contributions in the estimation should vary (Fig. 7.4). Therefore, a correlation function should be used, where the correlation function defines the interrelationship between the different stations observed and the stations being predicted. Normally, the influence of a distant point should be small. Therefore, the value of the function usually decreases with a growing distance and converges to zero.

In this study, a function with a finite gradient at the zero position was chosen since the author is mainly interested in the strain, the first derivative of the signal. Therefore, Shen *et al.* [1996] was applied with a weighted version of C_{ij}, which was used for constructing the local averages, where C_{ij} is the covariance matrix of the station velocity estimation uncertainties obtained from the geodetic data adjustment. The weighting function Wbeing as follows:

$$W_{ij} = C_{ij} \exp \frac{\delta R_i^2 + \delta R_j^2}{\sigma_D^2} \tag{7.19}$$

where i and j are the velocity components corresponding to the i^{th} and j^{th} stations. Also, δR_i^2 and δR_j^2 are the distances from the i^{th} and j^{th} stations to the predicted station and σ_D^2 is the distance decaying constant. Hence, this controls the contribution of the observation stations, so that distant stations contribute less than close stations. The author prepare figure 7.5 shown weighting functions for various σ_D^2.

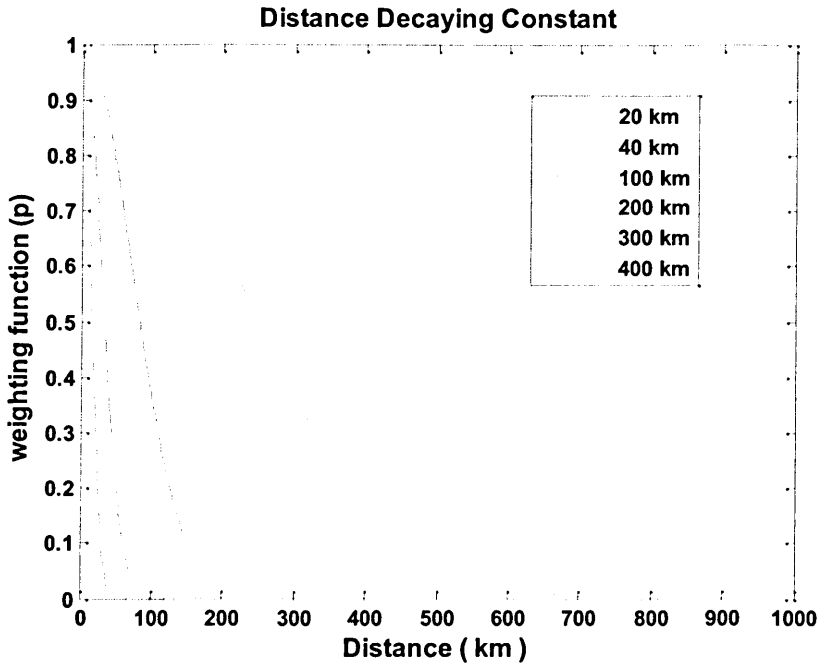

Figure 7.5. Weighting functions with various distance decaying constant.

The solution of the observation equations using the least squares estimation will be:

$$\hat{X} = (A^T W A)^{-1} A^T W L \tag{7.20}$$

and the covariance matrix of the parameters:

$$C_{\hat{x}\hat{x}} = (A^T W A)^{-1} \tag{7.21}$$

The strain rate algorithm developed by Shen *et al.* [1996] has an advantage when the model represents the strain rate field in a realistic way. For a local small region, the strain rate field is quasi uniform, but for a large region the strain rate field varies continuously. Therefore, the strain rate estimates are less biased as a result of proper weighting.

7.4 Strain rate accumulation within the Arabian plate

In order to study the strain rate accumulation, the number of stations and their distribution, as well as their location with regard to geological and geophysical criteria, are very important. In this study, there were two geodetic networks: the first is the regional network (Fig. 7.6), which covers most of the Arabian plate; the second is the local network (Fig. 7.7), which covers the south-western part of the Arabian plate. For more details of the two networks, the reader is referred to Chapter 4 and for more details of station the velocity estimations the reader should consult Chapter 5.

A general view of strain rate accumulation within the Arabian plate is estimated using the regional network, which covers two-thirds of the Arabian plate, where as a more detailed view of strain rate accumulation is estimated using the local network, in the south-western part of the Arabian plate. Algorithms and source code for the Shen *et al.* [1996] method, explained in Section 7.2, were used in this study.

One of the first and important steps in strain rate estimation is to make sure that there are no remaining station problems in the input data. It is known that if one of the components for the principal strain is compression, then the other component should be extensional. However, if both components of the principal strain are either compressions or extensional, then there is a station problem in that area. For this study, the first results showed that there were no station problems in the regional network, except for those stations reported before (F031, F041, F045 and P049). However, the stations O632, O628 and O641 in the local network did show station problems; hence they were excluded from any strain rate estimation.

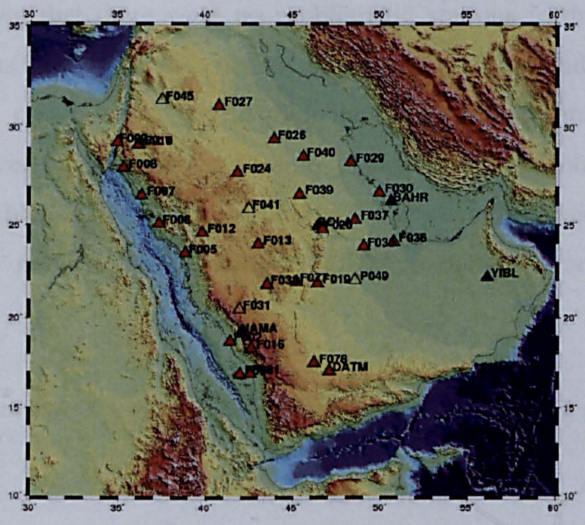

Figure 7.6. The 37 regional GPS stations on the Arabian plate. The red solid triangles are stations of the GCS network and the black solid triangles are IGS stations. The solid triangles (red and black) are stations used in the regional strain rate estimation and the open triangles are stations excluded from the regional strain rate estimation.

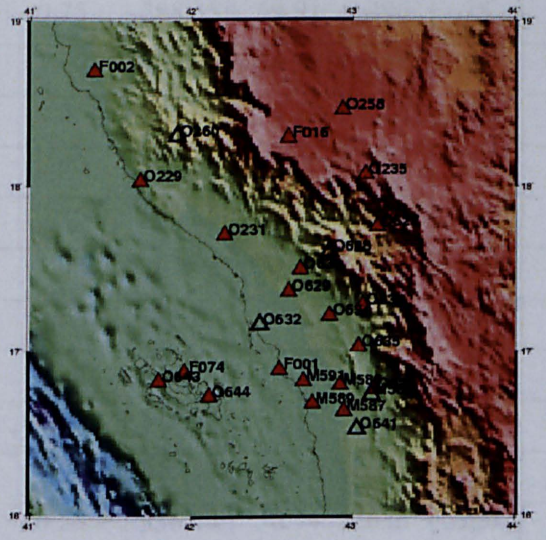

Figure 7.7. The 26 local GPS stations in the south-western part of the Arabian plate, where the red solid triangles are stations of the GCS network used for strain rate estimation in the south-western region and the open triangles are stations excluded from the local strain rate estimation.

7.4.1 Strain rate estimation for the regional network

After ensuring that there were no problematic stations in the input data, the next step was to find the best distance decaying constant and grid interval for the regional network that would give the best strain estimation. Therefore, many tests were carried out for different distances and grid node intervals. The statistical Table 7.1 shows a summary of the predicted grid node distances for the regional network when applying different distances and different grid intervals.

Table 7.1. Numerical tests with various distance decaying constants and grid intervals for the regional network.

		Grid node distances				
Distance (km)	Interval (Degree)	Mean (km)	S.dev. (km)	Max. (km)	Min. (km)	No. of stations predicted
75	0.25	290.20	67.38	518	75	2200
75	0.50	290.11	68.11	507	75	551
75	0.75	288.35	69.91	496	75	242
75	1.00	290.75	64.95	458	75	138
100	0.25	301.96	74.78	614	100	2552
100	0.50	300.94	74.95	580	100	637
100	0.75	300.85	75.65	539	100	283
100	1.00	304.03	75.35	602	100	156
200	0.25	315.69	76.30	636	200	2771
200	0.50	316.00	76.91	625	200	695
200	0.75	314.55	75.75	605	200	307
200	1.00	315.42	76.42	602	200	172
300	0.25	336.44	56.94	636	300	2771
300	0.50	336.72	57.70	625	300	695
300	0.75	335.79	55.81	605	300	307
300	1.00	336.09	57.27	602	300	172

Four different initial distances (75 km, 100 km, 200 km and 300 km) were tested because the regional network station distances vary widely between tens and hundreds of kilometres. Also, four grid intervals (0.25 ,0.50 , 0.75 and 1.0) were selected.

As can be seen in Table 7.2, when a distance of 75 km is applied, the mean of the grid distances for the four intervals are close to each other, at 290 ± 67 km. Furthermore, the maximum distance reaches 518 km (518, 507, 496 and 458 km) when applying the 0.25 interval and decreases systematically when the interval is increased; when applying 1.0 it reaches 458 km. Also, the number of computation grid nodes decreases dramatically (from 2200 to 551 to 242 and then 138).

When a distance of 100 km is applied, the mean of the grid distances for the four intervals are close to each other, at 300 ± 75 km, the maximum distances reach 614, 580, 539 and 602 km and the number of computation grid nodes again decreases dramatically (from 2552 to 637 to 283 and then 156). Whereas a distance of 200 km is applied, the mean of the grid distances for the four intervals are close to each other, at 315 ± 76 km, the maximum distances reach 636, 625, 605 and 602 km and the number of computation grid nodes again decreases dramatically (from 2771 to 695 to 307 and then 172). Whereas a distance of 300 km is applied, the mean of the grid distances for the four intervals are close to each other, at 336 ± 57 km, the maximum distances reach 636, 625, 605 and 602 km and the number of computation grid nodes again decreases dramatically (from 2771 to 695 to 307 and then 172).

When the results from using different distances are compared with each other, it is seen that the means and the associated standard deviations vary between 290 and 336 km and ± 55 to ± 76 km, respectively. Moreover, the maximum distances vary between 458 and 636 km. It can clearly be seen that when the selected distance is increased, the maximum distance increases as well. Furthermore, it can be seen that the results for the 200 and 300 km distances at

the four intervals are very close to each other, which means that increasing the distance does not improve or give more significant results. Also, the number of computation grid nodes increases when the distance increases, which means more coverage of the network area.

However, the value of the strain should be compared before selecting the best distance decaying constant and grid interval. Therefore, the differences in the principal strain rate components ($\varepsilon_1, \varepsilon_2$) at the common grid nodes for different distances at the interval 0.50° were computed. Table 7.2 shows the statistical analysis of these computations and it can be seen that there is not a significant difference between the distances 75 – 100 km. However, there are quite large difference between 75 – 200 km, 75 – 300 km, 100 – 200 km and 100 – 300 km, but the difference between 200 – 300 km is again small. Overall, the result shows that when the selected distance increases, the value of the strain decreases or, in other words, becomes smoother.

Table 7.2. The statistical analysis of the comparison of the strain rate at common grid nodes for different distances for the regional network.

Diff. of distances at Interval 0.50°	Mean Of diff ε_1	Standard dev. Of diff ε_1	RMS Of diff ε_1	Mean Of diff ε_2	Standard dev. Of diff ε_2	RMS Of diff ε_2
75 – 100	0.18	± 1.54	1.55	-0.11	± 0.86	0.86
75 – 200	0.80	± 4.21	4.28	-0.45	± 2.35	2.39
75 – 300	0.98	± 4.45	4.55	-0.70	± 2.73	2.82
100 – 200	0.62	± 3.28	3.34	-0.35	± 1.76	1.80
100 – 300	0.80	± 3.58	3.66	-0.59	± 2.20	2.28
200 – 300	0.18	± 0.72	0.74	-0.25	± 8.09	1.06

Therefore, it can be concluded that the strain value is more significant when the selected distance is short, but this will leave some gaps in the coverage of the area since the observed network stations are sparse. Hence, a distance of 100 km was selected to be the best, since it is a compromise between the significant strain value and the network area coverage. Also, the grid node interval of 0.50° was selected to be the most suitable interval, since it is a compromise regarding the density of the network (figure 7.8).

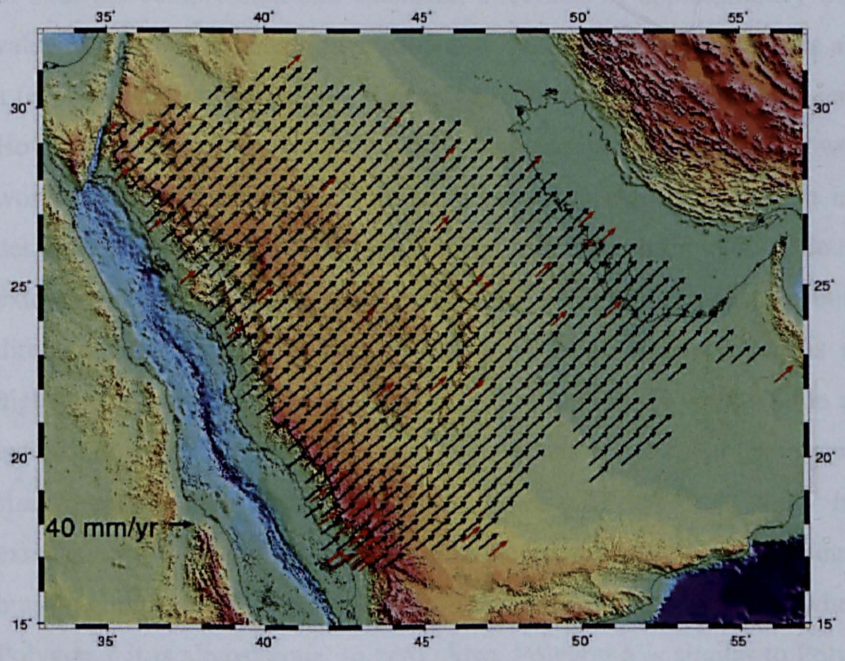

Figure 7.8. The regional velocity field network used in the strain rate computations The black arrows indicate the predicted grid node velocity field and the red arrows show the observed velocity field.

Figure 7.9 shows that the principal strain rate is in general, a compression in the north-east to south-west directions and an extension in the north-west to south-east direction, except for two areas: the first in the north-west, close to the Aqaba Gulf and the Dead Sea fault, where there is north to south compression and west to east extension, where this agree with Almendinger *et al.*, [2007], and the second in part of the south-west region ($42^{\circ}E$, $18^{\circ}N$) that shows a north to south extension and a west to east compression.

Furthermore, the whole region can be divided into different polygons according to the principal strain rate values and directions. Polygon 1 in the north-west of the Arabia plate along the Aqaba Gulf and the Dead Sea fault, shows a high principal strain rate compared to other regions, with a strain rate in both the compression and extension directions of approximately the same value of 8 nstr/yr and distributed smoothly over the region, since there are only a few observed stations in this regions with quite long distances between them. However, this result shows the region to be an active region; hence, it would be worthwhile having a denser network here, to be able to analyse it in more detail. Polygon 2 has a small strain value and the compression is double the extension. Also, the compression direction is along a north-east to south-west direction. Polygon 3 is similar to Polygon 2, but the strain rate is slightly higher. However, Polygon 4 has an extension double its compression and the extension strain rates are higher than in Polygons 1 and 2, but the compression strain rate decreases in the south-west direction. Polygons 5 and 7 have an extension strain rate of about 3 nstr/yr in the direction north-west to south-east, but the compression strain rate is very small at less than 1 nstr/yr, whereas in Polygon 7 it is almost equal to zero. Also, Polygon 6 is similar to Polygons 5 and 7, except that the extension rate reaches 5 nstr/yr. Polygons 8 and 9 show high extensions compared to other regions on the east of the Arabia plate where the highest extension rate is 6 nstr/yr in Polygon 9. Also, the extension rate is almost double the compression strain rate, which shows more investigation would be worthwhile here by establishing a denser network. Polygons 10 and 11 have the same extension strain rate of about 4 nstr/yr, but

the compression strain rate of Polygon 10 is double that of Polygon 11. Moreover, Polygons 12 and 13 have small strain rates in both the compression and extension directions and the extension strain rate decreases in the south direction.

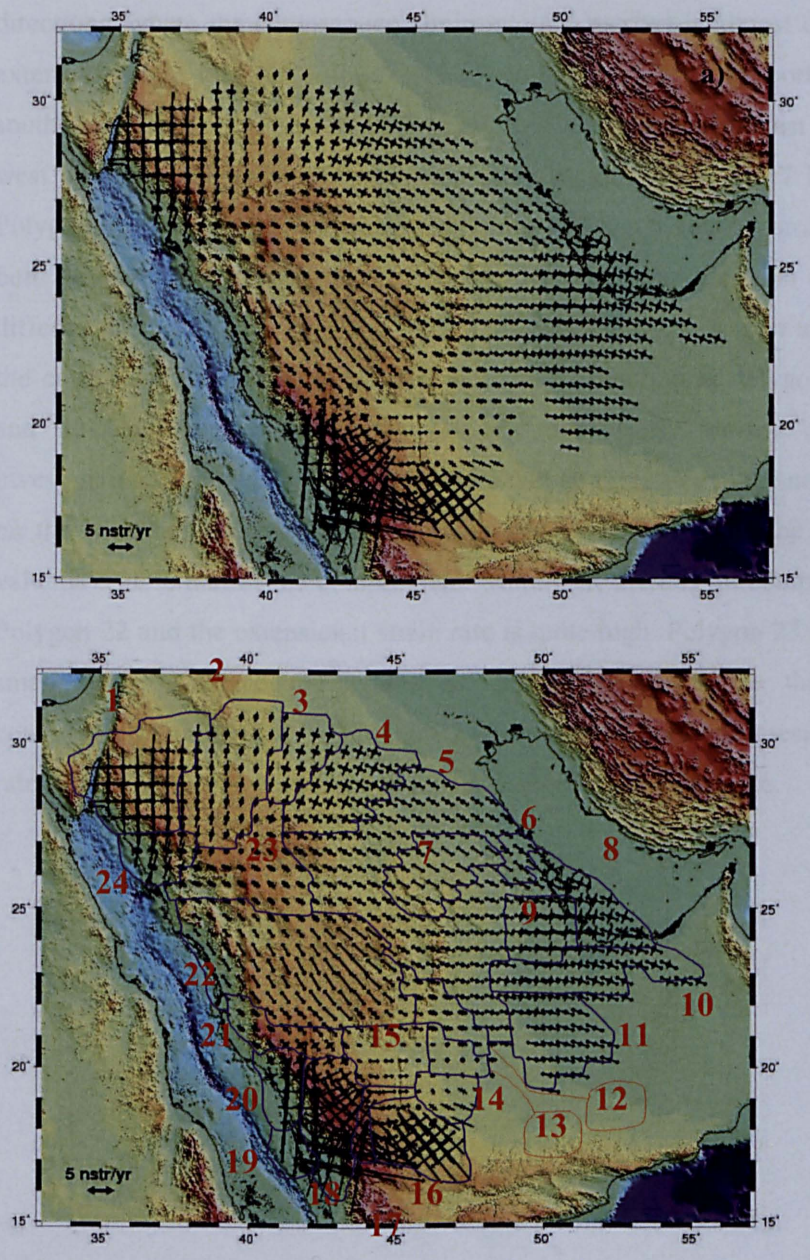

Figure 7.9. The principal strain rate components $(\varepsilon_1, \varepsilon_2)$ for the regional network. Compression is shown by the arrows directed inside and the extension by arrows directed outside. The polygons represent areas that have similar strain values. The unit is nano strain per year (nstr/yr).

Polygon 15 is an extension region in the direction west to east and there is no compression, because it is behind the mountain region. On the other hand, Polygon 14 is a compression region along the north-west to south-east direction and the compression strain rate decreases in the north direction. Polygon 16 shows quite a high strain in both the compression and extensional directions, where the compression strain rate (16 nstr/yr) is almost double the extension strain rate (10 nstr/yr). Also, compression is in the north-west to south-east direction, whereas the extension is along the north-east to south-west direction, which is different from other regions. Polygon 17 is west of Polygon 16 and east of the mountain region and has a smaller strain rate in both directions of approximately 5 nstr/yr. However, the direction is slightly different from Polygon 16, since the extensional direction is west to east and the compressional direction is north to south. Furthermore, Polygons 18, 19 and 20 have very high strain rates and are clearly worthy of further investigation using a denser network (there will be discussed in the next section on the local network). Polygon 21 has a small strain rate and the extension value is double that of the compression. Moreover, there is no compression in Polygon 22 and the extensional strain rate is quite high. Polygon 23 also has a small strain rate and the extensional strain rate is double that of the compression strain. Finally, Polygon 24 has quite a high compression strain rate (5 nstr/yr) and its compression rate is double its extension rate.

Figure 7.10 shows the rotation rates, where in general the rotation angle is anticlockwise and about 0.25 deg/Myr, except for a number of areas. For example, at approximately 36° E, 29° N the rotation angle is increasing gradually (to 0.35 deg/Myr) in the direction of the north-west (Dead Sea fault). Also, the region at approximately 50° E, 23° N shows a higher rotation rate compared to the surrounding areas. Furthermore, the region at approximately 46° E, 17° N shows a rotation rate that is anticlockwise to the west. Also, the value of the rotation in this area varies between 0 deg/Myr in the middle up to 3 deg/Myr in both the west and east directions. The south-west region also shows different rotation rate directions and values, which will be discussed in the next section on the local network.

Figure 7.11 shows the dilatation for the regional network, showing that the central, east and south-east areas of the Arabian plate are in compression, but the north and south areas are in extension. However, along the Red Sea coast the dilatation plot shows it changing between compression and extension, where at latitude 17° N there is extension, but at latitude 18.5° N there is compression, then at latitude 20.5° N there is extension and at latitude 25° N there is compression, then at latitude 27° N extension and finally at latitude 29° N there is compression. Furthermore, the figure shows the highest compressions and extensions because the network stations are denser here than in other areas.

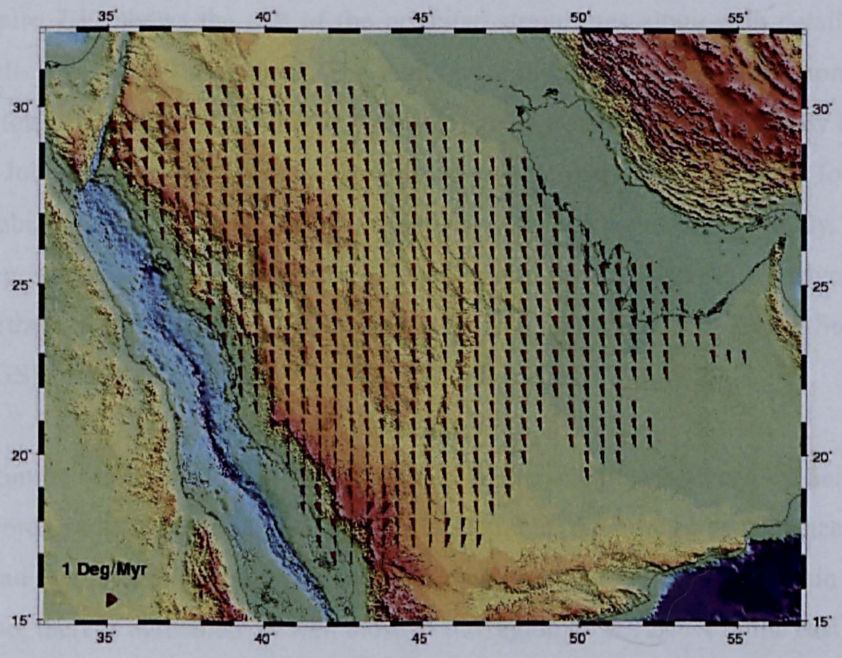

Figure7.10. Regional rigid body rotation rates for the regional network (in deg/Myr) computed at the grid nodes.

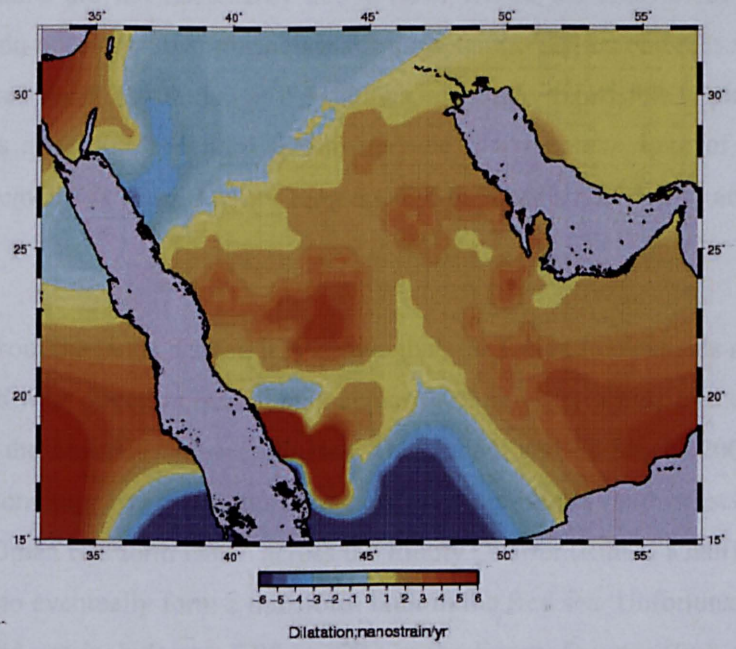

Figure 7.11. Regional dilatation rates for the regional network. Positive or negative values indicate extension and compression, respectively.

Figure 7.12 shows the plot of the principal strain rates along with details of, faults and the seismic record. The faults were digitized by the author from the tectonic map of Saudi Arabia and adjacent areas, which was compiled by Peter R. Johnson in 1998. There is no more up-to-date map of active faults for the Arabian plate that can be used for interpolation of the results of this study. This map shows the faults of the Precambrian period (545–4550 Myr/Bp). Furthermore, the seismic records were taken from the Saudi Geological Survey (SGS) archive, which were from the period from 1960 to July 2008.

It can be seen from Figure 7.12 that there is an agreement between the seismic records and the principal strain rate. For example, the north-west part near the Dead Sea fault shows an active seismic record and a high principal strain rate. Also, there is agreement as well close to the region 49° E, 24° N in the east.

However, Figure 7.12 does not show a strong relationship between the principal strain plot distribution and the faults plot; this is due to a variety of reasons. Firstly, the faults map available is from the Precambrian age, and these faults are not necessarily active now. Hence the analysis of the GPS results do not show any information for these faults. The second reason may be the quite sparse distribution of the stations, making it impossible to pick up any changes at faults. The third reason may be that the time span of the GPS measurements is short, i.e. not long enough to show strain due to any active faults.

Apart from the faults shown, it is known that, the Oman line extends north-east to south-west direction from Oman across the Strait of Hormuz in the Arabian gulf to the Makran mountain in Iran. Derkhshani and Farhoudi [2005] found indications suggesting that this lineament may represent a south-west extension of the Oman line form Oman across the Empty Quarter (Rub al Khali) of Saudi Arabia to eventually form a transform fault in the Red sea. Unfortunately, this study did not include any GPS stations in the Empty Quarter (Rub al Khali); however, the extent of the Oman line passes across the region around 46° E and

17° N, where the strain in this study is quite high which could be another indication of the extension of the Oman line in this area.

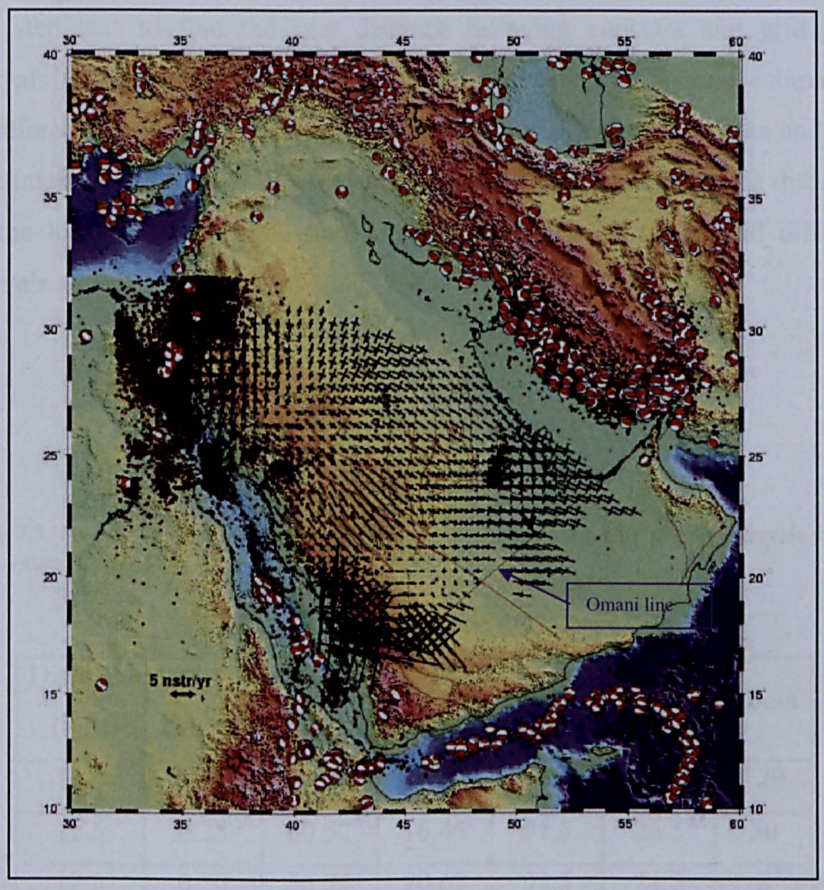

Figure 7.12. The principal strain rate components ($\varepsilon_1, \varepsilon_2$) for the regional network. Compression is shown by the arrows directed inside and the extension by arrows directed outside and the unit is nano strain per year (nstr/yr). The circles show all the seismic events from 1960 up to July 2008 from the Saudi Geological Survey (SGS) up to latitude 32° N. The peach ball show the seismic events from 1976 up to July 2008 from (http://www.globalcmt.org/CMTsearch.html) of magnitude > 4. The red lines show the faults from the Precambrian age, digitized from the tectonic map of Saudi Arabia and adjacent areas, compiled by Peter R. Johnson in 1998.

7.4.2 Strain rate estimation for the local network

After ensuring that there were no problematic stations in the input data, the next step was to find the best distance decaying constant and grid node intervals for the local network, in order to give the best strain estimation. Therefore, a number of tests were carried out for different distances and grid node intervals. Table 7.3 shows a summary of the predicted grid node distances for the local network when applying different distances and grid different intervals.

Table 7.3. Numerical tests with various distance decaying constants and grid intervals for the local network.

		Grid node distances				
Distance (km)	Interval Degree	Mean (km)	S.dev. (km)	Max. (km)	Min. (km)	Count
12.5	0.125	59.76	17.65	96.5	24.5	129
12.5	0.25	60.57	16.45	91.5	26.5	30
12.5	0.50	56.75	20.62	91.5	24.5	8
25	0.25	64.85	19.68	112	26	40
25	0.50	62.45	19.75	91	25	11
50	0.25	127.09	56.49	249	50	138
50	0.50	122.97	57.61	240	50	36
75	0.25	140.42	52.05	249	75	186
75	0.50	136.13	53.15	240	75	47

Four different initial distances (12.5 km, 25 km, 50 km and 75 km) were tested because the local network station distances were of the order of tens and two hundreds of kilometres. Also, three grid intervals (0.125°, 0.25° and 0.50°) were selected. As can be seen in Table 7.4, when a distance of 12.5 km is

applied, the mean of grid nodes distances for the three intervals are close to each other, at approximately 59 ± 18 km. Furthermore, the maximum distances reach 96.5 km when applying the 0.25° interval and 91.5 km when applying the 0.25° and 0.50° intervals. Also, the number of computation grid nodes decreases (from 129 to 30 and then 8).

When a distance of 25 km is applied, the mean of grid node distances for the two intervals are close to each other, at approximately 63 ± 19 km, the maximum distances reach 112 and 91 km, respectively, and the numbers of computation grid nodes are 40 and 11. Whereas, when a distance of 50 km is applied, the mean of grid node distances for the four intervals are close to each other at approximately 125 ± 57 km, the maximum distances reach 249 and 240 km, respectively, and the number of computation grid nodes decreases from 138 to 36. Finally, when a distance of 75 km is applied, the mean of grid node distances for the four intervals are close to each other at approximately 138 ± 52 km, the maximum distances reach 249 and 240 km, respectively and the number of computation grid nodes decreases from 186 to 47.

When the results from using different distances are compared with each other, it is seen that the means and the associated standard deviations vary between 56 and 140 km and ± 16 to ± 56 km, respectively. Moreover, the maximum distance varies widely as well, between 91 and 249 km. Therefore, the statistical result could be divided into two classes: the first class contains the distances of 12.5 and 25 km and the second class the 50 and 75 km distances. The number of computation grid nodes increases when the distance increases, which means more coverage of the network area.

As for the regional network, the value of the strain was compared before selection of the best distance decaying constant and grid interval. Therefore, the differences in the principal strain rate components ($\varepsilon_1, \varepsilon_2$) at the common grid nodes for different distances at the 0.25° interval were computed. Table 7.4 shows the statistical analysis of these computations and it can be seen that

the value of the strain at 12.5 and 25 km is almost the same, which is to be expected since the maximum and minimum distances for both are the same. Also, the strain values for 12.5 and 50 km are not significantly different. However, there are quite large differences between 12.5 and 75 km. Moreover, the strain values of 25 and 50 km are not significantly different, but the difference between 25 and 75 km is quite large and the differences between 50 and 75 km are quite large as well. These results show that when the selected distance increases the value of the strain decreases or, in other words, becomes smoother, similar to the case in the regional network. To futher investigate this, the differences in the principal strain rate components ($\varepsilon_1, \varepsilon_2$) at the common computation grid nodes of the regional network (distance 100 km and interval 0.5°) and the local network (distance 50 km and interval 0.5°) were computed. The results showed that the RMS of the principal strain rate components ($\varepsilon_1, \varepsilon_2$) were 9.0 and 6.9, respectively; the mean and the associated standard deviation being 4.2 ± 8.1 and -2.8 ± 6.4, respectively.

Table 7.4. Statistical analysis of the comparison of the strain rate at common grid nodes for different distances for the local network.

Diff. of distances at Interval 0.25°	Mean Of diff. ε_1	Standard dev. Of diff. ε_1	RMS Of diff. ε_1	Mean Of diff. ε_2	Standard dev. Of diff. ε_2	RMS Of diff. ε_2
12.5 – 25	0.0	± 0.6	0.5	-0.1	± 0.3	0.3
12.5 – 50	0.9	± 3.4	3.5	-0.4	± 2.3	2.3
12.5 – 75	5.1	± 8.8	10.0	-2.7	± 8.1	8.4
25 – 50	0.9	± 3.6	3.7	-0.3	± 2.3	2.3
25 – 75	5.1	± 9.0	10.2	-2.7	± 8.0	8.4
50 – 75	4.2	± 6.6	7.7	-2.3	± 6.3	6.6

Therefore, as with the regional network, it can be concluded that the strain value is more significant when the selected distance is short, but this will lead to some gaps in the coverage of the area. Hence, a distance of 50 km was selected to be the best, since it is a compromise between the significant strain value and the network area coverage. Also, the grid interval of 0.25° was selected to be the most suitable interval, since it is a compromise for the density of the network as well (figure 7.13).

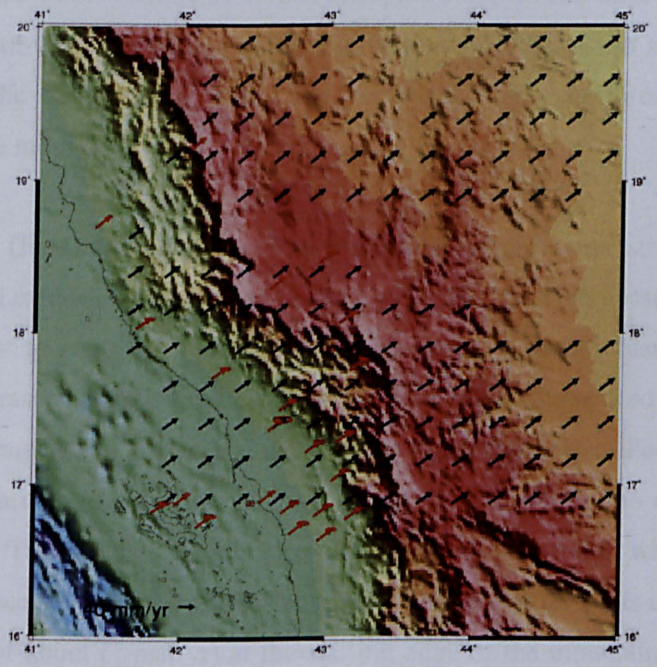

Figure 7.13. The local velocity field network used in the strain rate computations. The black arrows indicate the predicted grid node velocity field and the red arrows are the observed velocity field.

Figure 7.14 shows the principal strain rates for the local network. In Polygon 1 the principal strain rates in both the compression and extension directions are about 4 nstr/yr, the compression direction is north-east to south-west and the extension direction is north-west to south-east. Meanwhile, Polygon 2 only has an extension value of about 3 nstr/yr, there being no compression in this area. Polygon 3 shows variable principal strain, since in the direction from the west

to east there are quite large extensional strains and very small compressions at the edge, where the mountains start to build up. After that, the extension strain rate decreases and the compression strain rate increases in the mountain area until the strain rates in both directions are almost equal.

Polygon 4 has on average the same strain rate (4 nstr/yr) in both the compression and extensional directions, since this region is located beyond the mountains. However, Polygon 5 shows high strain rates in both the extensional (26 nstr/yr) and compression (13 nstr/yr) directions. So the extension strain rate is double that of the compression rate. Also, the compression direction is north-east to south-west and the extensional direction is north-west to south-east. In addition, the compression strain rate decreases in the north-east direction towards the mountains.

Polygon 6 (Farasan island) shows a very high compression strain rate (47 nstr/yr) and extensional strain rate (33 nstr/yr). Also, the compression direction is north-east to south-west, similar to the direction of the Arabian rigid plate motion. Farasan island is close to the opening ridge of the Red Sea, which would explain why Farasan island has very high strain rates. Polygon 7 has quite a high compression strain rate (22 nstr/yr) and there is no extension in this region. The compression direction is almost north to south, which is to be expected because of the Farasan island movement. Polygon 8 has an extension strain rate of about (7 nstr/yr) at the starting edge of the mountains. Also, the extension is double the compression and the value of the strain rate in both directions dramatically increases from west to east. Finally, Polygon 9 is similar to Polygon 8, where the extension strain rate is high (29 nstr/yr) in most of the area, but the compression strain rate is very small in the west and gradually increases in the east direction in the mountains. The extension direction is north to south and in the west the compression direction is west to east, but both directions change gradually in the east direction when the mountains build up, to where the extension direction becomes north-west to south-east and the compression direction north-east to south-west.

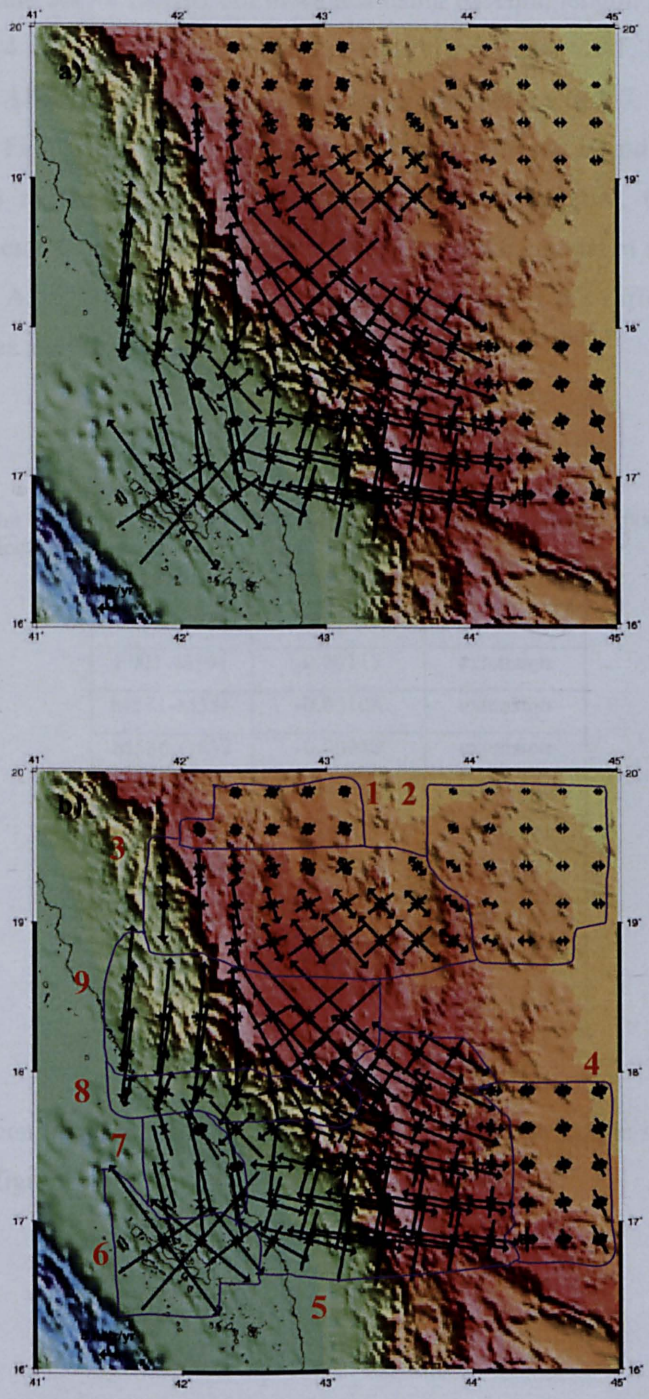

Figure 7.14. The principal strain rate components ($\varepsilon_1, \varepsilon_2$) for the local network. Compression is shown by pairs of arrows directed inwards and extension by pairs of arrows directed outwards. The polygons represent areas that have similar strain values. The unit is nano strain per year (nstr/yr).

Moreover, the author carried out more test using baseline length. From figures 7.7 and 7.14 show there is an extension along the stations F001, M591, M586 and O639. Also, there is a compression along the stations M587, M586, O635 and O633. Finally there is a compression between Farasan Island (f074, O643 and O644) to the direction of the coast (F001). Therefore, the baselines between these stations were computed using Jan 2006 campaign and Jan 2008 campaign. After that the baselines were compared and the differences were computed as shown in table.

Table 7.5. The baselines differences for a selected baselines in campaign 2006 and campaign 2008 for the local network.

Baseline	Difference (m)	
F001-O639	-0.00445	extension
F001-M591	-0.00117	extension
M591-M586	-0.00108	extension
M586-O639	-0.00248	extension
M587-M586	0.00122	compression
M586-O635	0.00045	compression
O635-O633	0.00035	compression
F074-F001	0.00330	compression
O643-F001	0.00236	compression
O644-F001	0.00377	compression

It can be seen that the result on table 7.5 agree with the principle strain analysis shown on figure 7.14.

Figure 7.15 shows the rotation rate for the local network in the south-west of the Arabian plate. The figure shows different rotation rate values and directions in different places. At 44.5° E, 19.5° N, the rotation rate direction is anticlockwise and the rotation rate is about 0.35 deg/Myr in the east, decreasing gradually to the west down to 0 deg/Myr at about 43.5° E. Then the rotation rate gradually increases again in the west direction. Also, at 44.5° E, 17.5° N there is an anticlockwise rotation direction with a rotation value of about 0.25 deg/Myr. However, at 42.8° E and between 17° N and 18.5° N, the rotation direction is different to the east and west of 42.8 E; in the west the rotation direction is anticlockwise and in the east it is clockwise. Also, the rotation value varies between 0 deg/Myr and 0.9 deg/Myr. Furthermore, the Farasan Island shows quite a anticlockwise rotation value.

Figure 7.16 shows the dilatation for the local network and shows that Farasan Island is in compression, but the coast along the Red Sea near Jazan city between latitudes of 17° N and 17.8° N is in extension. There is a compression between latitudes 18° N and 20° N, as well as in the mountains. Beyond the mountains in the easterly direction, the compression then decreases.

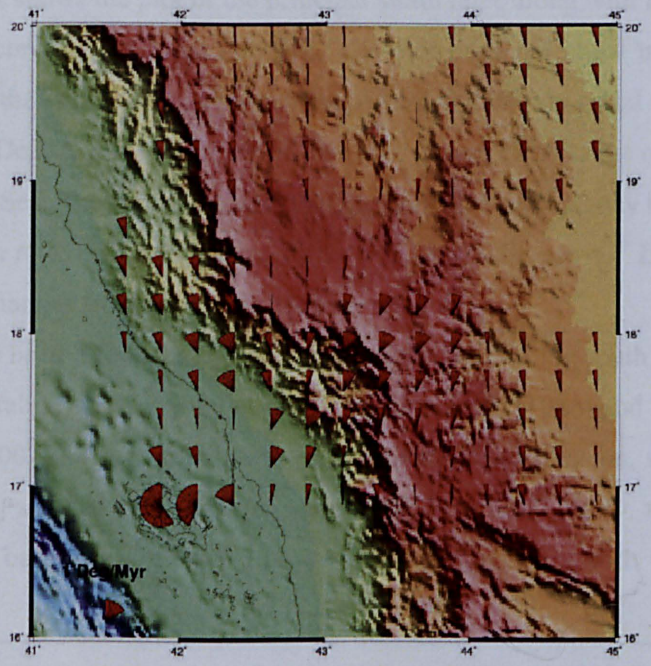

Figure 7.15. Rigid body rotation rates for the local network (in deg/Myr) computed at the grid nodes.

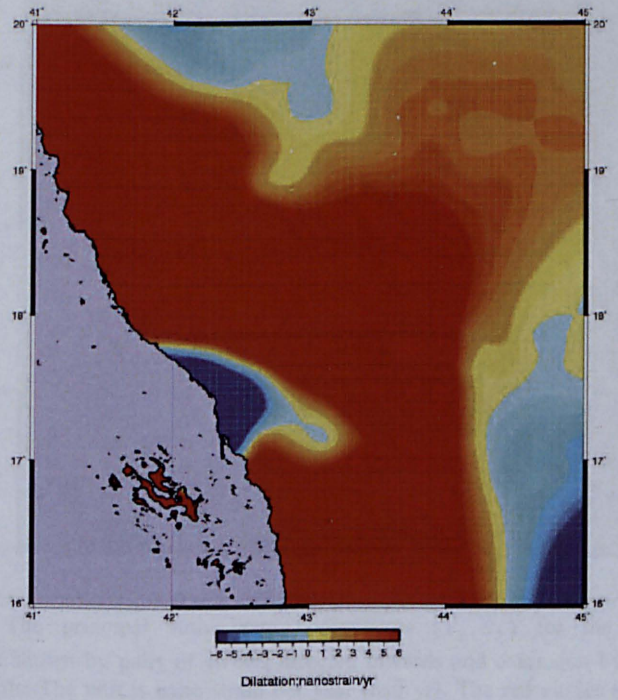

Figure 7.16. Dilatation rates for the local network.

Figure 7.17 shows the plot of the principal strain rates along with faults and the seismic record for the local network. The plot does not show many seismic records in the south-western part of the Arabian plate compared to the north-west part (Dead Sea fault); however, this area is very close to the opening ridge of the Red Sea. The results suggest that the fault along 43° E may be active and the rotation rate in Figure 7.12 confirms this, since close to 43° E the rotation direction changes from anticlockwise to clockwise.

There have been a few geological studies carried out on the south western part of Saudi Arabia, e.g. Coleman *et al.* [1979], Bohannan [1986] and Dwivedi and Hayashi [2007] all suggested north-east to south-west extension, while Giraud et al [1986] showed compression in the same direction. Clearly, the results of this study, based on GPS geodesy are more in agreement with Giraud *et al* [1986].

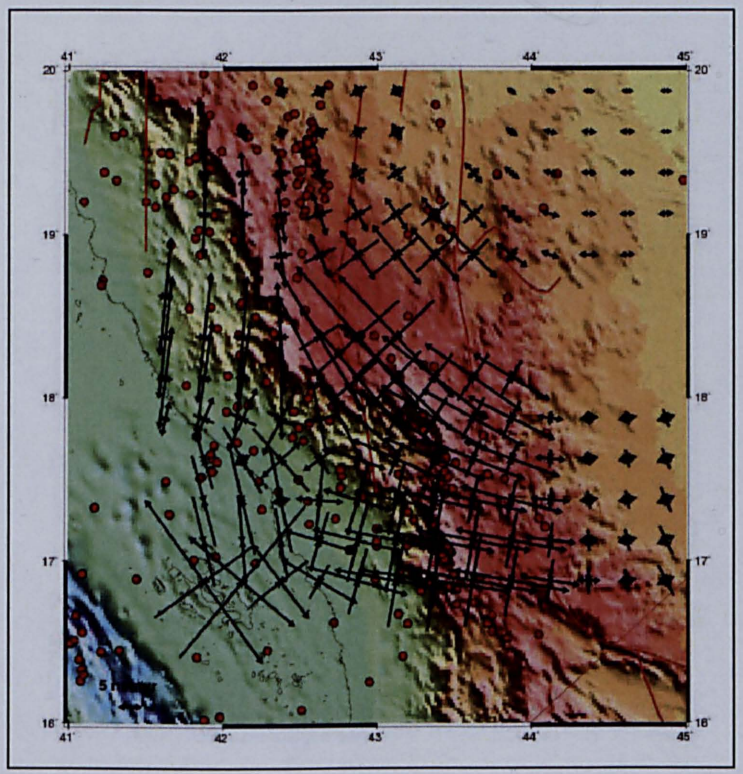

Figure 7.17. The principal strain rate components $(\varepsilon_1, \varepsilon_2)$ for the local network. Compression is shown by pairs of arrows directed inwards and extension by pairs of arrows directed outwards. The unit is nano strain per year (nstr/yr). The red circles show the seismic events from 1960 up to July 2008 from the Saudi Geological Survey (SGS). The red lines show the faults of Precambrian age digitized from the tectonic map of Saudi Arabia and adjacent areas, compiled by Peter R. Johnson in 1998.

7.5 Summary

This chapter has discussed the background theory of strain and its estimations. Strain rate accumulations within the Arabia plate at a regional scale, and at a local scale in the south-west part, have then been estimated and analysed. The results show that the strain rates on the Arabian plate are quite small, except in areas to the north-west, close to Dead Sea fault, in the eastern part and in the south-west. The results for the local network strain rate confirm that the south-west is an active region, with significant compressional strain associated with the opening of the Red Sea near to Farasan Island. Considering both scales of networks in this study, it is clearly worthwhile considering the establishment of more dense networks in the northwest and east of the Arabian plate.

Chapter 8: Conclusions and recommendations for further work

8.1. Summary

Previous investigations of the present-day kinematics of the Arabian plate using GPS measurements were primarily obtained from stations located on surrounding plates, often with few stations actually located on the Arabia plate itself. Due to the inhomogeneous distribution of these GPS stations and the fact that some of these were actually located in the plate boundary zone, the motion of the Arabian plate was only sensed in a few locations on the rigid plate interior

The aim of this study was to compute an updated estimate for the absolute and relative motion of the Arabian plate Euler pole and rotation rate. Then to investigates of the regional scale, the strain rate accumulation within the Arabian plate using the GPS network. Then, to investigate, at a local scale, the strain rate accumulation in the tectonically active south-western part of Saudi Arabia using a densified GPS network of stations in that area.

For this study the regional and local GPS networks were designed based on geological factors and geodetic factors, and the distribution of stations. A reference frame implementation was applied using a near global network 49 IGS stations, distributed around the Arabian plate and spanning five other plates (Africa, Somalia, India, Eurasia and Anatolia). Most of these stations being part of the ITRF2005 and IGS05 reference frames.

A processing strategy was adopted to avoid any inconsistent or unsuitable model used, or any incorrect computations carried out, which would affect the final result and its geodynamic interpretation. The processing strategy was designed to compute the daily station coordinates starting from 1 January 2000

up to 30 June 2007. The Bernese GPS Software version 5.0 (BSW 5.0) was used in double-difference mode, with the new absolute satellite and receiver antenna phase center models, together with newly available GPS products and those the first from a recent global re-processing effort [*Steigenberger et al.*, 2006]. Integer-ambiguities were resolved using the Quasi-Ionosphere-Free (QIF) strategy for baselines lengths less than 2000 km and the Melbourne-Wübbena strategy for baselines lengths greater than 2000 km.

For the continuous data, the daily coordinates computed using BSW 5.0 were used as input to CATS which allows taking into account for offsets and periodic signals and the uncertainties are estimated with full white plus flicker noise covariance based on a maximum likelihood estimation (MLE) noise analysis of the continuous GPS coordinate time series. For the episodic data, all campaigns were conducted between March and April for the regional network and in January for the local network in order to minimize biases from annual and semi-annual signals. Nevertheless, this study computed a regional filter using the continuous GPS coordinate time series and applied this to the episodic GPS coordinate time series. Then to obtain realistic uncertainties for the episodic data the equations given by Zhang *et al.* [1997] or Mao *et al.* [1999], with the average amplitudes of the white and flicker noise for the regional network taken from the CATS output for three (BAHR, YIBL and RAMO) of the IGS stations in the region.

8.2. Conclusions

The absolute motion model for the Arabian plate obtained from this study (50.420° N, 4.089° W and 0.533°/Ma) is significantly different from those obtained in previous studies, as a result of the number of stations used and their distribution. This does not mean that the previous studies were in error, but that they suffered from a lack of evenly distributed geodetic data for Arabia. Hence, this study result is a new contribution to the knowledge of Arabian plate motion.

The relative motion of the Arabian plate to Eurasian plate from this study (28.17° N, 18.93° E and 0.431 °/M) confirms the result from some previous studies using geodesy techniques. Furthermore, this study shows the significant difference in north direction to the geological model NUVEL-1A [*DeMets, et al.*, 1994]. However this agrees with other studies, in that the Arabian plate slows down in north direction as it moves to the north and collides to Eurasia.

The relative motion of the Arabian plate to Nubian plate from this study (31.42° N, 24.47° E and 0.407 °/M) confirms the result from most previous studies using geodesy or geology techniques. Moreover, this study has shown that the measured spreading rate averaged over the last 3 Myr modelled by Chu and Gordon, [1998] and Jestin, *et al.*, [1994] is systematically slightly faster than this study, but not significantly so. The rate in the northern red sea is reduced by 4% compared to Chu and Gordon, [1998] and by 7% compared to Jestin, *et al.*, [1994]. Also, the rate is reduced in the southern red sea by 9% compare with Chu and Gordon, [1998] and by 11% compared with Jestin, *et al.*, [1994]

The relative motion of the Arabian plate to Somalian plate from this study (22.79° N, 27.5° E and 0.430 °/M) and it is close to those of previous studies using geodetic techniques when using two stations. Whereas the result when using three stations (24.92° N, 26.05° E and 0.398 °/M) is close to those of previous studies using geological techniques.

Moreover, this study shows that at the regional scale, the principal strain rate is, in general, a compression in the north-east to south-west directions and an extension in the north-west to south-east direction, except for two areas: the first in the north-west, close to the Aqaba Gulf and the Dead Sea fault, where there is north to south compression and west to east extension, and the second in part of the south-west region ($42^{\circ}E$, $18^{\circ}N$) that shows a north to south extension and a west to east compression.

Also, this study shows that there is an agreement between the seismic records and the principal strain rate. For example, the north-west part near the Dead Sea fault shows an active seismic record and a high principal strain rate. Also, there is agreement as well close to the region 49° E, 24° N in the east.

This study does not show a strong relationship between the principal strain plot distribution and the faults plot. This may be due to a variety of reasons: firstly, the faults map available is from the Precambrian age, and these faults are not necessarily active now, hence the analysis of the GPS results does not show any information for these faults; the second reason may be the quite sparse distribution of the stations, making it impossible to pick up any changes at faults; the third reason may be that the time span of the GPS measurements is short, i.e. not long enough to show strain due to any active faults.

This study supports Derkhshani and Farhoudi [2005] who found indications suggesting that the Oman line extends in a north-east to south-west direction and may represent a south-west extension of the Oman line across the Empty Quarter (Rub al Khali) of Saudi Arabia to eventually form a transform fault in the Red sea.

The results in this study suggests that the fault along 43° E may be active and the rotation rate confirms this, since it is close to 43° E the rotation direction changes from anticlockwise to clockwise.

Furthermore, the results of this study, based on GPS geodesy are in agreement with Giraud *et al* [1986], who suggested north-east to south-west compression on the south-west of Saudi Arabia.

8.3. Recommendations for further work

The collaboration between the General Commission for Survey (GCS) in Saudi Arabia with the Institute of Engineering Surveying and Space Geodesy (IESSG) has resulted in establishing dense GPS networks in Saudi Arabia, in order to advance the knowledge of the dynamics of Arabia plate, from which this study is one of the collaboration results. Moreover, since in general the geodynamic studies depends greatly on the time span and quantity of data collected, the author recommends the following further works:

1. It will be greatly beneficial to advance more the knowledge of the dynamics of the Arabian plate, if this collaboration between GCS and IESSG continues in the future. Where more continuous GPS stations could be established, more GPS campaigns carried out, and more dense GPS networks be established.
2. It is suggested that this collaboration be extended to include other organizations in Saudi Arabia and other organizations in other countries on and surrounding Arabian plate.
3. It suggested that more continuous GPS stations to be established on the Arabia plate, where some of these are of them on the stable part, for reference frame implementation, and others are in the active area, for monitoring purposes. These would also enable the study of vertical motions in addition to horizontal motions.
4. It is recommended to establish a denser network in the north-west of Saudi Arabia to investigate the strain rate accumulation in that area.
5. It is suggested that two or more GPS campaigns are carried out for the local network in the south west to monitor the stability of the station velocities and their associated uncertainties.
6. It is recommended to establish continuous GPS stations on the south-west of Saudi Arabia, where one or two of them on the Farasan Island for more strain rate investigations.

7. It is recommended to establish more GPS stations along other side of the Red Sea (west coast of Red Sea), because there is a need to study more the opening of the red Sea.
8. It is recommended to establish more GPS stations along both side of Golf of Aden and Afar triple junction for more investigations.
9. It is recommended to estimate the relative motion of Arabian plate to Indian plate when more GPS stations are available on Indian plate and distributed evenly on land, since two third of Indian plate is covered by water.

Maximum Likelihood Estimation

Using Maximum Likelihood Estimation (MLE) a best fit model can be fit to the post-fit residuals $\hat{v}$ by maximizing the log-likelihood probability function [Zhang *et al.*, 1997; Mao *et al.*, 1999; Williams, 2003] as follows Williams:

$$lik(\hat{v}, C) = \frac{1}{(2\pi)^{N/2}(\det C)^{1/2}} \exp(-\frac{1}{2}\hat{v}^T C^{-1}\hat{v}) \tag{A.1}$$

$$\ln[lik(\hat{v}, C)] = -\frac{N}{2}\ln(2\pi) - \frac{1}{2}\ln(\det C) - \frac{1}{2}\hat{v}^T C^{-1}\hat{v} \tag{A.2}$$

Where the fully populated covariance matrix for observations is

$$C = a^2 I + b_k^2 J_k \tag{A.3}$$

Which accounts for a combination of white and power-law noise with amplitudes a and b_k. The identity matrix I is the covariance matrix of the white noise and the matrix J_k is the covariance matrix of the power-law noise that is computed by means of fractional differencing [Williams, 2003] as follow:

$$J_k = TT^T \tag{A.4}$$

where T is a transformation matrix obtained from

$$T = \Delta T^{-k/4} \begin{bmatrix} \psi_0 & 0 & 0 & 0 \\ \psi_1 & \psi_0 & 0 & 0 \\ \psi_2 & \psi_1 & \psi_0 & 0 \\ & & & \\ \psi_N & \psi_{N-1} & \psi_{N-2} & \psi_0 \end{bmatrix} \tag{A.5}$$

with sampling interval ΔT and with

$$\psi_N = \frac{-\frac{k}{2}(1-\frac{k}{2}) \quad (N-1-\frac{k}{2})}{N!} = \frac{\Gamma(N-\frac{k}{2})}{N!\Gamma(-\frac{k}{2})} \tag{A.6}$$

and Γ is the Gamma function.

Mao method

Mao *et al.*, [1999] and Dixon *et al.*, [2000] reported that there is a strong correlation between WRMS of their coordinate time series and the estimated noise amplitudes for white and flicker noise. From the data set they derived the following linear equations:

$$\begin{aligned} a(N) &= 0.613 WRMS(N) + 0.259 \\ a(E) &= 0.767 WRMS(E) - 0.183 \\ a(H) &= 0.843 WRMS(H) - 1.772 \\ b_{-1}(N) &= 1.139 WRMS(N) + 0.117 \\ b_{-1}(E) &= 1.041 WRMS(E) - 0.342 \\ b_{-1}(H) &= 0.668 WRMS(H) + 5.394 \end{aligned} \tag{A.7}$$

a is the white noise and b_{-1} the flicker noise amplitude for the north (N) , east (E) and height (H) components.

Williams method

Williams [2003] illustrated that when a linear combination of white and coloured noise of spectral index k with amplitudes a and b_{-k}, and equally spaced data that:

$$\mathrm{RMS} = \sqrt{a^2 + cb_k^2} \tag{A.8}$$

where

$$c = \frac{1}{sf}\frac{D_k}{f_s^{\frac{k}{2}+1}(k+1)}[(\frac{f_s}{2})^{k+1} - (\frac{1}{T})^{K+1}] \quad k \neq 1$$
$$c = \frac{D_{-1}}{\sqrt{f_s}}[\log(\frac{f_s}{2}) - \log(\frac{1}{T})] \qquad k = -1 \tag{A.9}$$
$$D_k = 2(2\pi)^k (24 \times 60 \times 60 \times 365.249)^{k/2}$$

f_s is the sampling frequency in Hz and T the total time span in years. The scaling factor sf is given by

$$sf = 0.5718k^2 + 1.0826k + 1.5838 \quad \text{for} \quad k < -1 \tag{A.10}$$
$$\text{and} \quad sf = -0.0681k + 1.0 \quad \text{for} \quad k \geq -1$$

Table B.1 all offsets applied in the first filter

STAT	Date	Details	Applied
ARTU	2000-02-02	ITRF2005 discontinuity	Up North East
BILI	2002-01-15	ITRF2005 discontinuity	Up North East
BILI	2002-03-03	ITRF2005 discontinuity	Up North East
BOR1	2002-03-06	Receiver change	Up North East
BRUS	2000-01-27	Receiver change	Up North East
BRUS	2000-03-27	Receiver change	Up North East
BRUS	2000-04-28	Antenna change	Up North East
BRUS	2001-03-21	Receiver change	Up North East
CAGL	2001-07-11	Antenna and receiver change	Up North East
CAGL	2004-03-01	Receiver change	Up North East
DGAR	2002-01-19	Receiver change	Up North East
DGAR	2002-11-02	Receiver change	Up North East
DGAR	2004-05-18	Antenna and receiver change	Up North East
DGAR	2004-12-26	Sumatra earthquake	Up North East
GLSV	2000-04-21	Receiver change	Up North East
GLSV	2002-06-26	Receiver change	Up North East
GLSV	2007-11-12	Antenna and receiver change	Up North East
GRAS	2003-04-22	Antenna and receiver change	Up North East
GRAS	2004-01-26	Receiver change	Up North East
GRAS	2004-10-20	Antenna and receiver change	Up North East
GRAS	2007-05-03	Receiver change	Up North East
GRAS	2007-05-14	Receiver change	Up North East
GRAS	2007-09-03	Receiver change	Up North East
HARB	2000-08-10	Antenna change	Up North East
HARB	2004-01-26	Receiver change	Up North East
HRAO	2000-04-16	Receiver change	Up North East
HRAO	2003-10-17	Antenna change	Up North East
HRAO	2004-11-19	Antenna change	Up North East
HRAO	2005-04-24	Antenna change	Up North East
HRAO	2006-02-14	Antenna change	Up North East
HRAO	2006-02-22	Antenna change	Up North East
HRAO	2006-12-28	Antenna and receiver change	Up North East
HYDE	2000-12-15	Receiver change	Up North East
HYDE	2001-07-13	Antenna and receiver change	Up North East
HYDE	2004-06-25	Receiver change	Up North East
HYDE	2004-12-26	Sumatra earthquake	Up North East
IFRN	2004-07-01	Receiver change	Up North East
IFRN	2004-08-23	Receiver change	Up North East
IFRN	2004-10-12	Receiver change	Up North East
IISC	2001-07-17	Receiver change	Up North East
IISC	2004-12-26	Sumatra earthquake	Up North East
JOZE	2004-12-06	ITRF2005 discontinuity	Up North East
JOZE	2006-01-01	ITRF2005 discontinuity	Up North East
KUNM	2002-11-11	Receiver change	Up North East
KUNM	2004-12-26	Sumatra earthquake	Up North East
LAUG	2002-11-18	Antenna change	Up North East
LAHZ	2001-11-28	Receiver change	Up North East
LAHZ	2003-10-19	Receiver change	Up North East
LAHZ	2003-11-24	Receiver change	Up North East
LAHZ	2006-05-16	Receiver change	Up North East
LAHZ	2007-02-28	Antenna change	Up North East

Cont. table B.1 all offsets applied in the first filter

STAT	Date	Details	Applied
MADR	2003-09-10	Antenna change	Up North East
MADR	2003-11-12	Antenna change	Up North East
MALI	2001-04-26	Receiver change	Up North East
MAS1	2000-11-21	Receiver change	Up North East
MATE	2001-09-24	Receiver change	Up North East
MATE	2004-02-10	Antenna change	Up North East
MATE	2004-04-19	Receiver change	Up North East
MBAR	2007-09-01	Receiver change	Up North East
MDVJ	2007-10-27	Receiver change	Up North East
METS	2000-05-24	Receiver change	Up North East
NICO	2000-03-01	Receiver change	Up North East
NICO	2006-01-17	Receiver change	Up North East
NICO	2007-03-07	Receiver change	Up North East
NRIL	2005-11-10	Receiver change	Up North East
ONSA	2003-08-19	Receiver change	Up North East
ONSA	2004-03-11	Receiver change	Up North East
ONSA	2007-11-01	Receiver change	Up North East
POL2	2001-06-11	Receiver change	Up North East
POTS	2000-08-19	Receiver change	Up North East
RABT	2004-04-14	Receiver change	Up North East
RAMO	2000-07-17	Antenna change	Up North East
RAMO	2003-02-16	Receiver change	Up North East
RAMO	2004-03-15	monument repair	Up North East
RAMO	2007-02-16	Receiver change	Up North East
REUN	2003-04-04	Antenna change	Up North East
REUN	2003-11-18	Receiver change	Up North East
SEY1	2003-02-06	Antenna and receiver change	Up North East
SEY1	2004-06-21	Receiver change	Up North East
SEY1	2005-04-01	Receiver change	Up North East
SEY1	2006-11-20	Antenna and receiver change	Up North East
SEY1	2007-04-11	Antenna and receiver change	Up North East
SEY1	2007-12-07	Receiver change	Up North East
SFER	2002-03-04	Antenna and receiver change	Up North East
SFER	2003-02-18	Receiver change	Up North East
SFER	2003-06-08	ITRF2005 discontinuity	Up North East
SFER	2005-11-28	Receiver change	Up North East
SOLA	2004-05-19	Antenna change	Up North East
SUTH	2001-01-12	Receiver change	Up North East
SUTH	2002-02-27	Antenna and receiver change	Up North East
SUTH	2004-06-01	Antenna and receiver change	Up North East
SUTH	2006-10-30	Receiver change	Up North East
TEHN	2004-01-16	Antenna and receiver change	Up North East
TEHN	2006-02-04	Receiver change	Up North East
TETN	2001-03-24	Receiver change	Up North East
TETN	2001-04-17	Receiver change	Up North East
TETN	2003-05-07	Receiver change	Up North East
TETN	2003-05-08	Receiver change	Up North East
TETN	2004-10-14	Receiver change	Up North East
TETN	2004-10-16	Receiver change	Up North East
TRO1	2000-06-19	Antenna change	Up North East
TRO1	2004-07-13	Antenna change	Up North East
TRO1	2007-08-24	Antenna change	Up North East

Cont. table B.1 all offsets applied in the first filter

STAT	Date	Details	Applied
MADR	2003-09-10	Antenna change	Up North East
MADR	2003-11-12	Antenna change	Up North East
MALI	2001-04-26	Receiver change	Up North East
MAS1	2000-11-21	Receiver change	Up North East
VILL	2000-07-18	Receiver change	Up North East
VILL	2001-04-23	Receiver change	Up North East
VILL	2004-09-28	Antenna change	Up North East
VILL	2004-12-03	Receiver change	Up North East
VILL	2005-01-18	Receiver change	Up North East
VILL	2006-11-29	Antenna change	Up North East
VILL	2007-04-18	Antenna change	Up North East
WSRT	2000-01-05	Receiver change	Up North East
WSRT	2000-08-15	Receiver change	Up North East
WSRT	2001-05-31	Receiver change	Up North East
WSRT	2005-04-05	Receiver change	Up North East
WTZR	2001-08-17	Receiver change	Up North East
WTZR	2002-06-25	Receiver change	Up North East
WTZR	2002-07-02	Antenna change	Up North East
WTZR	2005-05-04	Receiver change	Up North East
WTZR	2005-05-17	Receiver change	Up North East
WTZR	2005-12-01	Receiver change	Up North East
WTZR	2007-05-23	Receiver change	Up North East
WTZR	2007-05-30	Receiver change	Up North East
WTZR	2007-09-04	Receiver change	Up North East
WTZR	2007-12-14	Receiver change	Up North East
WUHN	2000-06-07	Antenna and receiver change	Up North East
WUHN	2002-01-23	Antenna change	Up North East
WUHN	2002-10-31	ITRF2005 antenna offset	Up North East
YIBL	2006-11-12	Receiver change	Up North East
ZIMM	2003-08-13	Receiver change	Up North East
ZIMM	2006-02-22	Receiver change	Up North East

Table B.2 the offsets applied in the second filter

STAT	Date	Details	Applied
BILI	2002-01-15	ITRF2005 discontinuity	Up
BILI	2002-03-03	ITRF2005 discontinuity	Up
BRUS	2001-03-21	Receiver change	Up
CAGL	2001-07-11	Antenna and receiver change	Up North East
DGAR	2004-12-26	Sumatra earthquake	Up North East
HYDE	2004-12-26	Sumatra earthquake	North East
IISC	2004-12-26	Sumatra earthquake	North East
KUNM	2002-11-11	Receiver change	Up
KUNM	2004-12-26	Sumatra earthquake	North East
SEY1	2004-06-21	Receiver change	Up North East
SFER	2002-03-04	Antenna and receiver change	North
SFER	2003-06-08	ITRF2005 discontinuity	North East
WUHN	2002-01-23	Antenna change	Up

Table B.3 the exclusions applied in the second filter

STAT	From	To	Applied
BRUS	2000-01-01	2000-04-28	Up North East
RAMO	2000-01-01	2004-03-17	Up North East

Table B.4 the offsets applied in the third filter

STAT	Date	Details	Applied
BRUS	2001-03-21	Receiver change	Up
CAGL	2001-07-11	Antenna and receiver change	Up North East
DGAR	2004-05-18	Antenna and receiver change	North
DGAR	2004-12-26	Sumatra earthquake	Up North East
GRAS	2003-04-22	Antenna and receiver change	Up North East
GRAS	2004-10-20	Antenna and receiver change	Up North East
HARB	2004-01-26	Receiver change	Up North East
HYDE	2004-12-26	Sumatra earthquake	North East
IISC	2004-12-26	Sumatra earthquake	North East
JOZE	2004-12-06	ITRF2005 discontinuity	North East
KUNM	2002-11-11	Receiver change	Up
KUNM	2004-12-26	Sumatra earthquake	North East
LAHZ	2007-02-28	Antenna change	Up North East
MATE	2004-02-10	Antenna change	Up North East
RAMO	2000-07-17	Antenna change	Up North East
RAMO	2004-03-15	monument repair	Up North East
REUN	2003-04-04	Antenna change	Up North East
SEY1	2003-02-06	Antenna and receiver change	Up North East
SEY1	2004-06-21	Receiver change	Up
SFER	2002-03-04	Antenna and receiver change	Up North East
SFER	2003-06-08	ITRF2005 discontinuity	North East
SUTH	2002-02-27	Antenna and receiver change	Up North
SUTH	2004-06-01	Antenna and receiver change	Up North
VILL	2001-04-23	Receiver change	Up North East
VILL	2004-09-28	Antenna change	Up North East
VILL	2006-11-29	Antenna change	Up North East
VILL	2007-04-18	Antenna change	Up North East
WTZR	2002-07-02	Antenna change	Up North East
WUHN	2000-06-07	Antenna & receiver change	Up
WUHN	2002-01-23	Antenna change	Up
WUHN	2002-10-31	ITRF2005 antenna offset	Up

Table B.5 the exclusions applied in the third filter

STAT	From	To	Applied
BRUS	2000-01-01	2000-04-28	Up North East
BILI	2002-01-15	2002-03-03	Up North East
IRKT	2000-01-01	2000-03-31	Up North East

Table B.6 The estimated offsets and their formal errors in the first filter

STAT	date	N_{off}	σ_N	E_{off}	σ_E	U_{off}	σ_U
ARTU	2000.091530	1.6694	0.3959	-2.7564	0.4742	21.2135	1.3214
BILI	2002.042466	3.7677	0.5770	2.1049	0.5242	-19.4119	1.5487
BILI	2002.171233	-1.5884	0.5847	-2.7607	0.5313	18.1122	1.5695
BOR1	2002.179452	-0.3723	0.1292	-0.3324	0.1312	-1.1120	0.3009
BRUS	2000.075137	2.2865	0.6684	-0.4257	0.8300	2.1894	1.3744
BRUS	2000.236339	-1.6990	0.6190	1.1209	0.7687	2.5234	1.2729
BRUS	2000.326503	-3.7246	0.4259	-1.7144	0.5289	-0.9134	0.8757
BRUS	2001.220548	-0.4326	0.1535	2.1292	0.1906	-4.9781	0.3156
CAGL	2001.524658	2.4395	0.1621	5.6339	0.1891	-4.4970	0.4176
CAGL	2004.170765	1.8801	0.1912	-0.9497	0.2230	-3.2932	0.4924
DGAR	2002.423288	6.2585	1.0383	-3.8771	1.0291	3.8957	2.5164
DGAR	2002.839726	-1.7295	1.0990	-1.8766	1.0893	-1.6727	2.6636
DGAR	2004.386612	2.0897	0.7401	-4.3359	0.7336	0.7926	1.7937
DGAR	2004.984973	6.8732	0.5008	8.1939	0.4964	-3.0718	1.2139
GLSV	2000.312842	-0.9524	0.2427	-2.2755	0.2519	-1.7832	0.6796
GLSV	2002.483562	-1.6887	0.1434	-0.6139	0.1488	-2.6515	0.4016
GRAS	2003.308219	1.6061	0.1895	4.7705	0.2083	-1.1460	0.4000
GRAS	2004.072404	-0.1521	0.1919	-0.2705	0.2110	-1.1880	0.4052
GRAS	2004.807377	3.6014	0.1657	-0.9924	0.1821	0.0483	0.3497
GRAS	2007.390411	-1.4263	0.3512	-1.3048	0.3860	0.3096	0.7415
HARB	2004.400273	2.5709	0.5312	-3.5426	0.5870	5.7328	0.9254
HYDE	2004.501366	2.5783	0.2983	-2.3521	0.3023	2.4117	0.6854
HYDE	2004.984973	-1.4023	0.3039	8.5174	0.3080	-2.7498	0.6983
IISC	2001.568493	0.3427	0.4198	-2.3588	0.5086	-8.0312	1.1311
IISC	2004.984973	-2.6397	0.3247	14.2151	0.3934	-12.1117	0.8750
JOZE	2004.930328	1.4779	0.1469	-3.3231	0.1432	0.4806	0.3756
JOZE	2006.047945	-2.0503	0.1593	1.3887	0.1553	2.4155	0.4074
KUNM	2002.861644	3.6873	0.3824	-0.0220	0.3964	24.3718	1.3792
KUNM	2004.984973	-7.0371	0.3544	-5.3006	0.3674	-4.7474	1.2783
MALI	2001.319178	-4.3374	0.3693	9.1865	0.6209	-2.8763	1.1512
MAS1	2000.968579	-0.7930	0.1934	-0.7203	0.2443	-0.3181	0.5850
MATE	2001.730137	2.0402	0.1438	0.3022	0.1479	-0.2760	0.3487
MATE	2004.110656	0.9816	0.2571	-0.2163	0.2644	-2.2686	0.6233
MATE	2004.301913	0.6622	0.2607	-0.3319	0.2681	0.2563	0.6321
METS	2000.394809	0.7038	0.2179	0.0056	0.1894	-2.1212	0.5795
NICO	2000.173497	-0.3474	0.3424	-2.3267	0.3810	-3.2487	1.0015
NICO	2006.047945	-1.9268	0.2517	2.5513	0.2800	0.7259	0.7361
NICO	2007.182192	-1.3304	0.3057	0.5072	0.3401	4.7768	0.8940
NRIL	2005.861644	-0.9159	0.1831	3.1261	0.2145	0.3962	0.5853
ONSA	2003.634247	0.0130	0.1661	-1.2878	0.1800	-2.5067	0.3902
ONSA	2004.192623	1.7836	0.1628	0.6074	0.1765	0.1805	0.3825
POL2	2001.442466	2.3734	0.1854	-2.3761	0.2249	-1.2655	0.5998
POTS	2000.632514	-0.3739	0.1583	-1.2114	0.1619	-2.6308	0.4084
RABT	2004.288251	-0.6437	0.1726	-1.8802	0.2057	-1.9907	0.4566
RAMO	2000.545082	-10.6237	0.2287	-15.0843	0.3786	-6.4019	0.6647
RAMO	2003.130137	1.9324	0.2084	0.0846	0.3449	1.1539	0.6055
RAMO	2004.209016	6.7274	0.2023	21.1786	0.3348	-9.0465	0.5878
RAMO	2007.130137	-1.7947	0.2872	5.1345	0.4753	-1.4605	0.8345
REUN	2004.157104	0.4837	0.7933	-9.2221	0.9894	21.6745	2.2720
SEY1	2003.146575	0.5773	1.0210	-0.3384	1.4391	-17.2804	3.2370
SEY1	2004.474044	-0.0203	0.5618	1.4478	0.7918	-16.4800	1.7811
SEY1	2006.182192	-8.1952	0.9340	-1.6810	1.3164	-7.0447	2.9611
SFER	2002.176712	-6.3306	0.1812	7.2547	0.2263	-0.0737	0.4129
SFER	2003.132877	0.0971	0.2460	0.4175	0.3072	-1.5973	0.5606
SFER	2003.434247	7.4462	0.2418	-8.3790	0.3020	-2.1843	0.5511

Cont. Table B.6 The estimated offsets and their formal errors in the first filter

STAT	date	N_{off}	σ_N	E_{off}	σ_E	U_{off}	σ_U
SFER	2005.910959	-0.7173	0.2034	0.0584	0.2540	1.1345	0.4635
SOLA	2004.381148	2.6057	0.2802	1.0680	0.2995	-9.9868	0.8945
SUTH	2001.034247	-1.3187	0.6194	-0.6265	0.6489	-1.2039	1.0330
SUTH	2002.160274	-2.1529	0.6646	-1.5933	0.6962	-3.6993	1.1083
SUTH	2004.416667	1.6313	0.7057	5.6239	0.7393	-4.5028	1.1768
SUTH	2006.845205	-1.8831	0.7458	0.2743	0.7813	-4.9553	1.2438
TEHN	2006.094521	-1.3894	0.3285	1.7008	0.3925	1.5330	1.0224
VILL	2000.545082	-0.7665	0.2221	-3.3214	0.2614	-2.0774	0.4914
VILL	2001.406849	-0.3218	0.1997	0.0440	0.2351	5.4727	0.4419
VILL	2004.744536	3.2433	0.3055	-2.9427	0.3597	2.3189	0.6762
VILL	2004.930328	-0.2083	0.4247	-1.7155	0.5000	-2.2914	0.9398
VILL	2005.050685	-0.4238	0.3415	2.5580	0.4020	4.4336	0.7556
VILL	2006.910959	0.5891	0.2242	5.7494	0.2640	0.5229	0.4962
VILL	2007.297260	-2.0022	0.3240	-1.0351	0.3815	2.4591	0.7171
WSRT	2000.015027	-1.0387	1.3022	0.7062	1.4720	8.0108	3.8298
WSRT	2000.621585	0.1561	0.1810	-1.3198	0.2046	-0.1559	0.5322
WSRT	2001.415068	-0.4035	0.1562	0.5614	0.1765	1.7484	0.4593
WSRT	2005.278082	-0.0742	0.1533	-0.0263	0.1733	-2.3428	0.4508
WTZR	2001.628767	0.2305	0.1624	0.4671	0.1613	-0.7087	0.3897
WTZR	2002.480822	-0.1751	0.8915	0.2304	0.8850	-1.5094	2.1388
WTZR	2002.500000	-0.9537	0.8899	1.4588	0.8834	-1.0896	2.1349
WTZR	2005.341096	1.2513	0.5820	-0.7264	0.5778	-7.1388	1.3962
WTZR	2005.373973	-0.5666	0.5925	0.8307	0.5882	3.8495	1.4214
WTZR	2005.919178	-1.1461	0.2029	1.3258	0.2014	4.2268	0.4867
WTZR	2007.390411	-2.0556	0.8165	-0.0772	0.8106	6.7674	1.9589
WUHN	2000.435792	9.3883	0.3951	2.0952	0.4317	-2.9978	0.9800
WUHN	2002.069863	0.9008	0.2912	-3.1862	0.3181	33.5678	0.7222
WUHN	2002.831507	0.7348	0.3097	-0.6182	0.3383	7.5904	0.7681
YIBL	2006.869863	-3.5875	0.3369	-1.4232	0.3198	2.6445	0.8681
ZIMM	2003.617808	0.9594	0.1600	0.0568	0.1757	1.0692	0.3520
ZIMM	2006.146575	-0.2492	0.1633	0.5594	0.1793	3.1876	0.3592

Table B.7 The estimated offsets and their formal errors in the second filter

STAT	date	N_{off}	σ_N	E_{off}	σ_E	U_{off}	σ_U
BILI	2002.042466	0.0000	0.0000	0.0000	0.0000	-19.4450	1.5524
BILI	2002.171233	0.0000	0.0000	0.0000	0.0000	18.0912	1.5732
BRUS	2001.220548	0.0000	0.0000	0.0000	0.0000	-4.9397	0.3139
CAGL	2001.524658	1.8077	0.1521	5.9548	0.1744	-3.4139	0.3882
DGAR	2004.984973	5.8193	0.4731	9.4035	0.4750	-3.5136	1.1176
HYDE	2004.984973	-0.5370	0.2939	7.8003	0.2991	0.0000	0.0000
IISC	2004.984973	-2.7200	0.2973	14.7600	0.3604	0.0000	0.0000
KUNM	2002.861644	0.0000	0.0000	0.0000	0.0000	26.8221	1.2111
KUNM	2004.984973	-8.6668	0.3148	-5.3126	0.3205	0.0000	0.0000
SEY1	2004.474044	0.0000	0.0000	0.0000	0.0000	-11.3559	1.5372
SFER	2002.176712	-5.9915	0.1541	0.0000	0.0000	0.0000	0.0000
SFER	2003.434247	7.7470	0.1685	-7.7039	0.2673	0.0000	0.0000
WUHN	2002.069863	0.0000	0.0000	0.0000	0.0000	36.1117	0.6696

Table B.8 The estimated offsets and their formal errors in the third filter

STAT	date	N_{off}	σ_N	E_{off}	σ_E	U_{off}	σ_U
BRUS	2001.220548	0.0000	0.0000	0.0000	0.0000	-4.9397	0.3139
CAGL	2001.524658	1.8077	0.1521	5.9548	0.1744	-3.4139	0.3882
DGAR	2004.386612	2.2732	0.6840	0.0000	0.0000	0.0000	0.0000
DGAR	2004.984973	5.8129	0.4712	9.4035	0.4750	-3.5136	1.1176
GRAS	2003.308219	1.6992	0.1665	4.7978	0.1828	-1.7047	0.3508
GRAS	2004.807377	3.5652	0.1563	-1.0643	0.1716	-0.3044	0.3293
HARB	2004.400273	2.5709	0.5312	-3.5426	0.5870	5.7328	0.9254
HYDE	2004.984973	-0.5370	0.2939	7.8003	0.2991	0.0000	0.0000
IISC	2004.984973	-2.7200	0.2973	14.7600	0.3604	0.0000	0.0000
JOZE	2004.930328	1.1122	0.1489	-3.0814	0.1420	0.0000	0.0000
KUNM	2002.861644	0.0000	0.0000	0.0000	0.0000	26.8221	1.2111
KUNM	2004.984973	-8.6668	0.3148	-5.3126	0.3205	0.0000	0.0000
MATE	2004.110656	0.6606	0.1515	-0.6132	0.1496	-1.9290	0.3532
RAMO	2000.545082	-10.7184	0.2305	-15.8103	0.3764	-6.3609	0.6454
RAMO	2004.209016	7.1821	0.2046	20.0150	0.3341	-8.6206	0.5729
REUN	2004.157104	0.4837	0.7933	-9.2221	0.9894	21.6745	2.2720
SEY1	2003.146575	5.2336	0.7525	-0.1427	0.9982	-10.5272	2.4830
SEY1	2004.474044	0.0000	0.0000	0.0000	0.0000	-14.3547	1.7099
SFER	2002.176712	-5.9884	0.1534	7.3163	0.1911	-1.1087	0.3572
SFER	2003.434247	7.7560	0.1677	-8.1011	0.2089	0.0000	0.0000
SUTH	2002.160274	-1.4994	0.5587	0.0000	0.0000	-1.4307	0.9368
SUTH	2004.416667	2.8071	0.6055	0.0000	0.0000	-2.3220	1.0152
VILL	2001.406849	-0.4812	0.1868	-1.0923	0.2276	4.5241	0.4151
VILL	2004.744536	2.8913	0.1840	-2.1183	0.2242	3.7892	0.4088
VILL	2006.910959	0.5944	0.2231	6.1526	0.2717	0.9964	0.4955
VILL	2007.297260	-2.0415	0.3242	-1.4350	0.3949	2.0803	0.7201
WTZR	2002.500000	-0.8779	0.1493	1.2497	0.1491	-3.0187	0.3636
WUHN	2000.435792	0.0000	0.0000	0.0000	0.0000	-3.2180	0.9859
WUHN	2002.069863	0.0000	0.0000	0.0000	0.0000	33.5407	0.7220
WUHN	2002.831507	0.0000	0.0000	0.0000	0.0000	7.5745	0.7679

Table C.1: Velocities and uncertainties for continuous GPS stations

Stations	Velocity		Uncertainty		Stations	Velocity		Uncertainty	
	V_N	V_E	U_N	U_E		V_N	V_E	U_N	U_E
	mm/yr	mm/yr	mm/yr	mm/yr		mm/yr	mm/yr	mm/yr	mm/yr
ARTU	6.31	24.42	0.20	0.29	MALI	16.72	26.21	0.42	0.55
ASC1	12.48	-5.85	0.65	0.68	MAS1	17.23	16.30	0.31	0.34
BAHR	30.43	31.20	0.26	0.28	MATE	18.90	23.00	0.24	0.23
BILI	-20.43	8.52	0.44	0.36	MBAR	18.22	23.82	0.50	0.42
BJFS	-10.64	30.16	0.37	0.38	MDVJ	11.95	22.63	0.31	0.34
BOR1	14.84	19.72	0.18	0.21	METS	12.78	19.67	0.23	0.20
BRUS	15.88	17.07	0.21	0.26	NAMA	28.58	33.36	0.45	1.60
CAGL	15.93	21.41	0.26	0.26	NICO	15.33	19.17	0.20	0.20
DAEJ	-12.49	26.45	0.42	0.40	NKLG	19.76	21.63	0.40	0.44
DGAR	33.04	46.72	0.72	0.49	NOT1	19.69	21.37	0.22	0.23
GLSV	12.98	22.05	0.22	0.23	NRIL	-2.22	21.71	0.28	0.36
GRAS	15.91	20.06	0.29	0.29	ONSA	14.54	16.73	0.20	0.24
GUAO	5.64	32.02	0.38	0.40	POL2	5.56	27.27	0.26	0.31
HALY	23.39	26.60	0.27	0.97	POLV	12.85	22.58	0.24	0.23
HARB	18.68	16.69	0.85	0.74	POTS	15.10	18.86	0.19	0.20
HYDE	34.66	40.80	0.61	0.54	RABT	17.84	15.96	0.27	0.29
IISC	35.24	42.34	0.40	0.45	RAMO	19.66	22.52	0.35	0.51
IRKT	-7.22	24.44	0.42	0.42	REUN	13.23	20.22	0.93	1.09
JOZE	14.19	20.73	0.24	0.24	SEY1	11.86	26.11	0.98	1.11
KIT3	5.78	27.59	0.24	0.31	SFER	17.04	14.00	0.32	0.36
KUNM	-18.06	30.69	0.50	0.49	SOLA	28.00	31.53	0.46	1.66
LHAZ	15.89	45.97	0.34	0.33	SUTH	21.02	16.64	0.93	0.60

V_N : velocity in northing (mm/yr)
V_E : velocity in easting (mm/yr)
U_N : Uncertainty in northing (mm/yr)
U_E : Uncertainty in easting (mm/yr)

Cont. table C.1: Velocities and uncertainties for continuous GPS stations

Stations	Velocity		Uncertainty	
	V_N	V_E	U_N	U_E
	mm/yr	mm/yr	mm/yr	mm/yr
TEHN	18.49	26.72	0.60	0.83
TRAB	13.55	25.01	0.17	0.19
TROM	15.23	14.17	0.33	0.27
ULAB	-8.30	27.60	0.36	0.39
VILL	16.56	18.69	0.37	0.41
WSRT	16.36	17.30	0.18	0.23
WTZR	15.56	19.67	0.27	0.26
WUHN	-11.29	32.43	0.45	0.40
YIBL	32.70	36.23	0.49	0.43
ZIMM	16.18	19.44	0.18	0.22

V_N : velocity in northing (mm/yr)
V_E : velocity in easting (mm/yr)
U_N : Uncertainty in northing (mm/yr)
U_E : Uncertainty in easting (mm/yr)

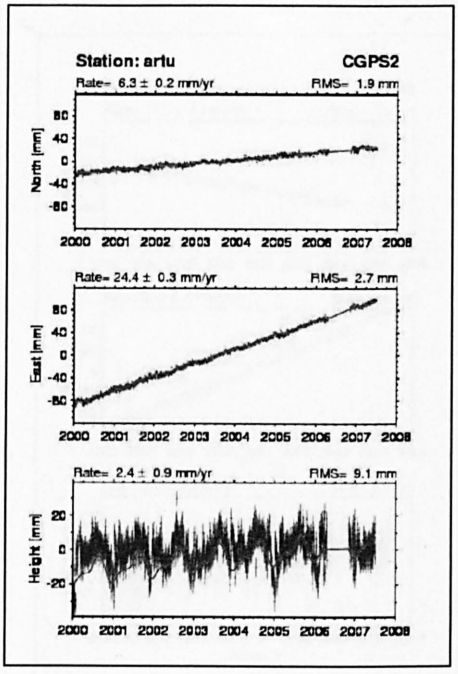
Station: artu
CGPS2
Rate= 6.3 ± 0.2 mm/yr
RMS= 1.9 mm
North [mm]
Rate= 24.4 ± 0.3 mm/yr
RMS= 2.7 mm
East [mm]
Rate= 2.4 ± 0.9 mm/yr
RMS= 9.1 mm
Height [mm]
2000 2001 2002 2003 2004 2005 2006 2007 2008

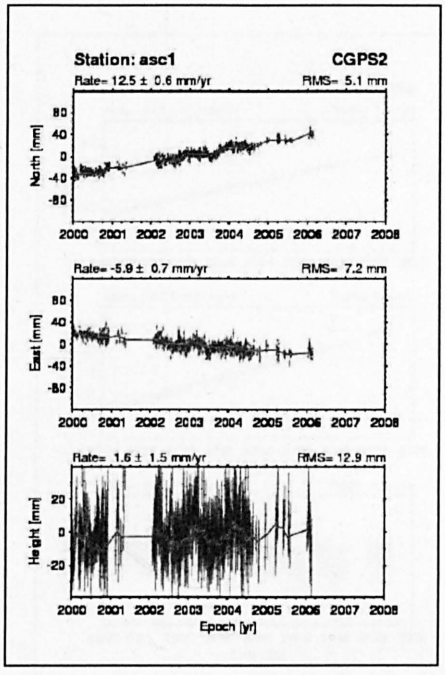
Station: asc1
CGPS2
Rate= 12.5 ± 0.6 mm/yr
RMS= 5.1 mm
North [mm]
Rate= -5.9 ± 0.7 mm/yr
RMS= 7.2 mm
East [mm]
Rate= 1.6 ± 1.5 mm/yr
RMS= 12.9 mm
Height [mm]
2000 2001 2002 2003 2004 2005 2006 2007 2008
Epoch [yr]

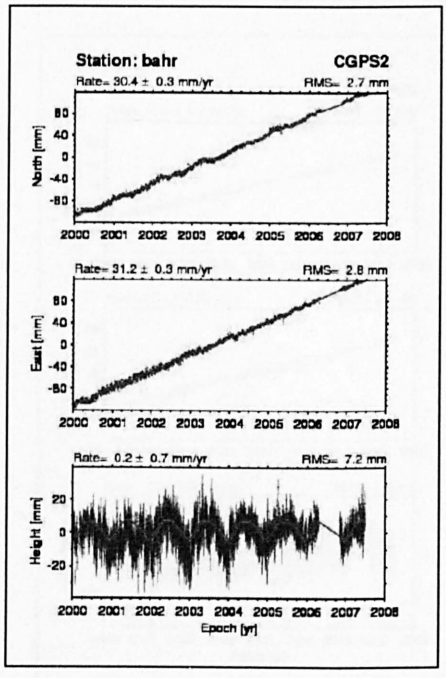
Station: bahr
CGPS2
Rate= 30.4 ± 0.3 mm/yr
RMS= 2.7 mm
North [mm]
Rate= 31.2 ± 0.3 mm/yr
RMS= 2.8 mm
East [mm]
Rate= 0.2 ± 0.7 mm/yr
RMS= 7.2 mm
Height [mm]
2000 2001 2002 2003 2004 2005 2006 2007 2008
Epoch [yr]

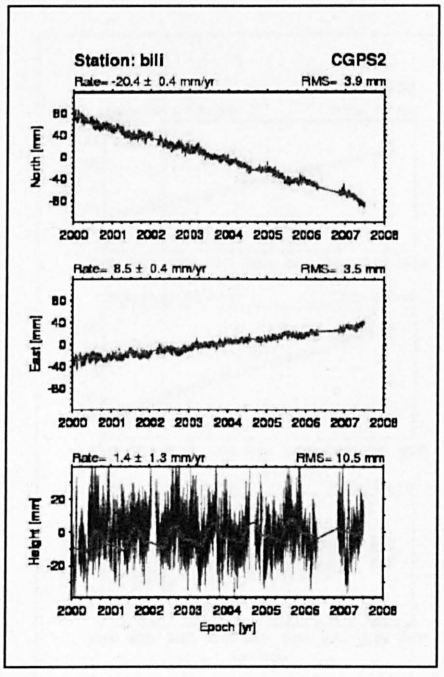
Station: bill
CGPS2
Rate= -20.4 ± 0.4 mm/yr
RMS= 3.9 mm
North [mm]
Rate= 8.5 ± 0.4 mm/yr
RMS= 3.5 mm
East [mm]
Rate= 1.4 ± 1.3 mm/yr
RMS= 10.5 mm
Height [mm]
2000 2001 2002 2003 2004 2005 2006 2007 2008
Epoch [yr]

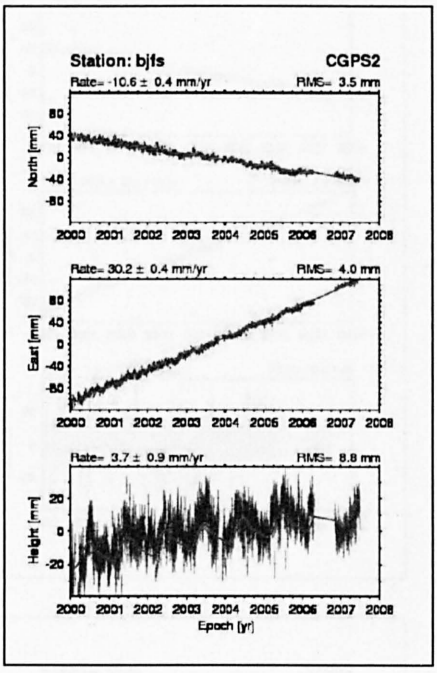
Station: bjfs
CGPS2
Rate= -10.6 ± 0.4 mm/yr
RMS= 3.5 mm
North [mm]
Rate= 30.2 ± 0.4 mm/yr
RMS= 4.0 mm
East [mm]
Rate= 3.7 ± 0.9 mm/yr
RMS= 8.8 mm
Height [mm]
2000 2001 2002 2003 2004 2005 2006 2007 2008
Epoch [yr]

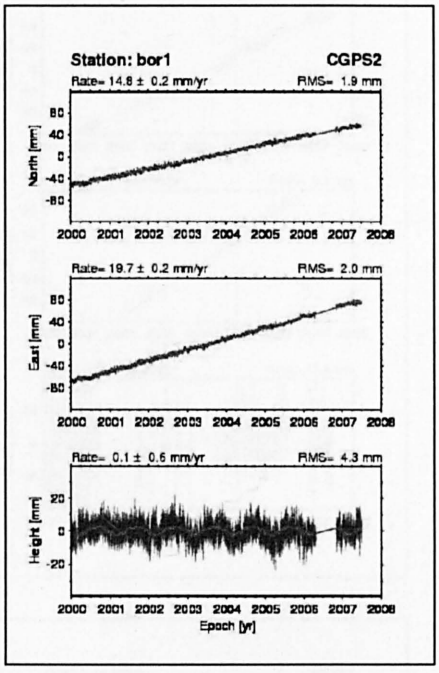
Station: bor1
CGPS2
Rate= 14.8 ± 0.2 mm/yr
RMS= 1.9 mm
North [mm]
Rate= 19.7 ± 0.2 mm/yr
RMS= 2.0 mm
East [mm]
Rate= 0.1 ± 0.6 mm/yr
RMS= 4.3 mm
Height [mm]
2000 2001 2002 2003 2004 2005 2006 2007 2008
Epoch [yr]

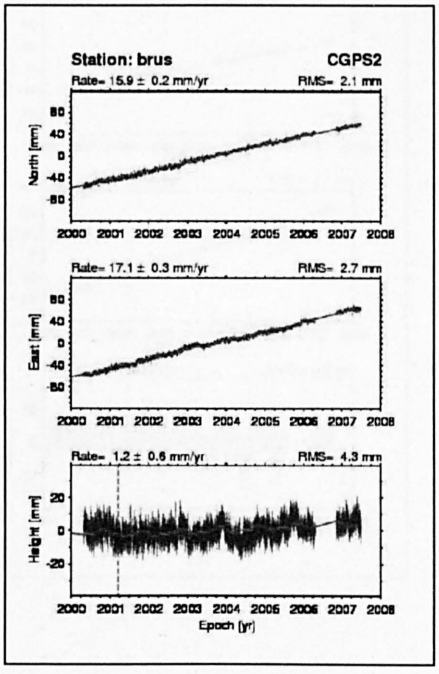
Station: brus
CGPS2
Rate= 15.9 ± 0.2 mm/yr
RMS= 2.1 mm
North [mm]
Rate= 17.1 ± 0.3 mm/yr
RMS= 2.7 mm
East [mm]
Rate= 1.2 ± 0.6 mm/yr
RMS= 4.3 mm
Height [mm]
2000 2001 2002 2003 2004 2005 2006 2007 2008
Epoch [yr]

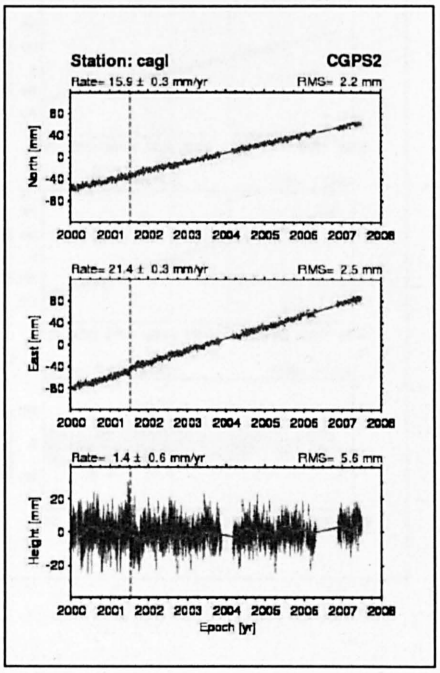
Station: cagl
CGPS2
Rate= 15.9 ± 0.3 mm/yr
RMS= 2.2 mm
North [mm]
Rate= 21.4 ± 0.3 mm/yr
RMS= 2.5 mm
East [mm]
Rate= 1.4 ± 0.6 mm/yr
RMS= 5.6 mm
Height [mm]
2000 2001 2002 2003 2004 2005 2006 2007 2008
Epoch [yr]

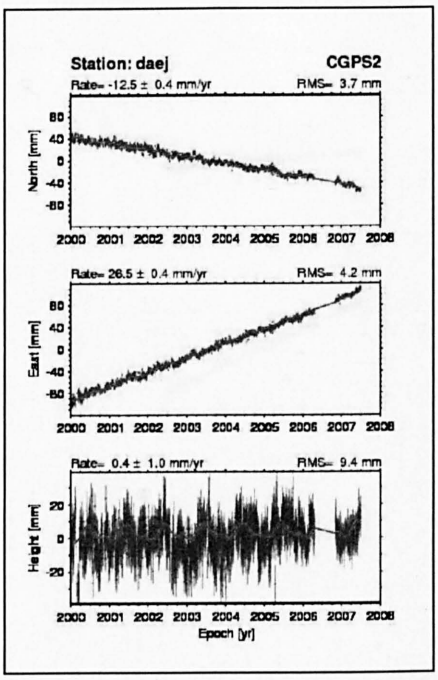
Station: daej
CGPS2
Rate= -12.5 ± 0.4 mm/yr
RMS= 3.7 mm
North [mm]
Rate= 26.5 ± 0.4 mm/yr
RMS= 4.2 mm
East [mm]
Rate= 0.4 ± 1.0 mm/yr
RMS= 9.4 mm
Height [mm]
2000 2001 2002 2003 2004 2005 2006 2007 2008
Epoch [yr]

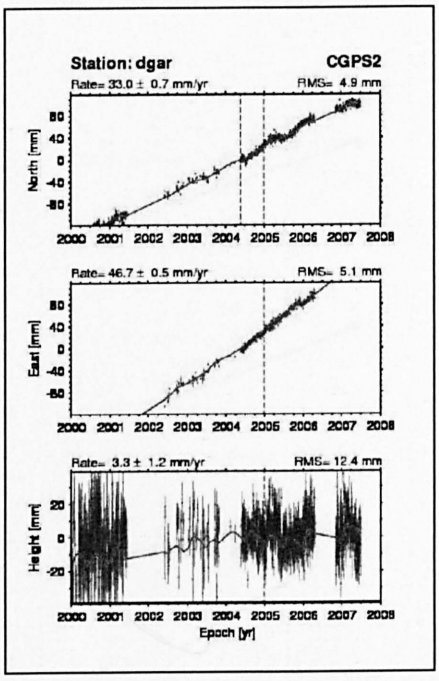
Station: dgar
CGPS2
Rate= 33.0 ± 0.7 mm/yr
RMS= 4.9 mm
North [mm]
Rate= 46.7 ± 0.5 mm/yr
RMS= 5.1 mm
East [mm]
Rate= 3.3 ± 1.2 mm/yr
RMS= 12.4 mm
Height [mm]
2000 2001 2002 2003 2004 2005 2006 2007 2008
Epoch [yr]

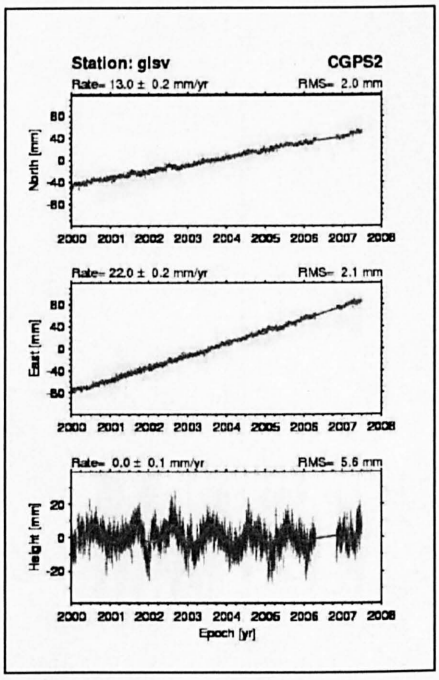
Station: glsv
CGPS2
Rate= 13.0 ± 0.2 mm/yr
RMS= 2.0 mm
North [mm]
Rate= 22.0 ± 0.2 mm/yr
RMS= 2.1 mm
East [mm]
Rate= 0.0 ± 0.1 mm/yr
RMS= 5.6 mm
Height [mm]
2000 2001 2002 2003 2004 2005 2006 2007 2008
Epoch [yr]

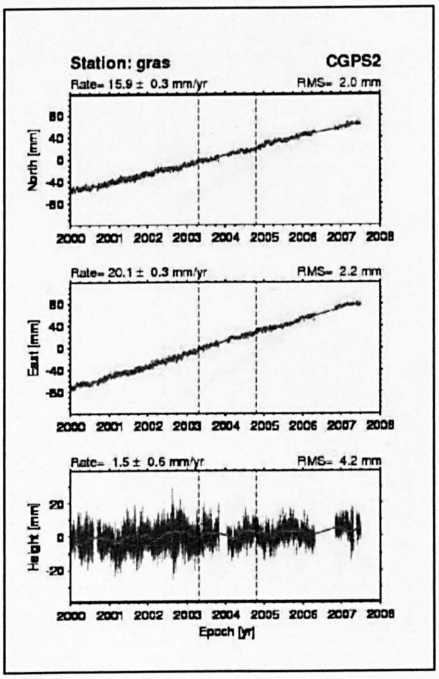
Station: gras
CGPS2
Rate= 15.9 ± 0.3 mm/yr
RMS= 2.0 mm
North [mm]
Rate= 20.1 ± 0.3 mm/yr
RMS= 2.2 mm
East [mm]
Rate= 1.5 ± 0.6 mm/yr
RMS= 4.2 mm
Height [mm]
2000 2001 2002 2003 2004 2005 2006 2007 2008
Epoch [yr]

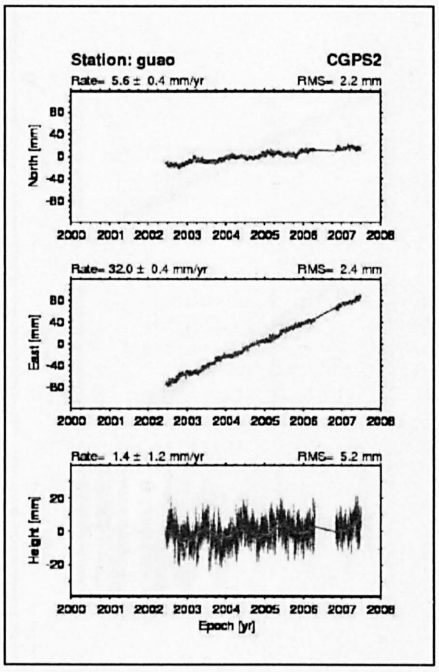
Station: guao
CGPS2
Rate= 5.6 ± 0.4 mm/yr
RMS= 2.2 mm
North [mm]
Rate= 32.0 ± 0.4 mm/yr
RMS= 2.4 mm
East [mm]
Rate= 1.4 ± 1.2 mm/yr
RMS= 5.2 mm
Height [mm]
2000 2001 2002 2003 2004 2005 2006 2007 2008
Epoch [yr]

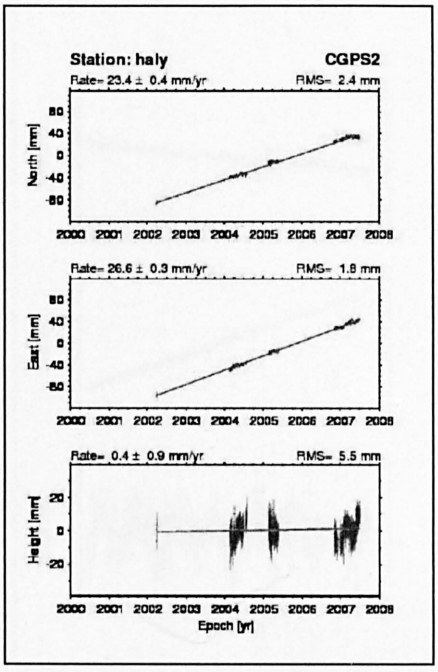
Station: haly
CGPS2
Rate= 23.4 ± 0.4 mm/yr
RMS= 2.4 mm
North [mm]
Rate= 26.6 ± 0.3 mm/yr
RMS= 1.8 mm
East [mm]
Rate= 0.4 ± 0.9 mm/yr
RMS= 5.5 mm
Height [mm]
2000 2001 2002 2003 2004 2005 2006 2007 2008
Epoch [yr]

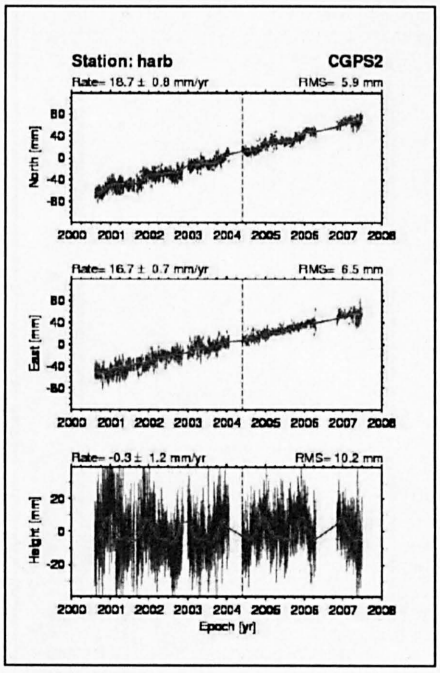
Station: harb
CGPS2
Rate= 18.7 ± 0.8 mm/yr
RMS= 5.9 mm
North [mm]
Rate= 16.7 ± 0.7 mm/yr
RMS= 6.5 mm
East [mm]
Rate= -0.3 ± 1.2 mm/yr
RMS= 10.2 mm
Height [mm]
2000 2001 2002 2003 2004 2005 2006 2007 2008
Epoch [yr]

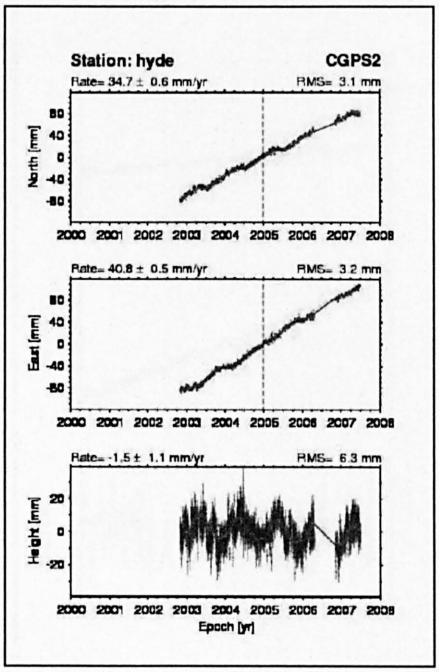
Station: hyde
CGPS2
Rate= 34.7 ± 0.6 mm/yr
RMS= 3.1 mm
North [mm]
Rate= 40.8 ± 0.5 mm/yr
RMS= 3.2 mm
East [mm]
Rate= -1.5 ± 1.1 mm/yr
RMS= 6.3 mm
Height [mm]
2000 2001 2002 2003 2004 2005 2006 2007 2008
Epoch [yr]

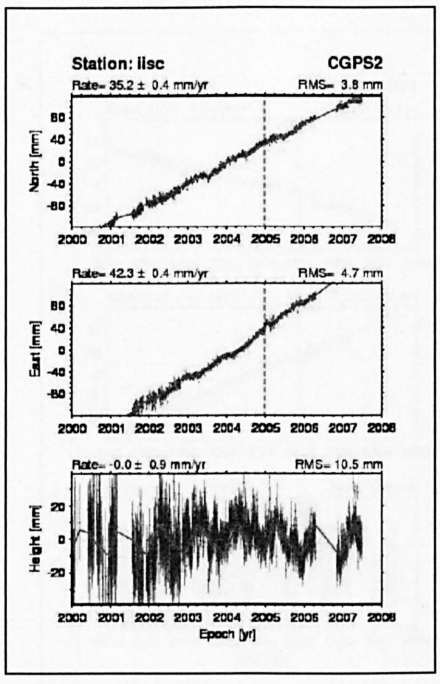
Station: ilsc
CGPS2
Rate= 35.2 ± 0.4 mm/yr
RMS= 3.8 mm
North [mm]
Rate= 42.3 ± 0.4 mm/yr
RMS= 4.7 mm
East [mm]
Rate= -0.0 ± 0.9 mm/yr
RMS= 10.5 mm
Height [mm]
2000 2001 2002 2003 2004 2005 2006 2007 2008
Epoch [yr]

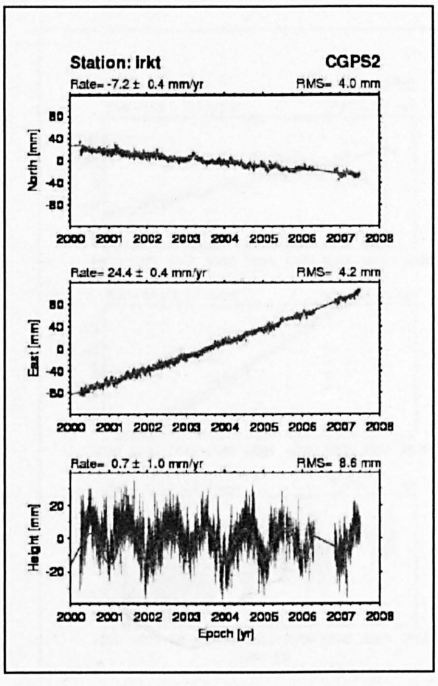
Station: irkt
CGPS2
Rate= -7.2 ± 0.4 mm/yr
RMS= 4.0 mm
North [mm]
Rate= 24.4 ± 0.4 mm/yr
RMS= 4.2 mm
East [mm]
Rate= 0.7 ± 1.0 mm/yr
RMS= 8.6 mm
Height [mm]
2000 2001 2002 2003 2004 2005 2006 2007 2008
Epoch [yr]

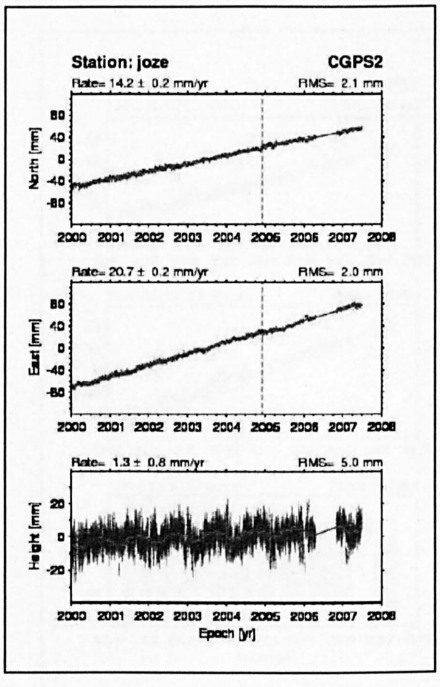
Station: joze
CGPS2
Rate= 14.2 ± 0.2 mm/yr
RMS= 2.1 mm
North [mm]
Rate= 20.7 ± 0.2 mm/yr
RMS= 2.0 mm
East [mm]
Rate= 1.3 ± 0.8 mm/yr
RMS= 5.0 mm
Height [mm]
2000 2001 2002 2003 2004 2005 2006 2007 2008
Epoch [yr]

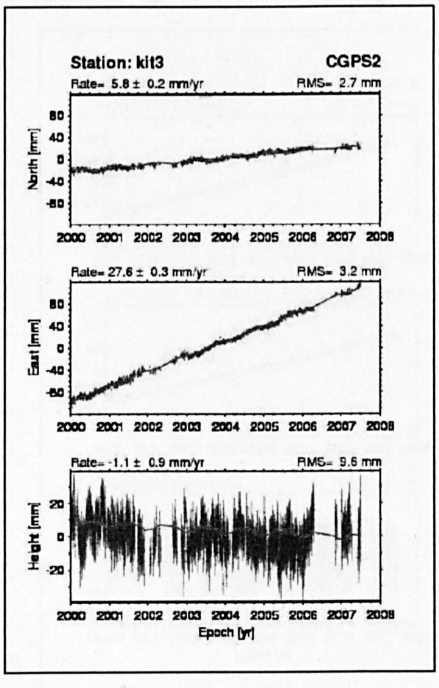
Station: kit3
CGPS2
Rate= 5.8 ± 0.2 mm/yr
RMS= 2.7 mm
North [mm]
Rate= 27.6 ± 0.3 mm/yr
RMS= 3.2 mm
East [mm]
Rate= -1.1 ± 0.9 mm/yr
RMS= 9.6 mm
Height [mm]
2000 2001 2002 2003 2004 2005 2006 2007 2008
Epoch [yr]

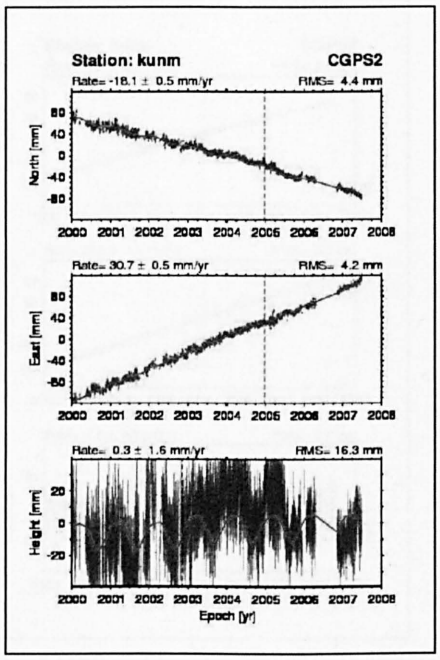
Station: kunm
CGPS2
Rate= -18.1 ± 0.5 mm/yr
RMS= 4.4 mm
North [mm]
Rate= 30.7 ± 0.5 mm/yr
RMS= 4.2 mm
East [mm]
Rate= 0.3 ± 1.6 mm/yr
RMS= 16.3 mm
Height [mm]
2000 2001 2002 2003 2004 2005 2006 2007 2008
Epoch [yr]

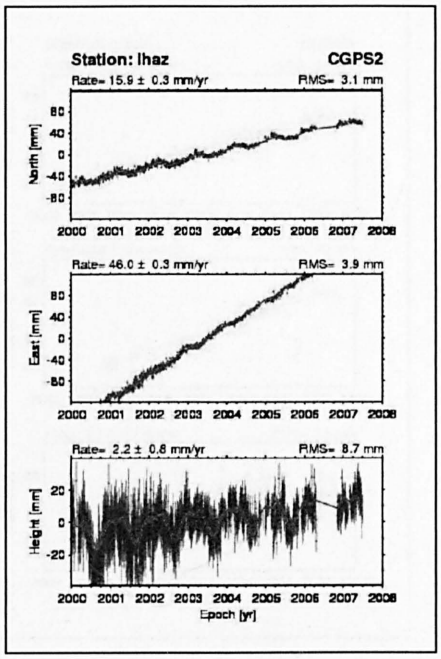
Station: lhaz
CGPS2
Rate= 15.9 ± 0.3 mm/yr
RMS= 3.1 mm
North [mm]
Rate= 46.0 ± 0.3 mm/yr
RMS= 3.9 mm
East [mm]
Rate= 2.2 ± 0.8 mm/yr
RMS= 8.7 mm
Height [mm]
2000 2001 2002 2003 2004 2005 2006 2007 2008
Epoch [yr]

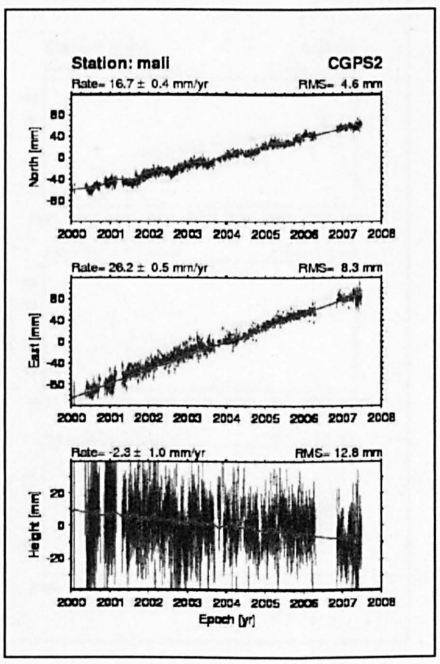
Station: mall
CGPS2
Rate= 16.7 ± 0.4 mm/yr
RMS= 4.6 mm
North [mm]
Rate= 26.2 ± 0.5 mm/yr
RMS= 8.3 mm
East [mm]
Rate= -2.3 ± 1.0 mm/yr
RMS= 12.8 mm
Height [mm]
2000 2001 2002 2003 2004 2005 2006 2007 2008
Epoch [yr]

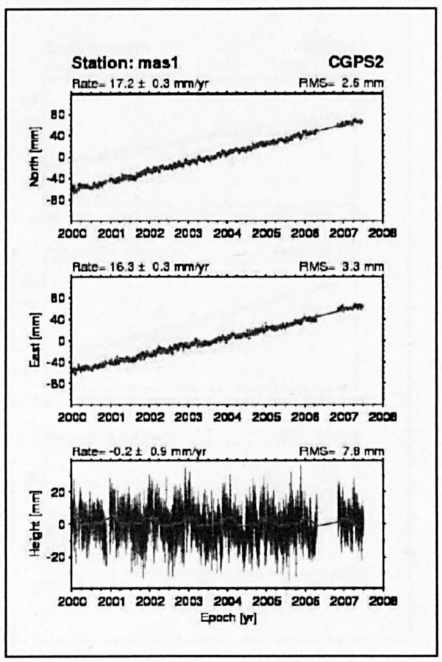
Station: mas1
CGPS2
Rate= 17.2 ± 0.3 mm/yr
RMS= 2.5 mm
North [mm]
Rate= 16.3 ± 0.3 mm/yr
RMS= 3.3 mm
East [mm]
Rate= -0.2 ± 0.9 mm/yr
RMS= 7.9 mm
Height [mm]
2000 2001 2002 2003 2004 2005 2006 2007 2008
Epoch [yr]

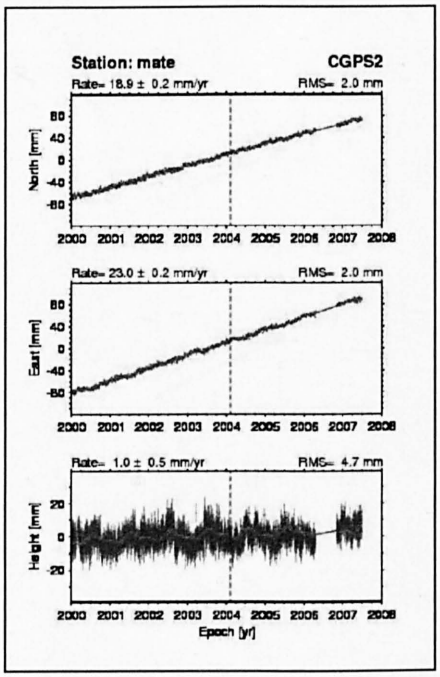
Station: mate
CGPS2
Rate= 18.9 ± 0.2 mm/yr
RMS= 2.0 mm
North [mm]
Rate= 23.0 ± 0.2 mm/yr
RMS= 2.0 mm
East [mm]
Rate= 1.0 ± 0.5 mm/yr
RMS= 4.7 mm
Height [mm]
2000 2001 2002 2003 2004 2005 2006 2007 2008
Epoch [yr]

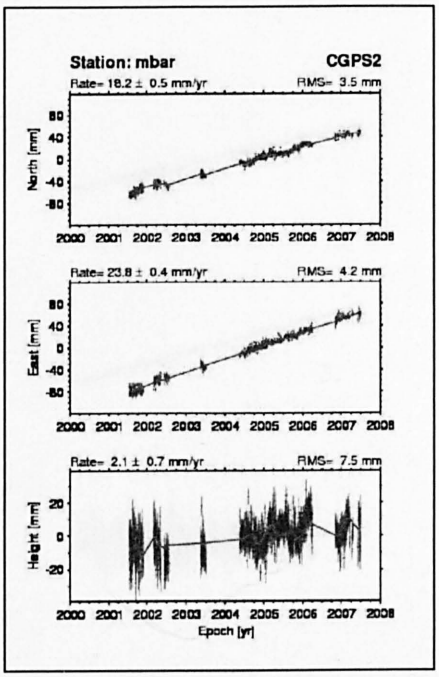
Station: mbar
CGPS2
Rate= 18.2 ± 0.5 mm/yr
RMS= 3.5 mm
North [mm]
Rate= 23.8 ± 0.4 mm/yr
RMS= 4.2 mm
East [mm]
Rate= 2.1 ± 0.7 mm/yr
RMS= 7.5 mm
Height [mm]
2000 2001 2002 2003 2004 2005 2006 2007 2008
Epoch [yr]

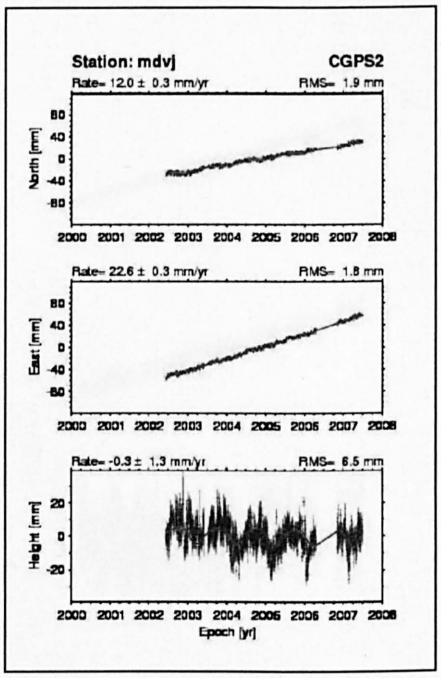
Station: mdvj
CGPS2
Rate= 12.0 ± 0.3 mm/yr
RMS= 1.9 mm
North [mm]
Rate= 22.6 ± 0.3 mm/yr
RMS= 1.8 mm
East [mm]
Rate= -0.3 ± 1.3 mm/yr
RMS= 6.5 mm
Height [mm]
2000 2001 2002 2003 2004 2005 2006 2007 2008
Epoch [yr]

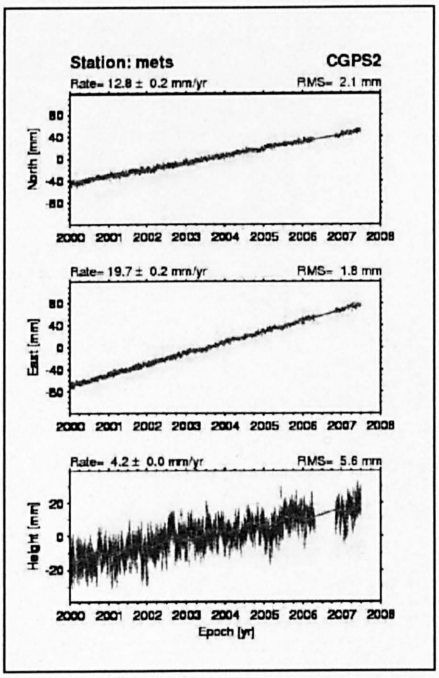
Station: mets
CGPS2
Rate= 12.8 ± 0.2 mm/yr
RMS= 2.1 mm
North [mm]
Rate= 19.7 ± 0.2 mm/yr
RMS= 1.8 mm
East [mm]
Rate= 4.2 ± 0.0 mm/yr
RMS= 5.6 mm
Height [mm]
2000 2001 2002 2003 2004 2005 2006 2007 2008
Epoch [yr]

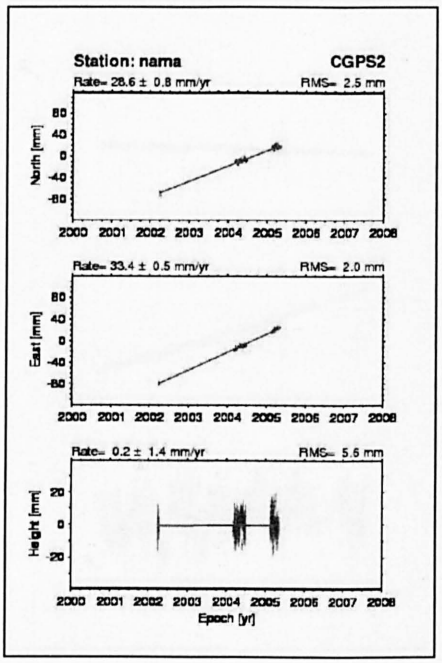
Station: nama
CGPS2
Rate= 28.6 ± 0.8 mm/yr
RMS= 2.5 mm
North [mm]
Rate= 33.4 ± 0.5 mm/yr
RMS= 2.0 mm
East [mm]
Rate= 0.2 ± 1.4 mm/yr
RMS= 5.6 mm
Height [mm]
2000 2001 2002 2003 2004 2005 2006 2007 2008
Epoch [yr]

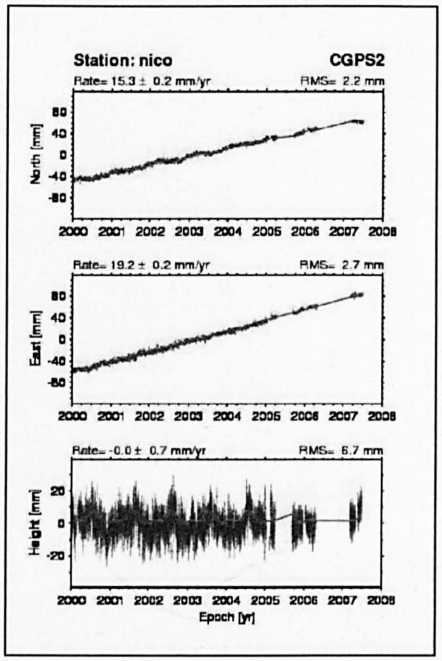
Station: nico
CGPS2
Rate= 15.3 ± 0.2 mm/yr
RMS= 2.2 mm
North [mm]
Rate= 19.2 ± 0.2 mm/yr
RMS= 2.7 mm
East [mm]
Rate= -0.0 ± 0.7 mm/yr
RMS= 6.7 mm
Height [mm]
2000 2001 2002 2003 2004 2005 2006 2007 2008
Epoch [yr]

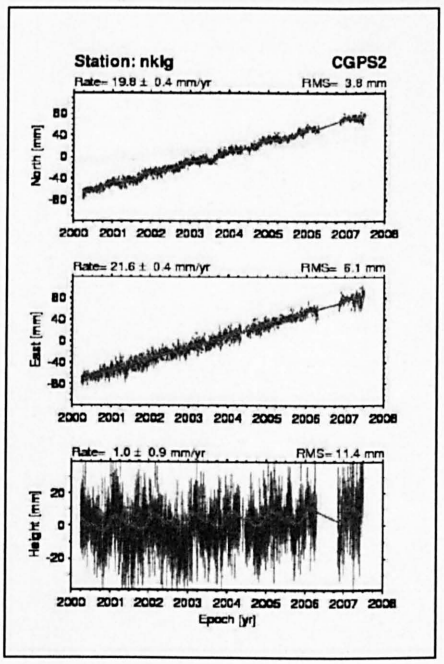
Station: nklg
CGPS2
Rate= 19.8 ± 0.4 mm/yr
RMS= 3.8 mm
North [mm]
Rate= 21.6 ± 0.4 mm/yr
RMS= 6.1 mm
East [mm]
Rate= 1.0 ± 0.9 mm/yr
RMS= 11.4 mm
Height [mm]
2000 2001 2002 2003 2004 2005 2006 2007 2008
Epoch [yr]

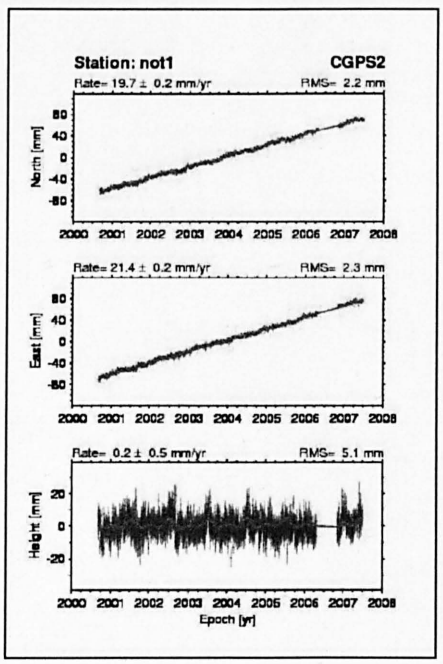
Station: not1
CGPS2
Rate= 19.7 ± 0.2 mm/yr
RMS= 2.2 mm
North [mm]
Rate= 21.4 ± 0.2 mm/yr
RMS= 2.3 mm
East [mm]
Rate= 0.2 ± 0.5 mm/yr
RMS= 5.1 mm
Height [mm]
2000 2001 2002 2003 2004 2005 2006 2007 2008
Epoch [yr]

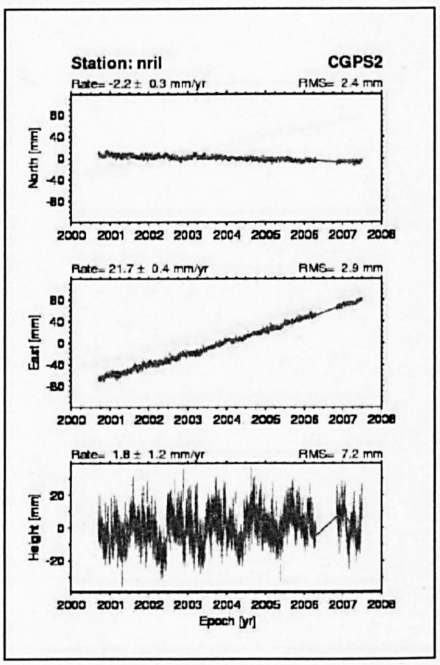
Station: nril
CGPS2
Rate= -2.2 ± 0.3 mm/yr
RMS= 2.4 mm
North [mm]
Rate= 21.7 ± 0.4 mm/yr
RMS= 2.9 mm
East [mm]
Rate= 1.8 ± 1.2 mm/yr
RMS= 7.2 mm
Height [mm]
2000 2001 2002 2003 2004 2005 2006 2007 2008
Epoch [yr]

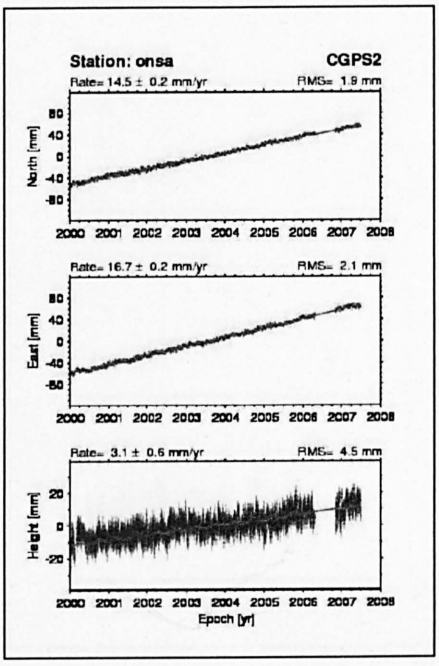
Station: onsa
CGPS2
Rate= 14.5 ± 0.2 mm/yr
RMS= 1.9 mm
North [mm]
Rate= 16.7 ± 0.2 mm/yr
RMS= 2.1 mm
East [mm]
Rate= 3.1 ± 0.6 mm/yr
RMS= 4.5 mm
Height [mm]
2000 2001 2002 2003 2004 2005 2006 2007 2008
Epoch [yr]

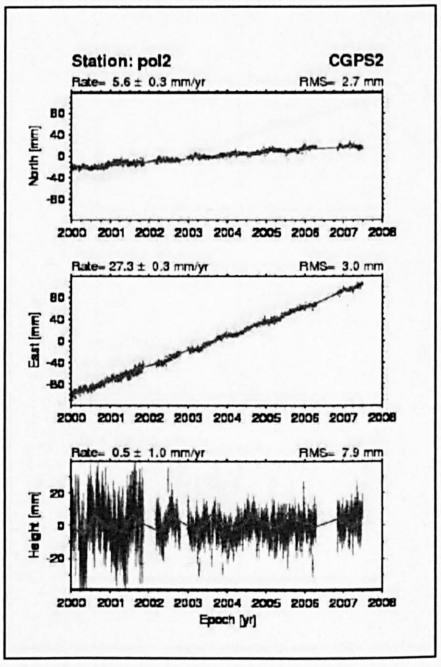
Station: pol2
CGPS2
Rate= 5.6 ± 0.3 mm/yr
RMS= 2.7 mm
North [mm]
Rate= 27.3 ± 0.3 mm/yr
RMS= 3.0 mm
East [mm]
Rate= 0.5 ± 1.0 mm/yr
RMS= 7.9 mm
Height [mm]
2000 2001 2002 2003 2004 2005 2006 2007 2008
Epoch [yr]

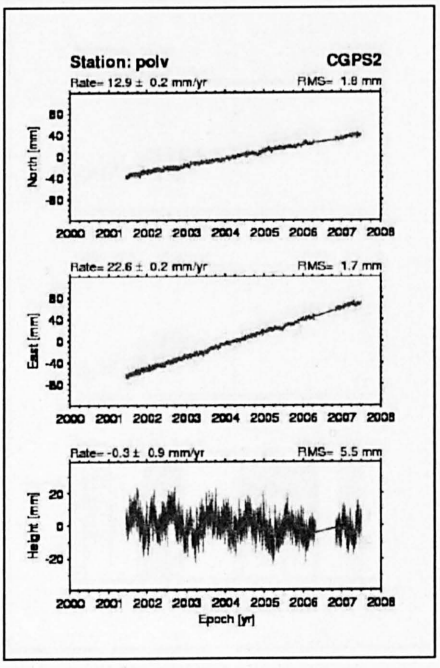
Station: polv
CGPS2
Rate= 12.9 ± 0.2 mm/yr
RMS= 1.8 mm
North [mm]
Rate= 22.6 ± 0.2 mm/yr
RMS= 1.7 mm
East [mm]
Rate= -0.3 ± 0.9 mm/yr
RMS= 5.5 mm
Height [mm]
2000 2001 2002 2003 2004 2005 2006 2007 2008
Epoch [yr]

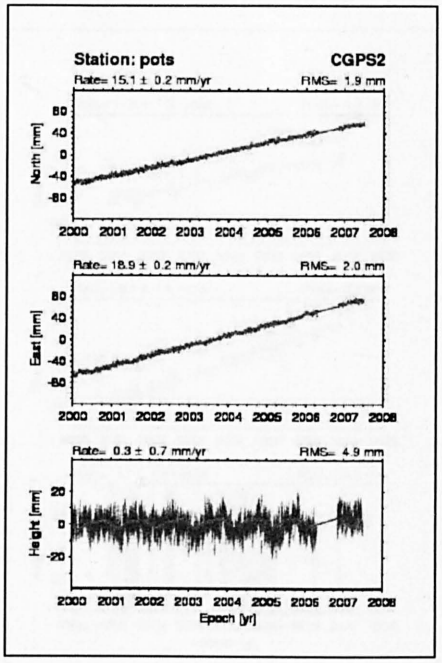
Station: pots
CGPS2
Rate= 15.1 ± 0.2 mm/yr
RMS= 1.9 mm
North [mm]
Rate= 18.9 ± 0.2 mm/yr
RMS= 2.0 mm
East [mm]
Rate= 0.3 ± 0.7 mm/yr
RMS= 4.9 mm
Height [mm]
2000 2001 2002 2003 2004 2005 2006 2007 2008
Epoch [yr]

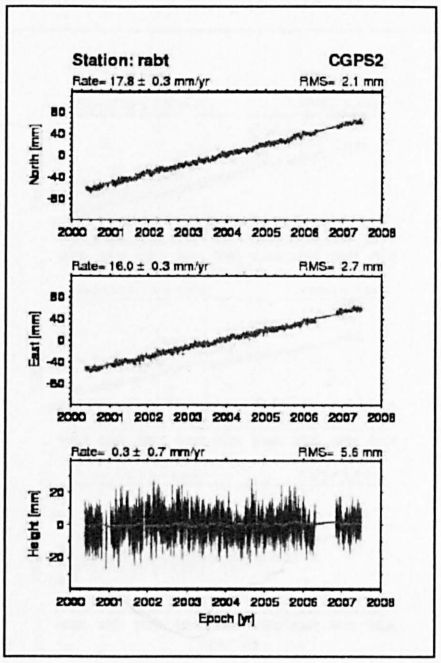
Station: rabt
CGPS2
Rate= 17.8 ± 0.3 mm/yr
RMS= 2.1 mm
North [mm]
Rate= 16.0 ± 0.3 mm/yr
RMS= 2.7 mm
East [mm]
Rate= 0.3 ± 0.7 mm/yr
RMS= 5.6 mm
Height [mm]
2000 2001 2002 2003 2004 2005 2006 2007 2008
Epoch [yr]

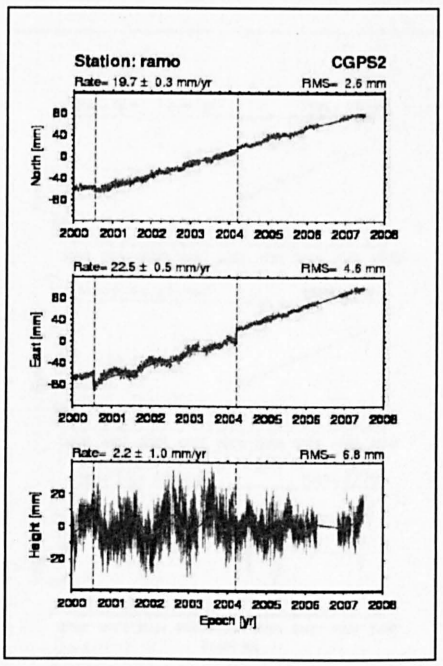
Station: ramo
CGPS2
Rate= 19.7 ± 0.3 mm/yr
RMS= 2.6 mm
North [mm]
Rate= 22.5 ± 0.5 mm/yr
RMS= 4.6 mm
East [mm]
Rate= 2.2 ± 1.0 mm/yr
RMS= 6.8 mm
Height [mm]
2000 2001 2002 2003 2004 2005 2006 2007 2008
Epoch [yr]

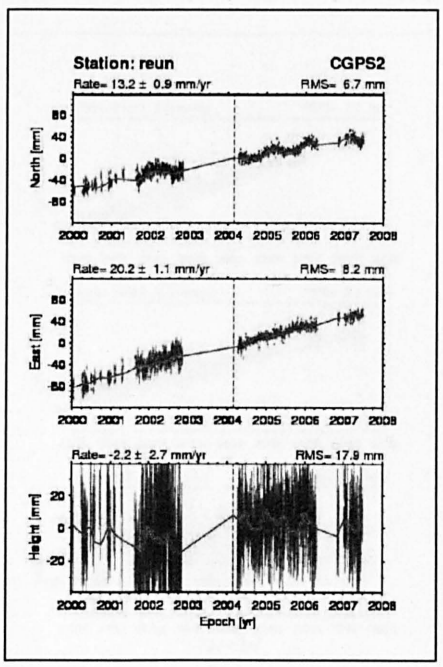
Station: reun
CGPS2
Rate= 13.2 ± 0.9 mm/yr
RMS= 6.7 mm
North [mm]
Rate= 20.2 ± 1.1 mm/yr
RMS= 8.2 mm
East [mm]
Rate= -2.2 ± 2.7 mm/yr
RMS= 17.9 mm
Height [mm]
2000 2001 2002 2003 2004 2005 2006 2007 2008
Epoch [yr]

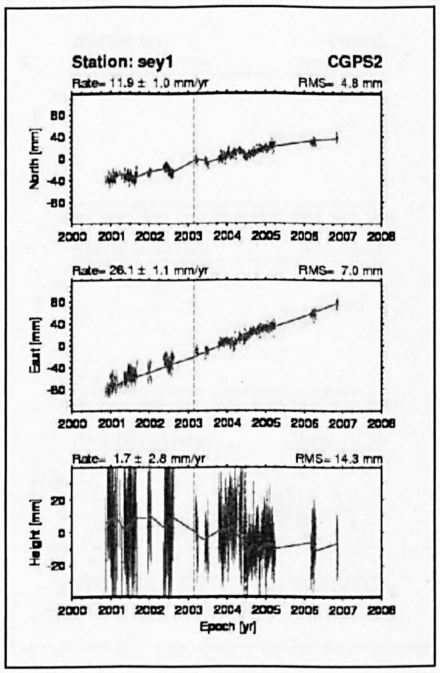
Station: sey1
CGPS2
Rate= 11.9 ± 1.0 mm/yr
RMS= 4.8 mm
North [mm]
Rate= 26.1 ± 1.1 mm/yr
RMS= 7.0 mm
East [mm]
Rate= 1.7 ± 2.8 mm/yr
RMS= 14.3 mm
Height [mm]
2000 2001 2002 2003 2004 2005 2006 2007 2008
Epoch [yr]

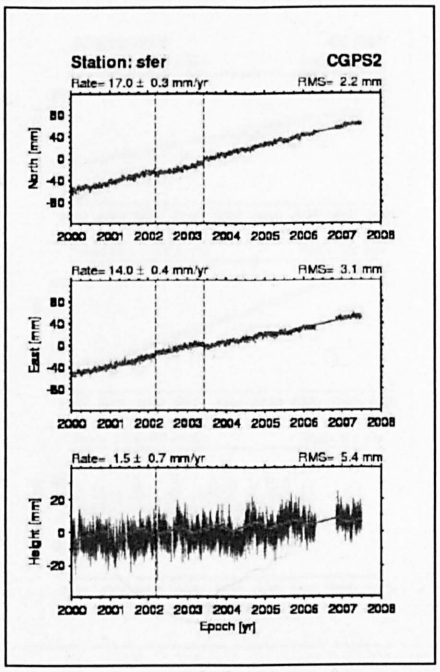
Station: sfer
CGPS2
Rate= 17.0 ± 0.3 mm/yr
RMS= 2.2 mm
North [mm]
Rate= 14.0 ± 0.4 mm/yr
RMS= 3.1 mm
East [mm]
Rate= 1.5 ± 0.7 mm/yr
RMS= 5.4 mm
Height [mm]
2000 2001 2002 2003 2004 2005 2006 2007 2008
Epoch [yr]

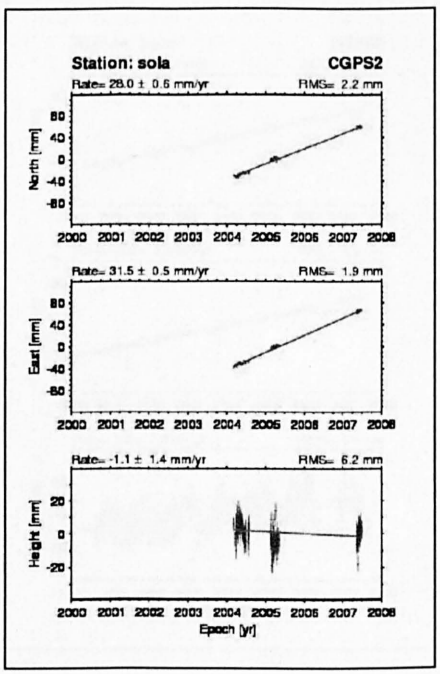
Station: sola
CGPS2
Rate= 28.0 ± 0.5 mm/yr
RMS= 2.2 mm
North [mm]
Rate= 31.5 ± 0.5 mm/yr
RMS= 1.9 mm
East [mm]
Rate= -1.1 ± 1.4 mm/yr
RMS= 6.2 mm
Height [mm]
2000 2001 2002 2003 2004 2005 2006 2007 2008
Epoch [yr]

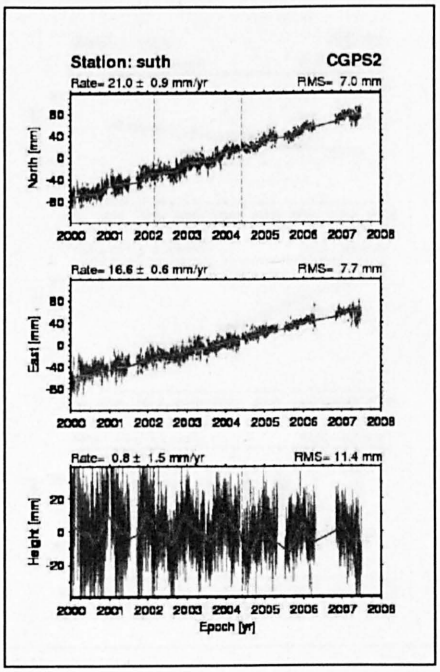
Station: suth
CGPS2
Rate= 21.0 ± 0.9 mm/yr
RMS= 7.0 mm
North [mm]
Rate= 16.6 ± 0.6 mm/yr
RMS= 7.7 mm
East [mm]
Rate= 0.8 ± 1.5 mm/yr
RMS= 11.4 mm
Height [mm]
2000 2001 2002 2003 2004 2005 2006 2007 2008
Epoch [yr]

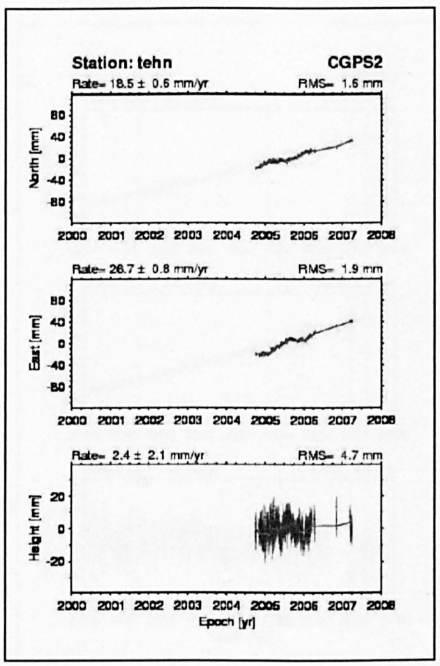
Station: tehn
CGPS2
Rate= 18.5 ± 0.6 mm/yr
RMS= 1.6 mm
North [mm]
Rate= 26.7 ± 0.8 mm/yr
RMS= 1.9 mm
East [mm]
Rate= 2.4 ± 2.1 mm/yr
RMS= 4.7 mm
Height [mm]
2000 2001 2002 2003 2004 2005 2006 2007 2008
Epoch [yr]

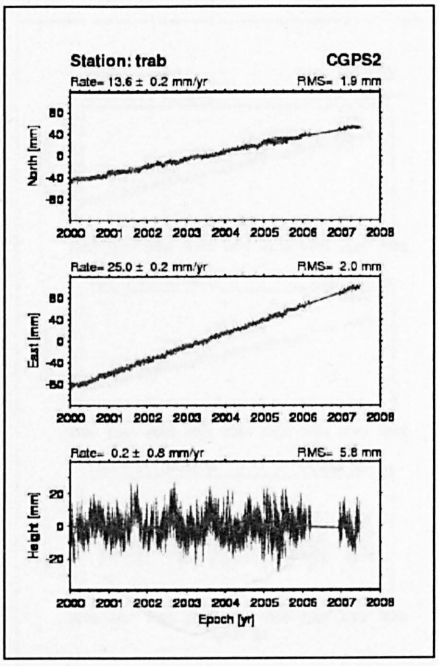
Station: trab
CGPS2
Rate= 13.6 ± 0.2 mm/yr
RMS= 1.9 mm
North [mm]
Rate= 25.0 ± 0.2 mm/yr
RMS= 2.0 mm
East [mm]
Rate= 0.2 ± 0.8 mm/yr
RMS= 5.8 mm
Height [mm]
2000 2001 2002 2003 2004 2005 2006 2007 2008
Epoch [yr]

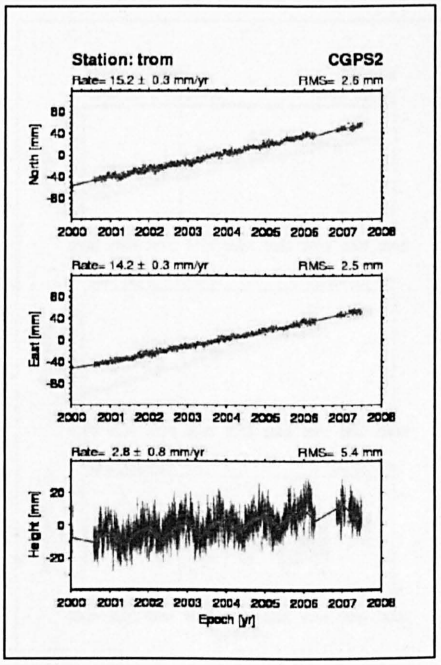
Station: trom
CGPS2
Rate= 15.2 ± 0.3 mm/yr
RMS= 2.5 mm
North [mm]
Rate= 14.2 ± 0.3 mm/yr
RMS= 2.5 mm
East [mm]
Rate= 2.8 ± 0.8 mm/yr
RMS= 5.4 mm
Height [mm]
2000 2001 2002 2003 2004 2005 2006 2007 2008
Epoch [yr]

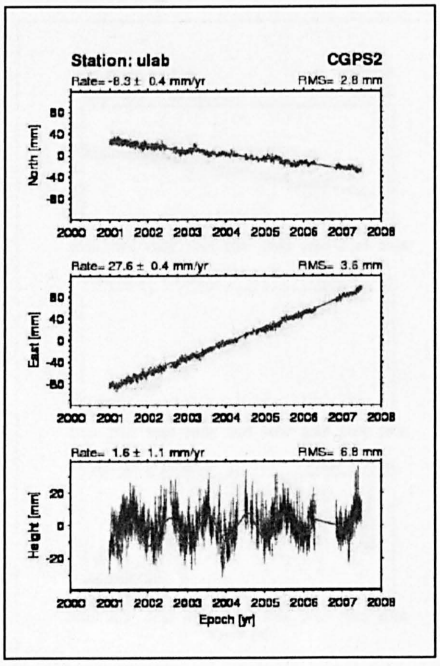
Station: ulab
CGPS2
Rate= -8.3 ± 0.4 mm/yr
RMS= 2.8 mm
North [mm]
Rate= 27.6 ± 0.4 mm/yr
RMS= 3.6 mm
East [mm]
Rate= 1.6 ± 1.1 mm/yr
RMS= 6.8 mm
Height [mm]
2000 2001 2002 2003 2004 2005 2006 2007 2008
Epoch [yr]

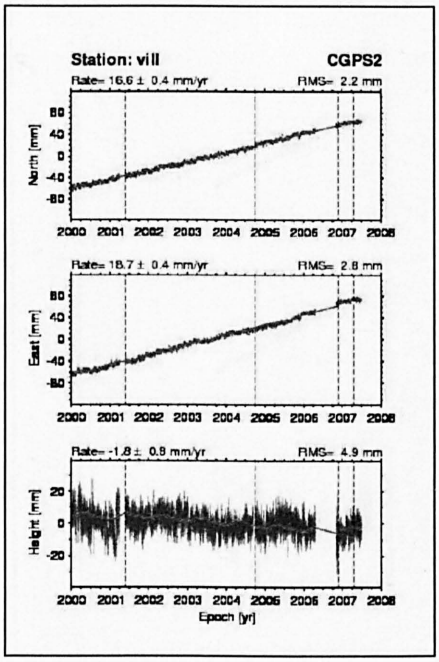
Station: vill
CGPS2
Rate= 16.6 ± 0.4 mm/yr
RMS= 2.2 mm
North [mm]
Rate= 18.7 ± 0.4 mm/yr
RMS= 2.8 mm
East [mm]
Rate= -1.8 ± 0.8 mm/yr
RMS= 4.9 mm
Height [mm]
2000 2001 2002 2003 2004 2005 2006 2007 2008
Epoch [yr]

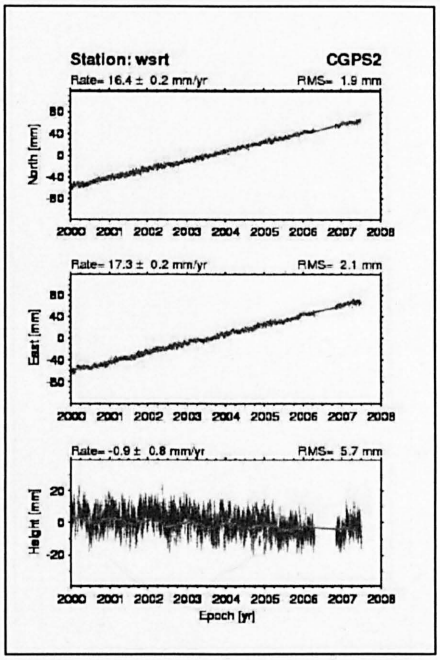
Station: wsrt
CGPS2
Rate= 16.4 ± 0.2 mm/yr
RMS= 1.9 mm
North [mm]
Rate= 17.3 ± 0.2 mm/yr
RMS= 2.1 mm
East [mm]
Rate= -0.9 ± 0.8 mm/yr
RMS= 5.7 mm
Height [mm]
2000 2001 2002 2003 2004 2005 2006 2007 2008
Epoch [yr]

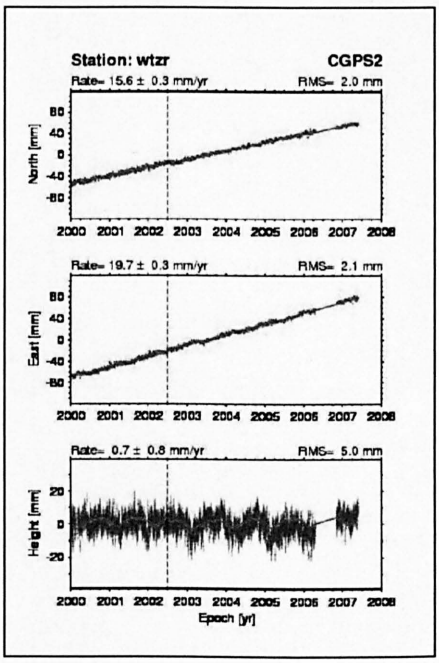
Station: wtzr
CGPS2
Rate= 15.6 ± 0.3 mm/yr
RMS= 2.0 mm
North [mm]
Rate= 19.7 ± 0.3 mm/yr
RMS= 2.1 mm
East [mm]
Rate= 0.7 ± 0.8 mm/yr
RMS= 5.0 mm
Height [mm]
2000 2001 2002 2003 2004 2005 2006 2007 2008
Epoch [yr]

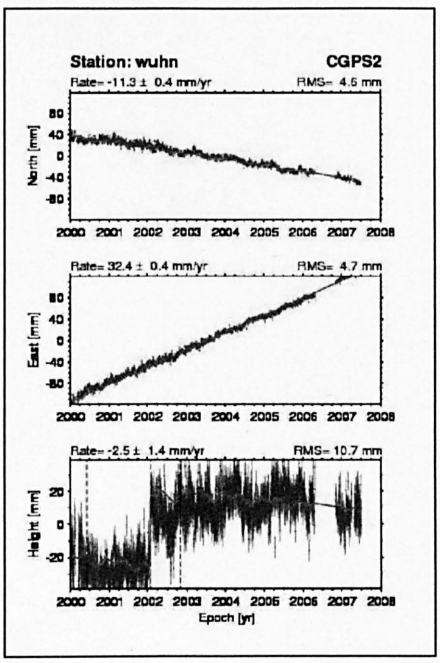
Station: wuhn
CGPS2
Rate= -11.3 ± 0.4 mm/yr
RMS= 4.6 mm
North [mm]
Rate= 32.4 ± 0.4 mm/yr
RMS= 4.7 mm
East [mm]
Rate= -2.5 ± 1.4 mm/yr
RMS= 10.7 mm
Height [mm]
2000 2001 2002 2003 2004 2005 2006 2007 2008
Epoch [yr]

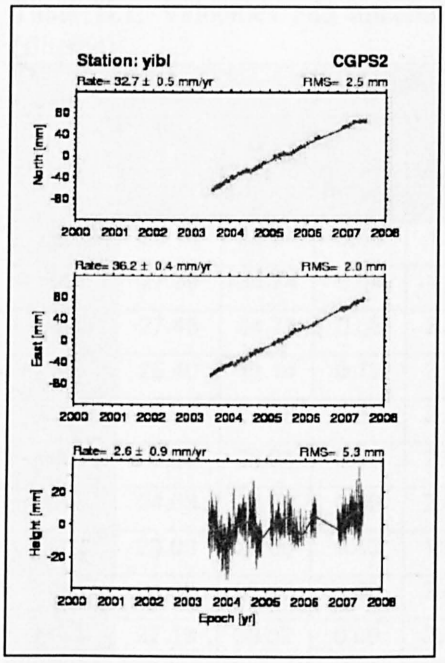
Station: yibl
CGPS2
Rate= 32.7 ± 0.5 mm/yr
RMS= 2.5 mm
North [mm]
Rate= 36.2 ± 0.4 mm/yr
RMS= 2.0 mm
East [mm]
Rate= 2.6 ± 0.9 mm/yr
RMS= 5.3 mm
Height [mm]
2000 2001 2002 2003 2004 2005 2006 2007 2008
Epoch [yr]

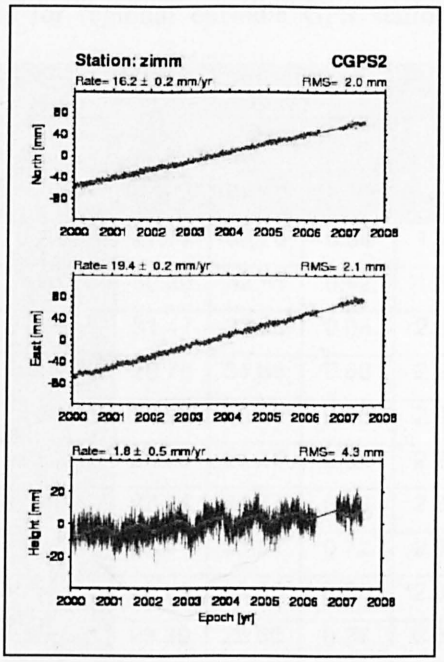
Station: zimm
CGPS2
Rate= 16.2 ± 0.2 mm/yr
RMS= 2.0 mm
North [mm]
Rate= 19.4 ± 0.2 mm/yr
RMS= 2.1 mm
East [mm]
Rate= 1.8 ± 0.5 mm/yr
RMS= 4.3 mm
Height [mm]
2000 2001 2002 2003 2004 2005 2006 2007 2008
Epoch [yr]

Table D.1: Velocities and uncertainties for regional episodic GPS stations (filtered)

Stations	Velocity		Uncertainty		Stations	Velocity		Uncertainty	
	V_N	V_E	U_N	U_E		V_N	V_E	U_N	U_E
	mm/yr	mm/yr	mm/yr	mm/yr		mm/yr	mm/yr	mm/yr	mm/yr
DATM	30.14	35.44	0.53	1.88	F033	27.77	32.78	0.54	1.91
F001	27.79	34.74	0.44	1.56	F035	30.20	32.55	0.42	1.51
F002	27.48	34.79	0.68	2.41	F036	31.47	33.60	0.68	2.39
F005	26.40	31.14	0.72	2.53	F037	29.78	31.66	0.68	2.38
F006	25.92	29.78	0.60	2.13	F039	28.99	30.25	0.58	2.06
F007	26.05	28.31	0.68	2.41	F040	28.99	28.85	0.64	2.26
F008	24.63	27.80	0.69	2.42	F074	27.44	34.77	0.66	2.31
F009	23.03	25.66	0.43	1.53	F077	29.43	33.01	0.72	2.52
F010	24.82	27.17	0.69	2.43	F078	29.29	36.55	0.58	2.05
F012	27.19	30.32	0.69	2.42	HALY	23.39	26.60	0.27	0.97
F013	28.38	30.96	0.58	2.05	NAMA	28.58	33.36	0.45	1.60
F016	27.77	34.64	0.63	2.23	SOLA	28.00	31.53	0.46	1.66
F019	29.18	33.17	0.66	2.32					
F020	29.06	31.29	0.43	1.55					
F024	27.99	28.46	0.55	1.97					
F026	28.20	27.23	0.72	2.54					
F027	26.61	25.87	0.57	2.04					
F029	29.72	29.25	0.53	1.90					
F030	30.94	30.64	0.68	2.40					

V_N : velocity in northing (mm/yr)
V_E : velocity in easting (mm/yr)
U_N : Uncertainty in northing (mm/yr)
U_E : Uncertainty in easting (mm/yr)

Table D.2: The regional network stations velocities before applying regional filtering (unfiltered)

Stations	V_N	V_E	Stations	V_N	V_E
	mm/yr	mm/yr		mm/yr	mm/yr
DATM	30.11	35.47	F027	26.58	25.91
F001	27.76	34.76	F029	29.75	29.23
F002	27.46	34.83	F030	30.91	30.69
F005	26.37	31.17	F033	27.79	32.79
F006	25.96	29.82	F035	30.21	32.51
F007	26.04	28.34	F036	31.42	33.62
F008	24.66	27.85	F037	29.8	31.61
F009	23.06	25.64	F039	28.96	30.29
F010	24.81	27.19	F040	29.04	28.82
F012	27.14	30.31	F074	27.46	34.73
F013	28.39	30.95	F077	29.39	32.98
F016	27.73	34.62	F078	29.33	36.5
F019	29.14	33.13			
F020	29.03	31.27			
F024	28.01	28.5			
F026	28.24	27.22			

V_N : velocity in northing (mm/yr)
V_E : velocity in easting (mm/yr)

Table D.3: The difference between regional network stations velocities when applying regional filtering (the difference between filtered and unfiltered)

Stations	ΔV_N	ΔV_E	Stations	ΔV_N	ΔV_E
	mm/yr	mm/yr		mm/yr	mm/yr
DATM	0.03	-0.03	F027	0.03	-0.04
F001	0.03	-0.02	F029	-0.03	0.02
F002	0.02	-0.04	F030	0.03	-0.05
F005	0.03	-0.03	F033	-0.02	-0.01
F006	-0.04	-0.04	F035	-0.01	0.04
F007	0.01	-0.03	F036	0.05	-0.02
F008	-0.03	-0.05	F037	-0.02	0.05
F009	-0.03	0.02	F039	0.03	-0.04
F010	0.01	-0.02	F040	-0.05	0.03
F012	0.05	0.01	F074	-0.02	0.04
F013	-0.01	0.01	F077	0.04	0.03
F016	0.04	0.02	F078	-0.04	0.05
F019	0.04	0.04	Mean	0.00	-0.00
F020	0.03	0.02	S.dev	0.03	0.03
F024	-0.02	-0.04	RMS	0.03	0.03
F026	-0.04	0.01			

ΔV_N : velocity difference in northing (mm/yr)
ΔV_E : velocity difference in easting (mm/yr)

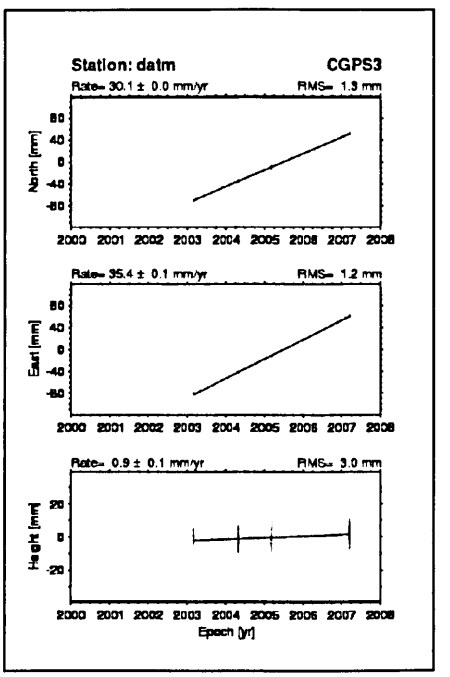
Station: datm
CGPS3
Rate= 30.1 ± 0.0 mm/yr
RMS= 1.3 mm
North [mm]
Rate= 35.4 ± 0.1 mm/yr
RMS= 1.2 mm
East [mm]
Rate= 0.9 ± 0.1 mm/yr
RMS= 3.0 mm
Height [mm]
2000 2001 2002 2003 2004 2005 2006 2007 2008
Epoch [yr]

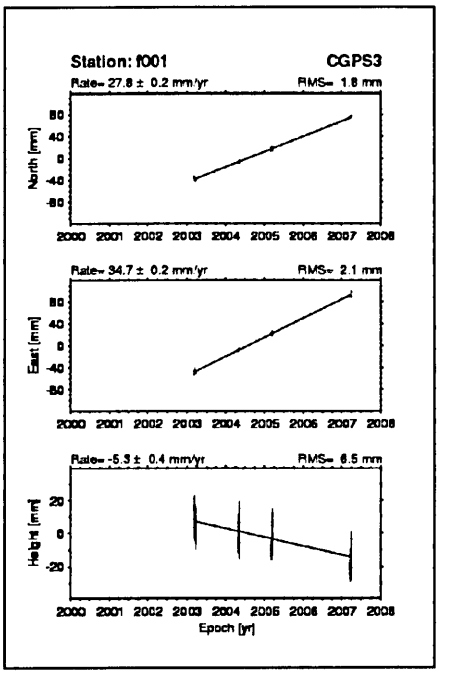
Station: f001
CGPS3
Rate= 27.8 ± 0.2 mm/yr
RMS= 1.8 mm
North [mm]
Rate= 34.7 ± 0.2 mm/yr
RMS= 2.1 mm
East [mm]
Rate= -5.3 ± 0.4 mm/yr
RMS= 6.5 mm
Height [mm]
2000 2001 2002 2003 2004 2005 2006 2007 2008
Epoch [yr]

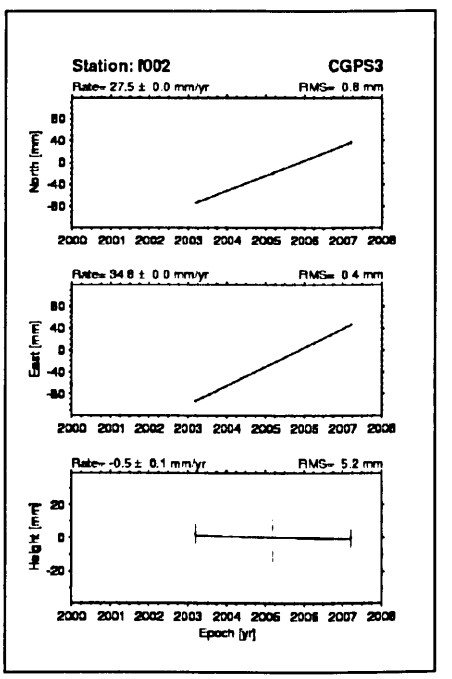
Station: f002
CGPS3
Rate= 27.5 ± 0.0 mm/yr
RMS= 0.8 mm
North [mm]
Rate= 34.8 ± 0.0 mm/yr
RMS= 0.4 mm
East [mm]
Rate= -0.5 ± 0.1 mm/yr
RMS= 5.2 mm
Height [mm]
2000 2001 2002 2003 2004 2005 2006 2007 2008
Epoch [yr]

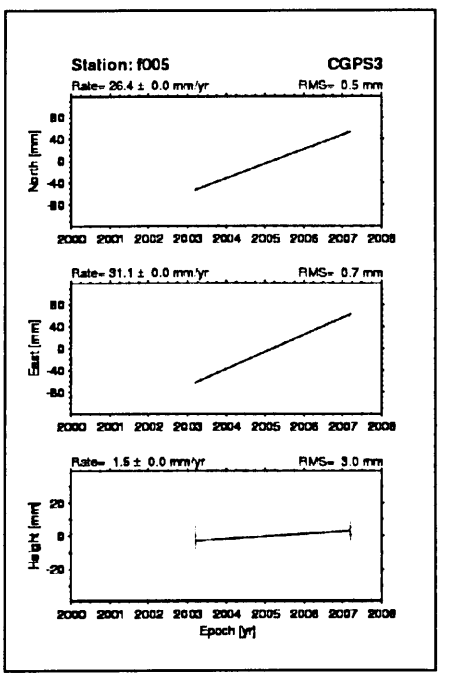
Station: f005
CGPS3
Rate= 26.4 ± 0.0 mm/yr
RMS= 0.5 mm
North [mm]
Rate= 31.1 ± 0.0 mm/yr
RMS= 0.7 mm
East [mm]
Rate= 1.5 ± 0.0 mm/yr
RMS= 3.0 mm
Height [mm]
2000 2001 2002 2003 2004 2005 2006 2007 2008
Epoch [yr]

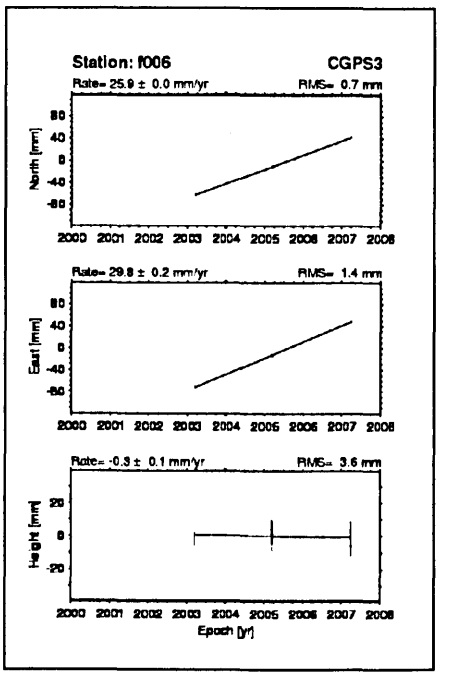
Station: f006
CGPS3
Rate= 25.9 ± 0.0 mm/yr
RMS= 0.7 mm
North [mm]
Rate= 29.8 ± 0.2 mm/yr
RMS= 1.4 mm
East [mm]
Rate= -0.3 ± 0.1 mm/yr
RMS= 3.6 mm
Height [mm]
2000 2001 2002 2003 2004 2005 2006 2007 2008
Epoch [yr]

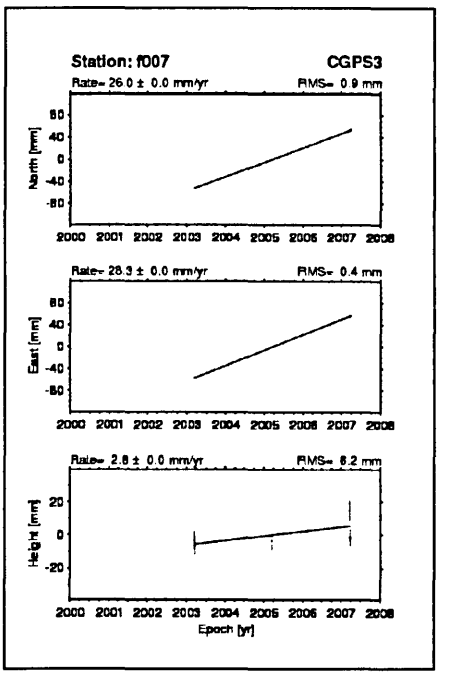
Station: f007
CGPS3
Rate= 26.0 ± 0.0 mm/yr
RMS= 0.9 mm
North [mm]
Rate= 28.3 ± 0.0 mm/yr
RMS= 0.4 mm
East [mm]
Rate= 2.8 ± 0.0 mm/yr
RMS= 8.2 mm
Height [mm]
2000 2001 2002 2003 2004 2005 2006 2007 2008
Epoch [yr]

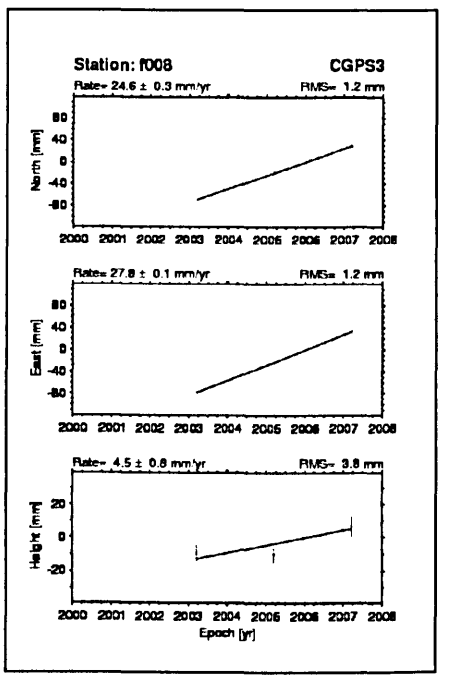
Station: f008
CGPS3
Rate= 24.6 ± 0.3 mm/yr
RMS= 1.2 mm
North [mm]
Rate= 27.8 ± 0.1 mm/yr
RMS= 1.2 mm
East [mm]
Rate= 4.5 ± 0.8 mm/yr
RMS= 3.8 mm
Height [mm]
2000 2001 2002 2003 2004 2005 2006 2007 2008
Epoch [yr]

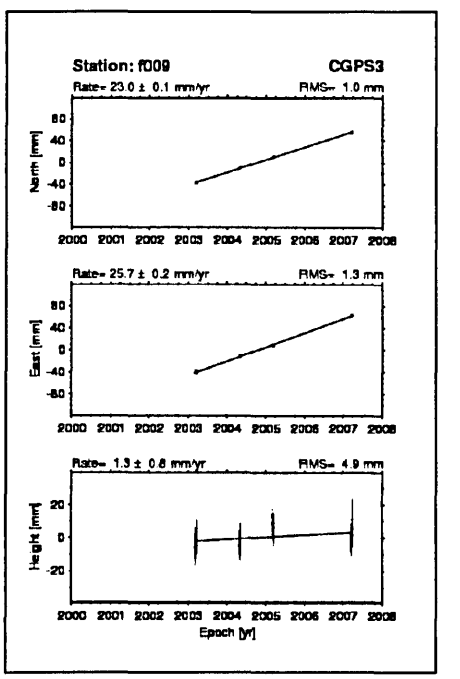
Station: f009
CGPS3
Rate= 23.0 ± 0.1 mm/yr
RMS= 1.0 mm
North [mm]
Rate= 25.7 ± 0.2 mm/yr
RMS= 1.3 mm
East [mm]
Rate= 1.3 ± 0.8 mm/yr
RMS= 4.9 mm
Height [mm]
2000 2001 2002 2003 2004 2005 2006 2007 2008
Epoch [yr]

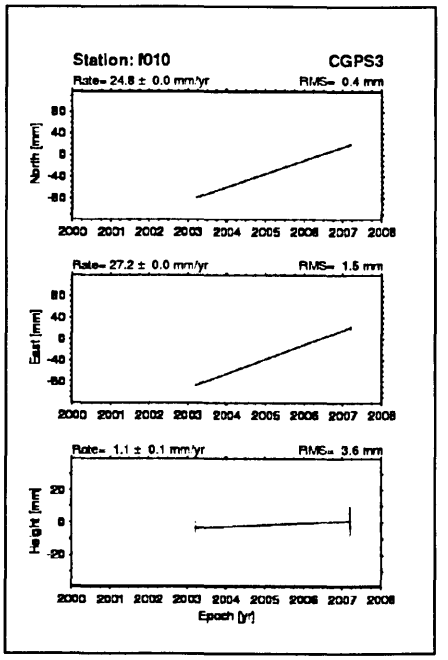
Station: f010
CGPS3
Rate= 24.8 ± 0.0 mm/yr
RMS= 0.4 mm
North [mm]
Rate= 27.2 ± 0.0 mm/yr
RMS= 1.5 mm
East [mm]
Rate= 1.1 ± 0.1 mm/yr
RMS= 3.6 mm
Height [mm]
2000 2001 2002 2003 2004 2005 2006 2007 2008
Epoch [yr]

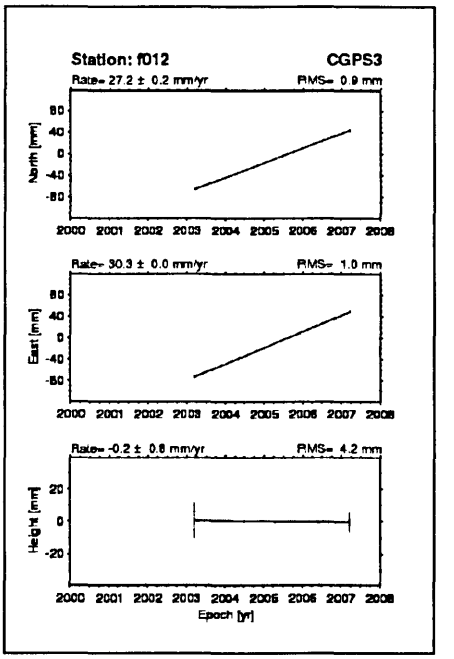
Station: f012
CGPS3
Rate= 27.2 ± 0.2 mm/yr
RMS= 0.9 mm
North [mm]
Rate= 30.3 ± 0.0 mm/yr
RMS= 1.0 mm
East [mm]
Rate= -0.2 ± 0.6 mm/yr
RMS= 4.2 mm
Height [mm]
2000 2001 2002 2003 2004 2005 2006 2007 2008
Epoch [yr]

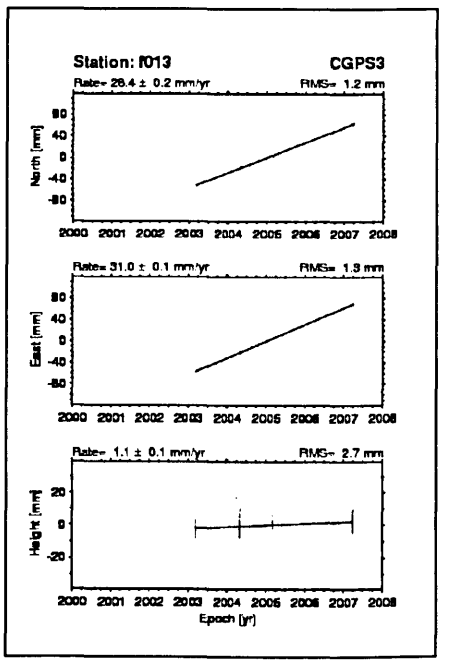
Station: f013
CGPS3
Rate= 26.4 ± 0.2 mm/yr
RMS= 1.2 mm
North [mm]
Rate= 31.0 ± 0.1 mm/yr
RMS= 1.3 mm
East [mm]
Rate= 1.1 ± 0.1 mm/yr
RMS= 2.7 mm
Height [mm]
2000 2001 2002 2003 2004 2005 2006 2007 2008
Epoch [yr]

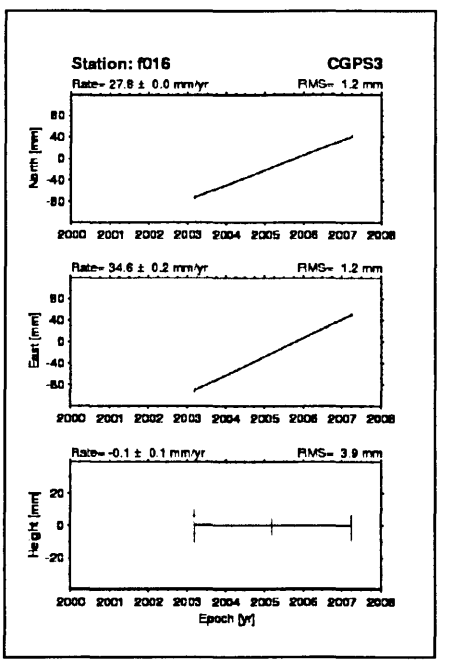
Station: f016
CGPS3
Rate= 27.8 ± 0.0 mm/yr
RMS= 1.2 mm
North [mm]
Rate= 34.6 ± 0.2 mm/yr
RMS= 1.2 mm
East [mm]
Rate= -0.1 ± 0.1 mm/yr
RMS= 3.9 mm
Height [mm]
2000 2001 2002 2003 2004 2005 2006 2007 2008
Epoch [yr]

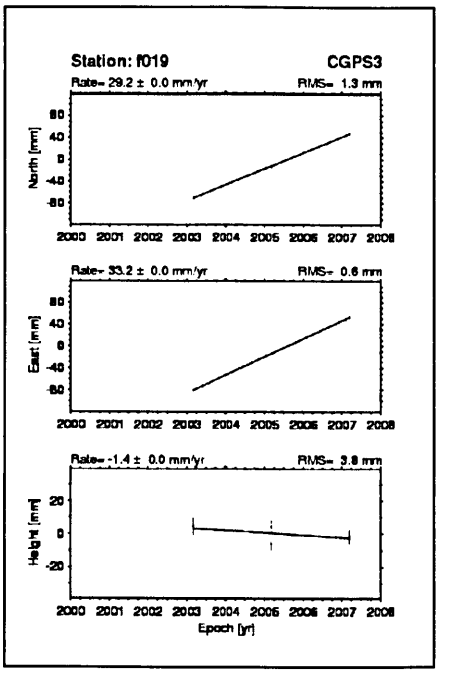
Station: f019
CGPS3
Rate= 29.2 ± 0.0 mm/yr
RMS= 1.3 mm
North [mm]
Rate= 33.2 ± 0.0 mm/yr
RMS= 0.6 mm
East [mm]
Rate= -1.4 ± 0.0 mm/yr
RMS= 3.8 mm
Height [mm]
2000 2001 2002 2003 2004 2005 2006 2007 2008
Epoch [yr]

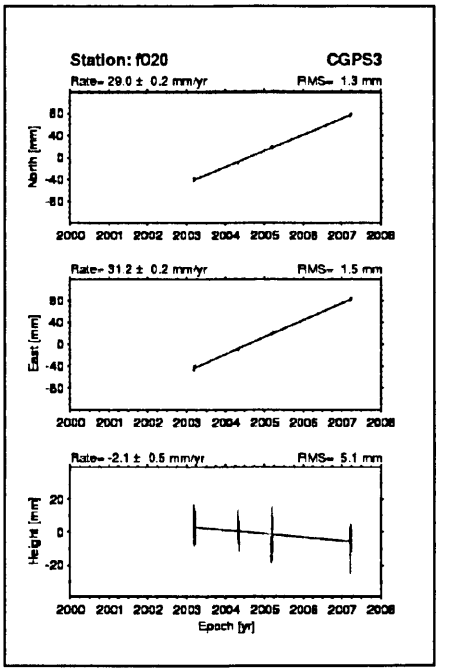
Station: f020
CGPS3
Rate= 29.0 ± 0.2 mm/yr
RMS= 1.3 mm
North [mm]
Rate= 31.2 ± 0.2 mm/yr
RMS= 1.5 mm
East [mm]
Rate= -2.1 ± 0.5 mm/yr
RMS= 5.1 mm
Height [mm]
2000 2001 2002 2003 2004 2005 2006 2007 2008
Epoch [yr]

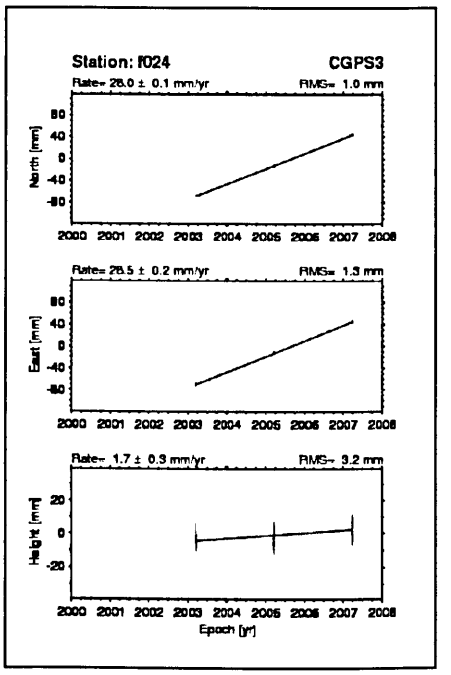
Station: f024
CGPS3
Rate= 26.0 ± 0.1 mm/yr
RMS= 1.0 mm
North [mm]
Rate= 26.5 ± 0.2 mm/yr
RMS= 1.3 mm
East [mm]
Rate= 1.7 ± 0.3 mm/yr
RMS= 3.2 mm
Height [mm]
2000 2001 2002 2003 2004 2005 2006 2007 2008
Epoch [yr]

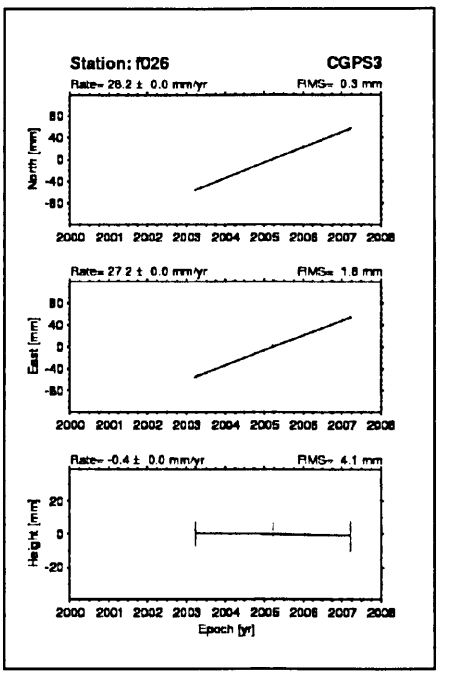
Station: f026
CGPS3
Rate= 26.2 ± 0.0 mm/yr
RMS= 0.3 mm
North [mm]
Rate= 27.2 ± 0.0 mm/yr
RMS= 1.8 mm
East [mm]
Rate= -0.4 ± 0.0 mm/yr
RMS= 4.1 mm
Height [mm]
2000 2001 2002 2003 2004 2005 2006 2007 2008
Epoch [yr]

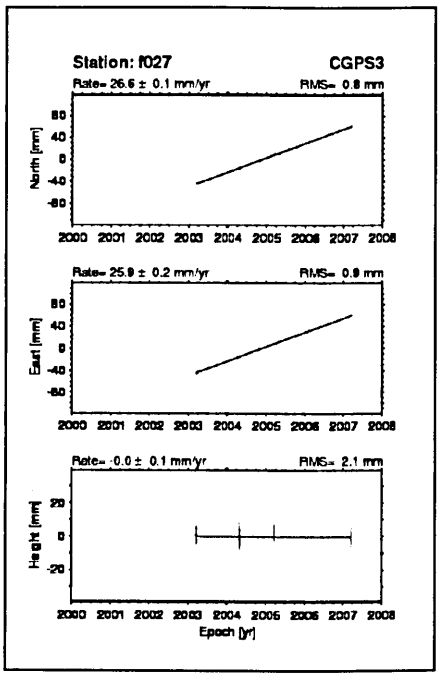
Station: f027
CGPS3
Rate= 26.6 ± 0.1 mm/yr
RMS= 0.8 mm
North [mm]
Rate= 25.9 ± 0.2 mm/yr
RMS= 0.9 mm
East [mm]
Rate= -0.0 ± 0.1 mm/yr
RMS= 2.1 mm
Height [mm]
2000 2001 2002 2003 2004 2005 2006 2007 2008
Epoch [yr]

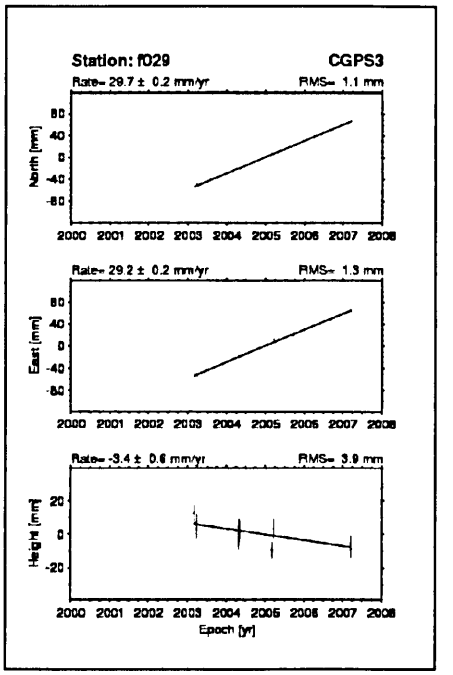
Station: f029
CGPS3
Rate= 29.7 ± 0.2 mm/yr
RMS= 1.1 mm
North [mm]
Rate= 29.2 ± 0.2 mm/yr
RMS= 1.3 mm
East [mm]
Rate= -3.4 ± 0.6 mm/yr
RMS= 3.9 mm
Height [mm]
2000 2001 2002 2003 2004 2005 2006 2007 2008
Epoch [yr]

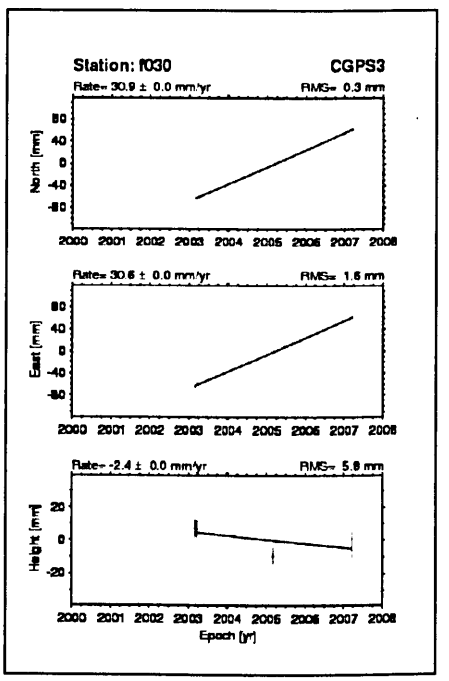
Station: f030
CGPS3
Rate= 30.9 ± 0.0 mm/yr
RMS= 0.3 mm
North [mm]
Rate= 30.6 ± 0.0 mm/yr
RMS= 1.6 mm
East [mm]
Rate= -2.4 ± 0.0 mm/yr
RMS= 5.8 mm
Height [mm]
2000 2001 2002 2003 2004 2005 2006 2007 2008
Epoch [yr]

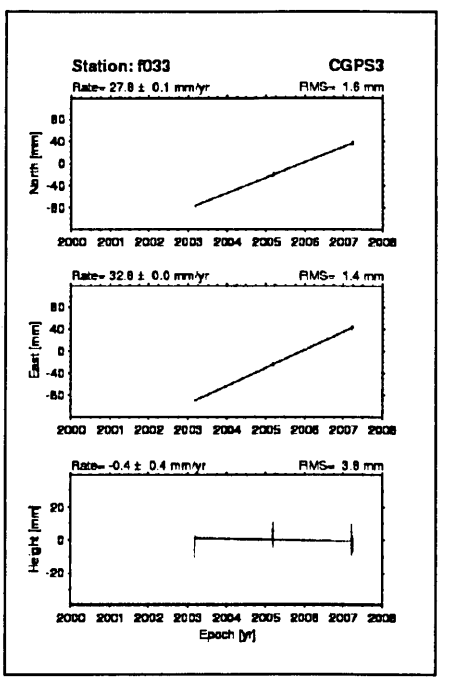
Station: f033
CGPS3
Rate= 27.8 ± 0.1 mm/yr
RMS= 1.6 mm
North [mm]
Rate= 32.8 ± 0.0 mm/yr
RMS= 1.4 mm
East [mm]
Rate= -0.4 ± 0.4 mm/yr
RMS= 3.8 mm
Height [mm]
2000 2001 2002 2003 2004 2005 2006 2007 2008
Epoch [yr]

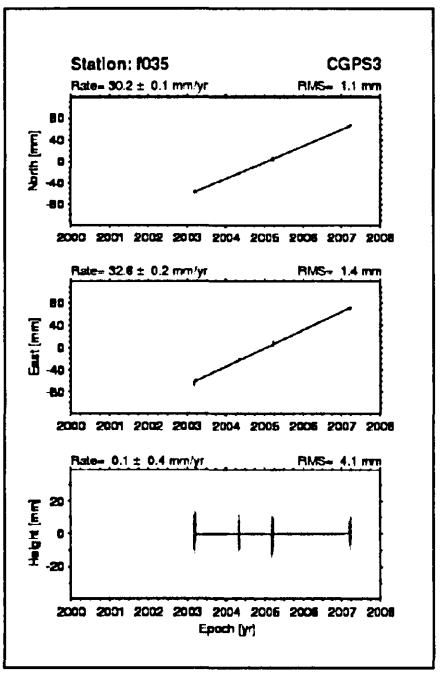
Station: f035
CGPS3
Rate= 30.2 ± 0.1 mm/yr
RMS= 1.1 mm
North [mm]
Rate= 32.6 ± 0.2 mm/yr
RMS= 1.4 mm
East [mm]
Rate= 0.1 ± 0.4 mm/yr
RMS= 4.1 mm
Height [mm]
2000 2001 2002 2003 2004 2005 2006 2007 2008
Epoch [yr]

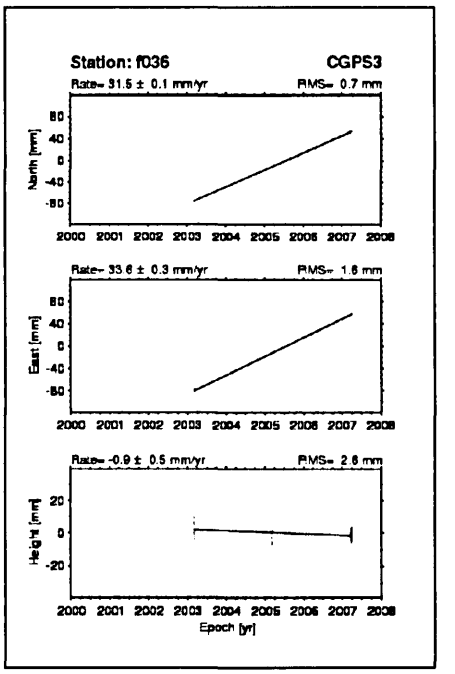
Station: f036
CGPS3
Rate= 31.5 ± 0.1 mm/yr
RMS= 0.7 mm
North [mm]
Rate= 33.6 ± 0.3 mm/yr
RMS= 1.6 mm
East [mm]
Rate= -0.9 ± 0.5 mm/yr
RMS= 2.6 mm
Height [mm]
2000 2001 2002 2003 2004 2005 2006 2007 2008
Epoch [yr]

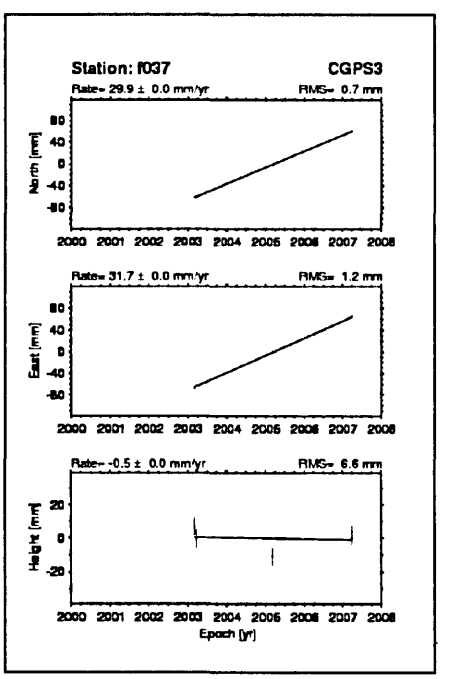
Station: f037
CGPS3
Rate= 29.9 ± 0.0 mm/yr
RMS= 0.7 mm
North [mm]
Rate= 31.7 ± 0.0 mm/yr
RMS= 1.2 mm
East [mm]
Rate= -0.5 ± 0.0 mm/yr
RMS= 6.6 mm
Height [mm]
2000 2001 2002 2003 2004 2005 2006 2007 2008
Epoch [yr]

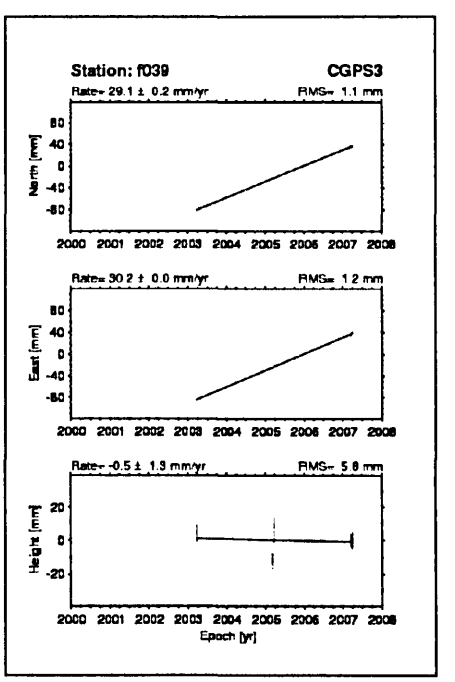
Station: f039
CGPS3
Rate= 29.1 ± 0.2 mm/yr
RMS= 1.1 mm
North [mm]
Rate= 30.2 ± 0.0 mm/yr
RMS= 1.2 mm
East [mm]
Rate= -0.5 ± 1.3 mm/yr
RMS= 5.8 mm
Height [mm]
2000 2001 2002 2003 2004 2005 2006 2007 2008
Epoch [yr]

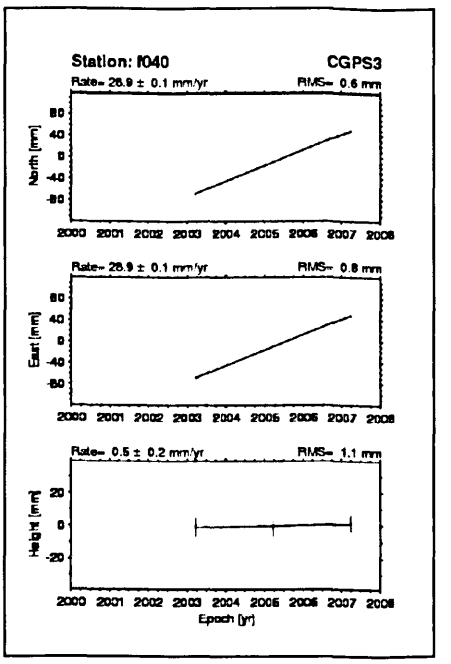
Station: f040
CGPS3
Rate= 26.9 ± 0.1 mm/yr
RMS= 0.6 mm
North [mm]
Rate= 26.9 ± 0.1 mm/yr
RMS= 0.8 mm
East [mm]
Rate= 0.5 ± 0.2 mm/yr
RMS= 1.1 mm
Height [mm]
2000 2001 2002 2003 2004 2005 2006 2007 2008
Epoch [yr]

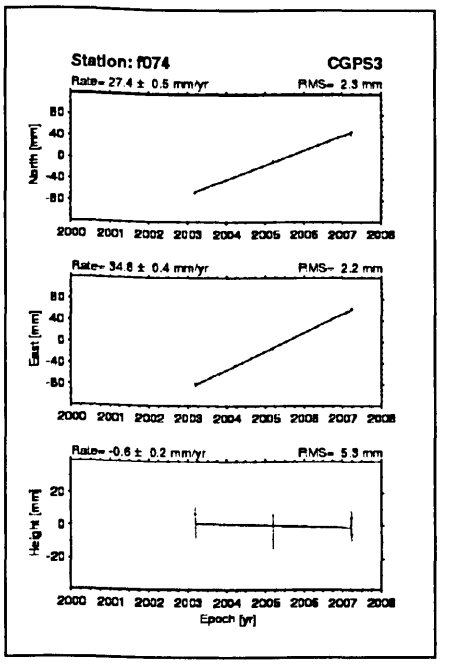
Station: f074
CGPS3
Rate= 27.4 ± 0.5 mm/yr
RMS= 2.3 mm
North [mm]
Rate= 34.8 ± 0.4 mm/yr
RMS= 2.2 mm
East [mm]
Rate= -0.6 ± 0.2 mm/yr
RMS= 5.3 mm
Height [mm]
2000 2001 2002 2003 2004 2005 2006 2007 2008
Epoch [yr]

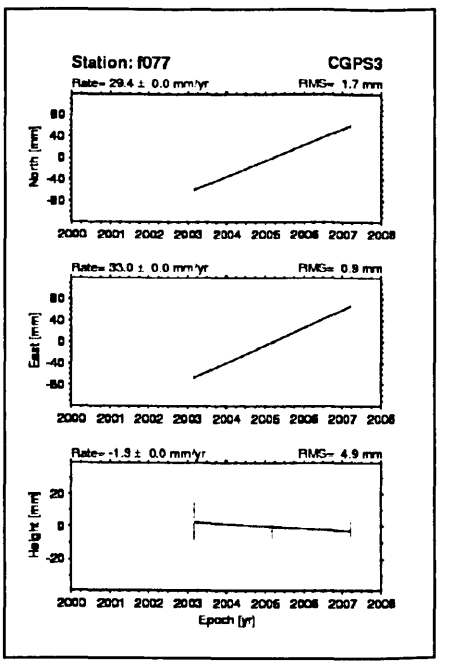
Station: f077
CGPS3
Rate= 29.4 ± 0.0 mm/yr
RMS= 1.7 mm
North [mm]
Rate= 33.0 ± 0.0 mm/yr
RMS= 0.9 mm
East [mm]
Rate= -1.9 ± 0.0 mm/yr
RMS= 4.9 mm
Height [mm]
2000 2001 2002 2003 2004 2005 2006 2007 2008
Epoch [yr]

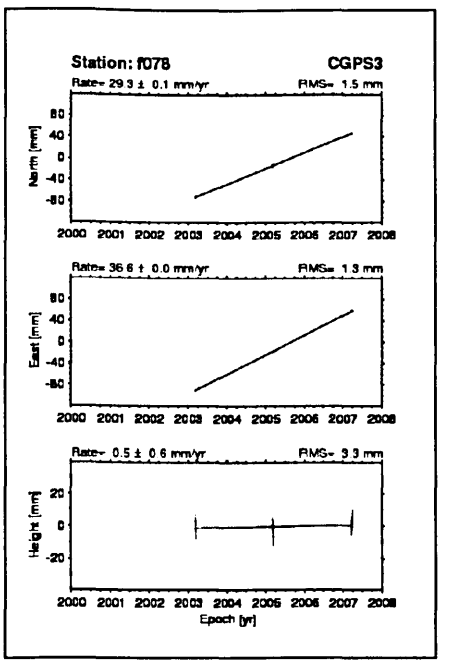
Station: f078
CGPS3
Rate= 29.3 ± 0.1 mm/yr
RMS= 1.5 mm
North [mm]
Rate= 36.6 ± 0.0 mm/yr
RMS= 1.3 mm
East [mm]
Rate= 0.5 ± 0.6 mm/yr
RMS= 3.3 mm
Height [mm]
2000 2001 2002 2003 2004 2005 2006 2007 2008
Epoch [yr]

Table E.1: Velocities and uncertainties for local episodic GPS stations

Stations	Velocity		Uncertainty	
	V_N	V_E	U_N	U_E
	mm/yr	mm/yr	mm/yr	mm/yr
o229	25.24	35.09	1.3711	4.8154
o231	25.06	35.2	1.3039	4.5870
o235	25.67	35.97	1.6016	5.5976
o258	26.39	33.86	1.6016	5.5976
o260	25.43	33.57	3.4838	12.1098
o627	28.73	36.29	1.3711	4.8154
o628	25.6	34.95	1.3039	4.5870
o629	27.78	35.33	2.7782	9.7184
o630	25.46	34.97	1.3101	4.6089
o632	25.51	36.48	1.1212	3.9651
o633	26.2	36.2	1.6154	5.6458
o634	26.16	35.4	1.6206	5.6636
o635	26.61	35.6	1.3177	4.6352
o639	27.33	36.85	1.3970	4.9060
o641	26.24	35.33	1.6366	5.7195
o643	25.11	35.78	1.6285	5.6914
o644	28.09	36.51	1.6366	5.7195
m586	27.05	35.35	1.3892	4.8785
m587	27.77	35.67	1.3241	4.6578
m588	24.75	36.55	3.6568	12.7095
m589	26.61	35.62	1.6366	5.7195
m591	27.06	34.94	1.3269	4.6678

V_N : velocity in northing (mm/yr)
V_E : velocity in easting (mm/yr)
U_N : Uncertainty in northing (mm/yr)
U_E : Uncertainty in easting (mm/yr)

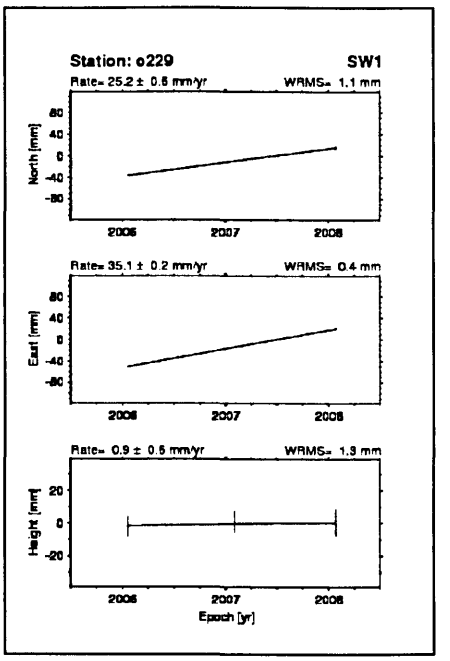
Station: o229
SW1
Rate= 25.2 ± 0.8 mm/yr
WRMS= 1.1 mm
North [mm]
Rate= 35.1 ± 0.2 mm/yr
WRMS= 0.4 mm
East [mm]
Rate= 0.9 ± 0.5 mm/yr
WRMS= 1.3 mm
Height [mm]
2006
2007
2008
Epoch [yr]

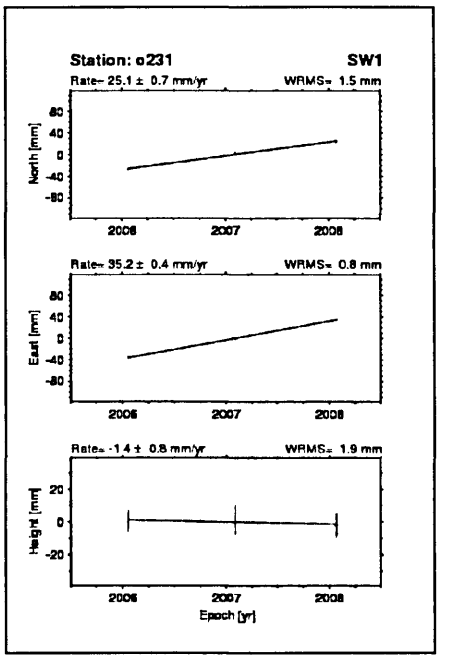
Station: o231
SW1
Rate= 25.1 ± 0.7 mm/yr
WRMS= 1.5 mm
North [mm]
Rate= 35.2 ± 0.4 mm/yr
WRMS= 0.8 mm
East [mm]
Rate= -1.4 ± 0.8 mm/yr
WRMS= 1.9 mm
Height [mm]
2006
2007
2008
Epoch [yr]

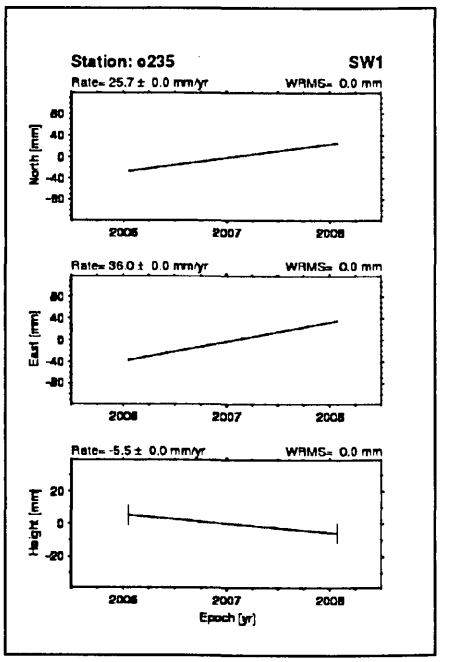
Station: o235
SW1
Rate= 25.7 ± 0.0 mm/yr
WRMS= 0.0 mm
North [mm]
Rate= 36.0 ± 0.0 mm/yr
WRMS= 0.0 mm
East [mm]
Rate= -5.5 ± 0.0 mm/yr
WRMS= 0.0 mm
Height [mm]
2006
2007
2008
Epoch [yr]

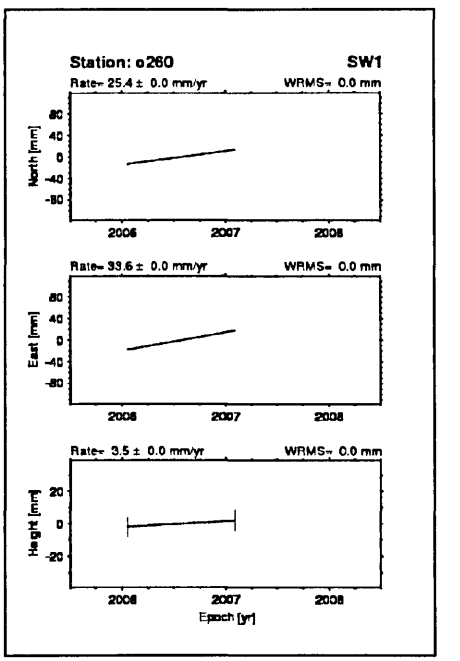
Station: o260
SW1
Rate= 25.4 ± 0.0 mm/yr
WRMS= 0.0 mm
North [mm]
Rate= 33.6 ± 0.0 mm/yr
WRMS= 0.0 mm
East [mm]
Rate= 3.5 ± 0.0 mm/yr
WRMS= 0.0 mm
Height [mm]
2006
2007
2008
Epoch [yr]

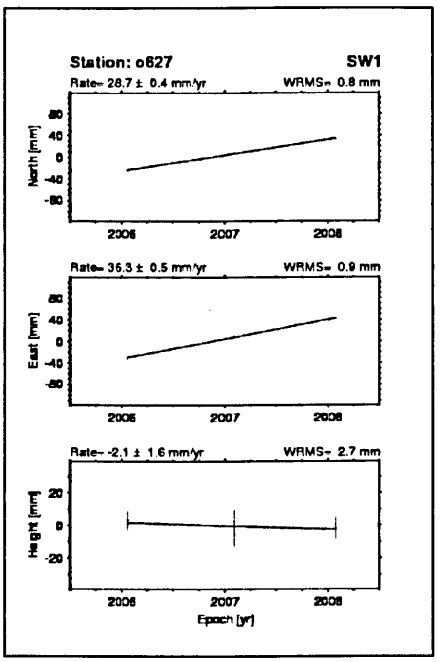
Station: o627
SW1
Rate= 28.7 ± 0.4 mm/yr
WRMS= 0.8 mm
North [mm]
Rate= 36.3 ± 0.5 mm/yr
WRMS= 0.9 mm
East [mm]
Rate= -2.1 ± 1.6 mm/yr
WRMS= 2.7 mm
Height [mm]
2006
2007
2008
Epoch [yr]

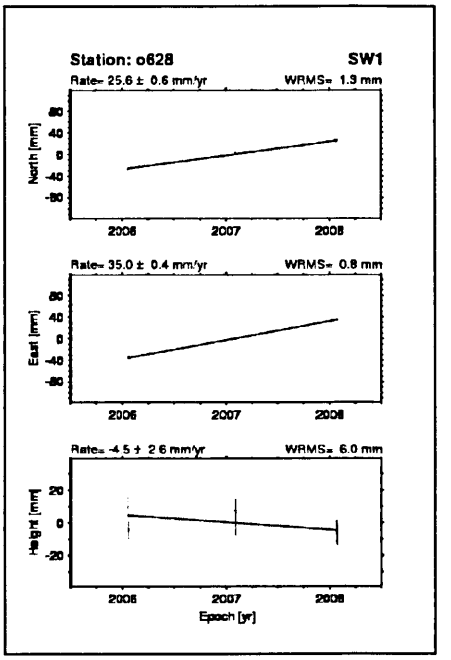
Station: o628
SW1
Rate= 25.6 ± 0.6 mm/yr
WRMS= 1.3 mm
North [mm]
Rate= 35.0 ± 0.4 mm/yr
WRMS= 0.8 mm
East [mm]
Rate= -4.5 ± 2.6 mm/yr
WRMS= 6.0 mm
Height [mm]
2006
2007
2008
Epoch [yr]

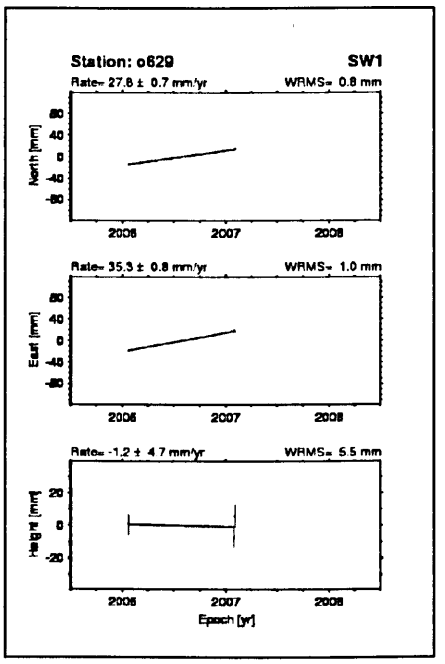
Station: o629
SW1
Rate= 27.8 ± 0.7 mm/yr
WRMS= 0.8 mm
North [mm]
Rate= 35.3 ± 0.8 mm/yr
WRMS= 1.0 mm
East [mm]
Rate= -1.2 ± 4.7 mm/yr
WRMS= 5.5 mm
Height [mm]
2006
2007
2008
Epoch [yr]

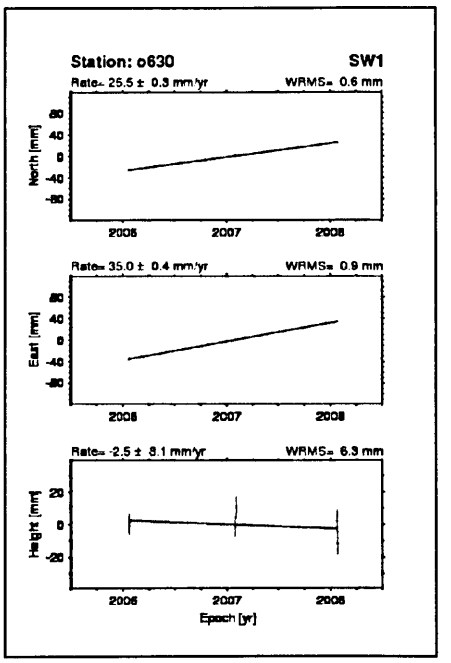
Station: o630
SW1
Rate= 25.5 ± 0.3 mm/yr
WRMS= 0.6 mm
North [mm]
Rate= 35.0 ± 0.4 mm/yr
WRMS= 0.9 mm
East [mm]
Rate= -2.5 ± 3.1 mm/yr
WRMS= 6.3 mm
Height [mm]
2006
2007
2008
Epoch [yr]

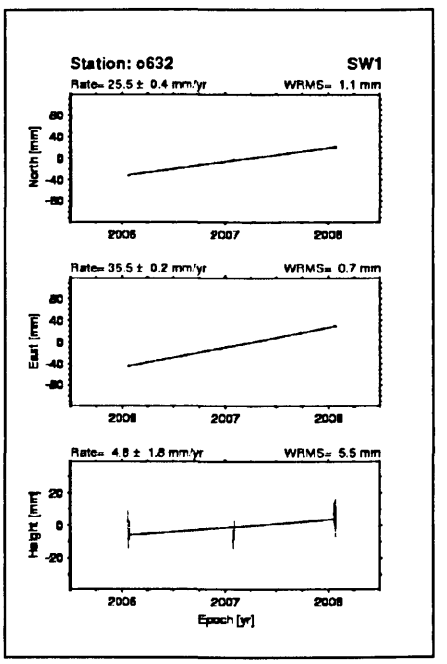
Station: o632
SW1
Rate= 25.5 ± 0.4 mm/yr
WRMS= 1.1 mm
North [mm]
Rate= 35.5 ± 0.2 mm/yr
WRMS= 0.7 mm
East [mm]
Rate= 4.8 ± 1.8 mm/yr
WRMS= 5.5 mm
Height [mm]
2006
2007
2008
Epoch [yr]

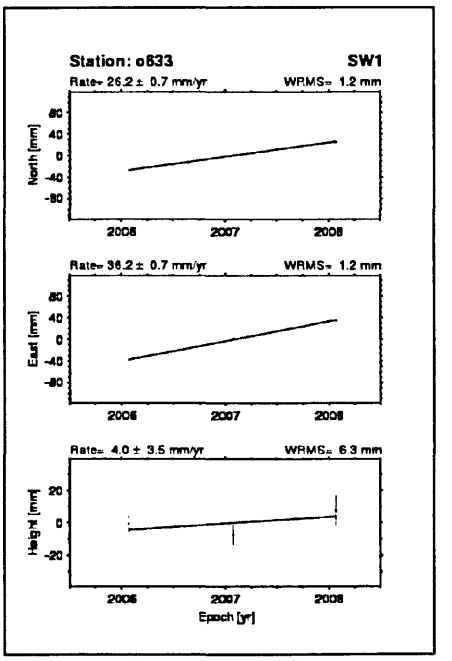
Station: o633
SW1
Rate= 26.2 ± 0.7 mm/yr
WRMS= 1.2 mm
North [mm]
Rate= 36.2 ± 0.7 mm/yr
WRMS= 1.2 mm
East [mm]
Rate= 4.0 ± 3.5 mm/yr
WRMS= 6.3 mm
Height [mm]
2006
2007
2008
Epoch [yr]

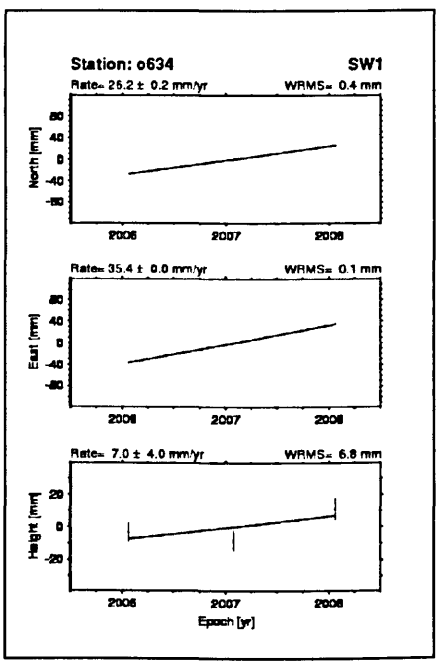
Station: o634
SW1
Rate= 25.2 ± 0.2 mm/yr
WRMS= 0.4 mm
North [mm]
Rate= 35.4 ± 0.0 mm/yr
WRMS= 0.1 mm
East [mm]
Rate= 7.0 ± 4.0 mm/yr
WRMS= 6.8 mm
Height [mm]
2006
2007
2008
Epoch [yr]

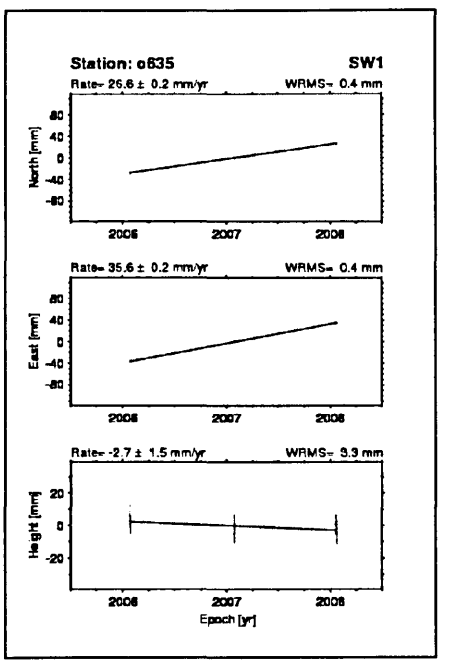
Station: o635
SW1
Rate= 25.6 ± 0.2 mm/yr
WRMS= 0.4 mm
North [mm]
Rate= 35.6 ± 0.2 mm/yr
WRMS= 0.4 mm
East [mm]
Rate= -2.7 ± 1.5 mm/yr
WRMS= 3.3 mm
Height [mm]
2006
2007
2008
Epoch [yr]

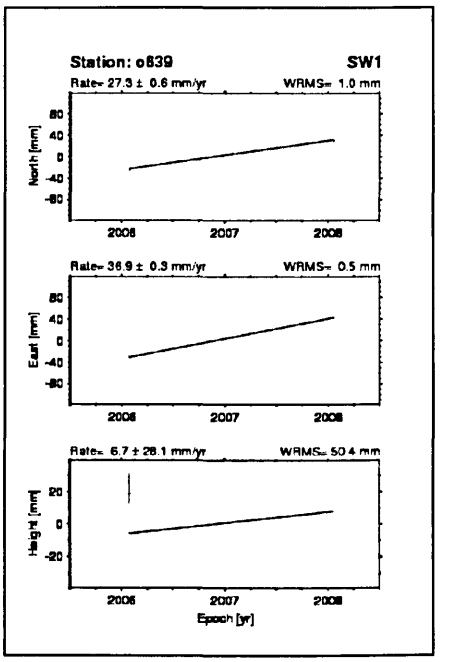
Station: o639
SW1
Rate= 27.3 ± 0.6 mm/yr
WRMS= 1.0 mm
North [mm]
Rate= 36.9 ± 0.3 mm/yr
WRMS= 0.5 mm
East [mm]
Rate= 6.7 ± 28.1 mm/yr
WRMS= 50.4 mm
Height [mm]
2006
2007
2008
Epoch [yr]

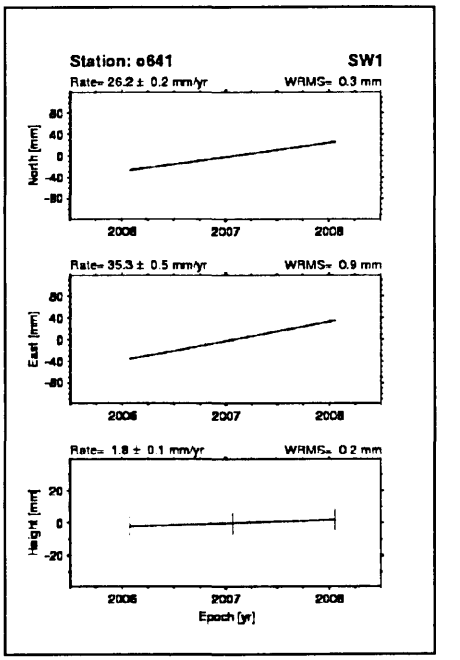
Station: o641
SW1
Rate= 26.2 ± 0.2 mm/yr
WRMS= 0.3 mm
North [mm]
Rate= 35.3 ± 0.5 mm/yr
WRMS= 0.9 mm
East [mm]
Rate= 1.8 ± 0.1 mm/yr
WRMS= 0.2 mm
Height [mm]
2006
2007
2008
Epoch [yr]

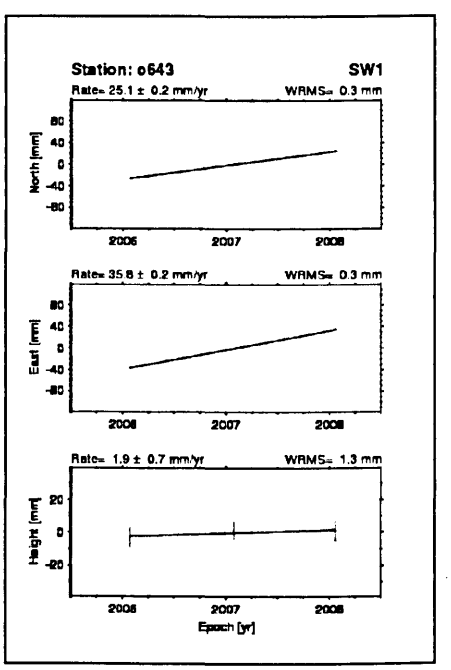
Station: o643
SW1
Rate= 25.1 ± 0.2 mm/yr
WRMS= 0.3 mm
North [mm]
Rate= 35.8 ± 0.2 mm/yr
WRMS= 0.3 mm
East [mm]
Rate= 1.9 ± 0.7 mm/yr
WRMS= 1.3 mm
Height [mm]
2006
2007
2008
Epoch [yr]

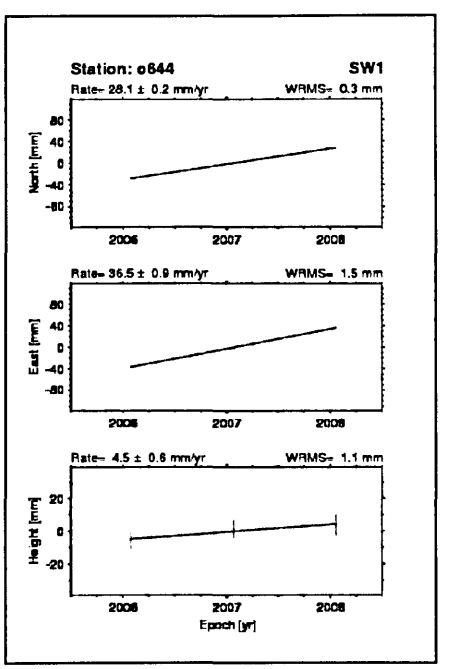
Station: o644
SW1
Rate= 28.1 ± 0.2 mm/yr
WRMS= 0.3 mm
North [mm]
Rate= 36.5 ± 0.9 mm/yr
WRMS= 1.5 mm
East [mm]
Rate= 4.5 ± 0.6 mm/yr
WRMS= 1.1 mm
Height [mm]
2006
2007
2008
Epoch [yr]

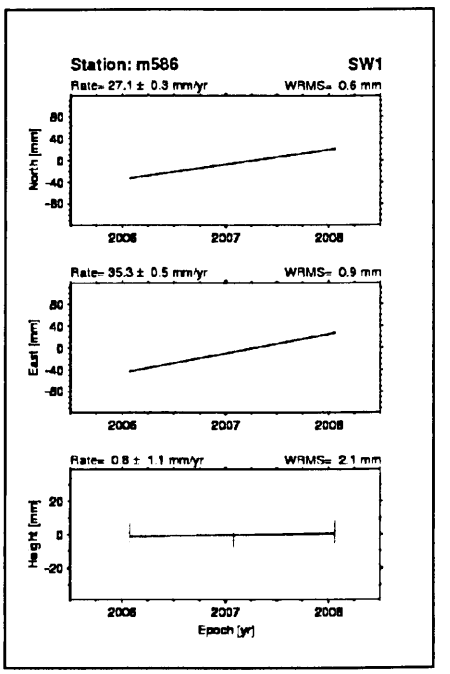
Station: m586
SW1
Rate= 27.1 ± 0.3 mm/yr
WRMS= 0.6 mm
North [mm]
Rate= 35.3 ± 0.5 mm/yr
WRMS= 0.9 mm
East [mm]
Rate= 0.8 ± 1.1 mm/yr
WRMS= 2.1 mm
Height [mm]
2006
2007
2008
Epoch [yr]

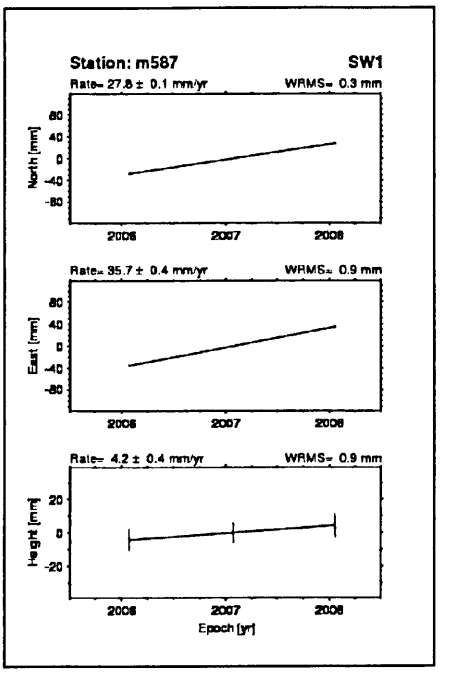
Station: m587
SW1
Rate= 27.8 ± 0.1 mm/yr
WRMS= 0.3 mm
North [mm]
Rate= 35.7 ± 0.4 mm/yr
WRMS= 0.9 mm
East [mm]
Rate= 4.2 ± 0.4 mm/yr
WRMS= 0.9 mm
Height [mm]
2006
2007
2008
Epoch [yr]

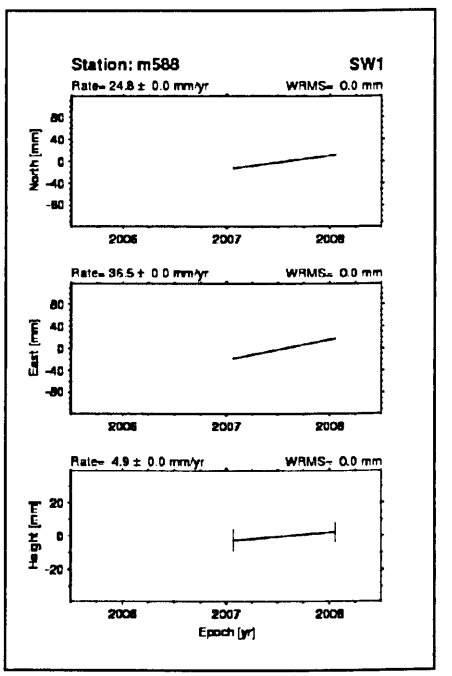
Station: m588
SW1
Rate= 24.8 ± 0.0 mm/yr
WRMS= 0.0 mm
North [mm]
Rate= 36.5 ± 0.0 mm/yr
WRMS= 0.0 mm
East [mm]
Rate= 4.9 ± 0.0 mm/yr
WRMS= 0.0 mm
Height [mm]
2006
2007
2008
Epoch [yr]

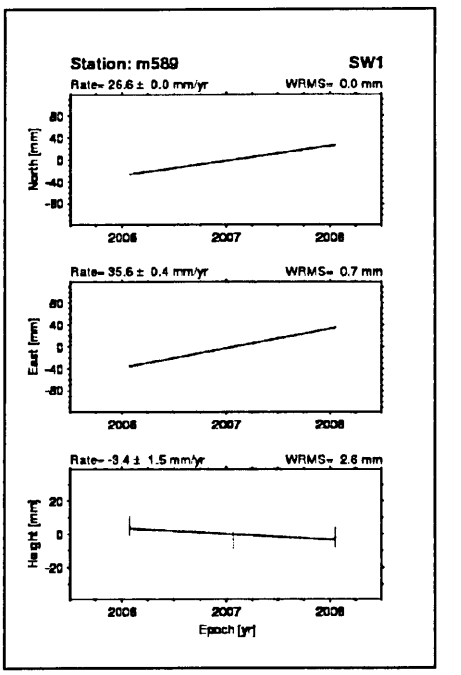
Station: m589
SW1
Rate= 26.6 ± 0.0 mm/yr
WRMS= 0.0 mm
North [mm]
Rate= 35.6 ± 0.4 mm/yr
WRMS= 0.7 mm
East [mm]
Rate= -3.4 ± 1.5 mm/yr
WRMS= 2.6 mm
Height [mm]
2006
2007
2008
Epoch [yr]

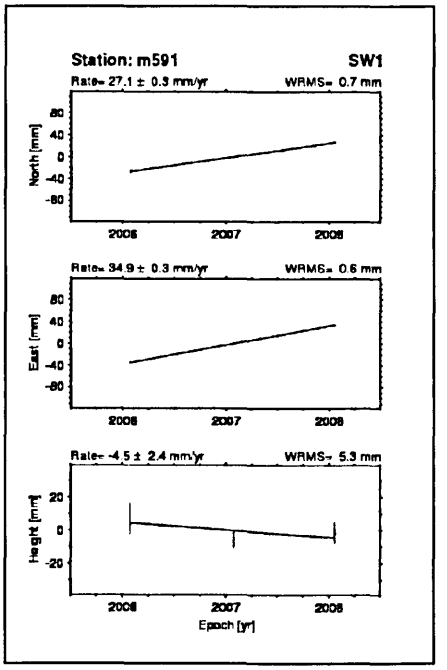
Station: m591
SW1
Rate= 27.1 ± 0.9 mm/yr
WRMS= 0.7 mm
North [mm]
80
40
0
-40
-80
2006
2007
2008
Rate= 34.9 ± 0.3 mm/yr
WRMS= 0.6 mm
East [mm]
80
40
0
-40
-80
2006
2007
2008
Rate= -4.5 ± 2.4 mm/yr
WRMS= 5.3 mm
Height [mm]
20
0
-20
2006
2007
2008
Epoch [yr]

Table F.1: Velocity uncertainties for episodic campaigns stations when using *Zhang et al.* [1997] or *Mao et al.* [1999] equations with the average amplitudes of the white and flicker noise for the regional network taken from this study when applying three and six stations.

	Method 2a3		Method 2a6			Method 2a3		Method 2a6	
Stations	U_N	U_E	U_N	U_E	Stations	U_N	U_E	U_N	U_E
	mm/yr	mm/yr	mm/yr	mm/yr		mm/yr	mm/yr	mm/yr	mm/yr
DATM	0.53	1.88	0.48	1.63	F033	0.54	1.91	0.49	1.66
F001	0.44	1.56	0.39	1.34	F035	0.42	1.51	0.38	1.30
F002	0.68	2.41	0.63	2.12	F036	0.68	2.39	0.63	2.10
F005	0.72	2.53	0.67	2.24	F037	0.68	2.38	0.63	2.10
F006	0.60	2.13	0.55	1.86	F039	0.58	2.06	0.53	1.80
F007	0.68	2.41	0.64	2.12	F040	0.64	2.26	0.59	1.98
F008	0.69	2.42	0.64	2.13	F074	0.66	2.31	0.61	2.03
F009	0.43	1.53	0.38	1.31	F077	0.72	2.52	0.67	2.22
F010	0.69	2.43	0.64	2.14	F078	0.58	2.05	0.53	1.79
F012	0.69	2.42	0.64	2.13	HALY	0.27	0.97	0.24	0.82
F013	0.58	2.05	0.53	1.78	NAMA	0.45	1.60	0.40	1.37
F016	0.63	2.23	0.58	1.96	SOLA	0.46	1.66	0.41	1.42
F019	0.66	2.32	0.61	2.04					
F020	0.43	1.55	0.39	1.33					
F024	0.55	1.97	0.50	1.71					
F026	0.72	2.54	0.67	2.24					
F027	0.57	2.04	0.52	1.77					
F029	0.53	1.90	0.48	1.64					
F030	0.68	2.40	0.63	2.11					

U_N : Uncertainty in northing (mm/yr)
U_E : Uncertainty in easting (mm/yr)
Method 2 & 3: *Zhang et al.* [1997] or *Mao et al.* [1999] equations were used with the average amplitudes of the white and flicker noise for the regional network taken from the CATS output for three station (BAHR, YIBL and RAMO) from this study.
Method 2 & 6: *Zhang et al.* [1997] or *Mao et al.* [1999] equations were used with the average amplitudes of the white and flicker noise for the regional network taken from the CATS output for six stations (BAHR, YIBL, RAMO, NICO, TEHN and TRAB) from this study.

Table F.2: Velocity uncertainties for episodic campaigns stations when using Geirsson et al., [2006] equations and *Zhang et al.* [1997] or *Mao et al.* [1999] equations with the average amplitudes of the white and flicker noise for the global model taken from Willams et al., [2004].

	Method 2b		Method 1			Method 2b		Method 1	
Stations	U_N	U_E	U_N	U_E	Stations	U_N	U_E	U_N	U_E
	mm/yr	mm/yr	mm/yr	mm/yr		mm/yr	mm/yr	mm/yr	mm/yr
DATM	0.71	2.47	0.59	0.59	F033	0.73	2.49	0.52	0.84
F001	0.59	2.11	0.62	0.69	F035	0.57	2.06	0.44	0.60
F002	0.92	2.96	0.88	0.36	F036	0.91	2.93	0.46	0.74
F005	0.97	3.07	0.46	0.98	F037	0.91	2.93	0.38	0.73
F006	0.81	2.71	0.29	0.62	F039	0.78	2.65	0.34	0.76
F007	0.92	2.96	0.41	0.63	F040	0.86	2.83	0.37	0.44
F008	0.92	2.97	0.18	0.57	F074	0.88	2.87	1.08	0.87
F009	0.58	2.08	0.48	0.61	F077	0.96	3.06	0.58	0.71
F010	0.93	2.98	0.19	0.41	F078	0.78	2.63	0.60	0.59
F012	0.92	2.97	0.37	1.10	HALY	0.36	1.34	0.44	0.34
F013	0.78	2.63	0.56	0.56	NAMA	0.61	2.21	0.77	0.59
F016	0.85	2.80	0.71	0.57	SOLA	0.63	2.29	0.69	0.61
F019	0.88	2.88	0.42	0.48					
F020	0.59	2.10	0.55	0.68					
F024	0.75	2.55	0.45	0.74					
F026	0.97	3.08	0.37	0.44					
F027	0.77	2.63	0.23	0.50					
F029	0.72	2.48	0.47	0.62					
F030	0.91	2.94	0.51	0.95					

U_N : Uncertainty in northing (mm/yr)
U_E : Uncertainty in easting (mm/yr)
Method 2b: Zhang *et al.* [1997] or Mao *et al.* [1999] equations were used with the average amplitudes of the white and flicker noise for the global network taken from Williams *et al.* [2004].
Method 1: Geirsson *et al.* [2006] equations were used.

Table F.3: The difference of Velocity uncertainties for episodic campaigns stations when *Zhang et al.* [1997] or *Mao et al.* [1999] equations with the average amplitudes of the white and flicker noise for the regional network taken from this study when applying three and six stations for and the global model taken from Willams et al., [2004].

	2a3- 2a6		2a3- 2b			2a3- 2a6		2a3- 2b	
Stations	ΔU_N	ΔU_E	ΔU_N	ΔU_E	Stations	ΔU_N	ΔU_E	ΔU_N	ΔU_E
	mm/yr	mm/yr	mm/yr	mm/yr		mm/yr	mm/yr	mm/yr	mm/yr
DATM	0.05	0.25	-0.18	-0.59	F033	0.05	0.25	-0.19	-0.58
F001	0.05	0.22	-0.15	-0.55	F035	0.05	0.21	-0.15	-0.55
F002	0.05	0.29	-0.24	-0.55	F036	0.05	0.29	-0.23	-0.55
F005	0.05	0.30	-0.25	-0.54	F037	0.05	0.29	-0.23	-0.55
F006	0.05	0.27	-0.21	-0.58	F039	0.05	0.27	-0.20	-0.58
F007	0.05	0.29	-0.24	-0.55	F040	0.05	0.28	-0.22	-0.57
F008	0.05	0.29	-0.24	-0.55	F074	0.05	0.28	-0.23	-0.56
F009	0.05	0.22	-0.15	-0.55	F077	0.05	0.30	-0.25	-0.53
F010	0.05	0.29	-0.24	-0.55	F078	0.05	0.26	-0.20	-0.58
F012	0.05	0.29	-0.24	-0.55	HALY	0.03	0.14	-0.10	-0.37
F013	0.05	0.26	-0.20	-0.58	NAMA	0.05	0.23	-0.16	-0.60
F016	0.05	0.28	-0.22	-0.57	SOLA	0.05	0.24	-0.16	-0.63
F019	0.05	0.28	-0.23	-0.56	Mean	0.05	0.26	-0.20	-0.56
F020	0.05	0.22	-0.15	-0.55	S.dev	0.00	0.03	0.04	0.04
F024	0.05	0.26	-0.19	-0.58	RMS	0.05	0.27	0.21	0.56
F026	0.05	0.30	-0.25	-0.54					
F027	0.05	0.26	-0.20	-0.59					
F029	0.05	0.25	-0.19	-0.58					
F030	0.05	0.29	-0.23	-0.55					

ΔU_N : Uncertainty in northing (mm/yr)

ΔU_E : Uncertainty in easting (mm/yr)

Table F.4: The difference of Velocity uncertainties for episodic campaigns stations when *Zhang et al.* [1997] or *Mao et al.* [1999] equations with the average amplitudes of the white and flicker noise for the regional network taken from this study when applying three and Geirsson *et al.*, [2006] and between when using six stations for regional network from this study and the global model taken from Willams et al., [2004].

	2a3- 1		2a6- 1			2a3- 1		2a6- 1	
Stations	ΔU_N	ΔU_E	ΔU_N	ΔU_E	Stations	ΔU_N	ΔU_E	ΔU_N	ΔU_E
	mm/yr	mm/yr	mm/yr	mm/yr		mm/yr	mm/yr	mm/yr	mm/yr
DATM	-0.06	1.30	-0.23	-0.84	F033	0.01	1.07	-0.24	-0.84
F001	-0.18	0.86	-0.20	-0.77	F035	-0.02	0.92	-0.19	-0.76
F002	-0.20	2.05	-0.28	-0.84	F036	0.22	1.65	-0.28	-0.83
F005	0.26	1.56	-0.30	-0.84	F037	0.30	1.65	-0.28	-0.83
F006	0.31	1.51	-0.26	-0.85	F039	0.24	1.30	-0.25	-0.85
F007	0.28	1.78	-0.29	-0.84	F040	0.27	1.82	-0.27	-0.85
F008	0.50	1.85	-0.29	-0.84	F074	-0.42	1.44	-0.28	-0.84
F009	-0.05	0.93	-0.20	-0.77	F077	0.14	1.81	-0.30	-0.83
F010	0.50	2.02	-0.29	-0.85	F078	-0.02	1.46	-0.25	-0.84
F012	0.32	1.32	-0.29	-0.84	HALY	-0.17	0.63	-0.13	-0.51
F013	0.01	1.49	-0.25	-0.84	NAMA	-0.32	1.02	-0.21	-0.84
F016	-0.07	1.66	-0.27	-0.84	SOLA	-0.22	1.05	-0.22	-0.87
F019	0.24	1.84	-0.28	-0.84	Mean	0.09	1.43	-0.25	-0.82
F020	-0.12	0.86	-0.20	-0.77	S.dev	0.24	0.39	0.04	0.06
F024	0.10	1.23	-0.24	-0.84	RMS	0.25	1.48	0.25	0.82
F026	0.35	2.10	-0.30	-0.84					
F027	0.34	1.54	-0.25	-0.85					
F029	0.07	1.27	-0.24	-0.84					
F030	0.17	1.45	-0.28	-0.84					

ΔU_N : Uncertainty in northing (mm/yr)

ΔU_E : Uncertainty in easting (mm/yr)

Table F.5: The difference of Velocity uncertainties for episodic campaigns stations when *Zhang et al.* [1997] or *Mao et al.* [1999] equations with the average amplitudes of the white and flicker noise for the regional network taken from this study when applying six stations and the global model taken from Willams et al., [2004] and Geirsson *et al.*, [2006].

	2a6- 1		2b- 1			2a6- 1		2b- 1	
Stations	ΔU_N	ΔU_E	ΔU_N	ΔU_E	Stations	ΔU_N	ΔU_E	ΔU_N	ΔU_E
	mm/yr	mm/yr	mm/yr	mm/yr		mm/yr	mm/yr	mm/yr	mm/yr
DATM	-0.11	1.05	0.13	1.88	F033	-0.03	0.82	0.20	1.65
F001	-0.23	0.64	-0.03	1.42	F035	-0.06	0.70	0.13	1.46
F002	-0.25	1.76	0.04	2.60	F036	0.17	1.36	0.45	2.20
F005	0.21	1.26	0.51	2.09	F037	0.25	1.36	0.53	2.20
F006	0.26	1.24	0.52	2.09	F039	0.19	1.03	0.44	1.88
F007	0.23	1.49	0.52	2.33	F040	0.22	1.54	0.49	2.39
F008	0.45	1.56	0.74	2.40	F074	-0.47	1.15	-0.20	2.00
F009	-0.10	0.71	0.10	1.47	F077	0.09	1.51	0.39	2.34
F010	0.45	1.73	0.74	2.58	F078	-0.07	1.20	0.18	2.04
F012	0.27	1.03	0.55	1.87	HALY	-0.20	0.48	-0.08	1.00
F013	-0.04	1.22	0.21	2.06	NAMA	-0.37	0.78	-0.16	1.62
F016	-0.12	1.39	0.15	2.23	SOLA	-0.28	0.81	-0.06	1.68
F019	0.19	1.56	0.46	2.40	Mean	0.04	1.17	0.29	1.99
F020	-0.16	0.65	0.04	1.42	S.dev	0.24	0.36	0.26	0.39
F024	0.06	0.97	0.30	1.81	RMS	0.24	1.22	0.39	2.03
F026	0.30	1.80	0.60	2.63					
F027	0.29	1.27	0.54	2.12					
F029	0.02	1.02	0.25	1.86					
F030	0.12	1.16	0.40	1.99					

ΔU_N : Uncertainty in northing (mm/yr)

ΔU_E : Uncertainty in easting (mm/yr)

Table G.1: Absolute station model velocities from this study

Stations	V_N	V_E	V_V	A_Z	Stations	V_N	V_E	V_V	A_Z
	mm/yr	mm/yr	mm/yr	°		mm/yr	mm/yr	mm/yr	°
BAHR	30.86	31.49	44.09	45.58	F031	27.22	33.77	43.37	51.13
DATM	29.46	36.86	47.19	51.37	F033	27.93	33.11	43.32	49.85
F001	27.50	36.31	45.55	52.86	F035	30.25	32.77	44.60	47.29
F002	26.97	34.92	44.12	52.32	F036	30.91	32.97	45.20	46.85
F005	25.75	31.02	40.31	50.31	F037	30.06	31.69	43.68	46.52
F006	25.01	29.54	38.70	49.75	F039	28.73	30.02	41.55	46.26
F007	24.51	28.17	37.34	48.98	F040	28.82	28.62	40.61	44.80
F008	23.99	26.82	35.98	48.19	F041	27.45	29.95	40.62	47.49
F009	23.81	25.67	35.01	47.16	F045	25.09	24.44	35.02	44.25
F010	24.43	26.03	35.70	46.81	F074	27.23	36.24	45.33	53.08
F012	26.21	30.37	40.12	49.21	F077	28.66	33.31	43.94	49.29
F013	27.69	31.46	41.91	48.64	F078	29.10	36.45	46.64	51.40
F016	27.53	35.38	44.83	52.11	HALY	24.40	26.02	35.67	46.84
F019	29.18	33.60	44.50	49.03	NAMA	27.28	34.68	44.12	51.81
F020	29.29	31.64	43.12	47.20	P049	30.06	33.89	45.30	48.42
F024	27.15	28.38	39.28	46.27	SOLA	29.18	31.46	42.91	47.16
F026	28.09	27.54	39.34	44.44	YIBL	32.82	35.34	48.23	47.12
F027	26.65	25.45	36.85	43.68					
F029	29.95	29.49	42.03	44.56					
F030	30.60	31.01	43.56	45.38					

V_N : velocity in northing (mm/yr)

V_E : velocity in easting (mm/yr)

V_V : vector velocity (mm/yr)

A_Z : azimuth in degree

Table G.2: Absolute station model velocities from *Almotairi.* [2006]

Stations	V_N	V_E	V_V	A_Z	Stations	V_N	V_E	V_V	A_Z
	mm/yr	mm/yr	mm/yr	°		mm/yr	mm/yr	mm/yr	°
BAHR	29.79	29.27	41.76	44.49	F031	26.24	31.45	40.96	50.16
DATM	28.43	34.43	44.65	50.45	F033	26.94	30.81	40.93	48.84
F001	26.51	33.89	43.03	51.96	F035	29.20	30.50	42.22	46.24
F002	26.00	32.55	41.66	51.39	F036	29.85	30.69	42.81	45.80
F005	24.80	28.80	38.01	49.27	F037	29.01	29.46	41.34	45.44
F006	24.09	27.38	36.47	48.66	F039	27.71	27.85	39.29	45.14
F007	23.60	26.07	35.17	47.85	F040	27.80	26.51	38.41	43.63
F008	23.09	24.77	33.87	47.01	F041	26.47	27.78	38.37	46.38
F009	22.92	23.68	32.95	45.93	F045	24.16	22.49	33.01	42.95
F010	23.52	24.02	33.62	45.59	F074	26.25	33.82	42.81	52.18
F012	25.26	28.18	37.85	48.13	F077	27.65	31.01	41.54	48.28
F013	26.70	29.23	39.59	47.59	F078	28.08	34.03	44.12	50.48
F016	26.54	33.00	42.35	51.19	HALY	23.49	24.01	33.59	45.62
F019	28.15	31.29	42.09	48.02	NAMA	26.30	32.32	41.67	50.86
F020	28.27	29.41	40.79	46.13	P049	29.01	31.56	42.87	47.41
F024	26.18	26.28	37.09	45.11	SOLA	28.15	29.23	40.58	46.08
F026	27.09	25.48	37.19	43.24	YIBL	31.71	32.97	45.74	46.12
F027	25.69	23.47	34.80	42.42					
F029	28.90	27.34	39.79	43.41					
F030	29.54	28.81	41.26	44.28					

V_N : velocity in northing (mm/yr)

V_E : velocity in easting (mm/yr)

V_V : vector velocity (mm/yr)

A_Z : azimuth in degree

Table G.3: Absolute station model velocities from *Altamimi et al.* [2007]

Stations	V_N	V_E	V_V	A_Z	Stations	V_N	V_E	V_V	A_Z
	mm/yr	mm/yr	mm/yr	°		mm/yr	mm/yr	mm/yr	°
BAHR	29.77	31.26	43.17	46.40	F031	25.03	34.43	42.57	53.98
DATM	27.93	37.94	47.11	53.65	F033	25.95	33.57	42.43	52.30
F001	25.39	37.45	45.25	55.86	F035	28.97	32.89	43.83	48.63
F002	24.72	35.83	43.53	55.40	F036	29.85	33.04	44.53	47.91
F005	23.18	31.32	38.97	53.50	F037	28.71	31.62	42.71	47.76
F006	22.26	29.66	37.09	53.11	F039	26.98	29.80	40.19	47.85
F007	21.64	28.12	35.48	52.42	F040	27.09	28.12	39.05	46.07
F008	21.00	26.60	33.89	51.71	F041	25.33	29.87	39.16	49.70
F009	20.78	25.29	32.73	50.60	F045	22.36	23.71	32.59	46.68
F010	21.54	25.63	33.48	49.95	F074	25.05	37.39	45.00	56.18
F012	23.76	30.51	38.67	52.09	F077	26.89	33.73	43.14	51.44
F013	25.64	31.63	40.72	50.97	F078	27.45	37.48	46.46	53.78
F016	25.43	36.33	44.35	55.01	HALY	21.51	25.63	33.45	49.99
F019	27.56	34.02	43.78	50.99	NAMA	25.11	35.51	43.49	54.73
F020	27.71	31.65	42.07	48.80	P049	28.71	34.26	44.70	50.04
F024	24.96	28.06	37.55	48.35	SOLA	27.56	31.46	41.82	48.78
F026	26.15	26.95	37.56	45.86	YIBL	32.45	35.65	48.21	47.70
F027	24.32	24.69	34.66	45.43					
F029	28.57	29.00	40.70	45.43					
F030	29.43	30.72	42.54	46.23					

V_N : velocity in northing (mm/yr)

V_E : velocity in easting (mm/yr)

V_V : vector velocity (mm/yr)

A_Z : azimuth in degree

Table G.4: Absolute station model velocities from APKIM2000 [*Drewes and Angermann*, 2001]

Stations	V_N	V_E	V_V	A_Z	Stations	V_N	V_E	V_V	A_Z
	mm/yr	mm/yr	mm/yr	°		mm/yr	mm/yr	mm/yr	°
BAHR	27.80	29.60	40.61	46.80	F031	25.06	31.30	40.09	51.32
DATM	26.76	33.89	43.18	51.70	F033	25.60	30.79	40.04	50.25
F001	25.27	33.37	41.86	52.86	F035	27.35	30.62	41.05	48.22
F002	24.87	32.23	40.70	52.34	F036	27.84	30.81	41.53	47.90
F005	23.92	28.99	37.58	50.47	F037	27.20	29.73	40.29	47.54
F006	23.35	27.74	36.26	49.91	F039	26.21	28.29	38.57	47.19
F007	22.96	26.58	35.13	49.18	F040	26.28	27.14	37.78	45.93
F008	22.55	25.44	33.99	48.44	F041	25.23	28.17	37.82	48.15
F009	22.41	24.48	33.19	47.52	F045	23.41	23.50	33.17	45.11
F010	22.90	24.80	33.75	47.28	F074	25.07	33.30	41.68	53.03
F012	24.28	28.47	37.42	49.54	F077	26.16	30.98	40.55	49.82
F013	25.42	29.43	38.89	49.18	F078	26.49	33.55	42.74	51.70
F016	25.30	32.62	41.28	52.21	HALY	22.88	24.79	33.73	47.30
F019	26.55	31.24	40.99	49.64	NAMA	25.11	32.04	40.71	51.92
F020	26.63	29.65	39.85	48.06	P049	27.21	31.51	41.63	49.19
F024	25.01	26.87	36.71	47.05	SOLA	26.55	29.49	39.68	48.01
F026	25.72	26.22	36.73	45.55	YIBL	29.22	32.83	43.95	48.33
F027	24.62	24.42	34.68	44.76					
F029	27.12	27.91	38.92	45.82					
F030	27.61	29.19	40.18	46.60					

V_N : velocity in northing (mm/yr)

V_E : velocity in easting (mm/yr)

V_V : vector velocity (mm/yr)

A_Z : azimuth in degree

Table G.5: Absolute station model velocities from APKIM2005 [*Drewes*, 2006]

Stations	V_N	V_E	V_V	A_Z	Stations	V_N	V_E	V_V	A_Z
	mm/yr	mm/yr	mm/yr	°		mm/yr	mm/yr	mm/yr	°
BAHR	30.87	32.08	44.52	46.10	F031	25.99	35.33	43.86	53.66
DATM	28.97	38.94	48.54	53.35	F033	26.93	34.44	43.72	51.97
F001	26.36	38.43	46.60	55.55	F035	30.04	33.75	45.19	48.33
F002	25.67	36.76	44.84	55.07	F036	30.95	33.91	45.91	47.62
F005	24.08	32.12	40.15	53.14	F037	29.78	32.44	44.04	47.46
F006	23.14	30.41	38.21	52.73	F039	27.99	30.57	41.45	47.52
F007	22.50	28.82	36.56	52.02	F040	28.11	28.84	40.28	45.73
F008	21.84	27.26	34.92	51.30	F041	26.30	30.63	40.37	49.35
F009	21.61	25.91	33.74	50.18	F045	23.24	24.29	33.62	46.26
F010	22.40	26.26	34.52	49.54	F074	26.01	38.36	46.35	55.86
F012	24.68	31.29	39.86	51.73	F077	27.90	34.61	44.46	51.12
F013	26.62	32.45	41.97	50.64	F078	28.49	38.47	47.86	53.48
F016	26.40	37.28	45.69	54.70	HALY	22.36	26.26	34.49	49.58
F019	28.59	34.91	45.12	50.68	NAMA	26.07	36.43	44.80	54.41
F020	28.75	32.48	43.37	48.49	P049	29.78	35.16	46.08	49.74
F024	25.91	28.77	38.72	47.99	SOLA	28.59	32.27	43.12	48.46
F026	27.15	27.64	38.74	45.51	YIBL	33.62	36.61	49.70	47.44
F027	25.26	25.31	35.76	45.05					
F029	29.63	29.75	41.98	45.11					
F030	30.52	31.52	43.88	45.93					

V_N : velocity in northing (mm/yr)

V_E : velocity in easting (mm/yr)

V_V : vector velocity (mm/yr)

A_Z : azimuth in degree

TableG.6: Absolute station model velocities from CGPS2004 [*Prawirodirdjo and Bock*, 2004]

Stations	V_N	V_E	V_V	A_Z	Stations	V_N	V_E	V_V	A_Z
	mm/yr	mm/yr	mm/yr	°		mm/yr	mm/yr	mm/yr	°
BAHR	27.76	31.25	41.80	48.38	F031	23.55	34.14	41.48	55.40
DATM	26.13	37.37	45.60	55.04	F033	24.37	33.35	41.31	53.85
F001	23.87	36.91	43.96	57.10	F035	27.05	32.75	42.47	50.44
F002	23.27	35.42	42.38	56.69	F036	27.83	32.89	43.09	49.77
F005	21.90	31.27	38.17	55.00	F037	26.82	31.57	41.43	49.65
F006	21.08	29.73	36.44	54.67	F039	25.28	29.88	39.14	49.77
F007	20.52	28.30	34.96	54.06	F040	25.39	28.34	38.05	48.14
F008	19.95	26.89	33.48	53.44	F041	23.82	29.94	38.26	51.50
F009	19.75	25.68	32.40	52.44	F045	21.16	24.23	32.17	48.86
F010	20.43	26.00	33.07	51.84	F074	23.57	36.85	43.74	57.40
F012	22.42	30.53	37.87	53.71	F077	25.20	33.51	41.93	53.05
F013	24.09	31.57	39.71	52.65	F078	25.71	36.95	45.01	55.17
F016	23.91	35.89	43.12	56.33	HALY	20.40	26.00	33.04	51.88
F019	25.80	33.78	42.50	52.63	NAMA	23.62	35.13	42.33	56.08
F020	25.93	31.60	40.88	50.63	P049	26.82	34.00	43.31	51.73
F024	23.48	28.27	36.75	50.28	SOLA	25.80	31.42	40.65	50.61
F026	24.55	27.25	36.68	47.98	YIBL	30.12	35.30	46.41	49.53
F027	22.92	25.15	34.02	47.66					
F029	26.69	29.15	39.53	47.52					
F030	27.46	30.75	41.23	48.23					

V_N : velocity in northing (mm/yr)

V_E : velocity in easting (mm/yr)

V_V : vector velocity (mm/yr)

A_Z : azimuth in degree

Table G.7: Absolute station model velocities from NNR-NUVEL-1A [*DeMets et al.*, 1994]

Stations	V_N	V_E	V_V	A_Z	Stations	V_N	V_E	V_V	A_Z
	mm/yr	mm/yr	mm/yr	°		mm/yr	mm/yr	mm/yr	°
BAHR	35.11	27.96	44.88	38.54	F031	31.02	30.17	43.27	44.20
DATM	33.54	33.50	47.40	44.96	F033	31.82	29.50	43.39	42.83
F001	31.34	32.86	45.40	46.36	F035	34.43	29.25	45.18	40.35
F002	30.74	31.37	43.92	45.58	F036	35.17	29.50	45.90	39.99
F005	29.37	27.23	40.05	42.84	F037	34.21	28.12	44.28	39.43
F006	28.54	25.66	38.38	41.96	F039	32.72	26.32	41.99	38.81
F007	27.97	24.21	37.00	40.87	F040	32.82	24.87	41.18	37.16
F008	27.39	22.78	35.62	39.75	F041	31.28	26.18	40.79	39.92
F009	27.19	21.58	34.71	38.44	F045	28.63	20.36	35.13	35.42
F010	27.89	21.97	35.50	38.24	F074	31.04	32.77	45.14	46.56
F012	29.89	26.57	39.99	41.64	F077	32.64	29.74	44.16	42.33
F013	31.56	27.76	42.03	41.34	F078	33.14	33.05	46.80	44.93
F016	31.37	31.88	44.73	45.46	HALY	27.85	21.96	35.47	38.26
F019	33.22	30.06	44.80	42.14	NAMA	31.09	31.12	43.99	45.03
F020	33.35	28.03	43.56	40.04	P049	34.21	30.40	45.77	41.62
F024	30.95	24.54	39.50	38.41	SOLA	33.22	27.83	43.34	39.96
F026	32.00	23.72	39.84	36.55	YIBL	37.30	32.07	49.19	40.69
F027	30.39	21.49	37.21	35.26					
F029	34.08	25.84	42.77	37.17					
F030	34.82	27.45	44.34	38.25					

V_N : velocity in northing (mm/yr)

V_E : velocity in easting (mm/yr)

V_V : vector velocity (mm/yr)

A_Z : azimuth in degree

Table G.8: Absolute station model velocities from GSRM v1.2 [*Kreemer et al.*, 2003]

Stations	V_N	V_E	V_V	A_Z	Stations	V_N	V_E	V_V	A_Z
	mm/yr	mm/yr	mm/yr	°		mm/yr	mm/yr	mm/yr	°
BAHR	31.14	32.28	44.85	46.03	F031	27.29	34.74	44.18	51.84
DATM	29.66	37.94	48.16	51.98	F033	28.05	34.03	44.10	50.51
F001	27.59	37.39	46.46	53.57	F035	30.50	33.64	45.41	47.80
F002	27.03	35.94	44.97	53.05	F036	31.20	33.84	46.02	47.32
F005	25.75	31.89	40.98	51.08	F037	30.29	32.51	44.44	47.03
F006	24.97	30.36	39.31	50.56	F039	28.89	30.79	42.22	46.83
F007	24.45	28.94	37.89	49.81	F040	28.98	29.32	41.23	45.33
F008	23.90	27.54	36.47	49.04	F041	27.54	30.74	41.27	48.14
F009	23.71	26.35	35.45	48.01	F045	25.06	25.04	35.42	44.98
F010	24.37	26.71	36.15	47.63	F074	27.31	37.31	46.24	53.80
F012	26.23	31.21	40.77	49.95	F077	28.82	34.23	44.75	49.91
F013	27.79	32.31	42.62	49.30	F078	29.28	37.52	47.59	52.03
F016	27.62	36.42	45.71	52.82	HALY	24.33	26.70	36.13	47.65
F019	29.36	34.52	45.32	49.62	NAMA	27.36	35.68	44.96	52.52
F020	29.48	32.47	43.86	47.76	P049	30.29	34.81	46.15	48.97
F024	27.23	29.11	39.86	46.91	SOLA	29.36	32.29	43.64	47.72
F026	28.21	28.22	39.90	45.00	YIBL	33.23	36.28	49.20	47.51
F027	26.70	26.07	37.31	44.31					
F029	30.17	30.20	42.69	45.03					
F030	30.87	31.78	44.31	45.84					

V_N : velocity in northing (mm/yr)

V_E : velocity in easting (mm/yr)

V_V : vector velocity (mm/yr)

A_Z : azimuth in degree

Table G.9: Absolute station model velocities from GSRM-NNR-2 [Kreemer, et al., 2006]

Stations	V_N	V_E	V_V	A_Z	Stations	V_N	V_E	V_V	A_Z
	mm/yr	mm/yr	mm/yr	°		mm/yr	mm/yr	mm/yr	°
BAHR	29.63	33.71	44.88	48.68	F031	25.91	36.22	44.53	54.42
DATM	28.20	39.35	48.42	54.37	F033	26.64	35.51	44.39	53.12
F001	26.20	38.83	46.84	55.99	F035	29.01	35.07	45.52	50.40
F002	25.66	37.41	45.37	55.55	F036	29.69	35.25	46.09	49.90
F005	24.42	33.42	41.39	53.84	F037	28.81	33.96	44.53	49.69
F006	23.68	31.92	39.74	53.43	F039	27.45	32.28	42.37	49.62
F007	23.17	30.52	38.32	52.80	F040	27.55	30.81	41.33	48.20
F008	22.64	29.14	36.90	52.15	F041	26.15	32.25	41.52	50.96
F009	22.46	27.97	35.87	51.23	F045	23.76	26.64	35.69	48.28
F010	23.09	28.31	36.53	50.80	F074	25.93	38.76	46.63	56.22
F012	24.89	32.74	41.13	52.75	F077	27.39	35.69	44.99	52.50
F013	26.40	33.81	42.90	52.02	F078	27.83	38.94	47.86	54.44
F016	26.23	37.88	46.07	55.30	HALY	23.06	28.30	36.51	50.83
F019	27.91	35.98	45.53	52.19	NAMA	25.98	37.15	45.33	55.04
F020	28.03	33.93	44.01	50.44	P049	28.81	36.24	46.30	51.51
F024	25.85	30.64	40.09	49.85	SOLA	27.91	33.75	43.80	50.41
F026	26.80	29.73	40.03	47.96	YIBL	31.66	37.63	49.18	49.93
F027	25.34	27.63	37.49	47.47					
F029	28.70	31.66	42.73	47.81					
F030	29.37	33.22	44.34	48.52					

V_N : velocity in northing (mm/yr)

V_E : velocity in easting (mm/yr)

V_V : vector velocity (mm/yr)

A_Z : azimuth in degree

Table G.10: Absolute station model velocities from PB2002 [*Bird et al.*, 2003]

Stations	V_N	V_E	V_V	A_Z	Stations	V_N	V_E	V_V	A_Z
	mm/yr	mm/yr	mm/yr	°		mm/yr	mm/yr	mm/yr	°
BAHR	37.88	32.22	49.73	40.39	F031	33.72	34.50	48.24	45.66
DATM	36.30	38.04	52.58	46.34	F033	34.54	33.80	48.33	44.38
F001	34.05	37.34	50.53	47.64	F035	37.19	33.58	50.11	42.07
F002	33.44	35.77	48.96	46.93	F036	37.95	33.85	50.85	41.73
F005	32.02	31.38	44.83	44.42	F037	36.97	32.38	49.15	41.21
F006	31.17	29.70	43.05	43.61	F039	35.46	30.45	46.74	40.66
F007	30.59	28.16	41.58	42.63	F040	35.56	28.92	45.83	39.12
F008	29.99	26.62	40.10	41.60	F041	33.99	30.28	45.52	41.70
F009	29.78	25.35	39.10	40.40	F045	31.26	24.06	39.45	37.58
F010	30.50	25.77	39.93	40.20	F074	33.74	37.25	50.26	47.83
F012	32.56	30.69	44.74	43.30	F077	35.38	34.07	49.12	43.92
F013	34.27	31.97	46.86	43.01	F078	35.88	37.57	51.95	46.31
F016	34.08	36.31	49.80	46.81	HALY	30.47	25.76	39.90	40.22
F019	35.97	34.42	49.78	43.73	NAMA	33.79	35.51	49.02	46.42
F020	36.10	32.27	48.42	41.79	P049	36.98	34.79	50.77	43.25
F024	33.65	28.54	44.12	40.30	SOLA	35.97	32.06	48.18	41.71
F026	34.72	27.68	44.41	38.56	YIBL	40.09	36.59	54.28	42.38
F027	33.07	25.28	41.63	37.40					
F029	36.85	29.96	47.49	39.11					
F030	37.59	31.68	49.16	40.12					

V_N : velocity in northing (mm/yr)

V_E : velocity in easting (mm/yr)

V_V : vector velocity (mm/yr)

A_Z : azimuth in degree

Table G11: Absolute station model velocities from REVEL-2000 [*Sella et al.*, 2002]

Stations	V_N	V_E	V_V	A_Z	Stations	V_N	V_E	V_V	A_Z
	mm/yr	mm/yr	mm/yr	°		mm/yr	mm/yr	mm/yr	°
BAHR	26.71	30.06	40.22	48.38	F031	22.75	32.78	39.90	55.24
DATM	25.17	35.85	43.80	54.92	F033	23.52	32.03	39.74	53.72
F001	23.05	35.40	42.24	56.93	F035	26.04	31.48	40.85	50.40
F002	22.48	33.99	40.75	56.51	F036	26.77	31.62	41.43	49.74
F005	21.19	30.04	36.76	54.81	F037	25.82	30.36	39.86	49.62
F006	20.41	28.58	35.12	54.46	F039	24.38	28.75	37.70	49.71
F007	19.89	27.22	33.71	53.85	F040	24.48	27.29	36.65	48.11
F008	19.34	25.88	32.31	53.22	F041	23.00	28.80	36.85	51.39
F009	19.16	24.73	31.28	52.24	F045	20.50	23.36	31.07	48.73
F010	19.81	25.04	31.92	51.65	F074	22.76	35.34	42.04	57.21
F012	21.68	29.34	36.48	53.54	F077	24.30	32.18	40.33	52.94
F013	23.26	30.34	38.23	52.53	F078	24.78	35.44	43.24	55.04
F016	23.08	34.43	41.45	56.16	HALY	19.77	25.03	31.90	51.69
F019	24.86	32.44	40.87	52.53	NAMA	22.81	33.71	40.71	55.91
F020	24.99	30.38	39.34	50.56	P049	25.83	32.66	41.64	51.67
F024	22.68	27.21	35.42	50.18	SOLA	24.86	30.21	39.12	50.55
F026	23.69	26.25	35.36	47.94	YIBL	28.92	33.91	44.57	49.54
F027	22.15	24.24	32.84	47.58					
F029	25.71	28.07	38.06	47.51					
F030	26.43	29.59	39.67	48.23					

V_N : velocity in northing (mm/yr)

V_E : velocity in easting (mm/yr)

V_V : vector velocity (mm/yr)

A_Z : azimuth in degree

TableG.12: Absolute station velocities from *Vigny et al.* [2006]

Stations	V_N	V_E	V_V	A_Z	Stations	V_N	V_E	V_V	A_Z
	mm/yr	mm/yr	mm/yr	°		mm/yr	mm/yr	mm/yr	°
BAHR	28.54	31.11	42.21	47.46	F031	26.34	32.42	41.76	50.91
DATM	27.73	34.84	44.52	51.49	F033	26.79	31.99	41.72	50.06
F001	26.51	34.29	43.34	52.28	F035	28.19	31.97	42.63	48.60
F002	26.18	33.24	42.31	51.78	F036	28.57	32.19	43.04	48.41
F005	25.39	30.24	39.49	49.99	F037	28.07	31.16	41.94	47.98
F006	24.90	29.06	38.27	49.41	F039	27.28	29.78	40.38	47.51
F007	24.57	27.98	37.23	48.71	F040	27.33	28.74	39.66	46.44
F008	24.22	26.89	36.19	47.99	F041	26.48	29.59	39.71	48.18
F009	24.10	25.99	35.44	47.16	F045	24.95	25.16	35.43	45.24
F010	24.52	26.32	35.97	47.03	F074	26.34	34.21	43.18	52.40
F012	25.69	29.80	39.34	49.24	F077	27.24	32.20	42.18	49.78
F013	26.64	30.75	40.68	49.10	F078	27.51	34.52	44.14	51.45
F016	26.54	33.62	42.83	51.72	HALY	24.50	26.31	35.95	47.04
F019	27.55	32.47	42.58	49.68	NAMA	26.38	33.09	42.31	51.44
F020	27.62	31.04	41.55	48.34	P049	28.08	32.76	43.15	49.40
F024	26.29	28.39	38.69	47.19	SOLA	27.55	30.90	41.40	48.28
F026	26.88	27.85	38.71	46.01	YIBL	29.61	34.12	45.18	49.04
F027	25.97	26.10	36.82	45.14					
F029	28.01	29.52	40.69	46.50					
F030	28.39	30.72	41.83	47.26					

V_N : velocity in northing (mm/yr)

V_E : velocity in easting (mm/yr)

V_V : vector velocity (mm/yr)

A_Z : azimuth in degree

Table G.13: The difference between the absolute station model velocities from this study and from *Almotairi.* [2006]

Stations	ΔV_N	ΔV_E	ΔV_V	ΔA_Z	Stations	ΔV_N	ΔV_E	ΔV_V	ΔA_Z
	mm/yr	mm/yr	mm/yr	°		mm/yr	mm/yr	mm/yr	°
BAHR	1.07	2.22	2.33	1.09	F031	0.98	2.32	2.41	0.97
DATM	1.03	2.44	2.54	0.92	F033	1.00	2.29	2.39	1.01
F001	0.99	2.42	2.52	0.90	F035	1.05	2.28	2.38	1.05
F002	0.97	2.37	2.46	0.93	F036	1.07	2.28	2.39	1.05
F005	0.94	2.22	2.30	1.04	F037	1.05	2.23	2.34	1.08
F006	0.92	2.16	2.23	1.09	F039	1.02	2.17	2.26	1.12
F007	0.91	2.10	2.17	1.13	F040	1.02	2.11	2.20	1.17
F008	0.89	2.05	2.11	1.18	F041	0.98	2.17	2.25	1.11
F009	0.89	2.00	2.06	1.23	F045	0.92	1.94	2.01	1.30
F010	0.91	2.01	2.08	1.22	F074	0.98	2.41	2.52	0.90
F012	0.95	2.19	2.27	1.08	F077	1.01	2.30	2.40	1.01
F013	0.99	2.23	2.32	1.05	F078	1.02	2.42	2.52	0.92
F016	0.99	2.38	2.48	0.92	HALY	0.91	2.01	2.08	1.22
F019	1.03	2.31	2.41	1.01	NAMA	0.98	2.36	2.45	0.95
F020	1.03	2.23	2.33	1.07	P049	1.05	2.32	2.43	1.01
F024	0.98	2.11	2.19	1.16	SOLA	1.03	2.23	2.33	1.08
F026	1.00	2.07	2.15	1.20	YIBL	1.11	2.37	2.49	1.00
F027	0.96	1.98	2.05	1.26	Mean	0.99	2.22	2.31	1.07
F029	1.04	2.14	2.24	1.15	S.dev	0.06	0.14	0.15	0.11
F030	1.06	2.20	2.30	1.10	RMS	0.99	2.22	2.31	1.08

ΔV_N : velocity in northing (mm/yr)

ΔV_E : velocity in easting (mm/yr)

ΔV_V : vector velocity (mm/yr)

ΔA_Z : azimuth in degree

Table G.14: The difference between the absolute station model velocities from this study and from *Altamimi et al.* [2007]

Stations	ΔV_N	ΔV_E	ΔV_V	ΔA_Z	Stations	ΔV_N	ΔV_E	ΔV_V	ΔA_Z
	mm/yr	mm/yr	mm/yr	°		mm/yr	mm/yr	mm/yr	°
BAHR	1.08	0.23	0.92	-0.82	F031	2.18	-0.66	0.80	-2.85
DATM	1.54	-1.08	0.08	-2.28	F033	1.99	-0.46	0.89	-2.45
F001	2.11	-1.14	0.30	-3.00	F035	1.29	-0.12	0.77	-1.34
F002	2.25	-0.91	0.59	-3.08	F036	1.07	-0.07	0.67	-1.06
F005	2.57	-0.30	1.34	-3.19	F037	1.35	0.07	0.97	-1.24
F006	2.75	-0.12	1.61	-3.36	F039	1.75	0.22	1.36	-1.59
F007	2.87	0.05	1.86	-3.44	F040	1.73	0.49	1.56	-1.27
F008	2.99	0.22	2.09	-3.52	F041	2.12	0.08	1.46	-2.21
F009	3.03	0.38	2.28	-3.44	F045	2.73	0.73	2.43	-2.43
F010	2.89	0.40	2.22	-3.14	F074	2.18	-1.15	0.33	-3.10
F012	2.45	-0.14	1.45	-2.88	F077	1.78	-0.42	0.80	-2.15
F013	2.05	-0.17	1.19	-2.33	F078	1.65	-1.03	0.18	-2.38
F016	2.10	-0.95	0.48	-2.90	HALY	2.89	0.39	2.22	-3.15
F019	1.62	-0.42	0.72	-1.96	NAMA	2.17	-0.83	0.63	-2.92
F020	1.59	-0.02	1.05	-1.60	P049	1.35	-0.38	0.60	-1.62
F024	2.20	0.32	1.73	-2.08	SOLA	1.62	0.00	1.09	-1.62
F026	1.94	0.59	1.78	-1.42	YIBL	0.37	-0.31	0.02	-0.58
F027	2.33	0.76	2.19	-1.75	Mean	1.98	-0.14	1.16	-2.21
F029	1.38	0.49	1.33	-0.87	S.dev	0.63	0.55	0.67	0.87
F030	1.17	0.29	1.02	-0.85	RMS	2.07	0.56	1.34	2.37

ΔV_N : velocity in northing (mm/yr)

ΔV_E : velocity in easting (mm/yr)

ΔV_V : vector velocity (mm/yr)

ΔA_Z : azimuth in degree

Table G.15: The difference between the absolute station model velocities from this study and from APKIM2000 [*Drewes and Angermann*, 2001]

Stations	ΔV_N	ΔV_E	ΔV_V	ΔA_Z	Stations	ΔV_N	ΔV_E	ΔV_V	ΔA_Z
	mm/yr	Mm/yr	mm/yr	°		mm/yr	mm/yr	mm/yr	°
BAHR	3.06	1.89	3.48	-1.22	F031	2.16	2.47	3.28	-0.19
DATM	2.70	2.97	4.01	-0.33	F033	2.33	2.32	3.28	-0.40
F001	2.23	2.94	3.69	0.00	F035	2.90	2.16	3.55	-0.93
F002	2.10	2.69	3.42	-0.02	F036	3.07	2.16	3.67	-1.05
F005	1.82	2.03	2.73	-0.16	F037	2.85	1.97	3.39	-1.02
F006	1.66	1.80	2.44	-0.16	F039	2.52	1.73	2.98	-0.93
F007	1.55	1.59	2.21	-0.20	F040	2.54	1.48	2.83	-1.13
F008	1.43	1.38	1.99	-0.25	F041	2.22	1.77	2.80	-0.66
F009	1.40	1.20	1.82	-0.36	F045	1.68	0.94	1.85	-0.86
F010	1.53	1.23	1.95	-0.47	F074	2.16	2.93	3.65	0.05
F012	1.93	1.90	2.70	-0.33	F077	2.50	2.33	3.39	-0.53
F013	2.27	2.03	3.02	-0.54	F078	2.61	2.91	3.90	-0.30
F016	2.23	2.76	3.55	-0.10	HALY	1.52	1.23	1.94	-0.46
F019	2.63	2.36	3.51	-0.61	NAMA	2.17	2.64	3.41	-0.11
F020	2.66	1.99	3.27	-0.86	P049	2.85	2.38	3.67	-0.77
F024	2.15	1.51	2.57	-0.78	SOLA	2.63	1.97	3.23	-0.85
F026	2.37	1.32	2.61	-1.11	YIBL	3.60	2.52	4.28	-1.21
F027	2.03	1.04	2.17	-1.08	Mean	2.32	2.00	3.05	-0.61
F029	2.83	1.57	3.11	-1.26	S.dev	0.53	0.57	0.66	0.41
F030	2.99	1.81	3.38	-1.22	RMS	2.38	2.08	3.12	0.73

ΔV_N : velocity in northing (mm/yr)

ΔV_E : velocity in easting (mm/yr)

ΔV_V : vector velocity (mm/yr)

ΔA_Z : azimuth in degree

Table G.16: The difference between the absolute station model velocities from this study and from APKIM2005 [*Drewes*, 2006]

Stations	ΔV_N	ΔV_E	ΔV_V	ΔA_Z	Stations	ΔV_N	ΔV_E	ΔV_V	ΔA_Z
	mm/yr	Mm/yr	mm/yr	°		mm/yr	mm/yr	mm/yr	°
BAHR	-0.01	-0.59	-0.43	-0.52	F031	1.22	-1.56	-0.49	-2.53
DATM	0.49	-2.08	-1.35	-1.98	F033	1.00	-1.33	-0.40	-2.12
F001	1.14	-2.12	-1.05	-2.69	F035	0.21	-0.98	-0.59	-1.04
F002	1.30	-1.84	-0.72	-2.75	F036	-0.03	-0.94	-0.71	-0.77
F005	1.66	-1.10	0.16	-2.83	F037	0.28	-0.75	-0.36	-0.94
F006	1.87	-0.87	0.49	-2.98	F039	0.74	-0.55	0.10	-1.26
F007	2.01	-0.65	0.78	-3.04	F040	0.71	-0.23	0.33	-0.93
F008	2.15	-0.44	1.06	-3.11	F041	1.15	-0.69	0.25	-1.86
F009	2.20	-0.24	1.27	-3.02	F045	1.85	0.15	1.40	-2.01
F010	2.03	-0.23	1.18	-2.73	F074	1.22	-2.13	-1.02	-2.78
F012	1.53	-0.92	0.26	-2.52	F077	0.76	-1.30	-0.52	-1.83
F013	1.07	-0.99	-0.06	-2.00	F078	0.62	-2.01	-1.22	-2.08
F016	1.13	-1.90	-0.86	-2.59	HALY	2.04	-0.24	1.18	-2.74
F019	0.59	-1.31	-0.62	-1.65	NAMA	1.21	-1.76	-0.68	-2.60
F020	0.55	-0.84	-0.25	-1.29	P049	0.28	-1.27	-0.78	-1.32
F024	1.24	-0.39	0.56	-1.72	SOLA	0.59	-0.81	-0.21	-1.30
F026	0.94	-0.09	0.60	-1.07	YIBL	-0.80	-1.26	-1.47	-0.32
F027	1.39	0.15	1.09	-1.37	Mean	0.99	-0.94	-0.09	-1.88
F029	0.32	-0.26	0.05	-0.55	S.dev	0.71	0.66	0.79	0.85
F030	0.08	-0.52	-0.32	-0.55	RMS	1.21	1.14	0.79	2.05

ΔV_N : velocity in northing (mm/yr)

ΔV_E : velocity in easting (mm/yr)

ΔV_V : vector velocity (mm/yr)

ΔA_Z : azimuth in degree

Table G.17: The difference between the absolute station model velocities from this study and from CGPS2004 [*Prawirodirdjo and Bock*, 2004]

Stations	ΔV_N	ΔV_E	ΔV_V	ΔA_Z	Stations	ΔV_N	ΔV_E	ΔV_V	ΔA_Z
	mm/yr	Mm/yr	mm/yr	°		mm/yr	mm/yr	mm/yr	°
BAHR	3.09	0.24	2.29	-2.80	F031	3.67	-0.37	1.89	-4.27
DATM	3.34	-0.51	1.59	-3.67	F033	3.57	-0.25	2.01	-4.00
F001	3.63	-0.60	1.59	-4.24	F035	3.20	0.03	2.13	-3.15
F002	3.70	-0.50	1.74	-4.37	F036	3.08	0.08	2.11	-2.92
F005	3.85	-0.25	2.14	-4.69	F037	3.24	0.12	2.25	-3.13
F006	3.93	-0.19	2.26	-4.92	F039	3.45	0.13	2.41	-3.51
F007	3.99	-0.13	2.38	-5.08	F040	3.43	0.28	2.56	-3.34
F008	4.04	-0.07	2.50	-5.25	F041	3.63	0.00	2.36	-4.01
F009	4.06	-0.01	2.61	-5.28	F045	3.92	0.21	2.85	-4.61
F010	4.00	0.03	2.63	-5.03	F074	3.66	-0.61	1.59	-4.32
F012	3.79	-0.15	2.25	-4.50	F077	3.46	-0.20	2.01	-3.76
F013	3.60	-0.11	2.20	-4.01	F078	3.39	-0.49	1.63	-3.77
F016	3.62	-0.50	1.71	-4.22	HALY	4.00	0.02	2.63	-5.04
F019	3.38	-0.18	2.00	-3.60	NAMA	3.66	-0.45	1.79	-4.27
F020	3.36	0.04	2.24	-3.43	P049	3.24	-0.12	1.99	-3.31
F024	3.67	0.11	2.53	-4.01	SOLA	3.38	0.04	2.26	-3.45
F026	3.54	0.29	2.66	-3.54	YIBL	2.69	0.04	1.82	-2.41
F027	3.73	0.31	2.83	-3.98	Mean	3.55	-0.085	2.20	-3.94
F029	3.25	0.33	2.50	-2.96	S.dev	0.32	0.28	0.36	0.75
F030	3.14	0.26	2.33	-2.85	RMS	3.57	0.28	2.23	4.01

ΔV_N : velocity in northing (mm/yr)

ΔV_E : velocity in easting (mm/yr)

ΔV_V : vector velocity (mm/yr)

ΔA_Z : azimuth in degree

Table G.18: The difference between the absolute station model velocities from this study and from NNR-NUVEL-1A [*DeMets et al.*, 1994]

Stations	ΔV_N	ΔV_E	ΔV_V	ΔA_Z	Stations	ΔV_N	ΔV_E	ΔV_V	ΔA_Z
	mm/yr	Mm/yr	mm/yr	°		mm/yr	mm/yr	mm/yr	°
BAHR	-4.25	3.53	-0.79	7.04	F031	-3.80	3.60	0.10	6.93
DATM	-4.08	3.37	-0.21	6.41	F033	-3.89	3.61	-0.07	7.02
F001	-3.84	3.45	0.15	6.50	F035	-4.18	3.52	-0.58	6.94
F002	-3.77	3.55	0.20	6.74	F036	-4.25	3.47	-0.70	6.86
F005	-3.62	3.79	0.26	7.47	F037	-4.15	3.57	-0.60	7.09
F006	-3.53	3.88	0.32	7.79	F039	-3.99	3.70	-0.44	7.45
F007	-3.47	3.96	0.34	8.11	F040	-4.00	3.74	-0.57	7.64
F008	-3.40	4.04	0.36	8.44	F041	-3.83	3.77	-0.17	7.57
F009	-3.38	4.09	0.30	8.72	F045	-3.54	4.08	-0.11	8.83
F010	-3.46	4.06	0.20	8.57	F074	-3.81	3.46	0.19	6.52
F012	-3.68	3.80	0.13	7.57	F077	-3.98	3.57	-0.22	6.96
F013	-3.86	3.69	-0.12	7.30	F078	-4.04	3.40	-0.16	6.47
F016	-3.84	3.51	0.10	6.65	HALY	-3.45	4.06	0.20	8.58
F019	-4.04	3.54	-0.30	6.89	NAMA	-3.81	3.55	0.13	6.78
F020	-4.06	3.61	-0.44	7.16	P049	-4.15	3.49	-0.47	6.80
F024	-3.80	3.84	-0.22	7.86	SOLA	-4.04	3.63	-0.43	7.20
F026	-3.91	3.82	-0.50	7.89	YIBL	-4.48	3.28	-0.96	6.43
F027	-3.73	3.97	-0.36	8.42	Mean	-3.88	3.68	-0.19	7.36
F029	-4.14	3.65	-0.74	7.39	S.dev	0.27	0.22	0.38	0.70
F030	-4.22	3.56	-0.78	7.13	RMS	3.89	3.69	0.42	7.39

ΔV_N : velocity in northing (mm/yr)

ΔV_E : velocity in easting (mm/yr)

ΔV_V : vector velocity (mm/yr)

ΔA_Z : azimuth in degree

Table G.19: The difference between the absolute station model velocities from this study and from GSRM v1.2 [*Kreemer et al.*, 2003]

Stations	ΔV_N	ΔV_E	ΔV_V	ΔA_Z	Stations	ΔV_N	ΔV_E	ΔV_V	ΔA_Z
	mm/yr	Mm/yr	mm/yr	°		mm/yr	mm/yr	mm/yr	°
BAHR	-0.28	-0.79	-0.76	-0.45	F031	-0.08	-0.97	-0.81	-0.71
DATM	-0.20	-1.08	-0.97	-0.61	F033	-0.11	-0.93	-0.78	-0.66
F001	-0.09	-1.08	-0.91	-0.71	F035	-0.25	-0.87	-0.81	-0.51
F002	-0.06	-1.02	-0.85	-0.73	F036	-0.29	-0.86	-0.82	-0.47
F005	0.00	-0.87	-0.67	-0.77	F037	-0.23	-0.82	-0.76	-0.51
F006	0.04	-0.82	-0.61	-0.81	F039	-0.16	-0.77	-0.67	-0.57
F007	0.06	-0.77	-0.55	-0.83	F040	-0.16	-0.70	-0.62	-0.53
F008	0.08	-0.72	-0.49	-0.85	F041	-0.09	-0.79	-0.65	-0.65
F009	0.09	-0.68	-0.44	-0.85	F045	0.03	-0.60	-0.40	-0.73
F010	0.06	-0.68	-0.45	-0.82	F074	-0.08	-1.08	-0.91	-0.72
F012	-0.02	-0.83	-0.65	-0.74	F077	-0.15	-0.92	-0.81	-0.62
F013	-0.10	-0.85	-0.71	-0.66	F078	-0.18	-1.06	-0.95	-0.63
F016	-0.09	-1.04	-0.88	-0.71	HALY	0.06	-0.68	-0.46	-0.81
F019	-0.18	-0.93	-0.82	-0.59	NAMA	-0.08	-1.01	-0.84	-0.71
F020	-0.19	-0.83	-0.74	-0.56	P049	-0.23	-0.92	-0.85	-0.55
F024	-0.07	-0.73	-0.58	-0.64	SOLA	-0.18	-0.83	-0.73	-0.56
F026	-0.12	-0.67	-0.56	-0.56	YIBL	-0.41	-0.93	-0.97	-0.39
F027	-0.05	-0.61	-0.46	-0.63	Mean	-0.11	-0.84	-0.71	-0.64
F029	-0.23	-0.72	-0.66	-0.47	S.dev	0.12	0.14	0.16	0.12
F030	-0.27	-0.77	-0.75	-0.46	RMS	0.17	0.86	0.73	0.65

ΔV_N : velocity in northing (mm/yr)

ΔV_E : velocity in easting (mm/yr)

ΔV_V : vector velocity (mm/yr)

ΔA_Z : azimuth in degree

Table G.20: The difference between the absolute station model velocities from this study and from GSRM-NNR-2 [Kreemer, et al., 2006]

Stations	ΔV_N	ΔV_E	ΔV_V	ΔA_Z	Stations	ΔV_N	ΔV_E	ΔV_V	ΔA_Z
	mm/yr	Mm/yr	mm/yr	°		mm/yr	mm/yr	mm/yr	°
BAHR	1.22	-2.22	-0.79	-3.10	F031	1.30	-2.45	-1.16	-3.29
DATM	1.26	-2.49	-1.23	-3.00	F033	1.29	-2.40	-1.07	-3.27
F001	1.30	-2.52	-1.29	-3.13	F035	1.24	-2.30	-0.92	-3.11
F002	1.31	-2.49	-1.25	-3.23	F036	1.22	-2.28	-0.89	-3.05
F005	1.32	-2.40	-1.08	-3.53	F037	1.25	-2.26	-0.85	-3.17
F006	1.33	-2.38	-1.04	-3.68	F039	1.28	-2.26	-0.82	-3.36
F007	1.34	-2.35	-0.98	-3.82	F040	1.27	-2.20	-0.72	-3.40
F008	1.34	-2.32	-0.92	-3.96	F041	1.30	-2.31	-0.90	-3.47
F009	1.34	-2.29	-0.86	-4.07	F045	1.33	-2.20	-0.67	-4.03
F010	1.34	-2.28	-0.83	-3.99	F074	1.30	-2.53	-1.30	-3.14
F012	1.32	-2.37	-1.01	-3.54	F077	1.28	-2.39	-1.05	-3.21
F013	1.30	-2.35	-0.99	-3.38	F078	1.27	-2.49	-1.22	-3.04
F016	1.30	-2.49	-1.24	-3.19	HALY	1.34	-2.28	-0.84	-3.99
F019	1.27	-2.38	-1.03	-3.16	NAMA	1.30	-2.48	-1.21	-3.23
F020	1.26	-2.30	-0.89	-3.24	P049	1.25	-2.36	-1.00	-3.09
F024	1.30	-2.26	-0.81	-3.58	SOLA	1.27	-2.29	-0.89	-3.25
F026	1.29	-2.19	-0.69	-3.52	YIBL	1.16	-2.29	-0.95	-2.81
F027	1.31	-2.17	-0.64	-3.79	Mean	1.29	-2.34	-0.96	-3.38
F029	1.25	-2.18	-0.70	-3.25	S.dev	0.04	0.11	0.19	0.33
F030	1.23	-2.21	-0.78	-3.14	RMS	1.29	2.34	0.98	3.40

ΔV_N : velocity in northing (mm/yr)

ΔV_E : velocity in easting (mm/yr)

ΔV_V : vector velocity (mm/yr)

ΔA_Z : azimuth in degree

Table G.21: The difference between the absolute station model velocities from this study and from PB2002 [*Bird et al.*, 2003]

Stations	ΔV_N	ΔV_E	ΔV_V	ΔA_Z	Stations	ΔV_N	ΔV_E	ΔV_V	ΔA_Z
	mm/yr	Mm/yr	mm/yr	°		mm/yr	mm/yr	mm/yr	°
BAHR	-7.02	-0.73	-5.64	5.19	F031	-6.50	-0.73	-4.87	5.47
DATM	-6.83	-1.17	-5.39	5.03	F033	-6.61	-0.70	-5.01	5.47
F001	-6.55	-1.03	-4.98	5.22	F035	-6.94	-0.81	-5.51	5.22
F002	-6.47	-0.85	-4.84	5.39	F036	-7.03	-0.87	-5.65	5.12
F005	-6.28	-0.36	-4.52	5.89	F037	-6.92	-0.69	-5.47	5.31
F006	-6.16	-0.16	-4.35	6.14	F039	-6.73	-0.43	-5.19	5.60
F007	-6.08	0.02	-4.24	6.35	F040	-6.74	-0.30	-5.22	5.68
F008	-6.00	0.19	-4.12	6.59	F041	-6.54	-0.34	-4.90	5.79
F009	-5.97	0.33	-4.09	6.76	F045	-6.17	0.38	-4.43	6.67
F010	-6.07	0.26	-4.23	6.61	F074	-6.51	-1.01	-4.93	5.25
F012	-6.35	-0.31	-4.62	5.91	F077	-6.72	-0.76	-5.18	5.37
F013	-6.58	-0.51	-4.95	5.63	F078	-6.78	-1.11	-5.31	5.09
F016	-6.55	-0.93	-4.97	5.30	HALY	-6.07	0.26	-4.23	6.62
F019	-6.79	-0.82	-5.28	5.30	NAMA	-6.51	-0.84	-4.90	5.39
F020	-6.81	-0.63	-5.30	5.41	P049	-6.92	-0.90	-5.47	5.17
F024	-6.49	-0.16	-4.84	5.97	SOLA	-6.79	-0.60	-5.27	5.45
F026	-6.63	-0.14	-5.07	5.88	YIBL	-7.27	-1.24	-6.05	4.74
F027	-6.42	0.17	-4.78	6.28	Mean	-6.59	-0.50	-5.00	5.65
F029	-6.90	-0.47	-5.46	5.45	S.dev	0.33	0.46	0.49	0.53
F030	-6.99	-0.67	-5.60	5.26	RMS	6.59	0.68	5.02	5.67

ΔV_N : velocity in northing (mm/yr)

ΔV_E : velocity in easting (mm/yr)

ΔV_V : vector velocity (mm/yr)

ΔA_Z : azimuth in degree

Table G.22: The difference between the absolute station model velocities from this study and from REVEL-2000 [*Sella et al.*, 2002]

Stations	ΔV_N	ΔV_E	ΔV_V	ΔA_Z	Stations	ΔV_N	ΔV_E	ΔV_V	ΔA_Z
	mm/yr	Mm/yr	mm/yr	°		mm/yr	mm/yr	mm/yr	°
BAHR	4.15	1.43	3.87	-2.80	F031	4.47	0.99	3.47	-4.11
DATM	4.29	1.01	3.39	-3.55	F033	4.42	1.07	3.58	-3.87
F001	4.45	0.91	3.31	-4.07	F035	4.21	1.30	3.75	-3.11
F002	4.48	0.93	3.37	-4.19	F036	4.14	1.36	3.77	-2.89
F005	4.56	0.98	3.55	-4.50	F037	4.23	1.33	3.82	-3.10
F006	4.60	0.96	3.58	-4.71	F039	4.35	1.27	3.85	-3.45
F007	4.62	0.95	3.63	-4.87	F040	4.34	1.33	3.96	-3.31
F008	4.64	0.94	3.67	-5.03	F041	4.45	1.15	3.77	-3.90
F009	4.65	0.94	3.73	-5.08	F045	4.59	1.08	3.95	-4.48
F010	4.62	0.99	3.78	-4.84	F074	4.47	0.90	3.29	-4.13
F012	4.53	1.03	3.64	-4.33	F077	4.36	1.13	3.61	-3.65
F013	4.43	1.12	3.68	-3.89	F078	4.32	1.01	3.40	-3.64
F016	4.45	0.95	3.38	-4.05	HALY	4.63	0.99	3.77	-4.85
F019	4.32	1.16	3.63	-3.50	NAMA	4.47	0.96	3.41	-4.10
F020	4.30	1.26	3.78	-3.36	P049	4.23	1.22	3.66	-3.25
F024	4.47	1.17	3.86	-3.91	SOLA	4.31	1.25	3.79	-3.39
F026	4.40	1.29	3.98	-3.50	YIBL	3.89	1.43	3.66	-2.42
F027	4.50	1.21	4.01	-3.90	Mean	4.40	1.13	3.68	-3.83
F029	4.24	1.42	3.97	-2.95	S.dev	0.17	0.17	0.20	0.68
F030	4.17	1.42	3.89	-2.85	RMS	4.40	1.14	3.69	3.88

ΔV_N : velocity in northing (mm/yr)

ΔV_E : velocity in easting (mm/yr)

ΔV_V : vector velocity (mm/yr)

ΔA_Z : azimuth in degree

Table G.23: The difference between the absolute station model velocities from this study and from *Vigny et al.* [2006]

Stations	ΔV_N	ΔV_E	ΔV_V	ΔA_Z	Stations	ΔV_N	ΔV_E	ΔV_V	ΔA_Z
	mm/yr	Mm/yr	mm/yr	°		mm/yr	mm/yr	mm/yr	°
BAHR	2.32	0.39	1.88	-1.88	F031	0.88	1.35	1.61	0.22
DATM	1.74	2.02	2.67	-0.12	F033	1.15	1.12	1.60	-0.21
F001	0.98	2.02	2.21	0.58	F035	2.06	0.80	1.97	-1.31
F002	0.79	1.68	1.81	0.54	F036	2.34	0.78	2.16	-1.56
F005	0.36	0.78	0.82	0.32	F037	1.98	0.53	1.74	-1.46
F006	0.11	0.48	0.43	0.34	F039	1.45	0.24	1.17	-1.25
F007	-0.06	0.20	0.11	0.27	F040	1.49	-0.12	0.95	-1.64
F008	-0.23	-0.07	-0.21	0.20	F041	0.97	0.35	0.91	-0.69
F009	-0.29	-0.31	-0.43	0.00	F045	0.14	-0.72	-0.41	-0.99
F010	-0.09	-0.29	-0.27	-0.22	F074	0.89	2.02	2.15	0.68
F012	0.52	0.57	0.78	-0.03	F077	1.42	1.10	1.76	-0.49
F013	1.06	0.71	1.23	-0.46	F078	1.59	1.94	2.50	-0.05
F016	0.99	1.76	2.00	0.39	HALY	-0.10	-0.29	-0.28	-0.20
F019	1.63	1.13	1.92	-0.65	NAMA	0.90	1.59	1.81	0.37
F020	1.67	0.60	1.57	-1.14	P049	1.98	1.12	2.15	-0.98
F024	0.86	0.00	0.59	-0.92	SOLA	1.63	0.56	1.51	-1.12
F026	1.21	-0.31	0.63	-1.57	YIBL	3.21	1.22	3.05	-1.92
F027	0.68	-0.65	0.03	-1.46	Mean	1.15	0.66	1.28	-0.60
F029	1.94	-0.03	1.34	-1.94	S.dev	0.83	0.79	0.93	0.83
F030	2.21	0.29	1.73	-1.88	RMS	1.41	1.02	1.57	1.02

ΔV_N : velocity in northing (mm/yr)

ΔV_E : velocity in easting (mm/yr)

ΔV_V : vector velocity (mm/yr)

ΔA_Z : azimuth in degree

Table H.1: Relative Arabian-Eurasian station model velocities from this study

Stations	V_N	V_E	V_V	A_Z	Stations	V_N	V_E	V_V	A_Z
	mm/yr	mm/yr	mm/yr	°		mm/yr	mm/yr	mm/yr	°
BAHR	22.19	4.53	22.65	11.54	F031	16.51	7.69	18.21	24.98
DATM	19.94	10.79	22.67	28.43	F033	17.58	6.84	18.87	21.27
F001	16.93	10.49	19.92	31.77	F035	21.20	6.03	22.04	15.88
F002	16.15	9.01	18.49	29.15	F036	22.28	6.11	23.10	15.35
F005	14.38	5.02	15.23	19.26	F037	20.88	4.91	21.45	13.23
F006	13.33	3.63	13.81	15.24	F039	18.80	3.42	19.11	10.31
F007	12.63	2.34	12.84	10.51	F040	18.95	1.96	19.05	5.92
F008	11.90	1.10	11.95	5.26	F041	16.87	3.59	17.24	12.02
F009	11.65	0.02	11.65	0.07	F045	13.44	-1.42	13.52	-6.04
F010	12.52	0.24	12.52	1.09	F074	16.53	10.45	19.56	32.28
F012	15.04	4.27	15.64	15.83	F077	18.70	6.93	19.94	20.33
F013	17.23	5.12	17.97	16.57	F078	19.37	10.38	21.97	28.18
F016	16.97	9.42	19.41	29.04	HALY	12.47	0.24	12.48	1.08
F019	19.49	7.15	20.76	20.13	NAMA	16.60	8.67	18.73	27.59
F020	19.68	5.01	20.30	14.27	P049	20.89	7.29	22.12	19.24
F024	16.43	2.05	16.56	7.12	SOLA	19.49	4.84	20.09	13.95
F026	17.83	1.03	17.86	3.30	YIBL	25.54	8.33	26.86	18.07
F027	15.70	-0.75	15.71	-2.73					
F029	20.71	2.63	20.88	7.22					
F030	21.77	4.07	22.14	10.60					

V_N : velocity in northing (mm/yr)

V_E : velocity in easting (mm/yr)

V_V : vector velocity (mm/yr)

A_Z : azimuth in degree

Table H.2: Relative Arabian-Eurasian station model velocities from CGPS2004 [*Prawirodirdjo and Bock*, 2004]

Stations	V_N	V_E	V_V	A_Z	Stations	V_N	V_E	V_V	A_Z
	mm/yr	mm/yr	mm/yr	°		mm/yr	mm/yr	mm/yr	°
BAHR	19.94	3.37	20.22	9.60	F031	13.91	6.89	15.52	26.35
DATM	17.54	10.04	20.21	29.80	F033	15.04	5.97	16.19	21.64
F001	14.36	9.80	17.38	34.32	F035	18.88	4.99	19.53	14.81
F002	13.53	8.27	15.86	31.44	F036	20.03	5.04	20.66	14.11
F005	11.66	4.17	12.39	19.69	F037	18.55	3.83	18.94	11.66
F006	10.57	2.76	10.92	14.66	F039	16.34	2.35	16.50	8.17
F007	9.83	1.45	9.94	8.42	F040	16.49	0.82	16.51	2.84
F008	9.07	0.19	9.08	1.20	F041	14.29	2.60	14.52	10.31
F009	8.81	-0.92	8.86	-5.95	F045	10.69	-2.48	10.97	-13.05
F010	9.72	-0.72	9.74	-4.24	F074	13.94	9.77	17.02	35.03
F012	12.37	3.37	12.82	15.22	F077	16.22	6.02	17.30	20.36
F013	14.67	4.18	15.25	15.92	F078	16.94	9.62	19.48	29.61
F016	14.40	8.69	16.82	31.10	HALY	9.67	-0.72	9.70	-4.27
F019	17.07	6.22	18.17	20.03	NAMA	14.00	7.91	16.08	29.47
F020	17.26	3.97	17.72	12.96	P049	18.55	6.33	19.60	18.84
F024	13.82	1.01	13.86	4.17	SOLA	17.07	3.81	17.49	12.57
F026	15.31	-0.11	15.31	-0.43	YIBL	23.54	7.25	24.63	17.13
F027	13.05	-1.87	13.19	-8.17					
F029	18.37	1.43	18.42	4.46					
F030	19.49	2.91	19.71	8.50					

V_N : velocity in northing (mm/yr)

V_E : velocity in easting (mm/yr)

V_V : vector velocity (mm/yr)

A_Z : azimuth in degree

Table H.3: Relative Arabian-Eurasian station model velocities from NUVEL-1A [*DeMets et al.*, 1994]

Stations	V_N	V_E	V_V	A_Z	Stations	V_N	V_E	V_V	A_Z
	mm/yr	mm/yr	mm/yr	°		mm/yr	mm/yr	mm/yr	°
BAHR	30.37	3.04	30.52	5.71	F031	23.93	6.22	24.72	14.57
DATM	27.83	9.85	29.52	19.49	F033	25.15	5.32	25.71	11.95
F001	24.41	9.38	26.15	21.03	F035	29.26	4.63	29.62	8.99
F002	23.51	7.68	24.74	18.10	F036	30.47	4.79	30.85	8.93
F005	21.47	3.11	21.69	8.24	F037	28.90	3.37	29.10	6.65
F006	20.26	1.48	20.32	4.18	F039	26.54	1.58	26.59	3.40
F007	19.45	-0.01	19.45	-0.03	F040	26.70	-0.03	26.70	-0.06
F008	18.61	-1.46	18.67	-4.48	F041	24.33	1.64	24.39	3.87
F009	18.32	-2.69	18.52	-8.37	F045	20.39	-4.19	20.82	-11.62
F010	19.32	-2.39	19.47	-7.05	F074	23.95	9.32	25.70	21.27
F012	22.24	2.29	22.36	5.89	F077	26.42	5.48	26.98	11.71
F013	24.74	3.38	24.97	7.77	F078	27.19	9.36	28.75	19.00
F016	24.46	8.19	25.79	18.51	HALY	19.27	-2.40	19.42	-7.08
F019	27.33	5.76	27.93	11.91	NAMA	24.03	7.33	25.12	16.96
F020	27.54	3.39	27.74	7.03	P049	28.91	6.00	29.52	11.74
F024	23.83	-0.11	23.83	-0.25	SOLA	27.33	3.20	27.51	6.68
F026	25.44	-1.15	25.46	-2.59	YIBL	34.12	7.44	34.92	12.31
F027	22.99	-3.28	23.22	-8.13					
F029	28.71	0.83	28.72	1.66					
F030	29.90	2.51	30.00	4.79					

V_N : velocity in northing (mm/yr)

V_E : velocity in easting (mm/yr)

V_V : vector velocity (mm/yr)

A_Z : azimuth in degree

Table H.4: Relative Arabian-Eurasian station model velocities from GSRM v1.2 [*Kreemer et al.*, 2003]

Stations	V_N	V_E	V_V	A_Z	Stations	V_N	V_E	V_V	A_Z
	mm/yr	mm/yr	mm/yr	°		mm/yr	mm/yr	mm/yr	°
BAHR	21.95	2.72	22.12	7.07	F031	16.01	6.02	17.10	20.61
DATM	19.59	9.18	21.63	25.12	F033	17.13	5.14	17.88	16.70
F001	16.45	8.89	18.70	28.38	F035	20.91	4.27	21.34	11.55
F002	15.63	7.37	17.28	25.25	F036	22.04	4.35	22.46	11.16
F005	13.78	3.30	14.17	13.48	F037	20.58	3.13	20.82	8.64
F006	12.69	1.89	12.83	8.46	F039	18.40	1.62	18.48	5.03
F007	11.96	0.58	11.98	2.78	F040	18.55	0.13	18.55	0.40
F008	11.21	-0.68	11.23	-3.48	F041	16.38	1.82	16.48	6.32
F009	10.95	-1.78	11.09	-9.24	F045	12.81	-3.26	13.22	-14.29
F010	11.85	-1.56	11.95	-7.51	F074	16.03	8.85	18.31	28.90
F012	14.48	2.52	14.70	9.88	F077	18.29	5.22	19.02	15.92
F013	16.76	3.38	17.09	11.40	F078	18.99	8.76	20.92	24.76
F016	16.49	7.79	18.24	25.30	HALY	11.80	-1.57	11.91	-7.56
F019	19.13	5.43	19.88	15.86	NAMA	16.10	7.03	17.57	23.58
F020	19.32	3.24	19.59	9.51	P049	20.58	5.57	21.32	15.14
F024	15.92	0.24	15.92	0.88	SOLA	19.13	3.07	19.37	9.11
F026	17.39	-0.81	17.41	-2.68	YIBL	25.47	6.60	26.31	14.52
F027	15.16	-2.60	15.38	-9.74					
F029	20.40	0.79	20.42	2.21					
F030	21.50	2.26	21.62	6.00					

V_N : velocity in northing (mm/yr)

V_E : velocity in easting (mm/yr)

V_V : vector velocity (mm/yr)

A_Z : azimuth in degree

Table H.5: Relative Arabian-Eurasian station model velocities from McClusky et al. [2003]

Stations	V_N	V_E	V_V	A_Z	Stations	V_N	V_E	V_V	A_Z
	mm/yr	mm/yr	mm/yr	°		mm/yr	mm/yr	mm/yr	°
BAHR	21.06	3.71	21.38	10.00	F031	15.77	6.61	17.10	22.74
DATM	18.96	9.50	21.21	26.60	F033	16.77	5.83	17.76	19.16
F001	16.17	9.20	18.60	29.65	F035	20.14	5.10	20.77	14.20
F002	15.44	7.83	17.31	26.88	F036	21.14	5.18	21.76	13.76
F005	13.78	4.13	14.39	16.67	F037	19.84	4.06	20.26	11.56
F006	12.81	2.83	13.12	12.47	F039	17.91	2.67	18.11	8.47
F007	12.15	1.64	12.26	7.67	F040	18.04	1.32	18.09	4.19
F008	11.48	0.48	11.49	2.38	F041	16.10	2.81	16.35	9.91
F009	11.25	-0.53	11.26	-2.68	F045	12.92	-1.85	13.05	-8.14
F010	12.05	-0.31	12.06	-1.49	F074	15.80	9.16	18.26	30.12
F012	14.41	3.43	14.81	13.39	F077	17.81	5.91	18.76	18.36
F013	16.44	4.23	16.98	14.44	F078	18.43	9.11	20.56	26.30
F016	16.21	8.22	18.17	26.89	HALY	12.01	-0.32	12.02	-1.51
F019	18.55	6.12	19.53	18.25	NAMA	15.86	7.52	17.55	25.37
F020	18.72	4.14	19.17	12.47	P049	19.85	6.26	20.81	17.51
F024	15.70	1.39	15.76	5.05	SOLA	18.55	3.98	18.97	12.12
F026	17.01	0.45	17.01	1.51	YIBL	24.17	7.25	25.23	16.69
F027	15.01	-1.21	15.06	-4.60					
F029	19.69	1.94	19.78	5.64					
F030	20.66	3.29	20.92	9.05					

V_N : velocity in northing (mm/yr)

V_E : velocity in easting (mm/yr)

V_V : vector velocity (mm/yr)

A_Z : azimuth in degree

Table H.6: Relative Arabian-Eurasian station model velocities from Reilinger et al. [2006]

Stations	V_N	V_E	V_V	A_Z	Stations	V_N	V_E	V_V	A_Z
	mm/yr	mm/yr	mm/yr	°		mm/yr	mm/yr	mm/yr	°
BAHR	22.32	4.78	22.83	12.08	F031	16.72	7.89	18.49	25.25
DATM	20.10	10.96	22.90	28.61	F033	17.78	7.05	19.13	21.63
F001	17.14	10.65	20.18	31.86	F035	21.35	6.26	22.25	16.34
F002	16.37	9.18	18.77	29.30	F036	22.41	6.34	23.29	15.81
F005	14.61	5.23	15.52	19.71	F037	21.04	5.15	21.66	13.75
F006	13.58	3.85	14.11	15.83	F039	18.99	3.67	19.34	10.93
F007	12.88	2.57	13.14	11.29	F040	19.13	2.22	19.26	6.63
F008	12.17	1.33	12.24	6.25	F041	17.07	3.83	17.50	12.64
F009	11.92	0.26	11.93	1.25	F045	13.69	-1.16	13.74	-4.83
F010	12.78	0.49	12.79	2.18	F074	16.75	10.61	19.82	32.36
F012	15.27	4.49	15.92	16.37	F077	18.88	7.14	20.18	20.71
F013	17.43	5.35	18.23	17.05	F078	19.54	10.55	22.21	28.37
F016	17.18	9.60	19.68	29.20	HALY	12.73	0.48	12.74	2.17
F019	19.67	7.36	21.00	20.51	NAMA	16.81	8.86	19.00	27.79
F020	19.85	5.24	20.53	14.79	P049	21.04	7.51	22.34	19.63
F024	16.64	2.30	16.80	7.87	SOLA	19.67	5.07	20.31	14.47
F026	18.03	1.29	18.07	4.10	YIBL	25.62	8.55	27.01	18.45
F027	15.92	-0.48	15.92	-1.72					
F029	20.87	2.89	21.07	7.87					
F030	21.91	4.33	22.33	11.17					

V_N : velocity in northing (mm/yr)

V_E : velocity in easting (mm/yr)

V_V : vector velocity (mm/yr)

A_Z : azimuth in degree

Table H.7: Relative Arabian-Eurasian station model velocities from Almotairi [2006]

Stations	V_N	V_E	V_V	A_Z	Stations	V_N	V_E	V_V	A_Z
	mm/yr	mm/yr	mm/yr	°		mm/yr	mm/yr	mm/yr	°
BAHR	25.20	5.38	25.77	12.06	F031	19.58	8.36	21.29	23.12
DATM	22.98	11.55	25.72	26.68	F033	20.65	7.54	21.98	20.06
F001	12.00	11.17	22.91	29.18	F035	24.23	6.84	25.18	15.77
F002	19.22	9.67	21.51	26.70	F036	25.29	6.96	26.23	15.39
F005	17.44	5.62	18.33	17.85	F037	23.92	5.72	24.59	13.44
F006	16.40	4.18	16.92	14.31	F039	21.86	4.15	22.25	10.76
F007	15.69	2.86	15.95	10.33	F040	22.00	2.70	22.16	7.00
F008	14.96	1.58	15.04	6.01	F041	19.93	4.26	20.38	12.06
F009	14.71	0.47	14.72	1.84	F045	16.51	-0.91	16.54	-3.17
F010	15.58	0.73	15.60	2.68	F074	19.60	11.12	22.54	29.57
F012	18.11	4.88	18.76	15.06	F077	21.75	7.66	23.06	19.39
F013	20.29	5.81	21.11	15.97	F078	22.42	11.12	25.03	26.38
F016	20.04	10.11	22.45	26.76	HALY	15.54	0.73	15.55	2.67
F019	22.54	7.90	23.89	19.31	NAMA	19.67	9.35	21.78	25.42
F020	22.72	5.77	23.45	14.24	P049	23.92	8.09	25.25	18.68
F024	19.50	2.70	19.68	7.87	SOLA	22.54	5.60	23.23	13.94
F026	20.89	1.72	20.97	4.702	YIBL	28.48	9.27	29.96	18.04
F027	18.76	-0.15	18.76	-0.45					
F029	23.75	3.43	24.00	8.22					
F030	24.79	4.91	25.27	11.22					

V_N : velocity in northing (mm/yr)

V_E : velocity in easting (mm/yr)

V_V : vector velocity (mm/yr)

A_Z : azimuth in degree

Table H.8: Relative Arabian-Eurasian station model velocities from REVEL-2000 [*Sella et al.*, 2002]

Stations	V_N	V_E	V_V	A_Z	Stations	V_N	V_E	V_V	A_Z
	mm/yr	mm/yr	mm/yr	°		mm/yr	mm/yr	mm/yr	°
BAHR	19.83	2.29	19.97	6.58	F031	13.92	5.68	15.03	22.19
DATM	17.48	8.76	19.55	26.62	F033	15.03	4.79	15.77	17.66
F001	14.35	8.51	16.69	30.67	F035	18.80	3.85	19.19	11.58
F002	13.54	7.02	15.25	27.41	F036	19.93	3.90	20.30	11.08
F005	11.71	3.03	12.10	14.50	F037	18.47	2.72	18.67	8.38
F006	10.63	1.65	10.76	8.84	F039	16.30	1.27	16.35	4.46
F007	9.91	0.38	9.92	2.18	F040	16.45	-0.21	16.45	-0.73
F008	9.17	-0.85	9.20	-5.31	F041	14.28	1.51	14.36	6.02
F009	8.91	-1.93	9.12	-12.22	F045	10.75	-3.43	11.29	-17.71
F010	9.80	-1.73	9.95	-10.04	F074	13.94	8.48	16.32	31.31
F012	12.40	2.24	12.60	10.26	F077	16.18	4.84	16.89	16.65
F013	14.66	3.05	14.97	11.75	F078	16.89	8.35	18.84	26.31
F016	14.40	7.43	16.20	27.29	HALY	9.75	-1.74	9.91	-10.09
F019	17.02	5.04	17.75	16.50	NAMA	14.01	6.67	15.51	25.47
F020	17.21	2.85	17.44	9.42	P049	18.47	5.15	19.17	15.58
F024	13.83	-0.04	13.83	-0.16	SOLA	17.02	2.69	17.23	8.99
F026	15.29	-1.12	15.33	-4.19	YIBL	23.37	6.07	24.14	14.57
F027	13.07	-2.84	13.38	-12.24					
F029	18.29	0.40	18.30	1.25					
F030	19.39	1.84	19.48	5.41					

V_N : velocity in northing (mm/yr)

V_E : velocity in easting (mm/yr)

V_V : vector velocity (mm/yr)

A_Z : azimuth in degree

Table H.9: Relative Arabian-Eurasian station model velocities from Vernant et al. [2004]

Stations	V_N	V_E	V_V	A_Z	Stations	V_N	V_E	V_V	A_Z
	mm/yr	mm/yr	mm/yr	°		mm/yr	mm/yr	mm/yr	°
BAHR	20.83	4.01	21.21	10.91	F031	15.38	7.06	16.92	24.65
DATM	18.66	10.01	21.18	28.21	F033	16.41	6.25	17.56	20.84
F001	15.79	9.73	18.54	31.64	F035	19.88	5.45	20.61	15.35
F002	15.04	8.32	17.18	28.95	F036	20.91	5.53	21.63	14.81
F005	13.34	4.52	14.08	18.71	F037	19.57	4.38	20.06	12.62
F006	12.33	3.19	12.74	14.51	F039	17.58	2.97	17.83	9.59
F007	11.66	1.97	11.83	9.58	F040	17.72	1.58	17.79	5.09
F008	10.97	0.78	11.00	4.08	F041	15.72	3.14	16.03	11.30
F009	10.73	-0.25	10.73	-1.33	F045	12.44	-1.63	12.55	-7.45
F010	11.56	-0.04	11.56	-0.19	F074	15.40	9.69	18.20	32.18
F012	13.98	3.79	14.48	15.18	F077	17.48	6.32	18.58	19.89
F013	16.07	4.60	16.71	15.99	F078	18.12	9.62	20.52	27.96
F016	15.83	8.71	18.06	28.84	HALY	11.52	-0.04	11.52	-0.21
F019	18.24	6.53	19.37	19.69	NAMA	15.47	8.00	17.41	27.34
F020	18.42	4.48	18.95	13.67	P049	19.58	6.66	20.68	18.79
F024	15.30	1.67	15.39	6.24	SOLA	18.24	4.32	18.75	13.33
F026	16.65	0.69	16.66	2.37	YIBL	24.05	7.63	25.23	17.62
F027	14.60	-1.00	14.63	-3.90					
F029	19.41	2.20	19.54	6.47					
F030	20.42	3.58	20.73	9.94					

V_N : velocity in northing (mm/yr)

V_E : velocity in easting (mm/yr)

V_V : vector velocity (mm/yr)

A_Z : azimuth in degree

Table H.10: Relative Arabian-Eurasian station model velocities from *Vigny et al.* [2006]

Stations	V_N	V_E	V_V	A_Z	Stations	V_N	V_E	V_V	A_Z
	mm/yr	mm/yr	mm/yr	°		mm/yr	mm/yr	mm/yr	°
BAHR	22.20	4.97	22.74	12.61	F031	17.73	7.23	19.15	22.17
DATM	20.44	9.84	22.68	25.70	F033	18.58	6.59	19.72	19.52
F001	18.07	9.49	20.41	27.70	F035	21.43	6.11	22.28	15.91
F002	17.44	8.27	19.31	25.36	F036	22.26	6.23	23.12	15.63
F005	16.03	4.98	16.78	17.26	F037	21.18	5.20	21.81	13.79
F006	15.18	3.80	15.65	14.06	F039	19.55	3.90	19.93	11.28
F007	14.62	2.72	14.87	10.54	F040	19.66	2.74	19.85	7.93
F008	14.03	1.67	14.13	6.78	F041	18.01	3.94	18.44	12.33
F009	13.83	0.77	13.85	3.19	F045	15.28	-0.31	15.28	-1.16
F010	14.53	1.00	14.56	3.93	F074	17.75	9.44	20.11	28.01
F012	16.56	4.40	17.14	14.87	F077	19.46	6.70	20.59	19.01
F013	18.30	5.19	19.02	15.83	F078	19.99	9.49	22.13	25.38
F016	18.10	8.64	20.06	25.50	HALY	14.49	0.99	14.53	3.92
F019	20.09	6.91	21.25	18.99	NAMA	17.80	8.02	19.53	24.25
F020	20.24	5.21	20.90	14.45	P049	21.18	7.09	22.34	18.51
F024	17.67	2.67	17.87	8.60	SOLA	20.09	5.07	20.72	14.17
F026	18.78	1.92	18.88	5.85	YIBL	24.78	8.14	26.08	18.20
F027	17.08	0.37	17.08	1.23					
F029	21.05	3.37	21.31	9.09					
F030	21.87	4.58	22.34	11.84					

V_N : velocity in northing (mm/yr)

V_E : velocity in easting (mm/yr)

V_V : vector velocity (mm/yr)

A_Z : azimuth in degree

Table H.11: The difference between the relative Arabian-Eurasian station model velocities from this study and from CGPS2004 [*Prawirodirdjo and Bock*, 2004]

Stations	ΔV_N	ΔV_E	ΔV_V	ΔA_Z	Stations	ΔV_N	ΔV_E	ΔV_V	ΔA_Z
	mm/yr	mm/yr	mm/yr	°		mm/yr	mm/yr	mm/yr	°
BAHR	2.25	1.16	2.43	1.94	F031	2.60	0.80	2.69	-1.37
DATM	2.40	0.75	2.46	-1.37	F033	2.54	0.87	2.68	-0.37
F001	2.58	0.69	2.54	-2.55	F035	2.32	1.04	2.51	1.07
F002	2.62	0.73	2.63	-2.29	F036	2.24	1.08	2.44	1.24
F005	2.71	0.85	2.84	-0.43	F037	2.34	1.09	2.51	1.57
F006	2.76	0.87	2.89	0.58	F039	2.47	1.08	2.61	2.14
F007	2.80	0.89	2.90	2.09	F040	2.46	1.15	2.54	3.08
F008	2.83	0.91	2.87	4.06	F041	2.58	0.99	2.72	1.71
F009	2.84	0.93	2.79	6.02	F045	2.76	1.05	2.55	7.01
F010	2.80	0.96	2.78	5.33	F074	2.60	0.68	2.54	-2.75
F012	2.68	0.90	2.82	0.61	F077	2.47	0.91	2.64	-0.03
F013	2.56	0.94	2.72	0.65	F078	2.43	0.76	2.49	-1.43
F016	2.58	0.74	2.59	-2.06	HALY	2.80	0.96	2.78	5.35
F019	2.43	0.92	2.59	0.10	NAMA	2.60	0.76	2.65	-1.88
F020	2.41	1.03	2.58	1.31	P049	2.34	0.96	2.52	0.40
F024	2.60	1.04	2.70	2.95	SOLA	2.43	1.04	2.60	1.38
F026	2.52	1.14	2.55	3.73	YIBL	2.00	1.08	2.23	0.94
F027	2.64	1.12	2.52	5.44	Mean	2.53	0.95	2.62	1.33
F029	2.35	1.19	2.46	2.76	S.dev	0.19	0.15	0.15	2.51
F030	2.28	1.16	2.43	2.10	RMS	2.54	0.96	2.62	2.81

ΔV_N : velocity in northing (mm/yr)

ΔV_E : velocity in easting (mm/yr)

ΔV_V : vector velocity (mm/yr)

ΔA_Z : azimuth in degree

Table H.12: The difference between the relative Arabian-Eurasian station model velocities from this study and from NUVEL-1A [*DeMets et al.*, 1994]

Stations	ΔV_N	ΔV_E	ΔV_V	ΔA_Z	Stations	ΔV_N	ΔV_E	ΔV_V	ΔA_Z
	mm/yr	Mm/yr	mm/yr	°		mm/yr	mm/yr	mm/yr	°
BAHR	-8.18	1.49	-7.87	5.83	F031	-7.42	1.47	-6.51	10.41
DATM	-7.89	0.94	-6.85	8.94	F033	-7.57	1.52	-6.84	9.32
F001	-7.48	1.10	-6.23	10.74	F035	-8.06	1.40	-7.58	6.89
F002	-7.36	1.32	-6.25	11.05	F036	-8.20	1.32	-7.75	6.42
F005	-7.09	1.91	-6.46	11.02	F037	-8.02	1.54	-7.65	6.58
F006	-6.93	2.15	-6.51	11.06	F039	-7.74	1.84	-7.48	6.91
F007	-6.82	2.35	-6.61	10.54	F040	-7.76	2.00	-7.65	5.98
F008	-6.71	2.56	-6.72	9.74	F041	-7.47	1.95	-7.15	8.15
F009	-6.67	2.71	-6.87	8.44	F045	-6.95	2.77	-7.30	5.58
F010	-6.80	2.63	-6.95	8.14	F074	-7.42	1.12	-6.14	11.01
F012	-7.20	1.97	-6.72	9.94	F077	-7.72	1.45	-7.04	8.62
F013	-7.52	1.75	-7.00	8.80	F078	-7.82	1.02	-6.78	9.18
F016	-7.48	1.24	-6.38	10.53	HALY	-6.80	2.63	-6.94	8.16
F019	-7.83	1.38	-7.17	8.22	NAMA	-7.43	1.35	-6.39	10.63
F020	-7.86	1.61	-7.44	7.24	P049	-8.02	1.29	-7.40	7.50
F024	-7.40	2.16	-7.27	7.37	SOLA	-7.83	1.64	-7.42	7.27
F026	-7.60	2.18	-7.60	5.89	YIBL	-8.58	0.89	-8.06	5.76
F027	-7.29	2.53	-7.51	5.40	Mean	-7.54	1.74	-7.09	8.23
F029	-7.99	1.80	-7.84	5.56	S.dev	0.47	0.53	0.53	1.90
F030	-8.13	1.57	-7.86	5.81	RMS	7.56	1.82	7.11	8.44

ΔV_N : velocity in northing (mm/yr)

ΔV_E : velocity in easting (mm/yr)

ΔV_V : vector velocity (mm/yr)

ΔA_Z : azimuth in degree

Table H.13: The difference between the relative Arabian-Eurasian station model velocities from this study and from GSRM v1.2 [*Kreemer et al.*, 2003]

Stations	ΔV_N	ΔV_E	ΔV_V	ΔA_Z	Stations	ΔV_N	ΔV_E	ΔV_V	ΔA_Z
	mm/yr	Mm/yr	mm/yr	°		mm/yr	mm/yr	mm/yr	°
BAHR	0.24	1.81	0.53	4.47	F031	0.50	1.67	1.11	4.37
DATM	0.35	1.61	1.04	3.31	F033	0.46	1.70	0.99	4.57
F001	0.48	1.60	1.22	3.39	F035	0.29	1.76	0.70	4.33
F002	0.52	1.63	1.21	3.90	F036	0.24	1.77	0.64	4.19
F005	0.59	1.72	1.06	5.78	F037	0.30	1.78	0.63	4.59
F006	0.64	1.74	0.98	6.78	F039	0.40	1.80	0.63	5.28
F007	0.66	1.76	0.86	7.73	F040	0.39	1.83	0.50	5.52
F008	0.69	1.78	0.72	8.74	F041	0.49	1.78	0.76	5.70
F009	0.70	1.80	0.56	9.31	F045	0.63	1.84	0.30	8.25
F010	0.67	1.80	0.57	8.60	F074	0.50	1.60	1.25	3.38
F012	0.56	1.74	0.94	5.95	F077	0.41	1.71	0.92	4.41
F013	0.47	1.74	0.88	5.17	F078	0.37	1.62	1.05	3.42
F016	0.48	1.63	1.17	3.74	HALY	0.67	1.80	0.57	8.64
F019	0.37	1.71	0.88	4.27	NAMA	0.50	1.65	1.16	4.01
F020	0.36	1.77	0.71	4.76	P049	0.30	1.72	0.80	4.10
F024	0.51	1.81	0.64	6.24	SOLA	0.37	1.77	0.72	4.84
F026	0.44	1.84	0.45	5.98	YIBL	0.07	1.73	0.55	3.55
F027	0.54	1.85	0.33	7.01	Mean	0.45	1.74	0.78	5.35
F029	0.31	1.84	0.46	5.01	S.dev	0.15	0.07	0.26	1.71
F030	0.26	1.81	0.52	4.60	RMS	0.48	1.75	0.83	5.61

ΔV_N : velocity in northing (mm/yr)

ΔV_E : velocity in easting (mm/yr)

ΔV_V : vector velocity (mm/yr)

ΔA_Z : azimuth in degree

Table H.14: The difference between the relative Arabian-Eurasian station model velocities from this study and from McClusky et al. [2003]

Stations	ΔV_N	ΔV_E	ΔV_V	ΔA_Z	Stations	ΔV_N	ΔV_E	ΔV_V	ΔA_Z
	mm/yr	Mm/yr	mm/yr	°		mm/yr	mm/yr	mm/yr	°
BAHR	1.13	0.82	1.27	1.54	F031	0.74	1.08	1.11	2.24
DATM	0.97	1.30	1.46	1.83	F033	0.81	1.02	1.11	2.11
F001	0.77	1.28	1.32	2.12	F035	1.06	0.94	1.27	1.68
F002	0.71	1.18	1.18	2.27	F036	1.14	0.94	1.34	1.59
F005	0.59	0.90	0.84	2.59	F037	1.04	0.85	1.19	1.67
F006	0.52	0.80	0.69	2.77	F039	0.90	0.75	1.00	1.84
F007	0.47	0.71	0.58	2.84	F040	0.91	0.64	0.96	1.73
F008	0.42	0.62	0.46	2.88	F041	0.76	0.78	0.89	2.11
F009	0.41	0.54	0.39	2.75	F045	0.53	0.42	0.47	2.10
F010	0.47	0.55	0.46	2.58	F074	0.74	1.28	1.30	2.16
F012	0.64	0.84	0.83	2.44	F077	0.89	1.02	1.18	1.97
F013	0.79	0.89	0.99	2.13	F078	0.93	1.27	1.41	1.88
F016	0.77	1.21	1.24	2.15	HALY	0.46	0.55	0.46	2.59
F019	0.94	1.03	1.23	1.88	NAMA	0.74	1.15	1.18	2.22
F020	0.96	0.87	1.13	1.80	P049	1.04	1.03	1.31	1.73
F024	0.73	0.67	0.80	2.07	SOLA	0.94	0.86	1.12	1.83
F026	0.83	0.58	0.85	1.79	YIBL	1.37	1.08	1.63	1.38
F027	0.68	0.46	0.65	1.87	Mean	0.81	0.87	1.02	2.06
F029	1.03	0.68	1.10	1.58	S.dev	0.23	0.25	0.32	0.40
F030	1.10	0.78	1.22	1.55	RMS	0.84	0.91	1.07	2.10

ΔV_N : velocity in northing (mm/yr)

ΔV_E : velocity in easting (mm/yr)

ΔV_V : vector velocity (mm/yr)

ΔA_Z : azimuth in degree

Table H.15: The difference between the relative Arabian-Eurasian station model velocities from this study and from Reilinger et al. [2006]

Stations	ΔV_N	ΔV_E	ΔV_V	ΔA_Z	Stations	ΔV_N	ΔV_E	ΔV_V	ΔA_Z
	mm/yr	Mm/yr	mm/yr	°		mm/yr	mm/yr	mm/yr	°
BAHR	-0.14	-0.25	-0.18	-0.54	F031	-0.21	-0.19	-0.28	-0.27
DATM	-0.17	-0.17	-0.23	-0.18	F033	-0.20	-0.21	-0.26	-0.36
F001	-0.21	-0.17	-0.26	-0.09	F035	-0.15	-0.23	-0.21	-0.46
F002	-0.22	-0.18	-0.28	-0.15	F036	-0.13	-0.23	-0.19	-0.46
F005	-0.24	-0.21	-0.29	-0.45	F037	-0.15	-0.24	-0.21	-0.52
F006	-0.25	-0.22	-0.30	-0.59	F039	-0.18	-0.24	-0.23	-0.62
F007	-0.26	-0.23	-0.30	-0.78	F040	-0.18	-0.26	-0.21	-0.71
F008	-0.27	-0.24	-0.29	-0.99	F041	-0.21	-0.23	-0.26	-0.62
F009	-0.27	-0.24	-0.28	-1.18	F045	-0.25	-0.27	-0.22	-1.21
F010	-0.26	-0.25	-0.27	-1.09	F074	-0.21	-0.17	-0.26	-0.08
F012	-0.23	-0.22	-0.28	-0.54	F077	-0.18	-0.21	-0.24	-0.38
F013	-0.20	-0.22	-0.26	-0.48	F078	-0.17	-0.17	-0.24	-0.19
F016	-0.21	-0.18	-0.27	-0.16	HALY	-0.26	-0.25	-0.26	-1.09
F019	-0.17	-0.21	-0.24	-0.38	NAMA	-0.21	-0.18	-0.27	-0.20
F020	-0.17	-0.23	-0.23	-0.52	P049	-0.15	-0.21	-0.22	-0.39
F024	-0.21	-0.25	-0.24	-0.75	SOLA	-0.17	-0.23	-0.22	-0.52
F026	-0.19	-0.26	-0.21	-0.80	YIBL	-0.09	-0.22	-0.15	-0.38
F027	-0.22	-0.27	-0.21	-1.01	Mean	-0.20	-0.22	-0.24	-0.55
F029	-0.16	-0.26	-0.19	-0.65	S.dev	0.04	0.03	0.04	0.31
F030	-0.14	-0.25	-0.19	-0.57	RMS	0.20	0.23	0.24	0.63

ΔV_N : velocity in northing (mm/yr)

ΔV_E : velocity in easting (mm/yr)

ΔV_V : vector velocity (mm/yr)

ΔA_Z : azimuth in degree

Table H.16: The difference between the relative Arabian-Eurasian station model velocities from this study and from Almotairi [2006]

Stations	ΔV_N	ΔV_E	ΔV_V	ΔA_Z	Stations	ΔV_N	ΔV_E	ΔV_V	ΔA_Z
	mm/yr	Mm/yr	mm/yr	°		mm/yr	mm/yr	mm/yr	°
BAHR	-3.01	-0.8	-3.12	-0.52	F031	-3.07	-0.67	-3.08	1.86
DATM	-3.05	-0.75	-3.05	1.76	F033	-3.06	-0.70	-3.11	1.21
F001	-3.07	-0.68	-2.99	2.59	F035	-3.03	-0.81	-3.14	0.11
F002	-3.07	-0.66	-3.02	2.45	F036	-3.01	-0.85	-3.13	-0.04
F005	-3.07	-0.59	-3.10	1.41	F037	-3.03	-0.80	-3.14	-0.21
F006	-3.07	-0.55	-3.11	0.93	F039	-3.05	-0.73	-3.14	-0.45
F007	-3.06	-0.52	-3.11	0.18	F040	-3.05	-0.74	-3.11	-1.08
F008	-3.06	-0.48	-3.09	-0.75	F041	-3.07	-0.67	-3.14	-0.04
F009	-3.06	-0.46	-3.07	-1.77	F045	-3.07	-0.51	-3.02	-2.87
F010	-3.06	-0.49	-3.08	-1.59	F074	-3.07	-0.67	-2.98	2.71
F012	-3.07	-0.61	-3.12	0.77	F077	-3.06	-0.73	-3.12	0.94
F013	-3.06	-0.68	-3.14	0.60	F078	-3.05	-0.74	-3.06	1.80
F016	-3.07	-0.68	-3.04	2.28	HALY	-3.06	-0.49	-3.07	-1.59
F019	-3.05	-0.75	-3.13	0.82	NAMA	-3.07	-0.67	-3.05	2.18
F020	-3.05	-0.76	-3.15	0.03	P049	-3.03	-0.79	-3.13	0.56
F024	-3.07	-0.64	-3.12	-0.75	SOLA	-3.05	-0.76	-3.14	0.01
F026	-3.06	-0.69	-3.11	-1.40	YIBL	-2.95	-0.94	-3.09	0.04
F027	-3.07	-0.60	-3.05	-2.28	Mean	-3.058	-0.69	-3.09	0.22
F029	-3.03	-0.80	-3.12	-1.00	S.dev	0.02	0.12	0.05	1.42
F030	-3.02	-0.84	-3.13	-0.62	RMS	3.05	0.70	3.09	1.42

ΔV_N : velocity in northing (mm/yr)

ΔV_E : velocity in easting (mm/yr)

ΔV_V : vector velocity (mm/yr)

ΔA_Z : azimuth in degree

Table H.17: The difference between the relative Arabian-Eurasian station model velocities from this study and from REVEL-2000 [*Sella et al.*, 2002]

Stations	ΔV_N	ΔV_E	ΔV_V	ΔA_Z	Stations	ΔV_N	ΔV_E	ΔV_V	ΔA_Z
	mm/yr	Mm/yr	mm/yr	°		mm/yr	mm/yr	mm/yr	°
BAHR	2.35	2.24	2.68	4.96	F031	2.60	2.02	3.18	2.79
DATM	2.46	2.03	3.12	1.81	F033	2.56	2.06	3.10	3.61
F001	2.58	1.97	3.23	1.10	F035	2.40	2.18	2.85	4.30
F002	2.61	1.98	3.24	1.74	F036	2.35	2.21	2.80	4.27
F005	2.67	1.99	3.13	4.76	F037	2.42	2.19	2.78	4.85
F006	2.70	1.98	3.05	6.40	F039	2.51	2.15	2.76	5.85
F007	2.72	1.97	2.92	8.33	F040	2.50	2.17	2.60	6.65
F008	2.74	1.95	2.75	10.57	F041	2.58	2.09	2.88	6.00
F009	2.74	1.94	2.53	12.29	F045	2.69	2.01	2.23	11.67
F010	2.72	1.97	2.57	11.13	F074	2.59	1.97	3.24	0.97
F012	2.64	2.02	3.04	5.57	F077	2.51	2.09	3.05	3.68
F013	2.57	2.08	3.00	4.82	F078	2.48	2.03	3.13	1.87
F016	2.58	2.00	3.21	1.75	HALY	2.72	1.97	2.57	11.17
F019	2.48	2.11	3.01	3.63	NAMA	2.59	2.00	3.22	2.12
F020	2.47	2.15	2.86	4.85	P049	2.42	2.14	2.95	3.66
F024	2.60	2.09	2.73	7.28	SOLA	2.48	2.15	2.86	4.96
F026	2.54	2.15	2.53	7.49	YIBL	2.17	2.26	2.72	3.50
F027	2.62	2.09	2.33	9.51	Mean	2.54	2.08	2.87	5.43
F029	2.42	2.23	2.58	5.97	S.dev	0.13	0.10	0.27	3.09
F030	2.37	2.24	2.66	5.19	RMS	2.55	2.08	2.88	6.23

ΔV_N : velocity in northing (mm/yr)

ΔV_E : velocity in easting (mm/yr)

ΔV_V : vector velocity (mm/yr)

ΔA_Z : azimuth in degree

Table H.18: The difference between the relative Arabian-Eurasian station model velocities from this study and from Vernant et al. [2004]

Stations	ΔV_N	ΔV_E	ΔV_V	ΔA_Z	Stations	ΔV_N	ΔV_E	ΔV_V	ΔA_Z
	mm/yr	Mm/yr	mm/yr	°		mm/yr	mm/yr	mm/yr	°
BAHR	1.36	0.52	1.44	0.63	F031	1.13	0.63	1.29	0.33
DATM	1.27	0.78	1.49	0.22	F033	1.17	0.60	1.31	0.43
F001	1.15	0.76	1.38	0.13	F035	1.32	0.58	1.43	0.53
F002	1.11	0.69	1.31	0.20	F036	1.37	0.59	1.47	0.54
F005	1.04	0.50	1.15	0.55	F037	1.31	0.53	1.39	0.61
F006	1.00	0.44	1.07	0.73	F039	1.22	0.45	1.28	0.72
F007	0.96	0.38	1.01	0.93	F040	1.23	0.39	1.26	0.83
F008	0.93	0.32	0.95	1.18	F041	1.14	0.45	1.21	0.72
F009	0.92	0.26	0.92	1.40	F045	1.00	0.21	0.97	1.41
F010	0.96	0.28	0.96	1.28	F074	1.13	0.75	1.36	0.10
F012	1.07	0.47	1.16	0.65	F077	1.22	0.61	1.36	0.44
F013	1.16	0.52	1.26	0.58	F078	1.25	0.76	1.45	0.22
F016	1.15	0.71	1.35	0.20	HALY	0.96	0.28	0.96	1.29
F019	1.25	0.62	1.39	0.44	NAMA	1.13	0.68	1.32	0.25
F020	1.26	0.53	1.35	0.60	P049	1.31	0.63	1.44	0.45
F024	1.13	0.38	1.17	0.88	SOLA	1.25	0.52	1.34	0.62
F026	1.18	0.34	1.20	0.93	YIBL	1.49	0.70	1.63	0.45
F027	1.10	0.25	1.08	1.17	Mean	1.17	0.51	1.27	0.65
F029	1.30	0.42	1.34	0.75	S.dev	0.14	0.16	0.18	0.36
F030	1.35	0.49	1.41	0.66	RMS	1.18	0.54	1.28	0.74

ΔV_N : velocity in northing (mm/yr)

ΔV_E : velocity in easting (mm/yr)

ΔV_V : vector velocity (mm/yr)

ΔA_Z : azimuth in degree

Table H.19: The difference between the relative Arabian-Eurasian station model velocities from this study and from *Vigny et al.* [2006]

Stations	ΔV_N	ΔV_E	ΔV_V	ΔA_Z	Stations	ΔV_N	ΔV_E	ΔV_V	ΔA_Z
	mm/yr	Mm/yr	mm/yr	°		mm/yr	mm/yr	mm/yr	°
BAHR	-0.01	-0.44	1.44	0.63	F031	-1.22	0.47	1.29	0.33
DATM	-0.50	0.96	1.49	0.22	F033	-1.00	0.26	1.31	0.43
F001	-1.13	1.00	1.38	0.13	F035	-0.23	-0.08	1.43	0.53
F002	-1.29	0.74	1.31	0.20	F036	0.01	-0.11	1.47	0.54
F005	-1.65	0.04	1.15	0.55	F037	-0.30	-0.29	1.39	0.61
F006	-1.85	-0.17	1.07	0.73	F039	-0.74	-0.48	1.28	0.72
F007	-1.99	-0.38	1.01	0.93	F040	-0.71	-0.77	1.26	0.83
F008	-2.13	-0.57	0.95	1.18	F041	-1.15	-0.35	1.21	0.72
F009	-2.18	-0.75	0.92	1.40	F045	-1.83	-1.11	0.97	1.41
F010	-2.01	-0.76	0.96	1.28	F074	-1.22	1.00	1.36	0.10
F012	-1.52	-0.13	1.16	0.65	F077	-0.77	0.22	1.36	0.44
F013	-1.07	-0.07	1.26	0.58	F078	-0.63	0.89	1.45	0.22
F016	-1.13	0.79	1.35	0.20	HALY	-2.02	-0.76	0.96	1.29
F019	-0.60	0.23	1.39	0.44	NAMA	-1.20	0.65	1.32	0.25
F020	-0.56	-0.21	1.35	0.60	P049	-0.30	0.20	1.44	0.45
F024	-1.24	-0.62	1.17	0.88	SOLA	-0.60	-0.23	1.34	0.62
F026	-0.95	-0.90	1.20	0.93	YIBL	0.76	0.19	1.63	0.45
F027	-1.38	-1.11	1.08	1.17	Mean	-0.99	-0.11	1.27	0.65
F029	-0.33	-0.74	1.34	0.75	S.dev	0.69	0.61	0.18	0.36
F030	-0.10	-0.51	1.41	0.66	RMS	1.21	0.61	1.28	0.74

ΔV_N : velocity in northing (mm/yr)

ΔV_E : velocity in easting (mm/yr)

ΔV_V : vector velocity (mm/yr)

ΔA_Z : azimuth in degree

Appendix I: Relative station model velocities between Arabian plate and Nubian plate

Table I.1: Relative Arabian-Nubian station model velocities from this study

Stations	V_N	V_E	V_V	A_Z	Stations	V_N	V_E	V_V	A_Z
	mm/yr	mm/yr	mm/yr	°		mm/yr	mm/yr	mm/yr	°
BAHR	17.02	5.97	18.04	19.31	F031	11.59	9.32	14.87	38.79
DATM	14.85	12.19	19.22	39.38	F033	12.61	8.46	15.18	33.84
F001	11.99	12.00	16.96	45.01	F035	16.07	7.50	17.73	25.01
F002	11.25	10.60	15.46	43.28	F036	17.11	7.52	18.69	23.72
F005	9.58	6.83	11.76	35.51	F037	15.77	6.41	17.02	22.14
F006	8.59	5.54	10.22	32.81	F039	13.78	5.07	14.68	20.21
F007	7.93	4.33	9.04	28.65	F040	13.91	3.64	14.38	14.67
F008	7.25	3.17	7.92	23.61	F041	11.93	5.34	13.07	24.10
F009	7.02	2.14	7.34	16.97	F045	8.70	0.66	8.73	4.35
F010	7.83	2.31	8.16	16.47	F074	11.62	11.97	16.68	45.86
F012	10.21	6.08	11.88	30.76	F077	13.67	8.49	16.09	31.84
F013	12.27	6.80	14.03	29.01	F078	14.31	11.81	18.56	39.53
F016	12.03	10.97	16.28	42.36	HALY	7.79	2.31	8.13	16.54
F019	14.43	8.67	16.83	30.98	NAMA	11.68	10.26	15.55	41.31
F020	14.61	6.57	16.02	24.22	P049	15.77	8.74	18.03	29.01
F024	11.52	3.86	12.15	18.55	SOLA	14.43	6.42	15.80	23.97
F026	12.85	2.79	13.15	12.26	YIBL	20.28	9.53	22.40	25.17
F027	10.82	1.19	10.89	6.26					
F029	15.60	4.18	16.16	15.01					
F030	16.62	5.54	17.52	18.45					

V_N : velocity in northing (mm/yr)

V_E : velocity in easting (mm/yr)

V_V : vector velocity (mm/yr)

A_Z : azimuth in degree

Table I.2: Relative Arabian-Nubian station model velocities from Chu and Gordon [1998]

Stations	V_N	V_E	V_V	A_Z	Stations	V_N	V_E	V_V	A_Z
	mm/yr	mm/yr	mm/yr	°		mm/yr	mm/yr	mm/yr	°
BAHR	17.71	6.16	18.76	19.19	F031	12.40	9.40	15.56	37.15
DATM	15.60	12.25	19.83	38.14	F033	13.40	8.56	15.90	32.56
F001	12.79	12.03	17.56	43.24	F035	16.78	7.65	18.45	24.51
F002	12.07	10.65	16.09	41.43	F036	17.80	7.69	19.39	23.36
F005	10.42	6.93	12.51	33.62	F037	16.49	6.59	17.76	21.78
F006	9.45	5.64	11.01	30.84	F039	14.54	5.24	15.46	19.83
F007	8.80	4.45	9.86	26.81	F040	14.67	3.84	15.17	14.67
F008	8.14	3.29	8.78	22.04	F041	12.73	5.48	13.86	23.30
F009	7.91	2.28	8.23	16.07	F045	9.56	0.84	9.60	5.03
F010	8.70	2.46	9.04	15.77	F074	12.42	12.00	17.27	44.02
F012	11.04	6.19	12.66	29.28	F077	14.44	8.60	16.80	30.78
F013	13.07	6.93	14.79	27.94	F078	15.07	11.87	19.18	38.23
F016	12.83	11.03	16.92	40.67	HALY	8.66	2.46	9.01	15.83
F019	15.18	8.78	17.54	30.05	NAMA	12.48	10.32	16.20	39.60
F020	15.36	6.73	16.77	23.66	P049	16.49	8.87	18.73	28.28
F024	12.33	4.03	12.97	18.11	SOLA	15.18	6.58	16.55	23.42
F026	13.63	2.99	13.96	12.38	YIBL	20.89	9.69	23.03	24.89
F027	11.64	1.39	11.73	6.79					
F029	16.33	4.40	16.91	15.07					
F030	17.32	5.75	18.25	18.35					

V_N : velocity in northing (mm/yr)

V_E : velocity in easting (mm/yr)

V_V : vector velocity (mm/yr)

A_Z : azimuth in degree

Table I.3: Relative Arabian-Nubian station model velocities from Jestin et al. [1994]

Stations	V_N	V_E	V_V	A_Z	Stations	V_N	V_E	V_V	A_Z
	mm/yr	mm/yr	mm/yr	°		mm/yr	mm/yr	mm/yr	°
BAHR	17.73	7.15	19.12	21.97	F031	12.26	10.55	16.17	40.72
DATM	15.55	13.49	20.58	40.95	F033	13.29	9.67	16.43	36.06
F001	12.66	13.28	18.35	46.37	F035	16.77	8.71	18.90	27.45
F002	11.91	11.85	16.80	44.86	F036	17.82	8.74	19.84	26.13
F005	10.22	8.00	12.98	38.07	F037	16.47	7.61	18.14	24.79
F006	9.22	6.68	11.39	35.90	F039	14.46	6.22	15.74	23.29
F007	8.56	5.44	10.14	32.46	F040	14.60	4.77	15.35	18.08
F008	7.87	4.25	8.94	28.35	F041	12.60	6.49	14.17	27.25
F009	7.64	3.19	8.28	22.70	F045	9.33	1.69	9.49	10.25
F010	8.45	3.38	9.10	21.77	F074	12.28	13.25	18.07	47.18
F012	10.86	7.23	13.05	33.68	F077	14.35	9.71	17.33	34.08
F013	12.94	7.99	15.21	31.69	F078	15.00	13.10	19.92	41.13
F016	12.70	12.24	17.64	43.94	HALY	8.41	3.37	9.06	21.85
F019	15.12	9.90	18.07	33.20	NAMA	12.34	11.51	16.88	43.02
F020	15.30	7.76	17.16	26.90	P049	16.47	9.98	19.26	31.22
F024	12.18	4.98	13.16	22.25	SOLA	15.12	7.60	16.93	26.70
F026	13.53	3.89	14.07	16.05	YIBL	21.00	10.80	23.62	27.21
F027	11.48	2.24	11.69	11.03					
F029	16.30	5.33	17.15	18.10					
F030	17.32	6.72	18.58	21.21					

V_N : velocity in northing (mm/yr)

V_E : velocity in easting (mm/yr)

V_V : vector velocity (mm/yr)

A_Z : azimuth in degree

Table I.4 Relative Arabian-Nubian station model velocities from McClusky et al. [2003]

Stations	V_N	V_E	V_V	A_Z	Stations	V_N	V_E	V_V	A_Z
	mm/yr	mm/yr	mm/yr	°		mm/yr	mm/yr	mm/yr	°
BAHR	14.94	4.64	15.64	17.25	F031	9.91	7.75	12.58	38.03
DATM	12.93	10.37	16.57	38.73	F033	10.85	6.95	12.89	32.65
F001	10.28	10.20	14.49	44.78	F035	14.05	6.05	15.30	23.29
F002	9.60	8.93	13.11	42.93	F036	15.02	6.06	16.19	21.98
F005	8.05	5.49	9.74	34.30	F037	13.77	5.06	14.67	20.17
F006	7.14	4.32	8.34	31.14	F039	11.93	3.84	12.53	17.86
F007	6.53	3.22	7.28	26.24	F040	12.06	2.54	12.32	11.88
F008	5.91	2.16	6.29	20.11	F041	10.22	4.10	11.02	21.87
F009	5.69	1.23	5.83	12.17	F045	7.24	-0.14	7.24	-1.09
F010	6.44	1.38	6.59	12.08	F074	9.93	10.18	14.23	45.72
F012	8.63	4.79	9.87	29.04	F077	11.83	6.98	13.74	30.52
F013	10.54	5.44	11.86	27.32	F078	12.43	10.02	15.96	38.88
F016	10.32	9.26	13.87	41.93	HALY	6.40	1.38	6.55	12.14
F019	12.54	7.13	14.42	29.64	NAMA	9.99	8.62	13.19	40.78
F020	12.70	5.21	13.73	22.31	P049	13.77	7.19	15.54	27.58
F024	9.84	2.76	10.22	15.67	SOLA	12.54	5.07	13.53	22.03
F026	11.08	1.77	11.22	9.07	YIBL	17.96	7.88	19.61	23.69
F027	9.20	0.32	9.21	2.00					
F029	13.62	3.02	13.95	12.49					
F030	14.56	4.25	15.17	16.29					

V_N : velocity in northing (mm/yr)

V_E : velocity in easting (mm/yr)

V_V : vector velocity (mm/yr)

A_Z : azimuth in degree

Table I.5: Relative Arabian-Nubian station model velocities from Reilinger et al. [2006]

Stations	V_N	V_E	V_V	A_Z	Stations	V_N	V_E	V_V	A_Z
	mm/yr	mm/yr	mm/yr	°		mm/yr	mm/yr	mm/yr	°
BAHR	15.99	5.73	16.99	19.71	F031	10.73	9.01	14.01	40.02
DATM	13.89	11.78	18.21	40.30	F033	11.72	8.17	14.28	34.88
F001	11.12	11.60	16.07	46.22	F035	15.07	7.22	16.71	25.60
F002	10.40	10.25	14.60	44.59	F036	16.08	7.24	17.63	24.23
F005	8.78	6.61	10.99	37.00	F037	14.78	6.17	16.01	22.68
F006	7.82	5.37	9.49	34.45	F039	12.84	4.88	13.74	20.82
F007	7.19	4.20	8.33	30.33	F040	12.98	3.50	13.44	15.09
F008	6.53	3.08	7.22	25.27	F041	11.06	5.15	12.20	24.99
F009	6.31	2.09	6.64	18.34	F045	7.93	0.65	7.96	4.67
F010	7.09	2.25	7.44	17.63	F074	10.75	11.58	15.80	47.12
F012	9.39	5.88	11.08	32.05	F077	12.74	8.20	15.15	32.75
F013	11.39	6.57	13.15	29.99	F078	13.37	11.41	17.58	40.49
F016	11.15	10.61	15.39	43.57	HALY	7.05	2.25	7.40	17.71
F019	13.48	8.36	15.87	31.81	NAMA	10.81	9.92	14.67	42.55
F020	13.65	6.33	15.05	24.88	P049	14.78	8.43	17.01	29.71
F024	10.66	3.73	11.29	19.29	SOLA	13.48	6.19	14.83	24.65
F026	11.95	2.68	12.25	12.65	YIBL	19.15	9.17	21.23	25.57
F027	9.98	1.14	10.05	6.52					
F029	14.62	4.01	15.16	15.35					
F030	15.60	5.32	16.48	18.84					

V_N : velocity in northing (mm/yr)

V_E : velocity in easting (mm/yr)

V_V : vector velocity (mm/yr)

A_Z : azimuth in degree

Table I.6: Relative Arabian-Nubian station model velocities from REVEL-2000 [*Sella et al.*, 2002]

Stations	V_N	V_E	V_V	A_Z	Stations	V_N	V_E	V_V	A_Z
	mm/yr	mm/yr	mm/yr	°		mm/yr	mm/yr	mm/yr	°
BAHR	13.67	5.15	14.61	20.65	F031	8.15	8.74	11.95	46.98
DATM	11.45	11.53	16.25	45.18	F033	9.18	7.84	12.07	40.48
F001	8.56	11.41	14.26	53.13	F035	12.69	6.74	14.37	27.97
F002	7.81	10.03	12.71	52.09	F036	13.75	6.72	15.31	26.04
F005	6.13	6.32	8.80	45.90	F037	12.39	5.66	13.62	24.56
F006	5.14	5.07	7.22	44.60	F039	10.36	4.39	11.25	22.97
F007	4.48	3.90	5.94	41.00	F040	10.50	2.95	10.91	15.69
F008	3.80	2.77	4.70	36.03	F041	8.49	4.74	9.73	29.14
F009	3.57	1.76	3.98	26.19	F045	5.25	0.21	5.25	2.31
F010	4.38	1.89	4.77	23.38	F074	8.18	11.40	14.03	54.34
F012	6.76	5.54	8.74	39.35	F077	10.25	7.83	12.90	37.37
F013	8.84	6.19	10.79	35.02	F078	10.90	11.16	15.60	45.66
F016	8.59	10.38	13.48	50.38	HALY	4.34	1.89	4.73	23.58
F019	11.03	7.98	13.61	35.90	NAMA	8.24	9.68	12.71	49.61
F020	11.21	5.87	12.65	27.63	P049	12.39	8.01	14.75	32.90
F024	8.08	3.28	8.72	22.10	SOLA	11.03	5.72	12.42	27.41
F026	9.43	2.14	9.67	12.82	YIBL	17.01	8.63	19.08	26.90
F027	7.38	0.63	7.41	4.92					
F029	12.22	3.42	12.69	15.62					
F030	13.25	4.74	14.07	19.69					

V_N : velocity in northing (mm/yr)

V_E : velocity in easting (mm/yr)

V_V : vector velocity (mm/yr)

A_Z : azimuth in degree

Table I.7: Relative Arabian-Nubian station model velocities from *Vigny et al.* [2006]

Stations	V_N	V_E	V_V	A_Z	Stations	V_N	V_E	V_V	A_Z
	mm/yr	mm/yr	mm/yr	°		mm/yr	mm/yr	mm/yr	°
BAHR	14.73	5.09	15.58	19.05	F031	10.76	7.43	13.07	34.63
DATM	13.15	9.61	16.29	36.17	F033	11.51	6.81	13.37	30.62
F001	11.05	9.42	14.52	40.43	F035	14.03	6.18	15.33	23.79
F002	10.51	8.37	13.43	38.54	F036	14.79	6.23	16.05	22.84
F005	9.27	5.54	10.80	30.86	F037	13.81	5.38	14.82	21.29
F006	8.54	4.55	9.68	28.06	F039	12.36	4.34	13.10	19.34
F007	8.05	3.64	8.84	24.32	F040	12.46	3.28	12.88	14.77
F008	7.55	2.75	8.04	20.03	F041	11.01	4.49	11.89	22.18
F009	7.38	1.98	7.64	15.01	F045	8.62	0.92	8.67	6.09
F010	7.98	2.13	8.26	14.94	F074	10.77	9.39	14.29	41.08
F012	9.74	4.99	10.94	27.14	F077	12.28	6.86	14.07	29.18
F013	11.26	5.58	12.57	26.38	F078	12.75	9.32	15.80	36.17
F016	11.08	8.66	14.06	38.01	HALY	7.95	2.13	8.23	14.99
F019	12.84	7.01	14.63	28.62	NAMA	10.82	8.13	13.53	36.92
F020	12.97	5.47	14.07	22.86	P049	13.81	7.10	15.53	27.19
F024	10.70	3.38	11.22	17.55	SOLA	12.84	5.35	13.91	22.62
F026	11.68	2.62	11.97	12.66	YIBL	17.08	7.78	18.77	24.49
F027	10.19	1.37	10.28	7.68					
F029	13.69	3.73	14.19	15.25					
F030	14.43	4.76	15.20	18.27					

V_N : velocity in northing (mm/yr)

V_E : velocity in easting (mm/yr)

V_V : vector velocity (mm/yr)

A_Z : azimuth in degree

Table I.8: The difference between the relative Arabian-Nubian station model velocities from this study and from Chu and Gordon [1998]

Stations	ΔV_N	ΔV_E	ΔV_V	ΔA_Z	Stations	ΔV_N	ΔV_E	ΔV_V	ΔA_Z
	mm/yr	mm/yr	mm/yr	°		mm/yr	mm/yr	mm/yr	°
BAHR	-0.69	-0.20	-0.72	0.12	F031	-0.81	-0.08	-0.69	1.64
DATM	-0.74	-0.05	-0.61	1.24	F033	-0.79	-0.10	-0.72	1.28
F001	-0.80	-0.04	-0.60	1.77	F035	-0.71	-0.16	-0.72	0.50
F002	-0.81	-0.05	-0.63	1.85	F036	-0.69	-0.17	-0.70	0.36
F005	-0.84	-0.10	-0.75	1.89	F037	-0.72	-0.17	-0.74	0.36
F006	-0.86	-0.11	-0.79	1.97	F039	-0.76	-0.17	-0.78	0.38
F007	-0.87	-0.12	-0.82	1.84	F040	-0.76	-0.20	-0.79	0.00
F008	-0.88	-0.12	-0.86	1.57	F041	-0.80	-0.15	-0.79	0.80
F009	-0.89	-0.14	-0.89	0.90	F045	-0.86	-0.18	-0.87	-0.68
F010	-0.87	-0.14	-0.88	0.70	F074	-0.81	-0.03	-0.59	1.84
F012	-0.83	-0.12	-0.78	1.48	F077	-0.77	-0.11	-0.71	1.06
F013	-0.79	-0.13	-0.76	1.07	F078	-0.75	-0.06	-0.62	1.30
F016	-0.80	-0.05	-0.64	1.69	HALY	-0.87	-0.14	-0.88	0.71
F019	-0.75	-0.12	-0.71	0.93	NAMA	-0.81	-0.06	-0.65	1.71
F020	-0.75	-0.16	-0.75	0.56	P049	-0.72	-0.13	-0.70	0.73
F024	-0.81	-0.17	-0.82	0.44	SOLA	-0.75	-0.16	-0.75	0.55
F026	-0.78	-0.20	-0.81	-0.12	YIBL	-0.61	-0.17	-0.63	0.28
F027	-0.82	-0.20	-0.84	-0.53	Mean	-0.78	-0.13	-0.74	0.87
F029	-0.72	-0.21	-0.75	-0.06	S.dev	0.06	0.05	0.08	0.73
F030	-0.70	-0.20	-0.73	0.10	RMS	0.79	0.14	0.75	1.13

ΔV_N : velocity in northing (mm/yr)

ΔV_E : velocity in easting (mm/yr)

ΔV_V : vector velocity (mm/yr)

ΔA_Z : azimuth in degree

Table I.9: The difference between the relative Arabian-Nubian station model velocities from this study and from Jestin et al. [1994]

Stations	ΔV_N	ΔV_E	ΔV_V	ΔA_Z	Stations	ΔV_N	ΔV_E	ΔV_V	ΔA_Z
	mm/yr	Mm/yr	mm/yr	°		mm/yr	mm/yr	mm/yr	°
BAHR	-0.71	-1.19	-1.08	-2.66	F031	-0.66	-1.23	-1.30	-1.93
DATM	-0.69	-1.30	-1.36	-1.57	F033	-0.67	-1.22	-1.25	-2.22
F001	-0.67	-1.28	-1.39	-1.36	F035	-0.70	-1.21	-1.17	-2.44
F002	-0.66	-1.25	-1.34	-1.58	F036	-0.71	-1.22	-1.15	-2.41
F005	-0.64	-1.17	-1.22	-2.56	F037	-0.70	-1.19	-1.12	-2.65
F006	-0.63	-1.14	-1.17	-3.09	F039	-0.68	-1.15	-1.06	-3.08
F007	-0.63	-1.11	-1.10	-3.81	F040	-0.68	-1.12	-0.97	-3.41
F008	-0.62	-1.08	-1.02	-4.74	F041	-0.67	-1.15	-1.10	-3.15
F009	-0.61	-1.05	-0.94	-5.73	F045	-0.63	-1.03	-0.76	-5.90
F010	-0.62	-1.06	-0.94	-5.30	F074	-0.66	-1.28	-1.39	-1.32
F012	-0.65	-1.16	-1.17	-2.92	F077	-0.68	-1.22	-1.24	-2.24
F013	-0.67	-1.18	-1.18	-2.68	F078	-0.69	-1.29	-1.36	-1.60
F016	-0.67	-1.27	-1.36	-1.58	HALY	-0.62	-1.06	-0.93	-5.31
F019	-0.69	-1.23	-1.24	-2.22	NAMA	-0.66	-1.25	-1.33	-1.71
F020	-0.69	-1.19	-1.14	-2.68	P049	-0.70	-1.24	-1.23	-2.21
F024	-0.66	-1.12	-1.01	-3.70	SOLA	-0.69	-1.19	-1.13	-2.73
F026	-0.67	-1.10	-0.92	-3.79	YIBL	-0.73	-1.27	-1.22	-2.04
F027	-0.66	-1.05	-0.80	-4.77	Mean	-0.67	-1.18	-1.14	-2.94
F029	-0.70	-1.14	-0.99	-3.09	S.dev	0.03	0.08	0.16	1.24
F030	-0.71	-1.18	-1.06	-2.76	RMS	0.67	1.18	1.15	3.19

ΔV_N : velocity in northing (mm/yr)

ΔV_E : velocity in easting (mm/yr)

ΔV_V : vector velocity (mm/yr)

ΔA_Z : azimuth in degree

Table I.10: The difference between the relative Arabian-Nubian station model velocities from this study and from McClusky et al. [2003]

Stations	ΔV_N	ΔV_E	ΔV_V	ΔA_Z	Stations	ΔV_N	ΔV_E	ΔV_V	ΔA_Z
	mm/yr	Mm/yr	mm/yr	°		mm/yr	mm/yr	mm/yr	°
BAHR	2.09	1.33	2.40	2.06	F031	1.68	1.57	2.29	0.76
DATM	1.93	1.82	2.65	0.65	F033	1.76	1.50	2.29	1.19
F001	1.71	1.79	2.47	0.23	F035	2.02	1.45	2.43	1.72
F002	1.66	1.67	2.35	0.35	F036	2.09	1.46	2.50	1.74
F005	1.53	1.34	2.02	1.21	F037	1.99	1.36	2.35	1.97
F006	1.45	1.22	1.88	1.67	F039	1.85	1.23	2.15	2.35
F007	1.40	1.11	1.76	2.41	F040	1.86	1.11	2.06	2.79
F008	1.35	1.01	1.63	3.50	F041	1.71	1.23	2.05	2.23
F009	1.33	0.91	1.51	4.80	F045	1.46	0.80	1.49	5.44
F010	1.39	0.94	1.57	4.39	F074	1.68	1.79	2.45	0.14
F012	1.58	1.28	2.01	1.72	F077	1.84	1.51	2.35	1.32
F013	1.73	1.36	2.17	1.69	F078	1.89	1.79	2.60	0.65
F016	1.72	1.71	2.41	0.43	HALY	1.39	0.94	1.58	4.40
F019	1.90	1.53	2.41	1.34	NAMA	1.69	1.65	2.36	0.53
F020	1.91	1.36	2.29	1.91	P049	1.99	1.55	2.49	1.43
F024	1.68	1.10	1.93	2.88	SOLA	1.90	1.34	2.27	1.94
F026	1.78	1.02	1.93	3.19	YIBL	2.32	1.65	2.79	1.48
F027	1.62	0.87	1.68	4.26	Mean	1.75	1.34	2.17	2.04
F029	1.98	1.17	2.21	2.52	S.dev	0.24	0.29	0.34	1.34
F030	2.06	1.29	2.35	2.16	RMS	1.77	1.37	2.19	2.43

ΔV_N : velocity in northing (mm/yr)

ΔV_E : velocity in easting (mm/yr)

ΔV_V : vector velocity (mm/yr)

ΔA_Z : azimuth in degree

Table I.11: The difference between the relative Arabian-Nubian station model velocities from this study and from Reilinger et al. [2006]

Stations	ΔV_N	ΔV_E	ΔV_V	ΔA_Z	Stations	ΔV_N	ΔV_E	ΔV_V	ΔA_Z
	mm/yr	Mm/yr	mm/yr	°		mm/yr	mm/yr	mm/yr	°
BAHR	1.03	0.24	1.05	-0.40	F031	0.86	0.31	0.86	-1.23
DATM	0.96	0.41	1.01	-0.92	F033	0.90	0.29	0.90	-1.04
F001	0.88	0.39	0.89	-1.21	F035	1.00	0.28	1.02	-0.59
F002	0.85	0.35	0.86	-1.31	F036	1.03	0.28	1.06	-0.51
F005	0.80	0.22	0.77	-1.49	F037	0.99	0.24	1.01	-0.54
F006	0.77	0.17	0.73	-1.64	F039	0.93	0.19	0.94	-0.61
F007	0.75	0.13	0.71	-1.68	F040	0.94	0.14	0.94	-0.42
F008	0.72	0.09	0.70	-1.66	F041	0.87	0.18	0.87	-0.89
F009	0.72	0.05	0.70	-1.37	F045	0.77	0.01	0.77	-0.32
F010	0.74	0.06	0.72	-1.16	F074	0.86	0.39	0.88	-1.26
F012	0.82	0.20	0.80	-1.29	F077	0.93	0.29	0.94	-0.91
F013	0.88	0.23	0.88	-0.98	F078	0.95	0.40	0.98	-0.96
F016	0.88	0.36	0.89	-1.21	HALY	0.74	0.06	0.73	-1.17
F019	0.95	0.30	0.96	-0.83	NAMA	0.87	0.34	0.88	-1.24
F020	0.96	0.24	0.97	-0.66	P049	0.99	0.31	1.02	-0.70
F024	0.86	0.14	0.86	-0.74	SOLA	0.95	0.23	0.97	-0.68
F026	0.90	0.11	0.90	-0.39	YIBL	1.12	0.36	1.17	-0.40
F027	0.84	0.05	0.84	-0.26	Mean	0.89	0.23	0.90	-0.90
F029	0.99	0.17	1.00	-0.34	S.dev	0.10	0.11	0.12	0.42
F030	1.02	0.22	1.04	-0.39	RMS	0.90	0.25	0.91	0.99

ΔV_N : velocity in northing (mm/yr)

ΔV_E : velocity in easting (mm/yr)

ΔV_V : vector velocity (mm/yr)

ΔA_Z : azimuth in degree

Table I.12: The difference between the relative Arabian-Nubian station model velocities from this study and from REVEL-2000 [*Sella et al.*, 2002]

Stations	ΔV_N	ΔV_E	ΔV_V	ΔA_Z	Stations	ΔV_N	ΔV_E	ΔV_V	ΔA_Z
	mm/yr	Mm/yr	mm/yr	°		mm/yr	mm/yr	mm/yr	°
BAHR	3.35	0.81	3.43	-1.34	F031	3.44	0.58	2.92	-8.19
DATM	3.40	0.66	2.97	-5.80	F033	3.43	0.62	3.11	-6.64
F001	3.44	0.59	2.70	-8.12	F035	3.38	0.76	3.36	-2.96
F002	3.44	0.57	2.75	-8.81	F036	3.35	0.80	3.38	-2.32
F005	3.45	0.51	2.96	-10.39	F037	3.38	0.75	3.40	-2.42
F006	3.45	0.47	3.00	-11.79	F039	3.42	0.68	3.43	-2.76
F007	3.45	0.44	3.10	-12.35	F040	3.41	0.69	3.47	-1.02
F008	3.45	0.40	3.22	-12.42	F041	3.44	0.60	3.34	-5.04
F009	3.45	0.39	3.36	-9.22	F045	3.45	0.45	3.48	2.04
F010	3.45	0.42	3.39	-6.91	F074	3.44	0.57	2.65	-8.48
F012	3.45	0.53	3.14	-8.59	F077	3.42	0.66	3.19	-5.53
F013	3.43	0.61	3.24	-6.01	F078	3.41	0.65	2.96	-6.13
F016	3.44	0.59	2.80	-8.02	HALY	3.45	0.42	3.40	-7.04
F019	3.41	0.68	3.22	-4.92	NAMA	3.44	0.58	2.84	-8.30
F020	3.40	0.71	3.37	-3.41	P049	3.38	0.73	3.28	-3.89
F024	3.44	0.59	3.43	-3.55	SOLA	3.41	0.70	3.38	-3.44
F026	3.43	0.65	3.48	-0.56	YIBL	3.26	0.90	3.32	-1.73
F027	3.44	0.55	3.48	1.34	Mean	3.42	0.62	3.21	-5.31
F029	3.38	0.77	3.47	-0.61	S.dev	0.04	0.13	0.25	3.75
F030	3.36	0.80	3.45	-1.24	RMS	3.42	0.63	3.22	6.47

ΔV_N : velocity in northing (mm/yr)

ΔV_E : velocity in easting (mm/yr)

ΔV_V : vector velocity (mm/yr)

ΔA_Z : azimuth in degree

Table I.13: The difference between the relative Arabian-Nubian station model velocities from this study and from *Vigny et al.* [2006]

Stations	ΔV_N	ΔV_E	ΔV_V	ΔA_Z	Stations	ΔV_N	ΔV_E	ΔV_V	ΔA_Z
	mm/yr	Mm/yr	mm/yr	°		mm/yr	mm/yr	mm/yr	°
BAHR	2.30	0.88	2.46	0.26	F031	0.84	1.89	1.80	4.16
DATM	1.71	2.58	2.93	3.21	F033	1.11	1.64	1.81	3.22
F001	0.94	2.58	2.44	4.58	F035	2.04	1.31	2.40	1.22
F002	0.75	2.23	2.03	4.74	F036	2.32	1.29	2.64	0.88
F005	0.31	1.29	0.96	4.65	F037	1.95	1.03	2.20	0.85
F006	0.05	0.99	0.54	4.75	F039	1.42	0.73	1.58	0.87
F007	-0.12	0.69	0.20	4.33	F040	1.45	0.36	1.50	-0.10
F008	-0.30	0.42	-0.12	3.58	F041	0.93	0.85	1.18	1.92
F009	-0.36	0.16	-0.30	1.96	F045	0.08	-0.26	0.06	-1.74
F010	-0.15	0.19	-0.10	1.53	F074	0.84	2.58	2.39	4.78
F012	0.47	1.08	0.94	3.62	F077	1.39	1.63	2.02	2.66
F013	1.02	1.22	1.46	2.63	F078	1.56	2.49	2.76	3.36
F016	0.95	2.31	2.22	4.35	HALY	-0.16	0.19	-0.10	1.55
F019	1.59	1.66	2.20	2.36	NAMA	0.86	2.13	2.02	4.39
F020	1.64	1.10	1.95	1.36	P049	1.95	1.65	2.50	1.82
F024	0.82	0.48	0.93	1.00	SOLA	1.59	1.07	1.89	1.35
F026	1.17	0.17	1.18	-0.40	YIBL	3.20	1.75	3.63	0.68
F027	0.63	-0.19	0.61	-1.42	Mean	1.10	1.17	1.60	2.13
F029	1.91	0.45	1.97	-0.24	S.dev	0.85	0.81	0.98	1.85
F030	2.19	0.78	2.32	0.18	RMS	1.38	1.42	1.87	2.81

ΔV_N : velocity in northing (mm/yr)

ΔV_E : velocity in easting (mm/yr)

ΔV_V: vector velocity (mm/yr)

ΔA_Z : azimuth in degree

Appendix K: Relative station model velocities between Arabian plate and Somalain plate

Table K.1: Relative Arabian-Somalain station model velocities from this study using two stations on Somalain plate

Stations	V_N	V_E	V_V	A_Z	Stations	V_N	V_E	V_V	A_Z
	mm/yr	mm/yr	mm/yr	°		mm/yr	mm/yr	mm/yr	°
BAHR	17.32	-1.18	17.36	-3.88	F031	11.00	2.52	11.28	12.92
DATM	14.79	5.62	15.82	20.82	F033	12.18	1.57	12.28	7.35
F001	11.46	5.45	12.69	25.41	F035	16.20	0.48	16.21	1.71
F002	10.60	3.92	11.30	20.31	F036	17.42	0.49	17.42	1.63
F005	8.66	-0.13	8.66	-0.87	F037	15.85	-0.68	15.87	-2.45
F006	7.53	-1.50	7.67	-11.29	F039	13.53	-2.09	13.69	-8.79
F007	6.76	-2.78	7.31	-22.32	F040	13.69	-3.62	14.16	-14.81
F008	5.98	-4.00	7.20	-33.77	F041	11.39	-1.78	11.53	-8.88
F009	5.72	-5.08	7.65	-41.65	F045	7.65	-6.68	10.16	-41.12
F010	6.65	-4.92	8.27	-36.51	F074	11.02	5.42	12.28	26.20
F012	9.39	-0.96	9.44	-5.82	F077	13.41	1.59	13.50	6.77
F013	11.78	-0.21	11.79	-1.01	F078	14.16	5.21	15.08	20.20
F016	11.50	4.32	12.29	20.58	HALY	6.60	-4.92	8.23	-36.70
F019	14.30	1.77	14.41	7.07	NAMA	11.09	3.55	11.64	17.74
F020	14.50	-0.49	14.51	-1.95	P049	15.85	1.84	15.96	6.62
F024	10.91	-3.34	11.41	-17.04	SOLA	14.30	-0.66	14.31	-2.62
F026	12.46	-4.51	13.25	-19.89	YIBL	21.14	2.64	21.30	7.11
F027	10.10	-6.17	11.84	-31.40					
F029	15.66	-3.06	15.96	-11.07					
F030	16.84	-1.62	16.92	-5.51					

V_N : velocity in northing (mm/yr)

V_E : velocity in easting (mm/yr)

V_V : vector velocity (mm/yr)

A_Z : azimuth in degree

Appendix K: Relative station model velocities between Arabian plate and Somalain plate

Table K.2: Relative Arabian-Somalain station model velocities from this study using three stations on Somalain plate.

Stations	V_N	V_E	V_V	A_Z	Stations	V_N	V_E	V_V	A_Z
	mm/yr	mm/yr	mm/yr	°		mm/yr	mm/yr	mm/yr	°
BAHR	16.68	0.72	16.70	2.47	F031	10.98	4.07	11.71	20.33
DATM	14.40	6.93	15.98	25.70	F033	12.05	3.20	12.47	14.89
F001	11.40	6.75	13.25	30.63	F035	15.68	2.23	15.83	8.11
F002	10.62	5.35	11.89	26.73	F036	16.77	2.25	16.92	7.66
F005	8.87	1.61	9.01	10.28	F037	15.36	1.17	15.40	4.34
F006	7.84	0.34	7.85	2.46	F039	13.27	-0.16	13.27	-0.67
F007	7.15	-0.85	7.20	-6.75	F040	13.41	-1.56	13.50	-6.64
F008	6.44	-1.98	6.74	-17.12	F041	11.33	0.12	11.33	0.59
F009	6.20	-2.99	6.88	-25.73	F045	7.96	-4.45	9.11	-29.21
F010	7.04	-2.83	7.59	-21.87	F074	11.00	6.73	12.90	31.43
F012	9.53	0.85	9.57	5.13	F077	13.16	3.23	13.55	13.79
F013	11.69	1.57	11.80	7.63	F078	13.83	6.55	15.30	25.34
F016	11.44	5.72	12.79	26.56	HALY	7.00	-2.83	7.55	-21.99
F019	13.96	3.40	14.37	13.70	NAMA	11.07	5.01	12.15	24.36
F020	14.14	1.32	14.21	5.35	P049	15.36	3.48	15.75	12.75
F024	10.90	-1.33	10.98	-6.96	SOLA	13.96	1.17	14.01	4.81
F026	12.30	-2.39	12.53	-11.00	YIBL	20.11	4.25	20.55	11.92
F027	10.17	-3.95	10.91	-21.21					
F029	15.19	-1.03	15.22	-3.89					
F030	16.25	0.30	16.25	1.07					

V_N : velocity in northing (mm/yr)

V_E : velocity in easting (mm/yr)

V_V : vector velocity (mm/yr)

A_Z : azimuth in degree

Appendix K: Relative station model velocities between Arabian plate and Somalain plate

Table K.3: Relative Arabian-Somalain station model velocities from CGPS2004 [*Prawirodirdjo and Yehuda Bock*, 2004]

Stations	V_N	V_E	V_V	A_Z	Stations	V_N	V_E	V_V	A_Z
	mm/yr	mm/yr	mm/yr	°		mm/yr	mm/yr	mm/yr	°
BAHR	19.01	-3.54	19.34	-10.55	F031	12.15	0.36	12.16	1.68
DATM	16.27	3.68	16.68	12.74	F033	13.44	-0.65	13.45	-2.78
F001	12.66	3.48	13.13	15.37	F035	17.80	-1.79	17.89	-5.74
F002	11.72	1.85	11.87	8.97	F036	19.12	-1.77	19.20	-5.29
F005	9.62	-2.48	9.93	-14.45	F037	17.42	-3.02	17.68	-9.85
F006	8.39	-3.94	9.27	-25.17	F039	14.90	-4.54	15.58	-16.94
F007	7.56	-5.30	9.23	-35.02	F040	15.08	-6.15	16.28	-22.20
F008	6.71	-6.60	9.41	-44.52	F041	12.58	-4.22	13.27	-18.53
F009	6.42	-7.75	10.06	-50.35	F045	8.52	-9.43	12.71	-47.89
F010	7.43	-7.57	10.61	-45.53	F074	12.18	3.45	12.66	15.83
F012	10.41	-3.35	10.94	-17.86	F077	14.77	-0.63	14.79	-2.43
F013	13.01	-2.55	13.26	-11.07	F078	15.58	3.24	15.91	11.73
F016	12.70	2.28	12.91	10.15	HALY	7.38	-7.57	10.57	-45.72
F019	15.73	-0.43	15.74	-1.56	NAMA	12.26	1.45	12.34	6.75
F020	15.96	-2.84	16.21	-10.08	P049	17.42	-0.35	17.43	-1.15
F024	12.06	-5.88	13.41	-26.00	SOLA	15.74	-3.01	16.02	-10.83
F026	13.74	-7.10	15.47	-27.33	YIBL	23.15	0.53	23.16	1.31
F027	11.19	-8.87	14.28	-38.43					
F029	17.22	-5.55	18.09	-17.88					
F030	18.50	-4.02	18.93	-12.26					

V_N : velocity in northing (mm/yr)

V_E : velocity in easting (mm/yr)

V_V : vector velocity (mm/yr)

A_Z : azimuth in degree

Appendix K: Relative station model velocities between Arabian plate and Somalain plate

Table K.4: Relative Arabian-Somalain station model velocities from NUVEL-1A [*DeMets, et al.*, 1994]

Stations	V_N	V_E	V_V	A_Z	Stations	V_N	V_E	V_V	A_Z
	mm/yr	mm/yr	mm/yr	°		mm/yr	mm/yr	mm/yr	°
BAHR	18.19	0.37	18.20	1.17	F031	12.50	3.60	13.01	16.07
DATM	15.92	6.50	17.20	22.20	F033	13.57	2.75	13.85	11.47
F001	12.92	6.28	14.37	25.91	F035	17.19	1.85	17.29	6.15
F002	12.15	4.87	13.09	21.87	F036	18.28	1.89	18.38	5.91
F005	10.39	1.12	10.45	6.14	F037	16.88	0.79	16.90	2.67
F006	9.36	-0.17	9.36	-1.04	F039	14.79	-0.56	14.80	-2.19
F007	8.66	-1.36	8.77	-8.94	F040	14.93	-1.96	15.06	-7.47
F008	7.95	-2.51	8.34	-17.53	F041	12.86	-0.33	12.86	-1.47
F009	7.71	-3.52	8.47	-24.54	F045	9.47	-4.94	10.68	-27.56
F010	8.56	-3.34	9.19	-21.34	F074	12.53	6.25	14.00	26.52
F012	11.05	0.38	11.06	1.94	F077	14.68	2.80	14.95	10.79
F013	13.22	1.12	13.26	4.84	F078	15.36	6.11	16.53	21.70
F016	12.96	5.25	13.99	22.06	HALY	8.51	-3.34	9.15	-21.45
F019	15.48	2.98	15.77	10.91	NAMA	12.59	4.54	13.39	19.83
F020	15.67	0.92	15.69	3.36	P049	16.88	3.08	17.16	10.34
F024	12.42	-1.78	12.55	-8.15	SOLA	15.48	0.77	15.50	2.84
F026	13.82	-2.81	14.11	-11.47	YIBL	21.60	3.92	21.95	10.30
F027	11.70	-4.40	12.50	-20.61					
F029	16.71	-1.40	16.77	-4.78					
F030	17.77	-0.05	17.77	-0.16					

V_N : velocity in northing (mm/yr)

V_E : velocity in easting (mm/yr)

V_V : vector velocity (mm/yr)

A_Z : azimuth in degree

Appendix K: Relative station model velocities between Arabian plate and Somalain plate

Table K.5: Relative Arabian-Somalain station model velocities from Jestin et al. [1994]

Stations	V_N	V_E	V_V	A_Z	Stations	V_N	V_E	V_V	A_Z
	mm/yr	mm/yr	mm/yr	°		mm/yr	mm/yr	mm/yr	°
BAHR	19.47	1.40	19.52	4.11	F031	13.53	4.79	14.35	19.47
DATM	17.10	7.84	18.81	24.64	F033	14.65	3.90	15.16	14.90
F001	13.97	7.61	15.91	28.56	F035	18.43	2.96	18.66	9.12
F002	13.16	6.12	14.52	24.96	F036	19.56	3.00	19.79	8.73
F005	11.32	2.16	11.53	10.80	F037	18.10	1.83	18.19	5.78
F006	10.24	0.80	10.28	4.45	F039	15.92	0.40	15.93	1.44
F007	9.52	-0.47	9.53	-2.80	F040	16.07	-1.07	16.11	-3.81
F008	8.78	-1.68	8.94	-10.85	F041	13.90	0.64	13.92	2.64
F009	8.52	-2.75	8.95	-17.88	F045	10.36	-4.25	11.20	-22.28
F010	9.41	-2.56	9.75	-15.21	F074	13.56	7.57	15.53	29.19
F012	12.02	1.38	12.09	6.55	F077	15.81	3.95	16.29	14.02
F013	14.28	2.17	14.44	8.65	F078	16.51	7.44	18.11	24.25
F016	14.01	6.53	15.46	24.97	HALY	9.36	-2.56	9.71	-15.29
F019	16.64	4.14	17.15	13.99	NAMA	13.62	5.78	14.80	22.97
F020	16.83	1.97	16.95	6.68	P049	18.10	4.25	18.59	13.21
F024	13.45	-0.89	13.48	-3.79	SOLA	16.64	1.81	16.74	6.21
F026	14.91	-1.97	15.04	-7.52	YIBL	23.01	5.15	23.58	12.62
F027	12.69	-3.66	13.21	-16.10					
F029	17.92	-0.47	17.93	-1.50					
F030	19.02	0.95	19.05	2.87					

V_N : velocity in northing (mm/yr)

V_E : velocity in easting (mm/yr)

V_V : vector velocity (mm/yr)

A_Z : azimuth in degree

Table K.6: Relative Arabian-Somalain station model velocities from Reilinger et al. [2006]

Stations	V_N	V_E	V_V	A_Z	Stations	V_N	V_E	V_V	A_Z
	mm/yr	mm/yr	mm/yr	°		mm/yr	mm/yr	mm/yr	°
BAHR	18.71	-3.39	19.01	-10.27	F031	11.91	0.49	11.92	2.35
DATM	15.98	3.78	16.43	13.30	F033	13.18	-0.52	13.19	-2.24
F001	12.41	3.58	12.92	16.11	F035	17.51	-1.65	17.59	-5.38
F002	11.48	1.97	11.65	9.73	F036	18.81	-1.63	18.88	-4.96
F005	9.40	-2.32	9.68	-13.88	F037	17.13	-2.87	17.37	-9.52
F006	8.18	-3.77	9.00	-24.76	F039	14.63	-4.37	15.27	-16.64
F007	7.36	-5.12	8.96	-34.81	F040	14.81	-5.98	15.97	-21.98
F008	6.52	-6.41	9.14	-44.51	F041	12.33	-4.05	12.98	-18.18
F009	6.23	-7.54	9.78	-50.45	F045	8.31	-9.22	12.41	-47.95
F010	7.23	-7.37	10.32	-45.55	F074	11.94	3.56	12.46	16.60
F012	10.18	-3.19	10.67	-17.40	F077	14.50	-0.49	14.51	-1.94
F013	12.76	-2.39	12.98	-10.63	F078	15.31	3.34	15.67	12.31
F016	12.45	2.39	12.68	10.86	HALY	7.18	-7.37	10.29	-45.75
F019	15.46	-0.30	15.46	-1.10	NAMA	12.01	1.57	12.11	7.46
F020	15.68	-2.69	15.91	-9.72	P049	17.13	-0.22	17.13	-0.74
F024	11.81	-5.70	13.12	-25.76	SOLA	15.46	-2.86	15.72	-10.47
F026	13.48	-6.91	15.15	-27.15	YIBL	22.81	0.64	22.82	1.62
F027	10.95	-8.67	13.97	-38.37					
F029	16.93	-5.38	17.76	-17.65					
F030	18.20	-3.86	18.60	-11.99					

V_N : velocity in northing (mm/yr)

V_E : velocity in easting (mm/yr)

V_V : vector velocity (mm/yr)

A_Z : azimuth in degree

Appendix K: Relative station model velocities between Arabian plate and Somalain plate

Table K.7: Relative Arabian-Somalain station model velocities from REVEL2000 [*Sella, et al.*, 2002]

Stations	V_N	V_E	V_V	A_Z	Stations	V_N	V_E	V_V	A_Z
	mm/yr	mm/yr	mm/yr	°		mm/yr	mm/yr	mm/yr	°
BAHR	17.14	-2.81	17.37	-9.31	F031	10.54	1.04	10.59	5.64
DATM	14.49	4.21	15.09	16.21	F033	11.77	0.05	11.77	0.25
F001	11.02	4.05	11.74	20.18	F035	15.98	-1.10	16.01	-3.92
F002	10.13	2.49	10.43	13.79	F036	17.24	-1.09	17.28	-3.62
F005	8.11	-1.67	8.28	-11.67	F037	15.61	-2.29	15.77	-8.34
F006	6.92	-3.07	7.57	-23.94	F039	13.18	-3.73	13.70	-15.78
F007	6.13	-4.37	7.53	-35.51	F040	13.35	-5.29	14.36	-21.63
F008	5.32	-5.62	7.74	-46.59	F041	10.95	-3.39	11.46	-17.19
F009	5.04	-6.73	8.41	-53.16	F045	7.05	-8.38	10.95	-49.90
F010	6.01	-6.57	8.90	-47.55	F074	10.56	4.03	11.31	20.88
F012	8.87	-2.53	9.22	-15.92	F077	13.06	0.06	13.06	0.28
F013	11.36	-1.78	11.50	-8.88	F078	13.84	3.79	14.35	15.33
F016	11.07	2.89	11.44	14.62	HALY	5.96	-6.57	8.87	-47.78
F019	13.98	0.25	13.98	1.01	NAMA	10.64	2.10	10.84	11.14
F020	14.20	-2.09	14.35	-8.37	P049	15.61	0.30	15.61	1.11
F024	10.45	-4.99	11.58	-25.53	SOLA	13.98	-2.25	14.16	-9.16
F026	12.06	-6.19	13.56	-27.18	YIBL	21.14	1.09	21.17	2.96
F027	9.61	-7.88	12.43	-39.34					
F029	15.41	-4.74	16.12	-17.10					
F030	16.64	-3.27	16.96	-11.11					

V_N : velocity in northing (mm/yr)

V_E : velocity in easting (mm/yr)

V_V : vector velocity (mm/yr)

A_Z : azimuth in degree

Table K.8: Relative Arabian-Somalain station model velocities from Vigny et al. [2006]

Stations	V_N	V_E	V_V	A_Z	Stations	V_N	V_E	V_V	A_Z
	mm/yr	mm/yr	mm/yr	°		mm/yr	mm/yr	mm/yr	°
BAHR	15.79	-2.59	16.00	-9.30	F031	10.53	0.34	10.53	1.84
DATM	13.69	2.93	14.00	12.06	F033	11.51	-0.43	11.52	-2.12
F001	10.91	2.75	11.25	14.12	F035	14.86	-1.26	14.92	-4.83
F002	10.20	1.48	10.30	8.28	F036	15.87	-1.23	15.92	-4.42
F005	8.58	-1.87	8.78	-12.30	F037	14.57	-2.21	14.74	-8.61
F006	7.62	-3.01	8.20	-21.54	F039	12.64	-3.40	13.09	-15.05
F007	6.99	-4.07	8.08	-30.20	F040	12.77	-4.64	13.59	-19.96
F008	6.33	-5.08	8.12	-38.74	F041	10.85	-3.18	11.31	-16.32
F009	6.11	-5.97	8.54	-44.35	F045	7.73	-7.24	10.59	-43.14
F010	6.89	-5.82	9.02	-40.20	F074	10.55	2.72	10.89	14.47
F012	9.19	-2.54	9.53	-15.44	F077	12.54	-0.39	12.55	-1.80
F013	11.18	-1.89	11.34	-9.58	F078	13.16	2.58	13.41	11.09
F016	10.95	1.82	11.10	9.43	HALY	6.85	-5.82	8.99	-40.37
F019	13.28	-0.23	13.28	-1.01	NAMA	10.61	1.18	10.67	6.35
F020	13.45	-2.08	13.61	-8.79	P049	14.57	-0.16	14.57	-0.61
F024	10.45	-4.46	11.37	-23.13	SOLA	13.28	-2.22	13.46	-9.47
F026	11.75	-5.38	12.92	-24.63	YIBL	18.95	0.58	18.96	1.75
F027	9.78	-6.78	11.90	-34.73					
F029	14.41	-4.15	15.00	-16.07					
F030	15.40	-2.96	15.68	-10.88					

V_N : velocity in northing (mm/yr)

V_E : velocity in easting (mm/yr)

V_V : vector velocity (mm/yr)

A_Z : azimuth in degree

Table K.9: The difference between the relative Arabian-Somalain station model velocities from this study (two stations) and from CGPS2004 [*Prawirodirdjo and Yehuda Bock*, 2004]

Stations	ΔV_N	ΔV_E	ΔV_V	ΔA_Z	Stations	ΔV_N	ΔV_E	ΔV_V	ΔA_Z
	mm/yr	mm/yr	mm/yr	°		mm/yr	mm/yr	mm/yr	°
BAHR	-1.69	2.37	-1.98	6.67	F031	-1.16	2.17	-0.88	11.24
DATM	-1.48	1.94	-0.86	8.08	F033	-1.26	2.22	-1.17	10.13
F001	-1.20	1.97	-0.44	10.04	F035	-1.60	2.27	-1.68	7.45
F002	-1.12	2.07	-0.57	11.34	F036	-1.70	2.26	-1.78	6.92
F005	-0.96	2.35	-1.27	13.58	F037	-1.57	2.35	-1.81	7.40
F006	-0.86	2.44	-1.60	13.88	F039	-1.37	2.45	-1.89	8.15
F007	-0.80	2.52	-1.92	12.70	F040	-1.39	2.54	-2.12	7.39
F008	-0.73	2.60	-2.21	10.75	F041	-1.19	2.44	-1.74	9.65
F009	-0.71	2.66	-2.41	8.70	F045	-0.87	2.75	-2.55	6.77
F010	-0.79	2.65	-2.34	9.02	F074	-1.16	1.97	-0.38	10.37
F012	-1.02	2.40	-1.50	12.04	F077	-1.36	2.22	-1.29	9.20
F013	-1.22	2.34	-1.47	10.06	F078	-1.43	1.97	-0.83	8.47
F016	-1.20	2.04	-0.62	10.43	HALY	-0.78	2.65	-2.34	9.02
F019	-1.44	2.20	-1.33	8.63	NAMA	-1.17	2.10	-0.70	10.99
F020	-1.46	2.34	-1.70	8.13	P049	-1.57	2.19	-1.47	7.77
F024	-1.15	2.54	-2.00	8.96	SOLA	-1.44	2.35	-1.71	8.21
F026	-1.28	2.60	-2.22	7.44	YIBL	-2.02	2.11	-1.86	5.80
F027	-1.08	2.71	-2.44	7.03	Mean	-1.25	2.34	-1.60	9.08
F029	-1.55	2.49	-2.13	6.81	S.dev	0.31	0.23	0.61	2.02
F030	-1.65	2.40	-2.01	6.75	RMS	1.29	2.35	1.71	9.30

ΔV_N : velocity in northing (mm/yr)

ΔV_E : velocity in easting (mm/yr)

ΔV_V : vector velocity (mm/yr)

ΔA_Z : azimuth in degree

Table K.10: The difference between the relative Arabian-Somalain station model velocities from this study (two stations) and from NUVEL-1A [*DeMets, et al.*, 1994]

Stations	ΔV_N	ΔV_E	ΔV_V	ΔA_Z	Stations	ΔV_N	ΔV_E	ΔV_V	ΔA_Z
	mm/yr	Mm/yr	mm/yr	°		mm/yr	mm/yr	mm/yr	°
BAHR	-0.87	-1.55	-0.84	-5.05	F031	-1.51	-1.08	-1.73	-3.15
DATM	-1.14	-0.88	-1.38	-1.38	F033	-1.39	-1.18	-1.57	-4.12
F001	-1.46	-0.83	-1.68	-0.50	F035	-0.99	-1.37	-1.08	-4.44
F002	-1.55	-0.95	-1.79	-1.56	F036	-0.86	-1.40	-0.96	-4.28
F005	-1.73	-1.25	-1.79	-7.01	F037	-1.03	-1.46	-1.03	-5.12
F006	-1.83	-1.33	-1.69	-10.25	F039	-1.26	-1.53	-1.11	-6.60
F007	-1.90	-1.41	-1.46	-13.38	F040	-1.24	-1.66	-0.90	-7.34
F008	-1.97	-1.49	-1.14	-16.24	F041	-1.47	-1.45	-1.33	-7.41
F009	-1.99	-1.56	-0.82	-17.11	F045	-1.82	-1.74	-0.52	-13.56
F010	-1.91	-1.58	-0.92	-15.17	F074	-1.51	-0.83	-1.72	-0.32
F012	-1.66	-1.33	-1.62	-7.76	F077	-1.27	-1.21	-1.45	-4.02
F013	-1.43	-1.33	-1.47	-5.85	F078	-1.20	-0.90	-1.45	-1.50
F016	-1.46	-0.93	-1.70	-1.48	HALY	-1.91	-1.57	-0.92	-15.25
F019	-1.19	-1.21	-1.36	-3.84	NAMA	-1.50	-0.99	-1.75	-2.09
F020	-1.16	-1.41	-1.18	-5.31	P049	-1.03	-1.24	-1.20	-3.72
F024	-1.52	-1.56	-1.14	-8.89	SOLA	-1.18	-1.42	-1.19	-5.46
F026	-1.37	-1.70	-0.86	-8.42	YIBL	-0.46	-1.29	-0.65	-3.19
F027	-1.59	-1.77	-0.66	-10.79	Mean	-1.39	-1.34	-1.24	-6.57
F029	-1.05	-1.67	-0.81	-6.29	S.dev	0.36	0.27	0.37	4.60
F030	-0.92	-1.57	-0.85	-5.35	RMS	1.43	1.37	1.29	7.99

ΔV_N : velocity in northing (mm/yr)

ΔV_E : velocity in easting (mm/yr)

ΔV_V : vector velocity (mm/yr)

ΔA_Z : azimuth in degree

Table K.11: The difference between the relative Arabian-Somalain station model velocities from this study (two stations) and from Jestin et al. [1994]

Stations	ΔV_N	ΔV_E	ΔV_V	ΔA_Z	Stations	ΔV_N	ΔV_E	ΔV_V	ΔA_Z
	mm/yr	Mm/yr	mm/yr	°		mm/yr	mm/yr	mm/yr	°
BAHR	-2.15	-2.57	-2.16	-7.99	F031	-2.54	-2.26	-3.07	-6.55
DATM	-2.32	-2.22	-2.99	-3.82	F033	-2.47	-2.33	-2.88	-7.55
F001	-2.51	-2.16	-3.22	-3.15	F035	-2.22	-2.48	-2.45	-7.41
F002	-2.56	-2.20	-3.22	-4.65	F036	-2.14	-2.51	-2.37	-7.10
F005	-2.66	-2.29	-2.87	-11.67	F037	-2.25	-2.51	-2.32	-8.23
F006	-2.72	-2.30	-2.61	-15.74	F039	-2.39	-2.49	-2.24	-10.23
F007	-2.76	-2.31	-2.22	-19.52	F040	-2.38	-2.55	-1.95	-11.00
F008	-2.79	-2.32	-1.74	-22.92	F041	-2.52	-2.42	-2.39	-11.52
F009	-2.81	-2.33	-1.30	-23.77	F045	-2.71	-2.43	-1.04	-18.84
F010	-2.76	-2.36	-1.48	-21.30	F074	-2.54	-2.15	-3.25	-2.99
F012	-2.62	-2.34	-2.65	-12.37	F077	-2.40	-2.36	-2.79	-7.25
F013	-2.49	-2.38	-2.65	-9.66	F078	-2.35	-2.23	-3.03	-4.05
F016	-2.51	-2.21	-3.17	-4.39	HALY	-2.76	-2.36	-1.48	-21.41
F019	-2.34	-2.37	-2.74	-6.92	NAMA	-2.53	-2.23	-3.16	-5.23
F020	-2.33	-2.47	-2.44	-8.63	P049	-2.25	-2.41	-2.63	-6.59
F024	-2.54	-2.45	-2.07	-13.25	SOLA	-2.34	-2.47	-2.43	-8.83
F026	-2.45	-2.54	-1.79	-12.37	YIBL	-1.88	-2.52	-2.28	-5.51
F027	-2.59	-2.51	-1.37	-15.30	Mean	-2.46	-2.38	-2.39	-10.42
F029	-2.26	-2.59	-1.97	-9.57	S.dev	0.21	0.13	0.59	5.81
F030	-2.18	-2.58	-2.13	-8.38	RMS	2.47	2.39	2.46	11.89

ΔV_N : velocity in northing (mm/yr)

ΔV_E : velocity in easting (mm/yr)

ΔV_V : vector velocity (mm/yr)

ΔA_Z : azimuth in degree

Table K.12: The difference between the relative Arabian-Somalain station model velocities from this study(two stations) and from Reilinger et al. [2006]

Stations	ΔV_N	ΔV_E	ΔV_V	ΔA_Z	Stations	ΔV_N	ΔV_E	ΔV_V	ΔA_Z
	mm/yr	Mm/yr	mm/yr	°		mm/yr	mm/yr	mm/yr	°
BAHR	-1.39	2.21	-1.65	6.39	F031	-0.91	2.04	-0.64	10.57
DATM	-1.20	1.84	-0.61	7.52	F033	-1.00	2.09	-0.91	9.59
F001	-0.95	1.86	-0.23	9.30	F035	-1.31	2.13	-1.38	7.09
F002	-0.88	1.95	-0.35	10.58	F036	-1.40	2.13	-1.46	6.59
F005	-0.74	2.19	-1.02	13.01	F037	-1.28	2.20	-1.50	7.07
F006	-0.65	2.27	-1.33	13.47	F039	-1.10	2.28	-1.58	7.85
F007	-0.59	2.34	-1.65	12.49	F040	-1.12	2.36	-1.81	7.17
F008	-0.53	2.40	-1.94	10.74	F041	-0.94	2.27	-1.45	9.30
F009	-0.51	2.46	-2.13	8.80	F045	-0.66	2.54	-2.25	6.83
F010	-0.58	2.45	-2.05	9.04	F074	-0.91	1.86	-0.18	9.60
F012	-0.79	2.23	-1.23	11.58	F077	-1.09	2.08	-1.01	8.71
F013	-0.97	2.19	-1.19	9.62	F078	-1.15	1.87	-0.59	7.89
F016	-0.95	1.93	-0.39	9.72	HALY	-0.58	2.45	-2.06	9.05
F019	-1.16	2.07	-1.05	8.17	NAMA	-0.92	1.98	-0.47	10.28
F020	-1.18	2.19	-1.40	7.77	P049	-1.28	2.06	-1.17	7.36
F024	-0.91	2.36	-1.71	8.72	SOLA	-1.16	2.20	-1.41	7.85
F026	-1.02	2.41	-1.90	7.26	YIBL	-1.68	1.99	-1.52	5.49
F027	-0.85	2.50	-2.13	6.97	Mean	-1.00	2.19	-1.32	8.72
F029	-1.26	2.32	-1.80	6.58	S.dev	0.28	0.20	0.58	1.93
F030	-1.35	2.24	-1.68	6.48	RMS	1.04	2.20	1.44	8.92

ΔV_N : velocity in northing (mm/yr)

ΔV_E : velocity in easting (mm/yr)

ΔV_V : vector velocity (mm/yr)

ΔA_Z : azimuth in degree

Appendix K: Relative station model velocities between Arabian plate and Somalain plate

Table K.13: The difference between the relative Arabian-Somalain station model velocities from this study (two stations) and from REVEL2000 [*Sella, et al.*, 2002]

Stations	ΔV_N	ΔV_E	ΔV_V	ΔA_Z	Stations	ΔV_N	ΔV_E	ΔV_V	ΔA_Z
	mm/yr	Mm/yr	mm/yr	°		mm/yr	mm/yr	mm/yr	°
BAHR	0.18	1.63	-0.01	5.43	F031	0.46	1.48	0.69	7.28
DATM	0.29	1.41	0.73	4.61	F033	0.41	1.52	0.51	7.10
F001	0.44	1.39	0.95	5.23	F035	0.23	1.58	0.20	5.63
F002	0.47	1.44	0.87	6.52	F036	0.17	1.59	0.14	5.25
F005	0.56	1.54	0.38	10.80	F037	0.24	1.61	0.10	5.89
F006	0.60	1.57	0.10	12.65	F039	0.35	1.63	-0.01	6.99
F007	0.63	1.60	-0.22	13.19	F040	0.34	1.67	-0.20	6.82
F008	0.66	1.62	-0.54	12.82	F041	0.44	1.61	0.07	8.31
F009	0.68	1.64	-0.76	11.51	F045	0.60	1.70	-0.79	8.78
F010	0.64	1.65	-0.63	11.04	F074	0.46	1.39	0.97	5.32
F012	0.53	1.57	0.22	10.10	F077	0.35	1.53	0.44	6.49
F013	0.42	1.57	0.29	7.87	F078	0.32	1.42	0.73	4.87
F016	0.44	1.43	0.85	5.96	HALY	0.64	1.65	-0.64	11.08
F019	0.31	1.53	0.43	6.06	NAMA	0.45	1.45	0.80	6.60
F020	0.30	1.60	0.16	6.42	P049	0.24	1.54	0.35	5.51
F024	0.46	1.65	-0.17	8.49	SOLA	0.31	1.60	0.15	6.54
F026	0.39	1.69	-0.31	7.29	YIBL	0.00	1.54	0.13	4.15
F027	0.50	1.71	-0.59	7.94	Mean	0.40	1.57	0.14	7.52
F029	0.25	1.68	-0.16	6.03	S.dev	0.16	0.09	0.50	2.48
F030	0.20	1.64	-0.04	5.60	RMS	0.43	1.57	0.51	7.91

ΔV_N : velocity in northing (mm/yr)

ΔV_E : velocity in easting (mm/yr)

ΔV_V : vector velocity (mm/yr)

ΔA_Z : azimuth in degree

Table K.14: The difference between the relative Arabian-Somalain station model velocities from this study (two stations) and from Vigny et al. [2006]

Stations	ΔV_N	ΔV_E	ΔV_V	ΔA_Z	Stations	ΔV_N	ΔV_E	ΔV_V	ΔA_Z
	mm/yr	Mm/yr	mm/yr	°		mm/yr	mm/yr	mm/yr	°
BAHR	1.53	1.41	1.36	5.42	F031	0.47	2.18	0.75	11.08
DATM	1.10	2.70	1.82	8.76	F033	0.66	2.00	0.76	9.47
F001	0.55	2.70	1.44	11.29	F035	1.34	1.74	1.29	6.54
F002	0.40	2.44	1.00	12.03	F036	1.55	1.72	1.50	6.05
F005	0.09	1.74	-0.12	11.43	F037	1.28	1.53	1.13	6.16
F006	-0.10	1.51	-0.53	10.25	F039	0.89	1.31	0.60	6.26
F007	-0.22	1.29	-0.77	7.88	F040	0.92	1.02	0.57	5.15
F008	-0.35	1.08	-0.92	4.97	F041	0.53	1.40	0.22	7.44
F009	-0.39	0.89	-0.89	2.70	F045	-0.08	0.56	-0.43	2.02
F010	-0.24	0.90	-0.75	3.69	F074	0.47	2.70	1.39	11.73
F012	0.21	1.58	-0.09	9.62	F077	0.87	1.98	0.95	8.57
F013	0.60	1.68	0.45	8.57	F078	0.99	2.63	1.67	9.11
F016	0.55	2.50	1.19	11.15	HALY	-0.25	0.90	-0.76	3.67
F019	1.02	2.01	1.13	8.08	NAMA	0.48	2.37	0.97	11.39
F020	1.05	1.59	0.90	6.84	P049	1.28	1.99	1.39	7.23
F024	0.45	1.12	0.04	6.09	SOLA	1.02	1.56	0.85	6.85
F026	0.71	0.88	0.33	4.74	YIBL	2.18	2.06	2.34	5.36
F027	0.32	0.61	-0.06	3.33	Mean	0.66	1.64	0.62	7.33
F029	1.25	1.09	0.96	5.00	S.dev	0.61	0.61	0.85	2.79
F030	1.45	1.33	1.24	5.37	RMS	0.90	1.75	1.04	7.83

ΔV_N : velocity in northing (mm/yr)

ΔV_E : velocity in easting (mm/yr)

ΔV_V : vector velocity (mm/yr)

ΔA_Z : azimuth in degree

Appendix K: Relative station model velocities between Arabian plate and Somalain plate

Table K.15: The difference between the relative Arabian-Somalain station model velocities from this study (three stations) and from CGPS2004 [*Prawirodirdjo and Yehuda Bock*, 2004]

Stations	ΔV_N	ΔV_E	ΔV_V	ΔA_Z	Stations	ΔV_N	ΔV_E	ΔV_V	ΔA_Z
	mm/yr	Mm/yr	mm/yr	°		mm/yr	mm/yr	mm/yr	°
BAHR	-2.33	4.26	-2.64	13.02	F031	-1.17	3.71	-0.45	18.65
DATM	-1.87	3.25	-0.70	12.96	F033	-1.39	3.86	-0.98	17.67
F001	-1.26	3.27	0.12	15.26	F035	-2.13	4.02	-2.06	13.85
F002	-1.10	3.50	0.02	17.76	F036	-2.35	4.02	-2.28	12.95
F005	-0.75	4.09	-0.92	24.73	F037	-2.06	4.19	-2.28	14.19
F006	-0.55	4.28	-1.42	27.63	F039	-1.64	4.38	-2.31	16.27
F007	-0.41	4.45	-2.03	28.27	F040	-1.67	4.59	-2.78	15.56
F008	-0.27	4.61	-2.67	27.40	F041	-1.25	4.33	-1.94	19.12
F009	-0.22	4.76	-3.18	24.62	F045	-0.57	4.98	-3.60	18.68
F010	-0.39	4.74	-3.02	23.66	F074	-1.18	3.27	0.24	15.60
F012	-0.88	4.21	-1.37	22.99	F077	-1.61	3.86	-1.24	16.22
F013	-1.32	4.11	-1.46	18.70	F078	-1.75	3.32	-0.61	13.61
F016	-1.27	3.44	-0.12	16.41	HALY	-0.38	4.74	-3.02	23.73
F019	-1.78	3.83	-1.37	15.26	NAMA	-1.19	3.56	-0.19	17.61
F020	-1.81	4.16	-2.00	15.43	P049	-2.06	3.83	-1.68	13.90
F024	-1.16	4.55	-2.43	19.04	SOLA	-1.78	4.18	-2.01	15.64
F026	-1.44	4.71	-2.94	16.33	YIBL	-3.04	3.72	-2.61	10.61
F027	-1.01	4.93	-3.37	17.22	Mean	-1.39	4.12	-1.81	17.78
F029	-2.03	4.52	-2.87	13.99	S.dev	0.67	0.49	1.08	4.58
F030	-2.25	4.32	-2.68	13.33	RMS	1.54	4.15	2.10	18.34

ΔV_N : velocity in northing (mm/yr)

ΔV_E : velocity in easting (mm/yr)

ΔV_V : vector velocity (mm/yr)

ΔA_Z : azimuth in degree

Table K.16: The difference between the relative Arabian-Somalain station model velocities from this study(three stations) and from NUVEL-1A [*DeMets, et al.*, 1994]

Stations	ΔV_N	ΔV_E	ΔV_V	ΔA_Z	Stations	ΔV_N	ΔV_E	ΔV_V	ΔA_Z
	mm/yr	Mm/yr	mm/yr	°		mm/yr	mm/yr	mm/yr	°
BAHR	-1.51	0.35	-1.50	1.30	F031	-1.52	0.47	-1.30	4.26
DATM	-1.52	0.43	-1.22	3.50	F033	-1.53	0.45	-1.38	3.42
F001	-1.53	0.47	-1.12	4.72	F035	-1.52	0.38	-1.46	1.96
F002	-1.52	0.47	-1.20	4.86	F036	-1.51	0.36	-1.46	1.75
F005	-1.52	0.49	-1.44	4.14	F037	-1.52	0.38	-1.50	1.67
F006	-1.52	0.51	-1.51	3.50	F039	-1.52	0.41	-1.53	1.52
F007	-1.51	0.52	-1.57	2.19	F040	-1.52	0.40	-1.56	0.83
F008	-1.51	0.53	-1.60	0.41	F041	-1.52	0.45	-1.53	2.06
F009	-1.51	0.53	-1.59	-1.19	F045	-1.52	0.49	-1.57	-1.65
F010	-1.51	0.52	-1.60	-0.53	F074	-1.52	0.47	-1.10	4.91
F012	-1.52	0.48	-1.49	3.19	F077	-1.52	0.43	-1.40	3.00
F013	-1.53	0.45	-1.46	2.79	F078	-1.52	0.44	-1.23	3.64
F016	-1.53	0.47	-1.20	4.50	HALY	-1.51	0.52	-1.60	-0.54
F019	-1.52	0.42	-1.40	2.79	NAMA	-1.53	0.47	-1.24	4.53
F020	-1.52	0.40	-1.48	1.99	P049	-1.52	0.40	-1.41	2.41
F024	-1.52	0.45	-1.57	1.19	SOLA	-1.52	0.41	-1.49	1.97
F026	-1.52	0.42	-1.58	0.47	YIBL	-1.49	0.32	-1.40	1.62
F027	-1.52	0.45	-1.59	-0.60	Mean	-1.52	0.44	-1.44	2.13
F029	-1.52	0.37	-1.55	0.89	S.dev	0.01	0.05	0.14	1.76
F030	-1.52	0.35	-1.52	1.23	RMS	1.52	0.44	1.45	2.75

ΔV_N : velocity in northing (mm/yr)

ΔV_E : velocity in easting (mm/yr)

ΔV_V : vector velocity (mm/yr)

ΔA_Z : azimuth in degree

Appendix K: Relative station model velocities between Arabian plate and Somalain plate

Table K.17: The difference between the relative Arabian-Somalain station model velocities from this study (three stations) and from Jestin et al. [1994]

Stations	ΔV_N	ΔV_E	ΔV_V	ΔA_Z	Stations	ΔV_N	ΔV_E	ΔV_V	ΔA_Z
	mm/yr	Mm/yr	mm/yr	°		mm/yr	mm/yr	mm/yr	°
BAHR	-2.79	-0.68	-2.82	-1.64	F031	-2.55	-0.72	-2.64	0.86
DATM	-2.70	-0.91	-2.83	1.06	F033	-2.60	-0.69	-2.69	-0.01
F001	-2.57	-0.86	-2.66	2.07	F035	-2.75	-0.72	-2.83	-1.01
F002	-2.54	-0.78	-2.63	1.77	F036	-2.79	-0.75	-2.87	-1.07
F005	-2.45	-0.55	-2.52	-0.52	F037	-2.74	-0.67	-2.79	-1.44
F006	-2.40	-0.46	-2.43	-1.99	F039	-2.65	-0.56	-2.66	-2.11
F007	-2.37	-0.38	-2.33	-3.95	F040	-2.66	-0.49	-2.61	-2.83
F008	-2.33	-0.30	-2.20	-6.27	F041	-2.57	-0.53	-2.59	-2.05
F009	-2.32	-0.24	-2.07	-7.85	F045	-2.41	-0.20	-2.09	-6.93
F010	-2.36	-0.27	-2.16	-6.66	F074	-2.56	-0.85	-2.63	2.24
F012	-2.49	-0.52	-2.52	-1.42	F077	-2.65	-0.72	-2.74	-0.23
F013	-2.59	-0.61	-2.64	-1.02	F078	-2.68	-0.89	-2.81	1.09
F016	-2.58	-0.81	-2.67	1.59	HALY	-2.36	-0.27	-2.16	-6.70
F019	-2.68	-0.74	-2.78	-0.29	NAMA	-2.56	-0.77	-2.65	1.39
F020	-2.69	-0.65	-2.74	-1.33	P049	-2.74	-0.77	-2.84	-0.46
F024	-2.55	-0.44	-2.50	-3.17	SOLA	-2.68	-0.64	-2.73	-1.40
F026	-2.61	-0.42	-2.51	-3.48	YIBL	-2.91	-0.91	-3.03	-0.70
F027	-2.52	-0.29	-2.30	-5.11	Mean	-2.59	-0.60	-2.60	-1.72
F029	-2.73	-0.56	-2.71	-2.39	S.dev	0.15	0.20	0.24	2.67
F030	-2.77	-0.65	-2.80	-1.80	RMS	2.60	0.63	2.61	3.15

ΔV_N : velocity in northing (mm/yr)

ΔV_E : velocity in easting (mm/yr)

ΔV_V : vector velocity (mm/yr)

ΔA_Z : azimuth in degree

Table K.18: The difference between the relative Arabian-Somalain station model velocities from this study (three stations) and from Reilinger et al. [2006]

Stations	ΔV_N	ΔV_E	ΔV_V	ΔA_Z	Stations	ΔV_N	ΔV_E	ΔV_V	ΔA_Z
	mm/yr	Mm/yr	mm/yr	°		mm/yr	mm/yr	mm/yr	°
BAHR	-2.03	4.11	-2.31	12.74	F031	-0.93	3.58	-0.21	17.98
DATM	-1.58	3.15	-0.45	12.40	F033	-1.13	3.72	-0.72	17.13
F001	-1.01	3.16	0.33	14.52	F035	-1.83	3.88	-1.76	13.49
F002	-0.86	3.38	0.24	17.00	F036	-2.05	3.89	-1.96	12.62
F005	-0.53	3.93	-0.67	24.16	F037	-1.77	4.04	-1.97	13.86
F006	-0.34	4.11	-1.15	27.22	F039	-1.37	4.22	-2.00	15.97
F007	-0.21	4.27	-1.76	28.06	F040	-1.39	4.42	-2.47	15.34
F008	-0.07	4.42	-2.40	27.39	F041	-1.00	4.17	-1.65	18.77
F009	-0.03	4.56	-2.90	24.72	F045	-0.36	4.77	-3.30	18.74
F010	-0.19	4.54	-2.73	23.68	F074	-0.93	3.17	0.44	14.83
F012	-0.65	4.05	-1.10	22.53	F077	-1.35	3.72	-0.96	15.73
F013	-1.06	3.96	-1.18	18.26	F078	-1.48	3.21	-0.37	13.03
F016	-1.02	3.33	0.11	15.70	HALY	-0.18	4.54	-2.74	23.76
F019	-1.50	3.70	-1.09	14.80	NAMA	-0.95	3.44	0.04	16.90
F020	-1.54	4.01	-1.70	15.07	P049	-1.77	3.70	-1.38	13.49
F024	-0.91	4.37	-2.14	18.80	SOLA	-1.50	4.03	-1.71	15.28
F026	-1.18	4.52	-2.62	16.15	YIBL	-2.70	3.60	-2.27	10.30
F027	-0.78	4.72	-3.06	17.16	Mean	-1.13	3.97	-1.53	17.42
F029	-1.74	4.35	-2.54	13.76	S.dev	0.64	0.46	1.05	4.66
F030	-1.94	4.17	-2.35	13.06	RMS	1.29	4.00	1.84	18.01

ΔV_N : velocity in northing (mm/yr)

ΔV_E : velocity in easting (mm/yr)

ΔV_V : vector velocity (mm/yr)

ΔA_Z : azimuth in degree

Appendix K: Relative station model velocities between Arabian plate and Somalain plate

Table K.19: The difference between the relative Arabian-Somalain station model velocities from this study (three stations) and from REVEL2000 [*Sella, et al.*, 2002]

Stations	ΔV_N	ΔV_E	ΔV_V	ΔA_Z	Stations	ΔV_N	ΔV_E	ΔV_V	ΔA_Z
	mm/yr	Mm/yr	mm/yr	°		mm/yr	mm/yr	mm/yr	°
BAHR	-0.46	3.53	-0.67	11.78	F031	0.44	3.03	1.12	14.69
DATM	-0.09	2.72	0.89	9.49	F033	0.28	3.15	0.70	14.64
F001	0.38	2.70	1.51	10.45	F035	-0.30	3.33	-0.18	12.03
F002	0.50	2.86	1.46	12.94	F036	-0.48	3.35	-0.36	11.28
F005	0.76	3.28	0.73	21.95	F037	-0.25	3.45	-0.37	12.68
F006	0.92	3.41	0.28	26.40	F039	0.08	3.57	-0.43	15.11
F007	1.02	3.53	-0.33	28.76	F040	0.06	3.73	-0.86	14.99
F008	1.13	3.64	-1.00	29.47	F041	0.39	3.50	-0.13	17.78
F009	1.16	3.74	-1.53	27.43	F045	0.90	3.93	-1.84	20.69
F010	1.04	3.74	-1.31	25.68	F074	0.44	2.70	1.59	10.55
F012	0.66	3.38	0.35	21.05	F077	0.10	3.17	0.49	13.51
F013	0.33	3.34	0.30	16.51	F078	0.00	2.76	0.95	10.01
F016	0.37	2.83	1.35	11.94	HALY	1.04	3.74	-1.32	25.79
F019	-0.02	3.16	0.39	12.69	NAMA	0.43	2.91	1.31	13.22
F020	-0.05	3.41	-0.14	13.72	P049	-0.25	3.17	0.14	11.64
F024	0.45	3.66	-0.60	18.57	SOLA	-0.02	3.43	-0.15	13.97
F026	0.24	3.80	-1.03	16.18	YIBL	-1.03	3.15	-0.62	8.96
F027	0.56	3.93	-1.52	18.13	Mean	0.27	3.35	-0.07	16.22
F029	-0.22	3.71	-0.90	13.21	S.dev	0.52	0.36	0.95	5.85
F030	-0.39	3.57	-0.71	12.18	RMS	0.58	3.37	0.94	17.21

ΔV_N : velocity in northing (mm/yr)

ΔV_E : velocity in easting (mm/yr)

ΔV_V : vector velocity (mm/yr)

ΔA_Z : azimuth in degree

Appendix K: Relative station model velocities between Arabian plate and Somalain plate

Table K.20: The difference between the relative Arabian-Somalain station model velocities from this study (three stations) and Vigny et al. [2006]

Stations	ΔV_N	ΔV_E	ΔV_V	ΔA_Z	Stations	ΔV_N	ΔV_E	ΔV_V	ΔA_Z
	mm/yr	Mm/yr	mm/yr	°		mm/yr	mm/yr	mm/yr	°
BAHR	0.89	3.31	0.70	11.77	F031	0.45	3.73	1.18	18.49
DATM	0.71	4.01	1.98	13.64	F033	0.53	3.63	0.95	17.01
F001	0.48	4.00	2.00	16.51	F035	0.81	3.49	0.91	12.94
F002	0.43	3.86	1.59	18.45	F036	0.90	3.48	1.00	12.08
F005	0.29	3.48	0.23	22.58	F037	0.79	3.37	0.66	12.95
F006	0.22	3.35	-0.35	24.00	F039	0.63	3.24	0.18	14.38
F007	0.16	3.22	-0.88	23.45	F040	0.64	3.08	-0.09	13.32
F008	0.11	3.10	-1.38	21.62	F041	0.48	3.29	0.02	16.91
F009	0.09	2.98	-1.66	18.62	F045	0.23	2.80	-1.48	13.93
F010	0.16	2.99	-1.43	18.33	F074	0.45	4.00	2.01	16.96
F012	0.34	3.39	0.04	20.57	F077	0.62	3.62	1.00	15.59
F013	0.51	3.45	0.46	17.21	F078	0.67	3.97	1.89	14.25
F016	0.49	3.90	1.69	17.13	HALY	0.15	2.99	-1.44	18.38
F019	0.68	3.64	1.09	14.71	NAMA	0.46	3.83	1.48	18.01
F020	0.69	3.40	0.60	14.14	P049	0.79	3.63	1.18	13.36
F024	0.45	3.13	-0.39	16.17	SOLA	0.68	3.39	0.55	14.28
F026	0.55	2.99	-0.39	13.63	YIBL	1.16	3.67	1.59	10.17
F027	0.39	2.83	-0.99	13.52	Mean	0.53	3.42	0.41	16.03
F029	0.77	3.12	0.22	12.18	S.dev	0.25	0.34	1.09	3.42
F030	0.86	3.26	0.57	11.95	RMS	0.59	3.44	1.15	16.38

ΔV_N : velocity in northing (mm/yr)

ΔV_E : velocity in easting (mm/yr)

ΔV_V : vector velocity (mm/yr)

ΔA_Z : azimuth in degree

Double-Difference Processing (WIDQIF.PCF) used in BPE

PID	Script		Descriptions
Copy required files and Create a priori CRD file			
001	R2S_COP	R2S_GEN	1. Copy all needed files to respective campaign directories. 2. file names will be changed according to the BPE variable V_B.
002	COOVEL	R2S_GEN	1. Propagates coordinates of stations to the current session's epoch.
Prepare Pole, Orbit and Clock information			
101	POLUPD	R2S_GEN	1. The IERS formatted pole file (IEP) provided by IGS is converted to Bernese format (ERP).
111	PRETAB	R2S_GEN	1. The precise orbit file (PRE) by IGS is converted to a Bernese tabular orbit file (TAB). 2. Satellite clock corrections are extracted and stored in a Bernese satellite clock file (using a polynomial representation).
112	ORBGEN	R2S_GEN	1. From tabular orbit file a standard orbit file is created by means of numerically integrating of motion.
Convert and synchronize observation data			
201	RNXGRA	R2S_GEN	1. Summary of all available observation data is created (satellites and stations) as well as their performance. 2. this file help to identify possible data tracking problems of observing sites 3. Stations showing large data gaps are detected and listed in a deletion file.
211	RXOBV3AP	R2S_GEN	1. This script does not start any programs. 2. It deletes already existing zero-difference observation files for current session. 3. It prepares the parallel execution of the next script.
212	RXOBV3_P	R2S_GEN	1. It converts RINEX to Bernese observation files. 2. It compares the data records in the RINEX header with the entries in the station information file.
221	CODSPPAP	R2S_GEN	1. Prepares the parallelization

222	CODSPP_P	R2S_GEN	1. CODSPP performs a code-based zero-difference point positioning 2. Mainly to synchronize the receiver clocks to GPS time on a sub-microsecond level.
223	CODXTR	R2S_GEN	1. It creates a summary from the output files written in the CODSPP 2. Stations showing a large rms are detected and listed in a deletion file
Form Baselines, pre-process and screen phase data, save cluster NEQ files			
301	SNGDIF (P)	R2S_GEN	1. it selects a complete of independent baselines and creates phase single-difference observation 2. The adopted strategy for the selection is the "OBS-MAX".
302	SNGDIF (C)	R2S_GEN2	3. it selects the same baselines selected in pervious step (301) and creates code single-difference observation 4. The adopted strategy for the selection is the "OBS-MAX".
311	MAUPRPAP	R2S_GEN	1. Prepares the parallel run for program MAUPRP.
312	MAUPRP_P	R2S_GEN	1. MAUPRP pre-processes the phase single-difference file. 2. Cycle slips are detected and repaired. 3. If the size of a cycle slip can not reliably be determined a new ambiguity is set up.
313	MPRXTR	R2S_GEN	1. it creates a summary of the previous pre-processing step 2. This file is included in the processing summary. 3. if rms > 20mm and/or baseline corrections > 0.5m as well as a lot of ambiguities may point out a possible data problem
321	GPSEDTAP	R2S_GEN	1. Prepares the parallel run of the GPSEDT_P script
322	GPSEDT_P	R2S_EDT	1. This script performs a double-difference phase residual screening using four Bernese programs: • GPSEST to create residual files. • RESRMS to screen these files for outliers. • SATMARK to mark identified

			outliers. • GPSEST to create final (clean) residual files and store normal equation files.
331	GPSCHK	R2S_GEN	1. Checks the screening results from the previous step and rejects data of misbehaving stations if need be using two programs: • RESRMS to create summaries from the first (unscreened) and final residual files. • RESCHK to create residual screening statistics and detect bad stations based on their overall performance.
Compute ambiguity-float network solution, resolve phase ambiguities			
401	ADDNEQ2	R2S_GEN	1. A network solution with real valued ambiguities is computed based on NEQ stored in the GPSEST after the residual screening. 2. Coordinates and troposphere estimates are saved for further use in the ambiguity resolution step.
402	GPSXTR	R2S_GEN	1. Creates a short overview of the float solution. 2. it is included in the processing summary (solution name P1_yyssss). 3. the a posteriori rms should be not higher than about 1.4mm.
409	GPSQIFAP	R2S_QIF3	1. Prepares the parallel execution of the ambiguity resolution steps. 2. Program BASLST is used to select baselines up to a maximum length of 2000 km.
410	GPSQIF_P	R2S_QIF3	1. One GPSEST for each baseline to be processed. 2. L1 & L2 ambiguities are resolved using QIF.
411	GPSQIFAM	R2S_QIF2	1. Prepares the parallel execution of the ambiguity resolution steps. 2. Program BASLST is used to select baselines greater than of 2000 km.
412	GPSQIF_M	R2S_QIF2	1. One GPSEST for each baseline to be processed. 2. Wide-line ambiguities are resolved using MELWUBB.
413	GPSQIFAN	R2S_QIF	1. Prepares the parallel execution of

			the ambiguity resolution steps. 2. Program BASLST is used to select the same baselines selected in step (411).
414	GPSQIF_N	R2S_QIF	1. One GPSEST for each baseline to be processed. 2. Narrow-lane ambiguities are resolved using L3 and introduce wide-lane ambiguities from step (412).
415	GPSXTR	R2S_QIF	1. Creates a summary of the previous step e.g. percentage of successfully resolved ambiguities (on average, about 70% of ambiguities are resolved)

References

Agnew, D. C., 1992. The time-domain behaviour of power-law noises. *Geophysical Research Letters 19* (4), 333–336.

Al-Amri A.M, F.R Schult, and C.G. Bufe (1991). Seismicity and aeromagnetic feature of the Gulf of Aqabah region. *Journal of Geophysical Research, 96,* 20179-20185.

Al-Amri A., M. (1994), Seismicity of the south-western region of the Arabian Shield and southern Red Sea, *journal of African Earth Sciences, 19,* 17-25.

Al-Amri, A. M. (1995). Premilinary seismic hazard assessment of the Southern Red Sea region, European Earthquake Engineering, 3, 33-38.

Al-Amri A. M. (1998), The crustal structure of the western Arabian platform from the spectral analysis of long-period P-wave amplitude ratios, *Tectonophysics,* 290, 271-283.

Al-Amri A. M. (1999), The crustal and upper-mentle structure of the interior Arabian platform, *Geophysical Journal International, 136,* 421-430.

Al-Amri, A. M. and Alkhalifah, T., (2004). Improving seismic hazard assessment in Saudi Arabia using earthquake location and magnitude calibration. King Abdulaziz City Science and Technology, AR-20-68, Final report.

Al-Damegh, K., Sandvol, E., Al-Lazki, A., and Barazangi, M., (2004), Regional seismic wave propagation (Lg and Sn) and Pn attenuation in the Arabian Plate and Surrounding regions, *Geophysics Journal International, 157,775-795.*

Al-Damegh, K., Sandvol E. and Barazangi, M., (2005), Crustal structure of the Arabian plate: New constraints from the analysis of teleseismic receiver functions, *Earth and Planetary Science Letters* 231, 177-196.

Almotairi, E. (2006), A study of Plate Motion and Large-Scale crustal Deformation of the Arabian Plate Using GPS, 300 pp, PhD Thesis, The Unversity of Nottingham, Nottingham.

Allmendinger, R. W., Reilinger, R., Loveless, J., (2007), Strain and rotation rate from GPS in Tibet, Anatolia, and the Altiplano, *Tectonics,* 26, TC3013, doi:10.1029/ 2006TC002030.

Altamimi, Z., Sillard, P., Boucher, C., (2002). ITRF2000: A new release of the International Terrestrial Reference Frame for Earth science applications. *Journal of Geophysical Research 107 (B10),* 2214, doi:10.1029/2001JB000561.

Altamimi, Z., Sillard, P. and Boucher, C., (2003). The impact of a No-Net-Rotation Condition on ITRF2000, *Geophysical Research Letter*, 30, 2, 36-1 – 36-4.

Altamimi, Z., Collilieux, X., Legrand, J., Garayt, B., and Boucher, C., (2007), ITRF2005: A new release of the International Terrestrial Reference Frame based on time series of site positions and Earth Orientation Parameters, *J. Geophys. Res., 112,* B09401, doi:10.1029/2007JB004949.

Ambraseys, A., (1988). Seismicity of Saudi Arabia and adjacent areas, Report 88/11, ESEE, *Imperial Coll. Sci. Tech.*, 88/11, London, UK.

Amiri-Simkooei, A. R. (2009). Noise in multivariate GPS position time-series, *Geodesy,* 83:175–187, doi:10.1007/s00190-008-0251-8

Argus, Donald F., (2007). Defining the translational velocity of the reference frame of the Earth, *Geophysical Journal International,* 169, 830–838 doi: 10.1111/j.1365-246X.2007.03344.x

Argus, D. F., Gordon, R. G., Heflin, M. B., Chopo Ma, Eanes., R. J., Willis, P., Peltier, W. R. and Owen, S. E. (2010). The angular velocities of the plates and the velocity of Earth's centre from space geodesy, *Geophysical Journal International,* 180, 913–960 doi: 10.1111/j.1365-246X.2009.04463.x.

Ayhan, M. E., Demir, C., Lenk, O., Kilicoglu, A., Altiner, Y., Baraka, A. A., Ergintav, S., Ozener, H., (2002). Interseismic Strain Accumulation in the Marmara Sea Region, *Bulletin of the seismological society of America*, 92, 1, pp 216-229.

Baker, T. F., (1984). Tidal deformations of the Earth, Pergamon Press Oxford., 69, 197-233,

Baker, H. C., (1998). GPS water vapour estimation for meteorological applications, Ph.D. thesis, University of Nottingham, UK.

Badri, M. (1991), Crustal structure of central Saudi Arabia determined from seismic refraction profiling, *Tectonophysics*, 185, 357-374.

Bail, K. L., (2006). Estimating the noise in space-geodetic positioning: the case of DORIS, *Geodesy,* 80:541-565,doi:10.1007/s00190-006-0088-y

Bassiri S., and Hajj, GA. (1993). Higher-order ionospheric effects on the global positioning system observables and means of modeling them, *Manuscripta Geodetica* 18:280–289.

Beavan, J., Tregoning, P., Bevis, M., Kato, T., and Meertens, C., (2002). Motion and rigidity of the Pacific Plate and implications for plate boundary deformation, *Journal of Geophysical Research,* 107(B10), 2261, doi:10.1029/2001JB000282.

Ben Menahem, A (1979). Earthquak catalogue of the Middle East (92BC- 1980 AD). *Boll. Geofisica Teorica de Applicata*, 21, 245-310.

Beutler, G., M. Rothacher, S. Schaer, T. A. Springer, J. Kouba, and R. E. Neilan (1999), The International GPS Service (IGS): An Interdisciplinary Service in Support of Earth Sciences, *Advance Space Research, 23*(4), 631-653.

Bird, P., (2003), An updated digital model of plate boundaries, *Geochem. Geophys. Geosyst.*, *4*(3), 1027, doi:10.1029/2001GC000252.

Blewitt, G., and Lavall'ee, D., (2002). Effect of annual signals on geodetic velocity. *Journal of Geophysical Research* 107 (B7), ETG9–1/9–11, DOI:10.1029/2001JB000570.

Boehm, J., Werl, B., and Schuh, H., (2006). Troposphere mapping functions for GPS and very long baseline interferometry from European Centre for Medium Range Weather Forecasts operational analysis data, *Journal of Geophysical Research*, 111, B02406, doi:10.1029/2005JB003629.

Bohannon, R. G., Naeser, C. W., Scmidt, D. L., and Zimmerman, R. A., (1989). The timing of the uplift and rifting peripheral to the Red Sea: a case for passive rifting? *Journal of Geophysical Research, 94*, 1683-1701.

B¨ohm, J., Niell, A. E., Tregoning, P., and Schuh, H., (2006). Global Mapping Function (GMF): A new empirical mapping function based on numerical weather model data, *Geophysical Research Letters*, **33**, L07304, doi: 10.1029/2005GL025546.

Bos, M. S., Fernandes, R. M. S., Williams, S. D. P., Bastos, L. (2008). Fast error analysis of continuous GPS observations, *Geodesy*, 82:157-166, doi:10.1007/s00190-007-0165-x.

Bouille, F., Cazenave, A., Lemoine, J. M. and Cretaux, J. F., (2000). Geocentre motion from the DORIS space system and laser data to the Lageos satellites: comparison with surface loading data, *Geophysical Journal International*, 143, 71-82.

Braitenberg, C., Nagy, I., Negusini, M., Romangnoli, C., Zadro, M., and Zerbini, S., (2001). Geodetic measurements at the northern border of the Adria plate. *Geodynamics 32* (1-2), 267–286.

Bruyninx, C., Kenyeres, A., and Takacs, B., (2002). EPN data an product analysis for improved velocity estimation: First results. In: 'Ad'am, J., Schwarz, K. P. (Eds.), Vistas for Geodesy in the New Millennium. Vol. 125 of International Association of Geodesy Symposia. Springer-Verlag, Berlin Heidelberg, pp. 47–52.

Calais, E., (1999). Continuous GPS measurements across the Western Alps, 1996 1998. *Geophysical Journal International 138* (1), 221–230.

Camp, V. E., and Roobol, M. J. (1992). Upwelling asthenosphere beneath western Arabian and its regional implications. *Journal Geophysical Research, 97*, 15255-15271.

Chapman R (1978). General information on the Arabian peninsula (Geology), Quaternary period in Saudi Arabia, ed (Al-Sayari S and Zoltl J).

Chen, J. L., Wilson, C. R., Chambers, D. P., Nerem, R. S. and Tapley, B. D., (1998). Seasonal Global Water Mass Budget and Mean Sea Level Variations, *Geophysical Research Letter*, 25, 3555-3558.

Chu, D., and Gordon, R. G. (1998), Current plate motions across the Red Sea, *Geophysical Journal International, 135*, 313-328.

Cross, P. A., (1994). Advanced least squares applied to position fixing. Tech. Rep. Working Paper No. 6, University of East London, Department of Land Surveying.

Dach, R., Hugentobler, U., Fridez, P., and Meindl, M., (2007), *Bernese GPS Software Version 5.0*, Astronomical Institute, University of Bern, Bern.

Dana P.H. (2000). www. Colorado.edu/geography/gcraft/notes/ps/gps.html.

DeMets, C., Gordon, R. G., Argus, D., and Stein, S., (1994), Effect of recent revisions to the geomagnetic reversal time scale on estimates of current plate motions, *Geophysical Research Letter, 21*, 2191–2194.

DeMets, C., Gordon, R. G., and Argus, D. F., (2010). Geologically current plate motions, *Geophysical Journal International,*. doi: 10.1111/j.1365-246X.2009.04491.x, 1-80

Derkhshani R. and Farhoudi G. (2005). Existence of the Oman Line in the Empty Quarter of Saudi Arabia and its Continuation in the Red Sea. *Journal of Applied Sciences 5(4)*: 754-752

Dixon, T. H., and Mao, A., (1997). A GPS estimate of relative motion between North and SouthAmerica. *Geophysical Research Letters 24* (5), 535–538.

Dixon, T. H., Miller, M., Farina, F., Wang, H., Johnson, D., (2000). Present-day motion of the Sierra Nevada block and some tectonic implications for the Basin and Range province, North American Cordillera, *Tectonics,* 19 (1), 1–24.

Dodson, A. H., Shardlow, P. J., Hubbard, L. C. M., Elgered, G., and Jarlemark, P. O. J., (1996). Wet tropospheric effects on precise relative GPS height determination. *Journal of Geodesy 70 (4)*, 188–202.

Donald, T., and Schubert, G., (2002), *Geodynamics*, 456 pp., Cambridge University press.

Dong, D., Gross, R. S. and Dickey, J. O., (1996). Seasonal variations of the Earth's gravitational field: An analysis of atmospheric pressure, ocean tidal, and surface water excitation, *Geophysical Research Letter*, 23, 725-728, 1996.

Dong, D., Fang, P., Bock, Y., Cheng, M. K., and Miyazaki, S., (2002). Anatomy of apparent seasonal variations from GPS derived site position time series. *Journal of Geophysical Research* 107 (B4).

Dong, D., Fang, P., Bock, Y., Webb, F. H., Prawirodirdjo, L., Kedar, S., & Jamason, P., (2006). Spatiotemporal filtering using principal component analysis and Karhunen-Loeve expansion approaches for regional GPS network analysis, *Journal Geophysical Research*, **111**, B03405, doi: 10.1029/2005JB003806.

Dragert, H., James, T. S., Lambert, A., (2000). Ocean loading corrections for continuous GPS: A case study at the Canadian coastal site Holberg. *Geophysical Research Letters*, 27 (14), 2045–2048.

Drewes, H., and Angermann, D. (2001), The Actual Plate Kinematic and Crustal Deformation Model 2000 (APKIM2000) as a Geodetic Reference System, In: Ádam J., and K. P. Schwarz (Eds.) *Vistas for Geodesy in the New Millennium*. IAG Symposia, 125, Springer, Berlin Heidelberg New York, 329–334.

Drewes, H. (2006), The APKIM2005 as a basis for a non-rotating ITRF, IAG Symposia.

Dwivedi S.K., and Hayashi D. (2007). Neotectonic stress analysis of the Red Sea rift by Finte Element Modeling. *Bull. Fac. Sci. Univ. Ryukyus, No83*:3-28.

Dye, S., and Baylin, F., (1997). The GPS Manual Principles and Applications. USA, Baylin publications.

Dziewonski, A. M., and Anderson, D. L., (1981). Preliminary Reference Earth Model. *Phys. Earth Planet. Inter. 25*, 297–356.

Estey, L. H., and Meertens, C.M., (1999). TEQC: The multi-purpose toolkit for GPS/GLONASS data. *GPS Solutions*, 3 (1), 42–49.

Fernandes, R. M. S., Ambrosius, B. A. C., Noomen, R., Bastos, L., Combrinck, L., Miranda, J. M., and Spakman, W., (2004), Angular velocities of Nubia and Somalia from continuous GPS data: Implications on present-day relative kinematics, *Earth and Planetary Science Letters, 222*, 197-208.

Flouzat, M., Bettinelli, P., Willis, P., Avouac, J.-P., H'eritier, T. and Gautam, u., (2009). Investigating tropospheric effects and seasonal position variations in GPS and DORIS time-series from the Nepal Himalaya, *Geophysical Journal International*, doi: 10.1111.1365-246.2009.04252.

Forsyth, D. W. and Uyeda, S., (1975). On the relative importance of driving forces of plate motions, Geophys. J. R. Astro. Soc., 43, 63-200, 1975.

Fowler, C. M. R. (2005), *The Solid Earth: An Introduction to Global Geophysics*, Cambridge University Press, Cambridge.

Frank, F. C., (1966). Deduction of earth strains from survey data, *Bulletin of the seismological society of America*, 56, pp. 35–42.

Garfunkel, Z., and Z. Ben-Avraham (1996), The structure of the Dead Sea basin, *Tectonophysics, 266*, 155-176.

Geirsson, H., Arnadottir, T., Volksen, C., Jiang, W., Sturkell, E., Villemin, T. Einarsson, P., Sigmundsson, F. and Stefansson, R., (2006). Current plate movements across the Mid-Atlantic Ridge determined from 5 years of continuous GPS measurements in Iceland, Journal of Geophysical Research, 111, B09407, doi:10.1029/2005JB003717.

Grünthal, G., Bosse, C, Sellami, S., Mayer-Rosa, D., and Giardini, D., (2006), Compilation of the GSHAP regional seismic hazard for Europe, Africa and the Middle East edited, http://www.seismo.ethz.ch/gshap/eu-af-me/euraf.html.

Heki, K., 2001. Seasonal modulation of interseismic strain buildup in Northeastern Japan driven by snow loads. *Science 293*, 89–92.

Herna´ndez-Pajares, M., Juan, J. M., Sanz, J. and Oru´s, R. (2007), Second-order ionospheric term in GPS: Implementation and impact on geodetic estimates, *Journal Geophysical Research*, 112, B08417, doi:10.1029/2006JB004707.

Hofmann-Wellenhof, B.H. Lichtengger, and J. Collins (2001). GPS Theory and Practise, New York: Springer-Verlage Wein.

IGS (2006), International GNSS service, edited, http://igscb.jpl.nasa.gov/.

Martha, K. (1996), This Dynamic Earth: the story of plate tectonics, edited, http://pubs.usgs.gov/gip/dynamic/dynamic.html.

Jackson, J., and Fitch, T., (1981). Basement faulting an d the focal depth of the larger earthquakes in the Zagros mountain (Iran), *Geophys. J R. Astron. Soc.*, 64, 561-586.

Jakowski,N., Mayer, Ch., Wilken,V., and Hoque, M.M., (2008).Ionospheric Impact on GNSS Signals, *Física de la Tierra*, 11-25.

Jaldehag, R. T. K., Johansson, J. M., Davis, J. L., and El´osegui, P., (1996). Geodesy using swedish permanent GPS network: Effects of snow accumulation on estimates of site positions. *Geophysical Research Letters 23* (13), 1601–1604.

Jestin, F., Huchon, P. and Gaulier, J. M. (1994), The Somalia plate and the East African Rift System: Present-day kinematics, *Geophysical Journal International, 116*, 637-654.

Johnson, H. O., and Agnew, D. C., (2000). Correlated noise in geodetic time series. Final Technical Report 1434-HQ-97-GR-03155, Institute of Geophysics and Planetary Physics, University of California.

Johansson, J. M., Davis, J. L., Scherneck, H. G., Milne, G. A., Vermeer, M., Mitrovica, J. X., Bennett, R. A., Jonsson, B., Elgered, G., El'osegui, P., Koivula, H., Poutanen, M., R¨onn¨ang, B. O., and Shapiro, I. I., (2002). Continuous GPS measurements of postglacial adjustment in Fennoscandia 1. Geodetic Results. *Journal of Geophysical Research 107* (B8), ETG 3/1–3/27.

Kaplan, E. D. (1996). Understanding GPS Principles and Applications. USA: Artech House, INC.

Kaniuth, K., and Stuber, K., (2002). The impact of antenna radomes on height estimates in regional GPS networks. In: Drewes, H., Dodson, A. H., Fortes, L. P. S., S'anchez, L., Sandoval, P. (Eds.), Vertical Reference Systems. Vol. 124 of International Association of Geodesy Symposia. Springer-Verlag, Berlin Heidelberg, pp. 101–106.

Kasdin, N. J., (1995). Discrete simulation of colored noise and stochastic processes and 1/f α power law noise generation. Proc IEEE 83(5):802–827

Kedar, S., Hajj, G. A., Wilson, B. D. and Heflin, M. B. (2003). The effect of the second order GPS ionospheric correction on receiver positions, *Geophysical Research Letter*, 30(16), 1829, doi:10.1029/2003GL017639.

Kreemer, C., Holt, W. E. and Haines, A. J. (2003), An integrated global model of present-day plate motions and plate boundary deformation, *Geophysical Journal International, 154*, 8-34.

Kreemer, C., Lavallée, D. A., Blewitt, G. and Holt, W. E. (2006), On the stability of a geodetic no-net-rotation frame and its implication for the International Terrestrial Reference Frame, *Geophysical Research Letter*, 33, L17306, doi:10.1029/2006GL027058.

Kenyeres, A., Bosy, J., Brockmann, E., Bruyninx, C., Caporali, A., Hefty, J., Jivall, L., Kosters, A., Poutanen, M., Fernandes, R., and Stangl, G., (2001). EPN Special Project on "Time series analysis ..." preliminary results and future prospects. In: Proceedings of EUREF Symposium. Dubrovnik, Croatia, May 2001.

Kleijer, F., (2002). Time series analysis of the daily solutions of the AGRS.NL reference stations. In: Drewes, H., Dodson, A. H., Fortes, L. P. S., S'anchez, L., Sandoval, P. (Eds.), Vertical Reference Systems. Vol. 124 of International

Association of Geodesy Symposia. Springer-Verlag, Berlin Heidelberg, pp. 60–65.

Langbein, J., Svarc, J., Murray-Moraleda, J., (2008). Comparison of noise characteristics of GPS position time-series between the San Francisco Bay area and Southern California networks, American Geophysical Union, Fall Meeting 2008, G51A-0594

Langley, R. B., 1996. Propagation of GPS signals. In: Teunissen, P. J. G., Kleusberg, A. (Eds.), GPS for Geodesy, 2nd Edition. Springer-Verlag, Berlin Heidelberg, pp. 111–150.

Lavall'ee, D. A., (2000). Tectonic plate motions from global GPS measurements. PhD. thesis, Newcastle University.

Lavall'ee, D. A., (2006). TANYA software user manual, Newcastle University, UK.

Leonard, L. J., Hyndman, R. D., Mazzotti, S., Nykolaishen, L., Schmidt, M. and Hippchen, S., (2007). Current deformation in the northern Canadian Cordillera inferred from GPS measurements, Journal Geophysical Research, 112, B11401, doi:10.1029/2007JB005061.

Looseveld R. J. H., Ball A., and Terken J. J. M (1996). The tectonic evolution of interior Oman. *GeoArabia,* 1(1), 28-51.

Lutz, S., Schaer, S., Meindl, M., Dach, R., Steigenberger, P., (2010). Higher-Order Ionosphere Modeling for CODE's Next Reprocessing Activities, IGS Workshop 2010, Newcastle upon Tyne, England.

Mader, G. L., and Czopek, F. M., (2001). Calibrating the L1 and L2 phase centers of a Block II antenna. In: Proc. of the 14th International Technical Meeting of the Satellite Division of the Institute of Navigation ION GPS 2001, 11-14 September 2001, Salt Lake City, Utah. Institute of Navigation, Washington D. C., pp. 1979–1984.

Mao, A., Harrison, C. G. A., and Dixon, T. H., (1999). Noise in GPS coordinate time series. *Journal of Geophysical Research 104* (B2), 2797–2818.

Mazzotti, S., Dragert, H., Henton, J., Schmidt, M., Hyndman, R., James, T., Lu, Y., and Craymer, M., (2003). Current tectonics of northern Cascadia from a decade of GPS measurements, *Journal Geophysical Research,* 108(B12), 2554, doi:10.1029/2003JB002653.

McCarthy, D., and Petit G. (2004). IERS Conventions (2003), IERS Technical Note No 32, Verlag des Bundesamts fur Kartographie und Geodasie, Frankfurt am Main127 pp.

McClusky, S., Reilinger, R., Mahmoud, S., Ben Sari, D. and Tealeb, A., (2003), GPS constraints on Africa (Nubia) and Arabia plate motions, *Geophysical Journal International, 155*, 126-138.

McClusky ,S., Reilinger,R., Ogubazghi,G., Amlesom,A., Haileab,B. , Sholan, J., Vernant,P., and ArRajehi,A., (2009). Active kinematics of the southern Red Sea, EGU General Assembly *2009*,Vol. 11, EGU2009-12316-2.

McKenzie, D. P., Davies D., and Molnar, P., 1970. Plate Tectonics of the Red Sea and east Africa, *Nature*, vol. 226, p 243-248.

Melchior, P., 1983. The Tides of the Planet Earth, Pergamon Press, Oxford, U.K

Minster, J. F., Cazenave, A., Serafini, Y. V., Mercier, F., Gennero, M. C and Rogel, P., (1999). Annual cycle in mean sea level from Topex-Poseidon and ERS-1: inference on the global hydrological cycle, *Global and Planetary Change*, 20, 57-66.

Nehlig, P., Genna, A., and Asfirane, F., (2002), A review of the Pan-African evolution of the Arabian Shield, *GeoArabia, 7.*

Nikolaidis, R. M., (2002). Observation of geodetic and seismic deformation with the Global Positioning System. PhD. Thesis, University of California.

Niell, A. E., (1996). Global mapping functions for the atmospheric delay at radio wavelenghts. *Journal of Geophysical Research* 101 (B2), 3227–3246.

Neil, A., (2000). Improved atmospheric mapping functions for VLBI and GPS, *Earth Planets Space*, 52(10):699-702

Onsala Space Observatory (2006), Ocean Tidal Loading edited, http://www.oso.chalmers.se/~loading/.

Penna, N. T., and Stewart, M. P., (2003). Aliased tidal signatures in continuous GPS height time series, *Geophysical Research Letter*, 30(23), 2184, doi:10.1029/2003GL018828.

Penna, N. T., King, M. A., and Stewart, M. P., (2007). GPS height time series: Short-period origins of spurious long-period signals, *Journal Geophysical Research*, 112, B02402, doi:10.1029/2005JB004047.

Penna, N. T., Bos, M. S., Baker, T. F., Scherneck H. G., (2008). Assessing the accuracy of predicted ocean tide loading displacement values, *Journal of Geodesy*, 82:893–907 doi:10.1007/s00190-008-0220-2.

Petrie, E. J., King, M. A., Moore, P., and Lavallée, D. A. (2010). Higher order ionospheric effects on the GPS reference frame and velocities, *Journal of Geophysical Research*, 115, B03417, doi:10.1029/2009JB006677.

Petrov, L., Boy, J. P., (2004). Study of the atmospheric pressure loading signal in VLBI observations, *Journal of Geophysical Research,* 10.1029/2003JB002500, Vol. 109, No. B03405.

Pireaux, S., Defraigne, P., Wauters , L., Bergeot, N., Baire, Q., Bruyninx, C., (2010). Higher-order ionospheric effects in GPS time and frequency transfer, *GPS Solutions,* 14:267–277 doi: 10.1007/s10291-009-0152-1

Ponte, R. M., D. A. Salstein, Rosen,R. D., (1991). Sea level response to pressure forcing in a barotropic numerical model, *Journal of Physical Oceanographic,* 21, 1043-1057.

Poutanen, M., Koivula, H., and Ollikainen, M., (2001). On the periodicity of GPS time series. In: Proceedings of the IAG 2001 Scientific Assembly "Vistas for Geodesy in the New Millennium". Budapest, Hungary, 2-7 September, 2001, p. 4.

Powers R. W., Ramirez, L. F., Redmond, C. D., Elberg, E. L., (1966). Geology o the Arabian Peninsula, Sedimentary geology of Saudi Arabia: U.S Geological Survey professional paper 560-D D1-D147

Prawirodirdjo, L., and Bock, Y., (2004), Instantaneous global plate motion model from 12 years of continuous GPS observations, Journal of *Geophysical. Research., 109,* B08405, doi: 10.1029/2003JB002944.

Prawirodirdjo, L., Ben-Zion, Y., and Bock, Y., (2006). Observation and modeling of thermoelastic strain in Southern California Integrated GPS Network daily position time series, *Journal of Geophysical Research,* 111, B02408, doi:10.1029/2005JB003716.

Prescott, W. H., (1976). An extension of Frank's for obtaining crustal shear strains from survey data, *Bulletin of the seismological society of America,* 66, 1847-1853, 1976.

Reilinger, R., McClusky, S., Vernant, P., Lawrence, S., Ergintav, S., Cakmak, R., Ozener, H., Kadirov, F., Guliev, I., Stepanyan, R., Nadariya, M., Hahubia, G., Mahmoud, S. Sakr, K., ArRajehi, A., Paradissis, D., Al-Aydrus, A. Prilepin, M., Guseva, T., Evren, E., Dmitrotsa, A., Filikov, S. V., Gomez, F. Al-Ghazzi, R., and Karam, G., (2006), GPS constraints on continental deformation in the Africa-Arabia-Eurasia continental collision zone and implications for the dynamics of plate interactions, *Journal of Geophysical Research, 111.* B05411, doi:10.1029/2005JB004051.

Rodell, M. and Famiglietti, J. S., (1999). Detectability of variations in continental water storage from satellite observations of the time dependent gravity field, *Water Resources Research,* 37, 2705-2723.

Rodell, M., and Famiglietti, J. S., (2001). An analysis of terrestrial water storage variations in Illinois with implications for the Gravity Recovery and Climate Experiment (GRACE), *Water Resources Research.,* 37(5), 1327–1339.

Rodell, M., and Famiglietti, J. S., (2002). The potential for satellite-based monitoring of groundwater storage changes using GRACE: the High Plains aquifer, Central US, *Journal of Hydrology*, 263(1–4), 245–256, 2002.

Rodgers, A. J., Walter, W. R., Mellors, R. J., Al-Amri, A. M., and Zhang, Y. S., (1999), Lithospheric structure of the Arabian Shield and Platform from complete regional waverform modelling and surface wave group velocities, *geophysical, 138*, 871-878.

Rothacher, M., (2002). Estimation of station heights with GPS. In: Drewes, H., Dodson, A. H., Fortes, L. P. S., S'anchez, L., Sandoval, P. (Eds.), Vertical Reference Systems. Vol. 124 of International Association of Geodesy Symposia. Springer-Verlag, Berlin Heidelberg, pp. 81–90.

Sanvol, E., Seber, D., Barazangi, M., Vernon, F., Mellors, R., Al-Amri, A., (1998), Lithospheric seismic velovity discontinuities beneath the Arabian Shield, *journal of Geophysical Research, 25*, 2873-2876.

Saudi Geological survey (2006), Arabian Plate geological setting, edited, http://www.sgs.org.sa/index.cfm?sec=1&page=home.cfm.

Schmidt, D.L., Haley, D. G. and Stoeser, D. B., (1979). Late Proterozoic crustal history of the Arabian Shield, Southern Najd province, Kingdom of Saudi Arabia, evolution and mineralization of the Arabian-Nubian Shield. *I.A.G. Bull., 3,* 41-58.

Schmid R., and Rothacher M., (2003). Estimation of elevation-dependent satellite antenna phase center variaions of GPS satellites. *Geodesy*, 77(7-8):440-446,doi:10.1007/s00190-003-0339-0

Scherneck, H. G., Johansson, J. M., Mitrovica, J. X., and Davies, J. L., (1998). The BIFROST project: GPS determined 3-D displacement rates in Fennoscandia from 800 days of continuous observations in the SWEPOS network. *Tectonophysics* 294 (3-4), 305–321.

Schupler, B. R., and Clark, T. A., 1991. How different antennas affect the GPS observable. GPS World (11-12), 32–36.

Seeber, G. (1993), *Satellite Geodesy*, 531 pp., Berlin; New York: de Gruyter.

Sella, G. F., Dixon, T. H. and Mao, A., (2002), REVEL: A model for recent plate velocities from space geodesy, *J. Geophys. Res., 104*, B4, 2081, doi:10.1029/2000JB000033.

Shen, Z. K., Jacksona, D. D., and Ge, B., X., (1996). Crustal deformation across and beyond the Los Angeles basin from geodetic measurements, *Journal of Geophysical Research*, vol.101 no. B12, 7,957-27,980.

Solomon, S. C., Sleep, N. H., and Richardson, R. M., (1975). On the forces driving plate tectonics: Inference from absolute plate velocities and intraplate stress, Geophys. J. R. Astro. Soc., 42 , 769-801, 1975.

Stamps D. S., Calais, E., Saria, E., Hartnady, C., Nocquet, J.-M., Ebinger, C. J., and Fernandes, R. M. (2008), A kinematic model for the East African Rift, *Geophysical Research Letter, 35,* L05304, doi:10.1029/2007/GL032781.

Steigenberger, P., Rothacher, M., Dietrich, R., Fritsche, M., Rülke, A., and Vey, S., (2006), Reprocessing of a global GPS network, *Journal of Geophysical Research,* 111, B05402, doi:10.1029/2005JB003747.

Stewart, M. P., Penna, N. T., and Lichti, D. D. (2005). Investigating the propagation mechanism of unmodelled systematic errors on coordinate time series estimated using least squares, 79, 479–489, doi:10.1007/s00190-005-0478-6

Teferle, F. N. (2003), Strategies for Long-term Monitoring of Tide Gauges using GPS 390 pp, PhD. Thesis, The University of Nottingham, Nottingham.

Teferle, F. N., Bingley, R. M., Williams, S. D. P., Baker, T. F., and Dodson, A. H., (2006). Using continuous GPS and absolute gravity to separate vertical land movements and changes in sea level at tide gauges in the UK, *Phil. Trans. Roy. Soc., Part A,* 364, 917–930, doi: 10.1098/rsta.2006.1746.

Teferle F.N., Bingley R.M., Orliac E.J., Williams S.D.P., Woodworth P.L., McLaughlin D., Baker T.F., Shennan I., Milne G.A., Bradley S.L. and Hansen D.N. (2009). Crustal Motions in Great Britain: Evidence from Continuous GPS, Absolute Gravity and Holocene Sea-Level Data, *Geophysical Journal International,* 178, 1, pp. 23-46(24).

Teferle, F. N.,Williams, S. D. P., Kierulf, H. P., Bingley, R.M., and Plag, H. P., (2008). A continuous GPS coordinate time series analysis strategy for high-accuracy vertical land movements, *Physics Chemistry of the Earth,* **33**(3-4), 205–216, doi: 10.1016/j.pce.2006.11.002.

Thenhaus P., Algermisen S., Perkins D., Hansen S. and Diment W. (1986). Probabilistic estimates of the seismic ground-motion hazards in western Saudi Arabia, USGS Bull., 1986, 40p.

Turcotte, D. L. and Schubert, G., 2002. Geodynamics. 2nd edition, Cambridge University Press, United Kingdom

Van Dam, T. M., Blewitt, G. and Helfin, M. B., (1994). Atmospheric Pressure Loading Effects on Global Positioning System Coordinate Determinations, *Journal of geophysical research , vol. 99, No. B12, pages , 23,939-23,950.*

van Dam, T., Plag, H. P., Francis, O., and Gegout, P., (2002). GGFC Special Bureau for Loading: Current status and plans [online]. Position paper, GGFC

Special Bureau for Loading, Available at: http://www.sbl.statkart.no/aboutloading/pos_paper_final.pdf.

Vernant, P., Nilforoushan, F., Hatzfeld, D., Abbassi, M. R., Vigny, C., Masson, F., Nankali, H., Martinod, J., Ashtiani, A., Bayer, R., Tavakoli, F. and Chery, J. (2004), Present-day crustal deformation and plate kinematics in the Middle East constrained by GPS measurements in Iran and northern Oman, *Geophysical Journal International, 157*, 381-398.

Vespe, F., Rutigliano, P., Ferraro, C., and Nardi, A., (2002). Vertical motions from geodetic and geological data: a critical discussion of the results. In: Drewes, H., Dodson, A. H., Fortes, L. P. S., S´anchez, L., Sandoval, P. (Eds.), Vertical Reference Systems. Vol. 124 of International Association of Geodesy Symposia. Springer-Verlag, Berlin Heidelberg, pp. 66–71

Vey, S., Dietrich, R., Fritsche, M., Ru¨lke, A., Rothacher, M., and Steigenberger, P., (2006). Influence of mapping function parameters on global GPS network analyses: Comparisons between NMF and IMF, *Geophysical Research Letter*, 33, L01814, doi:10.1029/2005GL024361.

Vigny, C., Huchon, P., Ruegg, J.-C., Khanbari, K., and Asfaw, L. M. (2006), Confirmation of Arabia plate slow motion by new GPS data in Yemen, *Journal of Geophysical Research, 111*, B02402, doi:10.1029/2004JB003229.

Wahr, J. and Bryan, F., (1998). Time Variability of the Earth's Gravity Field: Hydrological and Oceanic Effects and their Possible Detection using GRACE, *Journal Geophysical Research*, 103, 30,205-30,229.

Watson, C., Tregoning, P., Coleman, R. (2006), The Impact of Solid Earth Tide Models on GPS Coordinate and Tropospheric Time Series , *the American Geophysical Union,0094-8276/06*

Wdowinski S., Bock, Y., Zhang, J., Fang, P., and Genrich, J., (1997), Southern California Permanent GPS Geodetic Array: Spatial filtering of daily positions for estimating coseismic and postseismic displacements induced by the 1992 Landers earthquake, *Journal Geophysical Research, 102* (B8), 18057-18070.

Wdowinski, S., Bock, Y., Baer, G., Prawirodirdjo, L., Bechor, N., Naaman, S., Knafo, R., Forrai, Y. and Melzer, Y., (2004), GPS measurements of current crustal movements along the Dead Sea Fault, *Journal Geophysical Research, 109*, B05403, doi:10.1029/2003JB002640.

Wessel, P., and Smith, W. H. F., (1998), New, improved version of Generic Mapping Tools released. *EOS Trans.*, AGU, 79 (47), 579.

Wessel, P., and Walter, H. F. S., (1999), The Generic Mapping Tools (GMT), edited, http://gmt.soest.hawaii.edu/.

Williams, S. D. P. (2003), The Effect of Coloured Noise on the Uncertainties of Rates Estimated From Geodetic Time Series, *Geodesy, 76,* 483-494, doi:410.1007/s00190-00002-00283-00194.

Williams, S. D. P., (2008). CATS: GPS coordinate time series analysis software, *GPS Solutions.*, **12**(2), 147–153, doi: 10.1007/s010291–10007–10086–10294.

Williams, S. D. P., Nikolaidis, R. M., Bock, Y., Fang, P., Miller, M., and Johnson, D., (2003). MLE error analysis of global and regional continuous GPS time series. *Journal of Geophysical Research.*

Williams, S. P., Bock, Y., Fang, P., Jamason, P., Nikolaidis, R. M., Prawirodirdjo, L., Miller, M., and Johnson, D. J. (2004), Error analysis of continuous GPS position time series, *Journal of Geophysical Research, 109,* B03412, doi:10.1029/2003JB002741.

Wolfgang, T. (2001), *Geodesy,* Walter de Gruyter GmbH & Co.KG, Berlin.

Woppelmann, G., Letetrel, C., Santamaria, A., Bouin, M.-N., Collilieux, X. Altamimi, Z., Williams, S. D. P., and Martin Miguez, B., (2009). Rates of sea-level changes over the last century in a geocentric reference frame. *Geophysical Research Letter, 36,* L1207, doi:10.1029/2009GL038720.

W¨ubbena, G., Menge, F., Schmitz, M., Seeber, G., and Voelksen, C., (1998). A new approach for field calibration of absolute antenna phase center variations. In: Proc. of the 11th International Technical Meeting of the Satellite Division of the Institute of Navigation ION GPS98, 15-18 September 1998, Nashville. Institute of Navigation, Washington D. C., pp. 1205–1214.

Wyatt, F. K., (1982). Displacement of surface monuments: horizontal motion, *Journal of Geophysical Research,* 87, 979-989.

Wyatt, F., (1989). Displacement of surface monuments: vertical motion. Journal of Geophysical Research, 94:1655–1664

Yan, H., Chen, W., Zhu, Y., Zhang, W., and Zhong, M., (2009). Contribution of theral expansion of monuments and nearby bedrock to observed GPS height changes. *Geophysical Research Letter, 36,* L13303, doi:10.1029/2009GL038152.

Zhang, J., Bock, Y., Johnson, H. O., Fang, P., Williams, S. D. P., Genrich, J., Wdowinski, S., and Behr, J., (1997). Southern California Permanent GPS Geodetic Array: Error analysis of daily position estimates and site velocities. *Journal of Geophysical Research 102* (B8), 18035–18055.

Ziegler M. A. (2001). Late Permian to Holocene paleofacies of the Arabian plate and its hydrocarbon occurrences. *GeoArabia,* 6(3), 445-504